

A.I.Ch.E. JOURNAL

CHEMICAL ENGINEERING RESEARCH AND DEVELOPMENT

JUNE, 1960

THE UNIVERSITY
OF MICHIGAN

AUG 5 1960

CONTENTS

- Heat or Mass Transfer in a Fluid in Laminar Flow in a Circular or Flat Conduit
Heat and Mass Transfer to Decelerating Finely Atomized Sprays
A Corresponding-States Correlation for Higher Molecular-Weight Liquids
Concurrent Gas Absorption Mass Transfer
- Plate Efficiencies in Multicomponent Distillation
Critical Temperatures and Pressures of Organic Compounds
- Correlating Vapor Pressures and Heats of Solution for the Ammonium Nitrate-Water System:
An Enthalpy-Concentration Diagram
Hydrocarbon Vapor-Liquid Equilibria and Solubility Parameter
- Elutriation of Solid Particles From a Dense-Phase Fluidized Bed
- Mass Transfer from a Solid Soluble Sphere to a Flowing Liquid Stream
- Simultaneous Mass Transfer and Equilibrium Chemical Reaction
Modified Law of Corresponding States for Gases
- Heat Transfer to Liquid Streams in a Packed Tube Containing Large Packings
Natural Convection Inside a Horizontal Cylinder
- The Compressibility of Carbon Dioxide-Argon Mixtures
- Miniature Hydroclones as Slurry Concentrators
The Thermal Entrance Region in Fully Developed Turbulent Flow
- Diffusion in Compressed Binary Gaseous Systems
- Velocity of Large Drops and Bubbles in Media of Infinite or Restricted Extent
Mass Transfer Coefficients for Solids Suspended in Agitated Liquids
Mechanisms by Which Ultrasonic Energy Affects Transfer Rates in Liquid-Liquid Extraction
- Burning Rates of Solid Propellants
- Continuous-Throughput Rectification of Organic Liquid Mixtures with Thermal-Diffusion Columns
Momentum and Heat Transfer in Laminar Boundary-Layer Flows of Non-Newtonian Fluids Past
External Surfaces
- Use of Momentum Balance in Calibrating Orifices for Flow of Gases
The Mechanics of Vertical Moving Fluidized Systems: IV. Application to Batch-Fluidized
Systems with Mixed Particle Sizes
Point Source Turbulent Diffusion in a Pipe
- Correlating Criteria for Liquid-Phase Adsorption
- Calculation Procedures for Binary Batch Rectification
- George Martin Brown
W. P. Manning and W. H. Gauvin
A. Bondi and D. J. Simkin
W. S. Dodds, L. F. Stutzman,
B. J. Sollami, and R. J. McCarter
H. L. Toor and John K. Burchard
J. Charles Forman and
George Thodos
Donald F. Othmer and
Gerhard J. Frohlich
J. M. Prausnitz, W. C. Edmister,
and K. C. Chao
Chin-Yung Wen and
Richard F. Hashinger
Robert L. Steinberger
and Robert E. Treybal
Donald R. Olander
Oscar T. Bloomer and
Ralph E. Peck
Balapa Chennakesavan
William R. Martini and
Stuart W. Churchill
William H. Abraham and
C. O. Bennett
F. C. Engel and Joel Weisman
Peter H. Abbrecht and
Stuart W. Churchill
V. J. Berry, Jr., and
R. C. Koeller
Tibor Z. Harmathy
James J. Barker and Robert E. Treybal
H. A. Woodle, Jr., and
F. C. Vilbrandt
J. M. Smith
David R. Longmire
Andreas Acrivos, M. J. Shah,
and E. E. Petersen
J. J. Martin and V. R. Pabbi
Robert F. Hoffman, Leon Lapidus,
and J. C. Elgin
Duane L. Flint, Hisao Kada,
and Thomas J. Hanratty
Herbert L. Jones, Jr., and
Edward B. Stuart
Charles E. Huckaba and
Donald E. Danly

From
Vulcan-Cincinnati

a
new
evaporator
for
the
concentration
of
heat-sensitive
materials

*Experimental hydraulic studies
are conducted in
this test model
Stora-Vulcan Evaporator.*

VULCAN-
Cincinnati, Inc.
ENGINEERS
AND
CONSTRUCTORS • 120 Sycamore St., Cincinnati 2, Ohio

The Stora-Vulcan Evaporator—an important new concept in the design of evaporation equipment for heat-sensitive materials—offers you improved product quality, low maintenance costs, minimum utilities consumption, and minimum capital investment. Here's why:

■ Unusually low retention time minimizes thermal degradation of heat-sensitive materials.

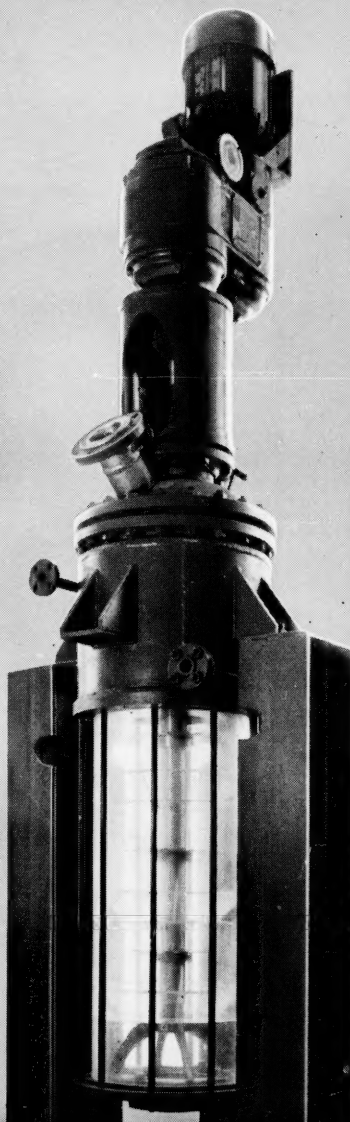
■ Highly turbulent action—with resulting high heat transfer coefficients—is achieved without the use of agitation equipment requiring close mechanical tolerances.

■ Channeling of process liquids, and non-uniform wetting of heat transfer surfaces, are prevented by centrifugal re-distribution at frequent intervals.

■ Efficient contact between liquid and vapor (or gas) assures high mass transfer rates in stripping operations, and when the evaporation process is augmented by the use of an inert carrier.

These are just a few of the reasons why the Stora-Vulcan Evaporator is ideal for the efficient evaporation or concentration of urea melt, tall oil and fatty acids, ammonium nitrate melt, plasticizers, monomers and polymers, as well as other heat-sensitive liquids.

If you'd like to know more about the Stora-Vulcan Evaporator—and how it can help solve your processing problems—write Vulcan today.



A.I.Ch.E. JOURNAL

JUNE, 1960

VOL. 6, NO. 2

The A.I.Ch.E. Journal, an official publication of the American Institute of Chemical Engineers, is devoted in the main to theoretical developments and research in chemical engineering and allied branches of engineering and science. Manuscripts should be submitted to the New York office.

PUBLISHER

F. J. Van Antwerpen

EDITOR

Harding Bliss

MANAGING EDITOR

Sylvia Fourdrinier

ADVERTISING MANAGER

P. A. Jolcuvar

ADVISORY BOARD

C. M. Cooper	R. H. Newton
O. E. Dwyer	R. L. Pigford
W. C. Edmister	E. L. Piret
E. R. Gilliland	J. M. Smith
A. N. Hixson	Theodore Vermeulen
H. F. Johnstone	R. R. White
W. R. Marshall, Jr.	R. H. Wilhelm

Publication Office, 215 Canal Street, Manchester, New Hampshire. Published quarterly in March, June, September, and December by the American Institute of Chemical Engineers, 25 West 45 Street, New York 36, New York. Manuscripts and other communications should be sent to the New York office. Correspondence with the editor may be addressed to him at Yale University, 225 Prospect Street, New Haven 11, Connecticut. Statements and opinions in the A.I.Ch.E. Journal are those of the contributors, and the American Institute of Chemical Engineers assumes no responsibility for them. Subscriptions: one year, member \$6.00; nonmember \$12.00; industrial libraries \$25.00; additional yearly postage, Canada 50 cents, Pan American Union \$1.50, other foreign \$2.00 (foreign subscriptions payable in advance). Single copies: \$4.00. Second-class mail. Postage paid at Manchester, New Hampshire. Copyright 1960 by the American Institute of Chemical Engineers. National headquarters of A.I.Ch.E. is concerned about nondelivery of copies of the A.I.Ch.E. Journal and urgently requests subscribers to give prompt notification of any change of address. Sixty days must be allowed for changes to be made in the records.

Postmaster: Please send form 3579 to A.I.Ch.E. Journal, 25 West 45 Street, New York 36, N. Y.

Conservation and Engineering IV. Industrial Raw Materials	177
Heat or Mass Transfer in a Fluid in Laminar Flow in a Circular or Flat Conduit	George Martin Brown 179
Heat and Mass Transfer to Decelerating Finely Atomized Sprays	W. P. Manning and W. H. Gauvin 184
A Corresponding-States Correlation for Higher Molecular-Weight Liquids	A. Bondi and D. J. Simkin 191
Concurrent Gas Absorption Mass Transfer	W. S. Dodds, L. F. Stutzman, B. J. Sollami, and R. J. McCarter 197
Plate Efficiencies in Multicomponent Distillation	H. L. Toor and John K. Burchard 202
Critical Temperatures and Pressures of Organic Compounds	J. Charles Forman and George Thodos 206
Correlating Vapor Pressures and Heats of Solution for the Ammonium Nitrate-Water System	Donald F. Othmer and Gerhard J. Frohlich 210
Hydrocarbon Vapor-Liquid Equilibria and Solubility Parameter	J. M. Prausnitz, W. C. Edmister, and K. C. Chao 214
Elutriation of Solid Particles From a Dense-Phase Fluidized Bed	Chin-Yung Wen and Richard F. Hashinger 220
Mass Transfer from a Solid Soluble Sphere to a Flowing Liquid Stream	Robert L. Steinberger and Robert E. Treybal 227
Simultaneous Mass Transfer and Equilibrium Chemical Reaction	Donald R. Olander 233
Modified Law of Corresponding States for Gases	Oscar T. Bloomer and Ralph E. Peck 240
Heat Transfer to Liquid Streams in a Packed Tube Containing Large Packings	Balapa Chennakesavan 246
Natural Convection Inside a Horizontal Cylinder	William R. Martini and Stuart W. Churchill 251
The Compressibility of Carbon Dioxide-Argon Mixtures	William H. Abraham and C. O. Bennett 257
Miniature Hydroclones as Slurry Concentrators	F. C. Engel and Joel Weisman 262
The Thermal Entrance Region in Fully Developed Turbulent Flow	Peter H. Abbrecht and Stuart W. Churchill 268
Diffusion in Compressed Binary Gaseous Systems	V. J. Berry, Jr., and R. C. Koeller 274
Velocity of Large Drops and Bubbles in Media of Infinite or Restricted Extent	Tibor Z. Harmathy 281
Mass Transfer Coefficients for Solids Suspended in Agitated Liquids	James J. Barker and Robert E. Treybal 289
Mechanisms by Which Ultrasonic Energy Affects Transfer Rates in Liquid-Liquid Extraction	H. A. Woodle, Jr., and F. C. Vilbrandt 296
Burning Rates of Solid Propellants	J. M. Smith 299
Continuous-Throughput Rectification of Organic Liquid Mixtures with Thermal-Diffusion Columns	David R. Longmire 304
Momentum and Heat Transfer in Laminar Boundary-Layer Flows of Non-Newtonian Fluids Past External Surfaces	Andreas Acrivos, M. J. Shah, and E. E. Petersen 312
Use of Momentum Balance in Calibrating Orifices for Flow of Gases	J. J. Martin and V. R. Pabbi 318
The Mechanics of Vertical Moving Fluidized Systems: IV.	Robert F. Hoffman, Leon Lapidus, and J. C. Elgin 321
Point Source Turbulent Diffusion in a Pipe	Duane L. Flint, Hisao Kada, and Thomas J. Hanratty 325
Correlating Criteria for Liquid-Phase Adsorption	Herbert L. Jones, Jr., and Edward B. Stuart 332
Calculation Procedures for Binary Batch Rectification	Charles E. Huckaba and Donald E. Danly 335
Communications to the Editor	Howard F. Rase and R. R. Padhye 343
	A. O. Converse 344
	Donald R. Olander 346
	Edgar B. Gutoff 347
Abstracts	
Symposium Series	350
Computer Interchange Program	8J
Books	2J

HEVI-DUTY

"Multiple Unit"

CRUCIBLE FURNACES

Temperatures to 2300° F.

Designed for

- ★ Melting Small Quantities of Metals
- ★ Pyrometer Calibrations
- ★ Heating All Materials Contained in Crucibles

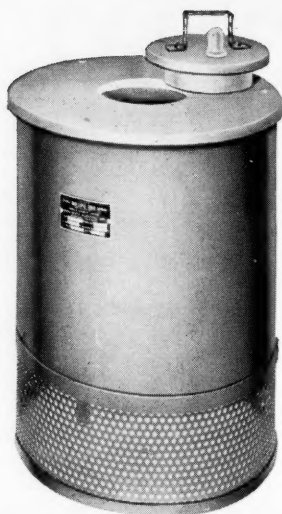
Laboratory technicians using Hevi-Duty Crucible Furnaces find they give the dependable service demanded by exacting research. Improved insulation and sturdy, long-life heating element construction are a few of the advantageous features.

Write for Bulletin 1246.

HOT CRUCIBLE FURNACES TO 2300° F.

Type	Size	Price
HDT-304*	3" x 4"	\$170.00*
HDT-506*	5" x 6"	270.00*
HDT-812*	8" x 12"	430.00*

*Requires a Transformer.



MU CRUCIBLE FURNACES TO 1850° F.

Type	Chamber Heating		Furnace Price
	Dia.	Deep	
82	2 3/4"	x 4"	\$ 47.50
84	3"	x 3 1/2"	58.00
86	3"	x 5"	71.00
506	5"	x 6"	110.00

FOR GENERAL AND SPECIALIZED LABORATORY APPLICATIONS

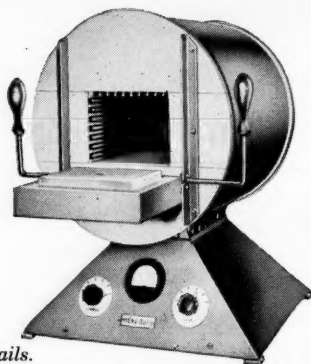
"Multiple Unit"

MUFFLE FURNACE

Temperatures to 1850° F.

This furnace is a complete self-contained unit with the temperature indicating and controlling devices conveniently located in the pyramidal base. Four interchangeable and reversible heating units of heavy gauge Nickel Chromium Wire installed in grooved refractory plates completely surround the heating chamber.

Write for Bulletin 849 for complete details.



Type	Watts	Chamber			Price
		W.	L.	H.	
051-PT	1150	5 1/4"	8	4	\$ 145.00
052-PT	1440	4 1/4"	10	3	210.00
054-PT	2070	5 1/4"	12	4	245.00
056-PT	3400	7 1/2"	14	5	315.00
012148-PT*	6500	11 1/4"	14	8	1050.00

Operating voltage either 115 or 230 volts A.C. only except 012148-PT is 230 volt only.
*Automatic temperature control \$230.00 additional.

HEVI-DUTY

A DIVISION OF



BASIC PRODUCTS CORPORATION

HEVI-DUTY ELECTRIC COMPANY, MILWAUKEE 1, WISCONSIN

Industrial Furnaces and Ovens, Electric and Fuel • Laboratory Furnaces • Dry Type Transformers • Constant Current Regulators

BOOKS

Chemical Process Principles, Part II, Thermodynamics, 2 ed., O. A. Hougen, K. M. Watson, and R. A. Ragatz. John Wiley and Sons, New York (1959). 537 pages. \$9.75.

The first edition of this excellent text has been revised to a considerable extent. Most of the recent advances in chemical engineering thermodynamics are included, particularly material on generalized thermodynamic properties, thermodynamics of fluid flow, and thermodynamics of separation processes. The recent developments in application of irreversible thermodynamics to chemical engineering are not discussed.

One of the major improvements in the new edition is contained in the opening chapter, which has been expanded and clarified, particularly with respect to the discussion of entropy. The result is a much better presentation for the beginning student in thermodynamics of the basic first-and second-law principles.

The added information on generalized thermodynamic properties consists of much of the material published previously by Lydersen, Greenkorn, and Hougen ("Generalized Thermodynamic Properties of Pure Fluids," University of Wisconsin Engineering Experimental Station Report 4, 1955). This section represents a valuable addition to the data available for calculation of thermodynamic properties; however the inclusion of such material is not without its disadvantages. The presentation of so many tables of generalized properties and related functions requires much of the discussion of the calculation of thermodynamic properties to be based wholly on generalized equations and methods involving precalculated values of functions. This is most convenient for ease in solution of problems, but for a beginning student this approach may tend to obscure somewhat the basic relationships of thermodynamic properties with p - v - t properties, rather than simplify matters. These concepts, however, are illustrated by the inclusion of numerous examples involving the use of generalized properties.

Material on the expansion and compression of fluids included in the first edition has been split into separate sections in the new volume, resulting in a much clearer presentation of the topics discussed. The added chapter on the thermodynamics of fluid flow presents an excellent treatment of this subject.

Additional material covered in the new edition includes the thermodynamics of solutions, vapor-liquid equilibrium (Continued on page 8f)

Conservation and Engineering

IV. Industrial Raw Materials

The major raw materials on which our whole industrial civilization is based are metals; nonmetallic minerals such as sand, gravel, cement rock, salt, and sulfur; coal, oil, and gas for the generation of energy; and renewable materials—wood, fibers, and other plants. Water and air, which belong in this classification, will be discussed later. The abundant earth has always before yielded up more and more as man has sought to develop its resources, but it is perfectly obvious that this sequence cannot continue forever. The supply of these materials is finite; there seems to be no such limitation to the demand for them. Two examples will make clear the fact that we have already gone a long way on the path to exhaustion:

1. Copper was first found as native 100 per cent metal. By 1900 the usual ore was about 5 per cent copper; now in this country it is about 0.5 per cent.

2. Colonel Drake's oil well was 69 feet deep; today such wells are commonly 10,000 to 15,000 feet deep.

High-grade, easily accessible raw materials make for cheap production. As we rely more on low-grade inaccessible substances, we shall find ever higher costs and much greater difficulties in enjoying the fruits of our industrialization.

In the past we have turned increasingly to other parts of the world for raw materials, and we have thus avoided the immediate consequences of excessive consumption of our own. The oil of the Middle East, the copper of Chile, and the iron ore of Venezuela are typical. The whole trend of the times, however, is to greater industrialization in other parts of the world, and when this trend has brought that industrialization to appreciable proportions we shall have much more difficulty in importing these raw materials. Again, costs will increase, or bartering systems will arise that will perhaps shut us off completely from such sources because of our probable inability to offer anything in exchange.

There are some things we can do, and they are all matters particularly suitable for us as engineers to do.

1. Obviously we must turn to the development of lower quality, less accessible materials. The research

and development required to permit economical processing will require chemical engineering of the finest quality.

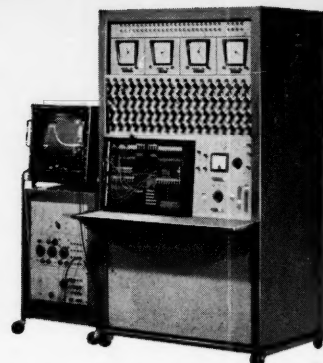
2. We must improve our exploration. The mining engineers, physicists, and oceanographers will be very important in such searching. The results of the International Geophysical Year showing rich deposits of manganese, iron, cobalt, and copper on the bottoms of the oceans are most reassuring. Estimates of the manganese found indicate that it is present to the extent of forty times the known world reserves.

3. We must make better use of materials, that is, waste less. We must keep *conservation* constantly in mind, and we must try to stop some of the appalling waste. In chemical processing we all know of the waste associated with pollution; we shall have to reduce this not only to eliminate the pollution but to recover materials. We ought also to try to reduce the waste associated with certain items over which we may have no direct control. It is difficult to imagine a greater dissipater of our national resources than the modern automobile—two tons of materials and 2 to 3 gallons of petroleum to transport a single individual to a ball game.

4. We must develop substitute materials. Over 5 per cent of the earth's crust is iron; aluminum is 800 times as abundant as copper. These will last a long time, and they will be more and more used. We must also develop additional synthetic materials from coal, oil, and gas to replace those now grown on land, since the land must be used more and more for food production. Coal, oil, and gas are certainly exhaustible as fuels, but as chemical raw materials they would last thousands of times as long. This suggestion is diametrically opposed to that of the President's Materials Policy Commission of 1952; that commission seemed to overlook the demands on the land which growing populations must make for food.

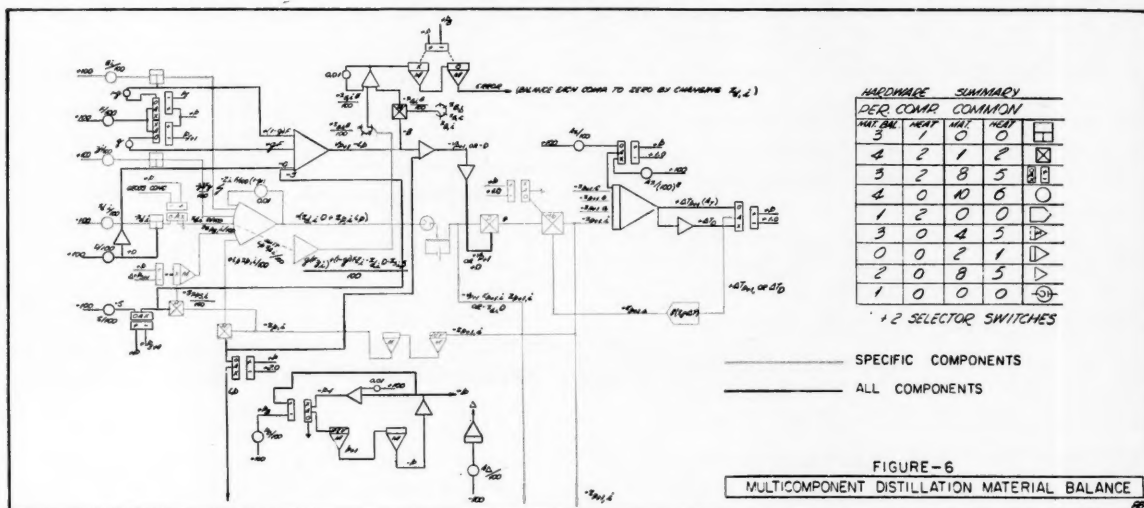
We engineers have the facts, the skills, and the methods to alleviate these problems. We should bring them to bear on our jobs, our communities, and our government.

H.B.



HOW TO SOLVE MULTI-COMPONENT DISTILLATION PROBLEMS IN 60 SECONDS

• AUTOMATICALLY • ACCURACY TO $\pm 0.05\%$ • FOR ANY SET OF SPECIFICATIONS



Multi-component Distillation Material Balance,
From 13-page design report available on request.

DYSTAC* completely obsoletes all other methods
for plate-to-plate calculations.

With DYSTAC computers you can now solve design and production problems, control limits, and optimize cost and materials! DYSTAC is truly an advancement in the state-of-the-art. Never before has there been an analog computer which combines the best features of both analog and digital machines.

Here's a partial list of just some of the applications of DYSTAC:

- Heat exchanger design
- Oil reservoir studies
- Transient process problems
- Distillation column design
- Multi-dimensional partials (steady state or transient)
- Regeneration and conversion design
- Fluid flow problems
- Pipelines and piping networks

Not only can DYSTAC solve problems which were previously unsolvable, but DYSTAC is also one of the easiest analog computers to program. Offers the greatest add-on capacity. Assures minimum down time. *Guarantees* its specifications as being minimum standard under actual operating conditions.

For the complete 13-page design digest of the multi-component distillation problem-solution, request CSI form #80-1-5-001.

*Dynamic memory STorage Analog Computer



COMPUTER SYSTEMS, INC., Culver Road, Monmouth Junction, N. J. • DAVIS 9-2351
A Schlumberger Subsidiary • formerly Mid-Century Instrument Corp.

Heat or Mass Transfer in a Fluid in Laminar Flow in a Circular or Flat Conduit

GEORGE MARTIN BROWN

Northwestern University, Evanston, Illinois

Accurate solutions to the Graetz equation and to the similar equation for flow between two parallel plates are presented including the first ten or eleven eigenvalues and important derivatives. The first six eigenfunctions are also presented at intervals of 0.05 from $y = 0$ to $y = 1$.

The similar problems of steady state conduction of heat and the steady state diffusion in a fluid flowing in a circular or flat duct have been studied by many investigators. The Fourier-Poisson equation for steady state heat conduction (11, 28) may be written

$$\nabla \cdot \nabla t = \alpha \nabla^2 t \quad (1)$$

or

$$V_x \frac{\partial t}{\partial x} + V_y \frac{\partial t}{\partial y} + V_z \frac{\partial t}{\partial z} = \alpha \left[\frac{\partial^2 t}{\partial x^2} + \frac{\partial^2 t}{\partial y^2} + \frac{\partial^2 t}{\partial z^2} \right] \quad (1a)$$

For one directional flow in a round tube with axial symmetry this equation becomes

$$\frac{V}{\alpha} \frac{\partial t}{\partial x} = \frac{1}{r} \frac{\partial}{\partial r} \left(r \frac{\partial t}{\partial r} \right) + \frac{\partial^2 t}{\partial x^2} \quad (2)$$

In laminar flow the velocity distribution is parabolic, and $V = V_{\max} [1 - (r/R)^2]$; $(\partial^2 t / \partial x^2)$ is usually so small in comparison with the other terms that it can be neglected without much error. Equation (2) can therefore be written in dimensionless form as

$$(1-y^2) \frac{\partial T}{\partial z} = \frac{1}{y} \frac{\partial}{\partial y} \left(y \frac{\partial T}{\partial y} \right) \quad (3)$$

where $z = 2\alpha x / D^2 V_{\max} = 2x / DN_{Re} N_{Pr}$
 $y = r/R$
 $T = (t - t_s) / (t_o - t_s)$

For one directional flow in a flat duct (between two parallel plates) the corresponding equation is

$$\frac{3}{8} (1-y^2) \frac{\partial T}{\partial z} = \frac{\partial^2 T}{\partial y^2} \quad (4)$$

where $z = \alpha x / 4 R^2 V_{\max} = x / R N_{Re} N_{Pr}$. The corresponding equations for mass transfer by diffusion are usually written with concentration or partial pressure in place of temperature, and diffusivity in place of thermal diffusivity.

The first published solution to Equation (3) was presented by Graetz (13, 14). The assumptions and boundary conditions made by Graetz are constant thermal diffusivity, constant tube wall temperature, temperature symmetrical about the axis, uniform temperature at tube inlet, fully developed parabolic velocity profile at tube inlet, and negligible conduction in direction of flow.

These assumptions correspond to the following boundary conditions:

1. $T = 1$ $0 \leq y \leq 1$ $-\infty \leq z < 0$
2. $T = 0$ $y = 1$ $0 < z \leq +\infty$
3. $\partial T / \partial y = 0$ $y = 0$ $-\infty \leq z \leq +\infty$
4. $T = 0$ $0 \leq y \leq 1$ $z = +\infty$

This solution to Equation (3) may be written as

$$T = \sum_{n=1}^{\infty} C_n Y_n \exp(-\lambda_n^2 z) \quad (5)$$

where λ_n is the n^{th} eigenvalue which is necessary for the solution to the differential equation

$$\frac{\partial^2 Y}{\partial y^2} + \frac{1}{y} \frac{\partial Y}{\partial y} + \lambda^2 (1-y^2) Y = 0 \quad (6)$$

corresponding to the boundary conditions $\dot{Y} = 0$ at $y = 1$, and $\partial Y / \partial y = 0$ at $y = 0$. The coefficients C_n , which make Equation (5) satisfy the boundary condition $T = 1$ at $z = 0$ and $0 \leq y < 1$, are obtained from

$$T = 1 = \sum_{n=1}^{\infty} C_n Y_n \quad (7)$$

by multiplying both sides of Equation (7) by $Y_m y (1-y^2) dy$ and integrating from $y = 0$ to $y = 1$. This procedure results in

$$C_n = \frac{\int_0^1 Y_n y (1-y^2) dy}{\int_0^1 Y_n^2 y (1-y^2) dy} = \frac{-2}{\lambda_n \left(\frac{\partial Y_n}{\partial \lambda_n} \right)_{y=1}} \quad (8)$$

which comes from

$$\int_0^1 Y_n Y_m y (1-y^2) dy = 0 \quad \text{if } n \neq m$$

$$\int_0^1 Y_n^2 y (1-y^2) dy =$$

$$\frac{1}{2\lambda_n} \left(\frac{\partial Y_n}{\partial y} \cdot \frac{\partial Y_n}{\partial \lambda_n} \right)_{y=1} \quad \text{if } n = m$$

$$\int_0^1 Y_n y (1-y^2) dy =$$

$$-\frac{1}{\lambda_n^2} \left(\frac{\partial Y}{\partial y} \right)_{y=1}$$

The function $Y_n(y)$ may be represented by the infinite series

$$Y_n = \sum_{i=0}^{\infty} a_{ni} y^i \quad (9)$$

where $a_{ni} = 0$ if $i < 0$

$$a_{ni} = 1 \text{ if } i = 0$$

$$a_{ni} = -\lambda_n^2 (a_{i-2} - a_{i-4}) / i^2$$

or the equivalent series

$$Y_n = \sum_{i=0}^{\infty} \sum_{j=0}^{\infty} A_{ij} \lambda_n^{2i} y^{2j} \quad (10)$$

TABLE 1. EIGENVALUES AND DERIVATIVES—ROUND CASE

n	λ_n	$(\partial Y_n / \partial \lambda)_y = 1$	$(\partial Y_n / \partial y)_y = 1$
1	2.70436 44199	-0.50089 91914	-1.01430 04587
2	6.67903 14493	0.37146 22734	1.34924 16221
3	10.67337 95381	-0.31826 44696	-1.57231 93392
4	14.67107 84627	0.28648 21001	1.74600 43350
5	18.66987 18645	-0.26449 06034	-1.89085 71240
6	22.66914 33588	0.24799 44920	2.01646 66530
7	26.66866 19960	-0.23496 76067	-2.12816 47501
8	30.66832 33409	0.22430 62663	2.22925 54182
9	34.66807 38224	-0.21534 85062	-2.32194 33391
10	38.66788 33469	0.20766 87724	2.40778 11647
11	42.66773 38055	-0.20097 87384	-2.48790 82547

TABLE 2. EIGENFUNCTIONS—ROUND CASE

y	Y_1	Y_2	Y_3	Y_4	Y_5	Y_6	y
0.00	1.00000000	1.00000000	1.00000000	1.00000000	1.00000000	1.00000000	0.00
0.05	0.99543708	0.97232998	0.93009952	0.87000981	0.79384934	0.70387285	0.05
0.10	0.98184469	0.89180935	0.73545009	0.53108099	0.30228888	0.07488082	0.10
0.15	0.95950842	0.76560457	0.45728832	0.11310661	-0.18271103	-0.36382498	0.15
0.20	0.92889268	0.60469973	0.15247311	-0.23303152	-0.40260123	-0.32121955	0.20
0.25	0.89062392	0.42260986	-0.12055081	-0.39912334	-0.29328114	0.03117856	0.25
0.30	0.84546827	0.23385711	-0.31521322	-0.35914102	0.00054293	0.28981991	0.30
0.35	0.79430462	0.05242653	-0.40611068	-0.16904247	0.24974768	0.22529155	0.35
0.40	0.73809441	-0.10959274	-0.39208452	0.06793183	0.29907438	-0.04765772	0.40
0.45	0.67784945	-0.24301831	-0.29305410	0.24985073	0.14844781	-0.24623845	0.45
0.50	0.61459912	-0.34214076	-0.14234190	0.31507157	-0.07973259	-0.20531795	0.50
0.55	0.54935825	-0.40482321	0.02279222	0.25703015	-0.24057455	0.00683579	0.55
0.60	0.48309693	-0.43218156	0.16968455	0.11416883	-0.25522963	0.19749710	0.60
0.65	0.41671327	-0.42794545	0.27593866	-0.05472615	-0.13791706	0.22889512	0.65
0.70	0.35100978	-0.39762949	0.33148788	-0.19604286	0.03610027	0.10372100	0.70
0.75	0.28667401	-0.34764861	0.33742641	-0.27757775	0.18482648	-0.07719162	0.75
0.80	0.22426362	-0.28449432	0.30272281	-0.29224076	0.25918362	-0.20893147	0.80
0.85	0.16419583	-0.21405616	0.24015828	-0.25200258	0.25273850	-0.24408867	0.85
0.90	0.10674088	-0.14113350	0.16262482	-0.17762079	0.18817264	-0.19521652	0.90
0.95	0.05201900	-0.06914371	0.08046102	-0.08916322	0.09629593	-0.10234372	0.95
1.00	0.00000000	0.00000000	0.00000000	0.00000000	0.00000000	0.00000000	1.00

where

$$A_{ij} = 0 \text{ if } j < i, j > 2i, \text{ or } i < 0$$

$$A_{ij} = 1 \text{ if } i = j = 0$$

and in general

$$A_{ij} = \frac{A_{i-1, j-2} - A_{i-1, j-1}}{(2j)^2}$$

These coefficients A_{ij} have been calculated for $0 \leq i \leq 7$ and $0 \leq j \leq 14$.

C_n and λ_n of Equation (5) have previously been calculated for only the first five values of n and to only a few significant figures (1, 5, 7, 13, 14, 17, 20, 21, 22, 23, 27, 30, 34). Y_n has been given only for $n = 1, 2, 3, 4$ (17, 21, 27, 34). Expressions have been derived for approximations to all the eigenvalues and related constants, which become increasingly accurate as $n \rightarrow \infty$ (20, 31). The need for accurate values for the eigenvalues and functions has recently been shown (24, 33).

SOLUTION TO GRAETZ EQUATION FOR ROUND DUCT

The eigenvalues of the Graetz equation can be calculated from Equation (9) by a trial-and-error procedure. A trial value of λ is used to obtain the coefficients, and Y is obtained for the

case $y = 1$. In addition to the calculation of Y the two partial derivatives $(\partial Y / \partial \lambda)_{y=1}$ and $(\partial Y / \partial y)_{y=1}$ are also calculated. The calculation of these quantities to any degree of accuracy with a desk calculator is extremely laborious, even for the first few eigenvalues, and practically impossible for values beyond about $n = 5$. This is due to the fact that the first few terms of the infinite series become progressively larger (until about the term $i = \sqrt{2\lambda}$) before becoming smaller. The largest term in this series is equal to about 10^{2n} , and the number of terms which have to be calculated is about $n^2 + m$ (where m is about equal to the number of significant figures desired in the answers).

To obtain accurate eigenvalues and related derivatives the computation was done on an IBM 650 electronic computer. The computation program was designed to handle terms which contained up to fifty significant figures (twenty to the left of the decimal point and thirty to the right). This program was used to compute λ_n , λ_n^2 , $(\partial Y_n / \partial \lambda)_n$, $(\partial Y_n / \partial y)_n$, and Y_n vs. y with an accuracy of about thirty significant figures for values of n up to 11.

The method of computation included calculation of Y_n and its derivatives by means of the following series:

$$Y_n]_{y=1} = a_0 + a_2 + a_4 + a_6 + \dots + a_i + \dots \quad (11)$$

where

$$a_i = -\lambda_n^2 (a_{i-2} - a_{i-4}) / i^2$$

$$\partial Y / \partial \lambda]_{y=1} = \frac{\partial a_2}{\partial \lambda} + \frac{\partial a_4}{\partial \lambda} + \dots \quad (12)$$

where

$$\frac{\partial a_i}{\partial \lambda} = \frac{-2\lambda}{i^2} (a_{i-2} - a_{i-4}) - \frac{\lambda^2}{i^2} \left[\frac{\partial a_{i-2}}{\partial \lambda} - \frac{\partial a_{i-4}}{\partial \lambda} \right]$$

$$\frac{\partial a_0}{\partial \lambda} = 0$$

$$(\partial Y / \partial y)_{y=1} = 2a_2 + 4a_4 + \dots + ia_i + \dots \quad (13)$$

The series was continued until $a_i < 10^{-30}$ and the sums taken. From each trial calculation were obtained Y , $\partial Y / \partial \lambda$, and $\partial Y / \partial y$ (all for $y = 1$). From these values the next trial $\lambda_{n,j+1}$ was obtained from the previous trial value $\lambda_{n,j}$ by

$$\lambda_{n,j+1} = \lambda_{n,j} - \frac{Y}{\partial Y / \partial \lambda} \quad (14)$$

By this procedure it was possible to obtain eigenvalues accurate to about thirty significant figures with as few as four trials. The results of these calculations rounded to ten decimal places are given in Table 1.

After each eigenvalue was determined with sufficient accuracy, Y_n was calculated for different values of y .

* Tabular material has been deposited as document No. 6126 with the American Documentation Institute, Photoduplication Service, Library of Congress, Washington 25, D. C., and may be obtained for \$1.25 for photoprints or \$1.25 for 35-mm. microfilm.

TABLE 3. COMPARISON OF EIGENVALUES—ROUND CASE

		λ_1	λ_2	λ_3	λ_4	λ_5
Graetz	(13,14)	2.7043	6.50			
Nusselt	(27)	2.705	6.66	10.3		
Drew	(7)	2.70436	6.6791			
Lee	(21)	2.704	6.679	10.673	14.671	
Yamagata	(34)	2.704365	6.67903	10.67340	14.6712	18.67
Brinkman	(5)	(2.704)*	(6.679)	(10.673)	(14.63)	
Lauwerier	(20)	(2.70434)*	(6.680)	(10.6734)	(14.67108)	
Schenk	(30)	2.70437	6.6790	10.6733		18.670
Abramowitz	(1)	2.7043644	6.679032	10.67338	14.67108	18.66987
Sellers	(31)	2 2/3	6 2/3	10 2/3	14 2/3	18 2/3
Sellers	(31)	2.71	6.69	10.62	14.58	
Lipkis	(23)	2.7043644	6.679032	10.67338	14.67108	18.66987
Brown		2.7043644199	6.6790314493	10.6733795381	14.6710784627	18.6698718645

*Values in parentheses were calculated from data reported in reference.

These calculations were made from the terms of Equation (11) already calculated by the use of Equation (9)

$$Y_n = a_0 + a_0 y^2 + a_1 y^4 + \dots \quad (9)$$

for values of y between 0 and 1 at increments of 0.05. Table 2 gives these results for the first six eigenfunctions rounded to eight decimal places.

Equation (5) gives T as a function of y and z . The average or cup-mixing temperature is

$$T_{AV} = \frac{\int_0^1 T V 2 \pi y dy}{\pi V_{av}}$$

Since

$$V = 2 V_{av} (1 - y^2)$$

and

$$T_{AV} = \int_0^1 4T (1 - y^2) y dy$$

$$T_{AV} = \sum_{n=1}^{\infty} \left[\frac{-8}{\lambda_n \left(\frac{\partial Y_n}{\partial \lambda_n} \right)_{y=1}} \right]$$

$$\left[\exp(-\lambda_n^2 z) \right] \int_0^1 Y_n y (1 - y^2) dy \Big]$$

$$T_{AV} = \sum_{n=1}^{\infty} \frac{8 \left(\frac{\partial Y_n}{\partial y} \right)_{y=1}}{\lambda_n \left(\frac{\partial Y_n}{\partial \lambda_n} \right)_{y=1}} \exp(-\lambda_n^2 z) \quad (15)$$

COMPARISON OF RESULTS

Equations (5), (8), and (15) have previously been derived by several writers (4, 5, 7, 14, 15, 17, 27, 34), and their applications to heat transfer (8, 9, 10, 17, 18, 19, 24, 26, 31, 33, 34) and mass transfer (2, 3, 6, 12, 32) have been discussed. A comparison of the eigenvalues with those previously calculated is given in Table 3. A comparison of the eigenfunctions $(\partial Y / \partial \lambda)$ and $(\partial Y / \partial y)$ with those previously calculated has been made.*

* See footnote on page 180.

TABLE 4. EIGENVALUES AND DERIVATIVES—FLAT CASE

f	λ_f	$(\partial Y_f / \partial \lambda)_y = 1$	$(\partial Y_f / \partial y)_y = 1$
1	1.68159 53222	-0.99043 69608	-1.42915 55060
2	5.66985 73459	1.17910 73461	3.80707 01070
3	9.66824 24625	-1.28624 87056	-5.92023 79188
4	13.66766 14426	1.36201 96175	7.89253 51208
5	17.66737 35653	-1.42132 56612	-9.77094 42849
6	21.66720 53243	1.47040 11597	11.57980 87072
7	25.66709 64863	-1.51246 03349	-13.33387 89738
8	29.66702 10447	1.54938 60066	15.04298 83445
9	33.66696 60687	-1.58238 01630	-16.71412 93950
10	37.66692 44563	1.61225 92197	18.35251 24063

The function $Y_n(y)$ has been previously calculated (17, 21, 27, 34) to only three or four significant figures and for only the first four values of n .

Although values of Y_n in Table 2 are given for only the first six values of n , at increments of 0.05, and reported to only eight significant figures, the program is capable of calculating Y_n for any n up to 11, any y between 0 and 1, and with an accuracy of nearly thirty significant figures. Results are now available for $n = 1$ to $n = 5$, $y = 0$ to $y = 1$ with increments of 0.02 with Y to thirty places.

SOLUTION TO EQUATION FOR FLAT DUCT

Equation (4) and its solution for the case with the same boundary conditions as for Equation (5) has been derived (29, 31). This solution is

$$T = \sum_{f=1}^{\infty} C_f \cdot Y_f \cdot \exp\left(-\frac{8}{3} \lambda_f^2 z\right) \quad (16)$$

where λ_f is the f^{th} eigenvalue, which is necessary for the solution to the differential equation

$$\frac{\partial^2 Y}{\partial y^2} + \lambda^2 (1 - y^2) Y = 0 \quad (17)$$

corresponding to the boundary conditions $Y = 0$ at $y = 1$, $\partial Y / \partial y = 0$ at $y = 0$. The C_f , which make Equation (16) satisfy the boundary condition $T = 1$ at $z = 0$ and $-1 \leq y \leq 1$ are obtained from

$$T = 1 = \sum_{f=1}^{\infty} C_f Y_f \quad (18)$$

Multiplying both sides by $Y_n (1 - y^2) dy$ and integrating from $y = 0$ to $y = 1$ one obtains

TABLE 5. EIGENFUNCTIONS—FLAT CASE

y	y_1	y_2	y_3	y_4	y_5	y_6	y
0.00	1.00000000	1.00000000	1.00000000	1.00000000	1.00000000	1.00000000	0.00
0.05	0.99646885	0.96010074	0.88546018	0.77552799	0.63468541	0.46854394	0.05
0.10	0.98591788	0.84377192	0.56853419	0.20356398	-0.19367528	-0.56064196	0.10
0.15	0.96847352	0.66076030	0.12249535	-0.45940625	-0.88289598	-1.00084872	0.15
0.20	0.94434300	0.42615789	-0.35125799	-0.92127048	-0.94139939	-0.39858805	0.20
0.25	0.91380933	0.15883318	-0.74804895	-0.98588465	-0.33711948	0.61543949	0.25
0.30	0.87722437	-0.12047066	-0.98430775	-0.63425823	0.50149201	1.01611220	0.30
0.35	0.83500029	-0.39113244	-1.01518005	-0.02144606	1.00745915	0.42451165	0.35
0.40	0.78759965	-0.63450596	-0.84140636	0.60158620	0.86317657	-0.57373954	0.40
0.45	0.73552430	-0.83542525	-0.50482523	0.99796998	0.18131026	-1.05774223	0.45
0.50	0.67930340	-0.98321739	-0.07498014	1.03501041	-0.61211784	-0.62716953	0.50
0.55	0.61948097	-1.07215385	0.36866934	0.71960900	-1.06882651	0.32311352	0.55
0.60	0.55660303	-1.10134778	0.75396988	0.17433415	-0.97130705	1.03602948	0.60
0.65	0.49120483	-1.07417239	1.02875272	-0.42445889	-0.40612604	1.02291537	0.65
0.70	0.42379830	-0.99732402	1.16687578	-0.91420090	0.34092183	0.35052804	0.70
0.75	0.35485987	-0.87967811	1.16760186	-1.19276885	0.96322186	-0.53240219	0.75
0.80	0.28481910	-0.73108692	1.04990111	-1.23289457	1.27030674	-1.16513731	0.80
0.85	0.21404783	-0.56124735	0.84407970	-1.06843948	1.23140209	-1.32944153	0.85
0.90	0.14285022	-0.37873136	0.58311581	-0.76562278	0.92849439	-1.07197987	0.90
0.95	0.07145363	-0.19022795	0.29544440	-0.39311565	0.48542365	-0.57342785	0.95
1.00	0.00000000	0.00000000	0.00000000	0.00000000	0.00000000	0.00000000	1.00

$$C_f = \frac{\int_0^1 Y_f (1-y^2) dy}{\int_0^1 Y_f^2 (1-y^2) dy} =$$

$$\frac{-2}{\lambda_f \left(\frac{\partial Y_f}{\partial \lambda_f} \right)_{y=1}} \quad (19)$$

The eigenvalues and related func-

tions can be easily calculated from the infinite series

$$Y_f = \sum_{i=0}^{\infty} b_{fi} y^i \quad (20)$$

in exactly the same manner as was done for the round duct with a single change. The recursion formulas for b_f

and $\partial b/\partial \lambda$ are slightly different from those for a_n in that i^2 is replaced by $i(i-1)$. These formulas are

$$b_{f,i} = -\lambda_f^2 (b_{f,i-2} - b_{f,i-1}) / i(i-1)$$

$$\frac{\partial b_i}{\partial \lambda} = \frac{-2\lambda}{i(i-1)} (b_{i-2} - b_{i-1}) -$$

TABLE 6. COMPARISON OF EIGENVALUES AND DERIVATIVES—FLAT CASE

f		1	2	3	4	5	6
λ_f							
Prins	(29)	1.6816	5.6699	9.6678			
Schenk	(30)	1.6816	5.6699	9.6678	13.6677	17.667	
Sellars	(31)	1 2/3	5 2/3	9 2/3	13 2/3	17 2/3	21 2/3
Harris	(16)	1.68159532	5.66985734	9.66824246	13.66766144	17.66737357	21.66720532
Brown		1.6815953222	5.6698573459	9.6682424625	13.6676614426	17.6673735653	21.6672053243
$(\partial Y/\partial \lambda)$							
Prins	(29)	-0.990	1.21	-1.35			
Sellars	(31)	(-0.95887185)*	(1.17581877)	(-1.28528242)	(1.36164181)	(-1.42116624)	(1.47034008)
Harris	(16)	-0.99043694	1.17910684	-1.28624824	1.36201795	-1.42132438	1.47039947
Brown		-0.9904369608	1.1791073461	-1.2862487056	1.3620196175	-1.4213256612	1.4704011597
$(\partial Y/\partial y)$							
Prins	(29)	-1.434	3.86	-5.9			
Sellars	(31)	(-1.36514243)*	(3.78509744)	(-5.90701347)	(7.88296340)	(-9.76336489)	(11.57348340)
Harris	(16)	-1.429155504	3.807070140	-5.920237920	7.892535140	-9.770944400	11.57980880
Brown		-1.4291555060	3.8070701070	-5.9202379188	7.8925351208	-9.7709442848	11.5798087072

*Values in parentheses were calculated from equations given by sellars (31), who also reported incorrect values for C_f and $-C_f (\partial Y/\partial y)$, which should be multiplied by 2.5. The corrected equations are:

$$C_f = (-1)^f 2.27114 \lambda_f^{-7/6} \quad \text{and} \quad -C_f (\partial Y/\partial y) = 2.02557 \lambda_f^{-1/3}$$

$$\frac{\lambda^2}{i(i-1)} \left(\frac{\partial b_{i-2}}{\partial \lambda} - \frac{\partial b_{i-4}}{\partial \lambda} \right)$$

The resulting calculated values rounded to ten decimal places for the eigenvalues λ_f and the derivatives $(\partial Y_f / \partial \lambda_f)_{y=1}$ and $(\partial Y_f / \partial y)_{y=1}$ are given in Table 4 for $f = 1$ to $f = 10$.

After the eigenvalues were obtained, the first six eigenfunctions Y_i were calculated for the interval $y = 0$ to $y = 1$ from Equation (20)

$$Y_f = b_0 + b_2 y^2 + b_4 y^4 + \dots \quad (20)$$

with increments of 0.05. These results were calculated to thirty decimal places and values rounded to eight places are given in Table 5.

Equation (16) gives T as a function of y and z . The average or cup-mixing temperature is

$$T_{AV} = \frac{\int_1^2 T V dy}{V_{AV}}$$

Since

$$V = \frac{3}{2} V_{Av}(1 - y^2)$$

$$T_{AV} = \int_0^1 \frac{3}{2} T (1 - y^2) dy$$

$$T_{av} = \frac{3}{2} \sum_{f=1}^{f=\infty} \left[\frac{-2}{\lambda_f \left(\frac{\partial Y_f}{\partial \lambda_f} \right)_{v=1}} \right]$$

$$\exp\left(-\frac{8}{3}\lambda_l^2 z\right) \int_0^1 Y_l(1-y^2) dy \Big]$$

$$T_{AV} = \sum_{f=1}^{f=\infty} \frac{3 \left(\frac{\partial Y_f}{\partial y} \right)_{y=1}}{\lambda_f^3 \left(\frac{\partial Y_f}{\partial \lambda_f} \right)_{y=1}} \exp \left(-\frac{8}{3} \lambda_f^2 z \right) \quad (21)$$

These eigenvalues, λ_f , and the derivatives $(\partial Y_f / \partial \lambda_f)_{y=1}$ and $(\partial Y_f / \partial y)_{x=1}$ have been previously estimated by an asymptotic solution (31) and calculated by a series expansion (16, 29, 30). A comparison with these values is given in Table 6. The values for the eigenfunctions Y_f in Table 5 are in substantial agreement with values previously calculated (16, 29) for $f = 1$ to $f = 6$ with increments in y of 0.01 and accurate to eight significant figures.

CONCLUSION

The eigenvalues and derivatives presented in Table 1 for the Graetz problem and in Table 4 for the similar problem in a flat duct together with the asymptotic values (31) for $n > 11$ and $f > 10$ should be accurate enough for all purposes which require the stated boundary conditions. For other boundary conditions and different ve-

locity distributions the problem solutions can be obtained by modification of the computation program.

ACKNOWLEDGMENT

The author wishes to express his thanks to Mrs. Alma Venters, who made many of the preliminary calculations, and to Dr. Daniel L. Harris, for his many suggestions and assistance in the programming of this problem and in the obtaining of results from the IBM 650 computer.

NOTATION

A	= coefficient in Graetz equation, Equation (10)
a	= coefficient in Graetz equation, Equation (9)
b	= coefficient, Equation (20)
C	= coefficient, Equation (8)
C_p	= heat capacity
D	= diameter of conduit, (=2R)
k	= thermal conductivity
R	= radius of conduit or half width of flat duct
r	= distance from center of duct
t	= temperature
T	= temperature, dimensionless [= $(t - t_s)/(t_o - t_s)$]
V	= velocity
Y	= functions, Equation (6)
x, y, z	= Cartesian coordinates
y	= relative coordinate, (=r/R)
z	= relative longitudinal coordinate, (=x/R $N_{Re} N_{Pr}$)
α	= thermal diffusivity, (= $k/C_p \rho$)
λ	= Eigenvalue, Equations (6), (17)
μ	= viscosity
ρ	= density

Dimensionless Groups

N_{Pr} = Prandtl number, ($= C_p \mu / k$)
 N_{Re} = Reynolds number,
 ($= DV_{AV} \rho / \mu$ for round duct;
 $= 4R V_{AV} \rho / \mu$ for flat duct)

Subscripts

i, j = integers, Equation (9)
 f, n, m = integers
 s = conduit wall
 o = conduit entrance
 x, y, z = Cartesian coordinate components
 av = average
 max = maximum
 V_{av} = average velocity, ($=V_{max}/2$ for round duct; $=2V_{max}/3$ for flat duct)

LITERATURE CITED

1. Abramowitz, M., *J. Math. Phys.*, **32**, 184 (1953).
2. Bird, R. B., "Advances in Chemical Engineering," Vol. I, p. 216, Academic Press, New York (1956).
3. Boelter, L. M. K., *Trans. Am. Inst. Chem. Engrs.* **39**, 557 (1943).
4. ———, V. H. Cherrv, and H. A.

Johnson, "Heat Transfer—Supp. Notes for M. E. 267A-B," X-18 to X-28 Univ. Calif. Press, Berkeley (1940).

5. Brinkman, H. C., *App. Sci. Res.*, **A2** 120 (1950).
6. Brown, C. G., et al., "Unit Operations," p. 517, John Wiley, New York (1950).
7. Drew, T. B., *Trans. Am. Inst. Chem. Engrs.*, **26**, 26 (1931).
8. ————*Ind. Eng. Chem.*, **24**, 152 (1932).
9. ————J. J. Hogan, and W. H. McAdams, *Trans. Am. Inst. Chem. Engrs.*, **26**, 81 (1931).
10. ————*Ind. Eng. Chem.*, **23**, 936 (1931).
11. Fourier, J. B. J., *Mem. Acad. Sci.*, **12**, 507, (1833).
12. Gilliland, E. R., and T. K. Sherwood, *Ind. Eng. Chem.*, **26**, 516 (1934).
13. Graetz, L., *Ann. Physik* (3), **18**, 79 (1883).
14. *Ibid.*, **25**, 337 (1885).
15. Grober, H., "Die Grundgesetze der Wärmeleitung und des Wärmeüberganges," p. 179, Springer, Berlin, Germany (1921).
16. Harris, D. L., and W. H. Reid, Private Communication (1958).
17. Jakob, Max, "Heat Transfer," p. 451, John Wiley, New York (1949).
18. Kays, W. M., *Trans. Am. Soc. Mech. Engrs.*, **77**, 1265 (1955).
19. Kirkbride, C. G., and W. L. McCabe, *Ind. Eng. Chem.*, **23**, 625 (1931).
20. Lauwerier, H. A., *App. Sci. Res.* **A2** 184 (1951).
21. Lee, A., W. O. Nelson, V. H. Cherry, and L. M. K. Boelter, "Proceedings Fifth International Congress for Applied Mechanics," p. 571, John Wiley, New York, (1939).
22. Lévêque, M. A., *Ann. mines (ser. 12)*, **13**, 201, 305, 381 (1928).
23. Lipkis, R. P., Discussion on reference (31).
24. Longwell, P. A. *A.I.Ch.E. Journal*, **3**, 353 (1957).
25. Lyche, B. C., and R. B. Bird, *Chem. Eng. Sci.* **6**, 35 (1956).
26. McAdams, W. H., "Heat Transmission," 3 ed., p. 230, McGraw-Hill, New York (1954).
27. Nusselt, W., *Z. Ver. deut. Ing.*, **54**, 1154 (1910).
28. Poisson, S. D., "Theorie Mathematique de la Chaleur," Bachelier, Paris, France (1835).
29. Prins, J. A., J. Mulder, and J. Schenk, *App. Sci. Res.*, **A2** 431 (1951).
30. Schenk, J., and J. M. Dumoré, *ibid.*, **A4**, 39 (1953).
31. Sellers, J. R., M. Tribus, and J. S. Klein, *Trans. Am. Soc. Mech. Engrs.*, **78**, 441 (1956).
32. Sherwood, T. K., and R. L. Pigford, "Absorption and Extraction," p. 81, McGraw-Hill, New York, (1952).
33. Tribus, M., and J. Klein, "Heat Transfer—A Symposium," p. 211, Engineering Research Institute, Univ. Michigan Ann Arbor (1953).
34. Yamagata, K., *Mem. Fac. Eng., Kyushu Univ.*, **8**, 365 (1940).

Manuscript received December 30, 1957; revision received February 2, 1959; paper accepted June 17, 1959.

Heat and Mass Transfer to Decelerating Finely Atomized Sprays

W. P. MANNING and W. H. GAUVIN

McGill University, Montreal, Quebec, Canada

The rate of heat and mass transfer in the nozzle zone of water sprays produced by internal-mixing pneumatic nozzles and hollow-cone pressure nozzles was determined for both concurrent and crosscurrent drying air-flow patterns. The Nusselt numbers for the evaporating drops were correlated by means of the equation proposed by Ranz and Marshall for stationary drops in a moving air flow. Methods of measuring the physical properties of the water-air system were developed, and special attention was devoted to the determination of drop velocities and air humidity.

An increasing number of physical and chemical operations depend on atomization for the production of large contact areas between liquid and gaseous phases. Of the many complex problems which must be solved before the nozzle range of a spray can be fully characterized, the two most important are the rate of evaporation from the droplets and their rate of momentum transfer during deceleration. It is with the former that this paper is principally concerned.

The rate of evaporation from a single, stationary liquid drop suspended in stagnant or moving air streams has been widely investigated (for a fairly complete bibliography on this subject, see reference 1). Of the several heat and mass transfer correlations proposed, those of Ranz and Marshall (2) are generally considered to be the most reliable:

$$N_{Su} = 2.0 + 0.60 (N_{Re})^{1/2} (N_{Pr})^{1/3} \quad (1)$$

$$N_{Su'} = 2.0 + 0.60 (N_{Re})^{1/2} (N_{Sc})^{1/3} \quad (2)$$

It should be mentioned that in his classic paper published fourteen years earlier Froessling (3) had presented an approximate solution for the Navier-Stokes equations which gave an expression for $N_{Su'}$ of identical form, but with a coefficient of 0.552 instead of 0.60.

In contrast with the above, very little information is available on the evaporation from sprays or freely falling drops. The published literature on this subject can be divided conveniently into three classes. First there are the purely

analytical approaches of Edeling (4), Sjenitzer (5), Miesse (6), and Daskin (7). Second there are several determinations of the evaporation rates under conditions of practically no relative velocity between the spray drops and the surrounding drying gases. The investigations of Dlouhy (8), Kesler (9), Kinzer and Gunn (10), and Marshall (11) have shown that the evaporation rates are analogous to those of stationary drops suspended in stagnant air; that is,

$$N_{Su} = N_{Su'} = 2.0 \quad (3)$$

Third there are several investigations in which the rate of evaporation from sprays injected into horizontal, turbulent, high-velocity air streams was de-

termined. Coldren (12) recorded the heat, mass, and momentum fluxes in the drying air stream but did not attempt to measure the spray-drop velocities; he was thus unable to calculate the heat and mass transfer coefficients. Hanson (13) and Fledderman and Hanson (14) assumed that Froessling's equation could be applied to the spray drops, which permitted them to calculate indirectly the drag coefficient of fuel spray drops. Ingebo (15) measured the evaporation rates and drop velocities of *iso*-octane sprays injected against a high-velocity air stream.

It is believed that the present investigation constitutes one of the first attempts at measuring the heat and mass transfer rates from decelerating spray drops produced by typical atomizing nozzles, under conditions similar to those encountered in conventional spray dryers. Two flow patterns were studied: crosscurrent flow (with the drying air passing at right angles to the spray) and downward concurrent flow.

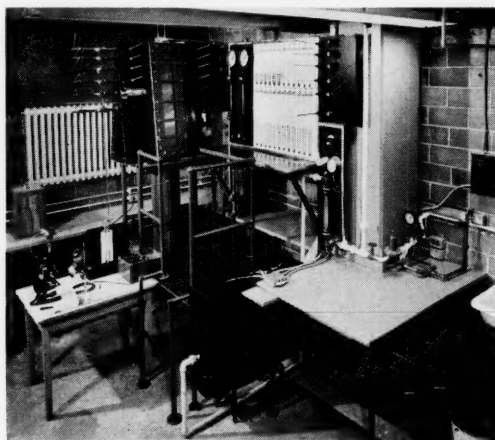


Fig. 1. Crossflow experimental equipment.

W. P. Manning is with Merck and Company, Incorporated, Rahway, New Jersey.

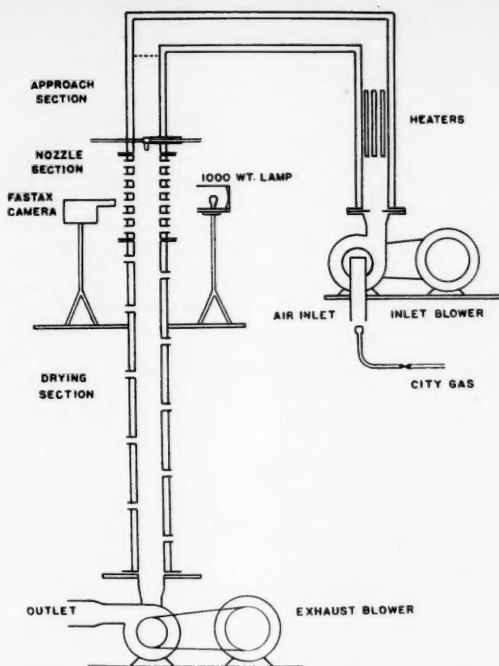


Fig. 2. Schematic diagram of concurrent-flow equipment.

EXPERIMENTAL

Methods of Measurement

The accurate determination of the individual, local physical properties of the separate phases in a spray of droplets is fraught with experimental difficulties. The presence of the liquid phase in the form of a finely divided suspension renders the conventional methods of measuring the velocity, humidity, and temperature of the drying gases completely useless. Consequently several experimental techniques had to be developed and these are now reviewed briefly.

Drop-Size Distribution. Drop-size determinations were carried out on samples obtained by traversing the spray with an immersion cell containing Varsol. The cell consisted of a hollow aluminum cylindrical tube 0.25-in. O.D., 0.20-in. I.D., and 0.20 in. deep and was fitted with a glass bottom. The samples were photographed under a microscope, and the drop sizes measured to within $1\ \mu$, with counts of up to 250 drops. Owing to the relatively high drop velocities, good impaction efficiencies were obtained, as shown by the large number of small drops (down to $1\ \mu$) collected.

Spray Evaporation. The progressive evaporation from the spray in the nozzle range was followed by measuring colorimetrically the increase in concentration of a powerful red dye added to the feed water. Differences corresponding to one part in ten million could be accurately detected, which permitted the use of a very low dye concentration in the feed water, of the order of one part per

ten thousand. Changes in the physical properties of the spray due to the presence of the dye were therefore negligible, and it was carefully ascertained that no surface active properties, such as depression of the surface tension, were imparted to the water.

Samples of the spray were collected under a nonvolatile silicone oil in small weighing bottles which were introduced into the spray by means of an aluminum holder. The holder was designed so that no evaporation of the drops could occur after collection.

Spray-Drop Temperature. There is considerable evidence in the literature to indicate that, once dynamic equilibrium conditions have been attained, evaporating spray drops remain at the wet-bulb temperature to the drying air (2, 8, 10, 11, 12, 13, 15).

In the nozzle range of a spray, however, an unsteady state period can be expected to occur before the drops attain a constant temperature. From theoretical step calculations El Wakil, Uyehara, and Myers (16) estimated that a $50\text{-}\mu$ drop of octane, issuing from a pressure nozzle with an initial velocity of 100 ft./sec., would require about 0.23 sec. to reach constant temperature. For large drops of water (2.7 mm.) Kinzer and Gunn (10) showed experimentally that 4.3 sec. elapsed while the temperature of the drop, which was freely supported by an air stream with a wet-bulb temperature of 14.9°C ., decreased from 22.4° to 17.6°C .

On the other hand Lyons (17) supplied in 1951 some experimental evidence which is much more pertinent to the present study. Using a copper-constantan ther-

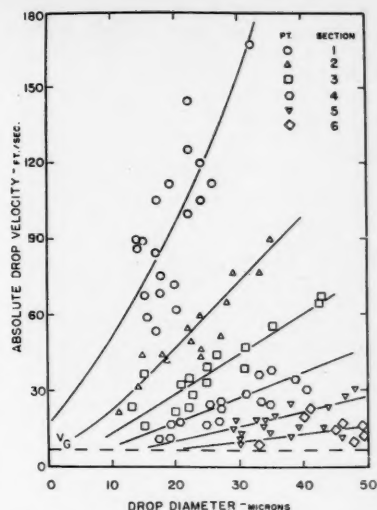


Fig. 3. Drop velocities for pneumatic nozzle JN number 12 in crosscurrent flow.

mocouple probe located $\frac{1}{8}$ in. from the orifice of an internal-mixing pneumatic nozzle, he recorded the following observations.

(1.) With air alone passing through the nozzle a temperature drop of 7.3°C . was observed, in contrast with the much higher decrease which had been predicted by Fogler and Kleinschmidt (18).

(2.) With a feed-water temperature of 81°F . the wet-bulb temperature of the air (65°F .) was attained within the distance of $\frac{1}{8}$ in., when the atomizing air pressure was sufficient to provide fine atomization. Coarser droplets, produced at lower atomizing air pressure, required a longer distance.

(3.) With increasing feed-water temperature and fine atomization, the wet-bulb temperature was again reached when the initial temperature did not exceed 102°F . The spray temperature was however 2°F . higher than the wet-bulb for a feed water of 114°F . and 12°F . higher for a feed water of 164°F .

These experimental results appear to indicate therefore that for fine droplets under the conditions prevailing in the nozzle range of a spray the unsteady state period is exceedingly short. It was assumed that, with feed-water temperature not too far removed from the wet-bulb temperature, the latter was probably attained by the droplets within 0.5 in. from the nozzle and certainly at higher distances.

To measure the spray temperature, a thermocouple probe was constructed, with a No. 16 hypodermic needle for mounting. The soldered end of the thermocouple protruded slightly beyond the end of the hypodermic needle, and its tip was bent slightly downward. When the device was inserted into the spray through a port in the test chamber, the liquid drops accumulated at the tip and then fell off under the effect of gravity, thus keeping

the thermocouple junction at the spray temperature. The latter agreed closely (within 1.0°F.) with the wet-bulb temperature of the drying air.

Spray-Drop Velocities. Few attempts at measuring the velocity of spray drops from atomizing nozzles have appeared in the literature, and the only extensive experimental study is that of York and Stubbs (19), who used direct photography to obtain the velocities of spray drops produced by hollow-cone pressure nozzles. For the present investigation a direct method involving the use of high-speed cinematography was developed.

The drop-velocity determinations were all performed in 8-in.-diameter columns fitted with optical glass windows. The camera used was a 16-mm. one equipped with a $f/3.5$ lens. Illumination of the spray

studies, however, the measurements had to be carried out in an 8-in. Lucite column, since the drying chamber did not lend itself to direct observations. However the flow rates, temperatures, and pressures of the fluid streams to the nozzle were regulated to correspond with the values used during the actual evaporation tests.

A suitable camera voltage—and consequently speed—was selected for the spray drops to appear on at least three consecutive frames. One 100-ft. reel of motion picture film was taken for each spray-velocity determination. When it was developed, the drops appeared as black streaks on a light background and were analyzed. The grain of the high-speed film was 54 lines/mm. and did not permit drops smaller than $10\ \mu$ to be photographed clearly. Accordingly the measurement of velocities for the very small drops had to be abandoned. A cathetometer was used to measure the thickness of the streaks. The instrument was fitted with a moving cross hair on a vernier scale, and the magnification so produced enabled drop diameters to be measured within 2 or 3 μ . Corresponding velocities were easily calculated from measurements of the distance travelled between successive frames.

Air Velocity in the Spray. The direct determination of the air velocity in a droplet-laden system is extremely difficult. Since there is no accurate method of direct measurement, an indirect approach was used, based on the fact that small drops may be considered excellent tracers for gas velocities in turbulent systems. As both their terminal settling velocity and initial kinetic energy are extremely low, the absolute velocities of the smallest droplets approach those of the air stream at a relatively short distance from the nozzle. Consequently a fairly accurate estimate of the air velocities in the spray may be obtained from the intercept on the velocity axis of the drop-diameter-drop-velocity graphs obtained by the photographic method described in the previous section. The main source of error is the actual determination of the drop velocities in this range. The air-velocity profiles obtained from graphical extrapolation in this manner were in agreement with those reported in the literature (12, 20, 21). They were also quite similar to those produced by pneumatic nozzles, with no water flowing, as experimentally measured with a standard Pitot tube and a special wedge-shaped velocity probe developed by Stachiewicz (22).

Air Temperature in Spray. In the concurrent flow experiments mercury thermometers were used, protected by two concentric aluminum-foil shields. In the concurrent flow experiments the shielding of the thermometers was very similar to that used by Dlouhy (8). A somewhat larger aluminum-foil shield was used, and the insulation of the thermometer stem was improved by means of a double-jacketed glass shield. The whole device was attached to a transite plug carefully machined to fit the sample port and to follow the inner contour of the drying chamber exactly. A radial temperature traverse could easily be obtained with it.

Determination of the Air Humidity.

Owing to the small changes in drying-air humidity observed in this work (about 0.005 to 0.015 lb. water/lb. dry air), a considerable degree of accuracy was required for the humidity measurements. The accuracy provided by conventional hygrometers, the dew-point method, or the wet- and dry-bulb method was found to be inadequate. Other techniques, such as thermal-conductivity measuring devices or conductance cells made of palladium wires coated with lithium chloride, were found to suffer from the additional disadvantages of a narrow range of application and necessity of frequent calibration. A volumetric method of determining the humidity of the air was therefore developed, based on the removal of the water vapor by contact with magnesium per-

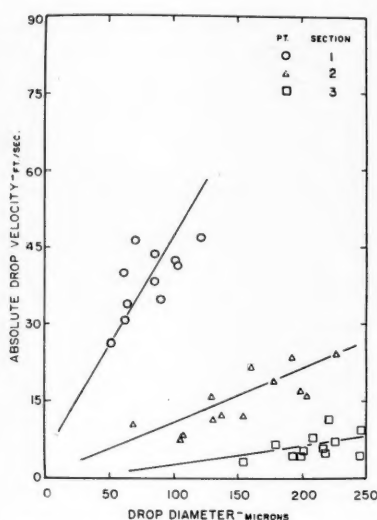


Fig. 4. Drop velocities for pressure nozzle LNN number 1 in crosscurrent flow.

was achieved by a 1,000-w. flood lamp. The optimum angle between the camera and the light beam was experimentally determined to be 135 deg.

The camera voltage and illuminating light was controlled, and a timing-light generator was incorporated into the circuit to activate the timing pulse of the camera, which flashed a light for the duration of a few microseconds every 1/100 or 1/1,000 of a second, so that the time which elapsed between successive frames might be measured.

The camera and illuminating light beam were directed onto the axis of the spray, and very small depths of focus could be photographed. No attempt was made to determine the velocity profile, radially. For the concurrent flow studies the velocity determinations were carried out in the drying chamber proper. For the crossflow

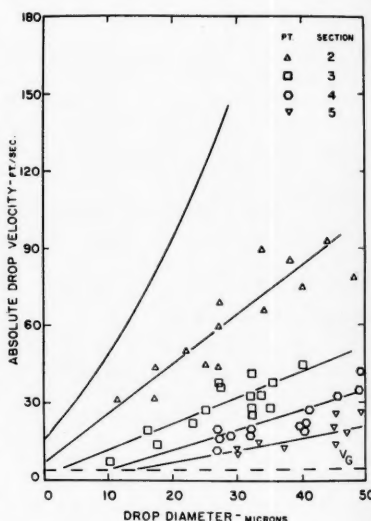


Fig. 5. Drop velocities for pneumatic nozzle JN number 12 in concurrent flow (low-atomizing air pressure).

chlorate. This dehydrating agent was chosen because of its high drying capacity and lack of absorption of carbon dioxide or other common gases.

Measurement of the air sample (collected through an impact separator to remove entrained droplets) was accomplished in a precision burette. The lowest and narrowest section (94 to 100 ml.) was graduated in 0.05-ml. divisions, and volume changes of 0.01 ml. could therefore be detected. The burette was surrounded by a water jacket in which a comparison tube was also installed. The latter was connected through a check valve and leveling tube to the burette. From the burette the air could be passed, by raising the leveling bulb, through the U tube containing the magnesium perchlorate and into a self-sealing mercury reservoir consisting of two interconnected

TABLE 1. COMPARISON OF SPRAY CHAMBERS

Section	Distance from nozzle, in.	Cross-sectional area available for flow		Location of sampling ports, in. from nozzle		
		Crosscurrent equipment, sq. ft.	Concurrent equipment, sq. ft.	Cross-current equipment	Concurrent pneumatic nozzles	Pressure nozzles
1	0-3	0.050	0.350	1.5	—	0.5
2	3-6	0.066	0.350	4.5	4.0	4.5
3	6-10	0.115	0.350	8.0	8.0	8.5
4	10-14	0.0147	0.350	12.0	12.0	12.5
5	14-18	0.0175	0.350	16.0	16.0	16.5
6	18-24	0.304	0.350	21.0	20.0	20.5

chambers, mounted one above the other. The air entering the lower compartment forced the mercury into the upper section.

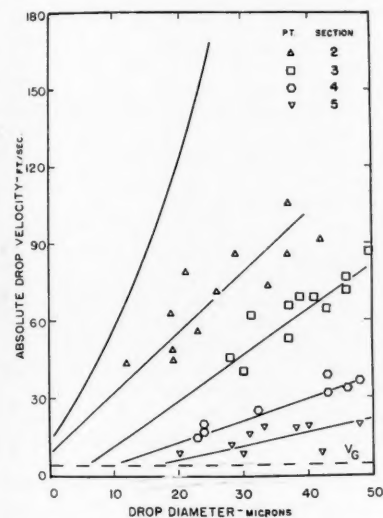


Fig. 6. Drop velocities for pneumatic nozzle JN number 12 in concurrent flow (high-atomizing air pressure).

When the air was sucked back into the burette, the mercury flowed back into the lower chamber. A fixed level of mercury in the lower chamber was obtained by means of a pilot-light circuit with contacts sealed into the mercury chamber. Three passes were found to be required for complete removal of the water vapor.

This method was tested painstakingly against a gravimetric determination, by means of molecular-sieve pellets attached to the end of a calibrated quartz spiral. This assembly was suspended in a 1.5-in.-I.D. by 50-in.-long glass tube, into which the air sample, containing the water vapor to be determined, was introduced. This method of determination was extremely accurate but was too ponderous for routine use. Since carbon dioxide was also absorbed, the apparatus was used for comparison only, by means of carbon dioxide-free air. The agreement between the two methods was excellent, as indicated by a number of comparative tests under various humidity conditions (1).

EQUIPMENT

Crosscurrent Flow Equipment

The use of a crosscurrent flow of drying air to measure the evaporation rates from a spray at small distances from the nozzle appeared to offer many advantages. Guiding the air at right angles to the vertical spray through horizontal compartments, in a specially constructed drying chamber, one might expect better contact and more rapid penetration of the spray by the drying air than could be achieved in conventional concurrent flow. The increase in the humidity of the drying air from each compartment would provide an accurate and simple method of determining the rate of evaporation at various distances from the nozzle.

A trapezoidal drying chamber consisting of six horizontal sections was therefore constructed (Figure 1). It was insulated with an internal layer of transite made impervious to water with several coats of high-temperature aluminum paint. Dividing partitions of transite were fitted into the chamber so that six horizontal sections were formed, two of them 3 in. high, three of them 4-in., and one 6 in. high. Circular holes of increasing diameters were cut in the partitions to permit the spray to pass downward from the nozzle, which was installed in the center of the top surface of the chamber.

The spray could be visually observed through a Pyrex glass plate in the front sloping side of the spray chamber. Inlet and outlet drying-air ports were cut in the center of the ends of each of the horizontal sections, and additional ports were provided for temperature determinations. Table 1 gives the physical measurements of the six horizontal sections comprising the drying chamber.

Drying air from a surge tank was delivered to each of the horizontal sections through individual lines, each containing a globe valve, a calibrated orifice, and a thermometer. The exit-air flow rates from the horizontal sections were similarly controlled and metered. Provisions for the close control of the atomization conditions and flow rate of the feed completed the experimental apparatus.

In operation, flow rates were so adjusted in each section as to provide equal velocities of the drying air in all the horizontal compartments. Distortion of the spray and wetting of the walls were prevented by the use of relatively low flow rates.

Concurrent Flow Equipment

This apparatus, which is shown diagrammatically in Figure 2, consisted of a continuous 8-in.-I.D. steel duct, covered with 2 in. of magnesia insulation. In the approach section, directly above the nozzle, straightening plates provided a uniform velocity profile for the drying air, as shown by traverses taken with a Pitot tube and the wedge-shaped probe previously mentioned. The nozzle section was 2 ft. high and fitted with six pairs of sampling ports, located as indicated in Table 1. These ports were also used to photograph the spray under actual operating conditions. The lower section (or drying section) was 12 ft. long and also contained sampling ports, but spaced farther apart.

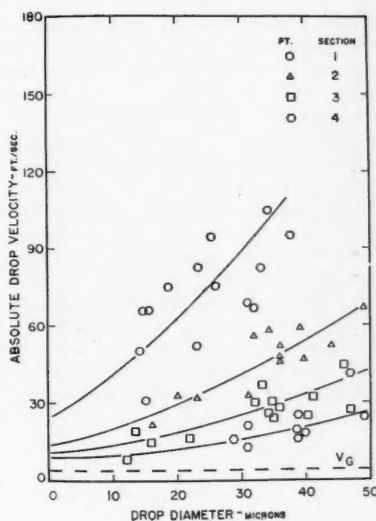


Fig. 7. Drop velocities for pneumatic nozzle JN number 22B in concurrent flow.

In addition to the conventional controls, a twelve-point temperature recorder was connected to copper-constantan thermocouples soldered at various points of the wall in the nozzle or drying sections. Any wetting of the wall by the spray or change in operating condition could thus be detected immediately. Provision was also made to heat the feed water containing the red dye over a wide range of temperature.

CALCULATIONS

In the crosscurrent flow experiment the rate of heat transfer to the spray from the drying air in each section was calculated from the increase in humidity of the individual drying-air streams, by means of an enthalpy balance on the system. When using pneumatic nozzles, one observed that the mass rate of outlet drying air was nearly always greater (particularly for the lower sections) than that of the inlet stream. This ef-

fect was due to the redistribution of the atomizing air and was of course absent when pressure nozzles were tested.

The surface area of the spray in a given section along the spray axis was calculated from the equation

$$A_s = W_s S_w \Delta x / 3,600 V_D \quad (4)$$

The average absolute drop velocity (that is, the absolute velocity of a drop of diameter equal to the Sauter mean diameter) was obtained from the graphs expressing the drop velocity in terms of the drop diameter for the appropriate nozzle operation, evaporation conditions, and the appropriate D_{vs} . Here the specific surface area was obtained from the particle count by substitution in

$$S_w = \Sigma n D^2 / (\rho_L \Sigma n D^3 / 6) \quad (5)$$

The driving force for heat transfer is the temperature difference between the average drying air and the evaporating spray. With pneumatic nozzles t_a was taken as the weighted average between the atomizing air and the drying air, while t_s was the average spray temperature in the section. Because of differences in the drying-air conditions between the various sections (temperature, heat losses, presence of atomizing air, etc.), t_a increased with distance from the nozzle but always remained at the wet-bulb temperature of the drying air in the section.

The heat transfer coefficient for the Sauter mean drop diameter of the spray was calculated from

$$h = q / A_s \Delta t \quad (6)$$

The Nusselt number was calculated from its definition:

$$N_{Nu} = h D_{vs} / k_f \quad (7)$$

Owing to the small content of water vapor in the surrounding gas film the thermal conductivity was taken as that of air alone at the arithmetic average temperature of the drying air and the drop surface (11).

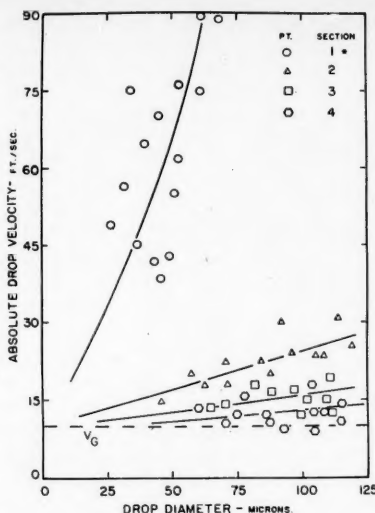


Fig. 8. Drop velocities for pressure nozzle LN number 1 in concurrent flow.

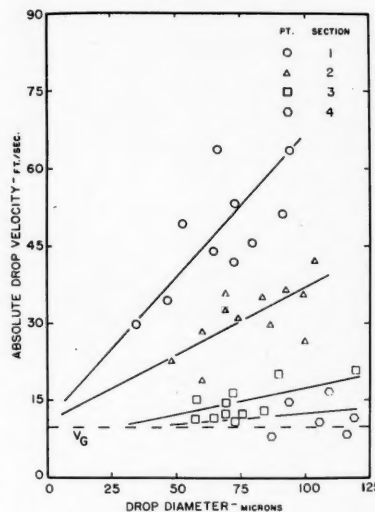


Fig. 9. Drop velocities for pressure nozzle LN number 1 in concurrent flow (high feed temperature).

The modified Nusselt number for mass transfer can be written as

$$N_{Nu'} = k_g D_{vs} RT / D_s = h D_{vs} / c_s D_s \rho_f \quad (8)$$

or in terms of the Nusselt number:

$$N_{Nu'} = N_{Nu} (k_f / c_s D_s \rho_f) \quad (9)$$

In the concurrent flow system analysis of the flow pattern was very much simpler, and calculations could be carried out more accurately. The evaporation was determined from the change in concentration of the dye dissolved in the spray. The average temperature of drops in spray remained constant at the wet-bulb temperature of the air. Values of the drying-air temperature, spray evaporation, Sauter mean diameter, and the velocity of a spray drop of the same diameter as the Sauter mean diameter, obtained at the various points shown in Table 1, were plotted against the distance from the nozzle as the abscissa. Average values of these quantities from section to section were obtained by the graphical integration of the area under the curve and the division of the values so obtained by the distance over which the integration was performed. These average values were then used for the calculations of h , N_{Nu} , and $N_{Nu'}$, as before.

RESULTS

A summary of the experimental conditions used is presented in Table 2. Two types of nozzles were tested in the crosscurrent flow equipment: an internal-mixing pneumatic nozzle and a hollow-cone pressure nozzle. The latter gave a much coarser degree of atomization.

These nozzles were again used in the concurrent drying chamber. In addition a second internal-mixing pneumatic nozzle was also used. This had a higher capacity and a somewhat larger spray angle.

In each of the seven sets of runs shown in Table 2, the atomizing air pressure and flow rate (for pneumatic

TABLE 2. EXPERIMENTAL CONDITIONS

Run	1 to 12	13 to 20	21 to 24	25 to 30	31 to 34	35 to 38	39 to 43
Flow pattern	crosscurrent	crosscurrent	concurrent	concurrent	concurrent	concurrent	concurrent
Nozzle type	pneumatic	pressure	pneumatic	pneumatic	pneumatic	pressure	pressure
Nozzle no.	JN 12	LNN 1	JN 12	JN 12	JN 22B	LN 1	LN 1
Spray angle, deg.	12	60	12	15	20	60	60
Atomizing—air pressure, lb./sq. in. gauge	25	—	25	35	25	—	—
Atomizing air flow rate, lb./hr.	5.45	—	5.45	7.2	20.5	—	—
Liquid feed pressure, lb./sq. in. gauge	14.9	99	14.9	25	6	95	95
Liquid feed flow rate, lb./hr.	2.0	5.1	2.0	4.4	6.0	12	12
Liquid feed temperature, °F.	76-92	76-90	76-92	62-75	62-81	85-101	78-250
Drying air flow rate, lb./hr.	42-81	25-46	300	300	300	750	750
Inlet drying—air temperature, °F.	138-214	144-220	145-230	145-230	145-230	150-250	250
Total evaporation, %	19-55	2-7	72-84	72-86	40-50	9-27	14-56
Sauter mean diameter, μ	14.1-35	65-169	16-23	12-23	16-28	59-82	40-92
Drop—velocity data, Figure no.	3	4	5	6	7	8	8-9

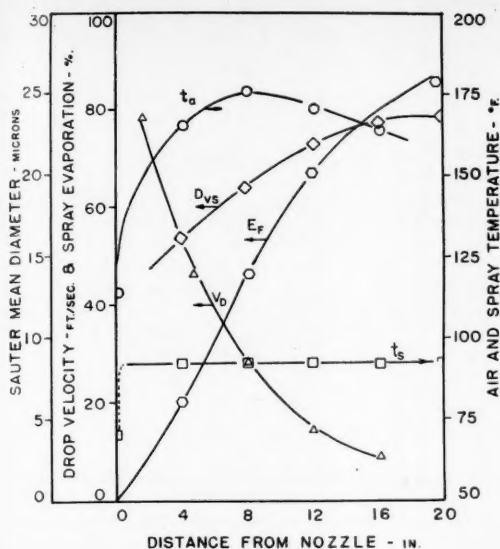


Fig. 10. Change in spray and air properties for run 29.

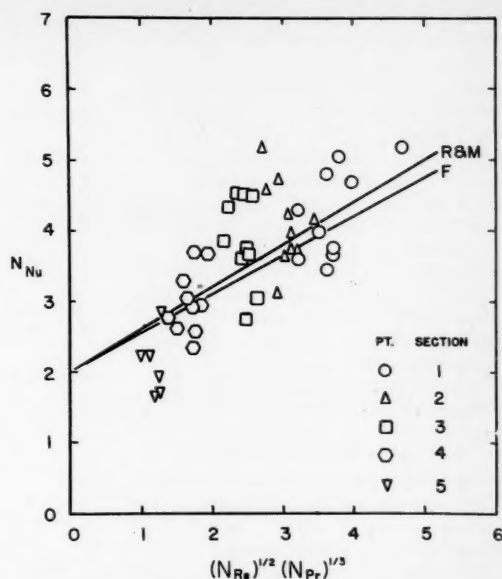


Fig. 11. Nusselt number for runs 21 through 30.

nozzles) and the liquid feed pressure and flow rate were kept constant. The variables studied were the drying-air flow rate and its inlet temperature. No attempt was made to control the feed temperature, which was allowed to fluctuate slightly from run to run, except in runs 39 to 43, where it was the variable studied. In run 39 the feed was preheated to 250°F. before the pressure nozzle and partially flashed at the nozzle opening.

The drop-velocity data are presented in Figures 3 to 9. In all these plots the air velocity is shown as a dotted line. The distances from the nozzle at which the measurements were made are indicated by the section number, as given in Table 1. Figures 3 to 8 cover the conditions shown in Table 2, as indicated in the bottom line. Figure 9 applies specifically to run 39, in which the feed was delivered to the nozzle at 250°F. Additional data can be found in reference 1.

Typical changes in spray air and drop temperatures, percentage of spray evaporation, drop velocity, and Sauter mean diameter as a function of the distance from the nozzle are shown in Figure 10 for concurrent drying with a pneumatic nozzle (run 29). A typical plot of calculated Nusselt numbers vs. $(N_{Re})^{1/2} (N_{Pr})^{1/3}$ is shown in Figure 11 (runs 21 to 30), on which the two lines representing the correlations of Ranz and Marshall (R and M) and of Froessling (F) are also indicated. Similar plots could be drawn for the calculated modified Nusselt numbers.

Finally the effect of variations in feed temperature on the rate of evaporation

from the spray is shown in Figure 12 (runs 39 to 43).

CONCLUSIONS

The development of suitable measuring techniques constituted an important phase of this investigation. Because of its importance in the calculation of heat and mass transfer rates, the determination of droplet velocities received particular attention. It is recognized, however, that the high-speed cinematographic method which was finally adopted presents a number of deficiencies, chief among which are its inability to determine velocities higher than about 180 ft./sec. or to permit measurements for drops smaller than 10 μ and the inherent inaccuracy in the estimation of the droplet diameter. It is also realized that, since the velocity of the droplet may depend to a significant extent on its radial position in the spray (19), the absolute droplet velocity at the axis of the spray (as measured in this work) is probably consistently higher than the true average velocity.

In spite of these various limitations, it was possible to make measurements as close as 1.5 in. from the pneumatic nozzle and 0.5 in. from the pressure nozzle. As expected, smaller drops and higher velocities are obtained with the pneumatic nozzles, and for a given nozzle the larger drops have a much higher initial velocity. The velocity data also indicate that the smaller droplets decelerate quite rapidly to the velocity of the air stream.

Generally speaking, an increased rate of evaporation, resulting from a higher

inlet drying-air temperature, will decrease the distance of penetration of the spray under otherwise identical operating conditions, since the reduction in the mass of the spray also reduces its kinetic energy. The true situation is, however, somewhat more complicated; for a given droplet diameter measured at a given distance from the nozzle the initial diameter of the corresponding droplet issuing from the atomizer must have been larger under conditions of higher evaporation rate. Its initial kinetic energy or velocity must therefore have been higher. On the other hand, this is offset by larger drag forces. At an appreciable distance from the nozzle the cumulative effect of the latter results in a lower droplet velocity in the presence of higher evaporation rates. Closer to the nozzle the opposite behavior is observed.

The initial increase in the value of the Sauter mean diameter of the spray with distance from the nozzle, as shown in Figure 10, may at first appear unusual. This is actually to be expected with a wide distribution in drop sizes, since the smaller drops evaporate much more quickly than the larger ones (8).

The equations proposed by Froessling (3) and by Ranz and Marshall (2) for stationary drops suspended in moving air streams were found to be generally applicable for correlating the Nusselt numbers in terms of the dimensional groups $(N_{Re})^{1/2} (N_{Pr})^{1/3}$, as shown in Figure 11. The scatter of the experimental data appears to be considerable but may be ascribed at least partially to the fluctuations inherent to the system: by this it is meant that in any part

of the nozzle zone drops of a given diameter, or of a given D_{v0} , may have different velocities depending on the effect of the turbulent-velocity fluctuations during deceleration. In Equation (4), however (and thus in the other equations which follow from it), only one average V_d value was used, read from the curves given in Figures 3 to 9. It might be expected that the intensity of turbulence encountered might result in an increase in the heat transfer rate (14, 23), but such effects are relatively small and thus are not likely to be apparent in the range of Reynolds numbers investigated.

The limited experimental data on the effect of an increase in feed temperature on the evaporation rate are summarized in Figure 12. The marked increase in the latter can be attributed to three separate factors: First, there is a certain amount of flashing as the drop temperature decreases to the wet-bulb temperature of the surrounding gas; second, the decrease in the liquid-sur-

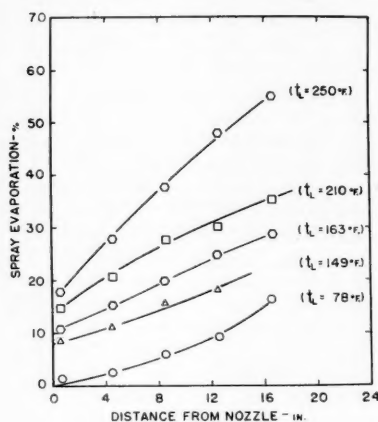


Fig. 12. Effect of feed temperature on evaporation.

face tension and viscosity at higher temperatures produces a decrease in the drop size (24, 25, 26) which results in an increase in the specific surface available for heat and mass transfer; third, there is a decrease in the drop velocity (Figures 8 and 9), which increases the residence time and hence the evaporation.

Dlouhy (8) has shown that the evaporation and drying time of a spray can be predicted with good accuracy from step-by-step calculations, with a procedure similar to that proposed by Marshall (11), provided that the drop-size distribution at the atomizing nozzle is known. A similar method, modified to take the changing drop velocity into account, can obviously be used to calculate the rate of evaporation in the nozzle range of a spray. Such calculations were carried out on five of the crosscurrent runs and four of the

concurrent ones and were generally in good agreement with the experimental values.

ACKNOWLEDGMENT

Financial assistance from the National Research Council of Canada in the form of a research grant and of the award of a fellowship to W. P. Manning is gratefully acknowledged. Recognition is due also to Jan Dlouhy for his collaboration in the development of many of the measuring techniques and particularly of the volumetric method of humidity determination.

NOTATION

A_s	= average total surface area of the spray drops, sq. ft.
C_D	= drag coefficient
c_s	= average humid heat of the gas film, (B.t.u.)/(lb. dry air) (°F.)
D	= diameter of drop, μ
D_{v0}	= Sauter mean diameter of spray drops, μ
D_v	= diffusivity of surrounding gas film, (sq. ft.)/(hr.)
E_f	= fraction of spray evaporated
h	= heat transfer coefficient, (B.t.u.)/(hr.) (sq. ft.) (°F.)
k_f	= average thermal conductivity of the gas film surrounding drop, (B.t.u.)/(hr.) (ft.) (°F.)
k_g	= mass transfer coefficient, (lb.-mole)/(hr.) (sq. ft.) (Δp)
n	= number of drops
N_{Nu}	= Nusselt number, hD_{v0}/k_f
$N_{Nu'}$	= Modified Nusselt number, $k_g M_m D_{v0} p_f / D_v p_f$
N_{Pr}	= Prandtl number, $C_p \mu_f / k_f$
q	= rate of heat transfer, (B.t.u.)/(hr.)
R	= gas constant 1,545 (ft.-lb. force)/(lb. mole) (°R.)
N_{Re}	= Reynolds number, $D_{v0} V_{sp} \rho_f / \mu_f$
N_{Sc}	= Schmidt number, $\mu_f / \rho_f D_v$
S_w	= specific surface area of spray drops, (sq. ft.)/(lb.)
Δt	= driving force = $t_a - t_s$, °F.
t_a	= average temperature of the drying air in the spray, °F.
t_s	= average temperature of drops in spray, °F.
t_L	= temperature of liquid feed, °F.
V_D	= absolute velocity of drop, (ft.)/(sec.)
V_a	= absolute velocity of drying air, (ft.)/(sec.)
V_R	= velocity of drop relative to drying air in spray, (ft.)/(sec.)
W_s	= average mass flow rate of spray water in a section in crosscurrent flow, lb./hr.
x	= axial distance from the source of the spray, ft.
μ_f	= absolute viscosity of gas film surrounding drop, (lb.)/(ft.) (sec.) or (lb.)/(ft.) (hr.)

ρ_f	= average density of the gas film surrounding drop, (lb.)/(cu. ft.)
ρ_L	= density of liquid feed, (lb.)/(cu. ft.)

LITERATURE CITED

- Manning, W. P., Ph.D. thesis, McGill Univ., Montreal, Quebec, Canada (1958).
- Ranz, W. E. and W. R. Marshall, *Chem. Eng. Progr.*, **48**, 141, 173 (1952).
- Froessling, N., *Gerlands Beitr. Geophys.*, **52**, 170 (1938).
- Edeling, C., *Beihfte angew. Chem.*, No. 57 (1949).
- Sjenitzer, F., *Chem. Eng. Sci.*, **1**, 101 (1952).
- Miesse, C. C., *J. Franklin Inst.*, **264**, No. 5, 391 (1957).
- Daskin, W., *Proc. Fourth Midwestern Conf. on Fluid Mechanics*, Purdue Univ., Lafayette, Indiana (Sept. 8-9, 1955).
- Dlouhy, Jan, Ph.D. thesis, McGill Univ., Montreal, Quebec, Canada (1957).
- Kesler, G. H., Sc.D. thesis, Mass. Inst. Technol. Cambridge (1952).
- Kinzer, G. D., and Ross Gunn, *J. Meteor.*, **8**, 71 (1951).
- Marshall, W. R., *Trans. Am. Soc. Mech. Engrs.*, **77**, 1377 (1955).
- Coldren, C. L., Ph.D. thesis, Univ. Illinois, Urbana (1954).
- Hanson, A. R., "Ohio State University Studies in Engineering," **21**, No. 3, 415 (1952).
- Fledderman, R. G. and A. R. Hanson, *Univ. Michigan, Eng. Research Dept.*, CM667 (1951).
- Ingebo, R. D., *Natl. Advisory Comm. Aeronaut. Tech. Note* 3265 (1954).
- El Wakil, M. M., O. A. Uyehara, and P. S. Myers, *ibid.*, 3179 (1954).
- Lyons, D. B., thesis McGill Univ., Montreal, Quebec, Canada (1951).
- Fogler, B. B., and R. V. Kleinschmidt, *Ind. Eng. Chem.*, **30**, 1372 (1938).
- York, J. L., and H. E. Stubbs, *Trans. Am. Soc. Mech. Engrs.*, **74**, 1157 (1952).
- Alexander, L. G., E. W. Comings, H. L. Grimmett, and E. W. White, *Chem. Eng. Progr. Symposium Ser. No. 10*, **50**, 93 (1954).
- Alexander, L. G., Arnold Kivnick, E. W. Comings, and E. D. Henze, *A.I.Ch.E. Journal*, **1**, 55 (1955).
- Stachiewicz, J. W., *Gas Dynamics Lab. Rept. R 41*, McGill Univ., Montreal, Canada (1954).
- Van der Hegge Zijnen, B. G., *App. Sci. Rev.*, **7A**, 205 (1958).
- Dorman, R. G., *Brit. J. App. Phys.*, **3**, 189 (1952).
- Tate, R. W. and W. R. Marshall, Jr., *Chem. Eng. Progr.*, **49**, 162, 226 (1953).
- Turner, G. M., and R. W. Moulton, *ibid.*, 185 (1953).

Manuscript received January 14, 1959; revision received June 1, 1959; paper accepted June 2, 1959. Paper presented at A.I.Ch.E. Cincinnati meeting.

A Corresponding-States Correlation for Higher Molecular-Weight Liquids

A. BONDI and D. J. SIMKIN

Shell Development Company, Emeryville, California

A corresponding-states correlation for the liquid-state properties of higher molecular-weight substances is presented which contains as reducing parameters the readily measurable (and correlatable) energy vaporization and van der Waals volume instead of the often inaccessible critical constants. One additional parameter characterizing molecular flexibility is introduced.

A single curve of the new reduced density ρ^* vs. the new reduced temperature T^* is shown to represent the atmospheric-pressure-density-temperature relations of paraffinic, naphthenic, and aromatic hydrocarbons with 10 or more carbon atoms per molecule to within $\pm 1\%$ between their melting and their atmospheric boiling points. The reduced surface tension is shown to be a unique function of ρ^* for many compounds, thus permitting prediction of surface tension over wide ranges of temperature. The heat-capacity difference between liquid and vapor proved to be easily correlatable with ρ^* . Finally the compression of numerous hydrocarbons proved to be well correlated in terms of T^* , ρ^* , and P^* . Extensive group data for V_∞ and E^* have been assembled in the appendix in order to enable others to use the proposed method without effort.

largely to hydrocarbons. Subsequent reports will show how the new correlations can be applied to nonhydrocarbons.

BASIC PRINCIPLES

The meaning of the critical constants in terms of molecular properties had first been elucidated by Lennard-Jones and Devonshire (11), who showed that the critical temperature is related to the potential energy between a pair of molecules (at the minimum of the potential energy-distance curve) by a universal constant, that the critical volume is a universal multiple of the cube of the molecular diameter and that the critical pressure is a universal multiple of the ratio ϵ/σ^3 . While no theory has as yet predicted the exact magnitude of the universal constants involved, the empirically determined multipliers proved to be universal for all those simple substances for which quantum mechanical corrections can be neglected (4). Furthermore ϵ and σ can be obtained fairly consistently from virial coefficients or the viscosity of the vapor (gas) and from the heat of sublimation and the lattice parameters of the crystal (9).

The parameters ϵ and σ are obviously insufficient to describe the properties of substances composed of larger polyatomic molecules. At least one additional molecular-structure parameter, such as the axis ratio, is needed to describe rigid anisometric molecules. They can be found in the theories of Trapeniers (21) and of Kihara (9). Since many molecules of interest to organic chemists are not rigid but flexible, the additional parameter is only of limited utility. The empirical corollary is the correction factor mentioned earlier, which has indeed been correlated with

GENERAL CORRELATIONS

Purpose and Scope

One of the most powerful methods for the correlation of the physical properties of fluids is that based on the principal of corresponding states. In its original form $V/V_c = f(T/T_c, P/P_c)$ it is valid only for very simple substances, such as the rare gases argon, krypton, xenon and substances composed of simple spherical molecules, such as methane, carbon tetrafluoride, etc. (13). In recent years its scope has been extended to many other substances through the introduction of a correction factor based on the deviation of the observed from the generalized vapor-pressure curve of liquids (14, 19). A more general equation of state then is $V/V_c = f(T/T_c, P/P_c, Y)$.

This modification has greatly increased the scope of accurate physical-property calculations; however it still requires a knowledge of the critical constants which are experimentally accessible only for hydrocarbons of up to 12 carbon atoms per molecule and not at all for many high-boiling nonhydrocarbons. While there are several fairly reliable methods to predict the critical constants (6, 18, 19), it is axio-

matic, at least in the authors' view, that one should use only those correlated constants which can be checked experimentally if doubts arise regarding the reliability of a correlation. The increasing technical interest in hydrocarbons with more than 12 carbon atoms per molecule and in high-boiling organic chemicals has motivated the search for a corresponding-states correlation based on reducing parameters which are directly accessible to experimental measurement. Recent developments in liquid-state theory have made such an enterprise more promising, and the following report gives an account of what has been accomplished to date. Progress in the correlation of equilibrium properties will be dealt with now. The more difficult task of correlating transport properties has not yet reached the reporting state.

The reader should be warned at the outset that no attempt has been made to develop a theory because no theory could describe the properties of highly complex molecules with sufficient accuracy for chemical engineering purposes. Instead an empirical correlation of dimensionless property parameters suggested by theory has been developed, which proved basically adequate for the description of the properties of high-boiling paraffin hydrocarbons (15, 16). The present report is restricted

D. J. Simkin is with Marquardt Aircraft Company, Van Nuys, California.

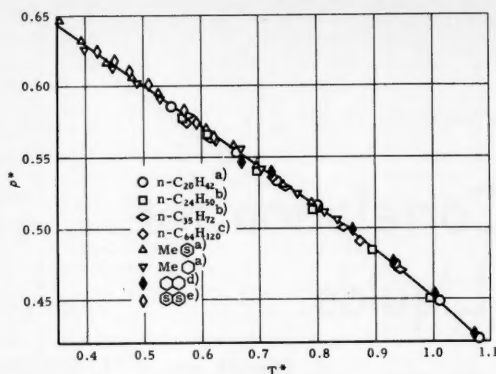


Fig. 1. Generalized density vs. temperature curve for hydrocarbon: (a) 26, (b) 30, (c) 31, (d) 32, (e) 27.

the axis ratio of cigar-shaped molecules and with the core radius of globular molecules.

A significant step forward was made by Prigogine and his collaborators (15) when they introduced the subdivision of larger flexible chainlike molecules into the number of chain links r and the total number of external degrees of freedom ($3c$) per molecule which result from the motions of the molecule as a whole and from the independent motions of the chain links. The physical properties of the condensed phase should then be determined by the molecular parameters ϵ and σ , the pair potential and the diameter characterizing a chain link, Z , the number of nearest neighbors around a chain link, r , the number of chain links per molecule, and $3c$, the number of external degrees of freedom per molecule. From statistical mechanics one can show that for rigid molecules $3c = 5$ or 6 , depending on the symmetry characteristics of the molecule; for flexible molecules (moderately hindered internal rotation) $3c = r + 3$; and for loose molecules (completely free internal rotation) $3c = 2r + 1$.

Several ways are open to determine ϵ and σ ; one way is to calculate them from p - v - T properties with the aid of theory. This has been done by Simha and Hadden (20). Their approach did not prove of sufficient generality for the authors' purposes. A second path was followed by Prigogine and Naar-Colin (16) who obtained ϵ , σ , and c/r by comparing the properties of many members of the n -paraffin series. Instead the authors decided to express ϵ in terms of the lattice energy taken as the energy of vaporization at a fixed value (1.70) of the reduced volume $V^* = V/V_w$, and to replace σ^* by V_w/r . V_w is calculated from the bond distances and van der Waals radii as outlined in Appendix I. The standard

energy of vaporization ΔE_v^* at $V^* = 1.70$, abbreviated as E^* in this report, is also easily correlated with molecular structure as outlined in Appendix II. Moreover for many small molecules $E^* \approx 10N_A\epsilon$, when ϵ is estimated from gas properties. This point was also considered in the choice of the standard state $V^* = 1.70$.

The definition of the dimensionless parameters is now straightforward. In accordance with Prigogine the reduced temperature $T^* = ckT/q\epsilon$, where q is defined by $qZ = rZ - 2r + 2$. Now $E^* = \frac{1}{2} qZ\epsilon f(V^*)$; hence if one sets $Z = 10$, (5), and $f(V^*) \approx 1$,† $T^* = cZRT/2E^* = 5cRT/E^*$. The reduced density $\rho^* = V_w/V$. The definition of the reduced pressure will be discussed in the p - v - T section of this report. The a priori calculation of c is possible only for the limiting cases mentioned previously. For most substances one has to determine it empirically by means of at least one property measurement, as will be shown in the next section. As c is now essentially an empirical constant, $3c$ can, and does, assume nonintegral values.

Generalized Density-Temperature Relation (at Atmospheric Pressure)

A test of the correct definition of reducing parameters in a corresponding states correlation is the universality of the curve ρ^* vs. T^* . For rigid molecules, such as those of the aromatic and the naphthenic ring series, this proved to be the case. The correlation was constructed by plotting ρ^* vs. T^* for toluene and other cyclic compounds. The value of ϵ/k (toluene)‡ = 460°K. was estimated from the published value ϵ/k (benzene) = 440°K. (9).

For the n -paraffin series one has a somewhat more complicated situation

† As turns out to be the case for $V^* = 1.70$ and the chosen lattice geometry.

‡ Owing to accidental cancellation of numerical data, in this case $5cRT/E^* = kT/\epsilon$.

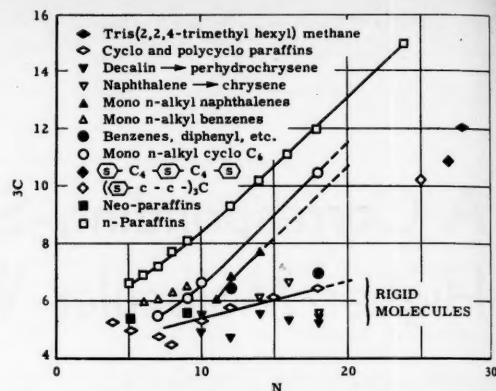


Fig. 2. Number of external degrees of freedom per molecule ($3c$) as function of molecule size for different hydrocarbon series.

because of the different flexibility of the methyl-methylene group as compared with the methylene-methylene linkage. Fortunately there is very little change beyond n -C₁₀, and the general correlation was constructed as follows. First p^* vs. T^* was plotted for propane for which ϵ/k is known (254°K.) (9) and for which a very long liquid range yields extensive density data. This curve crosses that of toluene at $V^* = 1.80$. Hence ρ^* vs. T^* was plotted on the assumption that all have the same value of T^* at $V^* = 1.80$ ($\rho^* = 0.5556$). The result, Figure 1, shows that all curves for n -paraffins with C_{10} to C_{60} , the naphthenes beginning with methyl cyclohexane and including tri-cyclohexyl methane, etc., and the aromatics from toluene through all the polyaromatic hydrocarbons for which data are available fit on a single curve, with no significant loss in accuracy.† (Needless to say, better than 0.5% accuracy cannot be expected from any corresponding states correlation.) Since for the hydrocarbons of interest (C_{12}^+) $\rho^* < 0.45$ is generally above the atmospheric boiling point and therefore not accessible experimentally without decomposition, the curves have not been carried beyond that point. The upper limit of the graph has been set up by the fact that practically all substances are solids when $\rho^* > 0.65$. All n -paraffins above C_8 are solid at $\rho^* > 0.59$.

The equation of the general correlation curve is

$$\rho^* = 0.726 - 0.249T^* - 0.019T^{*2}$$

(at atmospheric pressure)

The constant 0.726 has the physical meaning of a universal reduced density for all liquid hydrocarbons at $T = 0$.

† The n -paraffins below C_{10} do not fit the curve of Figure 2 but exhibit a smaller slope. Cyclohexane and benzene are not included in the correlations because their short liquid range does not permit a test of the fit.

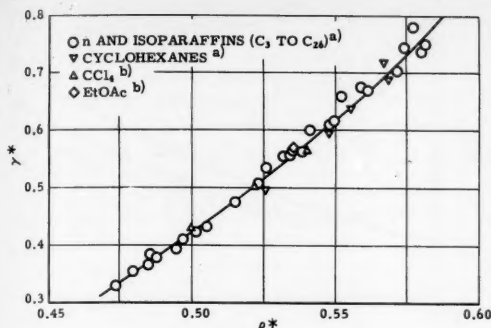


Fig. 3. Reduced surface tension as function of reduced density: (a) up to C_{20} (26), higher hydrocarbons (33); (b), 34.

The data of Table 1 show that the observed values of $\rho^* = \text{near } 0^\circ\text{K.}$ are of the order of 0.72.

The linearity of the curve at $T^* < 0.8$ is in agreement with the well-known linearity of the density vs. temperature curve of most liquids, much below their atmospheric boiling point (12). It is of practical interest that the existence of a single density measurement at a known temperature now permits the extrapolation of the entire density vs. temperature curve of a compound.

Reduced Density and Molecular Structure

As the reduced density is a unique function of the ratio of kinetic to potential energy per molecule it is relatively easy to locate the specific effects of molecular structure. The potential energy, given by the lattice energy E^* , is a relatively nonspecific property, as is evident from the narrow range of variations in the magnitude of E^* per carbon atom demonstrated in Appendix II. The kinetic energy by contrast is proportional to the number of external degrees of freedom per molecule and thus directly related to the flexibility of the molecular structure. This effect is more striking when one compares for a given series of

molecules the temperature at which $V^* = 1.70$ than the comparison of the degrees of freedom $3c$, also shown in Table 2. To state the case more directly, ρ^* is a direct measure of molecular flexibility; it is high for rigid molecules and is lower the more flexible a molecule.

A more general comparison is presented in Figure 2, where $3c$ is plotted for several groups of compounds as a function of molecular size. One sees rather clearly the difference between the flexible n -paraffins on the one hand and the stiff aromatic and naphthenic ring system on the other. The naphthenic ring systems of nearly spherical symmetry approach the rigid spheres in their small number of external degrees of freedom.

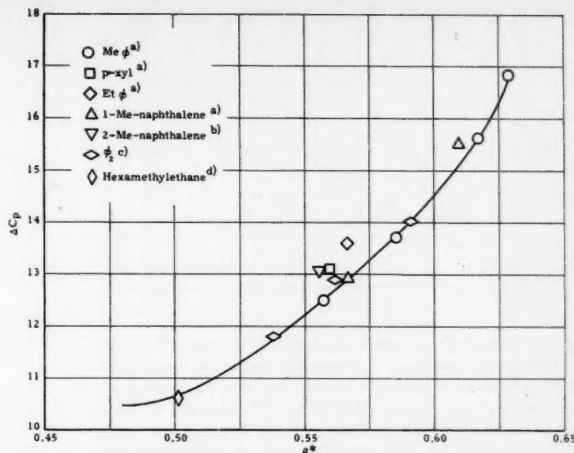


Fig. 4. Correlation of ΔC_p vs. reduced density for aromatic hydrocarbons, from heat-capacity data: (a) ΔC_p calculated from (35), (b) C_p (liq.) (36) and C_p (g.) (37), (c) C_p (liq.) (38) and C_p (g.) (39), (d) C_p (liq.) and C_p (g.) (40).

The prediction of $3c$ for hydrocarbons not covered by the data of Figure 2 may best be performed by interpolation between the existing data. Estimation of $3c$ for alkyl derivatives of specific ring systems may be carried out, for example by laying a curve paralleling the n -paraffin line through the particular ring compound.

Reduced Surface Tension

Molecular theory of surface energy shows that the reduced total surface energy $U^* = U A_s / E^*$ and the reduced surface free energy (surface tension) $\gamma^* = \gamma A_s / E^*$ of simple liquids are unique functions of the reduced density (7, 9). The plot of γ^* vs. ρ^* in Figure 3 shows that this prediction is valid for all the normal and isoparaffins,

TABLE 1. REDUCED DENSITY AT 0°K.

Substance	ρ_0^* Crystal (exp.) (22)	ρ_0^* Liq. (exp.) (22)	ρ_0^* Liq. (calc.) (23)
n -Pentane	0.710		0.702(24); 0.700(23)
iso-Pentane	0.701	0.683°	0.701(24)
n -Nonane	0.726		0.705(24); 0.714(23)
$(\text{CH}_2)_\infty$	0.757		0.716(24); 0.732(23)
Toluene	0.712		0.713(24)
CCl_4	0.690		0.711(23)

* This is probably not the equilibrium density, but, as is usual with glasses, the frozen-in density of a higher temperature.

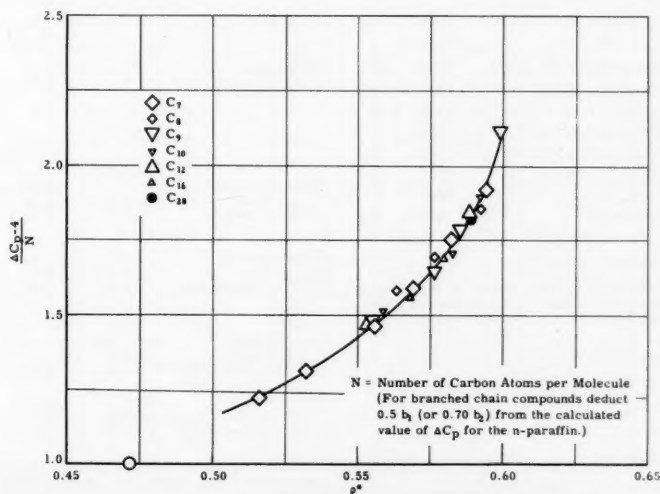


Fig. 5. Correlation of ΔC_p vs. reduced density for n -paraffins ($N \geq 7$) from heat-capacity data: C_p (liq.) (41), C_p (g.) (42).

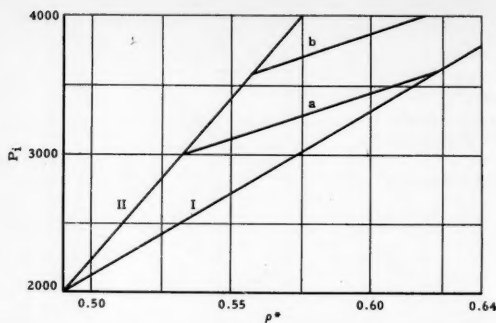


Fig. 6. Correlation of internal pressure with reduced density at atmospheric pressure: I *n*-paraffins (also for *iso*-paraffin and naphthenes), II aromatic nuclei (for alkyl aromatics use also the cross-over lines), *a* for $40 \pm 10\%$ aromatic C atoms per molecule, *b* for $80 \pm 10\%$ aromatic C atoms per molecule; *n*-paraffins (31, 43), aromatics (44), all classes (45, 46).

for monocyclic naphthenes, and for several nonpolar or slightly polar non-hydrocarbons.

This correlation can be valid only for molecules with isotropic force fields. Since a molecule with anisotropic force fields would orient in the surface such as to minimize the surface free energy, the term E^0/A_w would cease to describe the potential-energy contribution to the surface properties. The deviation of the behavior of a given compound from the curve of Figure 4 is by the same token a sensitive measure of orientation effects. Aromatic hydrocarbons exhibit a sufficiently anisotropic force field for their reduced surface tension to fall on curves below that of Figure 3. The reason for the deviations of the condensed cyclic naphthenes

from the basic correlation curve of Figure 3 is obscure at present. Since the extent of molecular orientation depends on the ratio of orientation energy to kT , the reduced surface tension of anisotropic systems is likely to depend on temperature explicitly and not only on density. Concurrently the extent of deviation from the general correlation should decrease with increasing temperature.

Heat-Capacity Difference

One of the most peculiar features of the liquid state is its high heat capacity as compared with both the solid and the vapor state. The heat capacity of the vapor in the ideal gas state is very well understood; the differences between the liquid and the vapor (as ideal gas) are therefore of particular interest.

TABLE 2. EFFECT OF MOLECULAR FLEXIBILITY ON THE TEMPERATURE AT WHICH $V^0 = 1.70$

Substance	<i>T</i> , °K.	3 <i>c</i>
1, 3, 5-Hexatriene (cis) (25)	199*	6.8
2, 3, 4-Hexatriene (25)	241	5.6
<i>n</i> -Nonane (26)	236	8.0
Tetraethyl methane (26)	286	5.6
1, 1-Dicyclohexyl heptane (27)	373	7.9
Tricyclohexyl methane (27)	425	6.4
<i>o</i> -Terphenyl (28)	397	6.8
Triphenylene (28)	565	5.4

* Extrapolated below *F_p*.

The references pertain mostly to the density data. The vapor-pressure data required to calculate *c* come from many additional sources.

TABLE 3. RECOMMENDED VAN DER WAALS RADII FOR CARBON AND HYDROGEN, Å.

Bond type	<i>r_w</i> (C)	<i>r_w</i> (H)
Single (aliphatic)	1.70	1.20
Olefinic double bond	1.70	1.20
Aromatic ring	1.77	1.00

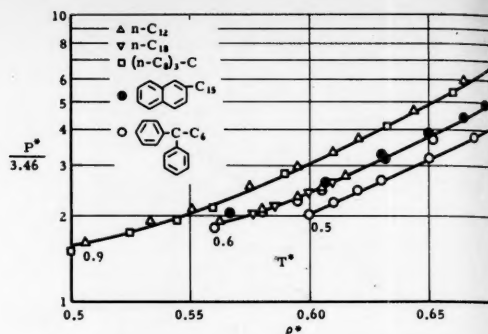


Fig. 7. Generalized $P^*-V^*-T^*$ correlation for different hydrocarbons (45).

Molecular theory tells us that ΔC_v of simple liquids is a unique function of T^* and therefore also of V^* (1, 17). The experimental heat capacity of liquid argon and mercury have been shown to conform rather closely to the predictions of theory. The maximum value of ΔC_v predicted by theory is identical with that for the ideal crystal, namely $(3/2)R$. Almost all organic substances exhibit ΔC_v 's significantly in excess of the value predicted by simple molecular theory, especially if $\rho^* > 0.5$. Assuming ΔC_v for argon at a given ρ^* as that for the perfect liquid one may consider $[\Delta C_v - \Delta C_v(A)]^* = \Delta C_v^*$ as the specific characteristic of the liquid under consideration.

A plot of ΔC_v^* vs. ρ^* for several liquids shows the same upward trend. But no other correlating feature of this highly specific property has as yet become apparent.

The physically less meaningful ΔC_v ,

TABLE 4. GROUP CONTRIBUTIONS TO V_w FOR HYDROCARBONS

Group	$-\dot{C}-$	$-\dot{CH}\dot{+}$	$>\dot{CH}_2\dot{+}$	$-\dot{CH}_2\dot{+}$	CH_3	n-paraffins†	
V_w (cc./mole)	3.33	6.78	10.23	13.67	17.12	6.88 + 10.23N	
A (10 ⁶ sq. cm./mole)	0	0.57	1.35	2.12	2.90	1.54 + 1.35N	
Group (aromatic)	$\geq CH$	$\geq C-$ (Alkyl)	$\geq C-$ (Condensation)	Benzene	Phenyl*	Naphthalene	Naphthyl*
V_w (cc./mole)	8.06	5.54	4.74	48.36	45.84	73.97	71.45
A (10 ⁶ cc./mole)	1.00	0.30	0.21	6.01	5.33	8.44	7.76
Group (olefinic)	$=CH$	$=CH_2$	$\equiv C-$	$\equiv CH$	$\equiv C-$ (in diacetylene)		
V_w (cc./mole)	8.47	11.94	6.87	10.42	6.65		
A (10 ⁶ sq. cm./mole)	1.08	1.86	0.85	1.64			
Group (olefinic)	$H_2C=CH_2$	$-HC=CH_2$	$>C=CH_2$	$>C=CH$	$C\equiv C$	$=C=$	
V_w (cc./mole)	23.87	20.41	16.95	13.49	10.02	6.96	
A (10 ⁶ sq. cm./mole)	3.72	2.94	2.17	1.39	0.61		
Group (olefinic)	$HC\equiv CH$	$-C\equiv CH$	$-C\equiv C-$				
V_w (cc./mole)	20.83	17.30	13.75				
A (10 ⁶ sq. cm./mole)	3.28	2.50	1.71				

† Correction for vicinal effects: Methyl or methylene group next to carboxyl or amide group: subtract 0.22 cc., methylene ring condensed to an aromatic system as in tetralin; subtract 0.52 cc./ring.

‡ *N* = number of carbon atoms per molecule.

* Subtract 2.52 cc./mole for each additional branch point on the ring.

proved far more readily correlated. The correlation for rigid molecules is shown in Figure 4. It appears here that ΔC_p can be described to a fair degree of approximation as a function of ρ^* (or of T^*). The flexible n -paraffins above C_7 are also well correlated as function of ρ^* by the scheme shown in Figure 5. The meaning of that correlation is most likely that the surrounding molecules increase the hindrance to the rotation of each chain link relative to that occurring in the gas. The origin of that increase, namely the strong tendency to parallel alignment due to polarization anisotropy of the C-H bond, has been discussed previously (1).

P-V-T Relations

One of the incentives to prepare the correlation at hand has been the availability of extensive compression data on higher molecular-weight hydrocarbons (2, 3), covering a pressure range up to 10,000 atm. and a temperature range from 0° to 200°C. The authors have yet to define a reduced pressure P^* . Simple molecular theory suggests

$$P^* = P \sigma^3 / \epsilon$$

and Prigogine's theory for polymers yields

$$P^* = P r \sigma^{*3} / q \epsilon^*$$

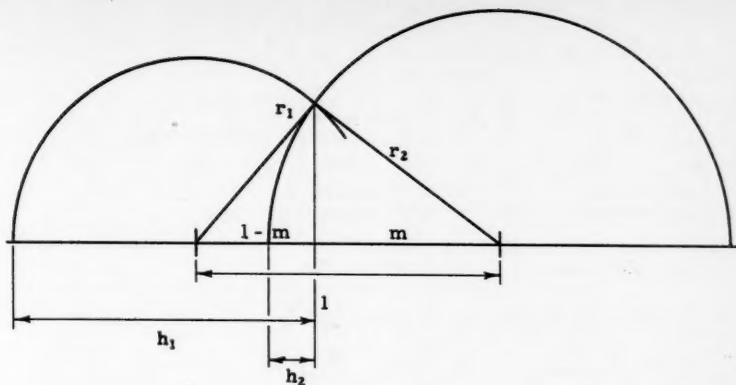
which in the language of the current work would be

$$P^* = P Z V_w / 2 E^*$$

However both of these definitions exhibit a serious inherent deficiency. They do not take into consideration that the external pressure is in reality additive to the intermolecular attractive forces. Specifically an external pressure of 1,000 atm. should not increase P^* by a factor of 1,000, as compared with atmospheric pressure, but only by a factor $(P_i + 1,000)/(P_i + 1)$. The experimental definition of P_i is $(\partial E / \partial V)_T$. The theoretical significance is not entirely clear. The attractive potential per unit volume is probably a reasonable interpretation (8). Hence the authors choose as the definition of reduced pressure $P^* = (P + P_i) Z V_w / 2 E^*$, which equals $(P + P_i) 5 V_w / E^*$ if $Z = 10$.

The internal pressure used here is that determined at atmospheric pressure and is hence experimentally accessible without direct compressibility measurement, for example via the sound velocity. But even that information is usually not available over the entire temperature range of interest. The ability to predict P_i in some other way is therefore important. An approximate empirical correlation of P_i with ρ^* is shown in Figure 6.

A few typical correlations of P^* vs.



r_1, r_2 = van der Waals radii

l = covalent bond distance

m = auxiliary parameter

h_1, h_2 = height of sphere segments

$$m = \frac{r_2^2 - r_1^2 + l^2}{2l}; h_1 = r_1 + l - m; h_2 = r_2 - m$$

$$V_1^* = \pi h_1^2 (r_1 - \frac{h_1}{3}); \Delta V_{2-1} = \pi h_2^2 (r_2 - \frac{h_2}{3}); V_2 = \frac{4\pi}{3} r_2^3$$

Example:

van der Waals volume of diatomic molecule:

$$V_w = N_A [V_1^* + V_2 - \Delta V_{2-1}] \text{ cm}^3/\text{mole}$$

where $N_A = 6.02 \times 10^{23}$ molecules/mole

and r 's are given in Angstrom units

Volume of center atom = Total volume of atom

Surface area = $2\pi r h$

Fig. 8. Method of calculation.

TABLE 5. STANDARD ENERGY OF VAPORIZATION E^* FOR n -PARAFFINS†

N°	2	3	4	5	6	7	8	9	10	12	
E^*	3.94	5.29	6.26	7.25	8.40	9.54	10.69	11.80	12.92	14.98	kcal./mole

* N = number of carbon atoms per molecule.

† Density and ΔH_{vap} from A.P.I. Project 44 Tables, ΔC_p from the references of Figure 6.

ρ^* and T^* are shown in Figure 7. The wide range of compounds covered by a single graph is rather gratifying; however the generality is not complete. Very rigid and nearly spherical molecules, such as perhydrochrysene, decalin, etc., do not fit into this scheme without extra effort. This peculiarity might have been predicted from the anomalously low value of 3c mentioned

earlier and tentatively ascribed to a smaller number of nearest neighbors than that obtained with flexible-chain substances. Such adjustment of Z moves the p - v - t curves of condensed cyclic polymethylenes in the right direction and yields plausible values for 3c.

Expression of these results in the form of an equation of state will only be attempted once a broader range of

TABLE 6. STANDARD ENERGY OF VAPORIZATION FOR ISO-PARAFFINS†
(KCAL./MOLE)

Substance	i -C ₄	i -C ₅	3-methylpentane	2, 2-dimethylbutane
E^*	6.02	7.00	8.15	7.78
Substance	3-ethylpentane	2, 4-dimethylpentane	2, 2-dimethylpentane	
E^*	8.94	8.87	8.79	
Substance	3-methyl, 3-ethylpentane	2, 5-dimethylhexane	2, 4-trimethylpentane	
E^*	9.30	9.97	9.38	
Substance	tetraethylmethane	2, 6-dimethylheptane		
E^*	9.98	11.25		

† Density and ΔH_{vap} from A.P.I. Project 44 Tables, ΔC_p from the references of Figure 6.

TABLE 7. CORRELATIONS FOR CALCULATING E°
(ALL IN KCAL./MOLE)

1. Paraffins	
a) <i>n</i> -Paraffins ($N > 12$)	$E^\circ = 14.98 + 1.07(N - 12)$
b) Isoparaffins*	$E^\circ = E^\circ(\text{n-paraffin}) - 0.30b_1 - 0.40b_2$
2. Olefins and diolefins	
a) Straight chain	$E^\circ = E^\circ(\text{n-paraffin})$
b) Branched chain	$E^\circ = E^\circ(\text{iso-paraffin}) + 0.90$
3. Cycloparaffins (one ring system per molecule)	
a) Rings without chains	$E^\circ = 3.27 + 0.76N$
b) Monoalkylcyclopentanes	$E^\circ = 5.90 - 0.20 \sum \frac{1}{N_b - 1} + \frac{1}{2}E^\circ(P_2)^\dagger$
c) Dialkylcyclopentanes	$E^\circ = 4.60 + \sum \frac{1}{2}E^\circ(P_2)$
d) Monoalkylcyclohexanes	$E^\circ = 6.60 - 0.20 \sum \frac{1}{N_b - 1} + \frac{1}{2}E^\circ(P_2)$
e) Dialkylcyclohexanes	$E^\circ = 5.25 + \sum \frac{1}{2}E^\circ(P_2)$
f) Monoalkyldecalins	$E^\circ = 9.12 + \frac{1}{2}E^\circ(P_2)$
4. Aromatics (one ring system per molecule)	
a) Monoalkylbenzenes	$E^\circ = 7.27 - 0.30 \sum \frac{1}{N_b - 1} + \frac{1}{2}E^\circ(P_2)$
b) Polyalkylbenzenes	$E^\circ = 7.27 - 1.2(b - 1) - 0.30 \sum \frac{1}{N_b - 1} + \sum \frac{1}{2}E^\circ(P_2) - 0.30b_{12} - 0.20b_{13}$
c) 2-Monoalkylnaphthalenes	$E^\circ = 10.65 + \frac{1}{2}E^\circ(P_2)$
d) 9-Monoalkylanthracenes	$E^\circ = 14.10 + \frac{1}{2}E^\circ(P_2)$
5. Polycyclic naphthenes	
a) Cyclopentanes**	$E^\circ = 5.22R_1 + 4.20R_2 + 1.1M - 2.25X + \frac{1}{2}E^\circ(P_2)$
b) Cyclohexanes**	$E^\circ = 6.22R_1 + 5.20R_2 + 1.05M - 2.25X - 1.0P_s - 0.30P_m + \frac{1}{2}E^\circ(P_2)$
c) Condensed cyclic polymethylenes: (except those containing endo methylene groups)	$E^\circ = 1.30M_c - 0.20T - 2.0$
6. Polycyclic aromatic	
a) Polyphenyls	$E^\circ = 6.85R_1 + 5.32R_2 - 1.0P_m - 2.3P$
b) Kata and peri condensed rings ^{††}	$E^\circ = 1.41S + 0.45T$

* b = total number of branches; b_1 = branches in isolated position; b_2 = branches in neo position.
[†] P_2 = appropriate paraffin hydrocarbon for which $N = 2N_b$, N_b = number of carbon atoms in alkyl chain.

** For systems where the rings are connected by chains of 6 carbon atoms or less.
 R_1 = number of rings with single attachment point.
 R_2 = number of rings with two attachment points.
 M = number of methylene groups between rings.
 M_c = number of methylene groups in a condensed ring system.
 T = number of tertiary carbon atoms in a condensed ring system.
 $X = 1$, 1 di-ring attachment to a chain or to a chain or ring system larger than 4 carbon atoms;
 P_o, P_m = ortho and meta attachments respectively.
^{††} $S = \text{CH group}$; T = carbon atom without hydrogen for phenanthrene and chrysene $E^\circ = 1.41S + 0.10T$.

compounds has been covered. In the meantime only qualitative considerations apply. Theory predicts an equation of the form

$$\frac{(P + P_s)V}{cRT} = \frac{1}{1 - A\rho^{*1/2}} + \frac{24}{T^\circ} [B\rho^{*4} - D\rho^{*2}]$$

when the constants A, B, D are given by the assumed packing geometry. The predicted linear relation between $P^\circ V^\circ/T^\circ$ and $1/T^\circ$ is quite well fulfilled. The location of the curves as function of ρ^* is also in qualitative

agreement with theory.

ACKNOWLEDGMENT

The assistance of J. Lielmesz and R. B. McConaughy with some of the calculations is gratefully acknowledged. Special thanks are due to D. W. Morecroft and A. L. Shellard of Shell Research, Ltd., Thornton, England, for carrying out many low-temperature vapor-pressure measurements on high-molecular-weight hydrocarbons, kindly lent by A.P.I. Project 42, with which to calculate the E° data presented in this report.

The authors are indebted to D. B. Marsland of the du Pont Experimental Station for valuable suggestions regarding the

improvement of the manuscript.

NOTATION

A_w	= surface area of a mole of molecules, sq. cm.
A, B, D	= constants in equation of state
c	= one-third of the number of external degrees of freedom per molecule
ΔC_p	= $C_p(\text{liq}) - C_p(\text{g})$ = heat-capacity difference between liquid and gas, cal. mole ⁻¹ °K ⁻¹
E°	= standard energy of vaporization = $(\Delta H_{vap} - RT)$ at $V^\circ = 1.70$, kcal./mole
l	= covalent bond distances
N	= number of carbon atoms per molecule
N_A	= Avogadro's number
P	= external pressure, atm.
P_i	= internal pressure, atm.
P_c	= critical pressure, atm.
P^*	= reduced pressure = $5V_w(P + P_i)/E^\circ$
q	= magnitude defined by $qZ = Zr - 2r + 2$
R	= gas constant
r	= number of chain links in a chainlike molecule = $(N + 1)/2$
r_w	= Van der Waals radius, Å.
T	= temperature, °K.
T_c	= critical temperature, °K.
T°	= reduced temperature = $5cRT/E^\circ$
U	= total surface energy, erg. cm. ⁻²
U^*	= reduced total surface energy = UA_w/E°
V	= molal volume, cc. mole ⁻¹
V_c	= critical molal volume, cc. mole ⁻¹
V_w	= Van der Waals volume, reducing parameter, cc. mole ⁻¹
V°	= reduced volume = V/V_w
Y	= correction constant
Z	= number of nearest neighbors

Greek Letters

γ	= surface free energy, erg. cm. ⁻²
γ°	= reduced surface free energy = $\gamma A_w/E^\circ$
ϵ	= pair potential at distance of potential minimum
ρ	= density, g. cm. ⁻³
ρ^*	= reduced density = V_w/V
σ	= molecular diameter at steepest ascent of repulsion curve

LITERATURE CITED

1. Bondi, A., *J. Phys. Chem.* **58**, 929 (1954).
2. Bradbury, D., M. Mark, and R. V. Kleinschmidt, *Trans. Am. Soc. Mech. Engrs.*, **73**, 667 (1951).
3. Cutler, W. G., R. H. Mickle, W. Webb, and R. W. Schissler, *J. Chem.*

- Phys.*, **29**, 727 (1958).
4. DeBoer, Jan, *Physica*, **14**, 139, 149, 520 (1948).
 5. ———, *Proc. Roy. Soc. (London)*, **A215**, 4 (1952).
 6. Forman, J. Charles, and George Thodos, *A.I.Ch.E. Journal*, **4**, 356 (1958).
 7. Harasima, A., *Adv. Chem. Phys.*, **1**, 203 (1958).
 8. Hildebrand, J. L. and R. L. Scott, "Solubility of Non-Electrolytes," Reinhold, New York (1951).
 9. Hirschfelder, J. O., C. F. Curtis, and R. B. Bird, "Molecular Theory of Gases and Liquids, Wiley, New York (1954).
 10. Kihara, T., *J. Phys. Soc. (Japan)*, **6**, 289 (1951).
 11. Lennard-Jones, J. E., and A. F. Devonshire, *Proc. Roy. Soc. (London)*, **A163**, 53 (1937); **A165**, 1 (1938).
 12. Lipkin, M. R., and S. S. Kurtz, *Ind. Eng. Chem. Anal. Ed.*, **13**, 291 (1941).
 13. Pitzer, K. S., *J. Chem. Phys.*, **7**, 583 (1939).
 14. ———, *et al.*, *J. Am. Chem. Soc.*, **77**, 3433 (1955).
 15. Prigogine, I., "Molecular Theory of Solution," Interscience, New York (1957).
 16. ———, A. Bellemans, and C. Naar-Colin, *J. Chem. Phys.*, **26**, 751 (1957).
 17. ———, and S. Raulier, *Physica*, **9**, 396 (1942).
 18. Reid, R. C., and T. K. Sherwood, "The Properties of Gases and Liquids," McGraw-Hill, New York (1958).
 19. Riedel, L., *Chem. Ing. Tech.*, **23**, 59, 321, 465 (1951).
 20. Simha, R., and S. T. Hadden, *J. Chem. Phys.*, **25**, 702 (1956).
 21. Trappeniers, N., *Physica*, **17**, 501 (1951).
 22. Biltz, W., *et al.*, *Z. Phys. Chem.*, **151**, 13 (1930).
 23. Doolittle, A. K., and D. B. Doolittle, *J. Appl. Phys.*, **28**, 901 (1954).
 24. Riedel, L., *Chem.-Ing.-Tech.*, **26**, 259 (1954).
 25. Faraday, Encyclopedia of Hydrocarbons.
 26. API-Project 44, Selected Properties of Hydrocarbons.
 27. API-Project 42.
 28. Andrews, J. N., and A. R. Ubbelohde, *Proc. Roy. Soc. (London)*, **A228**, 435 (1955).
 29. McLaughlin, E., and A. R. Ubbelohde, *Trans. Faraday Soc.*, **53**, 628 (1957).
 30. Nederbragt, G. W., and J. W. M. Boelhouwer, *Physica*, **13**, 305 (1947).
 31. Doolittle, A. K., and R. H. Peterson, *J. Am. Chem. Soc.*, **73**, 2145 (1951).
 32. Juravlev, D. I., *J. Phys. Chem. (U.S.S.R.)*, **9**, 875 (1937).
 33. Waterman, H. I., *et al.*, *J. Inst. Petrol.*, **25**, 801 (1939).
 34. Timmerman, J., "Physical Constants of Organic Compounds,"
 35. Pitzer, K. S., and D. W. Scott, *J. Am. Chem. Soc.*, **63**, 2419 (1941).
 36. McCullough, J. P., *et al.*, *J. Phys. Chem.*, **61**, 1105 (1957).
 37. Milligan, D. E., *et al.*, *J. Am. Chem. Soc.*, **78**, 2207 (1956).
 38. Spaght, M. E., *et al.*, *J. Phys. Chem.*, **36**, 882 (1932).
 39. Trevisoi, C., *Ann. chim. (Rome)*, **45**, 943 (1955).
 40. Scott, D. W., *et al.*, *J. Am. Chem. Soc.*, **74**, 3447 (1949).
 41. Finke, H. L., *et al.*, *ibid.*, **76**, 333 (1954).
 42. Thomson, G. W., *ibid.*, 620.
 43. Doolittle, A. K., unpublished data.
 44. Boelhouwer, J. M., private communication.
 45. Cutler, W. G., *et al.*, *J. Chem. Phys.*, **29**, 727 (1958).
 46. Bergmann, L., "Der Ultraschall," Springer, Germany (1950).

Manuscript received May 27, 1959; revision received September 9, 1959; paper accepted October 1, 1959.

APPENDIX I

Recommended Van der Waals Radii and Volumes

The calculation of V_w requires knowledge of the van der Waals radii and of the appropriate covalent bond distances between two bonded atoms in a molecule. A recent reevaluation of r_w data from X-ray diffraction patterns of crystals together with crystal density data at O°K, gas kinetic collision radii of small molecules, and critical densities,* has yielded the radii shown in Table 3.

The van der Waals volume and the molecular surface area are calculated by combination of r_w with the covalent bond distance (data for which can be found in most chemistry text books) according to the model shown in Figure 8. The results are presented in the form of V_w and A_w group increments in Table 4. Special effects due to bond contraction or expansion in cases of double-bond conjugation or hyperconjugation can be found in the footnotes to the table.

APPENDIX II

Energy of Vaporization Data

The reducing parameter for temperature proposed in this paper is E^*/R , where E^* is defined as $\Delta E_v = \Delta H_v - RT$ at the temperature where $V^* = 1.70$. This temperature and the appropriate heat of vaporization have been calculated from density and low-temperature vapor-pressure data for a large number of hydrocarbons. Tables 5, 6, and 7 contain the information necessary to estimate the energy of vaporization of a number of different hydrocarbons. The same scheme is being developed for nonhydrocarbon substances.

* It is noteworthy that for 100 out of 124 substances tried, $V_c = 5.3 \pm 0.3 V_w$. Details of this correlation will be published elsewhere.

Concurrent Gas Absorption Mass Transfer

W. S. DODDS, L. F. STUTZMAN, B. J. SOLLAMI, and R. J. McCARTER

General Food Corporation, Tarrytown, New York

Concurrent flow in gas absorption may be used to practical advantage when liquid partial pressure is minor. The higher transfer coefficients of this operation are reported and analyzed in reference to pertinent variables.

Gas absorption in packed towers with countercurrent flow of gas and liquid has been studied extensively. Several

investigators (1, 2, 4 to 9, 11 to 15) have reported on the materials of this study; however mass transfer in con-

current flow systems has received little attention.

The general preference for counter-

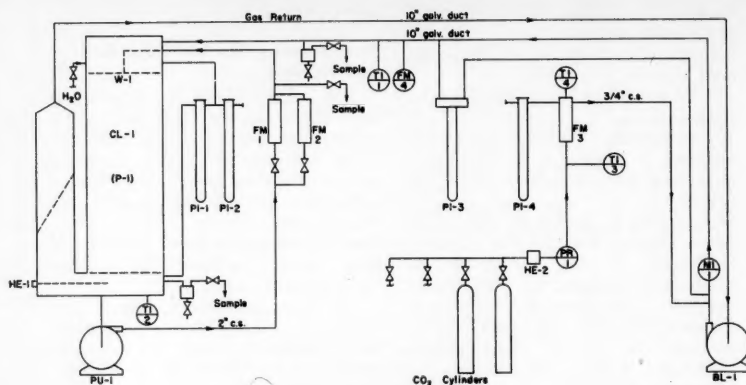


Fig. 3. Mass transfer coefficients.

current flow is apparent from inspection of the simplified equation for gas absorption:

$$N_L = K_g a V (\Delta p)_m$$

For a given system and conditions the amount of material transferred is proportional to the potential gradient or driving force, $(\Delta p)_m$, or its equivalent, $P_r (\Delta y)_m$. A more efficient operation results from the greater driving force of countercurrent flow (Figure 1a) than that of concurrent flow (Figure 1b) with the same terminal conditions when the liquid partial pressure varies with concentration. However when the liquid partial pressure is constant or negligible, this advantage ceases, and the driving force and transfer of the two systems tend to be equivalent (Figures 1c and d).

Such a system was used in this study, with carbon dioxide being absorbed in

caustic solutions. Thus it was possible to exploit without disadvantage the higher transfer coefficients that may be attained with concurrent flow. The flow rates in countercurrent operation are limited by the flooding point and probably cannot practically exceed the loading point. But in concurrent operation the flow rates are limited only by the feasible amount of power to be expended in pressure-drop losses. Thus high flow rates under stable operating conditions may be attained and used to yield high transfer coefficients. A wider range for design is in this way obtained, within which to optimize equipment and lower costs.

SCOPE OF INVESTIGATION

High flow rates were selected for this study at levels where countercurrent operation would be impossible and where the greater utility of concurrent flow could be attained. It was anticipated that the data would provide valuable design information in this higher range and be useful in improving over-all correlations. The range of these rates is generally higher than the flooding curves for countercurrent operation, according to the correlation of Lobo (10), and hence appreciably higher than the loading curves representing the practical limit in countercurrent operation.

The variables that were investigated were

Temperature (T) = 80° and 130°F.

Packing (P) = Berl saddles 1 and 1½ in., Intalox saddles 1 and 1½ in., and steel rings 2 in.

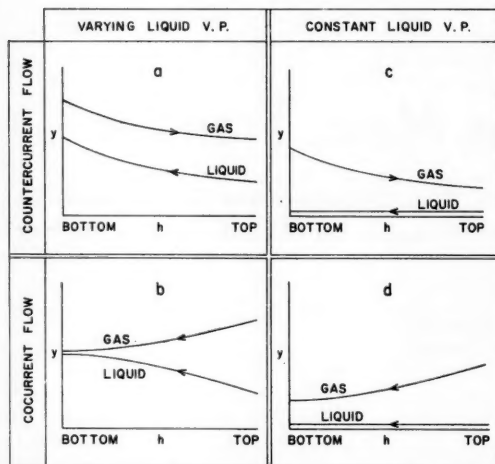
Liquid flow rate (L) = 17 and 59.4 gal./min./sq. ft. (9,330 and 32,600 lb./hr.) (sq. ft.) of 2.5N sodium hydroxide

Gas flow rate (G) = 22.7 and 56.6 lb. moles/(hr.) (sq.ft.)

Sodium normality (N) = 2.0, 2.5, 3.0, 3.5, and 4.0

Percentage of conversion (C) of hydroxyl to carbonate in entering solution = 0 to 100%

Material = sodium and potassium



$$N_L = K_g a V P_r (\Delta y)_m$$

Fig. 1. Driving force.

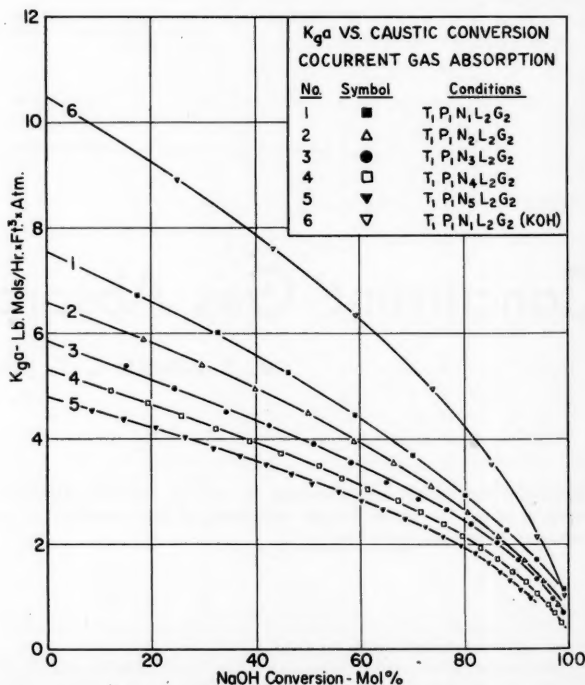


Fig. 2. Flow sheet for concurrent flow.

TABLE 1. $K_g a$ VALUES DERIVED FROM DATA CURVES

EQUIPMENT

The equipment used in this study is described in Figure 2.

EXPERIMENTAL PROCEDURE

The caustic solution was used to depletion in each run, so that transfer values were determined for the full range of caustic composition at a fixed concentration of sodium ions. The tower sump was first filled with a predetermined volume of caustic solution of the desired strength, which was maintained constant by the addition of water to replace evaporation losses. Liquid and gas streams were run until the packing was saturated and flow patterns were stabilized. Carbon dioxide was then introduced into the gas stream to constitute about 1 mole % concentration. During each run conversion of base to carbonate gradually progressed to completion, while all other conditions were maintained constant.

Recorded data included temperatures and flow rates of the liquid and gas streams. The liquid temperature varied less than 1°F. through the system because of the high flow rates. The temperature of the exit gas stream was within 1°F. of the liquid temperature. The recorded pressures included barometric pressure (mm.Hg), inlet gas-stream gauge pressure (mm.Hg), and pressure differential across the tower (inches of 0.827-gravity red oil). The carbon dioxide analyses of gas samples were obtained by measuring the weight increase resulting from absorption in Ascarite and anhydrous. As the gas stream was recirculated during the runs at the 130°F. temperature level, it was necessary to adjust the injection of replacement carbon dioxide as the run progressed and the rate of absorption decreased.

The transfer rate was calculated from the liquid analyses and liquid rates and was plotted against the mean of the time interval for sample collection. The smoothed values of N_L obtained from these curves were used for subsequent calculations. The carbon dioxide absorbed per hour also was calculated from the gas analyses and gas rates and the material balance afforded by comparison of N_L and N_G usually varied between 90 and 110% agreement. Deviations outside this range usually occurred when gas composition changed only slightly in transit through the tower and the accuracy of N_G was correspondingly low. The values of N_L were considered more reliable than those of N_G and were used to calculate $K_g a$ from the equation

$$N_L = K_g a V P_T (\Delta y)$$

An outlet gas composition was calculated from the liquid analyses and was used, rather than the analyzed composition, to obtain more consistent results.

The calculated values of $K_g a$ were plotted against the percentage conversion of hydroxide to carbonate, as exemplified by Figures 3 and 4. These figures summarize the runs involving solution normality, packing, and type of caustic as

% Conversion OH ⁻ to CO ₃ ⁼			0%		20%		40%		60%		80%	
			T ₁	T ₂	T ₁	T ₂	T ₁	T ₂	T ₁	T ₂	T ₁	T ₂
N ₁	L ₁	G ₁	3.9	8.4	3.6	7.3	3.1	6.1	2.5	4.9	1.7	3.4
		G ₂	4.4	8.8	3.9	7.7	3.3	6.6	2.7	5.2	1.9	3.6
	L ₂	G ₁	5.8	8.3	5.2	7.6	4.5	6.8	3.7	5.8	2.7	4.3
		G ₂	7.6	12.7	6.6	11.2	5.6	9.6	4.4	7.7	2.9	5.3
N ₂	L ₁	G ₁	4.2	6.9	3.8	6.3	3.2	5.7	2.5	4.7	1.6	3.2
		G ₂	4.4	9.5	3.8	8.2	3.3	6.8	2.6	5.4	1.8	3.7
	L ₂	G ₁	6.2	10.7	5.5	9.4	4.8	8.0	3.8	6.3	2.7	4.4
		G ₂	6.6	11.9	5.8	10.7	5.0	9.3	3.9	7.6	2.6	5.3
N ₃	L ₁	G ₁	3.7	8.7	3.2	7.4	2.8	6.1	2.2	4.7	1.5	3.1
		G ₂	3.8	7.0	3.4	6.3	2.9	5.6	2.3	4.6	1.5	3.2
	L ₂	G ₁	4.9	9.7	4.4	8.4	3.8	7.0	3.1	5.5	2.2	3.8
		G ₂	5.1	10.8	4.6	9.6	3.9	8.2	3.1	6.6	2.1	4.6
N ₂	L ₁	G ₁	3.6	6.7	3.1	5.9	2.7	5.1	2.1	4.1	1.4	3.0
		G ₂	3.6	7.3	3.2	6.4	2.8	5.5	2.2	4.3	1.5	3.0
	L ₂	G ₁	4.6	9.7	4.1	8.6	3.6	7.3	2.9	5.9	2.1	4.1
		G ₂	5.1	10.8	4.6	9.5	4.0	8.2	3.2	6.6	2.2	4.7

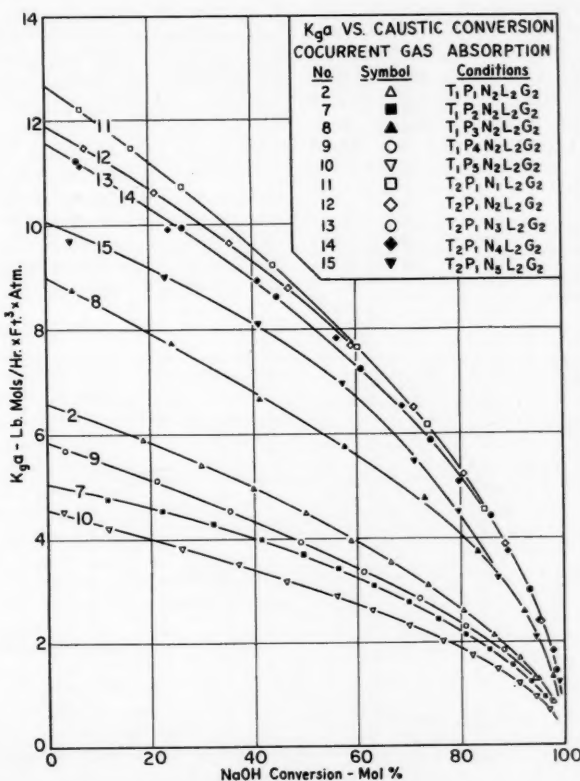


Fig. 4. Mass transfer coefficients.

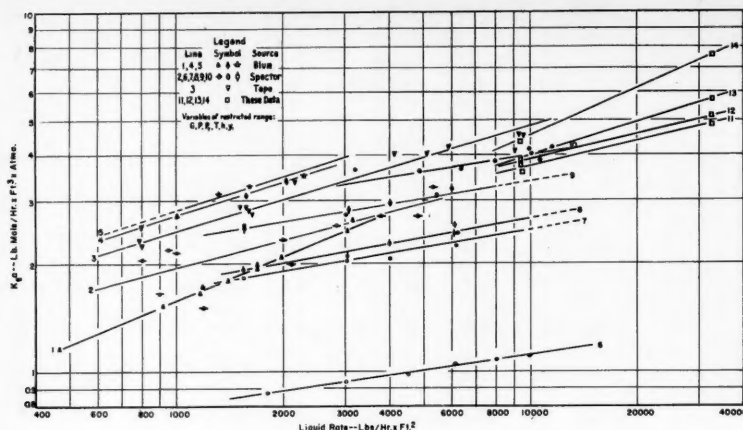


Fig. 5. Carbon dioxide absorption with sodium hydroxide solutions, liquid-rate effect.

individual variants. Similar curves were employed to derive the values of K_{ga} presented in Table 1, which summarizes the rest of the results.^o These runs form various factorial designs. The configuration of Table 1 evidences one such design with five variables at two levels and one variable at additional levels.

DISCUSSION

The simpler effects of the variables are apparent from inspection of Figures 3 and 4 and Table 1 and do not warrant discussion.

The data were compiled in factorial designs as a means toward extracting the most information per study and to facilitate statistical evaluation of the data. Various statistics could be used. The first treatment used was direct analysis of variance of the transfer co-

efficient. The procedure for such analysis is explained in Brownlee (3) and other texts on statistics. Against this additive model [$K_{ga} = f(T) + f(P) + f(N) + \dots$] numerous interactions of the variables were tested and found to be significant, but the results were unfortunately complex. As a next step the natural logarithm of the transfer coefficient was analyzed for variance. Against this multiplicative model [$\log K_{ga} = \log f(T) + \log f(P) + \log f(N) + \dots$] a simpler picture emerged. Results of a typical analysis are summarized in Table 2. In this set of data significance was indicated for the effects of temperature, packing, liquid rate, and gas rate, and for first-order interactions between temperature and packing and between liquid and gas rates. (In this case normality was not significant but would become so at higher values, as indicated by the data of Figures 3 and 4.) Although this process serves to identify effects of consequence and something of the nature of the relationship, it does not necessarily disclose the specific

^o Tabular material has been deposited as document 6047 with the American Documentation Institute, Photoduplication Service, Library of Congress, Washington 25, D. C., and may be obtained for \$5.00 for photoprints or \$2.25 for 35-mm. microfilm.

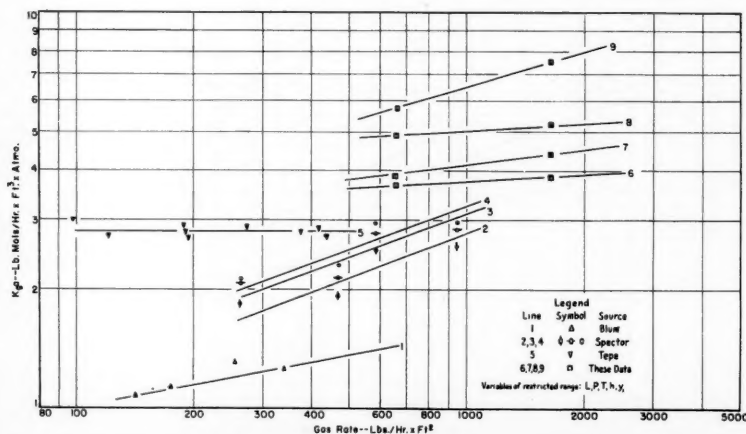


Fig. 6. Carbon dioxide absorption with sodium hydroxide solutions, gas-rate effect.

TABLE 2. STATISTICAL EXAMPLE
Dependent Variable: Natural Log of
 K_{ga} at 50% Conversion of Na Ion

			T_1	T_2
P_1	N_1	L_1 { G_1	1.06	1.70
		G_2	1.10	1.77
	L_2 { G_1		1.41	1.84
		G_2	1.61	2.16
N_2	L_1 { G_1		1.06	1.65
		G_2	1.10	1.81
	L_2 { G_1		1.46	1.97
		G_2	1.50	2.14
P_2	N_1	L_1 { G_1	0.92	1.69
		G_2	0.96	1.63
	L_2 { G_1		1.25	1.84
		G_2	1.25	2.00
N_2	L_1 { G_1		0.88	1.55
		G_2	0.96	1.59
	L_2 { G_1		1.19	1.89
		G_2	1.28	2.00

Summary of Analysis of Variance of
Dependent Variable

Source of variance	Un-coded mean	Degrees of freedom	Sums of squares	Probability of significant effect %
T	0.320	1	32,768.0	99.9
L	0.168	1	8,978.0	99.9
P	-0.077	1	1,891.1	99.9
G	0.047	1	703.1	99.9
N	-0.005	1	8.0	
TP	0.024	1	180.5	95
LG	0.021	1	144.5	95
PG	-0.018	1	105.1	
TL	-0.014	1	66.1	
TG	0.014	1	60.5	
PL	-0.010	1	32.0	
NL	0.009	1	28.1	
PN	-0.008	1	18.0	
TN	0.003	1	3.1	
NG	-0.001	1	0.5	
TPL	0.016	1	78.1	
NLG	-0.016	1	78.1	
Other				
2nd. Order		8	228.9	
Residual		6	82.8	
Total		31	45,454.5	

functions that may best relate the effects. It appears that additional data at more levels will be needed to delineate

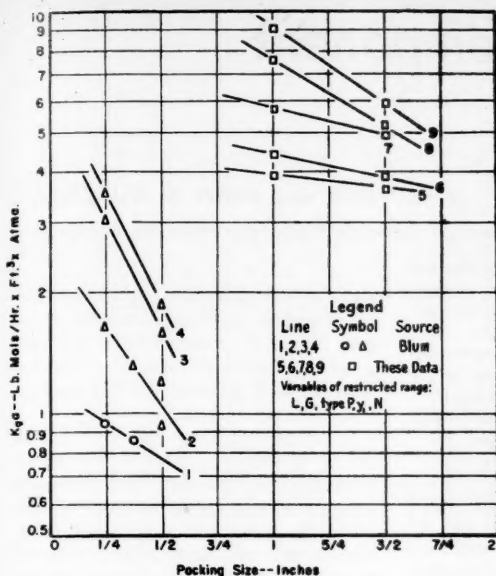


Fig. 7. Carbon dioxide absorption with sodium hydroxide, packing-size effect.

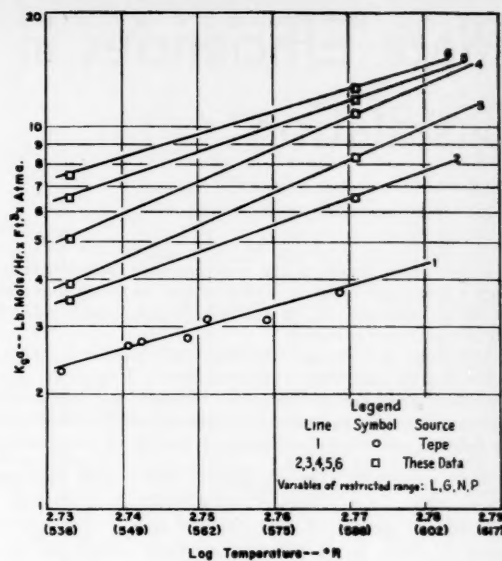


Fig. 8. Carbon dioxide absorption with sodium hydroxide solutions, temperature effect.

with confidence the best equation for the identified effects. Thus this work is a step toward a general correlation.

The data obtained in this study may be compared with other data of the field in the graphs of Figures 5 to 8. It was attempted to plot, against each of the major variables, values of K_{Ga} obtained under otherwise nearly similar conditions; the data were not entirely sufficient for this. Some ranges in the conditions had to be included, and lines, rather than points, are used in the graphs. Discrepancies within this variety of data make further resolution of effects difficult. The graphs respectively concern the effect of liquid rate, gas rate, packing size, and temperature.

CONCLUSIONS

High transfer coefficients were attained in this study of concurrent gas absorption, a demonstration that under some conditions this type of operation is advantageous. The data will be useful for design purposes. Reference ground is provided for a general correlation.

NOTATION

G = gas flow rate, lb. moles/(hr.) (sq. ft.)
 G_1 = gas flow rate of 40 lb moles/hr.
 G_2 = gas flow rate of 100 lb. moles/hr.
 h = height of packing, ft.
 K_{Ga} = over-all gas transfer coefficient, lb. moles/(hr.) (cu. ft.) (atm.)
 L = liquid flow rate, lb. moles/hr. sq. ft.
 L_1 = liquid flow rate of 30 gal./min.
 L_2 = liquid flow rate of 105 gal./min.

N = normality of sodium ion
 N_1 = normality of sodium ion of 2.0
 N_2 = normality of sodium ion of 2.5
 N_3 = normality of sodium ion of 3.0
 N_4 = normality of sodium ion of 3.5
 N_5 = normality of sodium ion of 4.0
 N_G = carbon dioxide transfer rate based on gas composition, lb. moles/hr.
 N_L = carbon dioxide transfer rate based on liquid composition, (smoothed values), lb. moles/hr.
 N_L' = carbon dioxide transfer rate based on liquid composition (original experimental data), lb. moles/hr.
 P = packing as a parameter
 P_1 = packing type, 1 in. Berl saddles
 P_2 = packing type, 1½ in. Berl saddles
 P_3 = packing type, 1 in. Intalox saddles
 P_4 = packing type, 1½ in. Intalox saddles
 P_5 = packing type, 2 in. steel rings
 P_T = pressure, total, in atm.
 p = partial pressure of transferring component
 T = temperature, °R.
 T_1 = temperature of 80°F.
 T_2 = temperature of 130°F.
 V = volume of packing in tower, cu. ft.

y = composition of transferring component, carbon dioxide, in gas stream
 Δ = difference between two quantities

Subscripts

m = log mean average of two quantities
 1 = inlet condition
 2 = outlet condition

3 = calculated outlet condition based on material balance

LITERATURE CITED

- Blum, H. A., Dissertation, Northwestern Univ., Evanston, Illinois (1949).
- , L. F. Stutzman, and W. S. Dodds, *Ind. Eng. Chem.*, **44**, 2969 (1952).
- Brownlee, K. A., "Industrial Experimentation," Chem. Pub. Co., New York (1952).
- Cooper, C. M., R. J. Cristl, and L. C. Peery, *Trans. Am. Inst. Chem. Engrs.*, **37**, 979 (1941).
- Cryder, D. S., and J. O. Maloney, *ibid.*, **37**, 827 (1941).
- Furnas, C. C., and F. M. Bellinger, *ibid.*, **34**, 251 (1938).
- Harte, C. R., Jr., E. M. Baker, and H. H. Purcell, *Ind. Eng. Chem.*, **25**, 528 (1933).
- Koch, H. A., Jr., L. F. Stutzman, H. A. Blum, and L. E. Hutchings, *Chem. Eng. Progr.*, **45**, 677 (1949).
- Landau, Ralph, C. E. Birchenall, G. C. Jeris, and J. C. Elgin, *ibid.*, **44**, 315 (1948).
- Lobo, W. E., Leo Friend, F. Hashmall, and F. Zenz, *Trans. Am. Inst. Chem. Engrs.*, **41**, 693 (1945).
- Sherwood, T. K., and F. A. L. Holloway, *ibid.*, **36**, 21 (1940).
- Ibid.*, p. 39.
- Sherwood, T. K., and R. L. Pigford, "Absorption and Extraction," McGraw-Hill, New York (1952).
- Spector, N. A., and R. F. Dodge, *Trans. Am. Inst. Chem. Engrs.*, **42**, 827 (1946).
- Tepe, J. B., and B. F. Dodge, *ibid.*, **39**, 255 (1943).

Manuscript received January 19, 1959; revision received April 20, 1959; paper accepted April 27, 1959.

Plate Efficiencies in Multicomponent Distillation

H. L. TOOR and JOHN K. BURCHARD

Carnegie Institute of Technology, Pittsburgh, Pennsylvania

A first approximation to the multicomponent plate-efficiency problem has been carried out with a film model combined with equations for steady state diffusion in a ternary gas mixture. Numerical integration of the equations through a plate yields the ternary efficiencies as functions of the binary efficiency.

The effects of diffusional interactions in a distillation column were studied by computing the efficiencies on each plate when a column is designed to separate a ternary mixture. In the example studied, the average column efficiency was 39% less than the binary efficiency.

Some criteria are suggested for comparing other multicomponent systems to the one studied in order to estimate the uncertainty in the use of binary correlations for these systems.

Plate efficiencies in distillation columns have been studied intensively and can be predicted adequately (2); however there is no information available on multicomponent systems, and the question arises as to how reliable the binary correlations may be when applied to a multicomponent system. In this paper a first approximation to the multicomponent problem will be carried out in order to explore the conditions under which a simple extrapolation of binary data is possible as well as the general magnitude of the error which may be caused by this extrapolation.

Mass transfer on a distillation plate is approached in a binary system by combining a rate equation for a single vapor bubble with a material balance on the bubble (4):

$$n_A = K_A (\bar{y}_A - y_A^*) = -\frac{m}{S} \frac{d\bar{y}_A}{d\theta} \quad (1)$$

m being constant for equimolar countercurrent transfer.

Although Equation (1) is rigorous in the sense that it merely defines the over-all mass transfer coefficient, it is usually integrated by assuming K_A , S , and y_A^* constant to yield

$$E_b = \frac{\bar{y}_{A1} - \bar{y}_{A11}}{\bar{y}_{A1} - y_A^*} = 1 - \exp\left(-\frac{K_A S}{m} \theta\right) \quad (2)$$

The assumptions made idealize the problem to one of complete liquid mixing in a vertical plane with a mass transfer mechanism such that $K_A S$ is independent of vertical position. When the above point efficiency is used as a plate efficiency, the constant K_A becomes some type of average across the plate. Notwithstanding the severe assumptions in Equation (2), its predictions on the additivity of resistances are found to be in reasonable accord

with experiment (2).

Although the hydrodynamics in a multicomponent system would not be expected to differ from a binary one which has the same physical properties, the mass transfer process is considerably more complicated. For steady state, equimolar, countercurrent diffusion in a three-component system the flux of species A and B from points 1 to 2 is approximated by (6)

$$n_j = \frac{D_{j0} p}{x} \phi_c (\delta_m y_{j1} - y_{j2}) \quad (3)$$

where

$$\delta_m = \exp\left(1 - \frac{D_{AO} + D_{BO}}{2D_{AB}}\right) (y_{e1} - y_{e2}) \quad (4)$$

$$\phi_c = \frac{y_{e1} - y_{e2}}{(1 - y_{e2}) - \delta_m (1 - y_{e1})} \quad (5)$$

n_c is obtained from the equation

$$n_A + n_B + n_C = 0 \quad (6)$$

which is usually valid in distillation. In this approximation species C is chosen to minimize $(D_{AO} - D_{BO})^2$; that is, species C is the odd component, normally the lightest or heaviest. When $D_{AO} = D_{BO}$, the above equations are exact solutions to the Maxwell-Stefan equations.

The equations differ considerably from the equivalent binary equations where the diffusional interaction terms δ_m and ϕ_c are 1.0. Since δ_m and ϕ_c are positive numbers, in a ternary system the direction of diffusion depends upon the generalized driving force $(\delta_m y_{j1} - y_{j2})$ rather than upon the binary driving force $(y_{j1} - y_{j2})$. Consequently in a ternary system diffusion may take

place in the direction opposite to the concentration gradient (reverse diffusion) when the concentration gradient is zero (osmotic diffusion), or in the presence of a gradient the flux may be zero (diffusion barrier).

In mass transfer, on a tray, of course, the flux is hardly likely to be controlled by steady state diffusion through a film. The transfer is undoubtedly complex with both convective and transient effects present. Furthermore generally there will be resistance in the liquid phase, and here even the diffusion problem has not been solved. (It would be expected however that the differences between binary and multicomponent transfer in the liquid phase are less marked than in the gas phase, since diffusional interactions appear to be less severe in liquids.)

Thus a complete solution to the mass transfer problem is not possible at present, but a first approximation can be obtained by resorting to the concept of steady state transfer through an effective gas film. It has been found recently that such a model does a surprisingly good job of predicting three-component mass transfer in a wetted-wall column (7). It will be assumed that the gas side is controlling. Since diffusional interactions in liquids and in turbulent fluids are expected to be relatively small, it appears probable that this approach will give the maximum deviation to be expected between binary and ternary transfer.

With this film viewpoint the mass transfer equations for A and B become

$$n_j = k_j \phi_c (\delta_m \bar{y}_j - y_{j1}) \quad (7)$$

The ϕ_c and δ_m are now given by Equations (4) and (5) with the compositions at point 1 taken as the mean composition and at point 2 as the interfacial composition. Combining with a material balance, one gets

$$-\frac{m}{S} \frac{d\bar{y}_j}{d\theta} = k_j \phi_c (\delta_m \bar{y}_j - y_{j1}^*) \quad (8)$$

where y_{j1} has been replaced by y_{j1}^* , since the gas side is assumed to be controlling. If the binary Equation (2) is interpreted in terms of an effective

TABLE 1. DIFFUSION COEFFICIENTS, SQ. FT./HR.

D_{AB}	D_{AC}	D_{BC}
0.422	0.7805	0.7805

TABLE 2. DIFFUSION COEFFICIENTS AT 95°C. AND 1 ATM. AND ACTIVITY COEFFICIENTS

A = Methanol, $D_{AB} = 0.422$	B = Isopropanol, $D_{BC} = 0.623$	C = Water, $D_{AC} = 0.938$
-----------------------------------	--------------------------------------	--------------------------------

$$\begin{aligned}\ln \gamma_A &= (1 - X_A)[0.13X_B + 0.9X_C - 4.2X_BX_C] \\ \ln \gamma_B &= (1 - X_B)[0.13X_A + 1.6X_C - 0.5X_C(3X_B - X_C) - 1.05X_AX_C] \\ \ln \gamma_C &= (1 - X_C)[0.9X_A + 1.6X_B - 0.5X_B(X_B - 3X_C)]\end{aligned}$$

film, it can be written for each component as

$$E'_{bj} = \frac{\bar{y}_{ji} - \bar{y}_j}{\bar{y}_{ji} - y^*_j} = 1 - \exp\left(-\frac{k_j S}{m} \theta'\right) \quad (9)$$

where the subscript II has been removed so that E'_{bj} is the plate efficiency at a contact time θ' for component j in a binary system of j and c operating under the same hydrodynamics conditions as the ternary system. The gas side is assumed to be controlling here also. When $\theta' = \theta$, the contact time on the plate \bar{y}_j becomes y_{ji} , and E'_{bj} becomes the actual binary plate efficiency.

Differentiating Equation (9) one obtains

$$d[\ln(1 - E'_{bj})] = -\frac{k_j S}{m} d\theta' = -dN'_j \quad (10)$$

and combining with (8) one gets

$$d\bar{y}_j = -\phi_c(\delta_m \bar{y}_j - y^*_j) dN'_j \quad (11)$$

It follows for the above equations that

$$\frac{dN'_A}{dN'_B} = \frac{N_A}{N_B} = \frac{k_A}{k_B} = \frac{D_{AC}}{D_{AB}} \quad (12)$$

But the ratio of the number of gas phase transfer units for two separate binary systems is not equal to the ratio of diffusion coefficients; rather it is found to be equal to the ratio of the square roots of the coefficients (2). This inconsistency is a result of the use of the present film model and will be avoided in later calculations by considering a ternary system in which there are two similar species, A and B, and one dissimilar one, C; so $D_{AC} = D_{BC} \neq D_{AB}$. The consequence of this restriction will be considered later, but it is interesting to note that these are the conditions under which Equation (3) is the exact solution of the Maxwell-Stefan equations.

Multicomponent plate efficiencies may be defined by

$$E_j = \frac{\bar{y}_{ji} - \bar{y}_{ji}}{\bar{y}_{ji} - y^*_j} \quad (13)$$

For a binary system the two efficiencies are equal, while in a multicomponent system there is one equation relating all the efficiencies (exclusive of

the mass transfer relationships). The equation for a ternary system is

$$E_c = \frac{(\bar{y}_{A1} - y^*_{A1}) E_A + (\bar{y}_{B1} - y^*_{B1}) E_B}{(\bar{y}_{A1} - y^*_{A1}) + (\bar{y}_{B1} - y^*_{B1})} \quad (14)$$

To compute the above plate efficiencies Equation (11) must be integrated from $N'_j = 0$ to $N'_j = N_j$.

If a system is considered in which $D_{AC} = D_{BC}$, $dN'_A = dN'_B = dN'$, Equation (11) becomes

$$d\bar{y}_j = -\phi_c(\delta_m \bar{y}_j - y^*_j) dN' \quad (15)$$

and, as the binary efficiencies of AC and BC mixtures are now the same, the integration is carried out from $N' = 0$ to $N' = N_A = N_B = N_b$. The binary efficiency is by definition the efficiency which would be measured, or predicted by standard correlations, for a binary system, in which the diffusivity is D_{AC} , operating on the same plate as the ternary system with all other physical properties, flow rates, and geometries the same as the ternary system.

Since, as far as species C is concerned, the AB mixture it is diffusing through is now a pure component, species C diffuses as if it were in a binary mixture. This means that species C will suffer no diffusional interactions and its efficiency will be equal to the binary efficiency.

CALCULATIONS OF PLATE EFFICIENCIES

Integration of Equation (15) necessitates the simultaneous integration of two nonlinear equations. Numerical integration was carried out on an IBM-650 digital computer by a modification of Newton's iteration method (1). With given values of y_{ji} and y^*_j , calculations were carried out in increments of N' from $N' = 0$ to the value

of N' corresponding to a binary plate efficiency of 99%. At each increment the multicomponent plate efficiencies were computed so that one integration yielded multicomponent efficiencies for each species in terms of the binary efficiency of the plate. The multicomponent efficiencies are shown as a function of the binary efficiency in Figure 1. The mole fractions used are also shown, and the diffusion coefficients used are given in Table 1.

As species C suffers no interaction effects, its efficiency is the same as the binary efficiency, while species A shows minor interaction effects, and species B very strong interaction effects. (The fact that E_A and E_B are both less than E_b is not significant; other types of interactions could be obtained with other plate inlet conditions.) The difference between E_A and E_B depends mainly on how the generalized driving force in Equation (15) differs from the binary driving force, and it is clear that the smaller the absolute value of the binary driving force $(\bar{y}_j - y^*_j)$ the larger will be the effect of the interaction term δ_m . Thus the difference between E_A and E_B in the calculations is caused entirely by the choice of a relatively small absolute value of $(\bar{y}_{B1} - y^*_{B1})$ and a relatively large absolute value of $(\bar{y}_{A1} - y^*_{A1})$.

Although E_A is always less than E_b , E_B is not only always much less than E_b , but it is actually negative for all plates whose binary efficiencies are less than about 60%. This negative efficiency is caused by reverse diffusion.

At a binary efficiency of 60% E_b returns to zero, and as the binary efficiency increases, the effect of the reverse diffusion gets increasingly smaller. As the binary efficiency approaches 100%, all the efficiencies also approach 100%. This is, of course, quit a general characteristic, since a plate which brings a binary system to complete equilibrium will also bring any multicomponent system to complete equilibrium.

CALCULATION OF NUMBER OF PLATES

Because the diffusional interactions depend on so many factors, a plate-to-plate calculation was carried out to examine the cumulative effects of the interactions in a column. To carry out the calculations vapor-liquid equilibrium data must be available, and the best example is an actual system. The system methanol-isopropanol-water was chosen, and the reported equilibrium data (3) were smoothed, extrapolated, and set up in analytical equations. Table 2 shows the equations used for the activity coefficients. They are only thermodynamically consistent for the

TABLE 3. DESIGN CONDITIONS

Reflux ratio = 5	Total condenser		
Pressure = 1 atm.	Single feed, distillate and bottoms streams		
Saturated liquid feed			
	Methanol,	Isopropanol,	Water,
	%	%	%
Feed composition	40	20	40
Desired distillate	98		
Desired bottoms	5		

binary pairs, since the available data as well as the requirements of this study do not justify further refinements.

The diffusivities for this system were calculated by Gilliland's method (5) and are given in Table 2 at an average temperature for the system. In the following work *A* refers to methanol, *B* refers to isopropanol, and *C* refers to water. The actual diffusivities used in the calculations below were not taken from Table 2 but rather from Table 1. (The values of D_{AC} and D_{BC} in Table 1 are the arithmetic average of D_{AC} and D_{BC} in Table 2.) This simplification means that a column design will be carried out for a hypothetical system which has the same equilibrium char-

acteristics as methanol-isopropanol-water but has $D_{AC} = D_{BC}$. This procedure, while simplifying the problem, retains its essential characteristics. The design conditions used are given in Table 3.

Plate-to-plate calculations were first carried out in the ordinary manner (4) with 100% efficiency assumed on each plate for all components. The usual operating lines and over-all balances hold (4) and constant molal overflow

was assumed. Terminal compositions were assumed, and calculations were carried out on the computer. The feed-plate location was obtained by trial and error so as to minimize the total number of plates after first matching the ratio of the liquid mole fractions of the key components on the plate to the ratio in the feed. An iteration procedure was used to obtain the terminal compositions, which are given in Table 4. Figure 2 shows the variation of liquid composition throughout the column. Thirty-five ideal plates are required, with the feed on the twenty-fifth plate.

Since the single-plate calculations indicated that interaction effects were most pronounced at a binary efficiency of 40%, this value was chosen for the column calculations to maximize these effects. Thus it was assumed that every plate in the column had a binary efficiency of 40%.

Two methods of calculating real plates were used. In the first method it was assumed that all the diffusional interactions were negligible, $\delta_m = \phi_c = 1.0$, so that all the individual ternary efficiencies were 40%. The vapor leaving a plate was then not the vapor in equilibrium with the liquid but the value given by Equation (13) with $E_i = 40\%$. The results of this calculation are given by the dotted line in Figure 3 and in Table 4. Terminal compositions were essentially the same as in the ideal-plate calculation. Eighty-four plates are required with the feed on the fifty-ninth plate. If the over-all column efficiency is taken as 40%, then the ideal-plate calculations yield eighty eight real plates with the feed on the sixty third plate.

equilibrium data yielded y^* . Equation (15) was then numerically integrated from $N' = 0$ to the value of N' corresponding to $E_b = 0.40$ to give the vapor composition leaving the plate. These calculations were repeated on each plate until the feed plate, at which point the upper operating line replaced the lower and calculations were continued until the desired methanol concentration in the distillate was obtained.

Figure 3 shows the resulting liquid compositions in the column, and Figure 4 gives the efficiencies on each plate. As before, the efficiency of component *C* is equal to the binary value. The efficiency of component *A* first

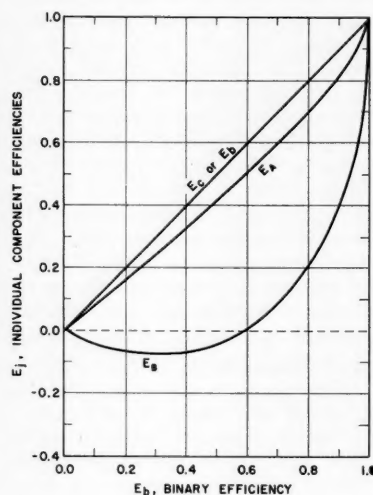


Fig. 1. Variation of efficiencies: $y_{AI} = 0.1$, $y^*_{AI} = 0.474$, $y_{BI} = 0.3$, $y^*_{BI} = 0.252$.

acteristics as methanol-isopropanol-water but has $D_{AC} = D_{BC}$. This procedure, while simplifying the problem, retains its essential characteristics. The design conditions used are given in Table 3.

Plate-to-plate calculations were first carried out in the ordinary manner (4) with 100% efficiency assumed on each plate for all components. The usual operating lines and over-all balances hold (4) and constant molal overflow

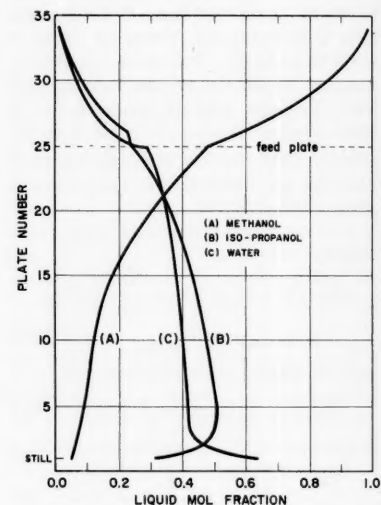


Fig. 2. Concentration profiles, ideal-plate column.

drops slightly and then remains fairly constant at 28%, except for the slight discontinuity at the feed plate. The efficiency of component *B* jumps sharply to above 100% on the sixth plate, then drops to a negative 44% on the seventh plate before leveling off at 24%. This wild fluctuation has little effect on the total number of plates and is due to the sensitivity to composition of component *B*'s very small generalized driving force. Thus component *B*'s average efficiency throughout the column is 40% lower than the binary efficiency, while component *A*'s average efficiency is 30% lower. The total number of plates needed to effect the separation is 117, equivalent to an over-all column efficiency of 30%. Thirty-three more plates are needed than would be required if all individual efficiencies were 40% and so the diffusional interactions can be said to have required an increase of 39% in the number of

TABLE 4. RESULTS OF DESIGN CALCULATIONS

Type of calculation	Total plates	Plate	Feed-plate location, Dis- tance up column, %	Over- all efficiency	Liquid terminal compositions					
					X_A	X_B	X_C	X_A	X_B	X_C
Ideal	35	25	71	100	0.050	0.315	0.635	0.976	0.012	0.012
Over-all 40%	88	63	72	40						
Each component 40%	84	59	70	42	0.050	0.315	0.636	0.981	0.0094	0.0094
Calculated with interactions	117	82	70	30	0.050	0.309	0.641	0.982	0.012	0.006
Over-all 30%	117	83	71	30						

plates.

Since the individual efficiencies are roughly constant throughout the column, the relative feed-plate location is about the same for all methods of calculation, roughly 70% of the distance up the column. The results of the various calculations are given in Table 4.

As the individual efficiencies are relatively constant with position, the concentration profiles within the column are not greatly different for the three cases considered, Figures 2 and 3, although they would have been significantly different if the number of plates had been taken as equal in all examples.

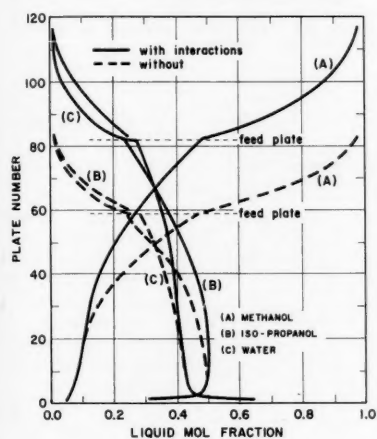


Fig. 3. Concentration profiles, column-design comparison.

It is clear that a column design which is carried out with all the individual column average efficiencies different from each other, as in the last calculation, will not yield the same terminal concentrations as a column designed with all the average efficiencies equal to each other, even though the terminal key component concentrations are equal in both designs. Thus in Table 4 the terminal compositions for the calculations with interactions differ from the results obtained when interactions were neglected. These differences could have been much larger if the terminal compositions had been chosen to be less pure. (The terminal compositions reported for the interaction case are not very accurate, since the iteration procedure used to calculate terminal compositions did not converge rapidly. Calculations were stopped before convergence, since the error had negligible effect on the other results and it was clear that the terminal compositions would not be the same as in the earlier calculations.)

In this example neglect of diffusional interactions in the design of a column would clearly lead to an underdesigned column (as compared to a design which included diffusional interactions). The rather surprising result is not that the over-all interactions were significant but rather that they were not larger, for a number of the conditions were chosen to emphasize the interaction effects. However it is not unlikely that in other systems or under other conditions the interactions may cause much more radical changes from ideal behavior than found here. If for example the wild fluctuation of the *B* efficiency persisted over a larger number of plates, and if a product of lower purity had been specified, then a product distribution very different from that predicted by an ideal-plate calculation could be obtained.

The above results are quite limited, and it is clear that there is a need for experimental work on multicomponent systems, especially in systems, where diffusion theory predicts strong interactions. For the time being a determination of the uncertainty in the extrapolation of binary correlations might be obtained by comparison of a system of interest with that studied here, with the results of the following section used.

GENERALIZATIONS

Unless stated otherwise the following comments would be expected to apply to any multicomponent system.

1. Highly efficient plates, that is plates which give high efficiencies for all the binary pairs, will tend to yield multicomponent efficiencies equal to each other and equal to the binary efficiencies.

2. As the fraction of the total transfer resistance in the liquid phase increases, the differences among the multicomponent efficiencies and between each multicomponent efficiency and the binary efficiency should generally tend to diminish.

3. If molecular diffusion in the gas phase plays a significant part in the transfer process, then the efficiency will in general be different for each component, and the differences among these efficiencies will increase as the differences between the diffusion coefficients of the binary pairs increase. If all the diffusion coefficients are equal, there will be no gas-side interactions (if, as is usual, equimolar countercurrent transfer takes place), and if there are also no liquid-side interactions, all the efficiencies will be equal to the binary efficiency.

4. In a ternary system where there are two similar species, and one dissimilar one, the dissimilar one will

have an efficiency close to the binary value, and the efficiencies of the similar species will differ from each other and from the binary value. The restrictions in (3) above apply here also.

5. If one species in a ternary system is dilute in both the gas and liquid, its efficiency may differ from the binary value, but the efficiencies of the other two species would be expected to approach the binary efficiency. This can be extended to a four component system where two species are dilute, a five component where three are dilute, etc.

6. Diffusional interactions depend strongly on composition of the terminal points of the diffusion path. A

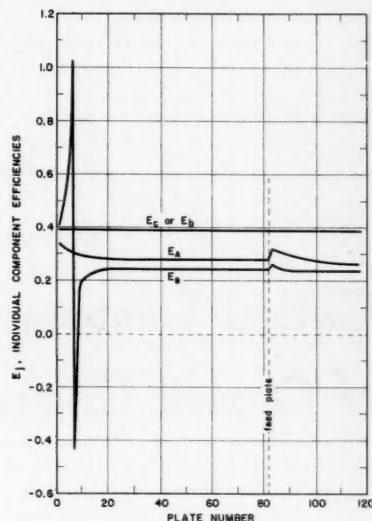


Fig. 4. Variation of efficiencies in column.

quick check of the possible magnitude of the interactions in a ternary system can be obtained by taking a few representative points in a column designed without inclusion of interactions and evaluating the ratio of the fluxes with and without interactions [Equations (1) and (7)]:

$$R = \phi_c \left[\frac{\delta_m \bar{y}_j - y_j^0}{\bar{y}_j - y_j^0} \right] \quad (16)$$

If this ratio is close to 1, it is probable that the interactions are small and that the binary correlations can be used with some confidence. If the ratio differs significantly from 1, the correlations should be used with trepidation.

ACKNOWLEDGMENT

The authors wish to acknowledge with thanks the assistance of L. N. Canjar in the calculation of the equilibrium data and the Standard Oil (Indiana) Foundation for fellowship assistance to J. K. Burchard.

NOTATION

D	= binary diffusion coefficient, sq.ft./hr.
E	= plate efficiency
k	= gas-side mass transfer coefficient, lb.moles/(hr.)(sq.ft.) (mole fraction)
m	= moles of vapor in bubble, lb. moles
n	= flux, lb.moles/(hr.)(sq.ft.)
N	= number of transfer units
R	= ratio of fluxes with and without interactions
S	= area, sq.ft.
x	= effective film thickness, ft.
X_i, X_e	= mole fraction in liquid
y	= mole fraction in gas

Greek Letters

γ	= activity coefficient
δ_m	= diffusional interaction term

θ	= time, hr.
ρ	= molar density, lb.moles/cu.ft.
ϕ_o	= diffusional interaction term defined by Equation (5)

Subscripts

A, B, C	= species A, B, and C, respectively
b	= binary value
i	= interface
j	= index which refers to species A or B
1, 2	= terminal points of diffusion path
I, II	= entering and leaving plate, respectively

Superscripts

o	= equilibrium value
$—$	= bulk mean value
$'$	= values at any vertical position on plate

tion on plate

LITERATURE CITED

1. Burchard, J. K., M. S. thesis, Carnegie Inst. of Technol., Pittsburgh, Pennsylvania (1958).
2. Final Report, A.I.Ch.E. Research Program on Distillation, New York (1958).
3. Dunlop, J. G., M. S. thesis, Brooklyn Polytech. Inst., New York (1948).
4. Robinson, C. S., and E. R. Gilliland, "Elements of Fractional Distillation," McGraw-Hill, New York (1950).
5. Sherwood, T. K., and R. L. Pigford, "Absorption and Extraction," McGraw-Hill, New York (1952).
6. Toor, H. L., A.I.Ch.E. Journal, 3, 198 (1957).
7. ———, and R. T. Sebulsky, *ibid.*, to be published.

Manuscript received June 17, 1959; revision received September 9, 1959; paper accepted September 14, 1959. Paper presented at A.I.Ch.E. San Francisco meeting.

Critical Temperatures and Pressures of Organic Compounds

J. Charles Forman and George Thodos

The Technological Institute, Northwestern University, Evanston, Illinois

The approach presented for the prediction of critical temperatures and pressures for hydrocarbons from the van der Waals' constants a and b (1) has been extended to permit the estimation of these constants for other organic compounds. Analogously, contribution values for a number of functional groups have been established, and the majority were found to depend on the size of the organic molecule. Information presently available in the literature (4) has permitted the establishment of values for functional groups in organic compounds of the following types: alcohols, phenols, ethers, ketones, carboxylic acids and esters, amines, nitriles, and halides. These functional group contributions, in conjunction with the values previously developed for the hydrocarbons, now make possible the calculation of both van der Waals' constants from only structural considerations. Once these van der Waals' constants have been established, the critical temperature and pressure are readily calculated.

With the approach developed in this investigation critical temperatures and pressures for eighty-one organic compounds have been calculated and when compared with literature values produced average absolute deviations of 1.36% for the critical temperature and 2.82% for the critical pressure.

The use of van der Waals' constants has been presented at length for the calculation of the critical temperatures and pressures of hydrocarbons (1, 5, 6, 7, 8). The most recent investigation (1) is concerned with the establishment of the van der Waals' constants a and b for hydrocarbons of all classes. These earlier studies permit the calculation of these constants from structural considerations alone, without the necessity

of utilizing any physical properties. The original work (5, 6, 7, 8) involves the successive building up of the molecular structure through the replacement of hydrogen by methyl groups along a definite prescribed pattern of substitution. The dependence upon a definite substitution pattern was later eliminated (1) through the introduction of structural group contributions, which when added together in any manner produced the van der Waals' constants directly. The latter approach has been

selected for the extension of this method beyond the hydrocarbons to include organic compounds of other classes.

For a pure substance the critical temperature and pressure are related to the van der Waals' constants a and b by the relationships

$$T_c = \frac{8a}{27Rb} \quad (1)$$

$$p_c = \frac{a}{27b^2} \quad (2)$$

Conversely Equations (1) and (2) enable the calculation of the van der Waals' constants from available critical temperatures and pressures:

$$a = \frac{27R^2T_c^2}{64p_c} \quad (3)$$

$$b = \frac{RT_c}{8p_c} \quad (4)$$

Critical values found in the litera-

J. Charles Forman is now with Abbott Laboratories, North Chicago, Illinois.

TABLE I. CONSTANTS FOR EQUATIONS WHICH ESTABLISH
FUNCTIONAL GROUP CONTRIBUTIONS FOR ORGANIC COMPOUNDS

Functional group	$\Delta a^{2/3} = \frac{m}{n} + k$		$\Delta b^{3/4} = \frac{s}{n} + t$	
	<i>m</i>	<i>k</i>	<i>s</i>	<i>t</i>
Alcohols —OH	30,200	14,000	8.96	7.50
Phenols —OH	0	8,500	0	4.19
Ethers (noncyclic) —O—	14,500	6,500	0	3.26
Ethers (cyclic) —O—	0	9,440	0	2.74
Ketones $\begin{array}{c} \text{O} \\ \parallel \\ \text{—C—} \end{array}$	62,800	16,700	27.20	4.55
Carboxylic acids $\begin{array}{c} \text{O} \\ \parallel \\ \text{—COH} \end{array}$	142,670	16,730	66.80	5.10
Acid anhydrides $\begin{array}{c} \text{O} \quad \text{O} \\ \parallel \quad \parallel \\ \text{—C—O—C—} \end{array}$	0	43,880	0	14.78
Esters $\begin{array}{c} \text{O} \\ \parallel \\ \text{—CO—} \end{array}$	35,140	26,800	2.29	15.80
Formates $\begin{array}{c} \text{O} \\ \parallel \\ \text{HCO—} \end{array}$	37,430	25,500	—3.00	12.20
Others $\begin{array}{c} \text{O} \\ \parallel \\ \text{—CO—} \end{array}$	4,800	18,900	0	10.15
Amines —NH ₂	51,800	0	19.60	—1.10
Primary $\begin{array}{c} \text{H} \\ \\ \text{—N—} \end{array}$	60,200	—4,300	29.20	—7.90
Secondary $\begin{array}{c} \text{H} \\ \\ \text{—N—} \end{array}$	86,000	25,900	39.70	12.10
Tertiary $\begin{array}{c} \text{H} \\ \\ \text{—N—} \end{array}$				
Nitriles —CN				
Aliphatic halides				
Fluorides —F				
First carbon	2,420	12,240	—3.70	10.92
Second carbon	—38,500	4,510	—48.50	12.86
Third carbon	0	3,450	0	6.92
Chlorides —Cl				
First carbon	0	22,580	0	11.54
Second carbon	66,000	—5,100	19.00	3.90
Third carbon	—60,250	29,100	—40.80	19.40
Fourth carbon	0	16,500	0	11.46
Bromides —Br				
First carbon	—2,720	23,550	—4.35	11.49
Second carbon	0	20,860	0	5.37
Iodides —I				
First carbon	0	33,590	0	13.91
Aromatic halides				
Fluoride —F	0	4,210	0	7.22
Chloride —Cl	0	17,200	0	10.88
Bromide —Br	0	24,150	0	12.74
Iodide —I	0	34,780	0	15.22

2. Values are defined for the entire functional group in an organic compound. Thus the functional group contributions $\Delta a^{2/3}$ and $\Delta b^{3/4}$ for the carboxylic-acid group represent the entire carboxylic portion of an acid molecule.

With these rules the results can be expressed in equations which produce the functional group contributions $\Delta a^{2/3}$ and $\Delta b^{3/4}$. These equations are of the basic form

$$\Delta a^{2/3} = \frac{m}{n} + k \quad (5)$$

$$\Delta b^{3/4} = \frac{s}{n} + t \quad (6)$$

The values of the constants for Equations (5) and (6) are summarized in Table I for the different types of organic compounds considered in this investigation.

The method of developing these constants for each class of organic compounds is discussed in the subsequent sections followed by illustrative examples.

ALCOHOLS

Critical temperatures and pressures for five primary alcohols permitted establishment of the functional group contributions, $\Delta a^{2/3}$ and $\Delta b^{3/4}$ for the hydroxyl group in alcohols. These values were obtained by subtracting from the values of $a^{2/3}$ and $b^{3/4}$ for the substance, the contributions for that portion not representing the functional group. This portion contains only carbon and hydrogen atoms and is accounted for by the method already presented by Forman and Thodos (1). For example the ethanol molecule contains two carbon atoms and one oxygen atom; thus $n = 3$. Of the two carbon atoms one is type-1, and the other is type-2. Subtracting these values from the values of $a^{2/3}$ and $b^{3/4}$ for ethanol one gets values of $\Delta a^{2/3}$ and $\Delta b^{3/4}$ for the hydroxyl functional group in this compound. This procedure was carried out for each alcohol for which experimental values of both critical temperature and pressure were available.

These contributions were found to vary with the size of the molecule in accordance with Equations (5) and (6).

Constants for the alcohol contributions were developed from data on primary alcohols. Since no reliable critical data are available for secondary and tertiary alcohols, this study cannot be reliably extended to these classes of compounds. With this limitation Equations (5) and (6) may be used until data become available to check their validity.

ture (4) permitted the calculation of van der Waals' constants for a number of classes of organic compounds and constitute the basis for the development of the group-contribution values of this study. When determined by the methods discussed below group-contribution values $\Delta a^{2/3}$ and $\Delta b^{3/4}$ for various types of organic functional groups can be combined with the values for the rest of the organic molecule in any manner desired to give the van der Waals' constants a and b .

To maintain consistency with the work upon which this study is based, the exponents of the van der Waals' constants a and b were assumed to be $2/3$ and $3/4$ respectively. For the reasons underlying the use of these exponents, reference should be made to the parent article (1).

GENERAL CONSIDERATIONS

In the original article (1) group contributions were developed for the various types of carbon atoms present in hydrocarbons of all classes. These group contributions were found to be either independent of the size of the molecule or to vary linearly with the inverse number of carbon atoms. The same procedure was extended to this study and was found to correlate group contributions successfully for various types of organic compounds if the following two rules are adopted:

1. The total number of functional atoms is used to represent the size of an organic molecule. In this investigation a functional atom is defined as any atom present in the substance, excluding hydrogen. Thus in methanol $n = 2$, and in acetic acid $n = 4$.

TABLE 2. DEVIATIONS RESULTING FROM THIS STUDY AND THAT OF LYDERSEN

	This investigation				Lydersen			
	No.	T_c % Dev.	No.	p_c % Dev.	No.	T_c % Dev.	No.	p_c % Dev.
Alcohols	7	1.74	5	4.50	7	1.07	5	3.67
Phenols	4	1.55	4	5.28	4	0.60	4	3.32
Ethers	5	0.84	5	1.48	5	0.41	5	2.69
Ketones	6	0.51	6	2.87	6	0.91	6	4.61
Carboxylic acids	6	1.04	2	1.30	6	0.88	2	7.16
Esters	10	0.85	10	1.76	10	0.58	10	3.81
Amines								
Primary	4	2.01	4	2.98	4	0.80	4	2.92
Secondary	4	2.64	4	6.78	4	0.62	4	7.26
Tertiary	3	2.91	3	1.45	3	0.51	3	4.14
Nitriles	5	0.84	5	2.68	5	0.73	5	3.87
Halides								
Fluorides	5	0.01	5	0.00	5	2.02	5	7.50
Chlorides	8	2.22	8	2.32	8	0.34	8	2.71
Bromides	4	0.00	3	0.00	4	1.72	3	6.45
Iodides	2	0.00	1	0.00	2	0.14	1	4.26
Fluorochloroalkanes	8	2.53	7	5.64	8	0.71	7	5.06
Total	81	1.36	72	2.82	81	0.80	72	4.39

PHENOLS

Group contributions for the phenolic hydroxyl group were obtained from data for phenol and the three isomeric cresols. These contributions were found to be constant at $\Delta a^{2/3} = 8,530$ and $\Delta b^{3/4} = 4.19$.

ETHERS

In the same manner as described above, data for four noncyclic ethers permitted establishment of functional group contributions for the oxygen group in noncyclic ethers.

Values of critical temperature and pressure for dioxane made possible the calculation of group contributions for the ether linkage in cyclic ethers. These values are $\Delta a^{2/3} = 9,440$ and $\Delta b^{3/4} = 2.74$. It should be noted that these values resulted from critical data on a single substance and therefore do not have the confidence factor possessed by the others. Additional experimental data are needed to corroborate these values.

KETONES

Functional group contributions for the carbonyl group in ketones were similarly obtained. More recent experimental data on several aliphatic ketones reported by Kobe, Crawford, and Stephenson (3) were included to obtain these contributions.

CARBOXYLIC ACIDS

An identical procedure was followed to produce group contributions for the carboxylic group in organic acids.

In addition, critical data for acetic anhydride permitted the calculation of the functional group contributions for

the acid anhydride group, $\begin{array}{c} \text{O} \quad \text{O} \\ \parallel \quad \parallel \\ -\text{C}-\text{O}-\text{C}- \end{array}$. These were $\Delta a^{2/3} = 43,880$ and $\Delta b^{3/4} = 14.78$. Since these anhydride contribution values were obtained from a single substance, the same conservatism exists as pointed out for the cyclic ethers.

CARBOXYLIC ACID ESTERS

Critical data on four formates, three acetates, and three butyrates permitted establishment of group contribution values for the ester group. On correlation of the data, the formates were found to deviate from the other esters and were treated separately. This is a logical classification, since only formate

esters contain the group $\begin{array}{c} \text{O} \\ \parallel \\ \text{HCO}- \end{array}$, whereas other esters have hydrocarbon portions attached to both sides of the ester group, $\begin{array}{c} \text{O} \\ \parallel \\ -\text{CO}- \end{array}$.

NITROGEN COMPOUNDS

Data from Kobe and Lynn (4) permitted the establishment of contributions for functional groups in amines and nitriles. For these classes of substances critical data were available for aromatic as well as aliphatic compounds. Analysis of these data showed that it made no difference whether the functional group was attached to an aliphatic or an aromatic hydrocarbon segment.

ORGANIC HALIDES

The method which successfully treated the classes of compounds already considered was found to apply

to halides as long as only one halogen atom is attached to a carbon atom in the molecule. A complication arises with halides, since it is possible to substitute more than one halogen atom on a single carbon atom. This behavior is not ordinarily encountered with other noncarbon-containing functional groups. Thus only one hydroxyl group can be attached to a single carbon atom to produce an alcohol. An attempt to attach two hydroxyl groups to the same carbon atom will cause dehydration with the formation of a ketone. However since multisubstituted behavior does exist with halides, it was found that the second and further halogen attachments required an extension of the method which could take into account not only the size of the molecule but also the extent of substitution. An additional factor to be considered is the existence of mixed halides such as the Freons, which contain more than one type of halogen atom on the same carbon atom. Thus when more than one halogen exists on a single carbon atom, not only must the group contributions for succeeding halogen substitutions be considered differently, but also their order of introduction onto the carbon atom must be recognized.

The method which was adopted considers different group contributions for the first and succeeding halogen substitutions on a single carbon atom. Sufficient data were available to establish contributions for the first, second, and third fluoride per carbon and the first, second, third, and fourth chloride per carbon. Inadequate information exists for bromides and iodides; both critical temperatures and pressures were available for two aliphatic bromides and no aliphatic iodides. However only critical temperatures were available for methyl bromide and methyl iodide. To utilize this information, critical pressures were calculated by the method of Lydersen (2). With these values approximate group contributions were obtained for the first and second bromide per carbon and for the first iodide per carbon.

For mixed halides the contributions must be used in order of increasing atomic number. Thus when both fluorine and chlorine are attached to a single carbon atom, the fluoride contributions should be considered first, followed by chloride contributions after all fluorides have been accounted for. For example in a compound containing one fluorine and one chlorine atom on the same carbon a first fluoride contribution is considered first, followed by a second chloride contribution. The procedure to be followed is presented later in an illustrative example.

Critical data for fluoro-, chloro-, bromo-, and iodobenzene permitted

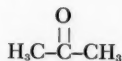
calculation of functional group contributions, $\Delta a^{2/3}$ and $\Delta b^{3/4}$ for halide substitutions in aromatic compounds. The resulting values were found not to correlate with the first halogen per carbon contributions in aliphatic halides. This is not unexpected, since as with other types of functional groups only one halogen atom can be attached to a single carbon atom in the aromatic nucleus.

ILLUSTRATIVE EXAMPLES

To illustrate the procedure used in obtaining van der Waals' constants a and b by the method of this investigation the critical temperature and pressure will be calculated for two organic compounds. The first one, acetone, is a ketone and is representative of all classes of compounds except the aliphatic halides. The compound trifluorotrichloroethane represents a typical halogen compound and in addition is a mixed organic halide.

Acetone

Structure:



This ketone contains two type-1 (methyl group) carbons (1), and one

carbonyl ($-\text{C}-$) functional group. The number of functional atoms is 4. From the group contributions presented in Table 1 of the parent article (1) and calculated by means of Table 1 of this study, $a^{2/3}$ and $b^{3/4}$ are calculated as follows:

2 carbon atoms (type-1)
1 carbonyl group

2(15,035) 2(11,453)
32,400 11.35

$a^{2/3} = 62,470$ $b^{3/4} = 34.256$

From these values the following calculated van der Waals' constants are produced:

$$a = 15.614 \times 10^6 \text{ (cc./g.-mole)}^2 \text{ atm.}$$

$$b = 111.26 \text{ cc./g.-mole}$$

to give the following values of critical temperature and pressure from Equations (1) and (2):

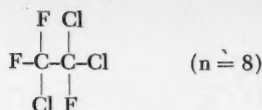
$$T_c = \frac{8(15.614 \times 10^6)}{27(82.055)(111.26)} = 506.8^\circ\text{K.}$$

$$p_c = \frac{15.614 \times 10^6}{27(111.26)^2} = 46.7 \text{ atm.}$$

Kobe and Lynn (4) report values of 508.7°K. and 46.6 atm. for acetone.

Trifluorotrichloroethane (Freon-113)

Structure:



In this compound there are two type-4 carbon atoms, two first fluorides (one per carbon), one second fluoride (on left-hand carbon), one second chloride (on right-hand carbon) and two third chlorides (one per carbon).

These contributions, when added together, produce values for $a^{2/3}$ and $b^{3/4}$ as follows:

Two type-4 carbons
Two first fluorides
One second fluoride
One second chloride
Two third chlorides

2(3480) 2(-8.837)
2(12,550) 2(10.46)
-300 6.80
3150 6.28
2(21,570) 2(14.30)

$a^{2/3} = 78,050$ $b^{3/4} = 44.926$

These values produce the following van der Waals' constants

$$a = 21.801 \times 10^6 \text{ (cc./g.-mole)}^2 \text{ atm.}$$

$$b = 159.71 \text{ cc./g.-mole}$$

and the critical temperature and pressure from Equations (1) and (2) become

$$T_c = \frac{8(21.801 \times 10^6)}{27(82.055)(159.71)} = 492.9^\circ\text{K.}$$

$$p_c = \frac{21.801 \times 10^6}{27(159.71)^2} = 31.7 \text{ atm.}$$

Critical values of 487.3°K. and 33.7 atm. are reported by Kobe and Lynn (4).

DISCUSSION

Critical temperatures and pressures were calculated for the eighty-one organic compounds of different classes available in the literature. Critical constants were also calculated for the same compounds by the method of Lydersen (2). The resulting deviations from comparison of calculated and experimental values by both methods are presented in Table 2. Of the eighty-one compounds examined, critical pressures were available for only seventy-five of them. In addition, excessive deviations were encountered for the critical pres-

ures of two acids and one fluorochloroalkane. For the two acids, similarly large deviations were found for the critical pressures resulting from the Lydersen method. Since these substances do not conform to the normal pattern, they were eliminated in the calculation of average deviations.

It will be noted from Table 2 that the Lydersen method produces somewhat better values for the critical temperature, whereas the method of this study predicts better critical pressures.

That the Lydersen method gives better critical temperatures is to be expected, since that method utilizes a physical property, the normal boiling point, in the calculation of the critical temperature. The method proposed by this investigation is independent in that no physical properties are required, and thus critical values can be calculated from structural considerations alone.

NOTATION

- a = pressure van der Waals' constant, (cc./g.-mole)² atm.
- b = volume van der Waals' constant, cc./g.-mole
- k = constant in Equation (5)
- m = constant in Equation (5)
- n = total number of functional atoms in organic compound
- p_c = critical pressure, atm.
- R = gas constant, 82.055 (atm.) (cc.)/(g.-mole) (°K.)
- s = constant in Equation (6)
- t = constant in Equation (6)
- T_c = critical temperature, °K.
- Δ = difference

LITERATURE CITED

1. Forman, J. C., and George Thodos, *A.I.Ch.E. Journal*, **4**, 356 (1958).
2. Hougen, O. A., K. M. Watson, and R. A. Ragatz, "Chemical Process Principles," p. 87, Wiley, New York (1954).
3. Kobe, K. A., H. R. Crawford, and R. W. Stephenson, *Ind. Eng. Chem.*, **47**, 1767 (1955).
4. ———, and R. E. Lynn, Jr., *Chem. Rev.*, **52**, 117 (1953).
5. Thodos, George, *A.I.Ch.E. Journal*, **1**, 165 (1955).
6. *Ibid.*, **1**, 168 (1955).
7. *Ibid.*, **2**, 508 (1956).
8. *Ibid.*, **3**, 428 (1957).

Manuscript received June 30, 1959; revision received August 31, 1959; paper accepted September 2, 1959.

Correlating Vapor Pressures and Heats of Solution for the Ammonium Nitrate—Water System:

An Enthalpy-Concentration Diagram

DONALD F. OTHMER and GERHARD J. FROHLICH

Polytechnic Institute of Brooklyn, Brooklyn, New York

The usual tedious method of construction of enthalpy-concentration charts for solutions of solids requires data seldom available. A new, simple method is therefore presented that utilizes more readily available data, that is vapor pressures of the solutions. These plot as straight lines on a logarithmic-reference substance plot. Differences from unity of the slopes of these lines represent heats of solution, and when this difference function is integrated between concentration limits the integral heat of solution is obtained. The enthalpy chart is then readily constructed by use of the specific heats of liquid and solid.

Ammonium nitrate is the solid used in this example, and water is the liquid because of the industrial importance of aqueous solutions. Vapor pressures were carefully determined experimentally, and the enthalpy chart was developed from the straight lines of the logarithmic plot and available heat data. Constants for the vapor-pressure curves for ammonium nitrate solutions and equations for enthalpies of solid ammonium nitrate are given for the temperature range 0° to 170°C.

With production of almost 3,000,000 tons/yr. in the United States, ammonium nitrate is of outstanding importance as a nitrogen fertilizer, more recently as an explosive, and in other major uses. Properties of the ammonium nitrate—water system are very important in the design of equipment to produce and use ammonium nitrate.

While more complex systems involving ammonium nitrate were being studied (4), pressures were measured above aqueous ammonium nitrate solutions; these were correlated with available vapor-pressure data as the logarithms of the vapor pressures vs. the vapor pressures of water at the same temperatures as previously described (11). From the slope of the lines of constant concentration, differential heats of dilution were calculated, and these were used together with integral heats of solution and heat capacity from the literature to construct an enthalpy-concentration diagram, as described by Othmer, Kowalski, and Napthali (12).

EXPERIMENTAL DETERMINATION OF VAPOR-PRESSURE DATA

Two ebulliometers, one containing the ammonium nitrate solution and the other pure water, were connected in parallel to a pressure system. The boiling-point difference was measured directly, and the temperature of the water was determined from the pres-

sure of the system. Pressure readings were accurate to ± 0.1 mm. Hg and temperature readings to $\pm 0.05^\circ\text{C}$. Below 50°C . and above 65 wt.% ammonium nitrate excessive bumping of the liquid made measurements unreliable. The experimental data are shown in Table I and plotted in Figure 1 according to the method previously described (11), no point deviating by more than 1% from the line representing all the points.

DISCUSSION OF VAPOR-PRESSURE DATA

After completion of these determinations Campbell *et al.* (1) published similar vapor pressures determined by

a static method. The experimental data and those of the literature (1, 3, 8) correlate well on the logarithmic-reference substance plot. The basic equation when vapor pressure of the solution is always taken at the same temperature as vapor pressure of water is

$$\log P = m \log P^\circ + C \quad (1)$$

where $m = L_B/L^\circ$.

Slopes and intercepts of the straight lines were plotted vs. concentration in Figure 2. Slopes derived from vapor-pressure data were calculated by statistical means (16), slopes have also been calculated from heats of dilution data (2, 10).

The slopes from the experimental

TABLE I. EXPERIMENTAL PARTIAL PRESSURE OF WATER ABOVE AMMONIUM NITRATE SOLUTIONS

20.6		40.1		46.6		60.3	
t, °C.	P _{H₂O} , mm. Hg	t, °C.	P _{H₂O} , mm. Hg	t, °C.	P _{H₂O} , mm. Hg	t, °C.	P _{H₂O} , mm. Hg
61.8	147.0	61.6	128.0	51.4	77.4	55.5	84.6
76.3	280.3	80.1	282.9	61.0	120.6	61.1	105.0
87.6	456.8	83.7	316.3	69.9	182.4	69.5	147.1
101.9	750.3	92.6	464.4	85.4	341.2	80.8	237.0
		94.6	479.9	97.5	520.3	85.1	278.5
		98.9	567.5	98.9	540.6	93.3	378.6
		99.4	578.8	103.9	647.6	98.9	461.3
		99.7	584.4	106.4	742.9	99.3	485.3
		102.1	634.7			104.9	593.2
		105.6	751.4			106.5	632.6
		105.8	727.9			113.1	749.1
		106.6	743.1				

Gerhard J. Frohlich is with St. Paul Ammonia Products, Inc., St. Paul, Minnesota.

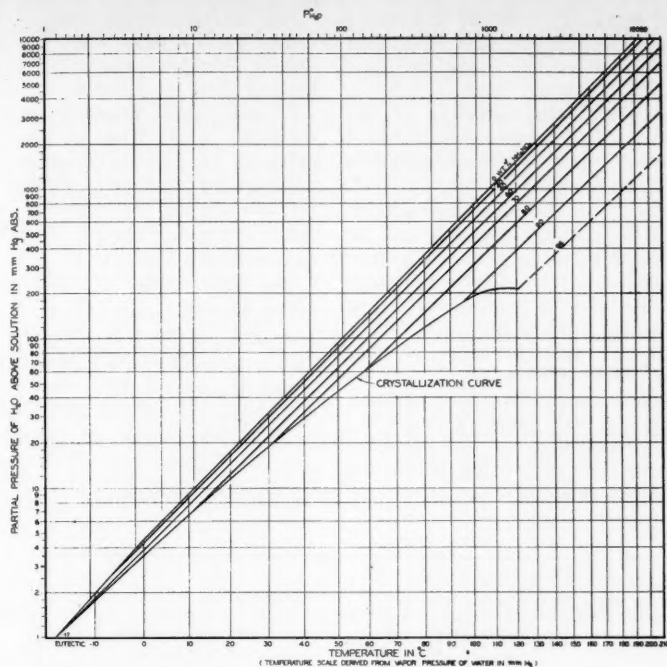


Fig. 1. Equilibrium vapor pressure of water above ammonium-nitrate solutions of constant concentration as a function of temperature.

data and those from Campbell *et al.* (1) for the high concentration range are within the confidence range of those calculated from heat of dilution data. Slopes from the Campbell *et al.* data for the lower concentration range are not consistent with those for high concentrations, nor with those presently found. They are disregarded in plotting the smooth curve of Figure 2a representing the slopes of the lines of constant composition of the best data as determined by the three indicated methods.

Constant C of Equation (1) was calculated for each concentration with mean values of the experimental data and the slope from Figure 2a. Data of Campbell *et al.* were used to establish C at 70, 80, and 90 wt.% ammonium nitrate. A smooth curve was drawn through the plotted points in Figure 2b.

Gerlach (5, 8, 9) gives the boiling points at 760 mm. also for 95 and 96 wt.% ammonium nitrate solutions. These may be used to estimate the pressures above the solution at concentrations higher than 90 wt.% by extrapolating the slope m in Figure 2a to the respective composition and then calculating C from Equation (1) to extend the correlation of Figure 2b. Equation (1) can then be used to calculate partial pressures at other conditions, also above 90 wt.% ammonium

nitrate. However further experimental verification of the pressures for solutions higher than 90 wt.% ammonium nitrate would be desirable. Table 2 summarizes the results.

The lines of Figure 1 correlate the experimental data, according to the vapor-pressure equations given in Table 2, on a temperature scale derived from the vapor pressure of pure water. At lower temperatures the lines intersect the liquid-solid saturation line, which was derived from data taken from D'Ans-Lax (2). Vapor pressures along this crystallization curve determine the operating conditions for vacuum and air-stripping crystallizers for ammonium nitrate; also they define humidity conditions under which solid ammonium nitrate will absorb moisture from the air.

CONSTRUCTION OF THE ENTHALPY-CONCENTRATION DIAGRAM

The enthalpy of a solution above a fixed datum temperature for two pure components mixed together is

$$H_s = x_A H_A + x_B H_B - x_A q \quad (2)$$

where the integral heat of solution q

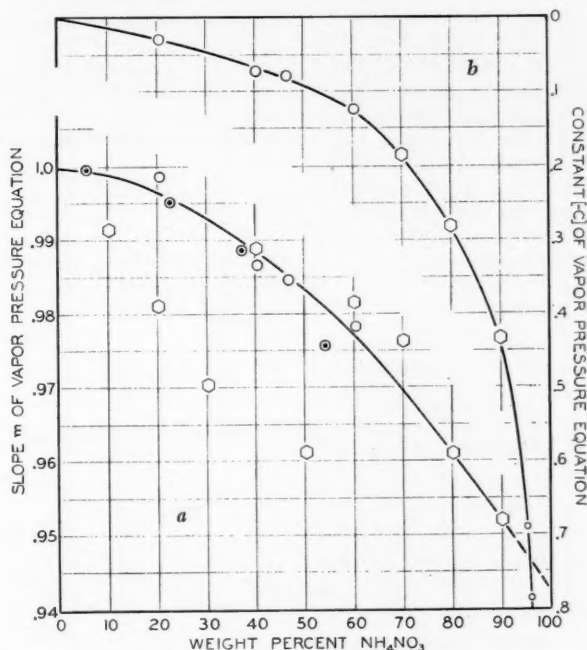


Fig. 2. The upper curve represents the intercept C of the vapor pressure Equation (1) as a function of the ammonium nitrate concentration. These values from Table 2 are all less than zero and hence are negative. The lower curve refers to the slope m of the vapor pressure Equation (1) as a function of the ammonium nitrate concentration. \circ This investigation, \odot Campbell *et al.* (1), \otimes Calculated from heats of dilution (2, 10), \circ Gerlach (5, 8, 9).

TABLE 2. PARTIAL PRESSURE OF WATER ABOVE AMMONIUM NITRATE-WATER SOLUTIONS

NH ₄ NO ₃ -Concentration, wt. %	Slope of isostere in Equation (1) <i>m</i>	Intercept of isostere in Equation (1) <i>C</i>
10	0.9988	-0.0125
20	0.9968	-0.0275
30	0.9935	-0.0460
40	0.9889	-0.0670
50	0.9837	-0.0910
60	0.9770	-0.1245
70	0.9693	-0.1853
80	0.9611	-0.2829
90	0.9523	-0.4360
95	0.9475	-0.6950

can be shown to be (12)

$$q = L^\circ_B \int_{x_B}^{x_B/x_A} (m-1) d\frac{x_B}{x_A} \quad (3)$$

The reference state for a solid solute is usually the state of infinite dilution, and Equation (2) becomes

$$H_s = x_A \bar{H}'_A + x_B H_B + x_A q_s \quad (4)$$

Here, instead of the enthalpy of the pure component H_A , the partial enthalpy of the solute at infinite dilution \bar{H}'_A has been used, and the infinite heat of solution is substituted by the infinite heat of dilution:

$$q_s = L^\circ_B \int_{x_B/x_A}^{\infty} (m-1) d\frac{x_B}{x_A} \quad (5)$$

For many systems of partial miscibility, such as salt-water systems, only Equations (4) and (5) can be used. However where vapor pressures at high concentrations can be determined, Equation (3) can be integrated at least as accurately as Equation (5); thus either may be used.

TABLE 3.

Enthalpies for solid NH₄NO₃ in kcal./kg.-mole ammonium nitrate derived from data of reference 8, 14

Temperature <i>t</i> , °C.	(base temperature 0°C.)
-60 to -17	$H^\circ_A = 3,890. - 3.10T - 0.0551T^2$
-17	$\Delta H_{TR} = 120 \quad (V \rightarrow IV)$
-17 to +32	$H^\circ_A = -5,580. + 9.54T + 0.0398T^2$
+32	$\Delta H_{TR} = 399. \quad (IV \rightarrow III)$
+32 to 83	$H^\circ_A = -5,452. + 14.11T + 0.0235T^2$
+83	$\Delta H_{TR} = 311 \quad (III \rightarrow II)$
+83 to +125	$H^\circ_A = -9,696. + 27.22T + 125 \Delta H^\circ_{TR} = 1,027 \quad (II \rightarrow I)$
+125 to +170	$H^\circ_A = -10,840 + 27.22T + 170 \Delta H^\circ_{fusion} = 1,460 \quad (I \rightarrow \text{liquid})$

Equations (2) and (3) were used in the present case. Liquid ammonium nitrate can exist only in its pure form above the melting point of 170°C. Below 170°C. the enthalpy of the molten salt in a subcooled state would be indicated and shall be designated as \bar{H}_A in contrast to H°_A .

The slope of the isosteres is a function of the concentration only and not of temperature; hence the integration of Equation (3) covers also the range of immiscibility at temperatures below the melting point of the solute.

It is necessary only that at some temperature the term $(m-1)$ can be extrapolated with reasonable accuracy to $x_B/x_A = 0$ in the same way as $(m-1)$ is extrapolated to $x_B/x_A = \infty$ when the reference state of infinite dilution for the solute is used.

The reference states of pure liquid water and of pure solid ammonium nitrate were both taken at 0°C. The integral heat of solution to dissolve solid ammonium nitrate in water isothermally at 25°C. can be taken from reference 15. The 25°C. isotherm may therefore be used as a starting point for constructing the enthalpy-concentration diagram, although the reference temperature is 0°C.

The steam tables (7) give the enthalpy of pure water. Heat capacities and heat of transformations for solid ammonium nitrate have been used as shown in Table 3. Heat capacity data of Rutskov (13) and Gucker *et al.* (6) for the ammonium nitrate solutions have been used. The 25°C. isotherm is thus calculated:

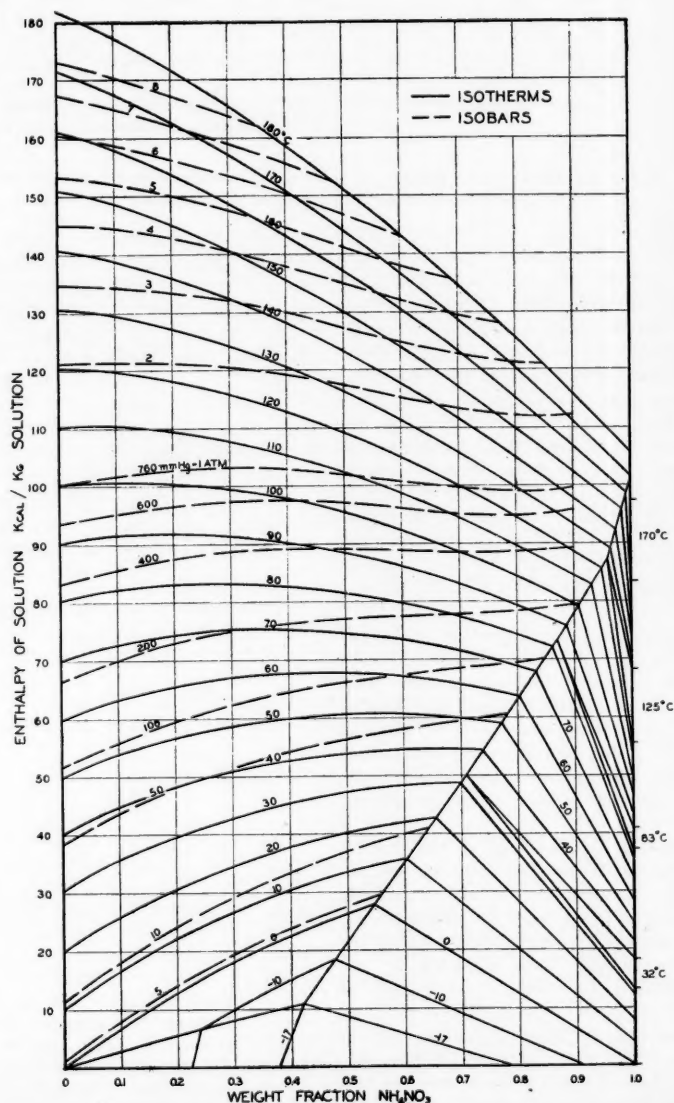


Fig. 3. Enthalpy-concentration diagram for the system water-ammonium nitrate.

TABLE 4. VALUES OF

$$\frac{x_A q}{L_B} = x_A \int_0^{x_B/x_A} (m-1) d \frac{x_B}{x_A} = x_A Z$$

Wt. % NH ₄ NO ₃	$x_A Z$
2.20	0.00186
5.0	0.00378
10.0	0.00687
20.0	0.01240
30.0	0.01760
40.0	0.02195
50.0	0.02525
60.0	0.02758
70.0	0.02785
80.0	0.02530
90.0	0.01900

First the enthalpy of a 9.09 mole % solution at 25°C. is calculated:

$$\begin{aligned} H_{s1} &= x_{A1} H^*_{A1} + x_{B1} H_B + x_{A1} Q \quad (6) \\ &= (0.0909 \times 805) + (0.9091 \times 451) \\ &\quad + (0.0909 \times 4,810) \\ &= 921.6 \text{ kcal./kg.-mole solution} \\ &= 38.92 \text{ kcal./kg. solution} \end{aligned}$$

The area under the curve $(m-1) x_B/x_A$ was evaluated by a step-by-step integration, and the values $x_A Z$ were calculated (Table 4), where

$$Z = \int_0^{x_B/x_A} (m-1) d \frac{x_B}{x_A} \quad (7)$$

Multiplication of Z by the molar heat of vaporization of pure water (7) gives the desired q value at any desired temperature and pressure.

The enthalpy of any solution along the 25°C. isotherm can now be calculated as

$$\begin{aligned} H_{s2} &= H_{s1} + (x_{A2} - x_{A1}) \bar{H}_A + \\ &\quad (x_{A1} - x_{A2}) H_B - x_{A2} q|_{x_{A2}}^{x_{A1}} + x_{A1} q|_{x_{A1}}^{x_{A2}} \quad (8) \end{aligned}$$

$$\begin{aligned} &= 921.6 + (x_{A2} - 0.0909) 3,540 - \\ &\quad (x_{A2} - 0.0909) 451 - 188.88 \\ &\quad - x_{A2} q|_{x_{A2}}^{x_{A1}} \end{aligned}$$

where \bar{H}_A is obtained from

$$\bar{H}_A = \frac{H_{s1} - x_{B1} H_B + x_{A1} q|_{x_{A1}}^{x_{A2}}}{x_{A1}} \quad (9)$$

and specifically for 25°C.

$$\bar{H}_A = \frac{921.6 - 0.9091 \times 451 - 188.88}{0.0909}$$

$$= 3,540 \text{ kcal./kg.-mole ammonium nitrate}$$

$$= 44.17 \text{ kcal./kg. ammonium nitrate}$$

TABLE 5. ENTHALPIES FOR THE WATER-AMMONIUM NITRATE SYSTEM

Temperature, °C	Concentration in Wt. % NH ₄ NO ₃									
	0	10	20	30	40	50	60	70	80	90
-17	-17.02			4.41	9.88	14.55				
-10	-10.10		4.30	9.16	15.19	19.42				
0	0.00	7.21	13.10	18.34	22.74	26.36	29.36			
10	10.06	16.54	22.26	25.52	30.30	33.30	35.70			
20	20.06	25.99	30.63	34.61	37.79	40.19	41.98	43.01		
30	30.04	36.24	39.34	42.71	45.27	47.06	48.27	48.70		
40	40.02	44.67	48.06	50.81	52.76	53.95	54.55	54.40	53.61	
50	49.99	54.01	56.76	58.90	60.24	60.82	60.83	60.09	58.72	
60	59.97	63.34	65.48	66.99	67.73	67.71	67.11	65.78	63.82	61.44
70	69.98	72.72	74.22	75.11	75.22	74.60	73.40	71.48	68.93	65.97
80	80.01	82.10	82.98	83.24	82.73	81.50	79.70	77.36	74.05	70.50
90	90.07	91.51	91.75	91.39	90.25	88.40	86.01	82.89	79.17	75.02
100	100.2	100.99	100.58	99.57	97.82	95.36	92.34	88.61	84.29	79.57
110	110.3	110.43	109.38	107.75	105.37	102.29	98.66	94.34	89.41	84.10
120	120.4	119.88	118.18	115.92	112.91	109.22	104.97	100.04	94.53	88.63
130	130.6	129.40	127.06	124.14	120.50	116.18	111.32	105.78	99.67	93.17
140	140.8	138.93	135.94	132.37	128.10	123.15	117.67	111.53	104.81	97.72
150	151.0	148.46	145.81	140.61	135.70	130.11	124.02	117.26	109.86	102.25
160	161.3	158.08	153.76	148.89	143.34	137.13	130.39	123.02	115.10	106.81
170	171.6	167.69	162.71	157.19	150.98	144.14	136.78	128.78	120.24	111.35
180	181.9	177.31	171.66	165.48	158.62	151.13	143.15	134.54	125.39	115.89

With the aid of heat capacity data for the solution, \bar{H}_A is calculated at any other temperature

$$\bar{H}_A = H_{s(25)} + \bar{C}_{ps} (t-25) - x_B H_B + x_A q|_{x_A}^{x_A} \quad (11)$$

At 170°C. \bar{H}_A should become equal to the enthalpy of pure molten ammonium nitrate. This value can be calculated independently by using heat capacities of the solid and heats of transition and fusion for pure ammonium nitrate. Within the accuracy of the heat-capacity data for solid ammonium nitrate and for the solutions there is calculated

$$\bar{H}_A = 2,744 + 31.67t \text{ (kcal./kg.-mole)}$$

With the above information the complete enthalpy-concentration diagram was calculated as shown in Figure 3. In addition to the isotherms, isobars for concentrations up to 90 wt.% ammo-

nium nitrate were calculated from the equation of Table 2 and plotted in the enthalpy-concentration diagram. Tables 5 and 6 show the values of enthalpy

along isotherms and isobars respectively; by use of these numbers, for more precise use, there may be prepared large-scale plots.

ACKNOWLEDGMENT

The support of Vulcan-Cincinnati, Incorporated, is gratefully acknowledged.

NOTATION

C = integration constant (intercept of partial-pressure equation)
 \bar{C}_{ps} = mean molar heat capacity for ammonium nitrate solutions, kcal./kg.-mole solution and °C.

TABLE 6. ISOBARS FOR THE WATER-AMMONIUM NITRATE SYSTEM (VALUES GIVEN ARE OF TEMPERATURES IN °C.)

Pressure mm. Hg.	Concentration in Wt. % NH ₄ NO ₃									
	0	10	20	30	40	50	60	70	80	90
5	1.2	1.3	1.4	1.5	1.7	1.9				
10	11.3	11.7	12.3	13.1	14.0	15.1	16.6			
50	38.1	38.8	39.6	40.6	41.9	43.4	45.4	49.0		
100	51.6	52.3	53.2	54.4	55.9	57.6	60.0	64.0	70.4	
200	66.5	67.2	68.3	69.8	71.4	73.4	76.2	80.8	88.0	99.6
300	75.9	76.7	77.9	79.4	81.2	83.4	86.6	91.6	99.4	112.0
400	83.0	83.9	85.1	86.6	88.7	91.0	94.3	99.7	108.0	121.5
500	88.7	89.6	90.9	92.6	94.7	97.1	100.6	106.2	115.0	128.9
600	93.6	94.5	95.8	97.6	99.8	102.3	105.9	111.8	120.9	135.6
700	97.7	98.8	100.1	101.9	104.2	106.8	110.6	116.7	126.0	141.0
(atmos.)										
1	100.0	101.0	102.5	104.2	106.6	109.3	113.1	119.3	128.9	144.1
1.25	106.6	107.2	108.9	110.8	113.3	116.2	120.2	126.7	136.7	152.8
1.5	111.8	112.9	114.4	116.4	119.0	122.0	126.1	132.9	143.4	160.0
2.0	120.7	121.9	123.4	125.6	128.3	131.6	136.1	143.4	154.6	172.4
2.5	127.9	129.1	130.8	133.1	136.0	139.4	144.1	151.8	163.6	182.5
3.0	134.0	135.3	137.0	139.4	142.5	146.0	151.0	159.0	171.4	191.1
3.5	139.3	140.7	142.5	144.9	148.1	151.8	157.0	165.4	178.2	198.6
4.0	144.1	145.5	147.3	149.9	153.2	157.0	162.4	171.0	184.3	
4.5	148.4	149.8	151.7	154.4	157.8	161.7	167.2	175.9	189.8	
5.0	152.3	153.8	155.7	158.5	162.0	166.0	171.7	180.8		
6.0	159.2	160.9	162.9	165.8	169.4	173.7	179.6	189.2		
7.0	166.0	167.1	169.2	172.1	175.9	180.4	186.6	196.6		
8.0	171.8	172.6	174.8	177.9	181.8	186.4	192.8			

Temperatures in degrees centigrade.

L°_B	= molar heat of vaporization for pure water, kcal./kg.-mole water
L_B	= molar heat of vaporization for water out of ammonium nitrate solutions, kcal./kg.-mole water
m	= slope of an isostere on a logarithmic partial-pressure plot
H	= enthalpy, kcal./kg.-mole (except if otherwise noted)
P	= partial pressure of water above ammonium nitrate solutions, mm. Hg abs.
P°	= vapor pressure of pure water, mm. Hg abs.
Q	= integral heat of solution for solid ammonium nitrate, kcal./kg.-mole
q	= integral heat of dilution, kcal./kg.-mole
t	= temperature, °C.
T	= absolute temperature, °K.
x	= mole fraction
Z	= abbreviation for the integral of Equation (7)

Subscripts

A	= ammonium nitrate
B	= water
s	= solution
TR	= transition

∞	= infinite dilution
1	= concentration where integral heat of solution Q is known
2	= any concentration

Superscripts

—	= partial quantity
∞	= infinite dilution
\circ	= solid state
\circ	= pure compound

LITERATURE CITED

1. Campbell, A. N., J. B. Fishman, G. Rutherford, T. P. Schaeffer, and L. Ross, *Can. J. Chem.* **34**, 151 (1956).
2. D'Ans-Lax, "Taschenbuch für Chemiker und Physiker," 2 edit., Springer Verlag, Berlin, Germany (1949).
3. Fricke, R., and L. Havestadt, *Z. Elektrochem.*, **33**, 441 (1927).
4. Fröhlich, G. J., D.Ch.E. dissertation, Polytechnic Inst. Brooklyn, New York (1957).
5. Gerlach, Z. *anal. Chem.*, **26**, 413 (1887).
6. Gucker, F. T., F. D. Ayres, and T. R. Rubin, *J. Am. Chem. Soc.*, **58**, 2118 (1936).
7. "Handbook of Physics and Chemistry," 37 ed. Chemical Rubber Publishing Company, Cleveland, Ohio (1955).

8. "International Critical Tables," Vol. V., McGraw-Hill, New York (1929).
 9. Kirk-Othmer, "Encyclopedia of Chemical Technology," Vol. I, p. 818, The Interscience Encyclopedia, Inc., New York (1947).
 10. Lerner-Steinberg, B., *Z. physik. Chem.*, **122**, 121 (1926).
 11. Othmer, D. F., *Ind. Eng. Chem.*, **32**, 841 (1940).
 12. ———, R. C. Kowalski, and L. M. Napthali, *Ind. Eng. Chem.*, **51**, 89 (1959).
 13. Rutskov, A. P., *J. Appl. Chem.*, (USSR), **21**, 820 (1948).
 14. Stephenson, C. C., D. R. Bentz, and D. A. Stevenson, *J. Am. Chem. Soc.*, **77**, 2161 (1955).
 15. U. S. National Bureau of Standards Circular 500.
 16. Volk, W., *Chem. Eng.*, **63**, 165 (March 1956).
- Previous articles in this series have appeared in *Ind. Eng. Chem.* during 1940, 1942 to 46, 1948 to 51, 1953, 1955, 1957, 1959 to 60; *Chem. Eng. Data*, 1956; *Chem. Met. Eng.*, 1940; *Chimie & Industrie (Paris)*, 1948; *Euclides (Madrid)*, 1948; *Sugar*, 1948; *Petrol. Refiner*, 1951 to 53; *World Petrol. Congr. Proc.*, 3 Congr., Hague, 1951; *Proc. Intern. Congr. Pure Appl. Chem.*, 11 Congr., London, 1947.

Manuscript received February 26, 1959; revision received July 21, 1959; paper accepted July 29, 1959.

Hydrocarbon Vapor-Liquid Equilibria and Solubility Parameter

J. M. PRAUSNITZ, W. C. EDMISTER, and K. C. CHAO

California Research Corporation, Richmond, California

Hydrocarbon vapor-liquid equilibria are expressed in terms of K values, which are functions of composition, as well as pressure and temperature. The composition effect in the liquid phase is calculated by the Hildebrand-Scatchard equation for regular solutions. The parameters in this equation, called *solubility parameters*, can be calculated simply from heat of vaporization for the heavier hydrocarbons, but an indirect method of calculation must be used for the lighter components. Solubility parameters for hydrogen, methane, ethane, and propane were computed from gas-solubility data in several hydrocarbon solvents at various temperatures and pressures. This computation also yielded simultaneously the fugacities of the hypothetical liquid-standard states.

The results presented are not complete for practical applications, owing to the scarcity of suitable solubility data, especially at high temperatures and pressures. However solubility parameters appear to give the right liquid-phase corrections in the correlation and prediction of hydrocarbon phase equilibria. Calculated K values for light hydrocarbons in paraffinic, naphthenic, and aromatic absorption oils are compared with experimental results. The average deviation for the forty-two values tested is 13%.

The composition dependence of the vaporization equilibrium ratio in hydro-

carbon systems has been frequently neglected in practical applications. While the composition-independent K values are approximately applicable to mixtures composed entirely of one class

of hydrocarbons, like the aliphatics, large deviations are encountered for mixtures composed of different classes of hydrocarbons, notably those containing aromatics and, to a lesser extent, naphthenes.

J. M. Prausnitz is at the University of California, Berkeley, California; W. C. Edmister, at Oklahoma State University, Stillwater, Oklahoma.

The composition-independent K values follow from the assumption of Raoult's law for the liquid phase and Dalton's law for the vapor phase. Lewis's fugacity rule leads, likewise, to composition-independent K values. Ideal K -value charts, such as those prepared by Lewis and Kay (15) and by Souders, Selheimer, and Brown (28), were derived therefrom.

Benedict, Webb, and Rubin developed composition-dependent K values from their equation of state (1, 2). Their results were simplified and correlated in reduced variables by Edmister and Ruby (5) for more convenient application. The B.W.R. equation of state K values are valuable at conditions of extreme temperature and pressure for aliphatic systems. An equation-of-state approach such as this, however, is limited by the rules of combination of the constants. The validity of these rules was established for hydrocarbon mixtures composed entirely of one class of compounds, specifically the aliphatics. Behavior of mixtures of different classes of compounds, such as mixtures of hydrocarbons and carbon dioxide, was shown not to follow these combination rules (3, 21).

The widely used Natural Gasoline Association of America K charts (31) seek to correlate composition effect on K values by the convergence pressure of the system. These K values apply only to aliphatic mixtures. Again their use in aromatic-containing systems may lead to large deviations.

The present work proposes to answer the need for correct K values of light hydrocarbons in different solvents. The following developments and results are for conditions where deviation from ideal solution arises mainly in the liquid phase. The liquid-phase nonideality is treated with the Hildebrand-Scatchard equation for regular solutions.

The K values for a component i are computed by the rigorous thermodynamic relationship

$$K_i = \frac{y_i}{x_i} = \frac{\gamma_i v_i}{\phi_i} \quad (1)$$

REGULAR SOLUTIONS

Much has been written on regular solutions (7), and only a few features pertinent to the problem under consideration will be mentioned here. A regular solution is one in which the nonideality is due entirely to the heat of mixing. Its entropy of solution is equal to that of an ideal solution. While no solutions are exactly regular, the properties of solutions of nonpolar fluids, such as the hydrocarbons, are approximated by the regular-solution equations. It was shown by Hildebrand

and Scott (7) and by Scatchard (25, 26) that the activity coefficient of a component i in a regular liquid solution containing n components is given by

$$\ln \gamma_i = \frac{V_i (\delta_i - \bar{\delta})^2}{RT} \quad (2)$$

The solubility parameter is the square root of an energy density. For a liquid it is defined by

$$\delta = \left(\frac{\Delta E}{V} \right)^{1/2} \quad (3)$$

At temperatures well below the critical this energy is essentially the enthalpy of vaporization minus RT .

In general, values of solubility parameters of the aromatic hydrocarbons are higher than those of the naphthenes; the latter are in turn higher than those of the paraffins. Among the normal paraffins the solubility parameter increases rapidly with molecular weight starting from methane but tends to level off for compounds heavier than n -pentane. Thus the difference in solubility parameters between a light and a heavy paraffin is less than that between the same light paraffin and an aromatic hydrocarbon. This explains the high K values of the light paraffins in aromatics.

It follows from Equation (3) that the solubility parameter decreases with temperature, but it is practically independent of pressure at a given temperature. The variation of solubility parameter with temperature was given by Hildebrand and Scott (7) to be approximately

$$\frac{d\ln \delta}{dT} \cong -1.25 \alpha \quad (4)$$

Over a moderate range of temperature where α may be taken to be approximately constant, Equation (4) states that $\log \delta$ varies linearly with temperature. The solubility parameters of several common hydrocarbons are shown in Figure 1. The lines are based on δ and its slope $(d\ln \delta)/dT$ at a temperature of 25°C. Determination of the lines for the light gases methane, ethane, propane, and hydrogen is discussed in the next section. Solubility parameters of a number of other hydrocarbons have been given (7) at 25°C.

Dependence of K values on solubility parameter is illustrated in Figure 2 for methane at 100°F. and 500 lb./sq. in. abs. The solubility-parameter equation accounts for the variation of K over a wide range because of the nature of the solvent and various dissolved quantities of other light hydrocarbons (ethylene and isobutane). Figure 2 also bears out the linear

relationship demanded by Equations (1) and (2). This linearity holds rigorously, barring significant variations in ϕ . Actually ϕ does not vary more than 3.3% for methane in these mixtures.

GASEOUS COMPONENTS

Since Equation (2) was derived for solutions of liquids mixing with no volume change, it does not in its present form have rigorous theoretical basis for solutions containing one component above its critical temperature. It was shown earlier (20) that Equation (2) can be modified to be theoretically applicable to gas-liquid solutions, but for the purpose of this paper it is more convenient to consider Equation (2) as a semiempirical relation with adjustable parameters suitable for all liquid-phase hydrocarbon solutions, including those containing both gaseous and liquid components.

For a gaseous solute in liquid solution the liquid molal volume is replaced by the partial molal volume of the dissolved gas, which can be estimated with fair accuracy from Watson's expansion factor, (30):

$$V = (V_i \omega_i) \left(5.7 + 3.0 \frac{T}{T_c} \right) \quad (5)$$

For a gaseous component i in a binary mixture Equation (1) is rewritten as

$$v_i = \frac{K_i \phi_i}{\gamma_i} \quad (1a)$$

There are two adjustable parameters for a component: the hypothetical liquid-phase fugacity, which is a function of temperature and pressure, and the solubility parameter, which at moderate pressures is a function of temperature only. By fitting Equation (1a) to the solubility data of a gas in at least two solvents at the same temperature and pressure, one can solve for the parameters f^L (or ν) and δ for the gaseous component.

The calculations for a given gas at a fixed temperature and pressure were of the trial-and-error type, with solubility data used in at least two solvents. To obtain sensitivity in the calculations, it was always necessary to choose solvents of different chemical nature; usually one solvent was a paraffin, the second an aromatic hydrocarbon, and so on. To start the calculation, a first estimate of δ was substituted into Equations (2) and (1a), one value of ν being obtained from each solution. The difference between them is designated by $\Delta \nu$. The calculation was repeated with new estimates of δ used until $\Delta \nu$ vanished. This then gave the correct values for ν and δ . This procedure is

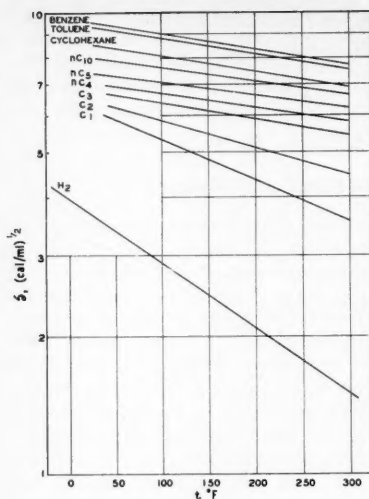


Fig. 1. Solubility parameters.

illustrated in Figure 3 for solutions of ethane in heptane and benzene at 110°F. and 400 lb./sq. in. abs. The fugacity coefficient in the vapor mixture was calculated from the Redlich and Kwong equation of state for this instance, as well as for all mixtures studied in this work. Discussions on vapor-phase correction are deferred to the next section.

Where solubility data for the same gas in more than two solvents are available, calculated ν 's are directly plotted against assumed values of δ , resulting in a group of curves, one for each solution. A single point of intersection is to be expected if the equations are exactly applicable and the data are perfectly precise. Figure 4 illustrates the result of calculation for H_2 at -25°C. and atmospheric pressure. The curves display a tendency toward conver-

gence, except for solution of H_2 in perfluoronormal heptane. The chosen point of convergence is marked with a large circle.

Some arbitrariness was unavoidable in the selection of this convergence point as shown in Figure 4. However the determined δ and ν , when applied consistently, will lead to K values correct to the extent indicated by the scattering of the ν curves at the chosen δ . Thus for the systems at the conditions shown the K values of H_2 will be reproduced to within 10% (except in perfluoronormal heptane), even though the K values vary by as much as 570% in different solvents.

Solubility parameters determined in this manner for methane, ethane, propane, and hydrogen are shown in Figure 1.

Values of ν for the three lightest paraffins and hydrogen are shown in Figures 5 to 8, respectively. Computed values of ν from solubility data correspond to conditions of high reduced temperature. At conditions of low reduced temperatures, where the pure substance exists as an actual liquid, values of ν were obtained from generalized correlations prepared by Lydersen, Greenkorn, and Hougen (16). The combination of computed and generalized values in the preparation of these ν charts is illustrated in Figure 9 for propane.

Sources of solubility data that were used in this work are recorded in Table 1.

Extension of ν to lower pressures is facilitated by the relation that ν tends to be inversely proportional to pressure when the pressure is sufficiently reduced. From the thermodynamic relation

$$\left(\frac{\partial \ln \nu}{\partial \ln P} \right)_T = \frac{PV^L}{RT} - 1 \quad (6)$$

it follows that

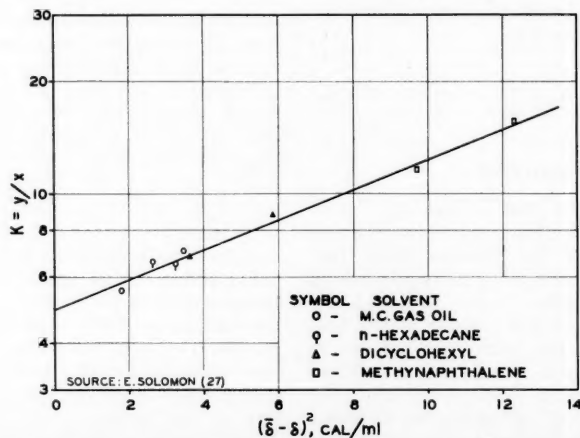


Fig. 2. Effect of solubility parameter on K value of methane at 100°F. and 500 lb./sq. in. abs.

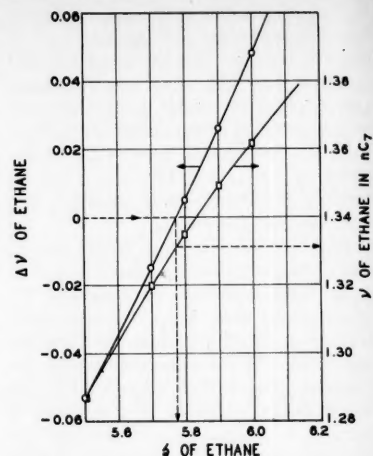


Fig. 3. ν from equilibrium data on ethane systems at 570°R. and 400 lb./sq. in. abs.

$$\lim_{P \rightarrow 0} \left(\frac{\partial \ln \nu}{\partial \ln P} \right)_T = -1 \quad (7)$$

since V^L changes but slightly with pressure. This situation apparently holds even when the liquid state is hypothetical, as illustrated in Figure 10 for propane. The points shown are taken from the curves in Figure 9.

The constants $V_{1\omega_1}$ in Equation (4) have been given (30) for the normal paraffins. Constants for methane and ethane were slightly adjusted to give better agreement with observed data on partial volumes in dilute hydrocarbon solutions (7). A plot of $V_{1\omega_1}$ against number of carbon atoms was connected smoothly from methane and ethane to the higher paraffins, resulting in slight adjustment for propane. The constants for the other normal paraffins were not changed. In Table 2 the constants for other hydrocarbons were evaluated to fit densities given in A.P.I. Project 44. For hydrogen, partial volumes in hydrocarbon solutions (8, 13,

TABLE 1. SOURCES OF SOLUBILITY DATA

Solute	Solvent	Reference
Hydrogen	Benzene	9
	Toluene	9
	Cyclohexane	9
	n-Hexane	18
	n-Heptane	4
	n-Octane	4
	iso-Octane	4
	Perfluoro-n-heptane	4
	Benzene	4
	Toluene	4
Methane	Carbon disulfide	4
	Carbon tetrachloride	4
	Trimethylbutane	24
	n-Nonane	24
	Cyclohexane	24
Ethane	Benzene	24
	Toluene	24
	n-Heptane	10
Propane	Benzene	11
	iso-Pentane	29
	Benzene	6

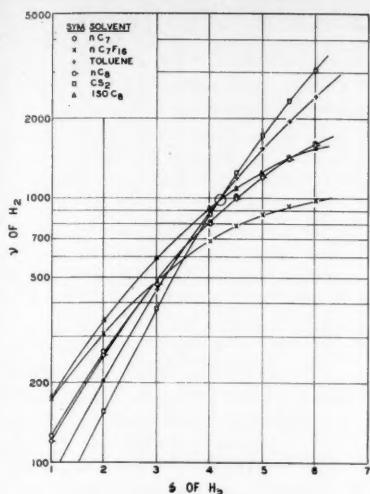


Fig. 4. Hydrogen systems at -25°C. , 14.7 lb./sq. in. abs.

14) under moderate pressures were the basis of the constant in Table 2.

VAPOR-PHASE CORRECTION

The fugacity coefficient in the vapor phase is, generally speaking, just as important as the liquid-phase activity coefficient in the determination of K values. There is however a point of distinction in emphasis, depending on the component. In systems composed of both light and heavy components the liquid activity coefficient is usually important for the light component but not for the heavy one, and the vapor fugacity coefficient is usually important for the heavy component but not for the light one.

The emphasis of this work is on liquid-phase correction and conse-

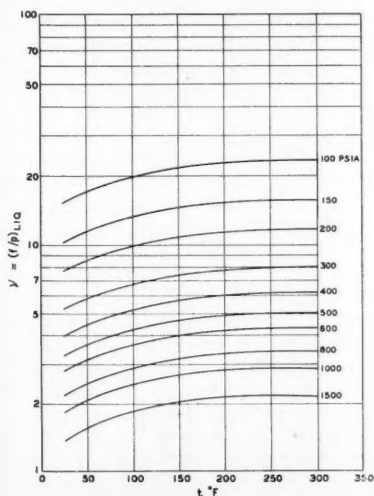


Fig. 5. Liquid fugacity for methane.

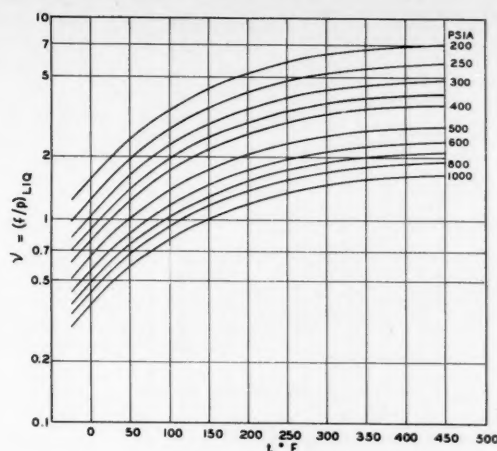


Fig. 6. Liquid fugacity for ethane.

quently on the K values of the light components. The vapor-phase fugacity coefficients for them are adequately given by the relatively simple Redlich and Kwong's equation of state (22) under the conditions investigated here. The characteristic constants in this equation are directly related to the critical temperature and pressure of the components. Other method for computing vapor-phase fugacity coefficients have been presented recently (19).

APPLICATIONS

Illustration 1

Application of the method outlined here to be the calculation of vapor-liquid equilibria in heavy-oil-absorption systems requires determination of the solubility parameter of the absorber oils. Strictly speaking, these oils should be broken down into narrow boiling cuts, the solubility parameter of the cuts evaluated according to Equation (3), and the over-all solubility param-

eter of the oil synthesized from that of the cuts as the volume-averaged mean value. This procedure is tedious, and the necessary information is often not available on the individual cuts, but it appears, fortunately, that sufficient accuracy is obtained by taking such oil as a single compound characterized by its average boiling point, A.P.I. gravity, and average molecular weight. These properties are included in standard inspections.

The solubility parameter is calculated at 25°C. of the hydroformer still bottoms used by Solomon in experimental studies of vaporization equilibrium ratios (27). The characteristics of this absorber oil are

Gravity, $^{\circ}\text{A.P.I.}$	4.8
Mole average boiling point, $^{\circ}\text{F.}$	634
Molecular weight	209
Solution: Density at 60°F.	$= 1.038$
g./ml., from given $^{\circ}\text{A.P.I.}$	
Density correction factor to 25°C. (77°F.)	$= 0.993$ (17)

TABLE 2. LIQUID-VOLUME CHARACTERISTIC CONSTANTS IN WATSON'S EQUATION

	$V_1\omega_{1s}$ cc./g.-mole
Hydrogen	1.05
Methane	5.00
Ethane	7.77
Propane	9.70
<i>n</i> -Butane	11.62
<i>n</i> -Pentane	14.07
<i>n</i> -Hexane	16.52
<i>n</i> -Heptane	18.96
<i>n</i> -Octane	21.39
<i>n</i> -Nonane	23.83
<i>n</i> -Decane	26.28
Cyclohexane	14.07
Benzene	11.64
Toluene	14.15

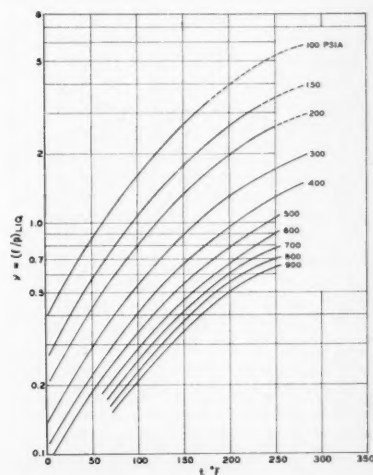


Fig. 7. Liquid fugacity for propane.

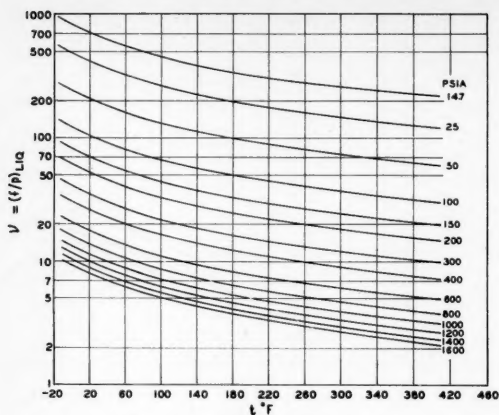


Fig. 8. Liquid fugacity for hydrogen.

Density at 25°C. = 0.993×1.038
= 1.030 g./ml.

V at 25°C. = $209/1.030 = 203$
ml./g.-mole.

ΔH at 634°F. = 13,060 cal./g.-mole,
from Kistiakowsky equation

ΔH correction factor to 25°C. =
1.369, according to Watson's 0.38
exponential correction (17) with T_c
= 1,066°F.

ΔH at 25°C. = $1.369 \times 13,060 =$
17,870 cal./g.-mole

RT at 25°C. = 592 cal./g.-mole

ΔE at 25°C. = $17,870 - 590 = 17,280$
cal./g.-mole

$\Delta E/V = 85.1$ cal./ml.

$\delta = 9.23$ (cal./ml.)^{1/2}

This is a high value for a solubility parameter, typical for aromatic hydrocarbons. (Refer to Figure 1 for comparison with the pure hydrocarbons.)

The pure-component property v of the heavy substances may be estimated from

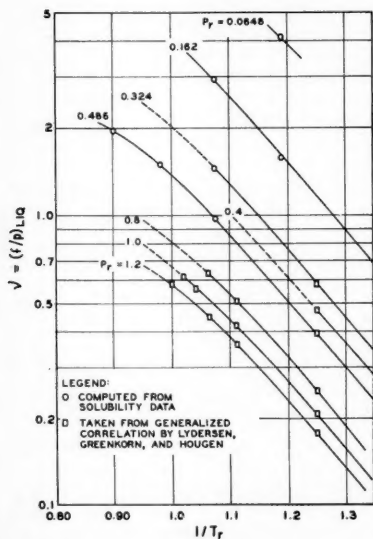


Fig. 9. Liquid fugacity for propane, combination of values from pure component and from solubility data ($z_c = 0.277$).

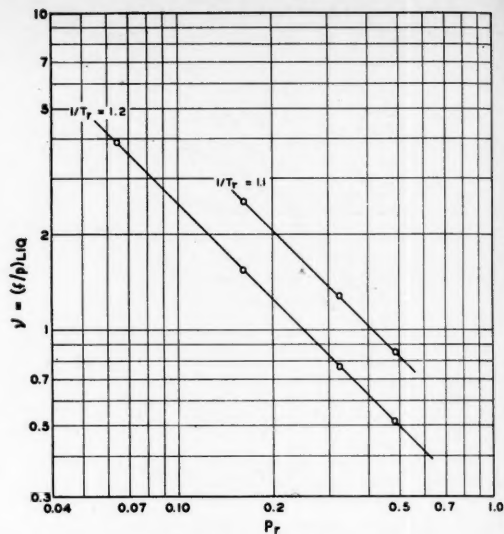


Fig. 10. Isothermal variation of v of propane at low pressure.

generalized correlations, such as the correlation prepared by Lydersen, Greenkorn, and Hougen (16).

Calculation of bubble and dew points of hydrocarbon mixtures according to K values given by Equation (1) involves double trial-and-error calculations. Both the temperature and the composition of the equilibrium phase must be assumed and checked through either $\sum K_i x_i = 1$, or

$$\sum (y_i/K_i) = 1.$$

COMPARISON WITH EXPERIMENTAL DATA

The solubility parameter and liquid fugacity coefficient presented in previous sections were developed from either pure-component properties or solubility data in binary mixtures. These values were used to compute K in multicomponent mixtures under conditions that had been experimentally studied. The results were compared with observed K values. Solomon's (27)

experimental studies of K values of light hydrocarbons were found the most suitable for the test because of the widely different character of the solvents, including aliphatic, naphthenic, and aromatic oils and compounds under comparable conditions of temperature and pressure. In addition Kirkbride and Bertetti's (12) low-pressure data were tested, but their high-pressure data were beyond the range of the v charts here developed.

Comparisons were made with the published vapor-liquid-equilibrium data of Kirkbride and Bertetti on the light hydrocarbons, methane through pentane, in naphthenic, paraffin, and aromatic absorption oils at 90 to 92°F. and 123 to 124 lb./sq. in. abs. The average absolute deviation was 15% for the light hydrocarbons. No trend of deviation is observed in the hydrocarbons from methane to pentane, in spite of the difference in source of v , which is taken from computed values for the

TABLE 3. SOLUBILITY PARAMETER AND LIQUID VOLUME OF SOLVENTS

Solvent	Investigator	t , °F.	δ , (cal./ml.) ^{1/2}	\bar{V}_L , ml./g.-mole
M.C. gas oil	27	100	7.41	324
		220	6.92	346
Hydroformer still bottoms	27	220	8.66	214
		220	7.02	316
<i>n</i> -Hexadecane	27	100	7.52	297
		220	8.20	190
Dicyclohexyl	27	100	7.68	202
		220	8.94	151
Methylnaphthalene	27	100	9.53	143
		220	8.94	151
Paraffinic lean oil	12	90	7.46	56
Naphthenic lean oil	12	90	7.81	61
Aromatic lean oil	12	92	9.66	94

lighter compounds and from a generalized correlation for the heavier compounds.

Another comparison was made of Solomon's K of methane with computed values. The experimental studies were on mixtures of methane, ethylene, isobutane, and the heavy solvents at 100° to 220°F. and 500 to 1,000 lb./sq. in. abs. Owing to a lack of suitable equilibrium data, the solubility parameter and liquid molal volume of ethylene were not available from data processing but were estimated from properties of the light paraffins at the same temperature. This admittedly was not accurate, but the estimated quantities were used only in the calculation of average solubility parameter of the liquid mixtures, to which the errors should not contribute to any significant extent. The lack of data also made it impossible to develop a correlation for ethylene. The average absolute deviation was 13%.

K values of isobutane at 100°F. in Solomon's mixtures were calculated by the use of Lydersen's generalized ν values. Results at 100°F. deviated only 5% from the observed.

The solubility parameter and liquid molal volume of the heavy solvents that were used in these calculations are given in Table 3.

DISCUSSION

Calculation of light hydrocarbon vapor-liquid equilibria by the use of solubility parameters appears to give correctly the liquid phase composition effects. Composition-corrected K values are not convenient to apply without electronic digital computers; this method is no exception.

However, simplification has been obtained by taking solubility parameter and liquid volume to be pressure insensitive. As demonstrated in the comparison with experimental data, this lack of sensitivity to pressure appears to be justified up to 1,000 lb./sq. in. abs. at usual temperatures. No trend in deviation was detected with pressure.

Another possibility of simplification may be to take solubility parameter and liquid volume to be temperature independent. There are indications that results of comparable accuracy may be obtained over a range of temperature of practical interest. Since the effect of solubility parameter on the liquid-phase correction is in the form of a difference term, the deviation incurred by taking the individual terms to be constant may be less than suggested by examination of the variation of the individual values with temperatures.

The results presented here are incomplete owing to the scarcity of suitable solubility data, especially at higher

temperatures. As more data become available, the correlation developed in this work can no doubt be improved. However the results summarized here indicate that the solubility parameter is a useful tool for the correlation and prediction of hydrocarbon vapor-liquid equilibria.

ACKNOWLEDGMENT

Grateful acknowledgement is due to L. Tornheim for aid in programming the computation on a Datatron computer, to W. S. Hanna for compiling gas-solubility data, and to J. D. Seader for constructive criticism.

NOTATION

E	= internal energy
f	= fugacity
H	= enthalpy
K	= vaporization equilibrium ratio
P	= pressure
R	= gas constant
T	= absolute temperature
t	= temperature
V	= molal volume
x	= mole fraction in liquid phase
x_v	= volume fraction in liquid phase; $x_v = \frac{x_i V_i}{\sum_{j=1}^n x_j V_j}$
y	= mole fraction in vapor phase

Greek Letters

ΔE	= energy required to vaporize the liquid to infinite volume
α	= coefficient of thermal expansion
γ	= activity coefficient in liquid phase, to be given by Hildebrand-Scatchard equation for regular solutions for component $i \equiv f_i/f^L_i x_i$
δ	= solubility parameter
$\bar{\delta}$	= volume average solubility parameter for the liquid solution = $\sum_{j=1}^n x_j \delta_j$
ν	= fugacity coefficient of pure liquid, for component $i \equiv f^L_i/P$
ϕ	= fugacity coefficient in vapor phase, for component $i \equiv f_i/P y_i$
ω	= Watson's expansion factor

Superscripts

L = pure liquid

Subscript

c	= critical property
i	= component i
j	= component j
r	= reduced property

LITERATURE CITED

1. Benedict, Manson, G. B. Webb, and L. C. Rubin, *J. Chem. Physics*, **8**, 334 (1940).

2. ———, *Chem. Eng. Progr.*, **47**, 419 (1951).
3. Cullen, E. J., and Kenneth Kobe, *A.I.Ch.E. Journal*, **1**, 452 (1955).
4. Cook, M. W., Ph.D. thesis, University of California, Berkeley, (January, 1954).
5. Edmister, W. C., and C. L. Ruby, *Chem. Eng. Progr.*, **51**, 95-F (1955).
6. Glanville, J. W., B. H. Sage, and W. N. Lacey, *Ind. Eng. Chem.*, **42**, 508 (1950).
7. Hildebrand, J. H., and R. B. Scott, "Solubility of Non-Electrolytes," Reinhold, New York (1950).
8. Horiuti, J., *Sci. Papers Inst. Phys. Chem. Research (Tokyo)*, **17**, 125 (1931).
9. Ipatiev, V. V., and M. I. Levina, *Zhur. Fiz. Khim.*, **6**, 632 (1935).
10. Kay, W. B., *Ind. Eng. Chem.*, **30**, 459 (1938).
11. ———, and T. D. Nevens, *Chem. Eng. Progr. Symposium Ser. No. 3*, **48**, 110 (1952).
12. Kirkbride, C. G., and J. W. Bertetti, *Ind. Eng. Chem.*, **35**, 1242 (1943).
13. Krichevskii, I. R., and G. D. Efremova, *Zhur. Fiz. Khim.*, **22**, 1116 (1948).
14. Lachowicz, S. K., D. M. Newitt, and K. E. Weale, *Trans. Faraday Soc.*, **51**, 1198 (1955).
15. Lewis, W. K., and W. C. Kay, *Oil Gas J.*, **32**, 40, 45, 114 (1934).
16. Lydersen, A. L., R. A. Greenkorn, and O. A. Hougen, *Univ. Wisconsin Eng. Expt. Sta. Rep. No. 4*, Madison, Wisconsin (1955).
17. Maxwell, J. B., "Data Book on Hydrocarbons," D. Van Nostrand, New York (1950).
18. Nichols, W. B., H. H. Reamer, and B. H. Sage, *A.I.Ch.E. Journal*, **3**, 262 (1957).
19. Prausnitz, J. M., *A.I.Ch.E. Journal*, **5**, 3 (1959).
20. *Ibid.*, **4**, 269 (1958).
21. ———, and R. D. Gunn, *ibid.*, No. 4, 430 (1958).
22. Redlich, Otto, and J. N. S. Kwong, *Chem. Rev.*, **44**, 233 (1949).
23. Sage, B. H., and W. N. Lacey, "Thermodynamic Properties of the Lighter Paraffin Hydrocarbons and Nitrogen," American Petroleum Institute, New York (1950).
24. Savvina, Y. D., and A. C. Velikovskii, *Zhur. Fiz. Khim.*, **30**, 1596 (1956).
25. Scatchard, G., *Chem. Rev.*, **8**, 321 (1931).
26. ———, *J. Am. Chem. Soc.*, **56**, 995 (1934).
27. Solomon, Ernest, *Chem. Eng. Progr. Symposium Ser. No. 3*, **48**, 93 (1952).
28. Souders, M., C. W. Selheimer, and G. G. Brown, *Ind. Eng. Chem.*, **22**, 517 (1932).
29. Vaughan, W. E., and F. C. Collins, *ibid.*, **34**, 885 (1942).
30. Hougen, O. A., and K. M. Watson, "Chemical Process Principles," Vol. II, p. 668, John Wiley, New York (1947).
31. "Equilibrium Ratio Data Book," Natural Gasoline Association of America, Tulsa, Oklahoma (1955).

Manuscript received December 30, 1958; revision received May 8, 1959; paper accepted May 13, 1959.

Elutriation of Solid Particles From a Dense-Phase Fluidized Bed

CHIN-YUNG WEN AND RICHARD F. HASHINGER

West Virginia University, Morgantown, West Virginia

The elutriation of fines from fluidized beds of two- and multiparticle systems is investigated. Materials used are glass beads and coal powder with air and helium as the elutriating gases.

A specific elutriation rate constant which takes into consideration the particle stratification and thus is nearly independent of the bed dimensions is employed in the correlation of the elutriation of fines.

The proposed generalized correlation applicable to a system of two particle sizes and to more complex ones is presented. Recorrelation of pertinent literature data by the dimensionless equation indicates good agreement in spite of a diversity of bed geometries. The effect of fluidized-bed parameters on the rate of elutriation is examined, and applications and limitations of the correlation are shown.

Elutriation is a process whereby smaller particles are continuously removed by means of a fluid current from a bed composed of a spectrum of particle sizes. The understanding of the process of elutriation of solid particles has in recent years become progressively important not only owing to the increased use of fluidized-bed technique in industrial plant operations but also because of the convenience of this process as a method of particle separation. In a continuous fluidized-bed operation the fine particles may be originally present, or they may in time be produced from large-size particles as a result of mechanical attrition or breakdown due to internal thermal stresses. The carry-over of fines must be either replaced with fresh particles or returned to the system through separation equipment such as cyclones or electrostatic precipitators. If the entrained solid particles are allowed to escape into the transfer line, a reduction in flow capacities and an erosion of pipelines will result. Furthermore the constantly changing particle-size distribution in the fluidized bed may alter the rate and extent of mass and heat transfer. These facts necessitate a thorough investigation of the rate of elutriation upon which design calculation can be made. Finally the importance of elutriation may be clearly seen in the possibility of adapting the fluidized-bed technique to nuclear reactors, where contamination by radioactive fines is a serious problem.

Several investigators (2, 5, 7) who have worked on two-particle size systems have made important contributions to the understanding of the mechanism of elutriation. The experimental

results of previous investigators agree qualitatively in major parts and differ in minor aspects. Leva (5) and Osberg and Charlesworth (7) studied the rate of elutriation from beds of two different particle sizes. They could express their data by a first-order rate equation, $C = C_0 e^{-kt}$. The system variables, such as gas velocity, fine particle size and concentration, solid and gas properties, etc., were empirically related to the elutriation constant. Leva considered the gas velocity as the driving force in elutriation and found the rate constant to be proportional to $u^{1.0}$. Osberg and Charlesworth, on the other hand, correlated k in terms of particle free-fall terminal velocity, the difference between the value of the linear gas velocity and particle free-fall terminal velocity being the elutriation driving force. Leva found that the fines concentrations ranging from 20 to 5% had a negligible effect on the elutriation constant; however Osberg and Charlesworth indicated that below 5% the fines concentration had a significant effect. The effect of coarse-particle size on the elutriation rate constant was reported to be negligible by Leva, whereas Osberg and Charlesworth noted a significant effect when the fines concentration was less than 1%. A discussion of bed mobility for multiparticle size system is given by Matheson (6) and Trawinski (11). Andrews (1) considered the kinetics of the system and a statistical function of the freeboard. The information currently available from these studies is only qualitative and rather fragmentary and therefore cannot support a generalization for prediction of elutriation rate.

The object of this investigation is to augment the present understanding of the mechanism to include multiparticle

size systems and to propose a generalized correlation for the elutriation rate constant.

EXPERIMENTAL METHOD

Equipment

Figure 1 is a schematic diagram of the equipment. A 4-in. I.D. glass column 72 in. high and a 2-in. standard steel pipe 82 in. high were used as the fluidization equipment. A cyclone separator for recovery of fines was attached to the top of the column. Glass containers were placed below this cyclone to collect the fines carried out from the column. A piece of filter cloth placed between the column and the base served as the gas distributor. A pressure tap at the base of the column connected to a manometer was used to indicate the gas pressure as it entered the column. The air used for elutriation of the fines was metered through a rotameter before entering the column.

Materials

Scotchlite glass beads and bituminous coal powder were the solids; air and helium were the gases used. The sizes of glass beads used were 0.0028, 0.0039, 0.0058, and 0.0110 in. in diameter. The material had an absolute density of 156 lb./cu. ft. The coal powder had average particle sizes of 0.0281, 0.0141, 0.0053 and 0.0038 in. in diameter. The absolute density of the coal powder was 81 lb./cu. ft.

Procedure

The gas was introduced at a velocity well below the free-fall velocity of the smallest particle in the bed and was kept at this rate for several minutes to assure mixing of the various particle sizes of the bed. The gas rate was then adjusted until the desired velocity was obtained. The carry-over of fines was collected by the cyclone for a suitable time interval and then separated into the various particle sizes by means of screens.

Occasional examination of the solids under the microscope indicated that no appreciable attrition had occurred. The electrostatic charges which accumulate on the particles during the course of elutriation frequently hinder considerably the accuracy and reproducibility of the results. To minimize this effect, a ground wire was inserted into the fluidized bed in addition to the wiring of the entire column from outside for grounding. This was found satisfactory in obtaining the reproducible data.

Richard F. Hashinger is with E. I. du Pont de Nemours and Company, Inc., Old Hickory, Tennessee.

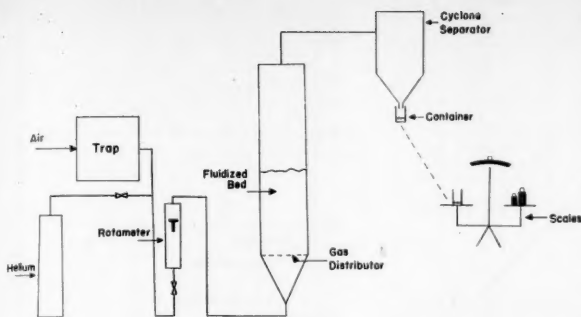


Fig. 1. Schematic diagram of equipment.

MECHANISM

In a fluidized bed of comparatively small diameter the solid particles move predominantly upward in the center of the column and considerably less vigorously downward near the vessel wall. In a large-diameter column, however, the pattern of flow is somewhat less well coordinated, and local vortices may prevail. At any rate the resulting fluidized bed is characterized by a turbulent bubbling surface similar to that of a boiling liquid. The elutriation of the fines from a bed composed of a size spectrum will occur only when the gas velocity above the bed exceeds the free-fall velocity of the fine particles. Since the actual local gas velocity in the bed is considerably higher than the superficial gas velocity, the gas bubbles carry with them the fines as well as coarse particles through the fluidizing bed. The kinetic energy of these particles moving through the bed can be ascribed to friction force and buoyancy force of the gas current and forces due to impact from the particles below. As the particles reach the surface of the bed, a sudden eruption of gas bubbles takes place, throwing particles up above the bed surface boundary. This sudden expansion of the gas reduces the gas velocity to below the free-fall terminal velocity of the coarse particles, causing the coarse particles to fall back into the bed. However the gas velocity is still larger than the free-fall velocity of the fines, and these will be carried out of the column. Thus above the bed Stokes's-law forces will prevail except in some instances when occasional collisions occur between the particles. In addition to the particle collisions, the development of a pronounced velocity gradient of the gas above the bed will also act to bring some fines situated near the column wall back into the bed. This effect can be seen from the velocity gradient of the gas above the bed as shown in Figure 2. The gas-velocity profiles immediately above the bed (A) and significantly farther above the bed

surface (B) are indicated in the figure. For a spherical particle traveling above the bed without collision, the particle velocity can be expressed as

$$u = (u_g - u_t)(1 - e^{-\alpha\theta}) + u_t e^{-\alpha\theta} \quad (1)$$

where α equals $18\mu/\rho_s D_p^2$. Since the value of $e^{-\alpha\theta}$ is very small, especially for small particles, $u \approx u_g - u_t$ and is practically independent of time. Accordingly, as the velocity gradient becomes progressively developed, the fine particles along the wall will be subjected to low-velocity gas and thus fall back into the bed while the particles in the center are being elutriated. A certain height is required for the gas to develop the velocity gradient fully. This height, called *critical height*, will be discussed later in some detail.

Since the rate of stratification of fine particles is considerably greater than that of coarse particles, accumulation of the fines on the surface of the bed will occur until a concentration gradient is

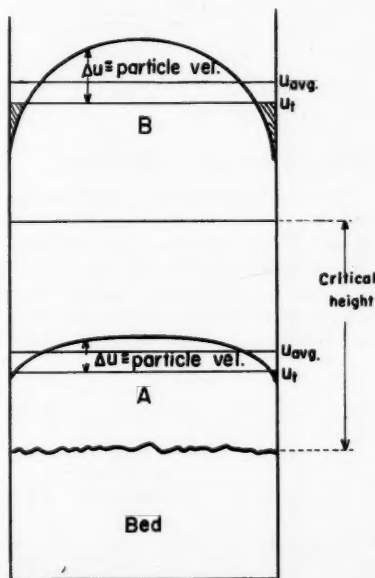


Fig. 2. Velocity distribution of gas above bed.

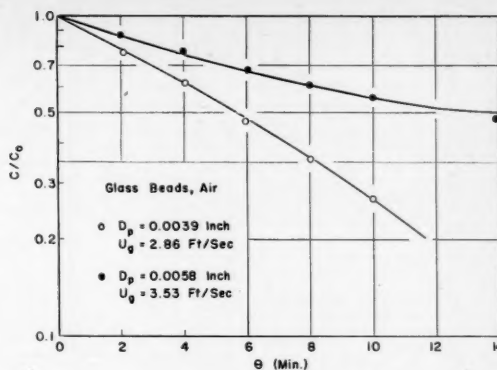


Fig. 3. Fines concentration vs. time.

reached throughout the bed with a maximum accumulation of the fines at the surface. Therefore during the elutriation the rate of fines thrown up above the bed as a result of eruption of gas bubbles will depend greatly on the population of the fines on the bed surface. Leva (5) employed a first-order rate equation to describe the rate of elutriation. If C is the concentration of the fines in the bed at any time, then

$$\frac{dC}{d\theta} = -kC \quad (2)$$

where k is a proportionality constant and is designated the elutriation constant. As the elutriation progresses, a reduction in fines population takes place which is in turn partially made up by the fines stratified from below. A plot of C/C_0 vs. θ , as shown in Figure 3, indicates that this relationship tends to deviate from linearity at large values of θ . This is due to the fact that the bed height is continually decreasing, and therefore the time of stratification required for the fine particles through the bed interior to the surface will be decreasing. At the same time the fines concentration is also decreasing, which may increase elutriation time. The curve in Figure 3 therefore can be either concave upward or downward, depending on the operating conditions. Thus when the amount of elutriation becomes appreciable, the line shows a substantial curvature. Since the effective time of stratification of the fines particles is governed by the height of the bed on one hand and the simultaneous decrease of fines concentration on the other, the effect of the bed height on the value of k cannot be accurately evaluated from Figure 3 unless the fines concentration is maintained constant throughout the operation. Consequently the change in fines concentration in the bed should be considered to be proportional to fines concentration and inversely proportional to the bed height through which the

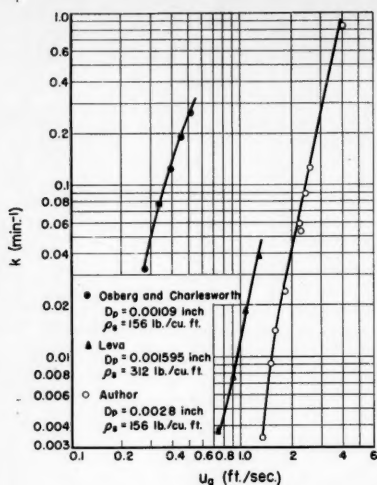


Fig. 4. Effect of linear gas velocity on elutriation constant.

fine particles must travel in order to emerge to the surface. For convenience in measurement the bed weight will be used instead of the bed height for the expression of the rate of elutriation. If A is the bed cross-sectional area, it follows that

$$\frac{dC}{d\theta} = -K \frac{A}{W} C \quad (3)$$

where K is a proportionality constant and has the unit of pounds per square foot per second. Yagi and Aoji (12) employed the same equation and attempted a correlation by means of a dimensionless empirical equation.

DIMENSIONAL ANALYSIS

Since the rate of elutriation is affected by the solid-particle characteristics, the gas properties, and the particle velocity above the bed, a dimensional analysis may be applied:

$$K = f[D_p, u_i, (u_g - u_i), \rho_g, (\rho_s - \rho_g), \mu, g] \quad (4)$$

The resulting equation is

$$\frac{K}{\rho_g(u_g - u_i)} = \beta \left[\frac{(u_g - u_i)^2}{g D_p} \right]^a \left[\frac{D_p u_i \rho_g}{\mu} \right]^b \left[\frac{\rho_s - \rho_g}{\rho_g} \right]^c \left[\frac{u_g - u_i}{u_i} \right]^d \quad (5)$$

The examination of the experimental data indicated that the power of $[(u_g - u_i)/u_i]$ was negligible, and the group was eliminated.

In all the free-fall terminal-velocity calculations Stokes's law or a modification of it was used. For particles with a Reynolds number less than 2 Stokes's law is applicable:

$$u_i = \frac{g D_p^2 (\rho_s - \rho_g)}{18\mu} \quad (6)$$

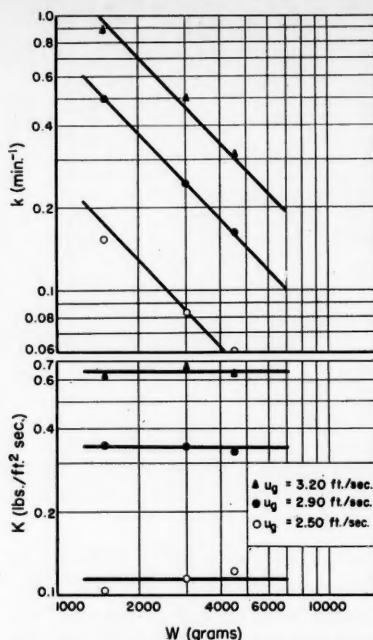


Fig. 5a. Effect of bed weight on elutriation constant and specific elutriation constant.

A correction-factor chart (8) was used with Stokes's law to correct for deviation as the particle size increased.

For Reynolds numbers larger than 2 a modified Stokes's equation is applicable:

$$u_i = \frac{0.153 g^{0.71} D_p^{1.14} (\rho_s - \rho_g)^{0.71}}{\rho_g^{0.29} \mu^{0.43}} \quad (7)$$

A correction was made for nonspherical particles according to the following equation (9):

$$Y = 0.843 \log \left(\frac{\phi}{0.065} \right) \quad (8)$$

The calculated value of the free-fall terminal velocity is multiplied by Y to make the correction.

CORRELATION AND DISCUSSION

The variables affecting the elutriation-rate constant can be classified into three general groups: gas variables (gas velocity, gas density, gas viscosity), bed variables (fine particle size, solid particle density, bed height, fines concentration, coarse particle size),

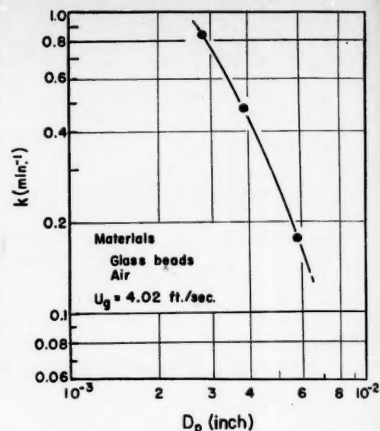


Fig. 5b. Effect of particle size on elutriation constant.

and column variables (column diameter, freeboard, baffling).

Gas Velocity

A significant effect of gas velocity on the value of the elutriation constant can be observed from Figure 4. The data of different investigators show that $k \propto u_g^{1.0-7.0}$. As indicated previously, the major factor affecting the rate of elutriation is the difference between the magnitude of the gas velocity and the particle free-fall terminal velocity, $(u_g - u_i)$. When the linear gas velocity is lower than the particle free-fall terminal velocity, the gas carries only a negligible amount of fines from the column; although the impact from below, induced by collisions with other particles, may throw up some particles above the bed, they will in due course fall back into the bed. However when the gas velocity exceeds the fine-particle terminal velocity, the gas stream will remove a significant number of particles from the column. If on the other hand the gas velocity is larger than the terminal velocity of one of the fine particle sizes in a multiparticle size system but lower than the terminal velocity of a second fine size, a significant amount of the smaller size alone will be removed from the bed. If the gas velocity is increased above the terminal velocity of the second fine particle size, a considerable amount of both sizes will be removed. Below is shown a typical run

Table 1

D_p , in.	Initial weight of particles, g.	u_i , ft./sec.	Grams of fines removed in 1 min.		
			$u_g = 1.45$ ft./sec.	$u_g = 2.21$	$u_g = 4.02$
0.0028	450	1.07	2.47	25.8	207
0.0039	450	1.88	0	4.45	145
0.0058	450	2.92	0	0	74.1
0.0110	4050	—	0	0	0

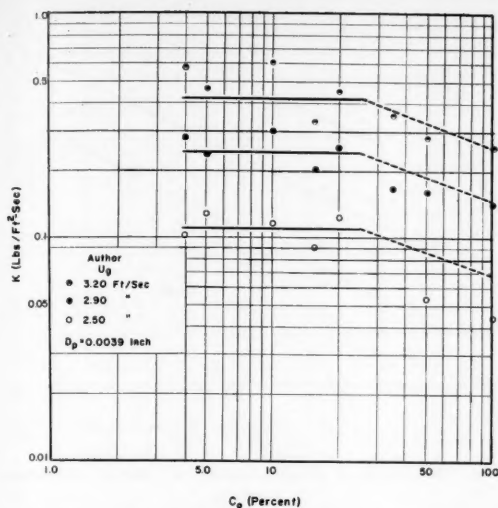


Fig. 6. Effect of fines concentration on the specific elutriation constant.

for a four-particle size system (Table 1).⁶ From this chart one observes that a considerable amount of fines was collected for those fines having a terminal velocity below the linear gas velocity and negligible amount for those fines having a terminal velocity above the gas velocity.

The velocity distribution in fully developed flow of the gas above the bed is shown in Figure 2. The velocity in the middle of the column of the gas reaches a maximum value of 1.25-2.0 times the average velocity. Near this region of maximum velocity the actual gas velocity might be larger than the terminal velocity of the coarse particle sizes, and therefore it is possible to remove a small amount of the coarse particles even though the average gas velocity is smaller than the terminal velocity of the particle.

Bed Weight

The elutriation constant for a given size column is shown to be inversely proportional to the bed weight in Figure 5a, where k is plotted against the bed weight at constant velocity. The concentration of fines is kept constant by taking the initial slope of the C/C_o vs. θ plot for different heights.

During elutriation of fine particles from a fluidized bed a concentration gradient is formed in the bed with the largest concentration of the fines found near the surface of the bed. The fine particles must travel to the surface of the bed before they can be removed, and the time of travel of the fines will be increased as the bed weight is in-

creased. An increase in the travel time of the fines will reduce the concentration gradient in the bed, and this will decrease the value of the elutriation constant.

In the same figure the specific elutriation constant is plotted against the bed weight for comparison. A negligible effect of bed weight is seen on K . Knowing the value of K , one can derive an equation to calculate the amount of fines removed from a bed in a specified time.

Fine Particle Size and Concentration

For a given gas rate the elutriation rates were observed to increase markedly with decreasing fines diameter. The value of k thus decreases sharply as fine size is increased, as illustrated in Figure 5b. This is due to the fact that the terminal velocity of the fine particles increases with increasing particle size, thereby reducing the driving force. The increase in fine-particle density will also cause a similar result.

The effect of fines concentration in a two-particle size system is shown in Figures 6 and 7, where the specific elutriation constant is plotted against the fines concentration in the bed. The

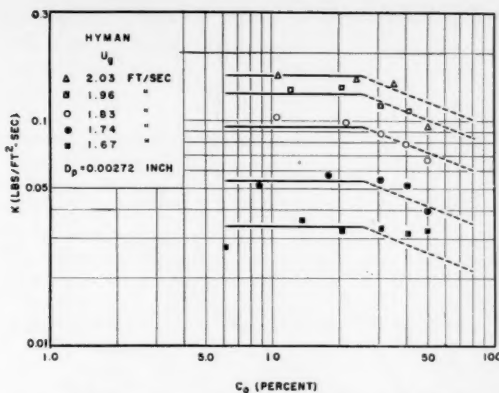


Fig. 7. Effect of fines concentration on the specific elutriation constant.

fines concentration has a small effect on the modified elutriation constant until a concentration of approximately 25% is used, and then the value of the modified elutriation constant seems to decrease as the fines concentration increases. The ratio of individual values of K to the average value obtained from Figures 6 and 7 was plotted in Figure 8. Although the trend is indicated, a further investigation is desirable to substantiate the variation of specific elutriation constant with respect to fines concentration.

In a multiparticle size system the effect of fines concentration can be considered to be similar to that for a two-particle size system because the correlation of the multiparticle size-system data showed that each of the fine components, when considered with coarse size as a two-particle size system, retained their individuality and acted as a two-particle size system. Therefore as long as the composition of each of the fine-particle sizes, when considered with the coarse-particle size, remains below 25%, the presence of the third particle size has no bearing on the rate of elutriation of that particular individual fine-particle size. This is analogous to Henry's law for the vapor pressure of a dilute solution.

Leva (5) found that the concentration of the fines had no effect on the

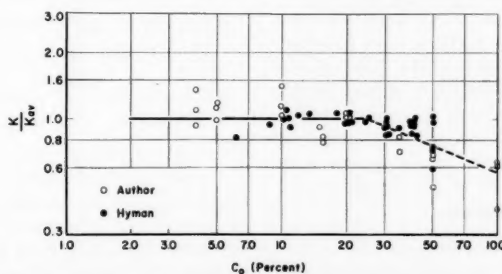


Fig. 8. Effect of fines concentration on the specific elutriation constant.

* Tabular material has been deposited as document No. 6259 with the American Documentation Institute, Photoduplication Service, Library of Congress, Washington 25, D. C., and may be obtained for \$1.25 for photoprints or for 35-mm microfilm.

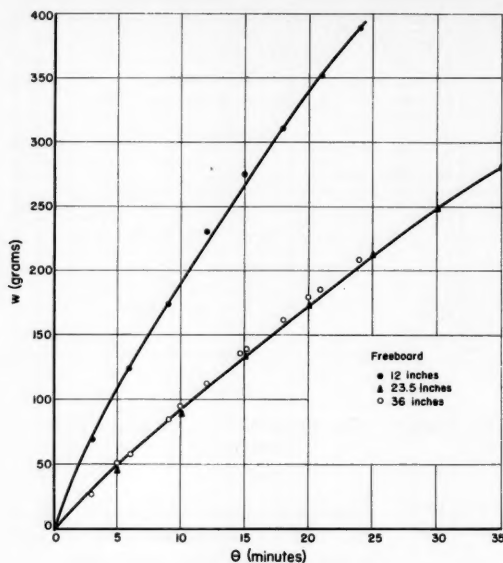


Fig. 9. Effect of freeboard on weight of fines collected.

value of the elutriation constant from 20 down to 5%, whereas Osberg and Charlesworth (7) noted a significant effect from 5 down to a few tenths %. No significant change on elutriation constant was observed as low as 4% of fines concentration in this investigation.

Based on Figure 8 a correction can be made to estimate roughly the value of K when fines concentration is above 25% with C_o expressed in percentages:

$$K_{>25\%} = K_{<25\%} \left(\frac{C_o}{25} \right)^{-0.48} \quad (9)$$

Freeboard

Freeboard is the distance between the expanded bed and the bed outlet. In Figure 9 the influence of freeboard on the weight of fines removed from a bed is shown. Three different heights, 12, 23.5, and 36 in., were used. The 12-in. height shows a definite increase in the amount of fines collected compared with the 23.5- and 36-in. heights, while equal amounts of fines were collected at the 23.5- and 36-in. heights. It can be seen that there is a critical height above the expanded bed, where the weight of fines collected remains constant. Similar findings were reported by Jolley and Stantan (3). The critical height can be estimated if the length of the column above the bed required to fully develop the gas flow profile is found. No attempt has been made to relate the location of this height to the other system variables.

Coarse-Particle Size

The effect of the coarse-particle size on the value of the elutriation constant was found to be insignificant. Leva (5)

concluded that coarse-particle size had a negligible effect on the elutriation constant. Osberg and Charlesworth (7) found that only below a fines concentration of 1% did the coarse-particle size have an effect on the elutriation constant.

Generalized Correlation

Figures 10, 11, and 12 are those used for the evaluation of the constants in the generalized equation. The results of the correlation indicated that the power of the Froude number, $(u_g - u_t)^2 / gD_p$, was 0.5; the Reynolds number, $D_p u_t \rho_g / \mu$, was 0.725; and the $(\rho_s - \rho_g) / \rho_g$ group was 1.15. Figure 12 is the final generalized plot including all the data taken in this investigation and the data of Leva (5), Hyman (2), and Yagi and Aoji (12). For fines concentration below 25% the final equation obtained is

$$\frac{K}{\rho_g(u_g - u_t)} = 1.52 \times 10^{-5} \left[\frac{(u_g - u_t)^2}{gD_p} \right]^{0.5} \left[\frac{D_p u_t \rho_g}{\mu} \right]^{0.725} \left[\frac{\rho_s - \rho_g}{\rho_g} \right]^{1.15} \quad (10)$$

where the limits of operation are

$$\begin{aligned} 0.001595 \text{ in.} < D_p < 0.0058 \text{ in.} \\ 0.0103 \text{ lb./cu. ft.} < \rho_g < 0.075 \text{ lb./cu. ft.} \\ 81 \text{ lb./cu. ft.} < \rho_s < 312 \text{ lb./cu. ft.} \\ 0.725 \text{ ft./sec.} < u_g < 4.33 \text{ ft./sec.} \end{aligned}$$

The data of Osberg and Charlesworth (7) were not included in this correlation because of the extremely small particle diameter (approximately 0.00102 in.) and the small fines concentration (below 1%) used. When a fluidized bed is operated at a low velocity, as was the case for Osberg and Charles-

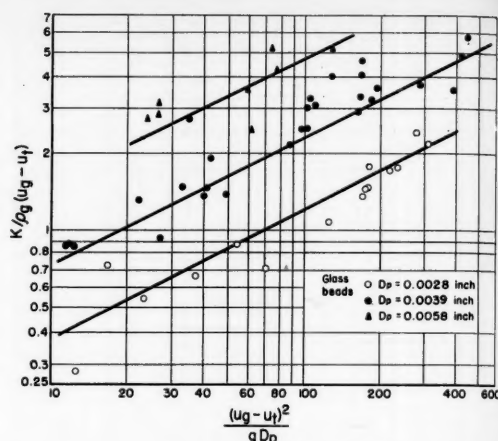


Fig. 10. Effect of Froude number on specific elutriation constant.

worth, there is a tendency for the gas to channel through the bed. The considerable effect of channeling and slugging on the rate of elutriation is evident from a comparison of the value of k operating a fluidized bed with and without a baffle. During the collection of the data for the 2-in. column, slugging was noticed, and a baffle was placed in the column to reduce the influence of slugging on the rate of elutriation. Screens with openings of 5 mesh and spaced approximately 5 in. apart were used as the baffle. The values of the elutriation constant obtained for a 1,500-g and a 1,000-g bed operated with and without the baffle are compared in Figure 13. In the 1,000-g. bed the use of the baffle had no effect on the value of k ; in the 1,500-g. bed the baffle increased the value of k . During the operation of the 1,000-g. bed there was insufficient slugging for the baffle to have any effect on the value of the elutriation constant.

The fines concentration used by Osberg and Charlesworth was of such magnitude that if an error were involved in the evaluation of the initial concentration, a much larger error in the value of the elutriation constant would result. If a larger fines concentration is utilized, an error of similar magnitude will have less effect on the value of k .

Lang (4) and Richards (10) reported elutriation of single-particle size system. The data reported by Lang (4) for single-particle size system are compared with two-particle size system of the present investigation in Figure 14. In spite of good agreement, the mechanism of the elutriation for a single-particle size system should be regarded as entirely different from that of multiparticle size system. In a single-particle size system, in order for the particles to be elutriated from the bed,

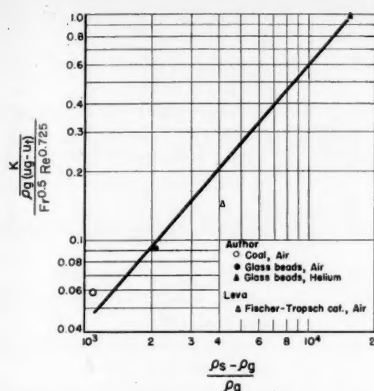


Fig. 11. Effect of solid and gas density on specific elutriation constant.

the gas velocity must be larger than the terminal falling velocity of the particle, and therefore a considerably large expansion of the bed will result. It has been known that the particle movement and the flow patterns for an excessively expanded bed, known as *dilute-phase fluidization*, are quite different from those of dense-phase fluidization. Since the fines concentration is relatively small for the multiparticle size system in the present investigation, the status of fluidization is essentially that of dense phase.

A potential source of experimental error which is frequently encountered in elutriation is an accumulation of an electric charge on the particles in the bed. When the particles become charged, they adhere to the equipment and reduce the accuracy of the work.

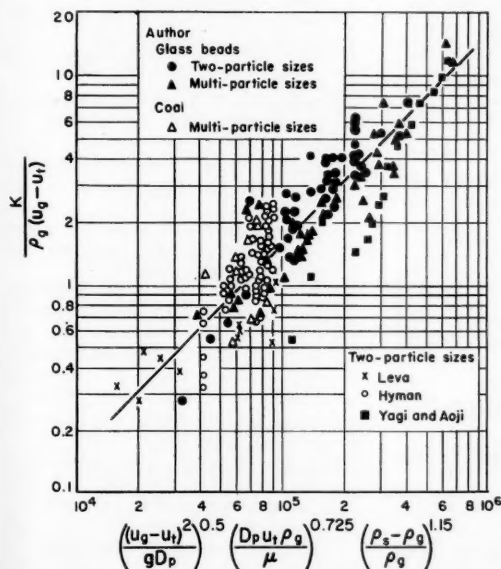


Fig. 12. Generalized plot of proposed correlation.

The smaller the particle, the greater the charge it will accumulate; since the particles employed by Osberg and Charlesworth were small, a static charge on them might have influenced the results. The column was grounded by wrapping the lead wires around the column and also introducing a ground wire into the moving fluidized particles. When the electrostatic charge was sufficiently eliminated from the column, reproducible data were obtained. A good electric conductor may be used as the fluidizing solids to reduce this effect further.

Column Diameter

The effect of column diameter was studied, and the results are shown in Figure 15, where

$$\frac{K}{\rho_g(u_g - u_t)} \left(\frac{\rho_g}{\rho_s - \rho_g} \right)^{1.15} \left[\frac{(u_g - u_t)^2}{gD_p} \right]^{0.5} \left(\frac{D_p u_t \rho_g}{\mu} \right)^{0.725}$$

is plotted against the column diameter. Each point on the plot represents an average of the above group for the corresponding column diameters. The work of Leva (5) in a 1.32-in.-diameter column, of this investigation in a 2- and 4-in. column, and of Hyman (2) in a 3-in. column are included on this plot. The dotted line represents the approximate trend of the column-diameter effect observed by Lang (4). More data on larger diameter columns are necessary to make conclusive statements for the effect of column diameter. It is believed that column diameter will have only small effect on the value of

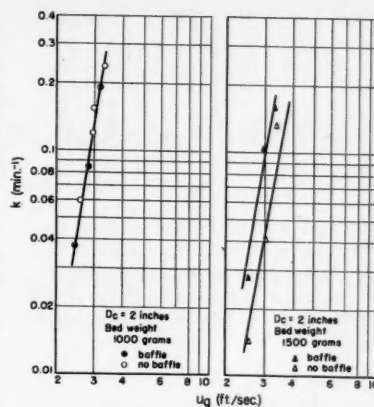


Fig. 13. Effect of a baffle on the elutriation constant.

the elutriation constant when the diameter of the column is large and whenever channeling and slugging can be eliminated.

APPLICATION

To use the new correlation one must be able to evaluate the value of K from the operating conditions and the bed variables. With the value of K known, an equation can be derived to calculate the amount of each size of fine particles elutriated for a specified length of time:

$$C = \frac{w_o - w}{W_i - w}$$

$$\frac{dC}{d\theta} = \frac{w_o - W_i}{(W_i - w)^2} \frac{dw}{d\theta} = -k \frac{w_o - w}{W_i - w}$$

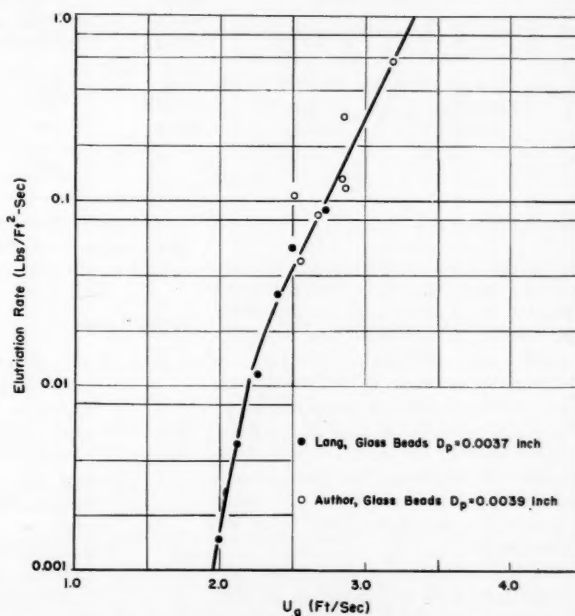


Fig. 14. Comparison of rate of elutriation for single particle size system.

Since $k = K A/W_i - w$

$$\frac{w_o - W_i}{(W_i - w)^2} \frac{dw}{d\theta} = -\frac{KA(w_o - w)}{(W_i - w)^2}$$

$$(w_o - W_i) \int_0^w \frac{dw}{(w_o - w)} = -KA \int_0^w d\theta$$

$$w = w_o [1 - \exp KA\theta / (w_o - W_i)] \quad (11)$$

For a multiparticle size system W_i is the weight of coarse particles and the weight of those fines in question.

The following example illustrates the application of the developed correlation.

Example

A four-particle size system of glass beads is to be elutriated for 2 min. with air at 70°F. and 1 atm. pressure. Compute the grams of each fine-particle size which will be carried out from the column.

$D_p = 0.0028, 0.0039, 0.0058$ in.
Weight of the coarse particles ($D_p = 0.0110$ in.) = 4,050 g.
Concentration of each fine size = 10% or 450 g.
 $u_g = 4.02$ ft./sec.

D column = 4 in.

$\rho_s = 156$ lb./cu. ft.

Solution

The terminal falling velocities of the fines are calculated by the use of Equations (6), (7), and (8). The values of K are evaluated from Equation (10). From Equation (11) the weight of fines elutriated can be calculated for each particle size:

D_p , in.	u_t , ft./sec.	K , lb./ (sq. ft.) (sec.)	Weight actually removed, g.	Weight calculated, g.
0.0028	1.07	1.061	414	320
0.0039	1.88	0.933	291	298
0.0058	2.92	0.354	148	153
			853	771

CONCLUSIONS

A generalized correlation for evaluation of the specific elutriation-rate constant in a two- and multiparticle size system is proposed. In a multiparticle size elutriation the rate of entrainment of each individual-size of fines is independent of the presence of other size particles if that fine size is considered with the coarse size as two-particle size systems. The final dimensionless equation obtained for fines concentration less than 25% is given by Equation (10).

For the fines concentration above approximately 25% a correction should be made.

The variables affecting the elutria-

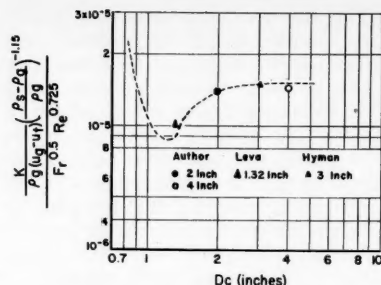


Fig. 15. Effect of column diameter.

tion constant are studied, and it is concluded that

1. The difference between the magnitude of the linear gas velocity and particle terminal velocity is the major factor influencing the value of the elutriation constant.

2. For large-diameter columns the bed dimensions and the coarse-particle size have a negligible effect on the value of the specific elutriation constant.

3. In a two-particle size system the initial fines concentration seems to have no effect on the elutriation constant until a concentration of approximately 25% is reached; above 25% the constant tends to decrease as the concentration increases.

4. Freeboard has an influence on the rate of elutriation only when the bed outlet is located below a certain height above the expanded bed.

5. The elutriation constant varies with the gas velocity approximately to the 7.0 power and inversely with the

- k = elutriation-rate constant ($1/\theta$)
- K = specific elutriation-rate constant ($M/\theta L^2$)
- K_{avg} = average value of $K(M/\theta L^2)$
- u_g = linear gas velocity (L/θ)
- u_o = initial velocity of the particle at the surface of the bed (L/θ)
- u_t = particle terminal velocity (L/θ)
- W = weight of the bed (M)
- w_o = initial weight of the fines in the bed (M)
- w = weight of the fines elutriated from the bed (M)
- W_i = total bed weight considered as two-particle system (M)

Greek Letters

- β = constant to be evaluated from experimental results, Equation (5).
- ρ_g = gas density (M/L^3)
- ρ_s = solid absolute density (M/L^3)
- θ = time (θ)
- ϕ = particle shape factor defined as area of a sphere divided by area of particle shape having same volume as sphere
- μ = gas viscosity ($M/L\theta$)

$$\frac{(u_g - u_t)^2}{gD_p} = \text{Froude number (Fr)}$$

$$\frac{D_p u_t \rho_s}{\mu} = \text{Reynolds number (Re)}$$

LITERATURE CITED

- Andrews, J. M., unpublished paper, Humble Oil and Refining Co., Baytown, Texas, (1957).
- Hyman, D., Master's thesis, Mass. Inst. Technol., Cambridge (1952).
- Jolley, L. J., and J. E. Stanton, *J. Appl. Chem. (London)*, **2**, Suppl. Issue 1, 562-568 (1952).
- Lang, P. M., Ph.D. thesis, Mass. Inst. Technol., Cambridge (1955).
- Leva, Max, *Chem. Eng. Progr.*, **47**, 39 (1951).
- Matheson, G. L., W. A. Herbst, and P. H. Holt, *Ind. Eng. Chem.*, **41**, 1099 (1949).
- Osberg, G. L., and D. H. Charlesworth, *Chem. Eng. Progr.*, **47**, 566 (1951).
- Perry, John H., "Chemical Engineers Handbook," pp. 1017-1021, McGraw-Hill, New York (1950).
- Pettyjohn, E. S., and E. B. Christensen, *Chem. Eng. Progr.*, **44**, 157 (1948).
- Richards, R. L., Jr., Ph.D. thesis, Mass. Inst. Technol., Cambridge (1955).
- Trawinski, H., *Chem. Ing. Tech.*, **25** (4), 201 (1953).
- Yagi and Aoji, paper presented at the Society of Chemical Engineers (Japan), Spring Meeting (1955).
- Zenz, F. A., and N. A. Weil, *A.I.Ch.E. Journal*, **4**, 472 (1958).

Manuscript received June 23, 1958; revision received September 17, 1959; paper accepted September 18, 1959.

Mass Transfer from a Solid Soluble Sphere to a Flowing Liquid Stream

ROBERT L. STEINBERGER and ROBERT E. TREYBAL

New York University, New York 53, New York

Solution rates of 1/2-, 3/4-, and 1-in. cast benzoic acid spheres were measured under natural- and forced-convection conditions. Upward-flowing streams of water and aqueous propylene glycol, in laminar and turbulent flow, were used to contact single spheres in either a 1.50- or 4.00-in.-diameter column. Sphere Reynolds numbers ranged from 10 to 16,920; Schmidt numbers from 987 to 69,680; sphere- to column-diameter ratios, d_s/d_c , from 0.123 to 0.497; and Grashof numbers from 5,130 to 125,200.

The Sherwood number was found independent of the laminar-turbulent transition for pipe flow and the sphere- to column-diameter ratio when the Reynolds number is based on the average fluid velocity and sphere diameter.

A correlation of the data based on the additivity of the natural and forced convection processes is proposed, and statistical analyses of the new experimental data result in equations which correlate other heat and mass transfer data for single spheres immersed in bounded and free-jet streams of gases and liquids for $N_{Re, s}$ from 1 to 30,000 and N_{Sc} from 0.6 to 3,000, within an average deviation of about 20%.

Dimensional analysis has been applied to problems involving the transfer of mass and heat from bodies immersed in fluid streams. In the case of a single sphere the results are

$$N_{Sh} = N_{Sh}(N_{Re}, N_{Sc}, N_{Gr}) \quad (1)$$

$$N_{Nu} = N_{Nu}(N_{Re}, N_{Pr}, N_{Gr}) \quad (2)$$

The actual form of the functions are not obtainable by dimensional analysis techniques, and resort must therefore be made to theory or experiment. The terms involved in Equations (1) and (2) are the result of a consideration of radial diffusion and natural and forced convection, the processes by which mass or heat may be transferred from from a sphere.

The first process, by radial diffusion, arises when $N_{Gr} = 0$ and $N_{Re} = 0$. Natural-convective transport arises when $N_{Gr} > 0$, and forced convection occurs when $N_{Re} > 0$. In an actual transport problem the above processes may act singly or in concert, depending upon the flow and diffusional characteristics of the system.

RADIAL DIFFUSION

The process of radial diffusion from a sphere to an infinite stagnant fluid has been treated theoretically by Langmuir (24), who shows that

$$N_{Sh,0} = N_{Nu,0} = 2 \quad (3)$$

Equation (3) has been verified experimentally with drops of relatively low-volatility liquids and solids vaporizing into low-temperature surroundings at near-atmospheric pressures (14, 25, 26, 38, 42).

In the case of air streams flowing past evaporating droplets a value of $N_{Sh,0}$ approaching 2 was observed as the Reynolds number was lowered to zero (5, 33); however in the case of liquid streams dissolving soluble spheres $N_{Sh,0}$ values from 44 to 100 have been observed which have been attributed to the influence of natural convection (6, 7).

NATURAL CONVECTION

Transfer by natural convection is attributed to a current of fluid flowing past a body because of a difference between the bulk and surface fluid densities resulting from concentration differences for the mass transfer problem and because of temperature differences in the case of heat transfer.

An approximate solution of boundary-layer equations is given by Merk and Prins (29) for the forward stagnation point of a sphere:

$$N_{Nu,0} = 0.597 (N_{Gr} N_{Pr})^{1/4} \quad (4)$$

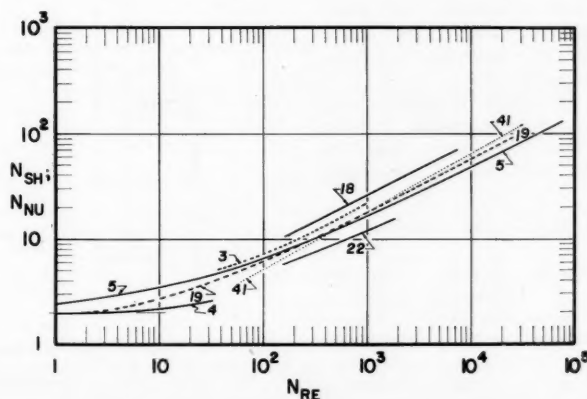


Fig. 1. Transfer from spheres ($N_{Sc} \approx N_{Pr} = 0.6$).

Robert L. Steinberger is with The Cooper Union, New York, New York.

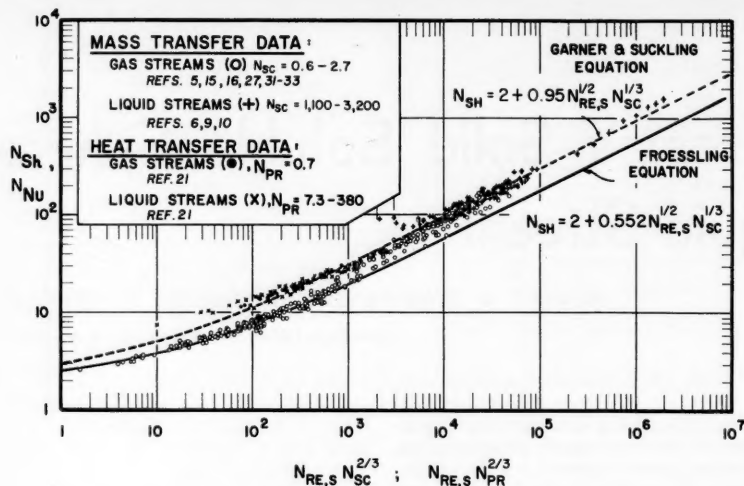


Fig. 2. Mass and heat transfer data for spheres.

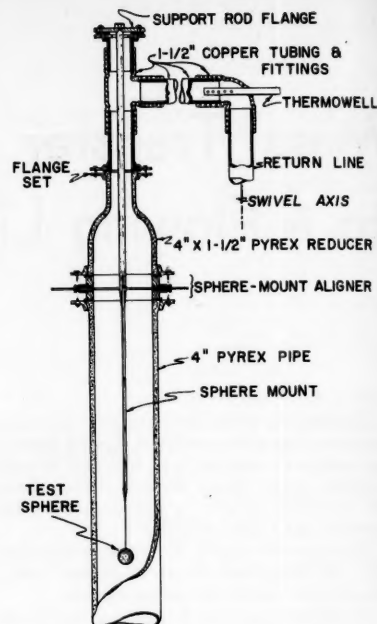


Fig. 3. Details of test section.

which is limited to laminar boundary-layer flow, that is $(N_{Gr}N_{Pr})$ less than 10^5 and N_{Pr} greater than 10. At present no analytical solutions are available for the entire surface of a sphere for either laminar or turbulent boundary-layer flow. Nusselt (30) indicates that $N_{Nu,0}$ may be related to $(N_{Gr}N_{Pr}^2)$ for fully turbulent boundary-layer flow, but no data are available.

Piret and co-workers (23, 28), working with heat and mass transfer from solid spheres to gases, propose

$$N_{Sh,0} = 2 + 0.5 (N_{Gr}N_{Sc})^{0.25} \quad (5)$$

for $(N_{Gr}N_{Sc})$ from 10^2 to 10^6 and somewhat similar expressions for heat transfer.

FORCED CONVECTION

Several analytical expressions have been developed by considering the hydrodynamics and diffusional characteristics for a sphere. A completely rigorous expression is not yet available. The problem is confounded by the development of flow separation and wake formation on the rear surface of a sphere even for Reynolds numbers, $N_{Re,s}$, as low as 20 (6).

Several analytical attempts have been made to characterize transfer rates. Potential-flow theory leads to functions for Equation (1) involving

$N_{Pr}^{1/2}$ (18, 19, 20), while boundary-layer theory involves $N_{Re}^{1/2}N_{Sc}^{1/3}$ (5, 7) or more complex functions (4). These relations are summarized in Figure 1 for the special case of $N_{Sc} = N_{Pr} = 0.6$.

Froessling (5) measured evaporation rates of spheres into air and correlated his data with a semiempirical equation:

$$N_{Sh} = 2 + 0.552 N_{Re,s}^{1/2} N_{Sc}^{1/3} \quad (6)$$

Others have correlated similar data by expressions of the same form (13, 16, 32, 33, 37, 39, 40, 41). The coefficients recommended range from 0.33 to 1.5 with exponents of the Reynolds number from 0.35 to 0.6. In some cases the radial diffusion term $N_{Sh,0} = 2$ of Equation (6) has been omitted; in others velocities other than the ap-

proach velocity have been used. These experiments cover the range of N_{Sc} from 0.6 to 2.7 and $N_{Re,M}$ from 0 to 48,000. Ingebo (17), working at temperatures up to 1,000°F., found it necessary to change the form of Equation (6) considerably. An excellent summary of atomization and evaporation of liquid fuels is presented by Graves and Bahr (12).

Liquid systems have received little attention. All work has involved the dissolution of benzoic and adipic acid spheres mounted in water streams flowing in either horizontal or vertical pipes. Gates and Shanks (10) mounted

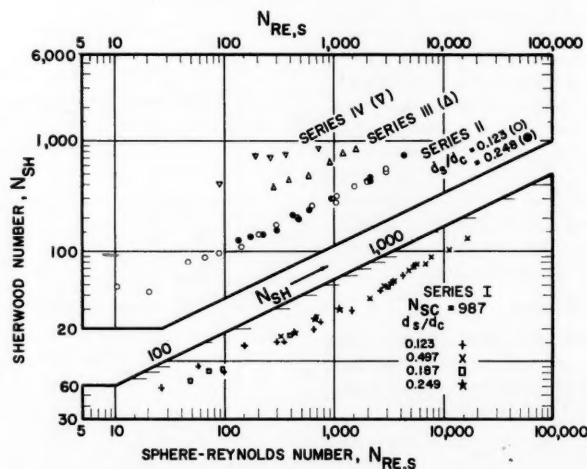


Fig. 4. Experimental data— N_{Sh} vs. $N_{Re,s}$.

TABLE 1. CAST SPHERE DIMENSIONS

Nominal size, in.	Number of spheres measured	Mean of average diameters, in.	Standard deviation from mean, in.
1/2	36	0.495	0.005
3/4	25	0.748	0.003
1	32	0.995	0.005

TABLE 2. RANGES OF PARAMETERS—FORCED-CONVECTION EXPERIMENTS

Series (N_{Re})	Subset	d_s/d_c	No. of runs	Reynolds number range $N_{Re,c}$	$N_{Re,s}$	($N_{Gr}N_{Sc}$) $\times 10^{-7}$
I (987)	A	0.123	11	218-35,400	26-4,340	1.50
	B	0.497	11	680-34,000	335-16,920	5.19
	C	0.187	5	264-16,400	49-3,060	5.23
	D	0.249	5	1,820-21,800	450-5,410	12.4
II (2,220)	A	0.123	18	84-24,640	10-3,000	1.14
	B	0.248	11	543-17,770	135-4,400	9.31
III (14,970)		0.185	6	1,510-8,610	280-1,600	12.5
IV (69,680)		0.247	5	371-2,970	92-733	94.5

cast spheres on shafts which were normal to the flow. The range of $N_{Re,s}$ was 1,500 to 11,000, with N_{Sc} approximately 3,000. Garner and Grafton (6) used pressed pellets mounted on the downstream side in a horizontal pipe. Local and over-all mass transfer rates were determined by taking photographs, which necessarily require that a substantial portion of the pellet be dissolved, thereby changing sphericity. Over-all rates were correlated by Garner and Grafton by

$$N_{Sh} = 44 + 0.48 N_{Re,s}^{1/2} N_{Sc}^{1/3} \quad (7)$$

where the limiting value of 44 was explained on the basis of natural convection.

Garner and Suckling (9), using the same apparatus and techniques and a variety of sphere sizes, gathered additional data and re-correlated the new and old results by replacing the 44 by 2 and the 0.48 by 0.95. Garner and Keey (7), using a vertical pipe, found a difference in rates depending upon

the direction of the liquid flow. Results are presented graphically. All of the Garner work is in the range of $N_{Re,s}$ from 2 to 840, N_{Sc} from 788 to 1,680, and laminar flow of the solvent stream.

Kramers (21) measured heat transfer rates from spheres to fluids in laminar flow and correlated the data with a modification of Equation (6) by using an additional N_{Pr} term.

In the case of spheres immersed in liquids flowing through pipes the sphere-to-column-diameter ratio, d_s/d_c , has been varied from 1/8 to 0.3 with no observable wall effect when the sphere-Reynolds number is used.

The data thus far available are exhibited in Figure 2. Two distinct belts of data are seen. The lower region, typified by Froessling's equation (6), contains most of the data for gas systems ($N_{Sc} = 0.6$ to 2.7). The liquid-system data ($N_{Sc} = 1,100$ to 3,200), exemplified by the equation of Garner and Suckling, give N_{Sh} values nearly twice those of the gas stream experi-

ments at the same value of $N_{Re,s}N_{Sc}^{2/3}$. No thorough experimental study of the effect of the Schmidt number has been made, and the effect of natural convection remains uncertain.

APPARATUS AND EXPERIMENTAL METHOD

In the present work spheres were cast from benzoic acid. After its dimensions and weight had been measured, a single sphere was mounted in a vertical, cylindrical test section of a flow apparatus. Solvent, flowing upward at constant temperature and flow rate, contacted the sphere for a measured time interval. Upon removing the sphere and reweighing when dry, one could determine the loss in weight.

Sphere Preparation

A length of 2-in.-diameter hot-rolled steel was faced in a lathe to a smooth finish. A round-end mill, mounted in the tailstock, was fed into the face of the rotating stock, thus forming a hemispherical depression. Drilling beyond the radial depth at a slow feed rate gave an extremely smooth finish to the cavity. To form a true hemisphere, face cuts were taken until depth-gauge measurements indicated radial depth of the cavity. The final facing was made to produce a smooth finish. The completed half mold was then cut from the stock. The other half of the mold was produced by repeating the entire procedure. To test for sphericity and to align the two halves, a steel ball bearing was placed in the spherical cavity formed by the molds. Remachining was done when necessary.

A sprue hole and support rod hole were drilled radially between the two clamped parts, the ball bearing serving to align the assembly. A thermocouple hole was

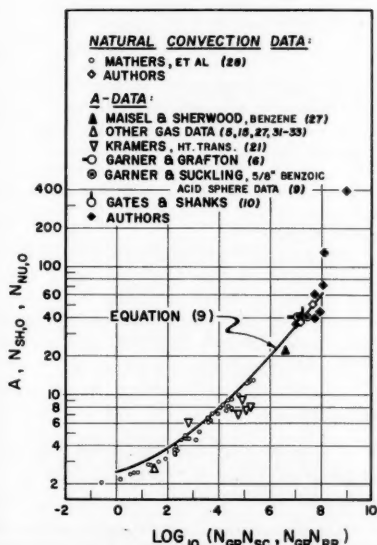


Fig. 5. Plot of $A = N_{Sh,0} = N_{Sh,0}$ vs. $(N_{Gr}N_{Sc}), (N_{Gr}N_{Pr})$.

TABLE 3. PHYSICAL PROPERTIES OF SOLUTIONS

Solubility

Benzoic acid in water (15.0° to 30.0°C.)

$$\log_{10} (C_s, \text{g./liter}) = 4.2066 \text{ to } 1.098/T$$

Benzoic acid in aqueous propylene glycol (15.0° to 25.0°C., $W = 40.0$ to 60.0 wt. % glycol on an acid-free basis):

$$\log_{10} (C_s, \text{g./liter}) = 6.898 + 0.0301(W-40) - 1.710/T$$

Kinematic viscosity

Aqueous propylene glycol solutions (15.0° to 25.0°C., $W = 40.0$ to 60.0 wt. % glycol on an acid-free basis):

$$\log_{10} (\nu, \text{centistokes}) = (26.86W + 463.4)/T - (1.6266 + 0.07467W)$$

Diffusion coefficient at 25.00 ± 0.005°C.

Benzoic acid,

in water:

$$D = (9.084 \pm 0.028)(10^{-6}) \text{ sq. cm./sec.}$$

in 40.0 wt. % propylene glycol:

$$D = (2.336 \pm 0.028)(10^{-6}) \text{ sq. cm./sec.}$$

in 60.0 wt. % propylene glycol:

$$D = (1.144 \pm 0.032)(10^{-6}) \text{ sq. cm./sec.}$$

Density

Benzoic acid-water solutions:

$$\log_{10} (\Delta\rho/C\rho_0) = 305/T - 1.745; \pm 10\%, \text{ max. in } \Delta\rho/\rho_0.$$

Benzoic acid in 40.0 wt. % propylene glycol, saturated, at 25.00°C.: $\Delta\rho/\rho_0 = 1.571 \times 10^{-3}$, $\pm 2.0\%$; $\rho_0 = 1.0293$.

Benzoic acid in 60.0 wt. % propylene glycol, saturated, at 25.00°C.: $\Delta\rho/\rho_0 = 5.052 \times 10^{-3}$, $\pm 2.7\%$; $\rho_0 = 1.0438$.

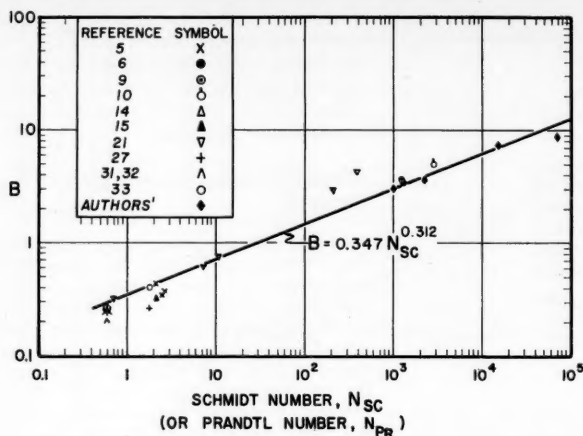


Fig. 6. Plot of B vs. N_{Sc} , N_{Pr} .

drilled behind the cavity. Molds for 1/2-, 3/4-, and 1-in. spheres were made.

A 4- to 6-in. length of 304 stainless steel rod 0.043 in. in diameter served as a support rod for each sphere. The rod, with a three-dimensional hook at the end to prevent its removal from the finished casting, was positioned between the mold halves. Spheres were then cast by charging the heated mold with molten benzoic acid. The cast spheres were inspected, excess sprue material was removed with a file, and the spheres were polished with a wad of absorbent cotton. The specimens thus obtained were shiny, white, nearly perfect spheres. Six micrometer measurements of diameter, to the nearest 0.0005 in., were taken at intervals on the equator. An average deviation of 0.002 in. from the mean was obtained for any one sphere. Table 1 shows the dimensions of the cast spheres prior to use in the mass transfer studies. The spheres were suspended in individual stoppered flasks containing Drierite by implanting their support rods into the face of the rubber stoppers.

Flow Apparatus

Fluid was circulated from a tank, through a heat exchanger and flow meters, and into the bottom of a test column, whence the solvent was returned to the tank. Pulsations were damped by a surge tank. The test columns were 15-ft. lengths of 1.50- and 4.00-in. I.D. Pyrex glass pipes. Inlet and exit temperatures at the test section were measured to indicate heat effects from the laboratory; the exit temperature, taken as that at the sphere, was measured to within 0.1°C.

Figure 3 shows the details of the method of mounting the test spheres in the 4-in. column. The swivel-pipe arrangement permitted connection to the 1.50-in. column. The tapered specimen mount had an over-all length of 32 in. and was composed of a 1/2-in. shaft axially connected to a 1/4-in. shaft. A 0.043-in.-diameter hole drilled into the end of the 1/4-in. shaft permitted the insertion of the test sphere support rod. A flange with slotted screw holes was bolted to the 1/2-in. shaft. The mount was streamlined by

turning a 5 deg. nose cone at one end of each shaft prior to assembly. The transitions were smoothed and polished with fine emery paper.

To align the sphere and mount at the center of the column and to provide stability during a run, another contact point was made. A 1.50-in. high, 4.00-in. I.D. by 5-in. O.D. Dural ring was flanged between the column and reducer. Three 1/4- by 5-in. brass slide rods in compression fittings, mounted 120 deg. apart in the midplane of the ring, centered the mount in the column. A similar tripod affair was made for the 1.50-in. column.

The above practices provided a stable, coaxial mounting for the test spheres. Disturbances in the flow pattern around the sphere were minor because the mount was streamlined and present on the downstream side of the test specimen. The sphere was located approximately 16 in. from the top of the cylindrical section, thus making a 13-2/3-ft.-long calming section available to the flowing solvent.

Procedure

Solvents used were water and aqueous propylene glycol solutions. The solvent level in the test column was lowered below the sphere position. A sphere, weighed to the nearest 0.05 mg. and measured to the nearest 0.0005 in., was mounted and the solvent circulation started. A stop watch was started when the rising solvent contacted the sphere. At the end of the test the site was drained rapidly and the sphere was removed and placed in its flask to dry. In the case of the glycol runs the spheres were vacuum washed five times with distilled water to remove the glycol. The washings were titrated for benzoic acid and the sphere was dried as for the water runs. The spheres were weighed during their drying periods.

Final sphere weights were not obtainable as such since the tested spheres never reached a final weight on drying. Sublimation of benzoic acid from the surface of the spheres took place continuously. Weight losses were plotted against time, and the resulting straight lines were extended to zero drying time to give the extrapolated weight losses due to solution.

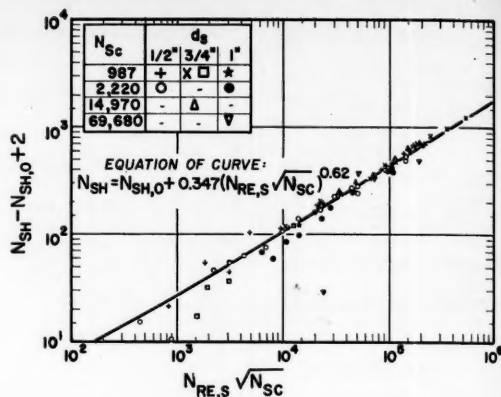


Fig. 7. Correlation of new experimental data.

The following represent the changes in the indicated quantities encountered in the forced convection experiments:

Sphere diameter: 0.012 in., maximum
Run temperature: $\pm 0.2^\circ\text{C}$., maximum
Flow rate: $\pm 1\%$ for water runs,
 $\pm 2\%$ for glycol runs

Average extrapolated weight losses were 58 mg. for the 1/2-in., 90 mg. for the 3/4-in., and 169 mg. for the 1-in. spheres. These weight changes are from 1.6 to 3% of the initial sphere weights and yield calculated diameter reductions of 0.5 to 1.6%. The ranges of operating conditions for the forced convection experiments are listed in Table 2.

Other Tests

The velocity distribution for water flowing in the 4.00-in. conduit was determined by pitot-static tube traverses. The velocity data indicate a distribution symmetrical about the column center line and agreed with the Nikuradse generalized velocity distribution (34) with a mean deviation of about 2%.

Two natural-convection experiments were performed. A 1 qt. Dewar flask was filled with water and allowed to stand for 8 hr. on a 1/4-in.-thick rubber pad to damp fluid circulations. A benzoic acid sphere was gently lowered into the stagnant fluid, a Lucite cover being used to support the sphere and a thermometer. The next day the sphere was gently removed from the flask, and the solution was mixed and titrated for its benzoic acid content.

The necessary physical properties of the benzoic acid solutions were measured, and the results are listed in Table 3. In the case of the diffusion coefficient the procedure of Gilliland, Baddour, and Goldstein (11) was used.

RESULTS

A summary of the computed results is given in Table 4^a; detailed data appear elsewhere (36).

^a Tabular material has been deposited as document 6264 with the American Documentation Institute, Photoduplication Service, Library of Congress, Washington 25, D. C., and may be obtained for \$1.25 for photoprints or \$1.25 for 35-mm microfilm.

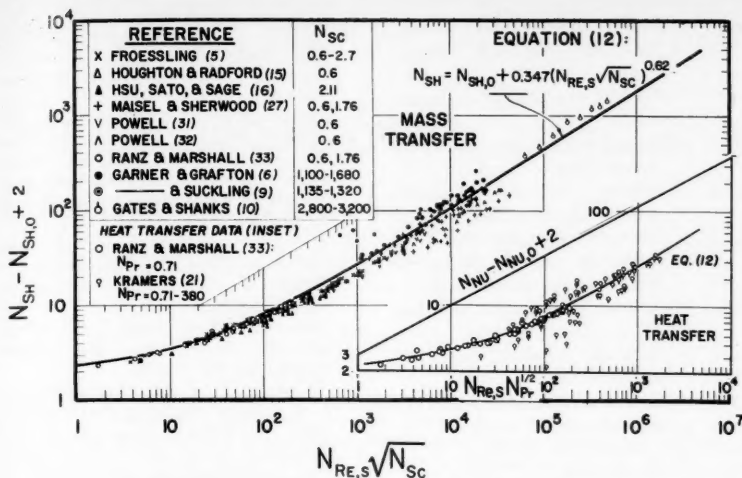


Fig. 8. Comparison of correlation equations with literature data.

Effect of Reynolds Number

The experimental data were first tested for dependence on flow rate by assuming the average fluid velocity in the pipe to be the correlating parameter. A plot of N_{sh} vs. $N_{Re,c}$ showed no effect of the laminar to turbulent transition for pipe flow. The data when plotted in this way showed a marked dependence on the ratio of the sphere-to-pipe diameter. This dependence disappeared, as shown in Figure 4, when the sphere-Reynolds number was used, and as a result subsequent correlations are based upon this. Reynolds numbers other than $N_{Re,s}$, based on d_s , were tried for correlating N_{sh} with N_{Re} . When the fluid velocity at the sphere axis (approach velocity), the average velocity intercepted by the projected sphere area, or the average velocity in the minimum flow area between the sphere and the column wall were used to calculate Reynolds numbers, the resulting N_{sh} vs. N_{Re} plots showed distinct separation according to d_s/d_c .

Proposed Correlation

It was possible to correlate the data by an expression of the form

$$N_{sh} = A + B(N_{Re,s})^n \quad (8)$$

The proposed-correlation equation predicts a value of $N_{sh,0} = A$ when $N_{Re,s} = 0$. This limiting case is significant since mass transport occurs by natural convection when $N_{Re} = 0$. The quantity A accounts for the curvature of the data plotted in Figure 4 and is taken to be a function of the Grashof and Schmidt moduli. At high $N_{Re,s}$ the forced-convection process predominates over the natural convection process, and N_{sh} becomes nearly equal to $B(N_{Re,s})^n$. The quantity B accounts for

the majority of the displacement between the data of series I, II, III, and IV at high $N_{Re,s}$ and is taken to be a function of N_{Re} . Equation (8) thus proposes the additivity of the natural- and forced-convection processes. Other interpretations of the natural- forced-convection phenomena are also possible as indicated by the recent theoretical paper of Acrivos (1). To extract the best value of A , B , and n from the experimental data, statistical analyses of the data were performed.

The forced-convection data of series I and II were applied to Equation (8), and statistical analyses of the data were performed. Since Equation (8) contains three unknowns, A , B , and n , and two knowns, values of n were assumed. The data for the various sphere sizes were pooled, and the criterion of least variance of the pooled estimate was used to find the best value of n .

With n taken as 0.5 or 0.7 the data should not be pooled with less than a 1% chance of being in error. For intermediate values of n the variance of the pooled estimate passed through a minimum at $n = 0.62$, and this value was therefore taken for further correlation. Correlation coefficients greater than 0.993 were obtained for the experimental data of series I, II, and III, indicating better than 99.9% confidence in Equation (8). A correlation coefficient of 0.811 for series IV indicated a 90 to 95% confidence in the equation. Values of A and B were then computed from the data with n taken as 0.62.

Least-square analyses were performed on the A data and $N_{sh,0}$ data by weighting the values of A and $N_{sh,0}$ according to the reciprocal of their variances to obtain A as a function of N_{Gr} and N_{Sc} . It was found necessary to

separate the data according to whether $(N_{Gr}N_{Sc})$ was less than or greater than 10^6 , probably because of the onset of a turbulent boundary layer in the higher range (8). For $(N_{Gr}N_{Sc})$ less than 10^6

$$A = N_{sh,0} = 2 + 0.569(N_{Gr}N_{Sc})^{(0.260)_2} \quad (9)$$

with an average deviation of the data of 12.7%, and for $(N_{Gr}N_{Sc})$ greater than 10^6

$$A = N_{sh,0} = 2 + 0.0254(N_{Gr}N_{Sc})^{1/3}(N_{Sc})^{0.244} \quad (10)$$

with an average deviation of 3.2%. The three points of series ID, III, and IV are the only data available for establishing Equation (10). In the case of Equation (9) a comparison of the equation, the new experimental data, and natural-convection mass transfer data (28) is shown in Figure 5. Also included are A values obtained from plots of N_{sh} (or N_{Nu}) vs. $N_{Re,s}^{0.62}$ with data used from the literature (5, 15, 16, 27, 31, 32, 33, 6, 9, 10, 21). The agreement is excellent.

Weighted least-square analyses were performed on the B data with the result that

$$B = 0.347 N_{Sc}^{0.312} \quad (11)$$

with an average deviation of 1.80%. It is interesting to note that the Colburn (2) exponent of 1/3 on the Schmidt number is included within one standard deviation (± 0.0204) of 0.312. The new B values, together with those determined from plots of N_{sh} (or N_{Nu}) vs. $N_{Re,s}^{0.62}$ with data used from the literature, are compared with Equation (11) in Figure 6. Again the agreement is excellent.

The final correlation is

$$N_{sh} = N_{sh,0} + 0.347(N_{Re,s}N_{Sc}^{1/2})^{0.62} \quad (12)$$

with $N_{sh,0}$ defined by Equations (9) and (10).

For purposes of graphical comparison of the experimental data and the correlation equations a logarithmic plot of $(N_{sh} - N_{sh,0} + 2)$ vs. $(N_{Re,s}N_{Sc}^{1/2})$ is proposed. This procedure reduces the experimental data to a natural-convection-free basis.

Equations (9) and (10) and the values of N_{Gr} and N_{Sc} were used to calculate values of $(N_{sh,0} - 2)$. These values were then subtracted from the experimental values of N_{sh} and the results plotted against $(N_{Re,s}N_{Sc}^{1/2})$ in Figure 7. The solid line is that of Equation (12). The data show excellent agreement with the final correlating equations. Errors in the low end of the scale are exaggerated because of the subtraction of $N_{sh,0}$ from N_{sh} .

Figure 8 is a plot of the experimental data from the literature computed in accordance with the relations proposed here. The ability of Equations (9) and (12) to correlate both gas- and liquid-stream data and heat as well as mass transfer data is most important; previous correlations, experimental and theoretical, are not capable of doing this.

It is interesting that the above equations, developed from the new data which range from $841 < (N_{Re,s} N_{Re}^{1/2}) < 531,000$, correlate other data ranging from $1 < (N_{Re,s} N_{Re}^{1/2}) < 500,000$. The low range is handled exceptionally well by the new equations with about a 3% average deviation. The new data of Garner and Keey (7) for $N_{Re,s}$ from 1 to 20, $N_{Re} = 788$, represent an exception to this. In the higher ranges the literature data scatter evenly above and below the curve of Figure 8 with an average deviation of about 20%.

Since the work reported here was completed, some additional data have appeared (35). The presently proposed equations correlate these data reasonably well, but distinct deviations due, it is felt, to inadequate diffusivities nevertheless remain.

ACKNOWLEDGMENT

The authors are grateful to the National Science Foundation for its support under Grant G-598. This paper is a condensation of a thesis submitted by Robert L. Steinberger in partial fulfillment of the requirements for the degree of Doctor of Engineering Science at New York University.

NOTATION

A	= value of N_{sh} extrapolated to $N_{Re} = 0$, dimensionless
B	= coefficient, dimensionless
C	= concentration of solute in solution, g./cc.
C_s	= saturation concentration, g./liter
D	= diffusion coefficient, sq. cm./sec.
d_c	= column or pipe diameter, cm.
d_s	= sphere diameter, cm.
g	= local acceleration due to gravity, cm./sec. ²
h	= heat transfer coefficient, cal./sq. cm. (sec.) (°C.)
K	= mass transfer coefficient, cm./sec.
k	= thermal conductivity, cal./cm. (sec.) (°C.)
L	= characteristic dimension of system, cm.
N_{Gr}	= Grashof number, $gd_s^3 (\rho_s - \rho_o) / (\rho_o \nu^2)$; dimensionless
N_{Su}	= Nusselt number, hL/k , dimensionless
$N_{Su,0}$	= value of N_{Su} at $N_{Re} = 0$, dimensionless

N_{Pe}	= Peclet number, equal to $(N_{Re} N_{Sc})$ or $(N_{Re} N_{Pr})$, dimensionless
N_{Pr}	= Prandtl number, ν/α , dimensionless
N_{Re}	= Reynolds number, LV/ν , dimensionless
$N_{Re,c}$	= column Reynolds number, $d_c U/\nu$, dimensionless
$N_{Re,M}$	= Reynolds number based on approach velocity at sphere axis, $d_s U_M/\nu$, dimensionless
$N_{Re,s}$	= sphere Reynolds number, $d_s U/\nu$, dimensionless
N_{Sc}	= Schmidt number, ν/D , dimensionless
N_{Sh}	= Sherwood number, Kd_s/D , dimensionless
$N_{Sh,0}$	= value of N_{Sh} at $N_{Re} = 0$, dimensionless
n	= exponent of $N_{Re,s}$, dimensionless
T	= absolute temperature, °K.
U	= average fluid velocity, cm./sec.
U_M	= approach velocity at axis of sphere, cm./sec.
V	= characteristic velocity of system, cm./sec.
W	= wt. % propylene glycol in water solutions, on a benzoic acid-free basis

Greek Letters

α	= thermal diffusivity, sq. cm./sec.
ν	= kinematic viscosity, sq. cm./sec.
ρ_o	= solvent density, g./cc.
ρ_s	= solution density, g./cc.
$\Delta\rho$	= solution minus solvent density $\rho_s - \rho_o$, g./cc.

LITERATURE CITED

1. Acrivos, Andreas, *A.I.Ch.E. Journal*, **4**, 285 (1958).
2. Colburn, A. P., *Trans. Amer. Inst. Chem. Engrs.*, **29**, 174 (1933).
3. Drake, R. M., P. M. Sauer, and S. A. Shaaf, *Inst. Eng. Res. Rept. He-150-74*, Univ. Calif., Berkeley (Nov. 15, 1950).
4. Friedlander, S. K., *A.I.Ch.E. Journal*, **3**, 43, (1957).
5. Froessling, Nils, *Gerland's Beit. zur Geophys.*, **52**, 170 (1938).
6. Garner, F. H., and R. W. Grafton, *Proc. Roy. Soc. (London)*, **A224**, 64 (1954).
7. Garner, F. H., and R. B. Keey, *Chem. Eng. Sci.*, **9**, 119 (1958).
8. *Ibid.*, **9**, 218 (1959).
9. Garner, F. H., and R. D. Suckling, *A.I.Ch.E. Journal*, **4**, 114 (1958).
10. Gates, R. P., and R. Shanks, S. M. thesis, Mass. Inst. Technol., Cambridge (1949).
11. Gilliland, E. R., R. F. Baddour, and D. J. Goldstein, *Can. J. Chem. Eng.*, **35**, 10 (1957).
12. Graves, C. C., and D. W. Bahr, *Natl. Advisory Comm. Aeronaut. Rept. 1300*, 1-31 (1957).

13. Gröber, H., S. Erk, and U. Grigull, "Grundgesetze der Wärmeübertragung," Springer-Verlag, Berlin, Germany (1957).
14. Houghton, H. G., *Physics*, **4**, 419 (1933).
15. ———, and W. H. Radford, *Papers Phys. Oceanog. Meteorol., Mass. Inst. Tech. and Woods Hole Oceanog. Inst.*, **6**, No. 3 (1938).
16. Hsu, N. T., K. Sato, and B. H. Sage, *Ind. Eng. Chem.*, **46**, 870 (1954).
17. Ingebo, R. D., *Chem. Eng. Progr.*, **48**, 403 (1952).
18. Johnstone, H. F., and R. V. Klein-schmidt, *Trans. Am. Inst. Chem. Engrs.*, **34**, 181 (1938).
19. Johnstone, H. F., R. L. Pigford, and J. H. Chapin, *Eng. Exp. Sta. Bull.* **330**, Univ. Ill., Urbana (June 17, 1941).
20. Johnstone, H. F., and G. C. Williams, *Ind. Eng. Chem.*, **31**, 993 (1939).
21. Kramers, H. A., *Physica*, **12**, 61 (1946).
22. Kudryashev, L. I., *Transl. No. 368, British R.A.E.* (March, 1951).
23. Kyte, J. R., A. J. Madden, and E. L. Piret, *Chem. Eng. Progr.*, **49**, 653 (1953).
24. Langmuir, Irving, *Phys. Rev.*, **12**, 368 (1918).
25. Langstroth, G. O., C. H. Diehl, and E. J. Winhold, *Can. J. Research*, **28A**, 580 (1950).
26. Luchak, G., and G. O. Langstroth, *ibid.*, **574** (1950).
27. Maisel, D. S., and T. K. Sherwood, *Chem. Eng. Progr.*, **46**, 131 (1950).
28. Mathers, W. G., A. J. Madden, and E. L. Piret, *Ind. Eng. Chem.*, **49**, 961 (1957).
29. Merk, H. J., and J. A. Prins, *Appl. Sci. Res.*, **A4**, 11, 195 (1954).
30. Nusselt, W., *Gesundheits Ing.*, **38**, 477 (1915).
31. Powell, R. W., *Proc. Brit. Assoc. Refrig.*, **36**, 61 (1939-40).
32. ———, *Trans. Inst. Chem. Engrs. (London)*, **18**, 36 (1940).
33. Ranz, W. E., and W. R. Marshall, Jr., *Chem. Eng. Progr.*, **48**, 141, 173 (1952).
34. Schlichting, Hermann, "Boundary-Layer Theory," McGraw-Hill, New York (1955).
35. Steele, L. R., and C. J. Geankoplis, *A.I.Ch.E. Journal*, **5**, 178 (1959).
36. Steinberger, R. L., D. Eng. Sci. thesis, New York Univ., New York (1959).
37. Tang, Y. S., J. M. Duncan, and H. E. Schweyer, *Natl. Advisory Comm. Aeronaut. Tech. Note 2867* (1953).
38. Topley, B., and R. W. Whytlaw-Gray, *Phil. Mag.*, **4**, 873 (1927).
39. Tverskaya, N. P., *Izvest. Akad. Nauk. SSSR. Ser. Geog. Geofiz.*, **14**, 164 (1950).
40. van Krevelen, D. W., and P. J. Hoftijzer, *J. Sci. Chem. Ind.*, **68**, 59 (1949).
41. Williams, G. C., Sc. D. thesis, Mass. Inst. Technol., Cambridge (1942).
42. Woodland, D. J., and E. Mack, Jr., *J. Am. Chem. Soc.*, **55**, 3149 (1933).

Manuscript received June 26, 1959; revision received October 9, 1959; paper accepted October 12, 1959. Paper presented at A.I.Ch.E. San Francisco meeting.

Simultaneous Mass Transfer and Equilibrium Chemical Reaction

DONALD R. OLANDER

University of California, Berkeley, California

Equations predicting the effect of various types of equilibrium chemical reactions on the liquid-phase mass transfer coefficient have been derived. In each case the reacting species were assumed to be present in equilibrium concentrations at all points along the diffusion path. Equations were derived for both the film and surface-renewal theories of simple mass transfer in conjunction with these equilibrium reactions.

The well-known Hatta equation for the rapid second-order irreversible reaction was shown to be a limiting case of the general equilibrium reaction $A + B \rightleftharpoons E$.

The calculated mass transfer coefficients were found to be functions of the concentration driving force and the average concentration level over the diffusion path as well as of the magnitude of the equilibrium constant and the diffusivities of the reacting species.

Ever since Hatta (5) modified the film concept of mass transfer to include simple simultaneous chemical reaction, there has been considerable theoretical work extending this analytical treatment to more complex reaction types. Each reaction is characterized by its kinetic order, degree of reversibility, and the relative rates of the diffusional and chemical-conversion steps. Thus Hatta's early investigation of the absorption of carbon dioxide by caustic solution pertained to a reaction the kinetics of which was second order, irreversible, and infinitely rapid compared with the diffusional rates involved. Subsequent studies have considered the slow (diffusion and chemical-conversion rates of comparable magnitudes), first order, reversible (2) or irreversible (8) reaction; the slow, irreversible reaction of n^{th} order in the transferring species (1); and the slow, second-order, irreversible reaction (10).

With the advent of the surface-renewal theories of Danckwerts and Kishinevsky, the diffusional step was no longer restricted to the oversimplified concept of the film theory, and a flurry of papers combining the same reaction types with these more realistic mass transfer models appeared (6, 2, 3).

However none of the previous studies have systematically examined the case of the infinitely rapid reversible reaction. It is the object of this paper to add the equilibrium reaction to the rogues' gallery of chemical interactions which can occur in conjunction with the mass transfer process.

The maintenance of chemical equi-

librium implies that throughout the diffusion path the reacting species are present in concentrations satisfying the mass action law. Consequently only the ratio of the forward and reverse chemical-rate constants appears as the equilibrium constant in the over-all transfer rate expression.

The reactions which will be considered are



Reactions (1) through (4) will be applied to the film theory and (1) through (3) to Danckwerts' surface-renewal theory.

Species A is assumed to transfer between an inert phase, in which no chemical reaction occurs, and a reacting liquid phase, in which any one of reactions (1) through (4) takes place. The inert phase can be a gas, another liquid immiscible with the reacting phase, or a solid. The restrictions on this phase are that it contain only A (and perhaps an inert diluent) and that it generate a known equilibrium concentration of A on the reacting-phase side of the interface.

Since for all cases the system includes more than two species (reactants, products, and inert solvent), a completely rigorous treatment of the problem would require the use of liquid multicomponent diffusion coefficients to characterize the transport rates. However in the following derivations it will be assumed that the re-

actants and products are sufficiently dilute such that Fick's Law is applicable; that is, the diffusion coefficients may be considered those of the binary system consisting of the particular species and the solvent.

Unlike the reactions previously studied, the method of approach to the equilibrium system is independent of the particular reaction under consideration; the differences in reaction type are reflected only in the boundary conditions and equilibrium restrictions. The development of the pertinent differential equations can be most easily illustrated by considering a particular reaction, for example the type exemplified by Equation (3).

If this reaction were not infinitely rapid, material balances for species A and E over a slice of fluid of thickness dx within the diffusion path would yield

$$D_A \frac{\partial^2 A}{\partial x^2} = kAB - k'E + \frac{\partial A}{\partial t} \quad (5)$$

$$D_E \frac{\partial^2 E}{\partial x^2} = -kAB + k'E + \frac{\partial E}{\partial t} \quad (6)$$

If the mass-action constant for the reaction is K , then

$$K = \frac{E}{AB} = \frac{k}{k'} \quad (7)$$

Equations (5) and (6) can be rewritten to yield

$$D_A \frac{\partial^2 A}{\partial x^2} = k(AB - E/K) + \frac{\partial A}{\partial t} \quad (5a)$$

$$D_E \frac{\partial^2 E}{\partial x^2} = -k(AB - E/K) + \frac{\partial E}{\partial t} \quad (6a)$$

If the reaction-rate constant is increased so that equilibrium conditions are approached at all points along the

diffusional path, the right-hand members of Equations (5a) and (6a) become indeterminate, since $(AB-E/K)$ approaches zero as k approaches infinity. This difficulty can be avoided by the addition of the two equations, which results in

$$D_A \frac{\partial^2 A}{\partial x^2} + D_E \frac{\partial^2 E}{\partial x^2} = \frac{\partial}{\partial t} (A + E) \quad (8)$$

Equation (8) can be viewed as the differential material balance of component A in all forms over a slab of thickness dx within the reacting phase. The first term on the left represents the contribution of unreacted A and the second term that of combined A. (In this case E represents the addition product of A and B.) Hereafter relations of the type represented by Equation (8) will be called *total-component material balances*; the total A component in this case denotes the sum of the concentrations of A+E. Equation (8) is directly applicable to the unsteady state processes of the penetration theory; in the film theory the time derivative is zero, since only steady state transfer is considered. In this example there would be an additional partial-differential equation representing the total B component material balance:

$$D_B \frac{\partial^2 B}{\partial x^2} + D_E \frac{\partial^2 E}{\partial x^2} = \frac{\partial}{\partial t} (B + E) \quad (9)$$

where the total B component = $B + E$.

Equations (8) and (9), in conjunction with the equilibrium restriction of Equation (7) and the appropriate boundary conditions, completely determine the concentration profiles of A, B, and E and the rate of transfer of species A between the inert phase and the reacting phase.

Following the total-component material-balance approach, one can derive the rate expressions for simultaneous mass transfer and each of the four types of equilibrium chemical reactions.

Mass transfer coefficients can be based on either the total driving force, $(C_i - C_L)$, or the driving force of unreacted solute $(A_i - A_L)$:

$$k_c \equiv \frac{J}{C_i - C_L}$$

$$k_A \equiv \frac{J}{A_i - A_L}$$

The most appropriate form depends on the particular reaction system and on the analytical techniques available. For many systems only the total A component can be determined, e.g., base titration of a partially ionized acid, and k_c is the only experimentally measurable coefficient possible. However for the last two cases [reactions (3) and

(4)] k_c is not a useful quantity, since C_i is a function of both the mass transfer and equilibrium characteristics of the system.

If the unreacted solute (species A) can be analytically differentiated from the reaction product (species E), then k_A is experimentally measurable. A_i is determined (and presumably known) by the physical distribution of A between the inert and reacting phases.

Case (1) Film-Theory Mass Transfer and the Reaction $A \rightleftharpoons E$

The total A component material balance is

$$D_A \frac{d^2 A}{dx^2} + D_E \frac{d^2 E}{dx^2} = 0 \quad (10)$$

The general solution of Equation (10) is

$$D_A A + D_E E = a_1 x + a_2 \quad (11)$$

With A and E subject to the equilibrium restriction

$$K = \frac{E}{A} \text{ for all } x \quad (12)$$

The boundary conditions are

$$\text{at } x = 0, A = A_i \quad (13a)$$

$$\text{at } x = x_L, A = A_L \quad (13b)$$

The transfer rate of species A from the inert phase is equal to the flux of the total A component within the reacting-phase film:

$$J = -D_A \frac{dA}{dx} - D_E \frac{dE}{dx} = -a_1 \quad (14)$$

Substituting Equations (12), (13), and (14) into Equation (11), one gets

$$J = \left(\frac{D_A}{x_L} \right) (A_i - A_L) \left(1 + \frac{D_E}{D_A} K \right) \quad (15)$$

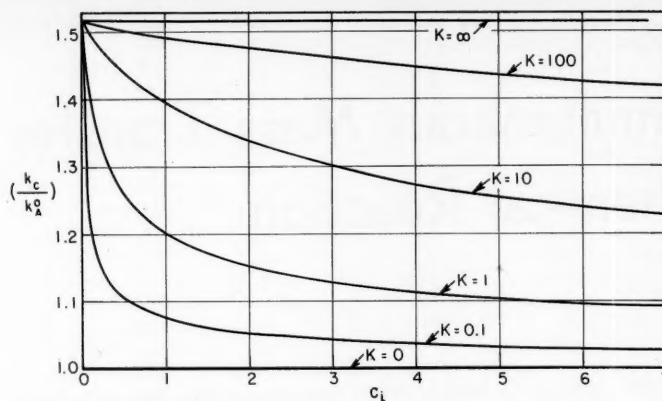


Fig. 1. Effect of interfacial concentration on the mass transfer coefficient for diffusion and the simultaneous equilibrium reaction $A \rightleftharpoons 2E$ as calculated from Equations (27) and (28): $0 \leq K \leq \infty$, $C_L = 0$, $D_E/D_A = 1.51$.

Or, with k_A defined as the flux divided by the driving force $(A_i - A_L)$ and k_A^0 as the mass transfer coefficient in the absence of chemical reaction (D_A/x_L)

$$k_A = k_A^0 \left(1 + \frac{D_E}{D_A} K \right) \quad (16)$$

If the concentrations at the film boundaries are specified in terms of the total A component, $C = A + E$:

$$\text{at } x = 0, C = C_i = (1 + K)A_i \quad (17a)$$

$$\text{at } x = x_L, C = C_L = (1 + K)A_L \quad (17b)$$

Then

$$J = \left(\frac{D_A}{x_L} \right) (C_i - C_L) \left[1 + \left(\frac{D_E}{D_A} - 1 \right) \theta \right] \quad (18)$$

where

$$\theta = \frac{K}{1 + K} \quad (19)$$

Again defining the mass transfer coefficient as the flux divided by the total A component driving force $(C_i - C_L)$, one obtains

$$k_c = k_c^0 \left[1 + \left(\frac{D_E}{D_A} - 1 \right) \theta \right] \quad (20)$$

Equation (15) has been derived by Peaceman (7) as a limiting case of the slow, first-order, reversible reaction. The concentration profiles are linear throughout the film for all values of K only for this case.

Case (2) Film-Theory Mass Transfer and the Reaction $A \rightleftharpoons 2E$

In this case A represents the dimer E_2 . A material balance on the total A component, $C = A + \frac{1}{2}E$, gives

$$D_A \frac{d^2 A}{dx^2} + \frac{1}{2} D_E \frac{d^2 E}{dx^2} = 0 \quad (21)$$

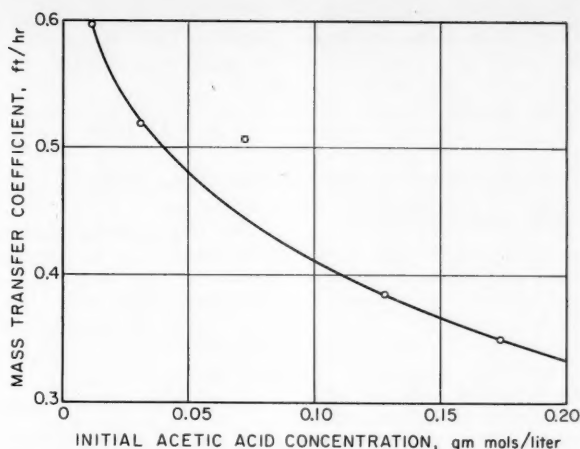


Fig. 2. Variation of the mass transfer coefficient with initial organic-phase solute concentration for the extraction of acetic acid from carbon tetrachloride into water (4).

the general solution of which is

$$D_A A + \frac{1}{2} D_E E = a_1 x + a_2 \quad (22)$$

The equilibrium condition is

$$K = \frac{E^2}{A} \quad (23)$$

and the boundary conditions are given by Equation (13). The flux of A is written as

$$J = -D_A \frac{dA}{dx} - \frac{1}{2} D_E \frac{dE}{dx} \quad (24)$$

The relation between the mass transfer coefficients with and without chemical reaction becomes^{*}

$$k_A = k_A^0 \left[1 + \frac{D_E}{D_A} \frac{\sqrt{K/4}}{\sqrt{A_i} + \sqrt{A_L}} \right] \quad (25)$$

If the boundary conditions are specified in terms of the total A component, then

$$\text{at } x = 0, C = C_i = A_i + \frac{1}{2} \sqrt{KA_i} \quad (26a)$$

$$\text{at } x = x_L, C = C_L = A_L + \frac{1}{2} \sqrt{KA_L} \quad (26b)$$

and

$$k_C = k_A^0 \left[1 + \left(\frac{D_E}{D_A} - 1 \right) \theta' \right] \quad (27)$$

where

* For the general polymerization reaction, $A \rightleftharpoons nE$, the relation between the mass transfer coefficients with and without chemical reaction can be determined by a simple extension of this method:

$$k_A = k_A^0 \left[1 + \frac{K^{1/n} D_E}{n D_A} \left(\frac{A_i^{1/n} - A_L^{1/n}}{A_i - A_L} \right) \right]$$

However an analytical expression for the mass transfer coefficient based on the total component C is not obtainable, since the solution of a polynomial of order greater than 2 would be required.

$$\theta' = \frac{\sqrt{K^2/16 + KC_i} - \sqrt{K^2/16 + KC_L}}{2(C_i - C_L)} \quad (28)$$

A plot of k_C/k_A^0 as a function of C_i is shown in Figure 1 for $C_L = 0$ and for various values of K. The ratio D_E/D_A was estimated by the assumption that the molecular volume of A is twice that of E and by the use of the Wilke correlation (11). Thus

$$\frac{D_E}{D_A} = \left(\frac{V_A}{V_E} \right)^{0.6} = (2)^{0.6} = 1.51$$

Figure 1 indicates that there is a maximum increase of 51% in k_C as the equilibrium constant increases from zero (no dissociation) to infinity (complete dissociation). Moreover k_C decreases markedly with increasing concentration owing to the increased amount of undissociated A present at higher concentrations. At $C_i = 0$ all the diffusing material is present as the dissociation products, for all nonzero values of K.

Acetic acid is one of the few solutes known to dimerize appreciably in non-polar solvents. Farmer (4) has investigated the effect of initial solute concentration on the mass transfer coefficient for the extraction of acetic acid from single drops of carbon tetrachloride into a dispersed water phase. These results, shown in Figure 2, show the same general behavior as the predicted curves of Figure 1.

Since the solute was stripped from the reacting phase (carbon tetrachloride) into an essentially solute-free inert phase (water), Equations (27) and (28), with $C_i = 0$, are applicable. The variation of the mass transfer coefficient with the acetic acid concentration of the carbon tetrachloride phase should be described by the curve of Figure 1 with C_i replaced by C_L in the

abscissa. However Farmer's data are not amenable to a direct analysis by this theory, since the solute concentration decreased by 30 to 40% during an experiment, and neither the dissociation constant nor the diffusivity ratio is known. The rapid decrease in k_C with concentration suggests an equilibrium constant in the range of 0.01 to 0.1 for this system. Since the mass transfer coefficient decreases by 70% between $C_L = 0.011$ and $C_L = 0.174$, the diffusivity ratio D_E/D_A must be larger than the value of 1.51 predicted by Wilke's correlation if these data are to be explained on the basis of simultaneous mass transfer and equilibrium dissociation. Farmer also attributed this behavior to partial dimerization of the acetic acid in the organic solvent.

The measured distribution coefficients (organic to aqueous) were less than 0.05 for all experiments, and so the observed mass transfer coefficients were essentially equal to the organic film coefficients. Thus the decrease in k_C cannot reasonably be attributed to the effect of increasing distribution coefficient on the sum of the individual resistances.

Although the curves of Figure 1 have been extended to a concentration of 7 molar, other effects probably become more important at high concentrations. Wilke (12) has cited the photographic studies of the carbon tetrachloride-acetic acid-water system reported by Sigwart and Nassenstein (9). They offer strong evidence of interfacial turbulence at concentrations beyond about 0.2 molar, although the water-carbon tetrachloride interface appeared to be quite stable during acetic acid transfer for the low-concentration region to which Farmer's investigation was restricted.

Equations (27) and (28) apply in principle to the transfer of a partially dissociated electrolyte, such as nitric acid, through an aqueous film. Despite their difference in sizes, the two ions will exhibit the same effective diffusivity, since by electrical neutrality the two must diffuse at the same rate. However the restriction that the solution be ideal is not true for aqueous electrolytes, even at very low concentrations. Consequently the theory is not applicable to this class of dissociating systems.

Equations (20) and (27) indicate that for cases (1) and (2) the mass transfer coefficient is given by an expression of the general type:

$$k_C = \frac{J}{C_i - C_L} = \left(\frac{D_A}{x_L} \right) \left[1 + \left(\frac{D_E}{D_A} - 1 \right) \theta \right] \quad (29)$$

Only the θ term depends upon the particular reaction type under consideration; the physical meaning of θ can be described as follows. The mass transfer rate of the total component is based on the driving force $(C_i - C_L)$. However for case (2) the nature of the equilibrium expression requires that the relative amount of unreacted solute (A) and reaction product (E) be an increasing function of the total concentration level (C) at any point along the diffusion path. Species A, because of its greater bulk, has lower diffusivity than the dissociated material. Hence the total flux, which is the sum of the transfer rates of A and one half that of E, depends upon the fraction of the total component in each form (which is in turn a function of the total concentration C) and of the diffusivity of each species. θ is a complex averaging parameter which accounts for the varying A to E ratio throughout the film, and $D_A \{1 + (D_E/D_A - 1)\theta\}$ is an average diffusivity for the transfer process.

Equation (29) shows that if $D_A = D_E$, then there is no effect of an equilibrium chemical reaction on the mass transfer coefficient if the reaction is of types (1) or (2). However it will be shown for cases (3) and (4) that C_i , and hence the driving force, depends on K. For these two cases equilibrium reaction will affect the transfer rate, even though $D_A = D_E$.

Case (3) Film Theory Mass Transfer and the Reaction $A + B \rightleftharpoons E$

Species E denotes the addition product of A and B. The total A component material balance gives

$$D_A \frac{d^2 A}{dx^2} + D_E \frac{d^2 E}{dx^2} = 0 \quad (30)$$

The total B component material balance gives

$$D_B \frac{d^2 B}{dx^2} + D_E \frac{d^2 E}{dx^2} = 0 \quad (31)$$

The general solutions to Equations (30) and (31) are

$$D_A A + D_E E = a_1 x + a_2 \quad (32)$$

$$D_B B + D_E E = a_3 x + a_4 \quad (33)$$

The equilibrium restriction, which applies throughout the film, is

$$K = \frac{E}{AB} \quad (34)$$

The four boundary conditions are

$$\text{at } x = 0, A = A_i \quad (35)$$

$$x = x_L, A = A_L \quad (36)$$

$$B = B_L \quad (37)$$

The final boundary condition reflects the inability of B or E to penetrate the interface:

$$D_B \frac{dB}{dx} + D_E \frac{dE}{dx} = 0 \quad (38)$$

With J given by Equation (14), Equations (32) and (33) can be solved for the mass transfer coefficient to give

$$k_A = k^{\circ}_A \left[1 + \left(\frac{D_B}{D_A} \right) \frac{B_L}{A_i + \frac{D_B/D_E}{K}} \right] \quad (39)$$

Even though a solution utilizing total component boundary conditions could also be obtained, this would not represent a useful description of the process. Although A_i is determined from the condition of physical equilibrium of species A between the inert and reacting phases at the interface, the total A component cannot be similarly specified. C_i is not a unique function of A_i , as it was for the two previous cases, [Equations (17) and (26)], but is given by

$$C_i = A_i + E_i = A_i (1 + KB_i) \quad (40)$$

C_i depends upon the concentration of reactant B at the interface as well as A_i . Owing to the chemical reaction occurring within the film, B_L is in general greater than B_i , the actual value of which is given by

$$B_i = B_L \left[\frac{\frac{D_B/D_E}{K} + A_L}{\frac{D_B/D_E}{K} + A_i} \right] \quad (41)$$

Thus

$$C_i = A_i \left[1 + KB_L \frac{\left[\frac{D_B/D_E}{K} + A_L \right]}{\left[\frac{D_B/D_E}{K} + A_i \right]} \right] \quad (42)$$

Since C_i is not a quantity which can be determined solely from equilibrium conditions but depends on both the mass transfer properties of the system and the bulk concentrations, it is not a useful boundary condition for this case. However A_i is fixed solely by the distribution coefficient of species A between the inert and reacting phases and is therefore an appropriate boundary condition.

If K becomes large, the system approaches that of the rapid, irreversible, second-order reaction, which has received considerable attention in the literature (5, 8). As K approaches in-

finity, the group $(D_B/D_E)/K$ in Equation (39) approaches zero, and the mass transfer coefficient is given by

$$k_A = k^{\circ}_A \left(1 + \frac{D_B B_L}{D_A A_i} \right) \quad (43)$$

which is the Hatta equation for this reaction type.

The concentration profiles of the three species can be determined from Equations (32), (33), and (34) and the known values of the constants a_1 , a_2 , a_3 , and a_4 . The variation of the concentration of A through the film is given by

$$A = \frac{1}{2} \{ [R - P(x)]^2 + 4\beta P(x) \}^{1/2} - \frac{1}{2} [R - P(x)] \quad (44)$$

where

$$R = \beta + \alpha \left(1 + \frac{A_L}{\beta} \right) \quad (45)$$

$$P(x) = A_i \left[1 + \frac{\alpha(1 + A_L/\beta)}{A_i + \beta} \right] - (A_i - A_L) \left[1 + \frac{\alpha}{A_i + \beta} \right] \left(\frac{x}{x_L} \right) \quad (46)$$

$$\alpha = \frac{D_B B_L}{D_A} \quad (47)$$

$$\beta = \frac{D_B/D_E}{K} \quad (48)$$

The concentration profiles of B and E are given by

$$B = B_L \left(\frac{\beta + A_L}{\beta + A} \right) \quad (49)$$

$$E = KAB \quad (50)$$

The behavior of the concentration profiles as K ranges from 10^{-3} to 10^{-4} is shown for a hypothetical system in Figure 3. The appearance of the characteristic reaction zone, at which $A = B = 0$, becomes evident at large values of K. As K approaches infinity, Equation (44) reduces to

$$A = A_i - (A_i + \alpha) \left(\frac{x}{x_L} \right) \quad (51)$$

which is identical to the result obtained from the Hatta model.

Similarly, as K approaches zero, the system reduces to the simple mass transfer of species A and Equation (44) becomes

$$A = A_i - (A_i - A_L) \left(\frac{x}{x_L} \right) \quad (52)$$

which is the film-theory expression for mass transfer in the absence of chemical reaction.

Another interesting limiting case is that in which K is large and A_i is small. This behavior is characteristic of the extraction of metallic salts by organic complexing or chelating agents. The metal salts are quite insoluble in

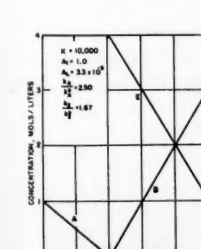
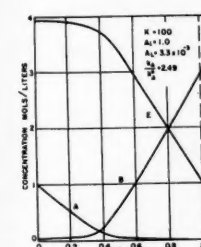
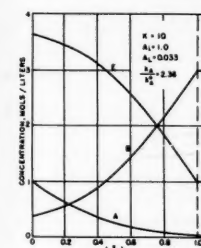
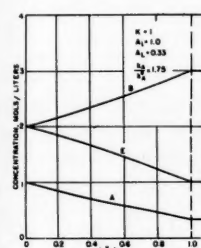
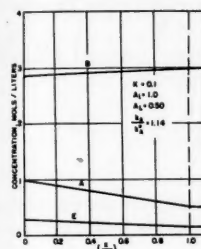
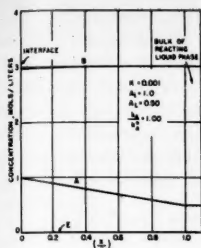
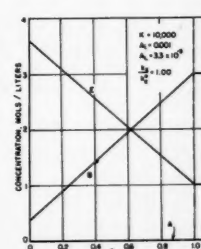
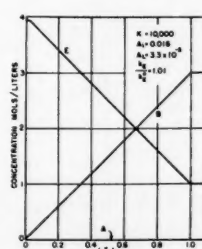
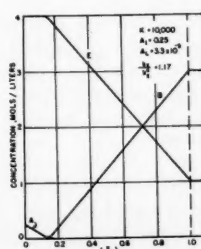
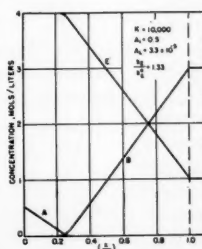


Fig. 3. Effect of the equilibrium constant on the concentration profiles for simultaneous mass transfer and the equilibrium chemical reaction $A + B \rightleftharpoons E$: $D_B/D_A = 0.5$, $D_B/D_E = 1.0$, $B_L = 3.0$, $A_i = 1.0$. A_L is adjusted to keep $T = E_L + B_L$ between 3 and 4, and $A_L \leq 0.5A_i$. k_E/k_A° is determined from Equation (39).

Fig. 4. Effect of decreasing A_i on the concentration profiles for simultaneous mass transfer and equilibrium chemical reaction $A + B \rightleftharpoons E$: $D_B/D_A = 0.5$, $D_B/D_E = 1.0$, $B_L = 3.0$, $K = 10,000$. A_L is adjusted to keep $T = E_L + B_L$ between 3 and 4, and $A_L \leq 0.5A_i$. k_E/k_A° is determined from Equation (58).



the inert solvent of the organic phase and are extractable only by virtue of the complexes or chelates formed with an active agent added to the diluent. For example uranyl nitrate is practically insoluble in kerosene but is quite extractable in a solvent composed of kerosene and the complexing agent tributyl phosphate. In these reactions K is large but not infinite, since generally all of the complexing agent is not consumed at equilibrium. The reduction of Equation (39) to Equation (43) does not apply to this case, since both $(D_B/D_E)/K$ and A_i approach zero. However Equation (39) can be rewritten as

$$J = \left(\frac{D_A}{x_L} \right) (KA_i - KA_L) \left[\frac{1}{K} + \frac{D_B}{D_A} \frac{B_L}{KA_i + D_B/D_E} \right] \quad (53)$$

By the equilibrium restrictions

$$KA_i = \frac{E_i}{B_i} \quad (54)$$

$$KA_L = \frac{E_L}{B_L} \quad (55)$$

If K is sufficiently large, $1/K \approx 0$, Equation (53) becomes

$$J = \left(\frac{D_B}{x_L} \right) \left[\frac{E_i}{B_i} - \frac{E_L}{B_L} \right] \left[\frac{B_L}{\frac{E_i}{B_i} + \frac{D_B}{D_E}} \right] \quad (56)$$

Upon elimination of B_i by Equations (41), (54), and (55), Equation (56) reduces to

$$J = \left(\frac{D_B}{x_L} \right) (E_i - E_L) \quad (57)$$

Furthermore since at all points along the diffusion path A is small, $C = E + A \approx E$, and

$$J = k^\circ_E (C_i - C_L) \quad (57a)$$

The change in the profiles of A , B , and E for $K = 10^4$ as A_i is decreased is shown in Figure 4. k_E/k_A° has been computed by the relationship

$$\frac{k_E}{k_A^\circ} = \frac{(D_B/D_E)}{(D_B/D_A)} \left(\frac{A_i - A_L}{E_i - E_L} \right) \left(\frac{k_A}{k_A^\circ} \right) \quad (58)$$

and presented along with the concentration profiles. E_i and E_L are the calculated values of E at the film boundaries, and k_A/k_A° is obtained from Equation (39). At $K = 10^4$ and $A_i = 10^{-2}$, the concentration of E is nearly linear across the film and $k_E/k_A^\circ = 1.00$, as would be expected from Equation (57).

Thus for the case of large K and small A_i , the system is equivalent to the simple mass transfer of reaction product E between the interface and the bulk. However the limitations on C_i previously discussed apply to this special case as well. It can be shown that only if $D_B = D_E$, is C_i a function of the equilibrium conditions at the interface (KA_i) and the total B component concentration, $T = B_L + E_L = \text{constant}$.

For the general case of $D_B \neq D_E$ the problem of determining either C_i or A_i may be the major obstacle in analyzing the mass transfer data. For the complexing of uranyl nitrate by tributyl phosphate, for example, no analytical technique has been devised for differentiating between the small amount of uncomplexed material and the complex in the organic phase; only their sum is experimentally available. In addition, the organic phase equilibrium constants are generally unknown, since only over-all aqueous to organic equilibrium constants (which include the distribution constant of species A) are measurable. Thus neither C_i nor A_i is known, and the rate equations are inapplicable for lack of sufficient equilibrium information.

Another variation of this case should also be noted. If in addition to large K and small A_i , B_L is also small, the $1/K$ term in Equation (53) is not negligible and the mass transfer coefficient is again given by Equation (43).

Case (4) Film-Theory Mass Transfer and the Reaction $A + B \rightleftharpoons E + F$

In order to determine clearly the requisite material balance reactions, it

$$\phi = \frac{1}{2} \left\{ \left[\left(\frac{D_F}{D_B} - 1 \right) \sqrt{K B_L A_L} + \frac{D_F}{D_B} A_i K \right]^2 + 4 \left[\frac{D_B}{D_F} B_L + \sqrt{K A_L B_L} \right] \left(\frac{D_F}{D_B} A_i K \right) \right\}^{1/2} - \frac{1}{2} \left[\frac{D_F}{D_B} \sqrt{K A_L B_L} + \frac{D_F}{D_B} K A_i \right] \quad (72)$$

is convenient to rewrite this exchange reaction in terms of the subspecies which constitute the reactants and products: $ab + cd \rightleftharpoons ad + cb$, where $A = ab$, $B = cd$, $E = ad$, $F = cb$. The material balances on each of the subspecies, a, b, c , and d are

Subspecies a :

$$D_A \frac{d^2 A}{dx^2} + D_B \frac{d^2 E}{dx^2} = 0 \quad (59)$$

Subspecies b :

$$D_A \frac{d^2 A}{dx^2} + D_F \frac{d^2 F}{dx^2} = 0 \quad (60)$$

Subspecies c :

$$D_B \frac{d^2 B}{dx^2} + D_F \frac{d^2 F}{dx^2} = 0 \quad (61)$$

Subspecies d :

$$D_B \frac{d^2 B}{dx^2} + D_E \frac{d^2 E}{dx^2} = 0 \quad (62)$$

However only three of these equations are independent; Equations (59), (61), and (62) have arbitrarily been chosen, although any other combination would have been equally valid. The general solutions of these three differential equations are

$$D_A A + D_B E = a_1 x + a_2 \quad (63)$$

$$D_B B + D_F F = a_3 x + a_4 \quad (64)$$

$$D_B B + D_E E = a_5 x + a_6 \quad (65)$$

By the restriction that B , E , and F must remain in the reacting phase, a_3 and a_5 are zero. Furthermore by Equation (14) $a_1 = -J$. The remaining boundary conditions are

$$\text{at } x = 0, A = A_i \quad (66)$$

$$\text{at } x = x_L, A = A_L \quad (67)$$

$$B = B_L \quad (68)$$

and, by the stoichiometry of the reaction

$$E_L = F_L \quad (69)$$

with

$$K = \frac{EF}{AB} \quad (70)$$

The effect of the reaction on the mass transfer coefficient is then given by

$$k_A = k_A^\circ \left[1 + \frac{D_B}{D_A} \frac{\phi}{A_i - A_L} \right] \quad (71)$$

where ϕ is

In all four cases considered, except the first, the mass transfer coefficients k_c or k_A are functions not only of the various diffusivities and equilibrium constants but of the concentrations at the interface and in the bulk of the reacting phase. Generally, the larger the driving force, the more pronounced is the effect of the chemical reaction, but even for small driving forces the mass transfer coefficient will depend on the concentration level. The effect of the concentration level for zero driving force can be obtained by calculating the limiting values of k_c and k_A as $C_i \rightarrow C_L$ and $A_i \rightarrow A_L$ respectively.

The equations are probably not valid at high concentrations where the effects of solution nonideality on the

$$J(t) = \left(\frac{D_A}{\pi t} \right)^{1/2} \left[\left(1 + K \frac{D_B}{D_A} \right) (1 + K) \right]^{1/2} (A_i - A_L) \quad (78)$$

diffusion coefficients become more pronounced. Moreover the reacting phase must contain an inert solvent which sufficiently dilutes the reacting species so that Fick's law is applicable to each. Otherwise each diffusivity must be estimated from untested and complex equations for multicomponent diffusion (1).

Another limitation to these derivations is their complete dependence on the somewhat antiquated concepts of the film theory, namely the assumption of a stagnant film in which molecular diffusion is the sole transport process. This assumption is implicit in the application of Fick's law to each species and in the assumption that (D_A/x_L) is equal to the mass transfer coefficient k_A° . However since only diffusivity ratios appear in the correction factors, it might be more realistic to replace them by ratios of the mass transfer coefficients of the particular species; e.g., k_A°/k_B° would be substituted for

D_B/D_A . If from available correlations the mass transfer coefficient were known to vary as some fractional power of the diffusivity, then the ratio $(D_B/D_A)^n$ would be appropriate. These devices are tantamount to replacing Fick's law for each species by rate expressions of the type $J = k^\circ x_L \left(\frac{dC}{dx} \right)$.

Case (1a) Surface Renewal Mass Transfer and the Reaction $A \rightleftharpoons E$

The unsteady state material balance of the total A component is

$$D_A \frac{\partial^2 A}{\partial x^2} + D_E \frac{\partial^2 E}{\partial x^2} = \frac{\partial}{\partial t} (A + E) \quad (73)$$

E and A are related by Equation (12), and the appropriate boundary conditions are

$$\text{at } t = 0, A = A_L \quad (74)$$

$$\text{at } x = \infty, A = A_L \quad (75)$$

$$\text{at } x = 0, A = A_i \quad (76)$$

Equation (73), subject to these boundary conditions, can be solved for the instantaneous absorption rate, defined by

$$J(t) = -D_A \left(\frac{\partial A}{\partial x} \right)_{x=0} - D_E \left(\frac{\partial E}{\partial x} \right)_{x=0} \quad (77)$$

to yield

In accordance with Danckwerts' surface renewal theory (3), the steady state absorption rate is related to $J(t)$ by

$$J = \int_0^\infty J(t) s e^{-st} dt \quad (79)$$

Combining Equations (78) and (79) one obtains

$$J = \sqrt{D_A s} (A_i - A_L) \sqrt{\left(1 + \frac{D_B}{D_A} K \right) (1 + K)} \quad (80)$$

with $k_A^\circ = \sqrt{D_A s}$

$$k_A = k_A^\circ \sqrt{\left(1 + \frac{D_B}{D_A} K \right) (1 + K)} \quad (81)$$

If the boundary conditions are expressed in terms of the total A components, then

$$k_c = k_A^\circ \sqrt{1 + \left(\frac{D_B}{D_A} - 1 \right) \theta} \quad (82)$$

where

$$\theta = \frac{K}{1 + K}$$

A comparison of Equations (20) and (82) indicates that the film theory predicts the effect of this type of equilibrium reaction on the mass transfer coefficient to be directly proportional to $\{1 + [(D_E/D_A) - 1] \theta\}$, while the surface-renewal theory predicts only a one-half power dependence of k_a on this group.

Case (2a) Surface Renewal Mass Transfer and the Reaction $A \rightleftharpoons 2E$

The appropriate material-balance equation is

$$D_A \frac{\partial^2 A}{\partial x^2} + \frac{1}{2} D_E \frac{\partial^2 E}{\partial x^2} = \frac{\partial}{\partial t} (A + \frac{1}{2} E) \quad (83)$$

E can be eliminated from the equilibrium relations of Equation (23) and Equation (83) rewritten as

$$D_A \frac{\partial^2}{\partial x^2} \left[A + \frac{\sqrt{K}}{2} \frac{D_E}{D_A} \sqrt{A} \right] = \frac{\partial}{\partial t} \left[A + \frac{\sqrt{K}}{2} \sqrt{A} \right] \quad (84)$$

where boundary conditions are given by Equations (74), (75), and (76). With $J(t)$ given by the relations

$$J(t) = -D_A \left(\frac{\partial A}{\partial x} \right)_{x=0} - \frac{1}{2} D_E \left(\frac{\partial E}{\partial x} \right)_{x=0} \quad (85)$$

and the steady state transfer rate by Equation (79), an approximate solution can be written as

$$J = \sqrt{D_A s} (A_i - A_L) \left[\frac{\sqrt{A_i} + \frac{\sqrt{K}}{4} \frac{D_E}{D_A}}{\left(\frac{A_i}{b} \right)^{1/2} e^{a^2/b} \operatorname{erfc} \left(\frac{a}{\sqrt{b}} \right)} \right] \quad (86)$$

where a and b are given by

$$a = \frac{\frac{\sqrt{K}}{4} \frac{D_E}{D_A} (A_i - A_L)}{A_i \left(2\sqrt{A_i} + \frac{\sqrt{K}}{2} \frac{D_E}{D_A} \right) e^{a^2/b} \left(\frac{\pi}{b} \right)^{1/2} \operatorname{erfc} \left(\frac{a}{\sqrt{b}} \right)} \quad (87)$$

and

$$b = \frac{1}{2} \left[\frac{\sqrt{A_i} + \sqrt{K/4}}{\sqrt{A_i} + \frac{\sqrt{K}}{4} \frac{D_E}{D_A}} \right] + a^2 \left(\frac{12\sqrt{A_i}}{\sqrt{K}} \frac{D_A}{D_E} + 1 \right) \quad (88)$$

The bracketed term in Equation (86) is a measure of the effect of the equilibrium chemical reaction $A \rightleftharpoons 2E$ on the surface-renewal mass transfer coefficient.

Case (3a) Surface Renewal Mass Transfer and the Reaction $A + B \rightleftharpoons E$

The total component material balances for surface renewal mass transfer

and the reaction $A + B \rightleftharpoons E$ have no analytical solutions except for the special case of $D_A = D_B = D_E$. With this simplification the flux can be described by

$$J = \sqrt{D_A s} (A_i - A_L) \left[1 + \frac{B_L}{A_i + 1/K} \right] \quad (89)$$

or

$$k_a = k^{\circ}_a \left(1 + \frac{B_L}{A_i + 1/K} \right) \quad (90)$$

Equation (90) is identical to the film-theory expression for equal diffusivities, Equation (39). Similarly the surface-renewal and film theories lead to identical rate expressions (except for the k°_a term) for the equal-diffusivity cases of reactions (1) and (2) as well. This phenomenon appears to be true for all surface-renewal expressions with unsteady state material-balance equations that can be solved by a similarity transformation, that is reduction of the partial differential equation to an ordinary differential equation by the substitution $\eta = x/\sqrt{t}$.

ACKNOWLEDGMENT

The author wishes to thank Andreas Acrivos for his assistance in solving the equations of the surface-renewal treatment of this theory.

NOTATION

- a_1, a_2, \dots, a_n = integration constants in Equations (11), (22), (32), (33), (63), (64), and (65)
- a, b, c, d = subspecies in the exchange reaction of case (4)
- a, b = constants defined by Equations (87) and (88)
- A, B, E, F = molar concentrations of the reacting species
- C = molar concentration of total A component, equal to $A + E$ or $A + \frac{1}{2}E$ (reaction 2)
- D = Fick's law diffusivity

the absence of chemical reaction

- k_a = mass transfer coefficient based on the driving force $(A_i - A_L)$
- k_c = mass transfer coefficient based on the driving force $(C_i - C_L)$
- k_E = mass transfer coefficient based on the driving force $(E_i - E_L)$
- $P(x)$ = defined by Equation (46)
- R = defined by Equation (45)
- s = hydrodynamic parameter in Danckwerts' surface-renewal theory
- t = time
- T = molar concentration of total B component in bulk of reacting phase, equal to $E_L + B_L$
- V = molar volume
- x = distance along diffusion path away from interface
- x_L = film thickness

Greek Letters

- α = defined by Equation (47)
- β = defined by Equation (48)
- θ, θ' = functions defined by Equations (19) or (28)
- ϕ = defined by Equation (72)

Subscripts

- A, B, E, F = one of the transferring species
- i = interfacial value
- L = bulk liquid-phase value

LITERATURE CITED

1. Bird, R. B., "Notes on Transport Phenomena," Wiley, New York (1958).
2. Danckwerts, P. V., and A. M. Kennedy, *Trans. Inst. Chem. Eng. (London)*, **32**, S49 (1954).
3. —, *Ind. Eng. Chem.*, **43**, 1460 (1951).
4. Farmer, W., *Atomic Energy Comm. Rept. ORNL 635* (1949).
5. Hatta, S., *Tohoku Imp. Univ. Tech. Repts.*, **8**, 1 (1928).
6. Kishinevsky, M., *J. App. Chem. (USSR)*, **24**, 593 (1951).
7. Peaceman, D., Sc.D. thesis, Mass. Inst. Technol., Cambridge (1951).
8. Sherwood, T. K., and R. L. Pigford, "Absorption and Extraction," McGraw-Hill, New York (1952).
9. Sigwart, K., and H. Nassenstein, *Z. Ver. deut. Ing.*, **98**, 453 (1956).
10. Van Krevelen, D. W., and P. J. Hoftijzer, *Rec. Trav. Chim.*, **67**, 132, 564 (1948).
11. Wilke, C. R., and Pin Chang, *A.I.Ch.E. Journal*, **1**, 264 (1955).
12. Wilke, C. R., *Ind. Eng. Chem.*, **49**, 577 (1957).

Manuscript received May 25, 1959; revision received August 17, 1959; paper accepted August 25, 1959.

Modified Law of Corresponding States for Gases

OSCAR T. BLOOMER and RALPH E. PECK

Institute of Gas Technology, Chicago, Illinois

A new correlation is presented for predicting the pressure-volume temperature relations of nonpolar (and slightly polar) gases. The correlation modifies the law of corresponding states in which a third parameter, the slope of the pseudocritical isometric in dimensionless form, is introduced. This parameter is introduced in a simple manner by multiplying the reduced pressure and temperature of the gas by a factor which can be easily calculated or read from a graph. This gives the corrected reduced pressure and temperature which can then be used with a generalized compressibility factor chart in place of the true values. The correlation is accurate for densities up to about 1.2 times the critical density.

A detailed comparison of the method with data on twelve pure gases showed that by introducing this parameter into the law of corresponding states the average error was decreased from 1.598 to 0.320%. The parameter S can readily be determined from experimental PVT data, and only one isotherm is required. S is related to the vapor-pressure curve for a substance as characterized by the critical pressure and the ratio of the critical temperature to the normal boiling temperature, and a simple method is proposed for predicting S when no experimental data are available.

A new set of generalized compressibility factor and fugacity to pressure ratio charts is presented for use with the proposed correlation. A method is also presented for determining the thermodynamics functions.

The basis for the correlation presented in this paper is two well-known properties of gases. The first is the linearity of the isometrics (lines of constant density) when plotted on a P-T diagram. At densities below the critical density the isometric curves slightly downwards toward the T axis (negative curvature). As the critical density is approached, the curvature becomes less until in the vicinity of the critical density the isometrics are almost exactly linear over a considerable temperature range.

The second property concerns the critical isotherm. When the critical isotherm of various gases is plotted on a plot of the compressibility factor vs. the reduced pressure, many gases will plot along the same line to a surprising degree of accuracy. This is by no means true for other isotherms either above or below $T_r = 1.0$.

It has been shown by Cope, Lewis, and Weber (3) that the modification to the law of corresponding states which results when the compressibility factor is plotted as a function of the reduced pressure and reduced temperature requires that the reduced density (d/dc) be replaced by the pseudoreduced density (d/d'_c), where

$$d'_c = \frac{P_c}{RT_c Z'_c} \quad (1)$$

Z'_c was arbitrarily given the value of 1.0 by Su (7) but will be given the value of 0.29 in this paper to make it correspond closely in value to the true critical density of many nonpolar gases.

Since the pseudocritical density is almost exactly linear for a pure gas,

its equation may be written as

$$P = I + sT \quad (2)$$

where

$$s = (\partial P / \partial T)_{d'_c}$$

When one writes Equation (2) in reduced form

$$P_r = I/P_c + (s T_c / P_c) T_r \quad (3)$$

When $T_r = 1.0$, $P_r = 1.0^*$, and

$$I/P_c = 1 - s T_c / P_c \quad (4)$$

Substituting (4) into Equation (3) one gets

$$P/P_c = 1 - (s T_c / P_c) + (s T_c / P_c) T / T_c \quad (5)$$

Now

$$Z = P/RTd'_c$$

Substituting into this equation the value of P obtained from Equation (5) one gets

$$Z = (P_c / RT_c d'_c) (T_c / T) - (s / R d'_c) (T_c / T) + (s / R d'_c) \quad (6)$$

and finally

$$Z = 1/T_r (Z'_c - S) + S \quad (7)$$

where

$$S = s / R d'_c \quad (8)$$

If the law of corresponding states were valid for all substances, then S would be a universal constant for all substances.

One should consider the requirements necessary to have the compressibility factors for two different gases

* This is not strictly true for the pseudocritical isometric. (It is true for the critical isometric.) The error is however negligibly small because at the critical temperature the pressure is equal to the critical pressure to within a fraction of a percentage over a wide range of densities (from a reduced density of about 0.8 to about 1.30).

equal along the pseudocritical isometric. This is obtained at once from Equation (7).

$$Z_1 = 1/T_{r1} (Z'_c - S_1) + S_1 = Z_2 =$$

$$1/T_{r2} (Z'_c - S_2) + S_2 \quad (9)$$

If there is available a compressibility-factor chart for substance one, then the above equation can be solved for T_{r1} which is the reduced temperature line on the chart for substance one which will have the same value of the compressibility factor that substance two has at T_{r2} . This equation then provides a method of using for any substance a compressibility-factor chart based on the data for a reference substance. Aside from the critical pressure and temperature it requires only that the slope of the pseudocritical isometric be known. This method will certainly be valid for the pseudocritical isometric.

It is now assumed that the above transformation equation is valid for all constant pseudoreduced density lines $d'_c = d/d'_c$, not just for the $d'_c = 1.0$ line. The justification for this assumption must rest on a detailed comparison with experimental data. It is immediately evident however that it is a very good approximation for the critical isotherm, since the above equation gives $T_{r1} = 1.0$ when $T_{r2} = 1.0$, and as previously pointed out the critical isotherms of different gases do indeed very nearly coincide, at least up to a reduced pressure of 1.0 (pseudoreduced density of 1.0). This fact furnishes a hint that this equation will probably be valid for all constant reduced density lines at least up to $d'_c = 1.0$. The detailed comparison of the method with experimental data on twelve pure gases is presented in a following section. It suffices for the present to state that the equation is very satisfactory for pseudoreduced densities up to about 1.2 but that above this serious errors may be introduced.

Since in engineering practice the pressure and not the density is usually known, it is necessary to develop an equation corresponding to Equation (9) for finding the correct reference chart reduced pressure to use. This is easily found as follows:

By definition

Oscar T. Bloomer, is with the Eastman Kodak Company, Rochester, New York.

$$d' = (P_r/T_r)(Z'_c/Z) \quad (10)$$

It is required that

$$d'_{r(\omega)} = d'_{r(\omega)}$$

and

$$Z_{(\omega)} = Z_{(\omega)}$$

Hence

$$P_{r1}/T_{r1} = P_{r2}/T_{r2} \quad (11)$$

or

$$P_{r1}/P_{r2} = T_{r1}/T_{r2} \quad (12)$$

which is the desired relationship.

Equation (9) can be rearranged into the following form:

$$P_r/P_r = T_r/T_r = (S' - Z'_c)/[(S - Z'_c) + T_r(S' - S)] \quad (13)$$

Here those symbols with the superscript refer to the reference substance and those without the superscript refer to the gas whose properties are desired. This equation is plotted for a series of constant values of S in Figure 1. For this plot Z'_c was taken as 0.2900, and $S' = 1.8329$. The latter is the value of the slope of the pseudocritical isometric in dimensionless form for nitrogen. This plot is thus intended for use with a generalized compressibility-factor chart based on the PVT data of nitrogen. A generalized chart for nitrogen is presented in Figure 3. (The low pressure region of this chart is presented in Figure 2.)* This chart covers the reduced-temperature range 0.75 to 3.0 and the reduced-pressure range 0.0 to 10.0. The compressibility factor is plotted as a function of the pseudoreduced density in Figure 4. It is important to remember when using Figure 4 that the pseudoreduced density is not multiplied by the correction factor. The data and method used for the construction of these charts are discussed in an unpublished thesis (2). The charts were restricted to a reduced temperature of 3.0 because experimental data much above this temperature are available only for such gases as hydrogen and helium. Accurate extrapolation cannot be based on these gases because quantum effects are important for these gases.

PROCEDURE FOR USING THE CORRELATION

To find the compressibility factor of a gas at a given pressure and temperature with Figures 1, 2, and 3 used, the following procedure is followed:

1. Using the known values of the critical pressure and temperature of the substance one can calculate the reduced temperature (T/T_c) and reduced pressure (P/P_c) for the gas at the desired condition of pressure and temperature.

2. Using the known value of S for the substance, one can determine the ratio $T_r/T_r = P_r/P_r$ from Figure 1 or Equation (13).

3. One can multiply the values of the reduced temperature and pressure for the substance (step 1) by the ratio determined in step 2. This gives the corrected reduced temperature and reduced pressure to be used with the reference substance Z chart.

4. One should look up the value of Z on the reference substance chart (Figures 2 or 3) using the corrected reduced temperature and reduced pressure determined in step 3.

When the density instead of the pressure is known, the pseudoreduced density is calculated from the equation $d_r = d/d'_c = 0.29 RT_r d/P_c$. Then Figure 4 is used to determine the compressibility factor. Note that d_r is not multiplied by the correction factor.

Values of S for a number of pure gases are presented in Table 1. A correlation for predicting S when it is not known is presented in the following section.

DETERMINATION OF THE PARAMETER S

The parameter S is readily determined from experimental PVT data

when they are available. Only one isotherm is required. The data along the isotherm are interpolated to find the pressure at the pseudocritical density. The slope of the critical isometric is then found from

$$s = \frac{P - P_c}{T - T_c}$$

Then

$$S = \frac{s}{Rd'_c} \quad (8)$$

Since the pseudocritical isometric is not quite linear at temperatures well removed from the critical temperature, the value of S will depend slightly on the isotherm used to determine it. The values of S tabulated in Table 1 are based on experimental data for the isotherm nearest to a reduced density of 1.40. For the higher hydrocarbons the highest temperature investigated was well below 1.4, and for these gases the highest experimental isotherm was used. It is believed that the maximum error in S resulting from using isotherms higher or lower than $T_r = 1.4$ to determine it will not exceed 1%.

For those gases where there are no experimental PVT data available, it is necessary to have a reliable means of predicting them. It has been found that the parameter S can be related to the

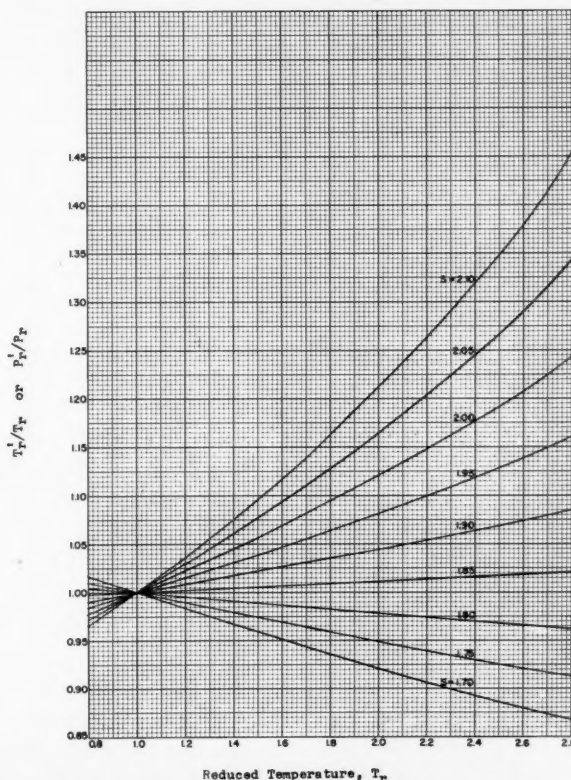


Fig. 1. Chart for determining the corrected reduced temperature and corrected reduced pressure.

* Larger scaled copies of the drawings in this paper can be obtained from the authors.

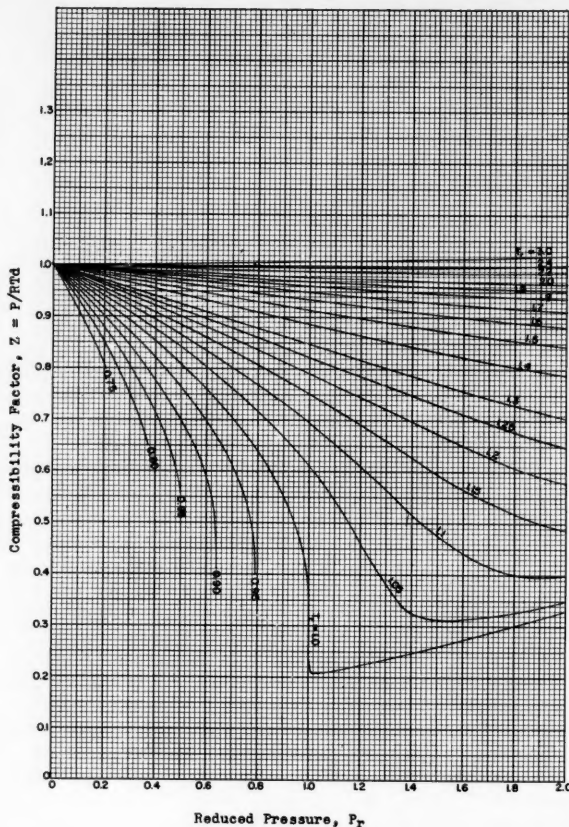


Fig. 2. Compressibility factor vs. reduced pressure (low-pressure range).

vapor-pressure curve as characterized by the ratio of the critical temperature to the normal boiling temperature (T_c/T_b). A correlation of this type is to be expected because the vapor-pressure curve is continuous with the critical isometric. The slope of the vapor-pressure curve at the critical point is equal to the slope of the critical isometric (4) (not the pseudocritical isometric).

The product $S \times T_c/T_b$ was found to be a constant for those substances having approximately the same critical pressure. This product would be expected to increase as the critical pressure increases, since T_b should be replaced by a higher temperature in order to still have the vapor pressure the same fraction of the critical pressure. The product $S \times T_c/T_b$ was found to correlate with the critical pressure. Table 1 presents the data on this correlation for nineteen gases. They include the thirteen gases whose PVT data are compared in detail below and in addition propylene isobutane, carbon dioxide, oxygen, water,* and hydrogen.*

* The correlation is not recommended for hydrogen because of quantum effects or for water because of its high dipole moment.

Below are tabulated recommended values for the product $S \times T_c/T_b$ as a function of the critical pressure.

Critical pressure, atm.	$S \times T_c/T_b$
25	2.975
30	2.995
40	3.040
50	3.080
60	3.125
70	3.170
80	3.210
100	3.280
125	3.350
150	3.405
175	3.445
200	3.475

The values of this product for all of the gases studied agree with the values in this table to within 1.1%. The average error is 0.45%. The values of S for the various gases differ among themselves by 16.5%, and the term T_c/T_b differs by 19.8%. Thus this correlation is quite satisfactory for predicting S when there are no experimental PVT data available.

COMPARISON WITH EXPERIMENTAL DATA

The proposed method of correlating the PVT relationships of gases has

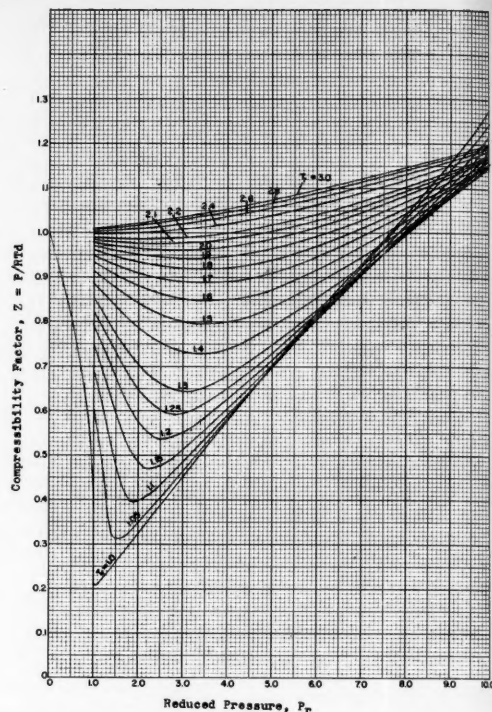


Fig. 3. Compressibility factor vs. reduced pressure (high-pressure region).

been compared with the experimental data for twelve pure gases (2). Table 2 presents data summarizing this comparison. The average error up to a pseudoreduced density of 1.2 was reduced from 1.60 to 0.32%.

The maximum error of any point was reduced from 3.43 to 1.01%. For all of the gases listed (except nitrogen) the comparison covers the entire range of the experimental data up to a pseudoreduced density of 1.2. Comparison was made along each of the experimental isotherms at evenly spaced values of the pseudoreduced density. (Most of the original data are reported along constant density lines, and in these cases the original isometrics were used.) It should be noted that if the pressure instead of the density is known, then in the vicinity of the critical point the error is somewhat larger than that tabulated.

The correlation is limited to a pseudoreduced density of 1.2. Above this limit the error for many of the gases increases quite rapidly. The error is generally larger than when the parameter S is not used. The magnitude of the error above a pseudoreduced density of 1.2 increases as the true critical point compressibility factor decreases.

THERMODYNAMIC FUNCTIONS

Following the method of Benedict,

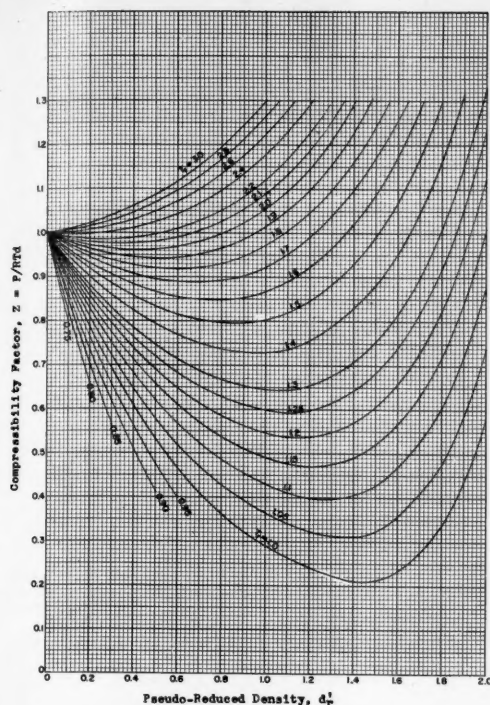


Fig. 4. Compressibility factor vs. pseudoreduced density.

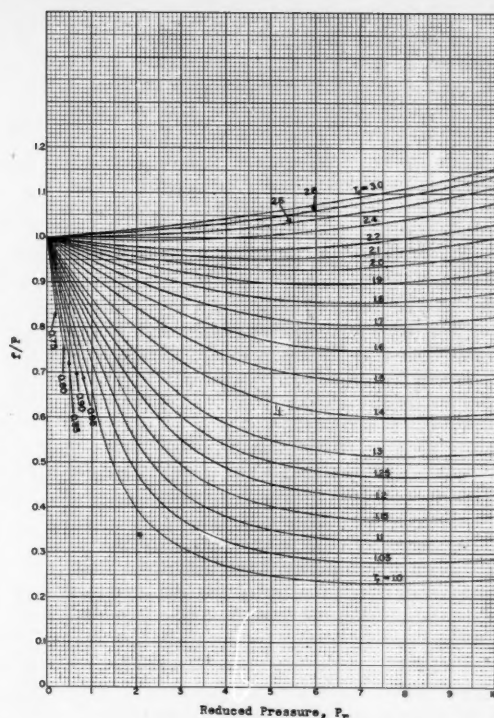


Fig. 5. Generalized chart for determining the fugacity to pressure ratio.

Webb, and Ruben (1) the effect of density (at constant temperature) on the thermodynamic properties of a real gas can be expressed in terms of the residual work content \bar{A} , which may be evaluated from the following gas law deviation function:

$$\bar{A} = \int_0^d [(P - RTd)/d^2]_T \delta d \quad (14)$$

A function of \bar{A} is also required. This is the residual entropy function \bar{S}_d , which may be evaluated from

$$\bar{S}_d = - \left(\frac{\partial \bar{A}}{\partial T} \right)_d \quad (15)$$

From the definition of \bar{A} one sees that

$$\frac{\bar{A}}{RT} = \int_0^d \left(\frac{P}{RTd} - 1 \right) (1/d) \delta d = \int_0^d (Z - 1)/d \delta d \quad (16)$$

or in a dimensionless form

$$\frac{\bar{A}}{RT} = \int_0^{d_r^*} (Z - 1)/d_r^* (\delta d_r^*) \quad (17)$$

Now if a plot of Z vs. d_r^* for two gases coincides along a given reduced-temperature isotherm, then the above integral will coincide for the two gases at all values of d_r^* . It is evident that a chart of the dimensionless function \bar{A}/RT vs. d_r^* with lines of constant T_r for a given gas can be used for a sec-

ond gas provided that the corrected reduced temperature is used instead of the true reduced temperature. Thus the method of using this chart would be the same as for the compressibility-factor chart.

When one considers \bar{S}_d , from Equations (14) and (15)

$$\bar{S}_d = - \int_0^d \left(\frac{\partial P}{\partial T} \right)_d - Rd \delta d \quad (18)$$

TABLE I. CORRELATION OF THE PARAMETER S WITH THE RATIO T_c/T_B

Gas	Critical temperature, °K.	Critical pressure, atm.	Pseudo-critical density g.-moles/liter	s/Rd'_c	Normal boiling temperature, °K.	T_c/T_B	$s/Rd'_c T_c/T_B$
Nitrogen	126.26	33.54	11.163	1.8329	77.36	1.632	2.995
Krypton	209.39	54.27	10.892	1.7623	120.26	1.741	3.065
Xenon	289.81	57.89	8.396	1.7700	166.06	1.745	3.09
Methane	190.56	45.50	10.040	1.7920	111.66	1.706	3.06
Ethane	305.43	48.20	6.631	1.8570	184.86	1.652	3.07
Propane	370.00	42.01	4.771	1.8951	230.99	1.602	3.04
n-Butane	425.17	37.48	3.704	1.9370	272.67	1.559	3.02
iso-Butane	408.14	36.00	3.707	1.9640	262.96	1.552	3.05
N-Pentane	469.78	33.31	2.980	1.9897	309.36	1.519	3.025
neo-Pentane	433.76	31.57	3.058	1.9660	282.66	1.534	3.015
n-Heptane	540.17	27.00	2.095	2.0520	371.68	1.453	2.98
Ethylene	282.41	50.05	7.447	1.8510	169.26	1.668	3.085
Propylene	364.56	45.40	5.233	1.8906	225.46	1.617	3.065
iso-Butylene	417.89	39.48	3.970	1.9374	267.16	1.564	3.03
Carbon Dioxide	304.16	72.90	10.072	1.9450	183.81†	1.655	3.215
Oxygen ^x	154.66	49.71	13.520	1.8115	90.16	1.715	3.10
Hydrogen*	33.19	12.98	16.434	1.565	20.42	1.626	2.55
Hydrogen Sulfide	373.56	88.87	9.998	1.845	213.56	1.749	3.225
Water‡	647.3	218.2	14.170	2.010	373.16	1.735	3.485

^x Based on data at 100 atm. and 0°C.; reduced density = 0.3575 and hence should be rechecked when new data is available at higher densities.

* At 17.17°K. the vapor pressure of hydrogen is equal to one-fortieth of the critical pressure. When one uses this value for T_B , the product $S \times T_c/T_B$ is equal to 3.025.

† Because of the high triple-point pressure of carbon dioxide the liquid phase is not stable at 1-atm. pressure. This value for the normal boiling point was obtained by extrapolation of the vapor-pressure curve for the liquid phase.

‡ The PVT correlation is not recommended for water.

or in dimensionless form

$$\frac{\bar{S}_d}{R} = - \int_0^{d_r} \left[\left(\frac{\partial P}{\partial T} \right)_d / R d - 1 \right] \frac{1}{d_r} \delta d_r \quad (19)$$

The term in the bracket is equal to $S - 1$ when the density is equal to the pseudocritical density. Thus the value of this quantity for two gases at the pseudocritical density is in the ratio of $(S - 1)_2 / (S - 1)_1$. It was found from experimental PVT data that this ratio applies for the term in the bracket at all densities within the limit of the correlation. Hence

$$\left(\frac{\bar{S}_d}{R} \right)_2 = \frac{(S - 1)_2}{(S - 1)_1} \left(\frac{\bar{S}_d}{R} \right)_1$$

The effect of pressure (or density) on the thermodynamic functions of the real gas can be obtained from the two functions \bar{A}/RT and \bar{S}_d/R for the reference gas nitrogen with the following equations used:

$$(S_{d,r} - S^\circ_r) / R =$$

$$[(S - 1) / 0.8329] \bar{S}_d / R - \ln P / Z \quad (20)$$

$$(H_{d,r} - H^\circ_r) / RT =$$

$$[(S - 1) / 0.8329] \bar{S}_d / R + \bar{A} / RT + (Z - 1) \quad (21)$$

$$(E_{d,r} - E^\circ_r) / RT =$$

$$[(S - 1) / 0.8329] \bar{S}_d / R + \bar{A} / RT \quad (22)$$

$$(A_{d,r} - A^\circ_r) / RT = \bar{A} / RT + \ln P / Z \quad (23)$$

$$(F_{d,r} - F^\circ_r) / RT =$$

$$\ln f = \bar{A} / RT + \ln P / Z + (Z - 1) \quad (24)$$

The functions \bar{S}_d/R and \bar{A}/RT for

TABLE 2. SUMMARIZED COMPARISON OF PROPOSED CORRELATION WITH EXPERIMENTAL DATA FOR TWELVE GASES

Gas	Average % error up to a pseudoreduced density of 1.0		Average % error up to a pseudoreduced density of 1.2		Maximum error of any point up to a reduced density of 1.2		Reduced temperature range of experimental data
	Proposed correlation	Without the parameter S	Proposed correlation	Without the parameter S	Proposed correlation	Without the parameter S	
Xenon	0.14	1.11	0.17	1.33	0.85	3.95	1.000-1.977
Nitrogen			basis of correlation				0.750-3.000
Krypton	0.15	1.72	—	—	0.69	3.34	1.305-2.737
Methane	0.22	1.08	0.30	1.22	1.76	3.04	1.066-2.483
Ethane	0.27	0.51	0.32	0.49	0.87	1.36	0.976-1.713
Propane	0.28	1.22	0.33	1.22	1.19	2.94	1.000-1.511
n-Butane	0.23	1.35	—	—	0.65	4.45	0.995-1.348
n-Pentane	0.28	2.08	0.37	2.21	1.13	4.85	1.007-1.220
neo-Pentane	0.22	1.72	0.27	1.87	1.23	4.98	1.000-1.264
n-Heptane	0.44	2.77	0.55	2.93	1.16	5.98	1.015-1.154
Ethylene	0.25	0.45	—	—	0.83	1.05	0.967-1.670
iso-Butene	0.23	1.45	0.25	1.51	1.10	3.37	1.013-1.312
Hydrogen Sulfide	0.26	0.43	—	—	0.72	1.86	0.744-1.189
Average	0.25	1.32	0.32	1.60	1.01	3.43	

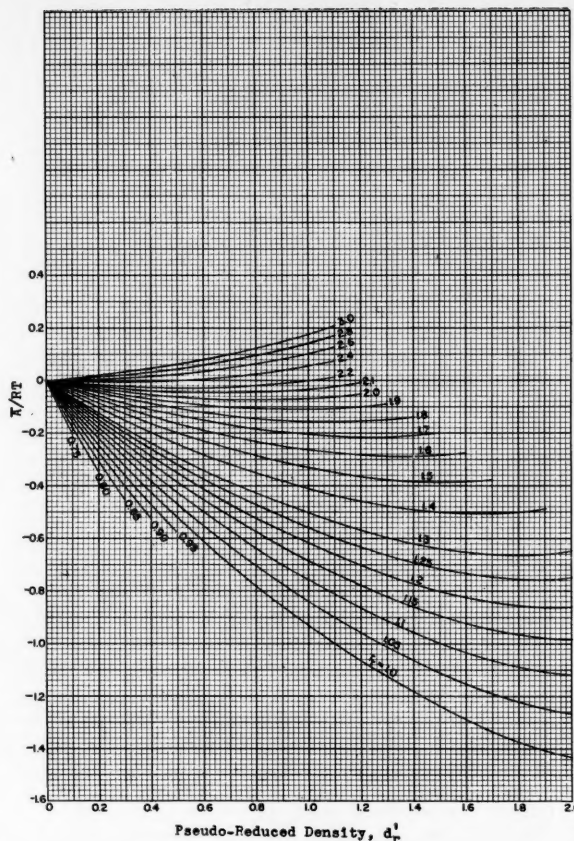


Fig. 6. Generalized chart for determining the residual work content.

nitrogen are plotted in Figures 6 and 7 against the pseudocritical density. The corrected reduced temperature and the pseudoreduced density are used with Figures 6 and 7 to determine the values of \bar{S}_d/R and \bar{A}/RT . However the value of \bar{S}_d/R must be corrected as noted in the equations. The value read from Figure 7 is multiplied by $(S - 1) / 0.8329$. The 0.8329 term is the value of $S - 1$ for the reference gas nitrogen.

Figure 5 plots the commonly used fugacity to pressure ratio chart vs. the pressure for nitrogen. The method of using this chart for other gases is the same as with the compressibility-factor chart. The corrected reduced temperature and corrected reduced pressure are used instead of the true values.

DISCUSSION

It is well known that the law of corresponding states applies rigorously only to the spherical nonpolar molecules. It is obvious that the correction factor S presented here takes into account the aspherical factor for nonpolar molecules. It thus may be regarded as a shape factor. If a polar molecule is very nearly spherical (as

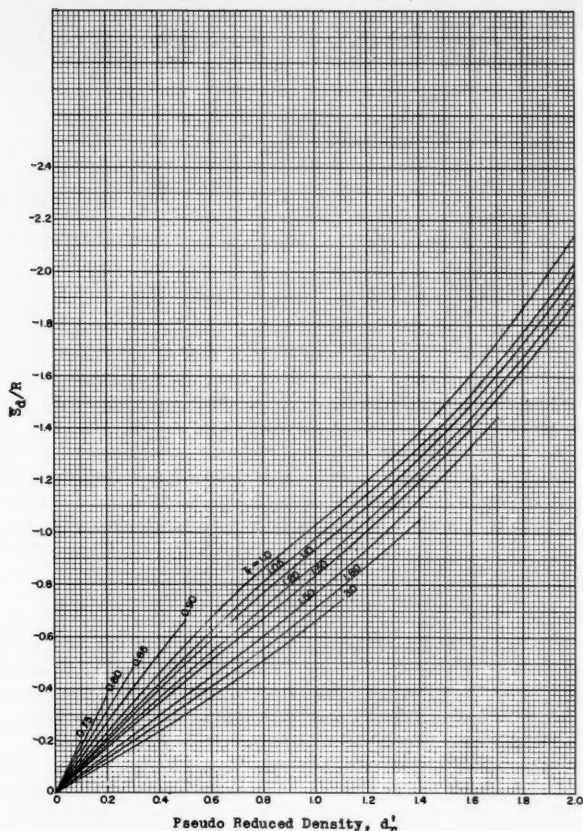


Fig. 7. Generalized chart for determining the entropy difference.

for example hydrogen sulfide), then the correction also does a good job of taking into account the dipole moment of the molecule. If the molecule is highly polar (as for example water) or both is aspherical and has a dipole moment (as for example the alcohols), then the correlation is probably not very satisfactory. However the later cases were not investigated in this work. Those few gases which have quantum correction were also not investigated, although it appears that the correlation should be satisfactory for them up to a reduced temperature of 3.0.

A correlation with a similar third parameter but different in the method of correcting for the third parameter has been presented by Pitzer *et al.* (6). They also related the third parameter to the vapor-pressure curve using a method very similar to that presented here. However the method presented here for taking into account the effect of the third parameter on the gas properties is considerably simpler to use and is at least as accurate over most of its range of applicability. The correlation of Pitzer *et al.* has a somewhat greater range of applicability.

The true critical point compressibility factor has also been proposed by

Meissner and Sefrian (5) as a third parameter. The use of this quantity as the third parameter however suffers from the fact that accurate data are seldom available for it. However a very simple relationship between the parameter S and the critical point compressibility factor has been found for the gases investigated in this work: $S \times Z_c = 0.5280$.

With the exception of carbon dioxide, hydrogen, and water, the values of S calculated from this equation agree with those tabulated in Table I to within an average of 1.13%. The maximum error is 2.6%. The error for carbon dioxide is 4.2% ($Z_c = 0.283$). Thus Z_c should be a satisfactory third parameter for nonpolar gases. However the correlation of S as a function of the ratio T_c/T_b and the critical pressure is much preferred because these data are usually available and are of higher accuracy than Z_c . It would appear that the above equation is a satisfactory method for estimating Z_c for nonpolar gases when no experimental data are available.

NOTATION

\bar{A} = work function per mole
 \bar{A} = difference between work con-

tent of real gas at given temperature and density and ideal gas at same temperature and density

E = energy content per mole
 F = free energy per mole
 H = enthalpy per mole
 I = intercept on P axis
 P = absolute pressure
 R = universal gas constant per mole
 S = entropy per mole, the slope of the pseudocritical isometric in dimensionless form ($s/R d_r^*$)
 \bar{S}_d = difference between entropy of real gas and ideal gas at same temperature and density
 T = absolute temperature
 Z = compressibility factor
 d = molar density
 f = fugacity
 s = slope of the pseudocritical isometric

Subscripts

c = the critical state
 P, d, T = a constant pressure
 r = reduced state, a state relative to the critical state

Superscripts

* = state of ideal gas-law behavior at 1-atm. pressure
 $-$ = differences between the value of a property and the value of the property if the substance behaved as an ideal gas at the same temperature and density as the real gas
 $'$ = reduced quantity which has been corrected by the proposed correlation

Abbreviations and other symbols

∂ = partial differential operator
 \int = integral operator
 ∂ = differential operator

LITERATURE CITED

1. Benedict, Manson, G. B. Webb, and L. C. Rubin, *J. Chem. Phys.*, **8**, 334 (1940).
2. Bloomer, O. T., Ph.D. thesis, Illinois Inst. Tech., Chicago (June, 1954).
3. Cope, J. Q., W. K. Lewis, and H. C. Weber, *Ind. Eng. Chem.*, **23**, 887 (1931).
4. Curtis, C. F., C. A. Boyd, and H. B. Palmer, *J. Chem. Phys.*, **19**, 663 (1951).
5. Meissner, H. P., and R. Seferian, *Ind. Eng. Chem.*, **27**, 302 (1935).
6. Pitzer, K. S., D. Z. Lippmann, R. F. Curl, C. M. Huggins, and D. E. Petersen, *J. Am. Chem. Soc.*, **77**, 3433 (1955).
7. Su, G. J., *Ind. Eng. Chem.*, **38**, 803 (1946).

Manuscript received March 17, 1959; revision received July 27, 1959; paper accepted August 4, 1959.

Heat Transfer to Liquid Streams in a Packed Tube Containing Large Packings

BALAPA CHENNAKESAVAN

A. C. College of Technology, University of Madras, Madras, India

Wall-area heat transfer coefficients based on bulk-mean temperatures of the liquids flowing upward in a steam-jacketed packed tube (4 ft. long and 2.25-in. I.D.) were determined. The tube was randomly packed in each of the experiments with spherical glass packings of uniform size (with diameters between 3/4 and 5/32 in.). The liquids used were water, toluene, 45% aqueous glycerine, and nitrobenzene.

Analogous correlations were developed for the heat transfer coefficients and for pressure drop, the dimensionless groups in the above being the same as for open tubes. The two relationships are applicable for the range in D_T/D_p ratio from 14 to 3 and in N_{Re} from 40,000 to 300. The first is satisfactory within $\pm 15\%$ for heating of liquids in the above packed tube, the second within $\pm 10\%$ for most of the data of packed tubes reported so far.

CRITERIA OF FLOW IN PACKED BEDS

The packed beds containing small packings have received much attention; the flow and transfer processes in them have been studied with different methods of approach, for example empirical correlations, analysis based on differential equations, and analysis by means of statistical concepts for turbulent diffusion. As shown in the following brief discussion, the available information provides the basis for a conclusion that is important for the present study; this is that the packed columns may be conveniently divided into two classes: the packed beds with D_T/D_p ratios greater than 10 or 12 and the packed tubes with smaller D_T/D_p ratios. In the former, analogy among the three transfer processes is found by the use of the modified Reynolds number $[N'_{Re}; (D_p w_o \rho) / \mu]$ as the criterion of flow. In the latter it appears that the Reynolds number based on tube diameter $[N_{Re}; (D_T w_o \rho) / \mu]$ can be used advantageously for satisfactory empirical correlations. In the above as well as in the following account the term packed bed is used to specify the packed systems containing (nonconducting) smooth, spherical, randomly packed packings of uniform size with D_T/D_p ratios greater than 12. The term packed tube is used for the packed systems of same properties with smaller D_T/D_p ratios.

Data and different empirical correlations for heat transfer coefficients at the tube wall of packed columns have been reported by Colburn (18) and Leva and co-workers (19, 20). These correlations are based on the dimensionless groups N_{su} and N'_{Re} and a complex function of the D_p/D_T ratio. Schumacher (10) used the above data to show a single comprehensive correlation represented in a plot of $\log N_{su}$ vs. $\log N'_{Re}$. The significant part of this

correlation, given as

$$N_{su} = 7.5(0.023)(N'_{Re})^{0.75}$$

is applicable when N_{Re} is greater than 9,500 and also pertains mostly to the data of packed tubes with small D_T/D_p ratios. The suitability of this simple relationship, without any need for a complex correction factor based on D_p/D_T ratio, indicated that the tube-diameter-based Reynolds number is to be preferred for the correlation of the heat transfer data of the present investigation in packed tubes.

It is remarkable that none of the available correlations for pressure drop [including that of Leva and co-workers (15, 16)] is satisfactory for the case of packed tubes, as is evident from a recent report (13). On the other hand, for (spherical) packed beds the two apparently different correlations of Chilton and Colburn (14) and Ergun (8) are equally suitable. The first one uses the group $(D_p w_o \rho) / \mu$ to characterize the flow; the second uses for the same purpose the group $(4r'_h w_o \rho) / \mu$ [generally represented as $(D_p w_o \rho) / [\mu(1-\epsilon)]$ (7)]. However it is evident as indicated by Mott (4) that the values of the two groups are identical if the terms ϵ , w , and r'_h are given appropriate values (9); $\epsilon = 0.34 + 0.4 D_p/D_T$ for $D_p/D_T < 0.08$, $w = w_o/\epsilon$, and $r'_h = D_p \epsilon / [6(1-\epsilon) + 4D_p/D_T]$. The above facts clearly show that the group $(D_p w_o \rho) / \mu$ or N'_{Re} is most satisfactory for correlations, as in the analogous field of heat transfer, only in the case of packed beds with D_T/D_p ratios > 12 .

Recently Baron (1) and Wilhelm and co-workers (2, 3) used the approaches based on differential equations and also on statistical concepts to interpret the mechanism of turbulent diffusion in the packed bed by reference to the theory of random-walk flow. This theory is valid owing to inherent assumptions only for packed beds with

D_T/D_p ratios > 10 and to $N'_{Re} > 200$. It predicts that the turbulent diffusivity for the lateral diffusion process is determined only by the product of w_o and D_p and that the modified Peclet number $[N'_{Pe}; (D_p w_o) / (E_T)]$ is constant and nearly equal to 10. References 2 and 3 present experimental data that are in accord with above predicted results, the former for lateral diffusion of mass in gas streams and water streams and the latter for the lateral diffusion of heat in gas streams. Thus these results show that the packed beds have unique characteristics different from those of the packed tubes. Besides in the former the mean fractional voids vary but slightly as the D_T/D_p ratios increase above 12 (4); the distribution of voids and velocity of flow across the cross section in the packed bed is nearly uniform. In all these properties the packed tubes show marked differences (5).

In the packed tube there is appreciable channeling of flow adjacent to the tube wall. Because of this the heat transfer process at the tube wall of the packed tube resembles that in open tubes, especially those provided with turbulence promoters. On the basis of this view Ranz (6) recommended the use of N_{Re} for correlation of heat transfer coefficients of packed tubes. This suggestion receives further support from the following observations of reference 3: heat transfer rates (as indicated from values of N'_{Pe}) are determined in the packed tubes, to an important degree, by the dimension D_T ; their values are of the same order of magnitude as those of open tubes.

The temperature gradients in the packed bed, in its core as well as in the vicinity of the tube wall, have been studied to obtain a direct insight into the mechanism of heat flow. From the analysis of the temperature profiles in packed beds (with gas streams) Argo and Smith (26) noted that a constant value of N'_{Pe} is found only in the core

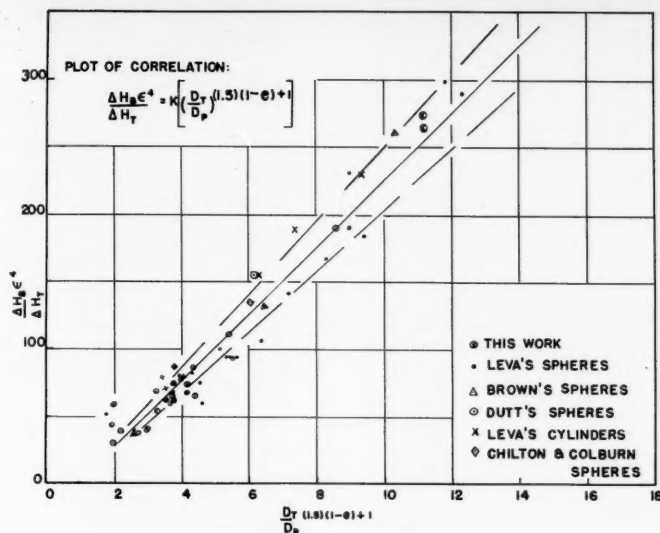


Fig. 1. Pressure drop in packed tubes.

of the bed. There is an appreciable temperature drop at the tube wall which indicates the presence of a convective type of boundary layer at the tube wall. Coberly and Marshall (22) and others (23, 24, 25) undertook special studies of this local resistance to heat flow at the tube wall. It is hence obvious that in packed tubes characterized by channeling of flow near the tube wall this boundary layer at the tube wall must assume a major role in controlling heat transfer as in the case of open tubes.

In summary the above cited results indicate that the choice of the criterion of flow, that is the selection of the length and velocity terms of the Reynolds group, is complicated for the case of the packed system. The lengths D_p , D_T and the ratios D_T/D_p and ϵ enter into the geometrical specification of the packed bed. But dimensional analysis can merely affirm that any characteristic length such as D_p , D_T , or $4r''$ (the equivalent diameter of the pores) must be a component of the Reynolds group. Similarly there is uncertainty as to the exact value of the velocity component. Under these circumstances the justification for the necessary choice of criterion of flow is a priori on the assumption of a plausible model of flow and a posteriori insofar as a simple and satisfactory correlation is obtained. It is interesting that the three models proposed so far for flow in packed beds all lead to the same criterion of flow: $(D_T w_{sp})/\mu$. These models are (1) external flow past assembly of spheres, (2) internal flow through the assembly of capillaries within the packed bed, and (3) random-walk model. However

it is evident that these models are satisfactory only for the case of uniform flow as in packed beds with D_T/D_p ratios greater than 12 and also that they are not consistent with the flow characteristics of packed tubes containing large packings. In the latter there is appreciable channeling of flow near the tube wall, and the pores are not comparable to capillaries since the pore system is more open in structure. Further, as found in the present experiments, the resistance to heat transfer is proportional to $1/w_{sp}^{0.8}$ as in open pipes. Consequently it seems more ap-

propriate to compare the flow to that in open tubes provided with turbulence promoters—which means that the criterion of flow would be the Reynolds number based on tube diameter. That this criterion is satisfactory is evidenced by the correlation of Schumacher for heat transfer to gases and the correlations presented in this paper for heat transfer to liquids and for pressure drop in packed tubes containing large packings.

PRESSURE-DROP CORRELATION

When one stipulates a similarity between the transfer processes in the packed tube and the open tube, a correlation for pressure drop in packed tubes can be expected which must be essentially a modified Fanning equation. Hence the following equations may be given:

$$\Delta H_T = f \cdot \frac{w_{sp}^2}{2g} \cdot \frac{L}{r_H}$$

for the open tube

$$\Delta H_T = K \cdot f \cdot \frac{w_{sp}^2}{\epsilon^2 \cdot 2g} \cdot \frac{L_H}{r''}$$

for the packed tube

In the above $r_H = D_T/4$ and $r'' = D_T/\epsilon(1-\epsilon)(D_T/D_p) + 4$, that is ratio of free volume and total frictional surface. Increased pressure drop in the packed tube is caused by the winding paths for the liquid in the core of the packed tube and by the consequent kinetic losses. The last mentioned effects would be prominent in tubes

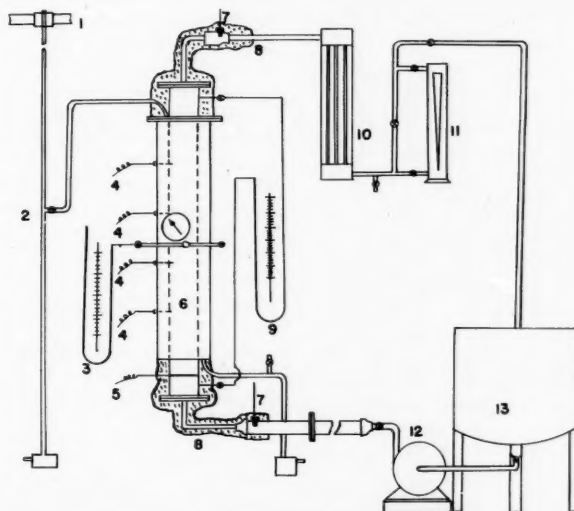


Fig. 2. Flow diagram: 1 and 2, steam main; 3 and 9, manometers; 4 and 5, thermocouples; 6, packed column; 7, thermometers; 8, insulation; 10, tubular cooler; 11, rotameter; 12, C.F. pump; 13, tank; 14, steam traps.

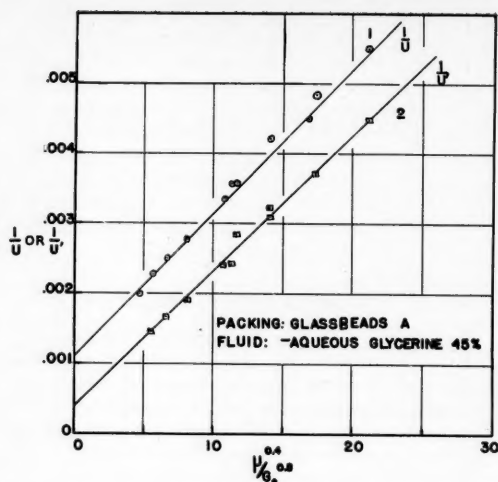


Fig. 3. Wilson plot for heating of liquid in packed tube.

packed densely but would disappear as the voids approach that of the open tube. Hence it may be tentatively assumed that L_b may be replaced by L/ϵ in the above equation for the packed tube. When one introduces these assumptions the same can be given as

$$\Delta H_b = K \cdot \frac{2f}{g} \cdot \frac{w_s^2 L}{\epsilon^4} \cdot \frac{1}{D_r}$$

$$\frac{1}{(1.5)(1-\epsilon)(D_r/D_p) + 1}$$

Comparison of this equation with that of Fanning gives with the introduction of an additive constant

$$\frac{\Delta H_{b\epsilon^4}}{\Delta H_r} = \frac{K[(1.5)(1-\epsilon)(D_r/D_p) + 1] + b}{\Delta H_r}$$

$$\frac{\Delta H_{b\epsilon^4}}{\Delta H_r} = K \left[\frac{\tau_{n\epsilon}}{\tau'_n} \right] + b$$

This relationship (12) for packed tubes, a plot of which is given in Figure 1, is found to be satisfactory within $\pm 10\%$ for the available data (11 to 17) of pressure drop in packed tubes with D_r/D_p ratios in the range between 14 and 3 and for a range in N_{Re} from 300 to 40,000. It may be noted that the constant K is a relative shape factor which might be justified by the complex geometry of packed tube. The constant b as also the lower limit of D_r/D_p ratio of 3 might be attributed to the behavior of ϵ which reaches a maximum at D_r/D_p ratio of approximately 2.

HEAT TRANSFER EXPERIMENTS IN PACKED TUBES

Only one tube size, a 2.25-in. I.D., was employed owing to limited equip-

ment and because priority was given to the objective of getting the data for heating of different liquids with varying Prandtl numbers. However the analogous correlations of Schumacher for heating of gases and that of this paper for pressure drop cover the range usually feasible in laboratory work. In view of the above and of the observations noted earlier in the discussion on criteria of flow, it is believed that the use of N_{Re} for correlation of heat transfer coefficients, determined in this single packed tube, is appropriate. The inference that the transfer process in the packed tube is similar to that in the open tube is of basic importance to this work. It has enabled the application of simple procedures, as in open tubes, for the experiments and for the treatment of the data, for example the resolution of over-all coefficients into liquid-film coefficients by means of Wilson's plot. Further, this method of correlation is of practical advantage since it permits the direct comparison of heat transfer and pressure-drop characteristics of packed tubes with those of open tubes. However it is recognized that further experiments for other tube sizes are necessary. Such an extension of this work is also in progress.

The packed tube employed was a steam-jacketed copper tube of inside and outside diameters 2.25 and 2.5 in. respectively, of packed length 5 ft. 6 in. ($L/D_r = 29.4$), and steam-jacketed length 4 ft. ($L/D_r = 21.4$). It was mounted vertically in a closed-circuit flow system consisting of a glass-lined tank, a centrifugal pump, an orifice meter, a rotameter for visual inspection for presence of air, and tubular cooler of ample capacity (Figure 2). The liquids flowed upward through the packed tube heater. The steam jacket

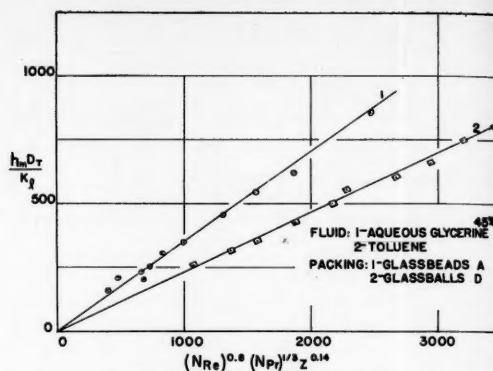


Fig. 4. Correlation of experimental heat transfer coefficients.

was provided with an air vent. Liquid temperatures were measured, at thermometer wells containing mercury, with certified and calibrated thermometers reading to 0.1°F . For measuring the temperature of the wall of the packed tube four copper-constantin thermocouples were inserted on the outer surface of the packed tube by adopting a simplified standard design with the tube wall itself forming one of the leads. In all the experiments the tube was first filled with the liquid, and the packings were then added a few at a time to ensure random packing and also the exclusion of air from the unit. The measurements for each experiment were liquid flow rate, inlet and outlet temperatures, saturated steam temperature, and tube wall temperature. In the heating experiments with liquids steady state conditions were reached by about 10 min. after setting the inlet valves for steam, for cooling water, and the discharge valve of the pump. Readings were then taken every 5 min. till three or four were in agreement. In most cases it took about 30 min. to complete an experiment. In a few orientating experiments the heat balance of the system was verified by collecting the condensate.

The treatment of the data was as follows. The total resistance is the sum of individual ones as in

$$\frac{1}{U} = \frac{A_i}{h_i A_o} + \frac{X A_i}{k_m A_m} + \frac{1}{h_m} + \frac{1}{h_a}$$

For computing the values of h_m the method of Wilson (27) involving extrapolation of the straight-line plot of $1/U$ vs. $1/(\text{velocity})^{0.8}$ is satisfactory provided $1/h_m$ is the controlling factor. In this work the resistance on the steam side is appreciable and increases with the heat flux, causing the above plot to bend slightly upward near the Y axis. Beatty and Katz (28) indicated that this difficulty can be overcome by fixing the slope of the same plot on the basis of a narrow interval of points in the high velocity range, and this procedure was found to be suitable in this case. However plots were made of $1/U$

TABLE 1. CHARACTERISTICS OF PACKINGS USED

Packing number	Shape	Diameter of sphere or nominal diameter (D_p)	Equivalent diameter (D_n)	Voids %	D_n/D_T
(A)	(Glass beads) sphere	0.257 in.	0.257 in.	41.1	0.1143
(B)	(Glass beads) sphere	5/32 in.	5/32 in.	40.8	0.0695
(C)	(Glass beads) sphere	5/16 in.	5/16 in.	—	0.1390
(D)	(Glass balls) sphere	0.671 in.	0.671 in.	48.4	0.2985
(E)	(Glass balls) sphere	0.585 in.	0.585 in.	45.2	0.2600
(F)	Berl saddles	1/4 in.	0.227 in.	61.1	0.1010
(G)	Raschig rings	0.230 in.	0.229 in.	43.5	0.1020
(H)	Raschig rings	1/4 in.	0.249 in.	52.3	0.1111
(I)	Raschig rings	3/8 in.	0.353 in.	58.8	0.1570

against $\mu^{0.4}/G_o^{0.8}$ to get comparable slopes with different liquids. A partial over-all heat transfer coefficient may be defined on the same lines as U by replacing the steam temperature by the tube wall temperature in the equation used for computing U . U' is independent of condensate film resistance. The intercept of the plot of $1/U'$ vs. $\mu^{0.4}/G_o^{0.8}$ is a measure of the dirt-factor resistance. The difference between the values of the two intercepts of the above two plots is indicative of the resistance of the condensate film. In this series of experiments the slopes of the two plots tallied (Figure 3). The values of the difference between the two intercepts were of the right order and were of the same magnitude at equal heat-flux rates. However the data of h_m were computed based on the former plots, since greater reliance can be placed on the value of T_s than on the averaged value of T_w .

RESULTS AND CORRELATION

The data relating to nearly 330 runs using the liquids water, distilled water, aqueous glycerine 45%, toluene, and nitrobenzene have been reported (11). Table 1 lists the packings used. Representative data are given in Tables 2 to 5.

Trial plots on logarithmic coordinates for the data for any one liquid and one D_p/D_T ratio indicated rough correlation on the basis of the dimensionless groups

$$\frac{h_m D_T}{k_i} \left/ \left(\frac{C_p \mu_i}{k_i} \right)^{0.4} \right. \text{ and } \frac{D_T w_o \rho}{\mu_i}$$

A better fit and a slope of 0.8 was indicated by the use of the groups

$$\left(\frac{h_m D_T}{k_i} \right) \left/ \left(\frac{C_p \mu_i}{k_i} \right)^{0.4} \right.$$

* Tabular material has been deposited as document No. 6269 with the American Documentation Institute, Photoduplication Service, Library of Congress, Washington 25, D. C., and may be obtained for \$1.25 for photoprints or 35-mm microfilm.

$$\left(\frac{C_p \mu_i}{k_i} \right)^{0.33} \left(\frac{\mu_i}{\mu_w} \right)^{0.14} \text{ and } \frac{D_T w_o \rho}{\mu_i}$$

To determine the effect of D_p/D_T ratio on the shape factor in the relation

$$N_{Su} = C (N_{Re})^{0.8} (N_{Pr})^{0.33} (Z)^{0.14}$$

(where $Z = \mu_i/\mu_w$), plots were made on linear coordinates based on N_{Su} vs. $(N_{Re})^{0.8} (N_{Pr})^{0.33} (Z)^{0.14}$. Representative graphs are given in Figures 4 and 5. These shape factors for each of the D_p/D_T ratios are given in Table 6*. A plot of the value of C vs. the D_p/D_T ratio indicated the simple linear relation

$$C = 0.41 - 0.5 D_p/D_T$$

The maximum variation in the value of C , for the same D_p/D_T ratio and different liquids, is within 15%, but the difference between the averaged value of C and that for any one liquid is less than 10%. Considering the approximations involved in computing the value

* See footnote to column 1.

of h_m from the value of U one cannot readily expect greater accuracy than $\pm 15\%$. Hence the relationship for the heat transfer coefficients of present experiments is given as

$$N_{Su} = (0.41 -$$

$$0.5 (D_p/D_T) (N_{Re})^{0.8} (N_{Pr})^{0.33} (Z)^{0.14}$$

as indicated in Figures 4 and 5, to within $\pm 15\%$ for the range in Reynolds numbers from 300 to 40,000 and D_p/D_T ratios from 0.07 to 0.299 for spheres. The same relation is also seen to hold for the few sizes (three) of Raschig rings and one size of Berl saddles when their nominal sizes are used.

The above results indicate that the heat transfer coefficients for heating liquids in the packed tube are greater than those in open tubes by a factor of 10 to 13. This may be compared with the results of Schumacher who found the coefficient to be constant at 7.5 for gas streams in the case of data of Colburn and Leva and co-workers but nearly 50% greater in the case of data of Kling (29). Chu and Storow (21) also reported higher values than those of Colburn. Again Colburn's correlation indicates a maximum for h_m at a D_p/D_T ratio of 0.15. In the present experiments this maximum is not exhibited in the D_p/D_T range studied. Hence it appears that the effect of this ratio is different in the case of liquids from that of gas streams.

One of the significant results of this work is that the same heat transfer characteristics are found even at very low Reynolds number down to 300, the lowest of the experiments. Similar effects are shown in the case of pressure drop. This result, though unexpected,

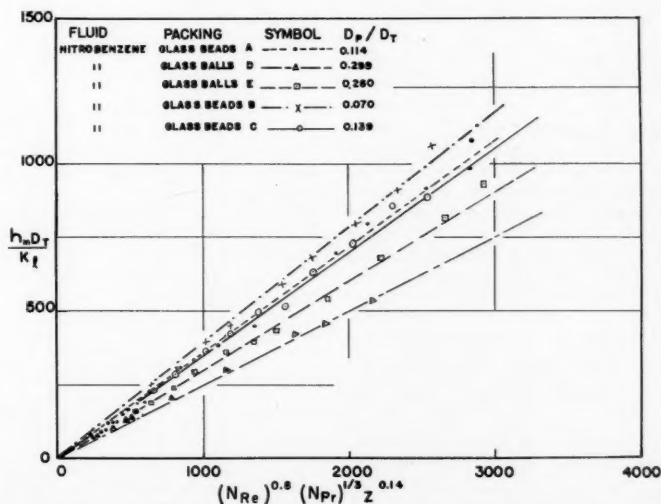


Fig. 5. Correlation of experimental heat transfer coefficients.

seems to be in line with the observations of Satterfield and co-workers (30) that turbulence persisted even at the low N_{Re} value of 10 in the packed beds studied by them.

The effect of L/D_T ratio to which reference has been made by Calderbank and Pogorski (31) could not be investigated with the present apparatus. Because of the similarity shown between the open tube and packed tube its effect might be small even as in the case of open tubes. However experimental data are needed for the case of downward flow of liquids, for cooling of liquids, for other tube sizes than the one used here, and for different L/D_T ratios.

CONCLUSION

Data on heat transfer for heating liquids flowing upward in a single packed tube and for a range in D_T/D_P ratios from 14 to 3.35 have been presented. For packed tubes of this ratio from 14 to 3 a satisfactory correlation for pressure drop has been developed by the use of the Reynolds number based on tube diameter, the Fanning friction factor, and a simple rationally derived function of fractional voids. This relationship

$$\frac{\Delta H_{\text{net}}}{\Delta H_T} =$$

$24.8[(1.5)(1-\epsilon)(D_T/D_P) + 1] - 22.3$ is applicable within $\pm 10\%$ for solid, nearly spherical packings in random-packed tubes. An analogous correlation has been found for heat transfer coefficients for the heating of liquids in a packed tube of L/D_T ratio 21.4. This is satisfactory within $\pm 15\%$ for the range in D_P/D_T ratio from 0.299 to 0.07, in N_{Re} from 40,000 to 300, and in N_{Pr} from 2.7 to 11.7 and is given as

$$\frac{h_m D_T}{k_i} = (0.4 - 0.5 D_P/D_T)$$

$$\left(\frac{D_T w_o \rho}{\mu_i} \right)^{0.5} \left(\frac{C_p \mu_i}{k_i} \right)^{0.33} \left(\frac{\mu_i}{\mu_w} \right)^{0.14}$$

ACKNOWLEDGMENT

The writer wishes to acknowledge his indebtedness to Professor G. S. Laddha, A. C. College of Technology, University of Madras for his valued interest and advice during this investigation. This paper forms a part of the Ph.D. thesis submitted to the University of Madras (1956).

Notation

- A_i = inside area of heat transfer surface of packed tube, sq. ft.
 A_m = mean area for packed tube
 A_o = outside area of heat transfer surface of packed tube, sq. ft.
 C = shape factor

- C_p = specific heat B.t.u./ (lb.) ($^{\circ}\text{F.}$)
 D_n = diameter of the equivalent volume sphere, ft.
 D_P = diameter of the packing, ft.
 D_T = diameter of the packed tube, ft.
 E_T = eddy diffusivity, sq. ft./sec.
 f = Fanning friction factor
 g = acceleration of gravity
 G_o = mass velocity of fluid based on area of cross section of empty tube, lb./ (sq. ft.) (hr.)
 h_d = dirt-factor coefficient
 h_m = mean heat transfer coefficient of the packed tube based on the area of the wall of the tube, B.t.u./ (hr.) (sq. ft.) ($^{\circ}\text{F.}$)
 h_s = condensing steam coefficient
 ΔH_B = loss of head accompanying fluid flow in packed tube
 ΔH_T = corresponding quantity in open tube
 k_i = thermal conductivity of liquid at average bulk temperature, B.t.u./ (hr.) (sq. ft.) ($^{\circ}\text{F./ft.}$)
 L = height of the packed bed, ft.
 L_B = equivalent length of flow path in packed tube
 N_{Nu} = Nusselt number, $h_m D_T / k_i$
 N_{Pe} = modified Peclet number, $D_T w_o / E_T$
 N_{Pr} = Prandtl number, $C_p \mu_i / k_i$
 N_{Re} = Reynolds number, $D_T w_o \rho / \mu_i$
 N'_{Re} = modified Reynolds number, $D_T w_o / \mu$
 r_H = hydraulic radius of tube, ft.
 r'_H = mean hydraulic radius of packed tube, ft.
 t_i = average mean bulk temperature of liquid, $^{\circ}\text{F.}$
 t_1 = liquid inlet temperature $^{\circ}\text{F.}$
 t_2 = liquid outlet temperature $^{\circ}\text{F.}$
 T_s = temperature of saturated steam, $^{\circ}\text{F.}$
 T_w = tube wall temperature
 U = over-all coefficient of heat transfer, B.t.u./ (hr.) (sq. ft.) ($^{\circ}\text{F.}$)
 U' = over-all coefficient of heat transfer from metal wall to liquid, B.t.u./ (hr.) (sq. ft.) ($^{\circ}\text{F.}$)
 w = velocity of the fluid, ft./sec.
 w_o = velocity of fluid based on area of cross section of tube, ft./sec.
 X = thickness of tube wall
 Z = ratio of viscosities of liquid at bulk temperature and wall temperature, (μ_i / μ_w)
 ϵ = mean fractional voids in packed bed
 μ_i = viscosity at bulk temperature of liquid, lb./ (hr.) (ft.)
 μ_w = viscosity at wall temperature of liquid, lb./ (hr.) (ft.)

LITERATURE CITED

1. Baron, Thomas, *Chem. Eng. Progr.*, **48**, 118 (1952).
2. Bernard, A. E., and R. H. Wilhelm, *ibid.*, **46**, 233 (1950).
3. Singer, Emanuel, and R. H. Wilhelm, *ibid.*, 343 (1950).
4. Mott, R. A., "Some Aspects of Fluid Flow," p. 242, Arnold, London, England (1951).
5. Schwartz, C. E., and J. M. Smith, *Ind. Eng. Chem.*, **45**, 1209 (1953).
6. Ranz, W. E., *Chem. Eng. Progr.*, **48**, 247 (1952).
7. Kozny, J., *Ber. Wien. Akad.*, **136** a, 271 (1927).
8. Ergun, Sabri, *Chem. Eng. Progr.*, **48**, 89 (1952).
9. Kramers, H., "Physische Transport ver Schijnsalen," Collegdictaat, Technische Hogeschool te Delft, Holland (1955).
10. Schumacher, R., *Erdol u. Kohle*, **2**, 189 (1949).
11. Chennakesavan, Balapa, Ph.D. thesis, Univ. Madras, India (1956).
12. ———, and G. S. Laddha, *Trans. Indian Inst. Chem. Engrs.*, to be published.
13. Dutt, D. K., and Roy Chowdhury, *ibid.*, **6**, 60 (1953-54).
14. Chilton, T. H., and A. P. Colburn, *Ind. Eng. Chem.*, **28**, 913 (1931).
15. Leva, Max, *Chem. Eng. Progr.*, **43**, 549 (1947).
16. ———, and Milton Grummer, *ibid.*, 633, 713 (1947).
17. Brown, G. G., et al., "Unit Operations," p. 213, Wiley, New York (1950).
18. Colburn, A. P., *Ind. Eng. Chem.*, **23**, 910 (1931); *Trans. Am. Inst. Chem. Engrs.*, **26**, 176 (1931).
19. Leva, Max., *Ind. Eng. Chem.*, **39**, 857 (1947).
20. ———, Milton Grummer, *ibid.*, **40**, 415 (1948).
21. Chu, Y. C., and J. A. Storrow, *Chem. Eng. Sci.*, **1**, 230 (1952).
22. Coberly, C. A., and W. R. Marshall, Jr., *Chem. Eng. Progr.*, **47**, 141 (1951).
23. Felix, J. R., and W. K. Neill, Preprints Heat transfer symposium, p. 125, Annual Meeting Am. Inst. Chem. Engrs., Atlantic City, December (1951).
24. Plautz, D. A., and H. F. Johnstone, *A.I.Ch.E. Journal*, **1**, 193 (1955).
25. Hanratty, T. J., *Chem Eng Sci.*, **3**, 209 (1954).
26. Argo, W. B., and J. M. Smith, *Chem. Eng. Progr.*, **49**, 443 (1953).
27. Wilson, E. E., *Trans. Am. Soc. Mech. Engrs.*, **37**, 47 (1915).
28. Beatty, K. O., Jr., and D. L. Katz, *Chem Eng. Progr.*, **44**, 55 (1948).
29. Kling, V. D. I., *Forschung*, **9**, 82 (1938).
30. Satterfield, C. N., Hyman Resmic, and R. L. Wentworth, *Chem. Eng. Progr.*, **50**, 460 (1954).
31. Calderbank, P. H., and L. A. Pogorski, *Trans. Inst. Chem. Engrs. (London)*, **35**, 195 (1957).

Manuscript received March 11, 1959; revision received August 3, 1959; paper accepted August 24, 1959. Paper presented at A.I.Ch.E. Atlantic City meeting.

Natural Convection Inside a Horizontal Cylinder

WILLIAM R. MARTINI and STUART W. CHURCHILL

The University of Michigan, Ann Arbor, Michigan

The two vertical halves of the wall of a 4.3-in. I.D. cylinder were maintained at different uniform temperatures. The rate of circulation of air inside the cylinder and the local rate of heat transfer between the wall and air were derived from measurements of the velocity and temperature fields in the air for wall-temperature differences from 3.5° to 367°F. The overall rate of circulation was found to increase quite rapidly and then to decrease slowly as the wall-temperature difference was increased. The over-all Nusselt number based on the wall-temperature difference was found to have an approximately constant value of 7.0.

Numerical solution of the partial differential equations describing the conservation of mass, momentum, and energy for this system was investigated with an IBM-650 magnetic drum computer. Instabilities in the computational procedure and limitations of this computer prevented solution of the general problem. However specification of the velocity field obtained from experiment yielded a numerical solution for the temperature field in good agreement with the experimental measurements.

The importance of natural convection in space heating and meteorology has long been recognized. More recently attention has been given to such applications as the emergency cooling of nuclear reactors, the cooling of gas turbine blades, and the recombination of the oxygen and hydrogen involved in water-boiler types of nuclear reactors. Nevertheless natural convection, particularly in enclosed spaces, has been a relatively neglected field of investigation.

Apparently natural convection in a horizontal cylinder has been studied experimentally only by Ostroumov (1), who discussed the determination of the temperature gradients in glycerine by an optical method but did not present any data. Zhukhovitskii and others (2, 3, 4) outlined a method for the approximate solution of the mass, energy, and momentum equations describing natural convection. Results in agreement with the unpublished experimental work of Ostroumov were claimed. The method appears to be applicable only for low temperature differences and/or for fluids of high viscosity, and only for very special boundary conditions.

In this investigation a long horizontal circular cylinder and a step function in temperature at the vertical diameter were chosen for simplicity. Since the primary purpose was to pro-

vide insight into the transfer processes, the temperature and velocity fields were measured rather than the heat flux at the wall.

Numerical solution of the partial differential equations for describing the conservation of mass, energy, and momentum in this system was investigated with an electronic digital computer. The possibilities of this technique are discussed and the computed values compared with the measured values.

Only representative data, final correlations, and conclusions are presented in this article. The complete data and additional details are included in reference (5).

EXPERIMENTAL APPARATUS

Figure 1 is a diagram of the experimental apparatus. A 3-ft. length of 4-in. standard iron pipe was cut in two lengthwise and welded into two iron jackets as shown. The inside surface of the pipe was machined to a uniform diameter of 4.3 in., and the two boxes were then positioned with a cylindrical template. A ¼- by 3-in. channel was constructed completely through one jacket, and a Lucite window was fitted in the pipe wall at the end of this channel to permit illumination of the inside of the pipe. The ends of the pipe were closed with glass plates.

The ½-in. space between the jackets above and below the pipe was filled with asbestos felt. With the exception of the windows, the jackets were covered with 4 in. of insulation and a layer of alumi-

num foil. A plug of insulation covered the Lucite window when it was not in use for velocity measurements.

Heat was supplied to one jacket by electrical resistance elements. The energy input was regulated by a variable transformer and measured by a wattmeter. The jacket was filled to a depth of 2 or 3 in. with acetone water, Dowtherm A or Dowtherm E and evacuated to remove air from the vapor space. A condenser was mounted in the top of the jacket so that the entire jacket was filled with vapor or liquid at the saturation temperature. The pressure was measured with a mercury manometer, which also served as a safety valve.

The other jacket was filled almost to the top with acetone. Originally it had been planned to allow the acetone to boil and then to condense on the cooling coils, but operation with the cooling coils immersed in the liquid yielded a more uniform wall temperature. To minimize leaks, a slight vacuum was maintained on the cooling jacket. The rate of heat removal through the cooling coils in the two jackets was determined by passing the cooling water through rotameters and measuring the inlet and outlet temperatures.

TEMPERATURE MEASUREMENT

Cooling water and wall temperatures were measured with calibrated, 30-gauge, copper-constantan thermocouples. Fourteen thermocouples located at various points in the cylinder wall indicated that longitudinal temperature gradients were negligible in the central half of the cylinder wall. Consequently a two-dimensional temperature and velocity field was assumed to exist in the air in the central region. The reported temperatures of the hot and cold wall were measured in thermowells that penetrated almost to the inside surface at the horizontal diameter. Thermocouples soldered to the outside of the walls at the top and bottom indicated that the temperature variation

William R. Martini is with Atomics International, Canoga Park, California.

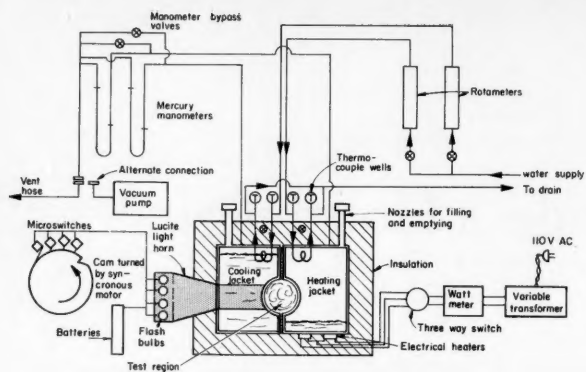


Fig. 1. Diagram of experimental apparatus.

over the walls was less than 10% of the temperature differences between the walls. The experimental boundary condition thus closely approached the idealized case of a step function in wall temperature.

The air temperature was measured with a calibrated, 40-gauge, chromel P-alumel thermocouple stretched parallel to the axis of the cylinder with the junction at the center. This single wire was supported by a rod across each end of the cylinder, just inside the glass end plates. A small spring at one end of the wire maintained tension. The two rods were allowed to slide in three horizontal and three vertical grooves. The location of the temperature traverses is indicated in Figure 2. To position the thermocouple, the rods were placed in corresponding grooves at the two ends; then each rod was moved by hand until the stretched wire was aligned with grid lines on the end plates. Energy balances for the 40-gauge thermocouple wires indicate that the effect of radiation on the air-temperature measurements and on the desired heat transfer rates was negligible.

VELOCITY MEASUREMENT

The velocity field was determined by photographing dust particles suspended in the air. A small quantity of titanium-dioxide pigment having particle diameters from 3 to 7 μ was blown into the center of the test space through a small tube. The flow pattern reestablished itself in about 30 sec. after introduction of the dust. The settling velocity of the particles was calculated to be 0.05 to 0.2 in./sec., which was negligible compared with the air velocity in most of the region.

The particles were illuminated through the Lucite window in one side of the cylinder. Fast-peaking flash bulbs were used so that the flow measurements would be completed before the flow could be affected by the thermal radiation. The time scale of the acceleration due to the bulbs was observed to be far greater than the period of exposure. A Lucite light horn directed the light from the bulbs into the center of the test regions as indicated in Figure 1. The bulbs were fired by microswitches riding on a wheel driven at 37.5 rev./min. by a synchronous motor. The time interval between the flashes was obtained from a triple exposure of a

radial mark on the wheel. In order to photograph the particles, the glass end plates on the cylinder were replaced with opaque plates, one of which had a hole at the axis of the cylinder. A short black cardboard tube leading from this hole to the camera acted as a lens shade and also shielded the test region from external drafts. A triple exposure was obtained at $f/4.5$.

An enlarged section of a photograph obtained as described above is shown in Figure 3. This photograph shows clearly the groups of three images from which the velocities and streamlines were deduced. Dust tracks very near the wall were obscured by wall reflections.

The photographs were analyzed by tracing the flow lines and measuring the distance between the images of each particle. The flow lines obtained for run 4 are sketched in Figure 4. The velocities along



Fig. 3. Dust tracks near cold wall, run 8, $T_h - T_c = 3.47^\circ\text{F}$.

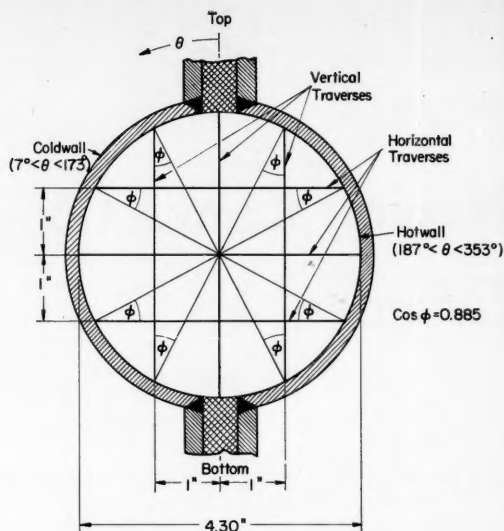


Fig. 2. Experimental geometry.

the horizontal and vertical diameters are drawn as curved vectors, and the ends of the vectors are connected by a heavy line.

FLOW FIELD

The major characteristics of the fluid motion are apparent from the streamlines and velocity vectors sketched in Figure 4 for a wall-temperature difference of 70°F. The flow patterns for all of the other experiments were quite similar. A narrow ring of gas circulates around the wall of the cylinder, but the gas in the central region is relatively stagnant. The velocity of the narrow ring of circulating gas increases up the hot wall as the gas is heated, decreases along the top of the cylinder, increases down the cold wall, and decreases again at the bottom of the cylinder. The width of the circulating ring of gas decreases up the hot wall, increases at the top, decreases down the cold side, and increases again along the bottom as required to conserve momentum. This increase and decrease in the amount of circulating gas produces large, slow eddies in the stagnant core. The motion near the wall was observed to be parallel to the wall (Figures 3 and 4), steady with time, and reproducible; therefore it can be considered laminar. The motion in the central region was also steady with time and reproducible.

Because of a positive vertical temperature gradient in the central core, the entire volume of gas does not circulate as a solid disk, as might otherwise have been expected. The central core resists rotation owing to its increasing density from top to bottom and can be considered analogous to a disk weighted at the bottom.

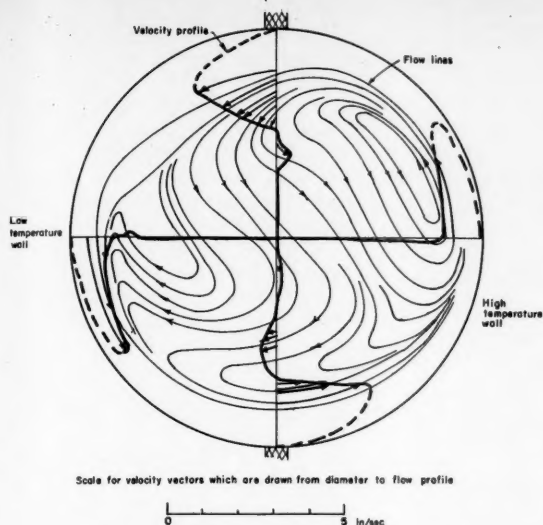


Fig. 4. Typical flow pattern, run 4, $T_h - T_c = 70^\circ\text{F}$.

The velocities were determined with the most confidence along the horizontal radius on the cold side, where the illumination was most intense. Figure 5 plots the horizontal velocity profiles for three wall-temperature differences. A decrease in the width of the circulating ring with increasing wall-temperature difference can be observed. The velocities at five points along this radius and at one point in the upper vertical radius are plotted vs. wall-temperature difference in Figure 6. The data show considerable scatter but indicate a maximum velocity at all points at a wall-temperature difference of approximately 40°F .

The total volumetric and mass rates of flow across the horizontal radius on the cold side were obtained by integration, with the three velocity and temperature profiles shown in Figure 5. The maximum velocities and hence the integrated flow rates were less certain in the other runs. The results are

plotted vs. temperature difference in Figure 7, indicating a rapid increase and then a slow decrease in the overall rate of circulation of gas with increasing wall-temperature difference.

TEMPERATURE FIELD

A typical set of temperature traverses is shown in Figures 8 and 9. Temperatures along the horizontal radius on the cold side are shown in Figure 5 for the same three wall-temperature differences for which the local velocities are plotted. The complete temperature data for thirteen different runs are given in reference 5. The temperature data for all thirteen runs are interpreted in the following paragraphs in terms of the local rates of heat transfer along the cylinder wall.

HEAT TRANSFER RATES

The local rate of heat transfer to or from an isothermal wall can be ex-

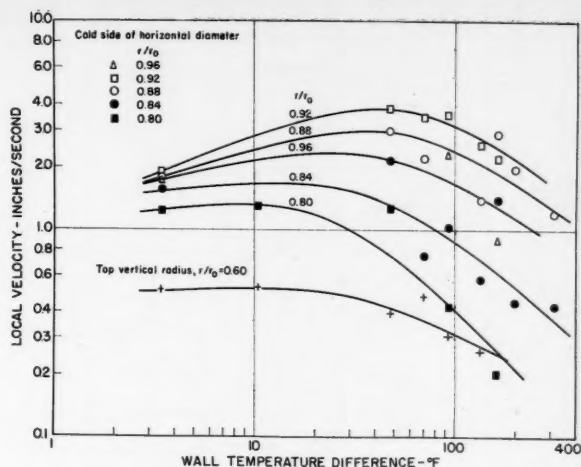


Fig. 6. Variation of local velocities with wall-temperature difference.

pressed in terms of the temperature gradient in the fluid: that is

$$\frac{dq}{dA} = -k \left(\frac{\partial T}{\partial r} \right)_{r=r_0} \quad (1)$$

As indicated in Figure 2, the air temperature was measured along a series of horizontal and vertical lines rather than along radii only. Therefore $\partial T / \partial r$ is not directly obtainable except along the vertical and horizontal radii. However as an approximation

$$\left(\frac{\partial T}{\partial r} \right)_{r=r_0} = -\frac{1}{\cos \phi} \left(\frac{\partial T}{\partial w} \right)_{w=0} \quad (2)$$

This approximation was used to estimate the local rates of heat transfer from the measured temperatures.

The temperatures along the horizontal and vertical traverses were observed to vary linearly with distance near the wall. Hence the gradient was determined by fitting a straight line through three to five points near the wall by least squares. The local rate, the local heat transfer coefficient based on the wall temperature difference

$$h = \left(\frac{dq}{dA} \right) \left(\frac{1}{T_h - T_c} \right) \quad (3)$$

and hD/k were then calculated from the gradients. The 50% confidence limits for these quantities were calculated by the method described in Duncan (7). The physical properties of the air were in all cases evaluated at the wall temperature with the values given in Eckert (8). The results are illustrated in Figure 10 for the set of data in Figures 8 and 9.

The local rates at each of the twelve positions around the wall were plotted vs. wall-temperature difference and smoothed as illustrated in Figure 11 for the horizontal radius on the cold side. The smoothed data for all positions and

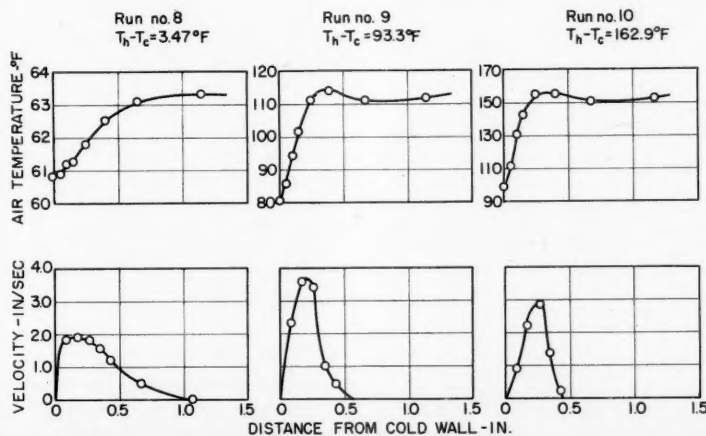


Fig. 5. Velocity and temperature distribution along horizontal radius on cold side.

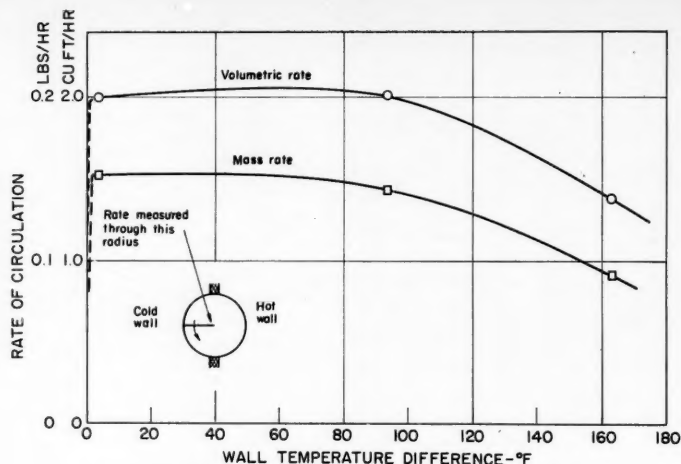


Fig. 7. Boundary-layer circulation through horizontal radius on cold side.

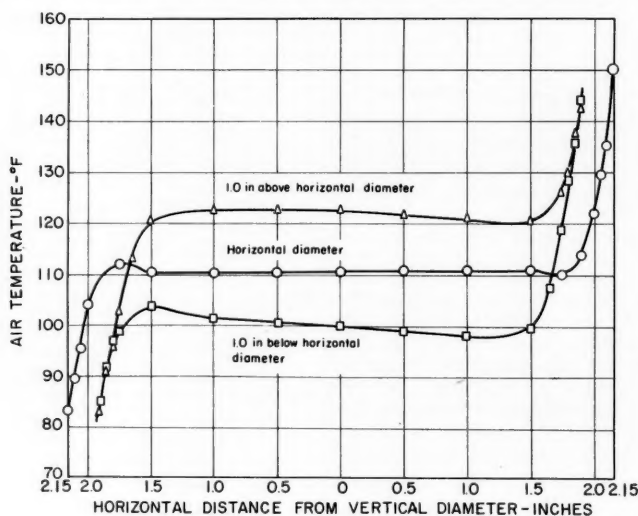


Fig. 8. Horizontal temperature profiles, run 4, $T_h - T_c = 70^\circ\text{F}$.

temperature differences are summarized in Figure 12. Since the temperature and velocity fields were not symmetrical on the hot and cold sides,

symmetry in the heat transfer rates was not to be expected.

The over-all rates of heat transfer were determined by graphical integra-

TABLE 1. OVER-ALL HEAT TRANSFER RATE DATA

Run	T_h °F.	T_c °F.	$T_h - T_c$ °F.	Cold side	Hot side	$\left[\frac{C_p \mu}{k} \right] \left[\frac{g D^3 \beta (T_h - T_c)}{\nu^2} \right] 10^{-6}$		h_m B.t.u./ (sq. ft.) (°F.)		$h_m D/k$	
						Cold side	Hot side	Cold side	Hot side	Cold side	Hot side
3	149.9	106.7	43.2	2.21	1.572	0.266	0.362	6.03	7.47		
4	146.1	76.1	70.0	4.58	2.62	0.328	0.411	7.82	8.74		
5	108.0	61.7	46.3	3.43	2.34	0.244	0.303	5.92	6.83		
6	104.4	67.1	37.3	2.66	1.954	0.224	0.270	5.42	6.13		
7	73.1	62.8	10.3	0.760	0.697	0.147	0.165	3.57	3.95		
8	64.63	61.16	3.47	0.258	0.250	0.249	0.283	6.07	6.85		
9	162.4	69.1	93.3	6.52	3.07	0.218	0.340	5.25	7.06		
10	241.9	79.0	162.9	10.44	2.64	0.332	0.449	7.87	8.13		
11	212.4	77.0	135.4	8.83	3.13	0.303	0.434	7.20	8.41		
12	297.1	98.2	198.9	10.90	1.868	0.253	0.439	5.79	7.04		
13	296.1	95.9	200.2	11.16	1.898	0.266	0.573	5.93	7.26		
14	428.5	115.1	313.4	15.09	1.052	0.274	0.637	6.09	7.32		
15	489.4	122.8	366.6	16.29	0.837	0.261	0.456	6.03	7.33		

tion of the local rates. For example the areas above the curve on the right and below the curve on the left in Figure 10 are divided by 180° to obtain the corresponding over-all Nusselt number $h_m D/k$ for the heated side and cooled sides, respectively. The over-all rates, heat transfer coefficients, and Nusselt numbers determined from these integrations are given in Table 1. Owing to significant heat losses through the insulation to the surroundings and owing to radiation from the hot wall to the cold, the data obtained from the wattmeter and the cooling water stream do not provide direct information on the rate of heat transfer by convection. Accordingly these data are not reproduced herein.

The over-all rates determined from the temperature field are plotted in Figure 13 as heat transfer coefficients vs. temperature difference. The coefficients show only a slight increase as the temperature difference increases from 3.5° to 367°F . Curves representing the correlations of Griffiths and Davis (9); Jakob (6); and Peck, Fagan, and Werlein (10) for natural convection in air between enclosed vertical plates are included in Figure 13. The observed coefficients for the cylindrical region are of the same order of magnitude. Since these three previous correlations represent data taken in rectangular regions where the height was at least three times the width, and since the data are not compared in dimensionless form, this agreement is rather surprising and perhaps coincidental.

The experimental data for heat transfer by natural convection for other geometries and boundary conditions have been correlated successfully in terms of the dimensionless groups Nu and $Pr \cdot Gr$ only. Therefore the results of this investigation can be interpreted with some justification in this general form even though the experiments were limited to a single diameter and to air at atmospheric pressure. The over-all coefficient is plotted as $Nu = h_m D/k$ vs. $Pr \cdot Gr = (C_p \mu/k) (g D^3 \beta [T_h - T_c]/\nu^2)$ in Figure 14 with all properties evaluated at the wall temperature. Although $Pr \cdot Gr$ was varied over two orders of magnitude, no significant trend in Nu is apparent. The experimental values of $h_m D/k$ have a mean value of approximately 7.0.

The data in Figures 6, 7, and 11 might similarly be reinterpreted in dimensionless terms.

MACHINE COMPUTATIONS

Numerical solution of the simultaneous partial differential equations describing conservation of mass, energy, and momentum in a gas inside an in-

finite horizontal cylinder with a vertical step in wall temperature was attempted on an IBM-650 magnetic drum computer. The details of this computational experience are presented in reference 5, and only the more significant features are reported herein.

The region within the cylinder was divided into a grid of points representing elemental volumes, and the differential equations were approximated by finite difference equations in terms of the temperatures and velocities at these points. The resulting set of algebraic equations was then solved by reiteration in real time, yielding an unsteady state solution with the steady state solution as an asymptote.

Because of storage limitations of the computer, an explicit representation was used; that is the spatial derivatives of temperature and velocity were written in terms of present and incrementally past values of the variables. Extensive exploratory calculations indicated that the explicit representation was unstable for any time increment. Solution of the mass and momentum equations only, with fixed values for the temperature field from the experimental measurements, was also unsuccessful owing to instability.

A convergent solution for the energy equations only was obtained by the use of fixed values for the velocity field taken from the experimental measurements. The computed dimensionless isotherms for conditions equivalent to run 4 are compared with the experimental values in Figure 15. Significant uncertainties in the measured velocities, as well as idealizations in the differential representation, the finite number of grid points, round-off errors, and failure to carry the computations completely to the steady state could be expected to introduce discrepancies between the experimental and computed temperatures. In view of these considerations the agreement is quite reasonable. The most apparent discrepancy in the temperature is the 20-deg. inclination of the computed isotherms toward the hot side in the central region as compared with the almost horizontal measured isotherms.

The temperature gradients at the wall which determine the rate of heat transfer are compared in Figure 16. This is a very critical test in which errors are magnified by an order of magnitude, and the agreement is surprisingly good. The saw-tooth behavior in the computed curve occurs because alternate points rather than consecutive points are associated in the computations. The construction of a smooth curve between the points would therefore have been justifiable if the objec-

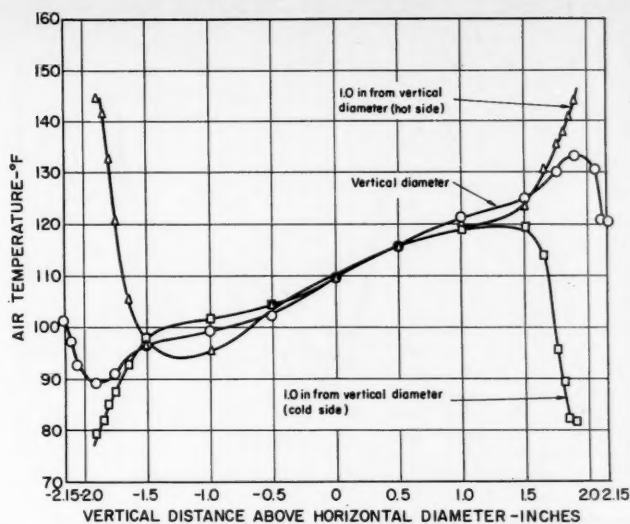


Fig. 9. Vertical temperature profiles, run 4, $T_h - T_c = 70^\circ\text{F}$.

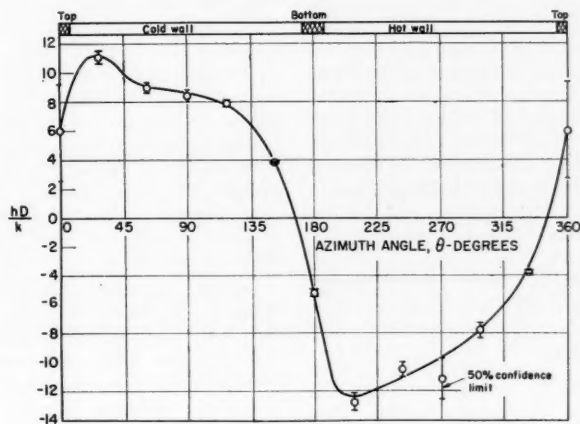


Fig. 10. Local Nusselt number, run 4, $T_h - T_c = 70^\circ\text{F}$.

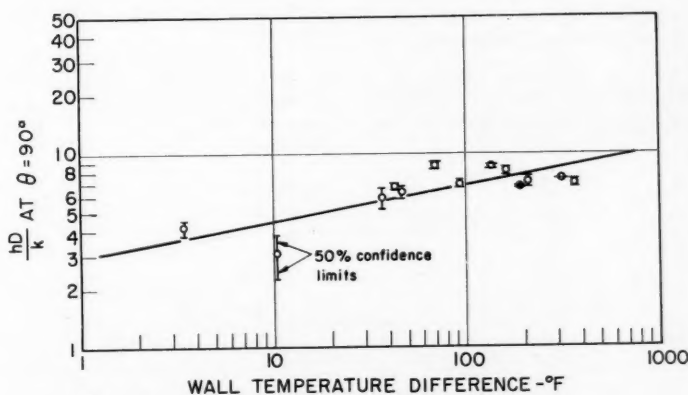


Fig. 11. Example of smoothing of local Nusselt number.

tive were to produce the best estimate of the gradient rather than to illustrate the results obtained by computation. If the thermal conductivity were constant, the net area under the curve

should be zero, since as much heat must leave the gas as enters. The experimental gradient integrates to very nearly zero, but the computed gradient shows a net heat input.

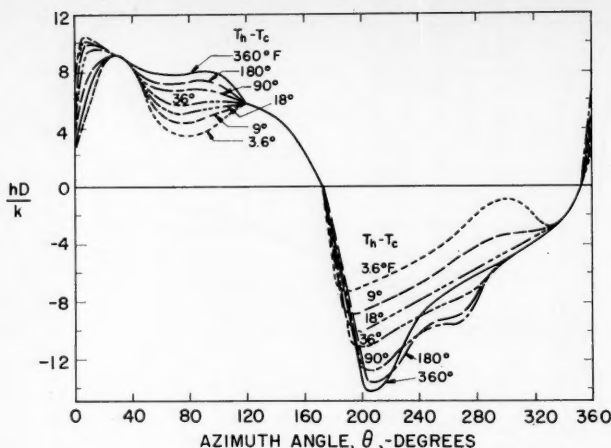


Fig. 12. Smoothed correlation for local Nusselt number.

This success with the energy equation and the failure with the momentum and mass equations suggests that the nonlinearity of the momentum equations is the key to the instability of the general problem. Linearization of the momentum equations by some transformation or idealization would undoubtedly yield stable difference equations. However such a procedure loses the very advantages of exactness promised by numerical integration. A stable procedure probably can be developed with implicit representations, but such a program is feasible only on a computer with much greater storage than the IBM-650.

CONCLUSIONS

Although the experimental investigation was exploratory rather than definitive, several general conclusions can be drawn concerning the fluid motion and the rate of heat transfer in a circular cylinder with a vertical step function in wall temperature:

1. The air circulates rapidly in a narrow band near the wall while the central core of air is essentially stagnant.

2. The circulation rate increases rapidly and then decreases slowly with increasing wall-temperature difference.

3. The local heat transfer coefficient varies considerably with angle and increases only slightly with increasing wall-temperature difference.

4. The over-all rate of heat transfer by convection for air at atmospheric pressure inside a 4.3-in. cylinder corresponds to a coefficient of approximately 0.3 B.t.u./ (hr.) (sq. ft.) (°F.) or a Nusselt number of approximately 7 over a range of wall-temperature difference from 3.5° to 367° F.

Several general conclusions can similarly be drawn from the exploratory computational investigation:

1. Explicit finite difference representations for the momentum, energy, and mass equations appear to be unstable for any size of the time increment.

2. The instability is apparently due to the nonlinear terms in the momentum equation.

3. A stable procedure probably can be developed with implicit representations, but such a program requires a computer with greater storage than the IBM-650.

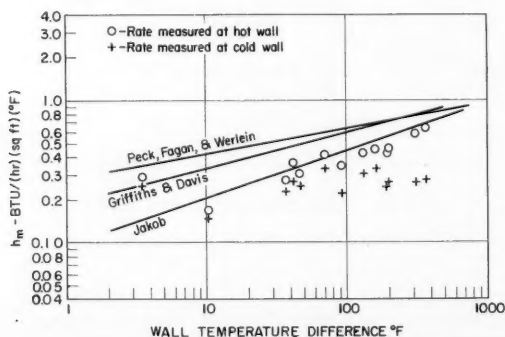


Fig. 13. Comparison of experimental correlations for natural convection.

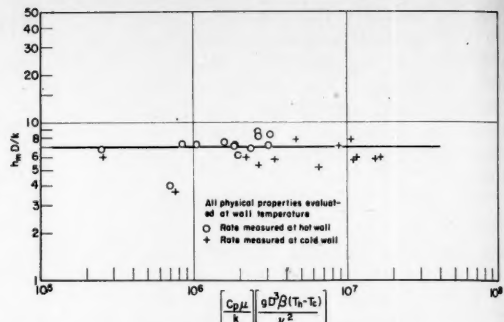


Fig. 14. Generalized correlation for natural convection inside a horizontal cylinder.

4. The agreement demonstrated between the measured temperatures and those computed by utilizing the measured velocities gives support to both the experimental values and to the numerical representation and computational procedure.

5. A method for a priori machine computation of natural convection for any boundary conditions and physical properties has real economic as well as scientific value. This computational experience is believed to be a significant step in developing such a method even though only partial success was realized.

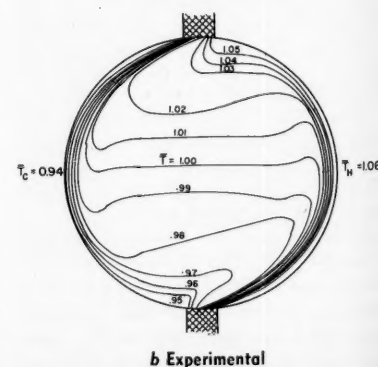
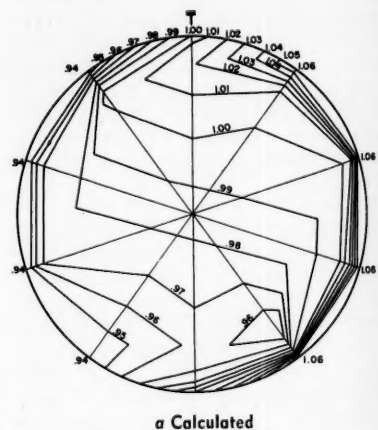


Fig. 15. Comparison of computed and measured isotherms, run 4, $T_h - T_c = 70^\circ \text{F}$.

NOTATION

- A = surface area, sq. ft.
 C_p = heat capacity, B.t.u./ (lb.) (°F.)
 D = diameter of cylinder, ft.
 g = acceleration due to gravity, (ft./hr.)/hr.
 Gr = $gD^3\rho(t_h - T_c)/\nu^2$ = Grashof number
 h = local heat transfer coefficient based on wall-temperature difference, B.t.u./ (hr.) (sq. ft.) (°F.)
 h_m = mean heat transfer coefficient over cold or hot wall based on wall-temperature difference, B.t.u./ (hr.) (sq. ft.) (°F.)
 k = thermal conductivity of gas, B.t.u./ (hr.) (sq. ft.) (°F./ft.)
 Nu = $h_m D/k$ = Nusselt number
 Pr = $C_p \mu/k$ = Prandtl number
 q = heat flux to wall, B.t.u./hr.
 r = radial distance from axis of cylinder, ft.
 r_s = radius of cylinder, ft.
 \bar{r} = r/D = dimensionless radial distance
 T = temperature, °R.
 T_c = temperature of cold wall, °R.
 T_h = temperature of hot wall, °R.
 T_o = $(T_h + T_c)/2$ = reference temperature, °R.
 \bar{T} = T/T_o = dimensionless temperature

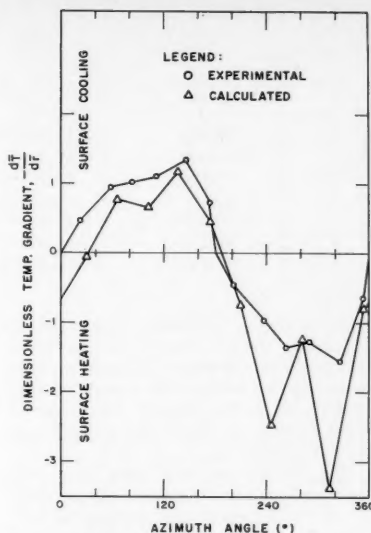


Fig. 16. Comparison of computed and measured temperature gradients, run 4, $T_h - T_c = 70^\circ\text{F}$.

w = distance from wall along a temperature traverse, ft.

Greek Letters

- β = volumetric coefficient of expansion, $^\circ\text{R}^{-1}$
 θ = azimuth angle from top of cylinder through cold side, deg.

- μ = viscosity, lb./ (ft.) (hr.)
 ν = kinematic viscosity, (sq. ft.)/hr.
 ϕ = angle between traverse line and radial line at cylinder wall, deg.

LITERATURE CITED

- Ostroumov, G. A., *Doklady Akad. Nauk S.S.S.R.*, **71**, 887 (1950).
- Zhukhovitskii, E. M., *Zhur. Tekh. Fiz.*, **22**, 832 (1952).
- Drakhlin, E., *ibid.*, **22**, 829 (1952).
- Shaposhnikov, I. G., *ibid.*, **22**, 826 (1952).
- Martini, W. R., Ph.D. thesis, Univ. Michigan, Ann Arbor (1956).
- Jakob, Max, "Heat Transfer," vol. I, John Wiley, New York (1949).
- Duncan, A. J., "Quality Control and Industrial Statistics," Richard D. Irvin, Inc., Homewood, Ill. (1953).
- Eckert, E. R. G., "Introduction to the Transfer of Heat and Mass," McGraw-Hill, New York (1950).
- Griffiths, E., and A. H. Davis, "The Transmission of Heat by Radiation and Convection," Food Investigation Board Special Report No. 9, His Majesty's Stationary Office, London, England (1922).
- Peck, R. E., W. S. Fagan, and P. P. Werlein, *Trans. Am. Soc. Mech. Engrs.*, **73**, 281 (1951).

Manuscript received May 1, 1957; revision received September 10, 1959; paper accepted October 12, 1959. Material presented at 1957 Nuclear Congress and A.I.Ch.E. Atlantic City meeting.

The Compressibility of Carbon Dioxide-Argon Mixtures

WILLIAM H. ABRAHAM and C. O. BENNETT

Purdue University, Lafayette, Indiana

The compressibility factor has been measured at 50°C. and 50 to 1,000 atm. for each of seven mixtures of carbon dioxide and argon containing 12.9 to 83.1 mole % carbon dioxide. The compressibility factors are reported as smoothed values at even pressures and also in the form of empirical smoothing expressions which fit the experimental values with an average absolute deviation of 0.1%. Various methods of predicting gas-mixture compressibility are tested, and activity coefficients calculated from the experimental data are reported.

Despite more than 200 previous high-pressure P - V - T studies (5), it is still not possible to predict accurately the compressibility at high pressures of a gas for which experimental compressibility data are not available. The best methods of predicting gas-mixture compressibilities, for example, may be in

error by 5% at only a few hundred atmospheres of pressure. As a corollary the prediction of properties derived from the compressibility, such as the fugacity of the component of a gaseous mixture, is still more uncertain.

The present experimental study of the compressibility of mixtures of carbon dioxide and argon provides new information about gas-mixture compress-

sibility at temperatures and pressures approaching the critical region, where previous experimental information is rather limited. Seven different mixtures of carbon dioxide and argon were investigated, at 50°C. and pressures of 50 to 1,000 atm. The use of a large number of mixtures permits the calculation of accurate values of the fugacity of the components of the mixture.

William H. Abraham is with E. I. du Pont de Nemours, Inc., Wilmington, Delaware. C. O. Bennett is with the Lummus Company, New York, New York.

TABLE I. COEFFICIENTS FOR SMOOTHING EQUATION (1)

Mole % CO ₂ in mixture	$A_1 \times 10^8$	$A_2 \times 10^8$	$A_3 \times 10^9$	$A_4 \times 10^{12}$	$A_5 \times 10^{15}$	$A_6 \times 10^{18}$
12.9	-0.807547	+2.349632	+3.337823	-14.969786	+40.005519	-24.913008
23.8	-1.144981	+3.995961	-9.656040	+43.430021	-76.748707	+61.698831
37.1	-1.510006	+2.976921	+4.676169	-13.777809	+20.459042	+5.0997600
46.4	-1.822606	+3.408848	+3.023837	-7.025959	+11.723338	+9.466274
62.4	-2.604265	+6.151487	-5.961679	+12.637514	-19.090902	+38.234449
72.1	-3.031094	+5.824879	+3.963679	-27.669235	+46.518088	+3.183392
83.1	-3.637742	+7.434813	+1.976118	-33.677804	+64.231621	-4.789510

The experimental fugacities in turn will assist the interpretation of diffusion studies to be made in the department of chemical engineering at Purdue University. It is planned to measure the rate of diffusion of argon and carbon dioxide in mixtures of the two at high pressures by a radioactive tracer technique currently being developed.

EXPERIMENTAL APPARATUS

A variety of methods has been used by previous investigators to measure the compressibility of gases and gas mixtures (1). One of the most successful investigators in the *P-V-T* field is Michels (15 to 22), who has reported *P-V-T* data to 3,000 atm. for a large number of pure gases. Michels estimates that densities measured in his laboratory are accurate to approximately 0.01% (21). He employs an elaborate and careful experimental approach, utilizing a glass cell supported from the outside by oil pressure equal to the gas pressure inside. However the equipment used in the present study resembles that used by Bartlett (2). An unknown quantity of gas of known composition is confined at a measured pressure in a high-pressure cell of fixed, known volume, which is immersed in a temperature-regulated bath. Then the quantity of gas in the cell is determined by expanding the high-pressure gas to a measured pressure near 1 atm. in a large, known volume of previously evacuated glassware immersed in a second constant-temperature bath. The density of the gas at the low pressure is calculated from the measured temperature and pressure.

Figure 1 is a schematic layout of the equipment, which consists of a supply of gas mixture, a high-pressure cell, a free piston gauge, low-pressure glassware, and ancillary equipment. The gas mixtures were purchased as mixtures and analyzed by Orsat analysis to 0.1% by volume. They are believed to contain less than 0.1% by weight of impurities. The gas mixtures are confined in standard carbon dioxide type of cylinders at sufficiently low pressure to be entirely gaseous at room temperature. The cylinder in use is enclosed in a steam-heated box maintained at approximately 50°C., and all the high-pressure gas lines are heated by steam in copper tubing taped to the lines in order to prevent condensation of liquid from the mixtures of carbon dioxide and argon. The critical temperature of carbon dioxide is 31°C., and preliminary investigation showed that

liquid is readily condensed from mixtures of carbon dioxide and argon at 25°C. However the experimental compressibility measurements confirm the expectation that mixtures of carbon dioxide and argon are incompressible at 50°C. and pressures up to 15,000 lb./sq. in.

The gas mixtures were dried by passage over analytical-grade magnesium perchlorate and compressed over mercury in a U-tube arrangement with high-pressure nitrogen as a source of pressure. The two vessels of the nitrogen-mercury-gas compressor are made from 4340 steel and provided with side-entering standard high-pressure fittings. The vessels are sealed at the top with O rings which swell only slightly when exposed to carbon dioxide at high pressure.

The high-pressure cell is made from a 60-in. length of stainless steel high-pressure tubing, 3/8-in. O.D. by 1/2-in. I.D., formed into the helical shape indicated in the layout. The valves of the high-pressure cell and other valves exposed to high-pressure gas mixture were made from Teflon-packed stainless steel. The volume of the high-pressure cell was determined by calibration with argon of known compressibility as reported by Michels (21). Complete details of the calibration procedure are reported in Reference 1. The calibration relies on the accuracy of Michels' data for argon in the pressure range from 50 to 1,000 atm. For eight pairs of calibration runs, each pair made at two argon densities in a ratio of two to one to each other, the average range of cell volumes in each pair was 0.04%, after computed corrections of less than 0.15% for elastic changes in cell volume with pressure. When a valve at the end of the cell was replaced, recalibration showed that the cell volume was increased by 0.8% or 0.09 cc.

The cell volume extends from valve 9 at the top of the cell to the free surface of a column of mercury near the bottom of the cell. A U-shaped mercury seal, with valve 10 at the trough of the U, separates the high-pressure gas from the oil used with the piston gauge. The position of the mercury column in the cell is determined with a special transformer (Figure 2). The transformer consists of three coils mounted on a common form, two balanced output coils connected in electrical opposition, and one input coil. An A.C. voltage of 4 v. is applied to the input coil, and the net output of the two other coils is measured with a vacuum-tube voltmeter. As the five 7/64-in.-diameter steel ball bearings floating on the mercury enter the core of the transformer, the output voltage first rises to 20

mv. and then passes through a null reading of less than 0.5 mv. when the float is centered in the core of the transformer. The ball bearings have negligible friction; the null position, which was used for all measurements, is reproducible to within approximately 0.003 in. No change in the composition of the mixture was detected in three cases for which it was analyzed before and after compression. As a precaution, new O rings were seasoned before use by an exposure to pure carbon dioxide at high pressure.

The general construction of the heavily insulated constant-temperature bath containing the high-pressure cell has been described previously (9). The bath used by Hagenbach was modified for the present work. It is now equipped with a Lightnin' portable, propeller type of mixer mounted independently of the bath, a commercial mercury-in-glass thermoregulator, and a knife-blade immersion heater. The temperature is measured to 0.01°C. by a thermometer calibrated by the National Bureau of Standards. The bath fluid is a light oil. The bath temperature is maintained at 50.00 ± 0.01°C. and is uniform within ± 0.01°C. in the vicinity of the high-pressure cell.

The piston gauge, of a design credited to Keyes (11, 12), was calibrated for this study against the known vapor pressure of carbon dioxide at 0°C., 505.45 lb./sq. in. abs. This value is the average of those values determined by three different careful investigators (3, 14, 23).

The glassware consists of eight Pyrex glass bulbs in series and an integral mercury-in-glass manometer, interconnected with pressure types of stopcocks, as shown in Figure 1. The eight available glassware volumes range from 600 to 6,000 ml. The entire glassware assembly is mounted on an angle-iron frame and immersed in a constant-temperature water bath provided with a large Plexiglas window, through which the manometer is viewed with a cathetometer reading to 0.01 cm. The temperature of the bath is maintained at a uniform 30.00 ± 0.01°C. by a mercury-in-glass thermoregulator, two propeller types of mixers, and four knife-blade immersion heaters. The glassware volumes were measured by a method described by Scott (24) which involves the displacement of air by mercury.

A vacuum pump, rated at 0.3 μ ultimate pressure with a leak-free system, is attached to the glassware with vacuum-type rubber tubing at stopcock *j*, and a tilting type of Stokes-McCloud vacuum gauge is attached at stopcock *b*.

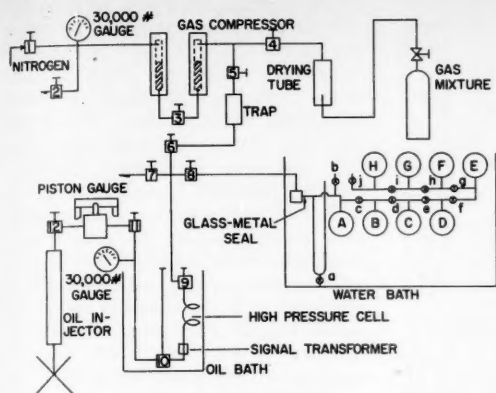


Fig. 1. Sketch of equipment.

PROCEDURE

A separate run is required for the measurement of each compressibility factor. Gas mixture of known composition is compressed over mercury and confined in the high-pressure cell for 10 to 15 min. The pressure of the gas is balanced against the oil pressure of the free piston gauge until the ball bearing float at the bottom of the cell is at the null position described earlier. Under the most unfavorable conditions, at the highest gas densities, a pressure unbalance of 0.01% can be detected, and the pressure required to bring the float to the null position appears to be reproducible within 0.02%. The temperature of the gas is assumed to be that of the constant-temperature bath in which the high-pressure cell is immersed. The high-pressure gas is then expanded through valves 9 and 8 into the low-pressure glassware, which has previously been evacuated to an absolute pressure less than 50 μ . The elevation of the mercury legs in the manometer is measured to 0.01 cm. with a cathetometer, and the barometric pressure is measured to 0.01 cm. with a conventional mercury-in-glass barometer.

In order to avoid such systematic experimental errors as creep in the cell over a long period of time, the order of experimental runs was a modified random one. The runs were divided into eighteen groups, a high- and low-pressure group for

each gas mixture. The order of groups and runs within a group was selected by use of a table of random numbers, although in a few cases the order of groups was changed for convenience.

CALCULATIONS

The calculation of results is straightforward. The independent variables of pressure, temperature, and composition are measured directly as explained earlier. Small corrections, amounting to less than 0.05% in all cases, are applied to the piston-gauge constant to correct for distortion of the piston gauge due to high pressures and changes in room temperature. The dependent variable, the high-pressure density, is calculated by a simple material balance, from the known volume of the high-pressure cell, the known volume of the glassware, and calculated values of the low-pressure density. Changes in volume of the cell, approximately 0.15%/1,000 atm., are computed according to a formula based on elastic theory developed by Love (13). Low-pressure densities are based on the known density of pure argon and pure carbon dioxide at low pressure (17, 18, 21) and the assumption of no volume change of mixing for these two gases. Data on the volume change which occurs on mixing two pure gases at atmospheric pressure and room temperature (14a) do not include the system argon-carbon dioxide; the system studied which is most comparable to argon-carbon dioxide was nitrogen-carbon dioxide. For this case the deviation from additive volumes, $\Delta PV/PV$, was 5×10^{-4} for a 50-50 mixture. Calculations based on the Lennard-Jones force law give a similar result for the argon-carbon dioxide system. The assumption of additive volume is therefore believed justified.

RESULTS

The general form of the experimental results is shown in Figure 3, a

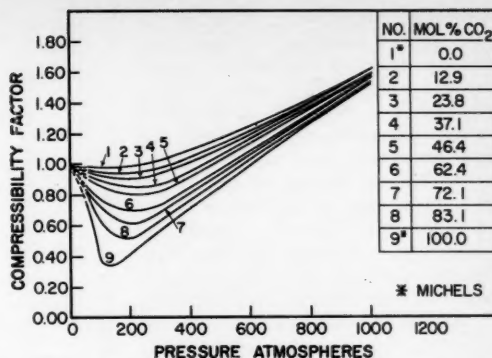


Fig. 3. The compressibility of carbon dioxide-argon mixtures at 50°C.

plot of compressibility factor vs. pressure at 50°C. for each of the seven experimental mixtures of carbon dioxide and argon. Plots for pure carbon dioxide and argon shown on the same plot are based on Michels' data. The general shapes of the curves closely resemble the familiar generalized compressibility charts (7). The lines for different gases do not cross; at any fixed pressure less than 1,000 atm., the compressibility factor increases continuously as the composition varies from pure carbon dioxide to pure argon.

The experimental compressibility factors were fitted to smoothing expressions of the form

$$C = PV/RT = 1 + A_1D + A_2D^2 + A_3D^3 + A_4D^4 + A_5D^5 + A_6D^6 \quad (1)$$

The constants A_i were determined by least-squares analyses of the twelve to fourteen experimental compressibility factors for each mixture, with the assistance of a digital computer. Table 1 lists the constants. For the six mixtures containing 12.9 to 72.1 mole % carbon dioxide the average absolute deviation of smoothed and experimental compressibility factors is 0.10%. For the 83.1 mole % carbon dioxide mixture the series is satisfactory at and below 378 atm., giving an average absolute deviation of 0.14%. At higher pressures the series does not fit the experimental data adequately, deviating by nearly 1% in one case. Michels has

TABLE 2. EMPIRICAL CORRECTION Δ_2 FOR EQUATION (2)

Δ_2	Pressure, atm.
-0.004	378
-0.003	400
+0.002	500
+0.006	600
+0.009	700
+0.008	800
+0.004	900
-0.003	1,000

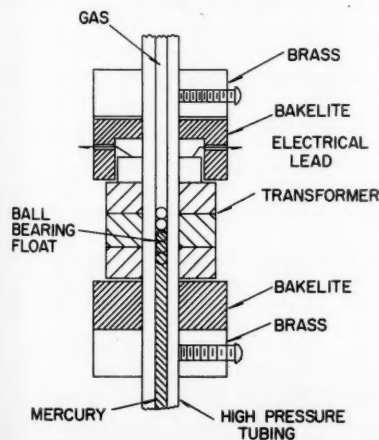


Fig. 2. Linear variable differential transformer.

found that an improved series of the same general form as that used here similarly fails to reproduce experimental compressibility factors of pure carbon dioxide (17, 18). Hirschfelder, Curtiss, and Bird (10) suggest that even the actual virial series, containing an infinite number of terms, will begin to diverge as the density of the gas approaches that of a liquid. Accordingly it is believed that the high-pressure data for the 83.1 mole % carbon dioxide mixture are as reliable as the rest of the data, even though the smoothing expression fails to reproduce the data adequately. Above 378 atm., the compressibility factor of the 83.1 mole % carbon dioxide mixture is given by

$$C = (1.2990 \times 10^{-3} P) + 0.2514 + \Delta_2 \quad (2)$$

Figure 4 is a plot of the residual compressibility factor vs. composition at various fixed pressures, where

$$\Delta C = C_M - X_A C_A - X_{CO_2} C_{CO_2} \quad (3)$$

The mixture data are taken from Table 3, whereas the compressibility factors for the pure gases are taken from the literature (17, 18, 21).

The maximum value of ΔC occurs at 125 atm. for a mixture containing 62.4 mole % carbon dioxide. Above 400 atm. $\Delta C/C_M$ is less than 2% in all cases.

Bartlett's rule of additive pressure (8) was also tested over the entire range of experimental pressures and compositions. The pressures predicted by Bartlett's rule are always low; for example the molar density experimentally measured with the 37.1 mole % carbon dioxide mixture at 585.81 atm. would be anticipated by Bartlett's rule to occur at 526 atm.

Kay's pseudocritical method (4) of predicting gas-mixture compressibilities works rather well for the mixtures of carbon dioxide and argon. The average deviation of the predicted compressibility factors from experimental values is only 2.2% for a representative selection of pressures and compositions.

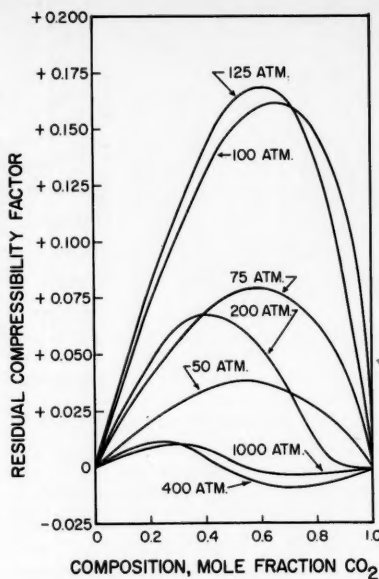


Fig. 4. Residual compressibility factors at 50°C. [Equation (3)].

As a check on the calibration of the equipment, measurements were made of the compressibility of carbon dioxide (99.95% by weight) at 50°C. and 50 to 1,000 atm. The results agree with values reported by Michels (17, 18), except in the pressure range 75 to 150 atm. Outside this range the average absolute deviation is 0.08%. The reason for disagreement in the pressure range of 75 to 150 atm., as discussed below, is not known. However the close agreement at other pressures was taken as evidence of the effectiveness of the equipment calibration. The experimental carbon dioxide measurements were not used in any calculations, since Michels' data (17, 18, 21) for pure carbon dioxide and argon are more precise than the present work.

Two series of carbon dioxide measurements were made, with carbon dioxide of the same grade (99.95% by weight) from two different cylinders. In both cases the experimental compressibility factors deviate smoothly

from the literature values in the pressure range of 75 to 150 atm. The experimental values are high in this range, exceeding the literature values by maxima of 4.5% and 1.2% at 100 atm. The reasons for these deviations have not been established. However the most plausible hypothesis seems to be that impurities in the carbon dioxide were responsible. In the case of the series showing a 4.5% deviation gross contamination of the carbon dioxide is suspected, as with a trace of oil for example. In the case of the 1.2% deviation it is at least conceivable that the anticipated impurities of 0.05% by weight of oxygen and nitrogen in the carbon dioxide are responsible for the observed deviations. Figure 4 shows that at 50°C. and 100 atm. the compressibility factor of carbon dioxide is very sensitive to small impurities of argon. A mixture containing only a small mole fraction of argon has a compressibility factor disproportionately larger than that of pure carbon dioxide. It seems reasonable that small amounts of nitrogen and oxygen should likewise raise the compressibility factor of carbon dioxide more than otherwise expected. Accordingly it is not surprising that the experimental values of the compressibility factor of carbon dioxide exceed the accepted values in a pressure range near 100 atm. Unfortunately additional experimental measurements with mixtures containing higher fractions of carbon dioxide would be required to prove that impurities of only 0.07 mole % do in fact cause the compressibility factor of carbon dioxide to increase by 1.2% at 50°C. and 100 atm.

Activity coefficients for carbon dioxide and argon in mixtures of the two have been calculated from the experimental data by a rigorous procedure described elsewhere (1) and are shown in Figures 5 and 6. The fugacity coefficients for the pure substances are given in Figure 7. The accuracy of the activity coefficients is difficult to estimate. It is thought that the activity coefficient for the major component of the

TABLE 3. SMOOTHED COMPRESSIBILITY FACTORS OF ARGON-CARBON DIOXIDE MIXTURES AT 50°C.

Mole % CO ₂ in mixture	Pressure in atm.												
	50	75	100	125	150	175	200	250	300	400	600	800	1,000
0°	0.9826	0.9768	0.9730	0.9715	0.9722	0.9753	0.9805	0.9973	1.0215	1.0867	1.2547	1.4412	1.6317
12.9	0.9695	0.9576	0.9483	0.9420	0.9387	0.9384	0.9412	0.9549	0.9783	1.0464	1.2259	1.4235	1.6229
23.8	0.9565	0.9387	0.9239	0.9124	0.9045	0.9006	0.9007	0.9125	0.9372	1.0112	1.2016	1.4083	1.6181
37.1	0.9384	0.9106	0.8861	0.8661	0.8514	0.8424	0.8393	0.8486	0.8741	0.9540	1.1594	1.3798	1.6007
46.4	0.9240	0.8882	0.8556	0.8278	0.8064	0.7928	0.7871	0.7967	0.8265	0.9169	1.1370	1.3659	1.5927
62.4	0.8896	0.8356	0.7849	0.7408	0.7073	0.6871	0.6803	0.6972	0.7375	0.8454	1.0879	1.3324	1.5724
72.1	0.8663	0.7967	0.7290	0.6698	0.6279	0.6078	0.6063	0.6365	0.6871	0.8078	1.0633	1.3156	1.5614
83.1	0.8350	0.7437	0.6496	0.5665	0.5187	0.5093	0.5217	0.5725	0.6351	0.7679	1.0370	1.2991	1.5471
100.0°	0.7710	0.6256	0.4135	0.3331	0.3530	0.3855	0.4212	0.4954	0.5700	0.7167	0.9992	1.2697	1.5308

* Michels (17, 21).

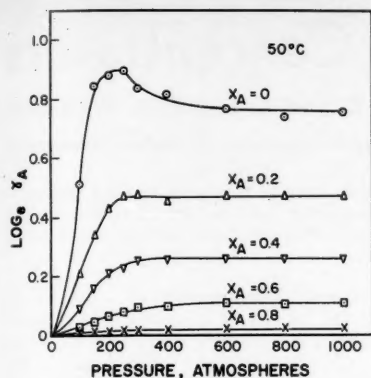


Fig. 5. Activity coefficients for argon at 50°C.

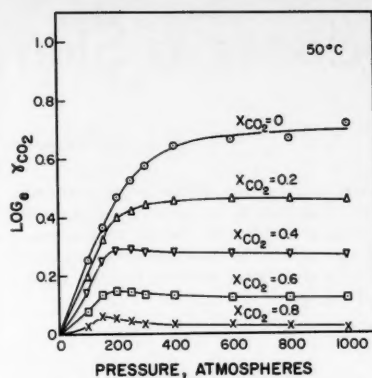


Fig. 6. Activity coefficients for carbon dioxide at 50°C.

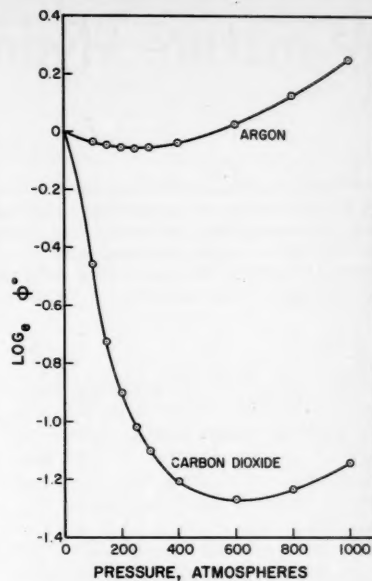


Fig. 7. Fugacity coefficients for pure argon and pure carbon dioxide at 50°C.

mixture is accurate within 0.5%, but the activity coefficients for the minor component for the limiting cases of very low concentration of a component may be in error by as much as 5%.

The fugacity coefficients of argon and carbon dioxide were calculated from Michels' (17, 18, 21) data.

Further details of this study and the original experimental data may be found in reference 1.

SUMMARY

The compressibility factor has been measured experimentally at 50°C. and 50 to 1,000 atm. for each of seven mixtures of carbon dioxide and argon containing 12.9 to 83.1 mole % carbon dioxide.

Plots of compressibility factor vs. pressure resemble closely the familiar generalized compressibility factor charts. At a fixed pressure a mixture richer in argon always has a higher compressibility factor.

The experimental compressibility factors have been fitted to smoothing expressions of the form

$$PV/RT = 1 + A_1 D + A_2 D^2 + A_3 D^3 + A_4 D^4 + A_5 D^5 + A_6 D^6 \quad (1)$$

The smoothing equations (1) predict the experimental values of compressibility factor with an average absolute deviation of 0.1% for the six mixtures containing 12.9 to 83.1 mole %. For the 83.1 mole % carbon dioxide mixture the series (1) is unsatisfactory above 378 atm., and a different empirical expression is given.

Kay's pseudocritical method predicts a sample of fifteen experimental compressibility factors with an average absolute deviation of only 2.2%.

Amagat's law of additive volumes is in error by as much as 20% at intermediate pressures, but the molar volume agrees with that predicted by Amagat's law within 2% in all cases for pressures above 400 atm.

Activity coefficients for argon and carbon dioxide in mixtures of the two have been calculated from the experimental data.

ACKNOWLEDGMENT

It is desired to acknowledge the generous financial support given by the National Science Foundation, the Proctor and Gamble Company, and the Lubrizol Corporation.

NOTATION

- A = coefficient in Equation (1)
- C = PV/RT compressibility factor, unity for an ideal gas
- D = density, the ratio of the gas density at the prevailing temperature, pressure, and composition to the density of an ideal gas at 0°C. and 1 atm.
- f_i = fugacity of a component of a gas mixture, atm.
- P = total absolute pressure, atm.
- X_i = mole fraction of a component in a gas mixture
- Δ_2 = graphical correction tabulated in Table 2 for even pressures
- ϕ_i = f_i/PX_i , fugacity coefficient
- γ_i = $f_i/f_i^0 X_i$, activity coefficient

Subscripts

- A = argon
- M = mixture

Superscript

- o = pure substance

LITERATURE CITED

1. Abraham, William H., Ph.D. thesis, Purdue Univ., Lafayette, Indiana (June, 1957).
2. Bartlett, E. P., *J. Am. Chem. Soc.*, **49**, 687 (1927).
3. Bridgman, O. C., *ibid.*, 1174 (1927).
4. Comings, E. W., "High Pressure Technology," pp. 304-309, McGraw-Hill, New York (1956).
5. *ibid.*, pp. 490-495.
6. *ibid.*, pp. 498-506.
7. Dodge, B. F., "Chemical Engineering Thermodynamics," p. 160, McGraw-Hill, New York (1944).
8. Gilliland, E. R., and T. E. Sullivan, *Chem. Eng. Progr. Symposium Ser. No. 2*, **48**, 18 (1952).
9. Hagenbach, W. P., Ph.D. thesis, Univ. Illinois, Urbana (1951).
10. Hirschfelder, J. O., C. F. Curtiss, and R. B. Bird, "Molecular Theory of Gases and Liquids," p. 132, John Wiley, New York (1954).
11. Keyes, F. G., *Ind. Eng. Chem.*, **23**, 1375 (1931).
12. ———, and J. Joubert, *J. Math. Phys.*, **1**, 195 (1922).
13. Love, A. E. H., "Mathematical Theory of Elasticity," 4 ed., p. 145, Dover Publications, New York (1945).
14. Meyers, C. H., and M. S. Van Dusen, *Bur. Standards J. Research*, **10**, 381 (1933).
- 14a. Michels, A., *Bull. Soc. Chim. Belge*, **62**, 119 (1953).
15. Michels, A., and R. Gibson, *Ann. Physik*, **87**, 850 (1928).
16. *ibid.*
17. Michels, A., and C. Michels, *Proc. Roy. Soc. (London)*, **A153**, 201 (1936).
18. *ibid.*, **A160**, 348 (1937).
19. ———, and H. Wouters, *ibid.*, **A153**, 214 (1936).
20. Michels, A., J. Otto, and H. Wouters, *Z. Physik*, **35**, 97 (1934).
21. Michels, A., H. Wijker, and W. J. Wijker, *Physica*, **15**, 627 (1948).
22. Michels, A., H. Wouters, and Jan deBoer, *ibid.*, **1**, 587 (1934).
23. Roebuck, J. R., and S. W. Cram, *Rev. Sci. Inst.*, **8**, 215 (1937).
24. Scott, G. A., *Proc. Roy. Soc. (London)*, **A125**, 330 (1929).

Manuscript received November 14, 1958; revision received May 4, 1959; paper accepted May 15, 1959.

Miniature Hydroclones as Slurry Concentrators

F. C. ENGEL and JOEL WEISMAN

Westinghouse Electric Corporation, Pittsburgh, Pennsylvania

Miniature hydroclones were evaluated for use with thorium-uranium slurries being considered as fuels for one type of homogeneous nuclear reactor. In addition to extensive room temperature data on concentrating performance, the results of tests with thorium slurries at a pressure of 2,000 lb./sq. in. and temperatures up to 550°F. are given. The data correlation presented allows prediction of the concentrating performance of a given clone provided that the properties and particle size distribution of the slurry feed are known.

The proposed homogeneous-slurry nuclear reactor, which is fueled with an aqueous thorium-uranium suspension, requires devices capable of both concentrating and diluting the slurry fuel during start-up and shut-down. Hydroclones seemed particularly suitable for such purposes, being easily designed for high pressures and temperatures, simple and durable, and devoid of moving parts to complicate remote maintenance. In addition they have proved highly efficient in the removal of micron-size particles from the uranyl sulfate solutions that are employed in one type of aqueous homogeneous reactor (11). Therefore the concentrating behavior of miniature hydroclones was investigated as one part of an extensive feasibility study of the homogeneous slurry reactor (14, 15).

Most previous investigations (4 to 8, 11, 16, 19) have been concerned primarily with the classification action of hydroclones. The solids-separation ability of the hydroclones was described in terms of the particle diameter at which 50% of the particles enter the underflow. Since the thorium-uranium slurry contains an appreciable quantity of submicron particles, use of the smallest miniature hydroclone practical (5 to 10 mm.) at reasonable pressure drops (20 to 40 lb./sq. in.) results in a d_{50} which is above the size of an appreciable fraction of the particles. To predict the concentrating effectiveness with thorium-uranium slurry it is therefore necessary to describe quantitatively the behavior of particles below the d_{50} size.

This problem was considered in the work of Yoshioka and Hotta (20) on full-sized hydroclones. These investigators studied the velocity distribution in several hydroclones and the classification of clay slurries in a 6-in. hydroclone with a 20-deg. included angle. The solids-removal efficiency at a given particle size was defined as the percentage of feed particles of a given size which is removed by the underflow. The ratio Q_u/Q_i was found to have a significant effect on the separation efficiency. For a specific clone at a

fixed feed rate, Yoshioka and Hotta found that

$$100 - E = K(1 - Q_u/Q_i) \quad (1)$$

To allow for the underflow effect, they defined d'_{50} as the particle size at which $(100 - E)/(1 - Q_u/Q_i)$ is equal to 50%. The values of d'_{50} they obtained are correlated by

$$d'_{50} = 2 \left(\frac{\mu_i}{\rho_p - \rho_i} \right)^{0.5} \frac{D^{0.1} F^{0.6} O^{0.8}}{Q^{0.5}} \quad (2)$$

Solids-removal efficiencies at other particle sizes were graphically correlated by a fractional recovery curve showing $(100 - E)/(1 - Q_u/Q_i)$ as a function of d/d'_{50} .

EXPERIMENTAL PROGRAM

The present experimental study of miniature hydroclone performance was divided into two phases. The first phase was a room-temperature investigation, aimed at providing enough basic information to allow the formulation of generalized correlations describing the concentrating action of miniature hydroclones. The second phase was the testing of prototype clones with thorium-uranium slurries at reactor plant conditions (550°F. and 2,000 lb./sq. in.)

The hydroclones tested in this program ranged from 5 to 50 mm. in diameter. The detailed dimensions of the units used are tabulated in Figure 1. It may be seen that both individual clones and assemblies of several clones in parallel were tested. (Owing to the small throughput of the individual clones, plant-sized units would consist of such assemblies.)

EXPERIMENTS AT ROOM TEMPERATURE

The concentrating action of 50- and 10-mm. clones (clone assemblies A and C of Figure 1) was investigated by the use of a bypass line of a 50 gal./min. test loop. The flow rates were measured by rotameters, and valved tees were provided for sampling. Samples were taken of overflow, underflow, and feed to determine concentrations, settling rates, and particle size

distributions. To ensure that the loop concentration was uniform, data were taken only after the slurry had circulated for 1 hr.

10-mm. Clone Assembly

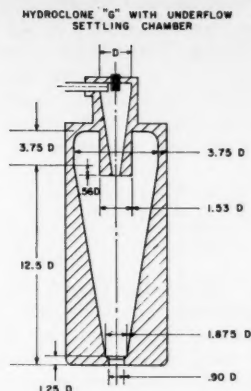
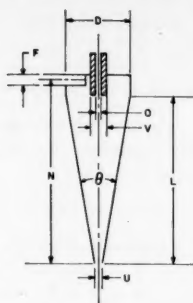
The 10-mm. clone assembly was tested with a thorium-uranium slurry of a type and composition similar to that proposed for the reactor plant (weight ratio of uranium to thorium = 0.03) used. Microscopic examination of the thorium-uranium showed that many of these particles were collected in large flocs having diameters of 20 to 150 μ . Particle-size determinations by the Andreasen sedimentation pipette method (1, 2) in the presence of a sodium-silicate dispersant showed these flocs to be composed of particles ranging from approximately 0.3 to 7 μ in size. The particle size so determined, rather than the floc size, was taken to be representative of the conditions within the hydroclones. This assumption is based on the results of Bennett and Thomas (3), which indicated that the high shearing force developed in the hydroclones reduces the large, loose thorium flocs into individual particles.

Test conditions for the 10-mm. clone assembly included pressure drops ranging from 10 to 50 lb./sq. in. and concentrations ranging from 30 to 300 g./liter. At each condition the flow distribution was varied over a large range by throttling the valve in the underflow line.

Separation efficiencies as a function of particle size were obtained in essentially the same manner as described by previous investigators (4, 19, 20). The Andreasen pipette technique was used to give the particle-size distribution in terms of weight fraction of particles having free-settling rates higher than any given free-settling rate. Multiplication of the respective particle-size distribution curves by the fraction of total feed solids in each stream yielded curves of the cumulative weight fraction of feed solids. The solids-removal efficiency at a given free-settling rate equals one hundred times the ratio of the slopes of the underflow and feed curves at that settling rate.

Figure 2 shows a typical set of data calculated by the above procedure. The pronounced effect of the underflow ratio should be noted. The general shapes of the curves are in agreement with the observations of Yoshioka and Hotta (20). At very small particle sizes the solids-removal efficiency approaches the underflow ratio, and the curves for the various underflow ratios approach each other as E approaches 100%. There exists a settling rate above which all particles enter the underflow. As expected, the settling rate at which this occurs decreases with increasing pressure drop.

The observed underflow-ratio effect was compared with the relationship by Yoshioka and Hotta [Equation (1)]. It was found that their relationship holds for



CLONE	NO. OF CLONES IN PARALLEL	D, MM	L/D	EQUIV. F/D	O/D	U/D	V/D	N/D	INCLUDED ANGLE, DEGREES	PRESSURE RATING, PSI
A	1	50	5.5	.286	.35	.22	—	5.5	8.125	80
B	1	25.4	6.0	.141	.125	.334	.25	6.4	6.00	50
C	4	10	8.2	.248	.22	.22	.4	8.09	5.45	300
D	7	10	8.0	.248	.22	.22	.4	8.11	5.20	2500
E	1	10	8.2	.248	.22	.22	.4	8.32	5.45	2500
F	7	5	8.9	.240	.22	.22	.44	9.0	5.03	2500
G	1	10	5.68	.295	.25	.25	.375	5.82	7.20	2500

Fig. 1. Dimensions of miniature hydroclones used in this investigation.

low values of r but gives poor agreement as r is increased. It was found that over the range of r used (0.03 to 0.3), $E/100-E$ is directly proportional to $r/1-r$. In the calculation of r it was assumed that the thoria particles were half water. By defining a concentration factor α such that

$$\alpha = \left(\frac{E}{100-E} \right) \cdot \left(\frac{1-r}{r} \right) \quad (3)$$

one can describe the hydroclone performance independently of the underflow ratio being used. It will be noted that α represents the ratio of the concentration of a given size particle in the underflow to the concentration of the same size particle in the overflow, or

$$\alpha = C^u/C^o \quad (4)$$

This concentration factor is quite similar to the concentration factor defined by Haas *et al.* (11) for hydroclone operation with an underflow pot.

The data indicate that α is a function of feed concentration as well as head loss across the clone. Figure 3 shows the effect of feed concentration on α with the pressure drop across the clone fixed at 40 lb./sq. in. Although there is appreciable scatter, there is an observable increase in α as the feed concentration is decreased. Fitch and Johnson (9) cited a similar dilution effect.

50-mm. Clone

The 50-mm. hydroclone was tested with a glass-bead-water slurry of suitable particle size (10 to 40 μ). The tests were conducted at feed concentrations of approximately 200 to 50 g./liter and fluid head losses ranging from 50 to 500 cm. Concentrations, settling rates, and particle-size distribution were measured in the manner previously described. These data

could be correlated in the same fashion as those obtained with thoria. It was found that the ratio Q_u/Q_o differed negligibly from r for the thoria slurries used but that there was an appreciable difference between those quantities for the glass slurries. A noticeably poorer correlation of the glass data results if r is replaced by Q_u/Q_o .

GENERALIZED CORRELATION OF ROOM-TEMPERATURE DATA

To arrive at a means for relating the glass- and thoria-slurry data and to develop a correlation for the concentration ratio in terms of system properties and operating conditions, it is desirable to consider the behavior of a particle within the hydroclone. The radial movement of a given particle is determined by the relative values of the water radial velocity and the radial

settling velocity of the particle generated by the centrifugal forces developed in the clone. It therefore seems plausible, for a given underflow ratio, that the ratio of the mass of a given particle-size class collected in the underflow to the mass of the same particle-size class collected in the overflow is related to the ratio of the particle radial settling velocity to the water radial velocity; that is

$$\frac{E}{100-E} = f\left(\frac{v_r}{U}\right) \quad (5)$$

At any radius in the hydroclone the radial settling velocity of the particle is given by

$$v_r = \frac{V^2}{R} \cdot \frac{v_p}{g} \quad (6)$$

provided that the particles are in the size range to which Stokes's law normally applies. Noting that the corresponding values of R are proportional to the hydroclone diameter and making use of Kelsall's (16) observation that U/V at any radius is independent of throughput, one may restate Equation (5) as

$$\frac{E}{100-E} = f^* \left[\frac{v_p}{g} \left(\frac{V}{D} \right) \right] \quad (7)$$

For hydroclones where the ratios of O/D and F/D are held constant the tangential velocity would be very nearly proportional to the square root of the product of the acceleration of gravity and the fluid head loss across the hydroclone. The experimental data of Kelsall (16) show this to be a very close approximation of the facts. Consequently the functional relationship is modified to

$$\frac{E}{100-E} = f^* \left[\frac{v_p}{D} \left(\frac{\Delta H}{g} \right)^{1/2} \right] \quad (8)$$

Since the experimental results show,

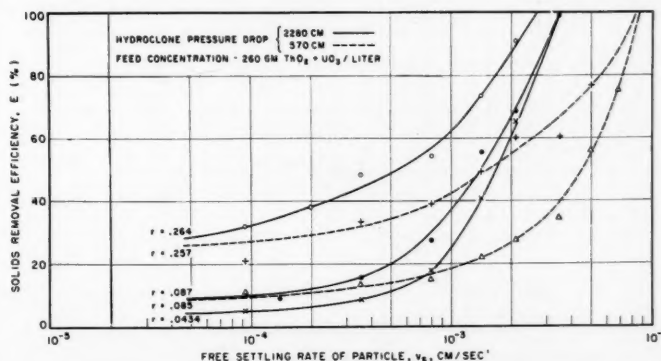


Fig. 2. Typical curves of separation efficiency as a function of particle settling rate and underflow ratio.

for a given slurry and hydroclone operating over a range of underflow to overflow ratios, that $E/(100-E)$ is directly proportional to $r/(1-r)$, this dependence is inserted explicitly. The correlation expression then becomes

$$\alpha = f''' \left[\frac{v_p}{D} \left(\frac{\Delta H}{g} \right)^{1/2} \right] = f'''(\Psi) \quad (9)$$

If one extends this correlation to include the effect of feed and overflow port sizes, one has

$$\alpha = f'''(\Psi) \times f''' \left(\frac{O}{D}, \frac{F}{D} \right) \quad (10)$$

It should be noted that Ψ is dimensionless.

In computing v_p , an allowance must be made for the effect of slurry concentration. For the glass-bead system this was done on the basis that v_p should show the same concentration dependence as the slurry hindered settling rate. The value of v_p at any concentration was then computed as the product of v_s and the ratio of the hindered settling rate at the given concentration to the extrapolated value at zero concentration.

The above procedure was not readily applicable to the thoria suspensions owing to the marked floc formation of these slurries. In this case the approximation was made that Stokes's law can be applied if the properties of the liquid are taken as those of the slurry mixture considered as homogeneous fluid medium. This does not strictly apply unless the particle under consideration is appreciably larger than those surrounding it. However Hap-

pel's (13) comparison of various sedimentation velocity correlations shows that this approach is in fairly good agreement with the available experimental data. Basing v_p on the properties of the slurry feed, one then has

$$v_p = v_s \cdot \left(\frac{\mu_l}{\mu_{ml}} \right) \left(\frac{\rho_p - \rho_{ml}}{\rho_p - \rho_l} \right) \quad (11)$$

The above relationship is not adequate for non-Newtonian fluids such as the thoria slurries investigated in this study. Since these slurries approximate Bingham plastic behavior and since the yield value may be disregarded at the high values of shear in the hydroclone, the slurry viscosity may be replaced by the modulus of rigidity:

$$v_p = v_s \left(\frac{\mu_l}{\eta_l} \right) \left(\frac{\rho_p - \rho_{ml}}{\rho_p - \rho_l} \right) \quad (12)$$

Values of η were measured for the thoria slurries, and the particle density was calculated on the basis that the thoria particles were half water.

In Figure 4 all the room-temperature data for both glass-bead and thoria slurries are plotted as $\alpha - 1$ vs. Ψ . The graph shows that the data for various concentrations and head losses are brought into agreement. At values of Ψ below 2×10^{-3} the data for the 10-mm. clone assembly can be represented by the equation

$$\alpha - 1 = 2.4 \times 10^5 (\Psi)^{1.5} \quad (13)$$

The data for the 50-mm. clone, which has O/D and F/D ratios higher than those of the 10-mm. units, are represented by

$$\alpha - 1 = 5.5 \times 10^4 (\Psi)^{1.5} \quad (14)$$

It would appear that the concentrating factor may therefore be expressed by equations of the form

$$\alpha - 1 = (K\Psi)^{1.5} \quad (15)$$

where K is dependent on the O/D and F/D ratios. To evaluate further the effect of O/D and F/D the data of Matschke and Dahlstrom (18, 19) on the classification of clay slurries by miniature hydroclones were recomputed. Happel's correlation (13) of hindered settling rate with void volume was used for calculation of v_p . From these data and the results of the present study it was found, as shown in Figure 5, that K is inversely proportional to the cube of (\sqrt{OF}/D) . Care should be used in extending this proportionality to values of (\sqrt{OF}/D) below 0.16. One would not expect hydroclone performance to improve continuously as (\sqrt{OF}/D) is decreased, but an optimum should be reached. This has been observed by other investigators (12, 19). The fact that the lowest value of (\sqrt{OF}/D) tested exhibits a K below the general correlation may indicate that the optimum is somewhat above this ratio. This would be in agreement with Fitch and Johnson's observation (9) that the

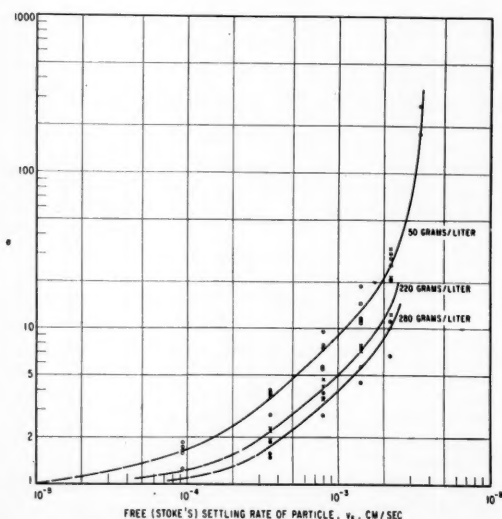


Fig. 3. Concentration factor as a function of particle settling rate and slurry concentration.

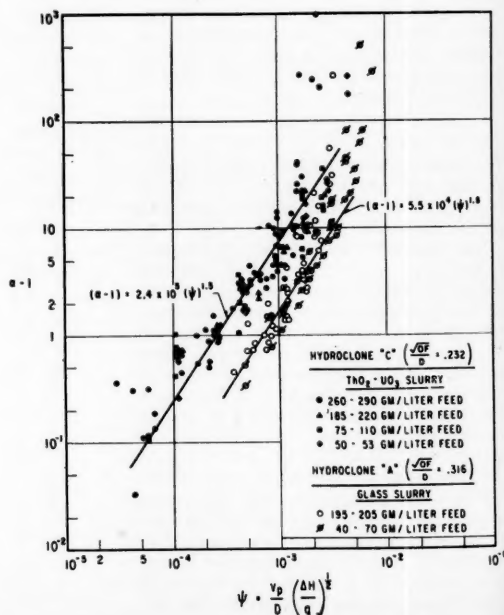


Fig. 4. Correlation of concentration factors obtained with thoria and glass-bead slurries.

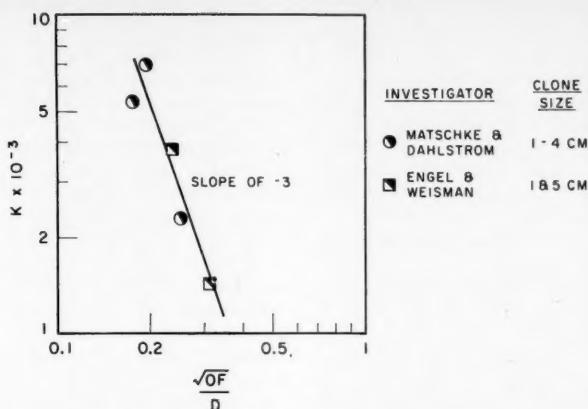


Fig. 5. Variation of coefficient of Equation (15) with hydroclone dimensions.

optimum occurs at (\sqrt{OF}/D) values between 1/5 and 1/6. Additional data at lower (\sqrt{OF}/D) ratios are needed to establish definitely this optimum for miniature clones.

The results of the generalized correlation are shown in Figure 6. It is seen that the data for the various miniature clones tested are brought into reasonable agreement. For values of $\Psi(\sqrt{OF}/D)^{-3}$ below 0.15 the data can be correlated by

$$\alpha - 1 = 350[\Psi(\sqrt{OF}/D)^{-3}]^{1.5} \quad (16)$$

At values of $\Psi(\sqrt{OF}/D)^{-3}$ above 0.22 α may, for all practical purposes, be considered infinite. From the dotted lines on Figure 8 it can be observed that for the vast majority of points the ratio of the experimentally determined value of E to the value predicted by Equation (16) lies between 0.65 and 1.35.

Use of Equation (16) allows one to predict the concentrating action of a given miniature hydroclone providing the properties and size distribution of the slurry feed are known. The simplest procedure is probably one similar to that used by Yoshioka and Hotta (20) with their fractional recovery curve. The feed size distribution is plotted in terms of weight percentage per size class. Values of α and E are then computed for each size class. The over-all solids-removal efficiency is the weighted average of the individual values of E . The values of E can also be used to compute the size distribution in the overflow and underflow.

To determine the utility of α and Ψ in correlating the performance of full-size hydroclones the data of Dahlstrom (4) and Yoshioka and Hotta (20) were recomputed in those cases where there was enough information to do

so. Again the correlation of Happel was used to estimate the hindered settling rate of the slurries used. The results of these recalculations are shown in Figure 7. The data of Dahlstrom for a 9-in. clone with a 20-deg. included angle was fairly well correlated by Equation (16). However a somewhat better fit is obtained with

$$\alpha - 1 = 1,000[\Psi(\sqrt{OF}/D)^{-3}]^2 \quad (17)$$

The data of Yoshioka and Hotta's 6-in. clone with a 20-deg. included angle fall to the right of Dahlstrom's data. Yoshioka and Hotta's data for the various values of (\sqrt{OF}/D) tested were brought into agreement and can be correlated by

$$\alpha - 1 = 250[\Psi(\sqrt{OF}/D)^{-3}]^2 \quad (18)$$

The reason for the discrepancy between these data and those of Dahlstrom is not known.

HYDROCLONE PERFORMANCE TESTS AT REACTOR-PLANT CONDITIONS

To test miniature hydroclones under conditions similar to those at which they might be used in a slurry reactor plant several units suitable for operation at temperatures up to 600°F. and pressures up to 2,500 lb./sq. in. were obtained (hydroclone assemblies D, E, and F of Figure 1). The units were all constructed of 300 series stainless steel, since tests had shown this material to be resistant to corrosion erosion by high temperature thoria slurries.

The high-pressure hydroclones together with the necessary test instrumentation were mounted on portable dollies. High-temperature rotameters were used for flow measurements, dif-

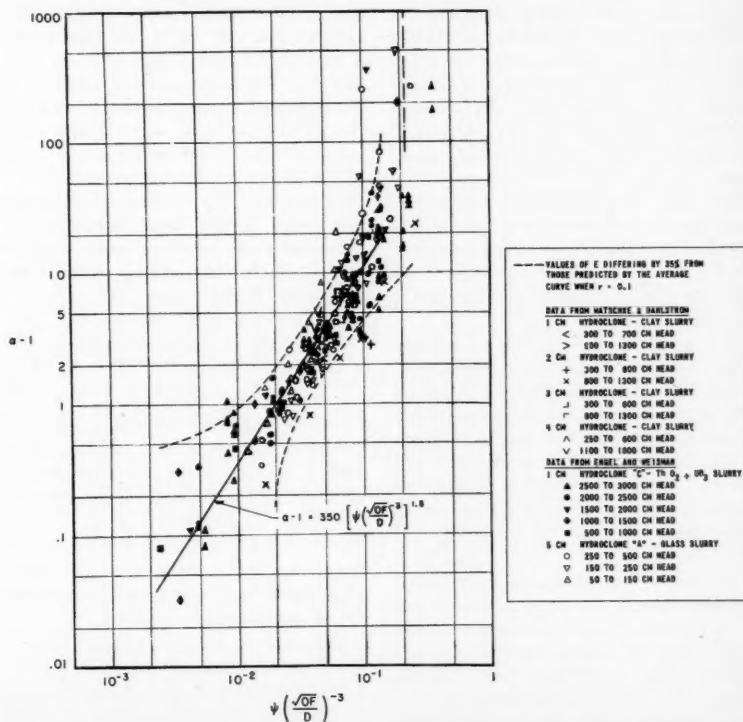


Fig. 6. Generalized correlation of miniature hydroclone concentration factors.

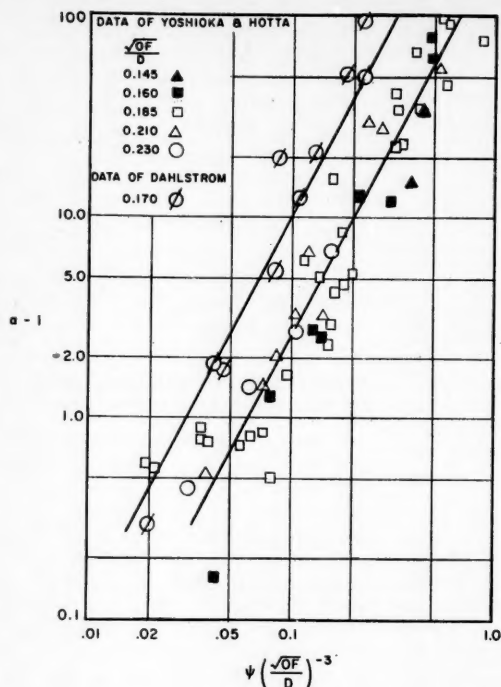


Fig. 7. Correlation of full size hydroclone concentration factors.

ferential pressure cells for measurement of head loss, and thermocouples for temperature measurements. Valved tees with cooling coils provided the means for withdrawing samples. A high-temperature thoria-slurry source was provided by connecting the dolly across one of the high-temperature corrosion test loops which have been described elsewhere (14). Since the test-loop volume was relatively low, most of the experiments were conducted by returning both the underflow and overflow to the loop. The temperature level was kept constant during each run but was varied from 250° to 550°F. during the course of these experiments.

For most of the operation a large (2-in. diameter) scalping clone preceded the miniature clones to insure the removal of any large particles. This is believed highly desirable, since examination of the scalping unit showed it had collected a number of large-size pieces of dirt which might have been capable of plugging the small clones.

Tests were conducted with a mixed thoria-uranium slurry (loop G runs) and a thoria slurry (loop B runs). The preparation of these slurries differed considerably, and the pure thoria slurry had a high temperature settling rate considerably greater than the mixed thoria-uranium slurry. As would

be expected the concentrating performance was appreciably better with the more rapidly settling material.

The Andreasen pipette technique (1, 2) for determining particle size distribution did not yield fruitful results when applied to samples taken from the high temperature hydroclone tests. This difficulty arose from the fact that the average particle size of the material in the high-temperature loop (99% below 1 μ) was appreciably less than encountered in the room-temperature tests. It was found however that the data could be represented approximately by the use of an overall concentration factor:

$$\alpha' = \left(\frac{E'}{100 - E'} \right) \left(\frac{1 - r}{r} \right) \quad (19)$$

It seems reasonable to assume that the hindered settling rate of the slurry flocs is related to the average settling rate of the particles which comprise the flocs. If this is the case, it would be expected for clones having a constant (\sqrt{OF}/D) ratio that the values of α' could be approximately correlated by an equation of the form

$$\alpha' - 1 = f \left(\frac{v_f}{D} \right) \left(\frac{\Delta H}{g} \right)^{1/2} \quad (20)$$

To determine the applicability of

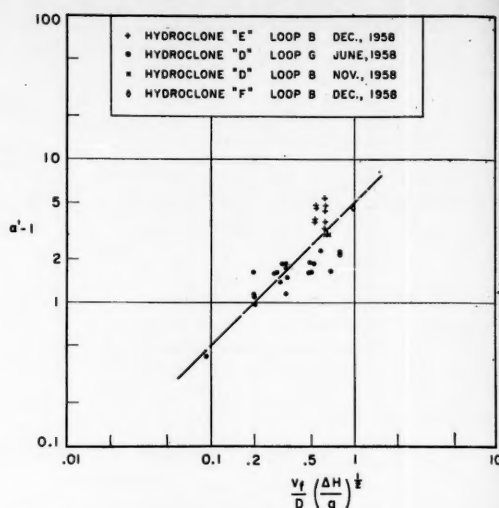


Fig. 8. Correlation of hydroclone performance with thoria slurries at elevated temperatures.

the above equation the high temperature settling rates of the slurries tested were determined as a function of concentration and temperature. Two methods were used for this determination. In the first of these a sample of slurry is placed in an agitated autoclave. Upon cessation of the agitation the slurry interface is followed by means of a float having a density intermediate between the slurry and the supernate. The position of the float is indicated by a magnetic follower located outside the autoclave. In the second of these methods the settling rate is determined in a vertical bypass line connected to the test loop itself. When flow through the line is stopped, settling occurs. The rate of movement of the slurry interface is determined by the time required to pass between two heated wire probes. The passage of the interface over one of the wires is observed by a change in temperature of the wires. Details of these procedures are described by Garber and Taylor (10) and Kivenson and Foster (17).

Figure 8 shows the high temperature performance data treated in the manner indicated by Equation (20). Although there is appreciable scatter in the data, they can be approximately fitted by

$$\alpha' - 1 = 5 \left[\frac{v_f}{D} \left(\frac{\Delta H}{g} \right)^{1/2} \right] \quad (21)$$

Comparison of the data of Figure 8 with those of the 10mm. clone in Figure 4 shows that equivalent values of α were obtained at particle settling rates approximately 1/900 of the floc settling rates. This is additional evidence that the high shear rates exist-

ing in the clone break down the flocs into their component particles. The action of a standard hydroclone in this case would appear to be somewhat self-defeating, since the high shear rates required to separate small particles produce even smaller particles for the clone to separate. Haas and Unger (12) have designed a hydroclone with a feature which partly counteracts the shearing of the slurry flocs. This unit, shown as hydroclone G in Figure 1, is equipped with an integral underflow settling tank. Here a low shear-stress region is provided where the flocs can reform and settle out. This unit was given preliminary tests under the same conditions used for the standard design. In all cases an underflow stream was continuously removed. These tests showed the unit with the integral underflow pot to provide values of α' approximately $1\frac{1}{2}$ times that of the standard hydroclone.

Operational experience with the high-temperature hydroclones was highly satisfactory. No clogging difficulty was encountered during normal operation. However with the rapidly settling pure-thoria slurry it was found that if stagnant slurry remained in the lines overnight, it was necessary to backflush the clones with water before taking the data. When this was not done, the hydroclones exhibited an appreciably lower efficiency than usual.

HEAD-LOSS STUDIES

Head loss across the clone, as a function of flow rate, was measured throughout the room-temperature and elevated-temperature tests. All of the clones shown in Figure 1 were used for these flow tests. It was found that Matschke and Dahlstrom's (19) empirical equation

$$Q = 14.8(0 \times F)^{0.3}(\Delta H)^{0.5} \quad (22)$$

fits the data for each clone with an average deviation of less than 5%.

CONCLUSIONS

This investigation has provided a generalized correlation which can be used to predict the concentrating effectiveness of a given miniature hydroclone providing the properties and particle size distribution of the slurry feed are known. Recalculation of the available literature data indicated that the same type of relationship is also applicable to full-size hydroclones.

The range of performance of miniature hydroclones handling thoria slurries at temperatures up to 550°F. was established. The applicability of the generalized correlation to the high-temperature data could not be established, since the available technique

for particle size determination was not adequate for the small sizes encountered. While it would have been desirable to use a centrifuge technique for particle size determinations, the termination of the contractual arrangements under which this program was pursued precluded this additional work.

ACKNOWLEDGMENT

The authors appreciate the advice and assistance obtained from many of the staff of the Westinghouse Atomic Power Department. In particular the authors wish to acknowledge the contributions of D. H. Fax, who suggested this study, and H. J. Garber, who furnished advice and guidance throughout the course of the work.

NOTATION

- C = total slurry concentration, g./liter of suspending fluid
 C^* = concentration of given size particle, g./liter of suspending fluid
 D = hydroclone diameter, cm.
 d = particle diameter, cm.
 d_{50} = particular particle diameter 50% of which goes into underflow of hydroclone, cm.
 E = solids-removal efficiency for given particle size = weight of given particle size in underflow/weight of same particle size in feed $\times 100$, %
 E' = over-all solids-removal efficiency = $(C_2/C_1)r$ = mass of solids in underflow/mass of solids in feed $\times 100$, %
 f, f' , etc. = functional relationship
 F = equivalent diameter of feed port, cm.
 g = local acceleration due to gravity (981 cm./sec.²)
 ΔH = head-feed to overflow- at feed concentration, cm.
 O = overflow port diameter, cm.
 Q = flow rate, (cc./sec.)
 r = underflow ratio = underflow liquid rate/feed liquid rate, dimensionless
 R = radial distance from center of hydroclone (cm.)
 U = water radial velocity (cm./sec.)
 v_r = hindered settling rate of slurry flocs, cm./sec.
 v_p = gravitational settling rate of individual particle in slurry feed (cm./sec.)
 v_r = radial settling rate of particle in hydroclone (cm./sec.)
 v_s = Stokes settling rate of particle in an infinitely dilute suspension in water at room temperature (cm./sec.)
 V = tangential liquid velocity in hydroclone (cm./sec.)

Greek Letters

- α = concentration factor for given particle size, $[(1-r)/r] \cdot [E/(100-E)]$, dimensionless
 α' = over-all performance factor, $[(1-r)/r] \cdot [E'/(100-E')]$
 η = coefficient of rigidity of slurry (g./sec. cm.)
 μ = viscosity (g./sec. cm.)
 Ψ = performance parameter $(v_p/D)(\Delta H/g)^{1/2}$
 ρ = density, g./cc.

Subscripts

- 1 = feed stream
 2 = overflow stream
 3 = underflow stream
 l = suspending liquid
 m = slurry mixture (mixture being considered as homogeneous medium)
 p = solid particle

LITERATURE CITED

- Andreasen, A. H., *Kolloidchem. Beih.*, **27**, 349 (1928).
- , *Ber. deut. keram. Ges.*, **11**, 675 (1930).
- Bennett, L. L., and D. G. Thomas, *Oak Ridge Natl. Lab. Rept.*, CF-58-2-7 (1958).
- Dahlstrom, D. A., *Trans. Am. Inst. Mining Met. Engrs.*, **184**, 331 (1949).
- , *Ibid.*, **190**, 153 (1951).
- Driessen, M. G., *J. Inst. Fuel*, **12**, 327 (1939).
- , *Ibid.*, **19**, 33 (1945).
- , *Trans. Am. Inst. Mining Met. Engrs.*, **177**, 240 (1948).
- Fitch, E. B., and E. C. Johnson, *Chem. Eng.*, **59**, No. 6, 172 (1952).
- Garber, H. J., and G. R. Taylor, *Westinghouse Electric Corp., Rept. WCAP-1150* (1959).
- Haas, P. A., E. O. Nurmi, M. E. Whatley, and J. R. Engel, *Chem. Eng. Progr.*, **53**, 203 (1957).
- Haas, P. A., and W. E. Unger, *Oak Ridge Natl. Lab., Personal communication* (August, 1958).
- Happel, John, *A.I.Ch.E. Journal*, **4**, 197 (1958).
- Johnson, W. E., D. H. Fax, and S. C. Townsend, *Proc. Am. Power Conf.*, **19**, 640 (1957).
- Johnson, W. E., and S. C. Townsend, *Nucleonics*, **17**, No. 2, 61 (1959).
- Kelsall, D. F., *Trans. Inst. Chem. Engrs. (London)*, **30**, 87 (1952).
- Kivenson, C., and W. E. Foster, *Westinghouse Electric Corp., Rept. WCAP-913* (1958).
- Matschke, D. E., *Northwestern Univ., Personal communication* (November, 1958).
- , and D. A. Dahlstrom, *Chem. Eng. Progr.*, **54**, No. 12, 60 (1958); **55**, No. 1, 79 (1959).
- Yoshioka, N., and Y. Hotta, *Chem. Eng. (Japan)*, **19**, 632 (1955).

Manuscript received April 20, 1959; revision received September 28, 1959; paper accepted October 1, 1959. Paper presented at A.I.Ch.E. St. Paul meeting.

The Thermal Entrance Region in Fully Developed Turbulent Flow

PETER H. ABBRECHT and STUART W. CHURCHILL

University of Michigan, Ann Arbor, Michigan

The temperature profile and the local rate of heat transfer from the wall were measured at 0.453, 1.13, 4.12, and 9.97 tube diameters downstream from a step increase in wall temperature for air in fully developed turbulent flow at Reynolds numbers of 15,000 and 65,000 in a 1.52-in. tube. The velocity profile and the pressure were also measured at these lengths.

Radial and longitudinal temperature gradients, radial heat fluxes, and eddy diffusivities for heat and momentum transfer were computed from the measurements. The longitudinal temperature gradients at all radii were found to differ significantly from the mixed mean temperature gradient. Although the radial heat flux was a maximum at the wall, the radial heat-flux density, in terms of which the eddy diffusivity for heat transfer is usually defined, was found to go through a maximum near the wall and then to decrease almost linearly across the thermal boundary layer. The eddy diffusivity for heat transfer was found to be independent of length in the thermal entrance region and hence a function only of the fluid motion, as previously hypothesized.

This paper presents the results of an experimental investigation of heat transfer in the region following a step change in wall temperature in fully developed turbulent flow in a tube. Following such a change in wall temperature, the temperature field in the fluid and the rate of heat transfer from the wall change rapidly, while the velocity field and rate of momentum transfer change only slightly, owing to changes in the physical properties of the fluid with temperature.

The length of tube required for the temperature of the fluid at the center of the tube to change some small arbitrary amount is called the *thermal entrance region*. The thermal entrance region has particular interest because of the high heat transfer coefficients attainable and has received recent attention in connection with heat transfer in nuclear reactors and other compact equipment. The step change in wall temperature in fully developed flow has particular theoretical interest since Tribus and Klein (20) have shown that a knowledge of the resulting temperature field permits computation of the rate of heat transfer for any wall-temperature distribution.

Previous experimental investigations of heat transfer in the thermal entrance region have apparently been limited to measurements of the surface temperature, the mixed mean temperature, and the heat flux at the wall. Analytical representations have all assumed that eddy diffusivities measured in fully developed boundary layers are directly applicable in the thermal entrance region.

In this investigation the time-mean temperature and velocity fields were measured as well as the heat flux at the wall in order to provide insight into

the mechanism of heat transfer in the entrance region and to test the postulates of previous investigators. The measurements were made in air at Reynolds numbers of approximately 15,000 and 65,000. Temperature differences of less than 30°F. were utilized to minimize changes in the physical properties of the air.

MATHEMATICAL RELATIONSHIPS

The conservation of momentum in the axial direction in fully developed turbulent flow of a fluid of constant physical properties can be written in terms of the time-mean pressure and velocity with the contribution of the fluctuating components of the velocity expressed as an eddy diffusivity as follows:

$$-\frac{g_c}{\rho} \frac{\partial P}{\partial x} + \frac{1}{r} \frac{\partial}{\partial r} \left[r(\nu + \epsilon_m) \frac{\partial u}{\partial r} \right] = 0 \quad (1)$$

Integrating for constant $\partial P/\partial x$ and rearranging yields

$$\frac{\epsilon_m}{\nu} + 1 = \frac{rg_c}{2\mu} \frac{\partial P}{\partial x} \frac{\partial r}{\partial u} = \frac{r}{a} \frac{dy^+}{du^+} \quad (2)$$

Since the eddy diffusivity is presumed to fall to zero at the wall, Equation (2) can be rewritten as

$$\frac{\epsilon_m}{\nu} + 1 = \frac{r}{a} \frac{(\partial u/\partial r)_w}{(\partial u/\partial r)} \quad (3)$$

In principle the eddy diffusivity for momentum transfer in fully developed flow can thus be computed for any radius from experimental measurements of the radial velocity profile

only. However the longitudinal pressure gradient can be measured more accurately than the radial velocity gradient at the wall, and Equation (2) is therefore more practical for computations than Equation (3).

The conservation of energy can similarly be written in terms of time-mean temperature and velocities, and axial and radial eddy diffusivities for heat transfer as follows:

$$u \frac{\partial t}{\partial x} = \frac{\partial}{\partial x} \left[(K + \epsilon_h) \frac{\partial t}{\partial x} \right] + \frac{1}{r} \frac{\partial}{\partial r} \left[r(K + \epsilon_h) \frac{\partial t}{\partial r} \right] \quad (4)$$

The first term on the right side of Equation (4) has been shown to be negligible under most circumstances (16) and will be dropped for simplicity. Integration then yields

$$\frac{\epsilon_h}{K} + 1 = \frac{1}{rK} \frac{\partial r}{\partial t} \int_0^r u \frac{\partial t}{\partial x} r dr \quad (5)$$

The radial eddy diffusivity for heat transfer can also be expressed in terms of the local radial heat-flux density:

$$\frac{\epsilon_h}{K} + 1 = \frac{q}{k} \frac{\partial r}{\partial t} \quad (6)$$

The radial heat-flux density is discussed in detail by Churchill and Balzhiser (5). Comparison of Equations (5) and (6) indicates that subject to the assumptions inherent in Equation (5)

$$q = \frac{\rho c}{r} \int_0^r u \frac{\partial t}{\partial x} r dr \quad (7)$$

For a constant heat flux at the wall and a fully developed temperature distribution $\partial t/\partial x$ is constant with respect to radius and length (16). For the thermal entrance region and for other boundary conditions $\partial t/\partial x$ varies with radius. Determination of the eddy diffusivity for heat transfer for such conditions thus requires measurement of the longitudinal temperature profile as well as the radial temperature and velocity profiles.

The local heat transfer rate at the wall is expressed in the customary form in terms of hD/k where

CHILL
Michigan

al pres-
ed more
velocity
Equation
tical for
(3).
ergy can
of time-
ties, and
vities for

$$\frac{dt}{dx} \quad (4)$$

side of
own to be
stances
r simpli-

$$\frac{r}{a} \quad (5)$$

for heat
in terms
ensity:

$$(6)$$

y is dis-
chill and
of Equa-
that sub-
herent in

$$(7)$$

t the wall
ature dis-
th respect
For the
for other
aries with
ddy dif-
such con-
ement of
profile as
ature and

ate at the
customary

ne, 1960

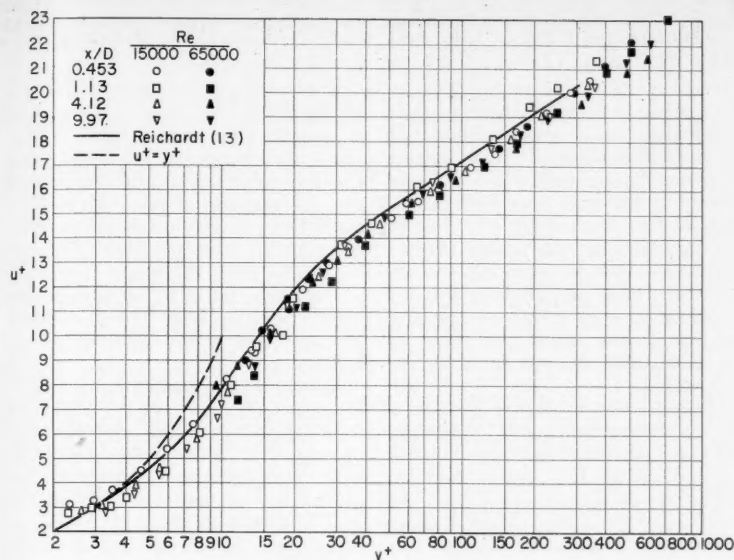


Fig. 1. Velocity-distribution data.

$$h = q_w / (T_w - T_b) \quad (8)$$

and

$$T_b = \int_0^1 T \left(\frac{u}{u_b} \right) d \left(\frac{r}{a} \right) \quad (9)$$

tions of tube were honed to an inside diameter of 1.520 in. with a 30- μ in. finish.

The nozzle and unheated tube yielded essentially fully developed turbulent flow. Four interchangeable heating tubes were utilized so that total heating distance to

EXPERIMENTAL APPARATUS

Air from a 90 lb./sq. in. gauge supply main passed through a filter; a flow-control valve; a calming section; a converging nozzle; a 66 in.-long unheated tube; a heated tube of variable length; a 1 in.-long, 0.19 in.-thick, heated copper tube serving as a calorimeter; another unheated tube containing an orifice; and finally into the atmosphere. The entrance and test sec-

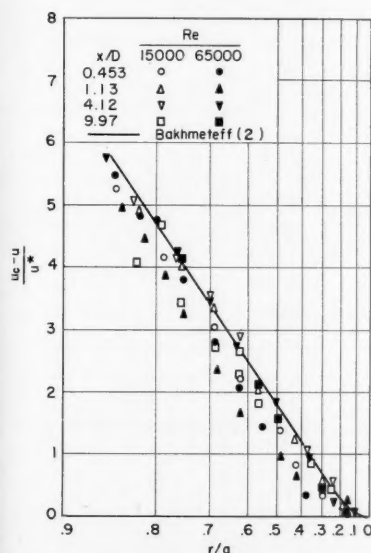


Fig. 2. Velocity deficiency.

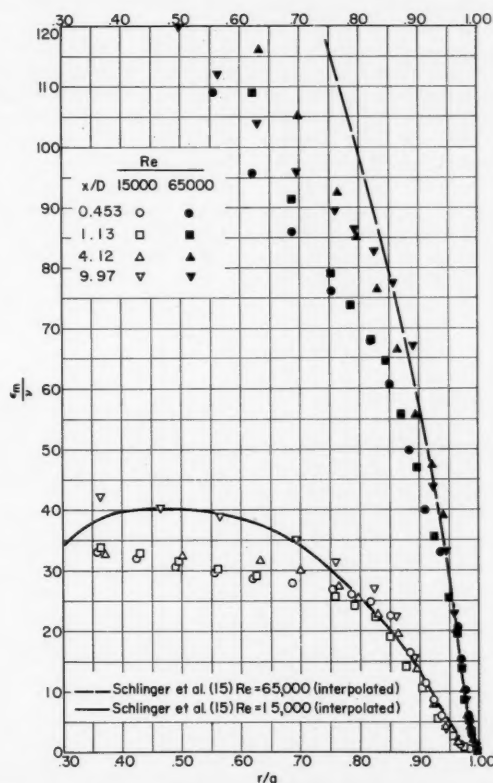


Fig. 3. Eddy diffusivity for momentum transfer.

the center of the calorimeter was 0.453, 1.13, 4.12, or 9.97 tube diameters. A steam jacket was used to heat the two longer tubes and electrical resistance coils to heat the two shorter tubes and the calorimeter. A 0.2 in. thick plastic disk insulated the entrance section from the heating section. The calorimeter was insulated from the adjacent sections of tube with 0.015 in. thick plastic disks and was surrounded by a guard heater. The sections of tube were aligned by means of carefully machined male and female joints.

A traversing mechanism was located downstream from the calorimeter with a probe extending upstream to the midplane of the calorimeter. The tip of the probe consisted of a 140-mil-long 3-mil wire, the center 40 mils of which were etched to 0.3 mil. This probe was used as a hot-wire anemometer to measure the velocity profile and as a resistance thermometer to measure the temperature profile. The heat flux through the calorimeter wall to the air stream was determined from voltage and current readings on the calorimeter heating coil.

The inlet air temperature was measured with a thermocouple in the calming section and the orifice temperature with a thermometer. Thermocouples were located at a number of azimuthal and longitudinal points in the wall of the heating section and calorimeter. Pressure-drop measurements were made with a micromanometer between taps located at 1, 3, 5, 15, 30, 44.5, 61, and 65 in. from the nozzle and at the outlet of the calorimeter.

Calibration of the measuring devices and further equipment details are given in reference 1. The raw data are preserved insofar as possible in the subsequent correlations to avoid prejudicing the results.

EXPERIMENTAL DATA

The heat flux at the wall and the radial temperature and velocity profiles were measured at the four stations at Reynolds numbers of approximately 15,000 and 65,000. No significant difference was observed in velocities measured during heating and nonheating runs, and the reported velocity data were obtained during the heating runs. The pressure gradient was determined for each run by averaging the differential measurements obtained at a number of positions along the tube. The experimental conditions and over-all data for the eight runs are summarized in Table 1.* The physical properties of air were taken from reference 9 except for density, which was computed from the ideal gas law.

The uncertainty in the measured velocities varied from about 0.5% at the center line up to perhaps 5% at a velocity of 7 ft./sec. The uncertainty in the measured temperatures is estimated at $\pm 0.2^\circ\text{F}$. The location of the probe was known within about ± 0.0005 in. The pressure gradient was reproducible to within less than 1% at a Reynolds number of 65,000 and less than 3% at 15,000. The heat flux obtained from the calorimeter is believed to be dependable within 3% at an x/D of 10 but to be somewhat less certain at lower values of x/D .

MOMENTUM TRANSFER

The measured pressure gradients agreed within 2% with the correlation of Moody (10) for fully developed flow in smooth pipe. Velocity data for all eight runs are plotted in

*Tabular material has been deposited as document 6260 with the American Documentation Institute, Photoduplication Service, Library of Congress, Washington 25, D. C., and may be obtained for \$2.50 for photoprints or \$1.75 for 35-mm. microfilm.

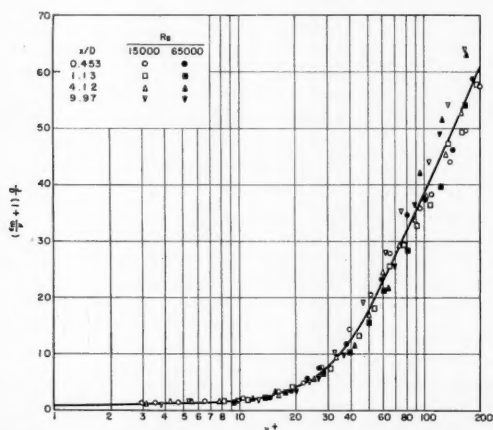


Fig. 4. Generalized correlation of eddy diffusivity for momentum transfer.

Figure 1 as u^+ vs. y^+ . Some overlying experimental points were omitted for clarity. The data for $y^+ > 3$ are in good agreement with those of previous investigations as indicated by the curve representing the measurements of Reichardt and others (13) and appear to extrapolate satisfactorily to zero velocity at the wall. The high velocities for $y^+ < 3$ are apparently due to heat transfer from the heated wire to the wall. Although empirical corrections have been proposed for this effect, their accuracy is questionable and such corrections would add little to the information obtained from this investigation.

The velocities in Figure 1 show a slight variation with x/D , indicating that the boundary layer was still developing even for these entrance lengths of 44 diam. and greater. As noted by Rothfus and Monrad (14) and others, a slight dependence on Reynolds number is also apparent. The incomplete development of the boundary layer can be examined more critically in Figure 2 in which the dimensionless velocity deficiency $(u_c - u)/u^*$ is plotted. Some development is indicated, but the data agree quite well with the curve given by Bakhmeteff (2) for fully developed flow.

The velocity data were differentiated graphically, and the velocity gradients

obtained from equal area curves were used to compute the eddy diffusivity for momentum transfer in Figure 3. Curves obtained by interpolating the results of Schlenger *et al.* (15) for flow in circular pipes are included in Figure 3 for comparison. The agreement between these curves and the data of this investigation is good. Figure 3 is a still more critical test of the development of the boundary layer. The scatter of the data below the curves for r/a less than 0.8 is to be expected because of the very small velocity gradient and is not believed to be significant.

Equation (2) suggests that a plot of $[(\epsilon_m/\nu) + 1] (a/r)$ vs. y^+ would not show dependence on the Reynolds number if u^+ were a function of y^+ only. The data in Figure 3 are replotted in this form in Figure 4. Despite the magnification of the actual dependence of u^+ on the Reynolds number for a given y^+ by the differentiation which leads from Figure 1 to Figure 4, a reasonably compact correlation is obtained.

HEAT TRANSFER

The heat fluxes obtained from the calorimeter were corrected for heat losses to the surroundings and through the plastic disks isolating the test sec-

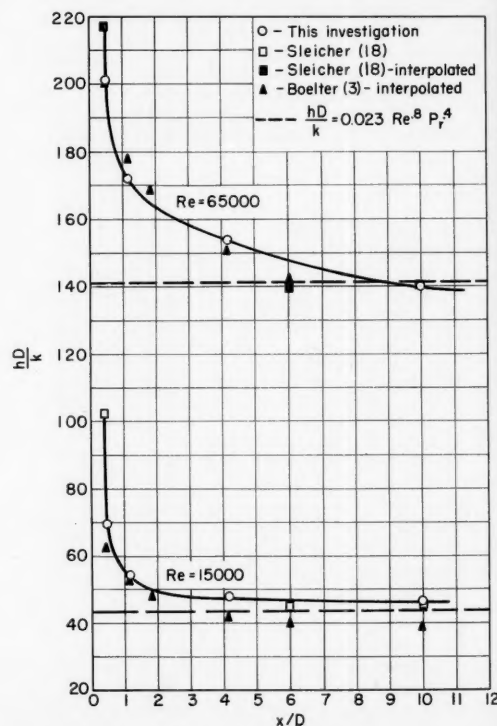


Fig. 5. Local Nusselt number.

ves were
diffusivity
Figure 3.
ating the
for flow
d in Fig.
reement
e data of
ure 3 is
develop-
The scat-
curves for
ected be-
velocity
d to be

a plot of
ould not
Reynolds
on of y'
are re-
e 4. De-
ne actual
Reynolds
differen-
ure 1 to
ct corre-

from the
for heat
through
test sec-

ropolated
olated
 P_r^4

0 11 12

ne, 1960

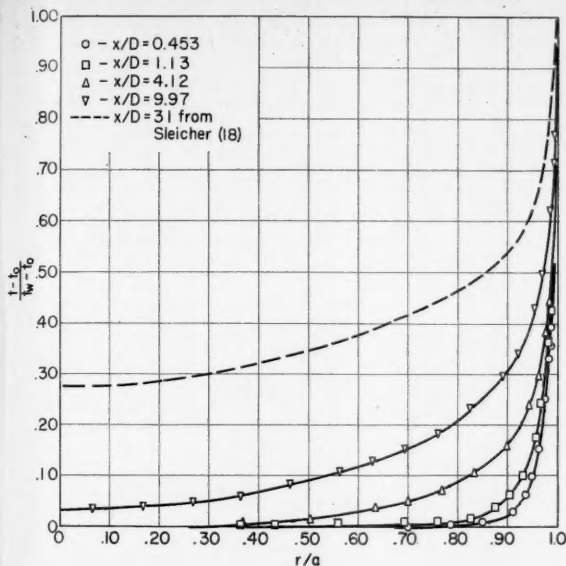


Fig. 6. Temperature distribution data for $N_{Re} = 15,000$.

tion. The computed loss through the plastic disks was in every case less than 3%. The heat losses to the surroundings were estimated from heat flux measurements with no flow. This correction was 12.5% or less at a Reynolds number of 15,000 and 4.3% or less at a Reynolds number of 65,000.

Since the corrected heat fluxes were for 1-in. segments of the tube, it was necessary to obtain the point fluxes from an equal-area curve through a plot of the segmental rate vs. length. The bulk temperature at each station was obtained by graphical integration of the temperature and velocity data according to Equation (9). The local heat transfer coefficient defined by Equation (8) and hD/k were then calculated. These quantities are all included in Table 1.

Figure 5 plots the local Nusselt number as a function of heated length. Excellent agreement with the data of Sleicher (18) and Boelter, Young, and Iverson (3) can be noted. The asymptotic values predicted by the empirical equation of Dittus and Boelter (8) for long tubes are also shown. The

Nusselt number appears to have attained close to its asymptotic value at an x/D of 10.

The temperature-distribution data is illustrated for N_{Re} of 15,000 in Figure 6. A curve representing the data of Sleicher (18) at an x/D of 31 is included. The radial temperature gradients were obtained by graphical differentiation of the data. The longitudinal temperature profiles shown in Figure 7 were obtained by cross plotting the temperature-distribution data. The longitudinal temperature gradients shown in Figure 8 were obtained by differentiating the longitudinal temperature profiles. The mixed mean temperature gradient was obtained from the smoothed heat flux; that is

$$\frac{\partial[(t_b - t_o)/(t_w - t_o)]}{\partial(x/a)} = \frac{2q_w}{\rho c u_b (t_w - t_o)} \quad (10)$$

It is apparent from Figure 8 that the longitudinal gradients at all radii differ from the mixed mean gradient even for an x/D of 10. Similar results were obtained at a Reynolds number of

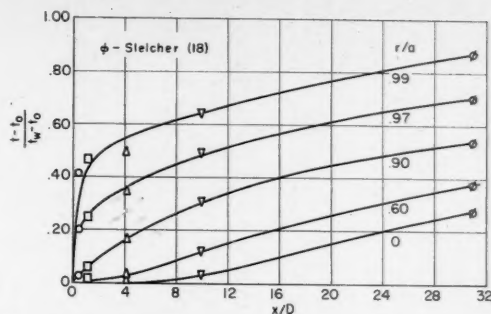


Fig. 7. Longitudinal temperature profiles for $N_{Re} = 15,000$.

65,000. However because of the absence of data for x/D greater than 9.97 the longitudinal gradients at x/D of 9.97 were defined with less certainty than at a Reynolds number of 15,000.

The radial heat flux density was computed from the following modified forms of Equation (7):

$$\frac{q}{q_w} \frac{r}{a} = 1 - \int_{r/a}^1 \frac{u}{u_b} \frac{(\partial t / \partial x)}{(\partial t_b / \partial x)} d\left(\frac{r}{a}\right) = \int_0^{r/a} \frac{u}{u_b} \frac{(\partial t / \partial x)}{(\partial t_b / \partial x)} d\left(\frac{r}{a}\right) \quad (11)$$

for the regions near the wall and center respectively. The results are illustrated for a Reynolds number of 15,000 in Figure 9. The data points are omitted since the integration which yields Figure 9 is inherently a smoothing process. Although the radial heat flux decreases monotonically from the wall, the radial flux density, in terms of which the eddy diffusivity for heat transfer can be defined [Equation (6)], is observed to go through a maximum and then to decrease almost linearly across the thermal boundary layer. This behavior is due to the opposing effects of longitudinal transfer and decreasing circumference.

The eddy diffusivity for heat transfer was next computed from a modified form of Equation (6),

$$\frac{\epsilon_h}{K} + 1 = \frac{q_w}{K} \cdot \frac{\partial r}{\partial t} \cdot \frac{q}{q_w} \quad (12)$$

by means of the heat flux density at the wall derived from the calorimeter measurements. The computed points are plotted vs. r/a in Figure 10. The data for x/D of 9.97 at a Reynolds number of 65,000 are omitted because of the previously noted uncertainty in the longitudinal temperature gradients. When the effect of the slightly changing velocity profile is considered, it is apparent that the eddy diffusivity for heat transfer is not a significant function of length in the thermal entrance region. Curves representing the data of Sleicher (18) for a fully developed thermal boundary layer in a tube and the data of Page *et al.* (11) for fully

TABLE 1. EXPERIMENTAL CONDITIONS AND RESULTS

Run No.	x/D	w lb/hr	t_o °F	t_w °F	t_b °F	$4w$ $\pi D \mu_b$	q_w Btu (in)(sq ft)	h Btu (in)(sq ft)°F	hD k_b
1	0.453	66.6	79.35	104.01	79.60	15000	207	8.45	69.4
2	1.13	66.0	82.17	109.70	83.02	14780	174	6.53	53.7
3	4.12	66.4	83.78	110.80	85.85	14860	147	5.87	47.8
4	9.97	65.8	83.49	108.48	87.35	14700	121	5.72	46.6
5	0.453	285.0	81.48	104.46	81.85	64100	551	24.4	201
6	1.13	287.0	84.24	113.65	84.74	64200	601	20.8	172
7	4.12	284.0	80.40	106.69	82.05	63800	462	18.7	154
8	9.97	290.0	81.81	107.49	84.55	64900	390	17.0	140

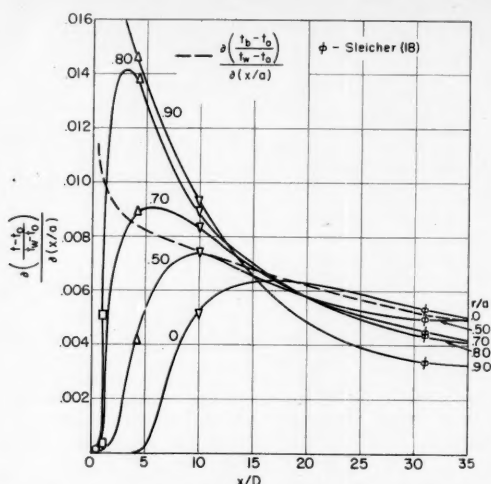


Fig. 8. Longitudinal temperature gradients for $N_{Re} = 15,000$.

developed heat transfer between parallel plates are included in Figure 10 for comparison. The curve of Sleicher for a Reynolds number of 14,500 is reproduced directly. The curves for a Reynolds number of 65,000 were obtained by cross plotting, interpolating, and converting the reported results of Sleicher and Page *et al.* The agreement with these previous experiments is excellent for r/a greater than 0.8 and is reasonable for smaller r/a , considering the smaller and hence more uncertain temperature gradients.

The data are replotted as $[(\epsilon_h/K) + 1] (a/r)$ vs. y^* in Figure 11. Again, as for momentum transfer, a reasonably general correlation for all Reynolds numbers is obtained in this form. The curve in Figure 11 coincides with the smoothed results of Cavers (4) for heat transfer between parallel plates which extend to y^* of 46.

Figure 12 plots the ratio of the eddy diffusivities for heat and momentum transfer as a function of position. Curves representing the results of Sleicher (18) and Page *et al.* (12) are included. This plot is a very critical test of the data since the ordinate involves the ratio of the derivatives of two independently measured quantities. Accordingly the scatter is not believed to be unreasonable; it appears to be random with respect to Reynolds number as well as to length, although Sleicher and Page *et al.* infer small effects for the Reynolds number from their data. The ratio ϵ_h/ϵ_m has a value of 1.0 to 1.5 in the turbulent core but increases rapidly near the wall.

DISCUSSION

The agreement of the velocity data for all four test stations with the correlations of previous investigators in Figure 1 indicates that essentially

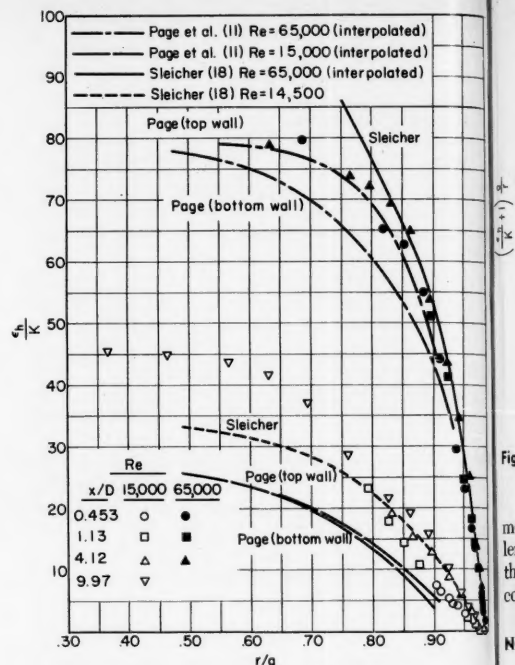


Fig. 10. Eddy diffusivity for heat transfer.

fully developed turbulent motion was established. The independence of the motion near the wall from x/D is further indicated in Figures 2, 3, and 4. The comparison in Figure 5 of the local heat transfer rate data with that of previous investigators for a step function in wall temperature in fully developed flow is evidence that the thermal boundary conditions as well as the flow conditions were representative.

The temperature-distribution data are difficult to interpret directly. However the deviation of the longitudinal temperature gradients at all radii from the mixed mean temperature gradient, even for an x/D of 10 where hD/k

has approached its asymptotic value, is significant since theoretical models frequently have postulated the form of these gradients. The radial variation of the heat flux density illustrated in Figure 9 is also of particular interest since temperature-distribution data and analytical results have apparently not been expressed in this form and since the radial heat flux density has been assumed to be constant in the theoretical developments of Deissler (6, 7) and others.

The eddy diffusivity for heat transfer in fully developed turbulent flow is shown in Figures 10, 11, and 12 to be invariant with length in the thermal entrance region following a step function in temperature and hence to be a function of the fluid motion only. The reasonable agreement noted in Figures 10, 11, and 12 with the results for heat transfer between parallel plates is further evidence of the independence of the eddy diffusivity from the temperature field. These observations confirm the hypothesis made by Deissler (7), Sleicher and Tribus (19), Seban and Shimazaki (17), Tribus and Klein (20), and others in theoretical derivations for the thermal entrance region.

The dimensionless groups $[(\epsilon_m/\nu) + 1] a/r$ and $[(\epsilon_h/K) + 1] a/r$ are observed in Figures 4 and 11 to be single valued functions of y^* for both Reynolds numbers within the certainty of the data. However the rapid increase indicated in Figure 12 for the ratio of the eddy diffusivities for heat and

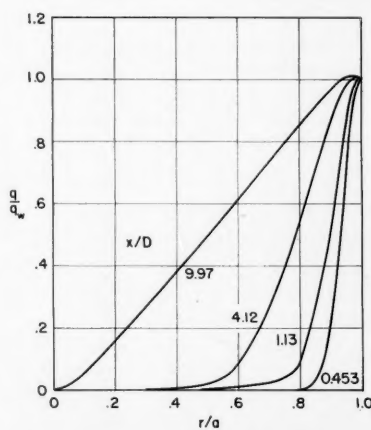


Fig. 9. Radial heat-flux density for $N_{Re} = 15,000$.

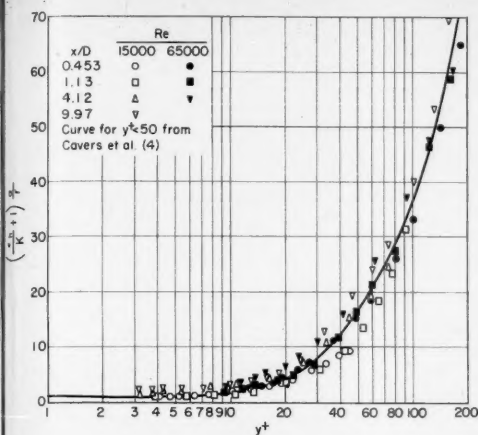


Fig. 11. Generalized correlation for eddy diffusivity for heat transfer.

momentum transfer near the wall challenges the validity and generality of theoretical models which postulate a constant ratio.

NOTATION

- a = radius of tube, ft.
 c = heat capacity, B.t.u./ (lb.) (°F.)
 D = diameter of tube, ft.
 g_c = conversion factor = 32.17 (lb.) (ft.) / (lb.-force) (sec.)²
 h = heat transfer coefficient, B.t.u./ (sec.) (sq.ft.) (°F.)
 k = thermal conductivity, B.t.u./ (sec.) (sq.ft.) (°F./ft.)
 K = $k/\rho c$ = thermal diffusivity, sq. ft./sec.
 N_{Pr} = $c\mu/k$ = Prandtl number
 N_{Re} = $4w/\pi D\mu$ = Reynolds number

- P = pressure, lb.-force/sq. ft.
 q = heat flux density, B.t.u./ (sec.) (sq.ft.)
 r = radial distance from axis of tube, ft.
 t = temperature, °F.
 u = velocity, ft./sec.
 u^* = $\sqrt{\frac{Dg_c}{4\rho} \left(-\frac{\partial P}{\partial x} \right)}$ = friction velocity, ft./sec.
 u^+ = u/u^* = dimensionless velocity
 x = heated length, ft.
 y = distance from wall, ft.
 y^+ = yu^*/ν = dimensionless distance from wall
 w = flow rate = lb./sec.

Greek Letters

- ϵ_h = radial eddy diffusivity for heat transfer, sq. ft./sec.
 ϵ_s = longitudinal eddy diffusivity for heat transfer, sq. ft./sec.
 ϵ_m = eddy diffusivity for momentum transfer, sq. ft./sec.
 θ = $(t-t_o)/(t_w-t_o)$ = dimensionless temperature

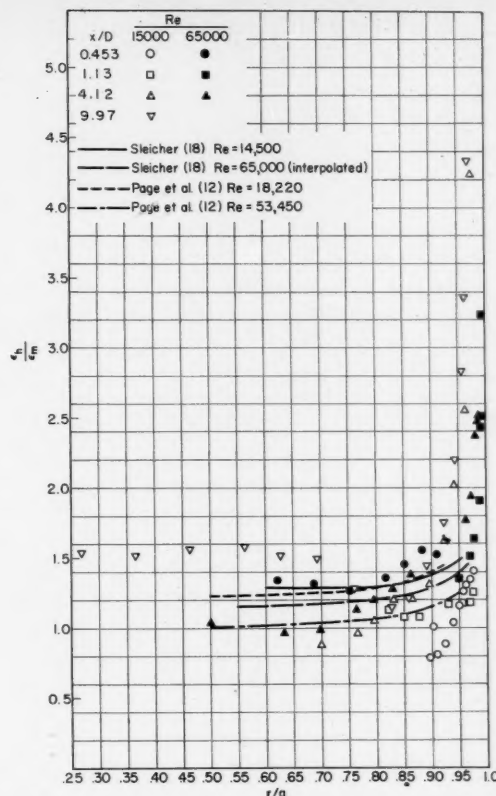


Fig. 12. Ratio of eddy diffusivities for heat and momentum transfer.

- μ = viscosity, lb./ (ft.) (sec.)
 ν = μ/ρ = kinematic viscosity, sq. ft./sec.
 ρ = density, lb./cu. ft.

Subscripts

- b = mixed mean
 c = center
 o = initial
 w = wall

LITERATURE CITED

- Abbreviated, P. H., Ph.D. thesis, Univ. Mich., Ann Arbor (1956).
- Bakhtmeteff, B., "Mechanics of Turbulent Flow," Princeton Univ. Press, Princeton, New Jersey (1941).
- Boelter, L. M. K., G. Young, and H. W. Iverson, *Natl. Advisory Comm. Aeronaut. Tech. Note 1451*, Washington, D. C. (1948).
- Cavers, S. D., N. T. Hsu, W. G. Schlenger, and B. H. Sage, *Ind. Eng. Chem.*, **45**, 2139 (1953).
- Churchill, S. W., and R. E. Balzhiser, *Chem. Eng. Progr. Symposium Ser. No. 29*, 55, 127 (1959).
- Deissler, R. G., *Natl. Advisory Comm. Aeronaut. Rept. 1210*, Washington, D. C. (1955).
- , *Trans. Am. Soc. Mech. Engrs.*, **77**, 1221 (1955).
- Dittus, F. W., and L. M. K. Boelter, *Univ. Calif. Pubs. Engr.*, **2**, 443 (1930).

- John Hopkins Univ., Applied Phys. Lab., Silver Spring, Md., "Handbook of Supersonic Aerodynamics," Navord Rept. 1488, Vol. 5, Washington Bureau of Ordnance (1953).
- Moody, L. F., *Trans. Am. Soc. Mech. Engrs.*, **66**, 671 (1944).
- Page, F., Jr., W. H. Corcoran, W. G. Schlenger, and B. H. Sage, *Ind. Eng. Chem.*, **44**, 419 (1952).
- Page, F., Jr., W. G. Schlenger, D. K. Breaux, and B. H. Sage, *ibid.*, **424** (1952).
- Reichardt, H., *Natl. Advisory Comm. Aeronaut. Tech. Memo. 1047*, Washington, D. C. (1943).
- Rothfus, R. R., and C. C. Monrad, *Ind. Eng. Chem.*, **47**, 1147 (1955).
- Schlenger, W. G., V. J. Berry, J. L. Mason, and B. H. Sage, *ibid.*, **45**, 662 (1953).
- Schneider, P. J., *Trans. Am. Soc. Mech. Engrs.*, **79**, 765 (1957).
- Seban, R. A., and T. T. Shimazaki, *ibid.*, **73**, 803 (1951).
- Sleicher, C. A., Jr., Ph.D. thesis, Univ. Mich., Ann Arbor (1955); *Trans. Am. Soc. Mech. Engrs.*, **80**, 693 (1958).
- , and Myron Tribus, *Trans. Am. Soc. Mech. Engrs.*, **79**, 789 (1957).
- Tribus, Myron, and J. S. Klein, "Heat Transfer," pp. 211-235, Univ. Press, Ann Arbor, Michigan (1953).

Manuscript received July 29, 1957; revision received September 30, 1959; paper accepted October 5, 1959. Paper presented at A.I.Ch.E. Baltimore meeting.

Diffusion in Compressed Binary Gaseous Systems

V. J. BERRY, JR., and R. C. KOELLER

Pan American Petroleum Corporation, Tulsa, Oklahoma

Apparatus is described for experimentally determining diffusion coefficients in dense-gas systems to pressures of 15,000 lb./sq. in. abs. Tests were made with the hydrogen-nitrogen and methane-ethane systems at 104°, 139°, and 171°F. to 10,000 lb./sq. in. abs. and with the nitrogen-methane and nitrogen-ethane systems at 104°F. to 2,500 lb./sq. in. abs. In all cases it was found that diffusion coefficients predicted on the basis of the Lennard-Jones model with Thorne's dense-gas correction diverged below the experimental data in the high-density region. Coefficients predicted from the Slattery-Bird reduced-state correlation showed better agreement with the experimental data. The temperature dependence of the results is better described by the exponential form for liquids than by the form of the dense-gas theory.

Fundamental physical data relating to molecular transport in gases at pressures above 1 atm. are not generally available. There is a growing need for such data for direct industrial application. Studies of gaseous diffusion at high pressures also provide data which can be used to evaluate the various theoretical relations available for predicting transport properties of dense gases. Not only do such comparisons aid the fundamental understanding of molecular interaction, but they are useful in demonstrating the accuracy of methods for predicting transport properties in regions for which no data are available.

A few studies have been made of diffusion in compressed gases, and the results compared with predictions based on the Chapman-Enskog (1) dense-gas theory. Drickamer and co-workers (2, 3, 4) have published self-diffusion coefficients for carbon dioxide at pressure up to 15,000 lb./sq. in. abs. The data indicate that in regions of high density the dense-gas approximation is not adequate for the prediction of the self-diffusion coefficient of carbon dioxide. It was concluded that at pressures above about 3,000 lb./sq. in. abs. (density above about 1.3 lb. mole/cu.ft) the temperature dependence is

more nearly described by the exponential form characteristic of liquids than by the Chapman-Enskog equations. O'Hern and Martin (5) have further studied self-diffusion in carbon dioxide at pressures to 3,000 lb./sq.in.abs. using a different experimental technique. Their results disagree even more with the theoretical predictions, and their opinion is that the diffusion coefficients published by Drickamer and co-workers are low.

Results for self-diffusion in methane were reported by Jeffries and Drickamer (6). Coefficients agreed with dense-gas predictions within about 10 to 20% at pressures to about 4,500 lb./sq.in.abs. Their measurements with mixtures of carbon dioxide and methane (7) over the same pressure range also show good agreement with theory, except near the critical point of carbon dioxide.

Studies of diffusion in a ternary system at pressures to 4,000 lb./sq.in.abs. were reported by Chou and Martin (8). The results show that the diffusion of traces of radioactive carbon dioxide in mixtures of unlabeled carbon dioxide with hydrogen, and with propane, varies with concentration in the manner predicted by Wilke (9) and by Curtiss and Hirschfelder (10). The nonideality of carbon dioxide is

again demonstrated by failure of the dense-gas approximation to predict diffusion coefficients at densities above about 0.6 lb.mole/cu.ft.

The relative scarcity of high-pressure diffusion data and the advantage of further evaluating the applicability of the dense-gas approximation suggest a need for additional measurements. This paper describes apparatus which has been constructed for such high-pressure diffusion studies. The results of some experimental measurements on the hydrogen-nitrogen, methane-ethane, nitrogen-ethane, and nitrogen-methane mixtures are presented together with an evaluation of several methods for predicting diffusion coefficients at elevated pressure in these binary gaseous systems.

THEORY

A lucid discussion of the various theoretical approaches to predicting diffusion coefficients in gases is given by Bird (11); a few pertinent results of the theoretical studies are summarized here.

Consideration of the kinetics of gaseous molecules by the Chapman-Enskog method leads to several different theoretical expressions for the diffusion coefficient in a binary mixture of gases 1 and 2, depending upon the particular molecular model chosen. If it is assumed that molecules act as rigid elastic spheres, then the expression derived is

V. J. Berry, Jr., is with Sinclair Research Laboratories, Inc., Tulsa, Oklahoma.

$$D_{12}^s = \frac{3}{8n\sigma_{12}^2} \left\{ \frac{\kappa T(M_1 + M_2)}{2\pi M_1 M_2} \right\}^{1/2} \quad (1)$$

Values of D_{12}^s computed from Equation (1) by the use of collision diameters $\sigma_{12} = (\sigma_1 + \sigma_2)/2$ from viscosity data are generally about 10 to 15% greater than experimental values of D_{12} at moderate temperatures. This disagreement is probably due to the assumption of rigid elastic spheres.

A more realistic description of molecular interactions is given by the Lennard-Jones (6-12) model. In the Lennard-Jones (6-12) model it is assumed that molecules attract one another with a force which is proportional to the -6 power of their separation and repel one another with a force proportional to the -12 power of separation. In addition to collision diameters, a force constant parameter is needed to describe a molecule in terms of the Lennard-Jones model. On the basis of this model the expression for D_{12}^s is given as (11)

$$D_{12}^s = \frac{3}{16n\pi\sigma_{12}^2\Omega^{(1,1)*}} \left\{ \frac{2\pi RT(M_1 + M_2)}{M_1 M_2} \right\}^{1/2} \quad (2)$$

Bird, Curtiss, and Hirschfelder (12) have tabulated values of σ and ϵ for a large number of pure compounds and also values of $\Omega^{(1,1)*}$ as a function of $T^* = \kappa T/\epsilon_{12}$, where $\epsilon_{12} = (\epsilon_1 \epsilon_2)^{1/2}$. The parameters σ and ϵ are best determined from pure-component viscosity data but may be empirically estimated from critical data. Slattery and Bird (13) show that for twenty-eight different binary gas mixtures the experimental diffusion coefficients are predicted to within an average deviation of 8.5% by the use of the Lennard-Jones model with parameters from viscosity data.

Both Equations (1) and (2) give first approximations to D_{12} which are independent of the relative proportions of the two molecular species. In such a situation it follows that $D_{12} = D_{21}$. Also these equations are known to be applicable only to gases at moderate pressures, since they are based upon only a first approximation of the probability of a binary molecular collision.

A dense-gas theory based on the solid-elastic-sphere model has been given by Enskog (14), but his results are not applicable to gas mixtures. Thorne (1) has extended Enskog's dense-gas theory to obtain a first-degree approximation for binary mixtures which can be applied to Equation (1) or (2) to determine diffusion coefficients at elevated pressures. Thorne's correction factor is simply applied as

$$D_{12}^{L*} = \frac{D_{12}^s}{\chi_{12}} \quad (3)$$

where

$$\chi_{12} = 1 + \frac{\pi}{12} n_2 \sigma_1^2 \left(8 - \frac{3\sigma_1}{\sigma_{12}} \right) + \frac{\pi}{12} n_2 \sigma_2^2 \left(8 - \frac{3\sigma_2}{\sigma_{12}} \right) + \dots \quad (4)$$

Thus from (1) or (2) and (3) it follows that

$$D_{12}^{L*} = \frac{(D_{12}^s)_0}{\chi_{12}} \cdot \frac{n_0}{n_p} \quad (5)$$

For an ideal gas, Equation (1) predicts that D_{12} should vary as $T^{3/2}$ at constant pressure. The dependence of D_{12} on temperature indicated by Equation (2) is masked by the variation of $\Omega^{(1,1)*}$ with temperature. Over a wide range of temperature for a given pair of molecules $\Omega^{(1,1)*}$ varies approximately as $e^{-1/T}$. Nevertheless both Equations (1) and (2) predict that the dependence of D_{12} on T should be independent of pressure. On the other hand, at elevated pressure where the dense-gas correction applies, it can be seen from Equation (4) that the effect of temperature on D_{12} depends upon the pressure level, because χ_{12} is a function of density.

It might be expected that the temperature dependence of the diffusion coefficient in highly compressed gases would be similar to that in liquids at moderate pressures. Although the theory of diffusion in the liquid state is not well developed, simple considerations (15) indicate that the diffusion coefficient can be expressed as follows at constant pressures:

$$D_L = b_L e^{-u/RT} \quad (6)$$

It has been found experimentally by Timmerhaus and Drickamer (4) that diffusion in compressed gases does depend upon temperature, approximately as indicated in Equation (6).

Slattery and Bird (13) have utilized a modified form of the Enskog dense-gas theory with generalized gas-viscosity and compressibility correlations to prepare a correlation chart. This chart can be used for predicting a reduced diffusion coefficient as a function of reduced temperature and reduced pressure. It was prepared from pure-component data, but it is anticipated that it might be used, with pseudocritical constants to predict diffusion coefficients in dense-gas mixtures.

PROCEDURE

Apparatus

For the determination of diffusion coefficients in gases under pressure the technique originally used by Loschmidt (16) appears to be the most satisfactory. Ap-

paratus used for determinations by this technique must provide for the separate filling of two diffusion cavities at a specified temperature and pressure. In addition the two cavities must be brought together at the initiation of an experiment in such a manner that the system undergoes no change in total volume. If the latter requirement is not met, it is found that turbulent mixing occurs as a result of the sudden volume change, obscuring the effects of simple diffusional transfer. The measurements reported here were made with a cell which meets these requirements.

Figure 1 is a sectional drawing of the working section. The cell is composed of two stainless steel pistons (A) and (B), enclosed within an outer stainless steel casing (C). The function of the shell (C) is to align properly and to support the pistons (A) and (B) and to provide a mass of high heat capacity to aid in stabilizing the temperature of the diffusing gases.

Diffusion occurs in the cylindrical cavities shown in the pistons. These cavities, each $1/4$ in. in diameter and 4 in. in length, are capable of confining fluids at pressures up to 15,000 lb./sq. in. abs. Figure 1 shows the configuration of the pistons when in the diffusing position. Rotating the piston (A) one quarter of a revolution about the axis of the cell brings the system to the fill or sampling position. The small lines for filling and sampling do not show in the sectional drawing. The line for filling the lower piston (B) is located in the upper piston (A), and the line for filling the upper piston (A) is located in the lower piston (B). The lower piston (B) receives an axial thrust from the end plug (D) and is pinned into the cell body (C) to prevent rotation about the cell axis. No pressure seal is necessary at the lower end of the cell body, since the region (E) is maintained at atmospheric pressure.

A disk of carbon-impregnated Bakelite (F) about $1/8$ -in. thick is pinned to the upper face of the lower piston. This disk provides a low-friction bearing surface for the rotating face of the upper piston and serves as a packing material to prevent leakage to the region (E) and to prevent communication between the diffusion chambers when these chambers are not in the diffusing position. Over a 16-hr. period there was no appreciable leakage between the two chambers with hydrogen at 10,000 lb./sq. in. abs. pressure in one chamber and a static vacuum of 0.1 mm. Hg in the other chamber.

The pressure on the Bakelite packing (F) is provided by a downward thrust from the upper piston. This thrust is generated by hydraulic action of oil within the annulus (G), the oil being confined by means of two O-ring seals (H). To eliminate the friction that would otherwise be generated at the O-ring-steel surface, bands of Teflon are inserted between the O rings and the body of the outer cell. The top of the upper piston is machined to receive a socket wrench and can be turned manually with ease, even when the oil pressure at (G) is 15,000 lb./sq. in. abs.

The small, unsupported area-seal plug (I) may be removed if desired to check

LER
homa

f the
predict
above

essure
ge of
ity of
gest a
ments.
which
high-
results
nts on
e-eth-
rogen-
d to-
veral
on co-
these

various
dicting
given
results
sum-

ics of
upman-
differ-
the dif-
ture of
on the
sen. If
act as
ne ex-

1960

alignment of the diffusion cavities. Under normal operating conditions the limits of rotation of piston (A) are fixed by a spring-loaded pin mounted externally on the cell body (C). This pin is not shown in Figure 1.

Figure 2 shows a flow diagram of the entire apparatus. Pressure was transmitted to the gas phase through floating pistons in two 450-ml. stainless steel pressure-transmitting cylinders. Pressure was generated within the oil phase by means of a conventional hydraulic pump and was measured by 0 to 3,750 and 0 to 15,000 lb./sq. in. Heise Bourdon-tube gauges connected directly to the oil line. These gauges were calibrated periodically in place against a dead-weight tester which was attached to the gas-phase side of the pressure transmitters.

The diffusion cell was mounted vertically in a cylindrical air bath. A slight positive temperature gradient (usually 0.1 to 0.2°F.) was maintained in the vertical direction as a safeguard against thermal disturbances which might give rise to natural convection. It was not found necessary to use a porous packing material in the cell to eliminate convection. The experiments reported by Boyd *et al* (17) in which the diffusion process was observed interferometrically indicate that with careful experimental procedures it is possible to eliminate initial convection even in a cell of moderately large cross-sectional area.

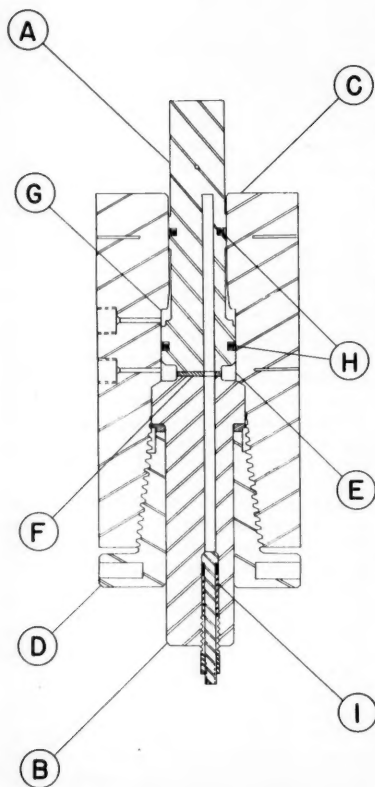


Fig. 1. Cross section of diffusion cell.

Experimental Procedure

Gases were introduced into the two chambers of the diffusion cell through separate manifolds. The more dense gas was placed in the lower chamber, since otherwise natural convective transfer, resulting from the gravitational instability, would completely overshadow that due to diffusion. After the gases had come to temperature equilibrium, the pressures on the two sides of the cell were balanced as nearly as possible by interconnecting the oil sides of the two pressure transmitters. The transmitters were then closed off completely, and the two gas chambers of the cell were directly interconnected through a long, auxiliary line of small diameter, permitting complete equalization of gas pressure. The length of line from the valve to each side of the cell was sufficiently great to prevent any diffusion or flow of gas through the line from one of the diffusion chambers into the other. It was found necessary to locate this valve at a point level with the center of the working section.

When the gas pressures were equalized, the upper piston was rotated 90 deg. to the diffusing position. It is estimated that the total time required to open the chambers to one another did not exceed 1 sec. Since the diffusion times generally exceeded 1,000 sec., this uncertainty in the starting time is considered negligible. The diffusion coefficient is known to depend at least weakly upon concentration. To achieve reproducibility all run times were chosen so that the diffusion process would proceed approximately half way to equilibrium.

Following the diffusion process, the diffusion chambers were again separated by rotation of the upper piston, and samples from each half of the cell were obtained by expansion of the gas into either 500- or 3,000-ml. glass vessels which had been evacuated to a pressure of less than 0.1 mm. Hg. Gas analyses were adjusted slightly to account for the fact that some of the gas, differing from the average sample composition, still remained in the cell and in the connecting lines.

Gas analyses were made on a mass spectrometer with an error of as much as $\pm 0.2\%$ by composition, resulting in an uncertainty of approximately $\pm 2\%$ in the calculated diffusion coefficients. The length of the diffusion path was known to within several thousandths of an inch over a total length of approximately 8 in. The area of the diffusion cavity did not vary more than $\pm 0.5\%$. Pressures were measured on Heise Bourdon-tube gauges calibrated throughout their entire ranges. Accuracy is estimated to be ± 5 lb./sq. in. over the range of conditions investigated. For cell-temperature measurements, thermocouples were calibrated in place against a conventional, strain-free platinum resistance thermometer. Temperatures at the point of measurement were known to about $\pm 0.02^\circ\text{F}$; the temperature difference between successive runs did not exceed 0.05°F .

During the process of initiating a diffusion run some pressure mixing of the gases must occur, first because of a shearing action which takes place as the open end

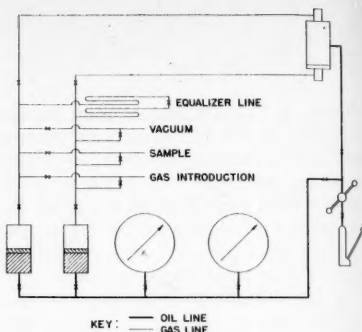


Fig. 2. Flow diagram of diffusion apparatus.

of one gas chamber passes over the open end of the other and second because of inertial forces which act to maintain the motion of the gas in the rotating chamber after the motion of the cell has ceased. Several experiments were made at a pressure of about 220 lb./sq. in. abs. to determine the magnitude of the effect of initial convection. This was done by comparing coefficients calculated for runs of different time duration.

Diffusion coefficients were measured at 3 temperatures at pressures up to about 10,000 lb./sq. in. abs. for the hydrogen-nitrogen and the methane-ethane systems. Measurements were made at one temperature at pressures up to about 2,500 lb./sq. in. abs. with the nitrogen-methane and nitrogen-ethane systems. Most of the methane-ethane measurements were made with one cell containing methane and the other containing a mixture having about 40 to 50 mole % ethane. Some of the low-pressure methane-ethane measurements were made with pure components in each of the two cells. This latter starting condition was used for all measurements with the other binary mixtures.

All gases used were commercial-grade cylinder gases, analyses of which were determined on a mass spectrometer.

Calculation of Observed Diffusion Coefficients

The definition of the diffusion coefficient is chosen as

$$\dot{N}_1 = -D_{12}A \frac{\partial n_1}{\partial z} \quad (7)$$

Application of this equation, together with a material balance on an element of volume, yields the following expression which must be satisfied throughout the system:

$$\frac{\partial}{\partial z} \left(D_{12} \frac{\partial n_1}{\partial z} \right) = \frac{\partial n_1}{\partial t} \quad (8)$$

The boundary conditions for the procedure used are equivalent to

$$\begin{aligned} \frac{\partial n_1}{\partial z} &= 0 & z &= \pm L, t > 0 \\ n_1 &= n_{10} & 0 < z < L, t &= 0 \\ n_1 &= 0 & -L < z < 0, t &= 0 \end{aligned}$$

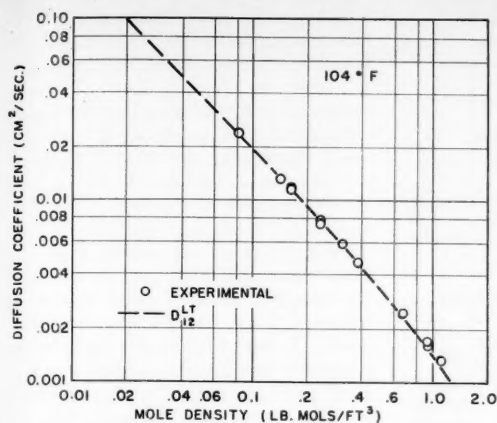


Fig. 3. Diffusion coefficients for the hydrogen-nitrogen system at 104°F.

If \mathcal{D}_{12} is assumed to be independent of concentration, Equation (8) may be integrated to yield

$$\frac{n_1}{n_{10}} = \frac{1}{2} + \frac{2}{\pi} \sum_{m=0}^{\infty} \frac{1}{(2m+1)} e^{-\frac{(2m+1)^2 \pi^2 D_{12} t}{4 L^2}} \sin \frac{(2m+1) \pi x}{2 L} \quad (9)$$

The average number density of component 1 in the upper chamber is then obtained by integrating Equation (9) over $0 \leq z \leq L$:

$$\frac{\overline{n_1}}{n_{10}} = \frac{1}{2} + \frac{4}{\pi^2} \sum_{m=0}^{\infty} \frac{1}{(2m+1)^2} e^{\frac{-(2m+1)^2 \pi^2 \mathcal{D}_{11} t}{4L^2}} \quad (10)$$

This relationship assumes that no volume change occurs on mixing. Although small volume change does occur in many situations, it is so slight that it may usually be ignored. Experimentally determined values of \bar{n}_1 , n_{10} , t , and L were used to establish average values of the diffusion coefficient according to Equation (10). Values of the series in Equation (10) have been tabulated as a function of the argument $(\mathcal{D}_{12}t/L^2)$ (18).

TABLE 1. EFFECT OF LENGTH OF TEST ON OBSERVED DIFFUSION COEFFICIENT

HYDROGEN-NITROGEN SYSTEM AT 104°F.

Pressure, lb./sq. in. abs.	Length of test, sec.	Diffusion coefficient, sq. cm./sec.	
		$\mathcal{D}_{12}^{\text{OBS.}}$	\mathcal{D}_{12}^{LT}
220	80	0.0552	
220	158	0.0559	
			0.0542
215	309	0.0560	
219	630	0.0567	

Calculation of Theoretical Diffusion Coefficients

Diffusion coefficients were predicted by the use of the Lennard-Jones model with Thorne's correction, Equations (2), (4), and (5). Predictions for the methane-ethane, nitrogen-methane, and nitrogen-ethane systems were also made by means of the reduced-state correlation of Slattery and Bird (13).

When converted to engineering units, Equations (2), (4), and (5) become

$$\mathcal{D}_{12}^L = \frac{0.01600}{p \sigma_{12}^2 \Omega^{(1,1)\bullet}} \quad 1/2$$

$$\left\{ \frac{T^0 (M_1 + M_2)}{2 M_1 M_2} \right\} \quad (11)$$

$$\chi_{12} = 1 + 2.3557 \times 10^{20} \frac{p}{Z_{12} T} \left[x_1 \sigma_1^3 \left(8 - \frac{3\sigma_1}{\sigma_{12}} \right) + x_2 \sigma_2^3 \left(8 - \frac{3\sigma_2}{\sigma_{12}} \right) \right] \quad (12)$$

$$\mathcal{D}_{12}^{LT} = \frac{(\mathcal{D}_{12}^L)_{\mathcal{Q}_0}}{\chi_{12}} \cdot \left(\frac{Z_{12}}{p} \right) p_0 \quad (13)$$

with p in pounds per square inch absolute, T in degrees Rankine, and σ_{12} in centimeters.

TABLE 2. SMOOTHED VALUES OF DIFFUSION COEFFICIENTS IN THE
HYDROGEN-NITROGEN SYSTEM (SQ. CM./SEC.)

lb./sq. in. abs.	lb.-mole/ cu. ft.	104°F. $D_{10}^{OBS.}$	D_{10}^{LT}	lb.-mole/ cu. ft.	139°F. $D_{10}^{OBS.}$	D_{10}^{LT}	lb.-mole/ cu. ft.	171°F. $D_{10}^{OBS.}$	D_{10}^{LT}
1000	.1606	.0115	.0116	.1512	.0125	.0130	.1436	.0135	.0141
2500	.3796	.00462	.00448	.3543	.00498	.00504	.3393	.00540	.00555
5000	.6810	.00240	.00223	.6474	.00251	.00251	.6132	.00283	.00277
7500	.9176	.00166	.00153	.8746	.00176	.00170	.8362	.00194	.00188
10000	1.1097	.00132	.00119	1.0609	.00140	.00132	1.0199	.00154	.00144
Average absolute error			5.73%			3.48%			4.12%

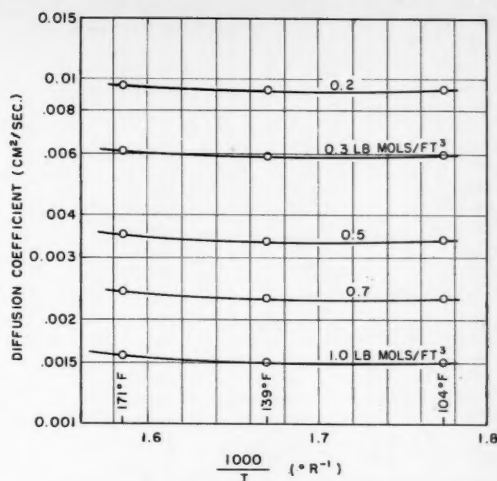


Fig. 4. Smoothed values of the diffusion coefficient for the hydrogen-nitrogen system.

Values of the collision diameters and force constants were taken from the tabulation of Bird, Curtiss, and Hirschfelder (12) as follows:

	σ , cm	ϵ/κ , °K.
H ₂	2.968	33.3
N ₂	3.681	91.5
C ₁	3.882	137
C ₂	4.418	230

Tables of $\Omega^{(1,1)*}$ vs. T^* given in the same reference were also used.

Compressibility data were taken from references 19 to 22. Data available for the methane-ethane system to only 3,000 lb./sq. in. abs. were extrapolated to 10,000 lb./sq. in. abs. through the use of a reduced-state correlation for the compressibility of natural gas (23). At 3,000 lb./sq. in. abs. this correlation agreed with the Sage-Lacey (20) experimental data to within better than 0.5%.

In all cases the diffusion coefficients were predicted for a mixture having a composition equal to the average composition in the test cell.

RESULTS AND DISCUSSION

Effect of Length of Test on Results

Results of four different diffusion experiments with the hydrogen-nitrogen system at 220 lb./sq. in. abs. and

TABLE 3. SMOOTHED VALUES OF DIFFUSION COEFFICIENTS IN THE METHANE-ETHANE SYSTEM

		(SQ. CM./SEC.) (80% methane) 104°F.		
lb./sq. in. abs.	lb.-mole/ cu. ft.	$D_{12}^{OBS.}$	D_{12}^{LT}	D_{12}^S
1000	.1945	.00210	.00164	.00179
2000	.4469	.00084	.000605	.000848
4000	.7855	.00043	.000286	.000431
8000	1.0465	.00030	.000190	—
10000	1.1172	.00027	.000173	—
Average absolute error			31.2%	5.3%

		140°F.			171°F.		
lb./sq. in. abs.	lb.-mole/ cu. ft.	$D_{12}^{OBS.}$	D_{12}^{LT}	lb.-mole/ cu. ft.	$D_{12}^{OBS.}$	D_{12}^{LT}	D_{12}^S
1000	.1764	.00233	.00193	.1630	.00249	.00221	
2000	.3895	.00099	.000757	.3499	.00113	.000904	
4000	.7121	.00050	.000345	.6569	.00058	.000403	
8000	.9931	.00034	.000216	.9482	.00039	.000241	
10000	1.0667	.00031	.000194	1.0252	.00036	.000216	
Average absolute error			29.1%			28.0%	

104°F. are shown in Table 1.* The time of duration of the tests ranged from 80 to 630 sec. The calculated diffusion coefficients are seen to vary by only about 3%, the largest value of the coefficients being calculated for the longest runs. If initial convection were present to any appreciable extent, apparent diffusion coefficients would be largest for the shortest runs. This is due to the fact that the total transfer would greatly exceed that attributable to diffusion. Furthermore the relative independence of the results on the length of the test suggests that gross convection is not appreciable. Table 1

also includes the value of the diffusion coefficient calculated from Equation (13). The calculated result is 2 to 4% less than the experimental value; however the coefficient calculated from Equation (13) at atmospheric pressure and 32°F. is also 2½% less than the experimental value reported for those conditions (24). Therefore on the basis of the information in Table 1 it is concluded that the apparatus and experimental technique are suitable for the determination of average diffusion coefficients in compressed binary gaseous mixtures which do not undergo large changes in volume on mixing.

Hydrogen-Nitrogen Diffusion Coefficients

Experiments were made at pressures up to 10,000 lb./sq. in. abs. for three

temperatures: 104°, 139°, and 171°F. Diffusion coefficients determined at 104°F. are shown plotted as a function of density in Figure 3. Data of similar quality were obtained at the two higher temperatures. The repeated measurements shown for the 104°F. isotherm indicate the degree to which the data for this system are reproducible. The maximum variation in coefficients from reproduced tests was ±2.5% from the mean value at 1500 lb./sq. in. abs. and 104°F. The dashed curve shown in Figure 3 was calculated from Equations (11) and (13). It is seen that the predicted data diverge from the experimental data beyond densities of about 0.2 lb.-mole/cu. ft. The predicted coefficients are low, indicating that Thorne's method results in an overcorrection. Without the dense-gas correction the theory predicts a simple inverse relationship between density and diffusivity.

Smoothed values of the observed coefficients at 104°, 139°, and 171°F. are compared in Table 2 with values calculated on the basis of the Lennard-Jones model with Thorne's correction. At equal values of density the error between observed and predicted coefficients is about the same at each of the three temperatures investigated. At a pressure of 10,000 lb./sq. in. abs. the error is -9.85% at 104°F., -5.72% at 139°F., and -6.49% at 171°F. It was not possible to obtain coefficients for the hydrogen-nitrogen system from the Slattery-Bird correlation because the reduced temperature is outside the range of the correlation chart.

Smoothed values of the observed data are plotted vs. 1/T in Figure 4 with density as a parameter. The nearly linear relationship shown between $\log D_{12}$ and 1/T indicates agreement with the form of Equation (6). This

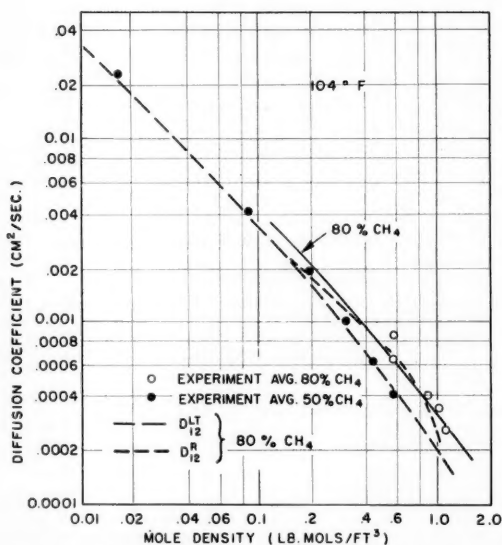


Fig. 5. Diffusion coefficients for the methane-ethane system at 104°F.

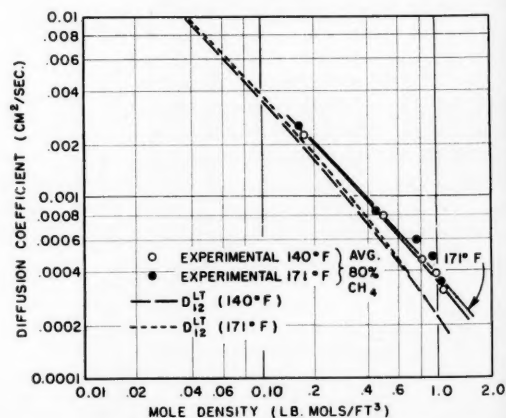


Fig. 6. Diffusion coefficients for the methane-ethane system at 140° and 171°F.

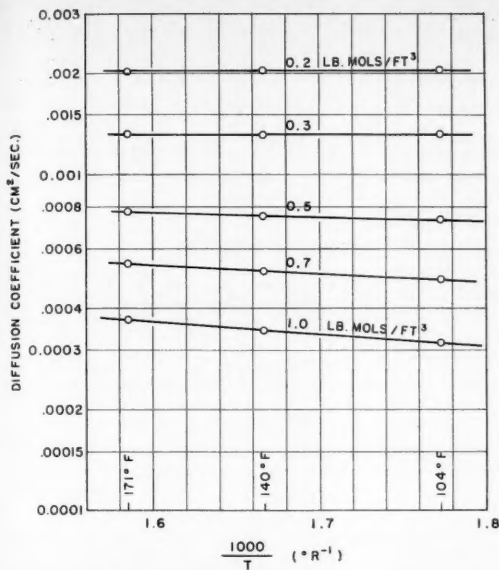


Fig. 7. Smoothed values of the diffusion coefficient for the methane-ethane system.

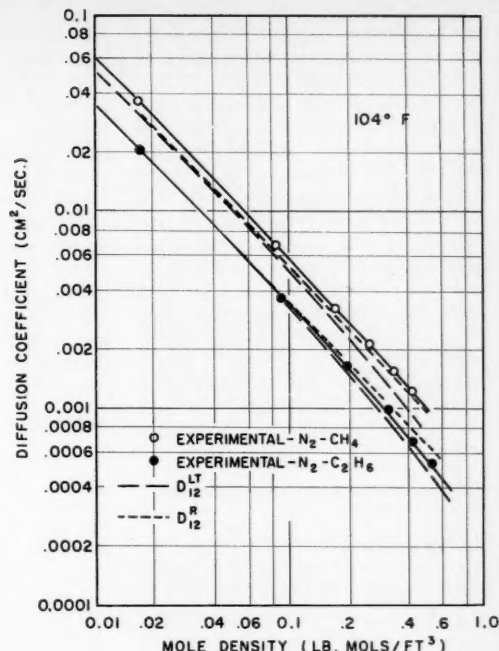


Fig. 8. Diffusion coefficients for the nitrogen-methane and nitrogen-ethane systems at 104°F.

further substantiates the conclusion that the actual temperature dependence of diffusion in dense gases is similar to that of liquids (4).

Methane-Ethane Diffusion Coefficients

Measurements were made with the methane-ethane systems at temperatures of 104, 140, and 171°F. and pressures to 10,000 lb./sq. in. abs. Experimental diffusion coefficients are shown plotted as a function of density at 104°F. in Figure 5 and at 140 and 171°F. in Figure 6. Data calculated with Equations (11) and (13) and those obtained from the Slattery-Bird reduced state correlation are also shown in Figure 5. The smoothed experimental and calculated and correlated diffusion coefficients are compared at 104°F. and various densities in Table 3.

From a comparison between Figures 3 and 5 it is seen that there is considerably more scatter in the experimental data for the methane-ethane system than for the hydrogen-nitrogen system. A plausible explanation for this difference might be found in the nonideal mixing in the methane-ethane system. Compressibility data indicate a 7.5% decrease in pressure when equal volumes of methane and ethane are mixed at 100°F. and 3,000 lb./sq. in. abs. The same experiment with hydrogen and nitrogen would show a 1.2% increase in pressure on mixing. The relatively large pressure defect in the methane-ethane system could give rise to a nonreproducible mass flux in the test cell which would have a pronounced effect on the precision and accuracy of observed diffusion coefficients.

The data points shown in Figure 5 as filled circles were determined from experiments in which each half of the cell initially contained a pure gas. The open circles pertain to experiments in which the upper half of the cell initially contained pure methane, and the lower half contained a mixture of methane and ethane such that the total cell content averaged about 80% methane. No effect of concentration is apparent in the data; this is surprising in view of the fact that the self-diffusion coefficient in methane is about five times as great as that in ethane.

Equation (13) does not predict a large effect of concentration on diffusion coefficients in binary systems, and this is apparently consistent with the experimental data. Thorne's dense-gas correction however does reflect a small effect of concentration through the weighting of terms in Equation (12) and through the mixture compressibility factor. The dense-gas correction used for D^{12}_{LT} in Figure 5 was calculated for a mixture containing 80 mole % methane.

In spite of the large divergence be-

tween experimental and calculated coefficients it is significant that both show about the same change in slope in the high-density region in Figure 5. This suggests that the dense-gas correction for density is satisfactory. It is surprising that this should be the case for a nonspherical molecule such as ethane in view of the fact that the dense-gas theory was derived for spherically symmetrical molecules.

Coefficients obtained from the reduced state correlation of Slattery and Bird fit the experimental data better than do the data calculated from kinetic theory. The Slattery-Bird correlation is based on extrapolated data beyond $p_r = 4.0$. This probably accounts for the anomalous shape of the curve of D^{12}_{12} in the high-density region. Over the range $0.3 < p_r < 4.0$ and $T_r = 1.262$ the average deviation of correlated factors from observed ones is about 10%. The average deviation of the calculated factors over this same range of conditions is about 25%. On the basis of these data, then, it is recommended that the reduced state correlation of Slattery and Bird be used to

TABLE 4. SMOOTHED VALUES OF DIFFUSION COEFFICIENTS IN THE METHANE-NITROGEN AND ETHANE-NITROGEN SYSTEMS

		104°F.							
		Methane nitrogen		Ethane nitrogen					
lb./sq. in. abs.	lb.-mole/cu. ft.	D^{12}_{12}	D^{12}_{LT}	D^{12}_{12}	D^{12}_{LT}	lb.-mole/cu. ft.	D^{12}_{12}	D^{12}_{LT}	D^{12}_{12}
100	.0166	.0364	.0312	.0311	.0168	.0208	.0207	.0204	.0204
500	.0843	.00680	.00587	.00612	.0898	.00370	.00366	.00364	.00364
1000	.1710	.00327	.00274	.00299	.1951	.00166	.00156	.00156	.00156
1500	.2579	.00211	.00173	.00195	.3117	.000985	.000897	.000897	.000897
2000	.3429	.00155	.00124	.00145	.4278	.000669	.000607	.000607	.000607
2500	.4256	.00122	.00095	.00116	.5279	.000522	.000463	.000463	.000463
Average absolute error		17.4%		8.7%		6.9%		9.1%	

predict diffusion coefficients in dense gases, at p_r less than 4.0, containing polyatomic asymmetric molecules.

Smoothed diffusion coefficients from the three methane-ethane isotherms are plotted vs. $1/T$ with density as a parameter in Figure 7. This graph confirms the observation from the hydrogen-nitrogen data that the dependence of diffusion on temperature in dense gases is of an exponential form. Since this relation was found for both a near-ideal system (hydrogen-nitrogen) and a relatively nonideal system (methane-ethane), it is thought safe to conclude that the diffusion coefficient in compressed binary gas mixtures varies with temperature approximately as $e^{-b_2/T}$.

Nitrogen-Methane and Nitrogen-Ethane Diffusion Coefficients

Diffusion coefficients determined for the nitrogen-methane and nitrogen-ethane systems at 104°F. and to a pressure of 2,500 lb./sq. in. abs. are plotted as a function of density in Figure 8. Curves of theoretical coefficients calculated from Equations (11) and (13) and determined from the Slattery-Bird correlation are also shown. Numerical values of the data are compared in Table 4. In these systems too it is seen that the coefficients calculated from kinetic theory diverge below the experimental data in the high-density region. The calculated data provide a better fit for the nitrogen-ethane system than for the nitrogen-methane system. There is a constant percentage difference between the calculated and observed data in the methane-nitrogen system at low densities. This indicates that the value of $(D_{12}^L)_0$ from Equation (11) is in error.

Over the experimental pressure range coefficients from the reduced state correlation show an average deviation of 8.7% from the observed data in the nitrogen-methane system and 9.1% from observed data in the nitrogen-ethane system. It is clear in Figure 8 that the Slattery-Bird correlation gives better agreement with the experimental diffusion coefficients than do the data calculated from Equations (11) and (13). A similar observation was made from the methane-ethane data above. On the basis of these observations it is concluded that the Slattery-Bird reduced state correlation provides slightly better estimates of diffusion coefficients in dense-gas mixtures than do kinetic-theory calculations based on the Lennard-Jones model with Thorne's binary dense-gas correction.

CONCLUSIONS

1. Apparatus and experimental techniques have been developed which are

suitable for the determination of average diffusion coefficients in compressed binary gaseous mixtures which do not undergo large changes in volume on mixing.

2. The diffusion coefficient in compressed binary gas mixtures varies with temperature approximately as $e^{-b_2/T}$.

3. The Slattery-Bird reduced state correlation provides slightly better estimates of diffusion coefficients in dense-gas mixtures than do kinetic-theory calculations based on the Lennard-Jones model with Thorne's binary dense-gas correction.

NOTATION

A	= cross-section area of diffusion cell
b_1, b_2, b_a	= arbitrary constants
D_{12}	= diffusion coefficient in binary gas mixture of components 1 and 2
D_L	= diffusion coefficient in the liquid state at temperature T
E	= activation energy
L	= half length of diffusion cell
M	= molecular weight
N	= Avogadro's number
N_1	= number flux of component 1
n	= number of molecules per unit volume = Np/ZRT
p	= pressure, lb./sq. in. abs.
R	= gas law constant
T	= absolute temperature, °R.
t	= time variable
V	= volume per mole of gas at p and T
x	= mole fraction
z	= position along axis of diffusion cell
Z	= compressibility factor = pV/RT

Greek Letters

ϵ	= force parameter for Lennard-Jones potential
κ	= Boltzmann constant
σ	= molecular collision parameter
χ_{12}	= Thorne's binary dense-gas correction factor
$\Omega^{(1,2)*}$	= collision integral given as a function of $\kappa T/\epsilon$

Superscripts

S	= calculated from the solid elastic sphere model
L	= calculated from the Lennard-Jones model
LT	= calculated from the Lennard-Jones model with Thorne's dense-gas correction
R	= obtained from Slattery-Bird reduced state correlation
—	= average value

Subscripts

1 or 2	= component 1 or 2
--------	--------------------

12	= mixture of components 1 and 2
0	= value at time = zero; value at $p_0 = 14.696$ lb./sq. in. abs.
r	= value of property divided by its critical or pseudocritical value

LITERATURE CITED

1. Chapman, S., and T. G. Cowling, "Mathematical Theory of Non-Uniform Gases," Cambridge Univ. Press, New York (1951).
2. Timmerhaus, K. D., and H. G. Drickamer, *J. Chem. Phys.*, **19**, 1242 (1951).
3. *Ibid.*, **20**, 981 (1952).
4. Robb, W. L., and H. G. Drickamer, *ibid.*, **19**, 1504 (1951).
5. O'Hern, H. A., and J. J. Martin, *Ind. Eng. Chem.*, **47**, 2081 (1955).
6. Jeffries, Q. R., and H. G. Drickamer, *J. Chem. Phys.*, **21**, 1358 (1953).
7. *Ibid.*, **22**, 436 (1954).
8. Chou, Chan-Hui, and J. J. Martin, *Ind. Eng. Chem.*, **49**, 758 (1957).
9. Wilke, C. R., *Chem. Eng. Progr.*, **46**, 95 (1950).
10. Hirschfelder, J. O., R. B. Bird, and E. L. Spotz, *J. Chem. Phys.*, **16**, 968 (1948).
11. Bird, R. B., "Advances in Chemical Engineering," Vol. 1, p. 182, Academic Press, New York (1956).
12. —, J. O. Hirschfelder, and C. F. Curtiss, *Trans. Am. Soc. Mech. Engrs.*, **76**, 1011 (1954).
13. Slattery, J. C., and R. B. Bird, *A.I.Ch.E. Journal*, **4**, 137 (1958).
14. Enskog, D., in "Mathematical Theory of Non-Uniform Gases," Cambridge Univ. Press, New York (1951).
15. Glasstone, Samuel, K. J. Laidler, and Henry Eyring, "The Theory of Rate Processes," McGraw-Hill, New York (1941).
16. Loschmidt, J., *Wien. Ber.*, **61**, 367 (1870).
17. Boyd, C. A., N. Stein, V. Steingrimmson, and W. F. Rumpel, *J. Chem. Phys.*, **19**, 548 (1951).
18. McKay, A. T., *Proc. Phys. Soc.*, **42**, 547 (1930).
19. Wiebe, R., and V. L. Gaddy, *J. Am. Chem. Soc.*, **60**, 2300 (1938).
20. Sage, B. H., and W. N. Lacey, "Thermodynamic Properties of the Lighter Paraffin Hydrocarbons and Nitrogen," Am. Petrol. Inst. Monograph, New York (1950).
21. Keyes, F. G., and H. G. Burks, *J. Am. Chem. Soc.*, **50**, 1100 (1928).
22. Sage, B. H., and W. N. Lacey, "Some Properties of the Lighter Hydrocarbons, Hydrogen Sulfide, and Carbon Dioxide," Am. Petrol. Inst. Monograph, New York (1955).
23. Standing, M. B., and D. L. Katz, *Trans. Am. Inst. Mining Engrs.*, **146**, 140 (1942).
24. "International Critical Tables," **5**, McGraw-Hill, New York (1929).

Manuscript received June 8, 1959; revision received August 12, 1959; paper accepted August 13, 1959. Paper presented at A.I.Ch.E. Kansas City meeting.

Velocity of Large Drops and Bubbles in Media of Infinite or Restricted Extent

TIBOR Z. HARMATHY

National Research Council of Canada, Ottawa, Canada

A new theory gives a simple method of calculating the terminal velocity of fluid particles moving in media of either infinite or restricted extent.

Empirical and semiempirical formulas [Equations (27) and (30)] and a graph (Figure 6) over the interval $0 \leq d/D \leq 1.3$ are shown to yield satisfactory results for gas or liquid particles moving in liquid media. In the case of liquid drops falling through gaseous media they give only a rough approximation.

Graphs showing the variation of the drag coefficient (Figure 1) and the shape (Figure 2) of fluid particles with the Eötvös number are given. A semiempirical equation for the terminal velocity of solid spheres in restricted media has also been developed [Equation (24)].

The necessity of studying the motion of large drops and bubbles in media of restricted extent has arisen in connection with an investigation into the throughput characteristics of packed liquid-extraction towers. Since the subject has been inspired by a special problem of liquid extraction, the liquid-liquid systems receive principal attention; however efforts have been made to develop a generalized theory of the behavior of drops and bubbles.

This paper deals only with drops and bubbles for which the Reynolds number is larger than 500. In practice these large drops and bubbles are by far the most interesting. The region of $N_{Re} > 500$ is characterized as the one in which the viscous effects are negligible. The shape of the fluid particles may be oblate ellipsoidal (regular or irregular), spherical cap, or cylindrical.

In the past decade several papers have been concerned with the motion of ellipsoidal drops in liquid media of practically infinite extent (12, 23, 25, 26, 27, 31, 50). A few other papers have dealt with the movement of drops in liquid media of more definitely restricted extent (46, 47, 48). To the writer's knowledge no attention has so far been paid to the motion of cylindrical drops.

The problem of velocity and behavior of liquid drops in gas has also attracted considerable interest (2, 15, 24, 29). These papers deal only with droplets moving or suspended in media of practically unlimited extent.

The most elaborate part of the hydrodynamics of fluid particles is that concerned with the motion of gas bubbles in liquids. An excellent review of the papers published before 1953 on this subject can be found in a report by Haberman and Morton (16). Since that time the motion of ellipsoidal (36, 42, 45), spherical cap-shaped (36,

45), and cylindrical (28) bubbles was further studied, and also the effect of wall proximity on the rise of bubbles (49).

From these papers and other sources it is learned that the small fluid particles are of spherical or slightly ellipsoidal shape and move in rectilinear paths. The larger ones assume a more definite ellipsoidal shape, becoming more and more distorted and less definite with increasing size, and move along zigzag or helical paths, the amplitude of which decreases with increasing deformation. The quite large fluid particles have a spherical cap shape, and their motion is practically rectilinear. The proximity of the channel wall reduces the velocity to an extent which is primarily a function of the size of the particle and of the channel (which is generally a circular tube). If the fluid particle is larger than the tube, it assumes a cylindrical shape, and its velocity depends mainly on the tube diameter.

Observations show that the oscillating motion of fluid particles moving in a relatively unrestricted medium appears around $N_{Re} = 500$; thus the appearance of the zigzagging or spiraling can be regarded as the beginning of the region of turbulent flow conditions, in which the author's correlations are applicable.

VELOCITY IN INFINITE MEDIA

It is a well-known fact that under turbulent flow conditions the drag coefficient of particles of identical shape is over a wide range practically independent of the Reynolds number. In the case of fluid particles this fact is however not immediately obvious. Several reports have been published (16, 23, 25, 27, 31, 36, 40) which seem to show that the drag coefficient is strongly dependent upon the Reynolds number, but this apparent con-

tradiction vanishes if one considers that for fluid particles the variation of the Reynolds number is generally accompanied by variation of the particle shape and that the drag coefficient does depend on the shape of the object. It is therefore the shape of the fluid particle, not the Reynolds number, that is responsible for the variation of the drag coefficient in the region of turbulent flow.

The drag coefficient is generally defined by

$$C = \frac{F}{\frac{1}{2} \rho_c u^2 A} \quad (1)$$

However when one is dealing with the motion of fluid particles, it is more convenient to regard the equivalent diameter of the particle as the characteristic length and to define a new drag coefficient with the following equation:

$$C^* = \frac{F}{\frac{1}{2} \rho_c u^2 \frac{d^2 \pi}{4}} \quad (2)$$

If a β factor defined as

$$\beta = \sqrt{\frac{A}{\frac{d^2 \pi}{4}}} \quad (3)$$

is introduced, then the correlation between the two kinds of drag coefficients becomes

$$C^* = \beta^2 C \quad (4)$$

From geometric correlations the following expressions can be obtained: for oblate spheroids

$$\beta = \sqrt{\frac{a}{b}} \quad (5)$$

for spherical caps

$$\beta = \frac{\frac{a}{b}}{\sqrt{1 + \frac{3}{4} \left(\frac{a}{b}\right)^2}} \quad (6)$$

If the particle is moving with its

terminal velocity, $F = (d^3\pi/6)\Delta\rho g$. A substitution into Equation (2) thus gives an expression for the terminal velocity:

$$u = K\sqrt{\frac{g\Delta\rho d}{\rho_o}} \quad (7)$$

where

$$K = \sqrt{\frac{4}{3C^*}} \quad (8)$$

or

$$K = \frac{1}{\beta} \sqrt{\frac{4}{3C}} \quad (9)$$

For spheres $\beta = 1$, and in infinite media $C_{\infty} = 0.44$ and $K_{\infty} = 1.74$, as is well known from various handbooks.

For the time being only the terminal velocity of the particles in infinite media will be considered. From Equations (7), (8), and (9) the following correlations can be obtained:

$$\frac{u_{\infty}}{u_{xx}} = \sqrt{\frac{C_{xx}}{C^*}} \quad (10)$$

or

$$\frac{u_{\infty}}{u_{xx}} = \frac{1}{\beta} \sqrt{\frac{C_{xx}}{C}} \quad (11)$$

Since, as mentioned earlier, in the region of turbulent flow the drag coefficient depends only on the particle shape, and since β is always a factor characteristic of the shape, Equation (11) is an expression of the fact that the terminal velocity of a fluid particle can be obtained from that of the equivalent sphere simply by applying a factor which is a function solely of the particle shape; that is,

$$\frac{u_{\infty}}{u_{xx}} = \phi_1(\text{shape}) \quad (12)$$

[The existence of this correlation was touched upon by the author in a previous paper (20).]

In Appendix 1 it is proved, on the other hand, that the shape of a fluid particle depends only on a dimensionless group, called hereafter *Eötvös number*. Thus combining Equation (12) and Equation (41) of Appendix 1 gives

$$\frac{u_{\infty}}{u_{xx}} = \phi_2(N_{Eo}) \quad (13)$$

and from Equations (10) and (13)

$$\frac{C^*}{C_{xx}} = \left[\frac{1}{\phi_2(N_{Eo})} \right]^2 = \phi_3(N_{Eo}) \quad (14)$$

It should be noticed however that the derivation of Equation (41) of Appendix 1 has been based on a fairly simplified model. Thus (1) the effect of finite viscosity of the particles has been neglected. This may affect the result both in case of small Eötvös numbers, because the circulation inside

the particles is known to depend on the viscosity of particle (5, 17, 41) and because the circulation has been found to reduce the viscous shear, which in this region contributes in a larger percentage to the total drag, and in case of large Eötvös numbers, because the increasing particle viscosity exerts an increasing damping on the shape oscillation and in this way reduces the form drag; and (2) the zig-zagging or spiraling of the particles which results in an apparent increase of the drag coefficient has also been disregarded. It will be seen later that these side motions of the particles are caused by a wake reaction and thus are dependent on the velocity and other factors influencing the shape of the wake.

Neglecting these factors has undoubtedly been responsible for the fact that, as will be seen, a u_{∞}/u_{xx} vs. N_{Eo} correlation established for liquid or gas particles moving in liquid media is only a rough approximation if applied to liquid droplets falling in gaseous media.

An experimental proof of the validity of Equation (14) for liquid-liquid systems was given by Licht and Narasimhamurthy (31), who found that for lower Eötvös numbers the C^*/C_{xx} vs. N_{Eo} correlation can be approximated by a straight line. For gas-liquid systems Haberman and Morton (16) yielded an indirect proof by plotting C^* against the Weber number and showing that the curves representing widely different systems can thus be brought close together. In Appendix 1 it has been pointed out that in the turbulent region the Eötvös and the Weber numbers are equivalent as variables.

A fairly rapid variation of the C^*/C_{xx} ratio is expected in the region of ellipsoidal particle shapes where, as observations show, the proportions of

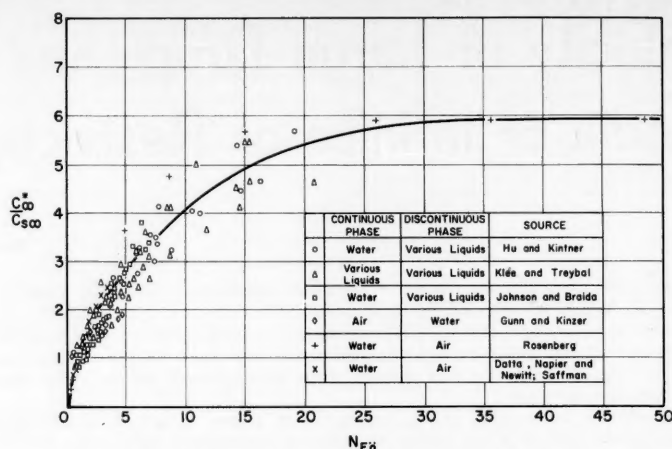


Fig. 1. Variation of drag coefficient with Eötvös number.

the particles vary markedly with size, that is with the Eötvös number. On the other hand, the dimension ratios of a spherical cap-shaped particle are practically independent of size (9, 40); therefore for large Eötvös numbers the C^*/C_{xx} ratio is expected to become constant.

Experimental data of several authors have been used to plot the C^*/C_{xx} ratio against the Eötvös number in Figure 1. Although the spread of the points is considerable, the expected tendency for variation of the C^*/C_{xx} ratio with the Eötvös number is obvious. C^*/C_{xx} values less than unity at very low Eötvös numbers indicate the effect of internal circulation. At higher Eötvös numbers the points for air bubbles are somewhat higher than those for liquid drops, probably because of the lack of damping effect of particle viscosity on shape oscillation.

Hu and Kintner (23) derived a correlation which, according to this terminology, states that liquid particles moving in liquid or gaseous media are not stable and will split up if $N_{Eo} > 14.2$. Based on Keith and Hixson's (26) estimations for liquid-liquid systems the disintegration takes place in the range $7 < N_{Eo} < 13$. For liquid particles falling through air Merrington and Richardson (33) have found the range of splitting up to be $8 < N_{Eo} < 25$. So far there seems to be fair agreement between the observations. The agreement suddenly vanishes however if one completes this brief survey of fluid particle stability with the case of gas bubbles rising in liquids. On the basis of the experimental results of Rosenberg (40) and Haberman and Morton (16) one may even assume that bubbles with Eötvös numbers as high as 450 can still be regarded as stable. Apparently the Eötvös number alone does not provide a satisfactory stability criterion. Nevertheless it seems proba-

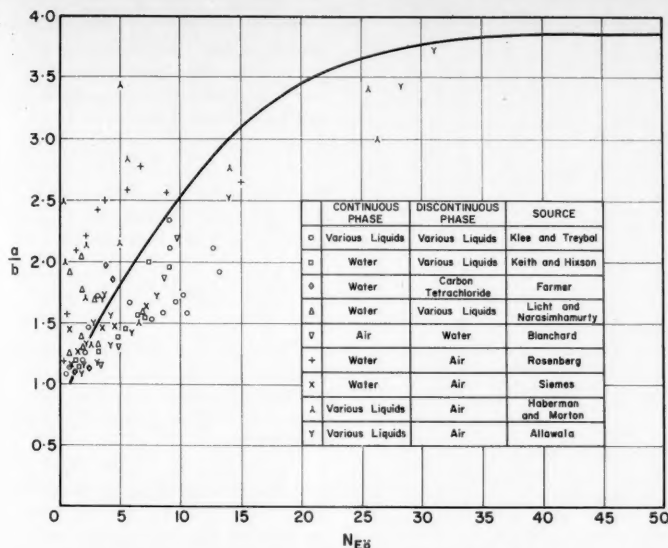


Fig. 2. Variation of particle shape with Eötvös number.

ble that the liquid drops never reach the region of spherical cap shape, which begins approximately at $N_{Eo} = 40$. In fact no point representing liquid particles can be found in Figure 1 above $N_{Eo} = 21$.

The spread of the points in Figure 1 cannot be attributed simply to the disregarded factors. There are strong signs that in some instances erroneous interfacial-tension determinations account for the discrepancies. In cases where the spread of points in noticeable, like the case seen in Figure 1, the best correlation of the points is the simplest one. In the range $N_{Eo} < 13$, which roughly corresponds to the region of moderately distorted ellipsoidal shapes, the approximation of

$$\frac{C^*}{C_{\infty}} = 1.29 N_{Eo}^{-1/2} \quad (N_{Eo} < 13) \quad (15)$$

offers certain practical advantages. By combining it with Equation (10) one obtains

$$\frac{u_w}{u_{\infty}} = \frac{0.88}{N_{Eo}^{1/4}} \quad (16)$$

which, after substitution for u_{∞} from Equation (7) with $K_{\infty} = 1.74$, becomes

$$u_w = 1.53 \left(\frac{g \Delta \rho \sigma}{\rho_o^2} \right)^{1/4} \quad (17)$$

It is seen that if one takes the C^*/C_{∞} ratio proportional to the square root of the Eötvös number, the particle diameter is eliminated from the expression of terminal velocity.

The fact that under turbulent flow conditions the terminal velocity of liquid particles moving in liquid media is practically independent of the particle size is well known from various publications (23, 26, 27). The velocity

of gaseous particles rising in liquid media seems to be somewhat more dependent on the particle size; however Equation (17) still yields satisfactory predictions if not applied to very small ($N_{Eo} < 1$) bubbles. The failure of Equation (17) in the region of very low Eötvös numbers is obviously a result of disregarding the effect of particle viscosity on the terminal velocity.

In the case of liquid particles falling through gaseous media the accuracy of Equation (17) is generally very poor. The velocity increases with the particle size throughout the whole region of turbulent flow, and although Equation

(17) gives a fairly good prediction for the middle of the region, the deviation between the measured and calculated values may be as high as 25% toward the ends. This discrepancy is not surprising if one considers the markedly different characteristics of this system and the average of fifty times higher values of the terminal velocity.

It is interesting to note that Peebles and Garber (36) derived a correlation similar to Equation (17) for the spherical cap-shaped bubbles. It was undoubtedly a significant wall effect which caused them to reach that result. It will be pointed out later that for very large bubbles the terminal velocity depends on the tube diameter rather than on the bubble size, even if the d/D ratio is as low as 0.3.

From Equation (16) $u_w \rightarrow \infty$ if $N_{Eo} \rightarrow 0$; therefore it might be thought that the applicability of this equation should be limited toward low Eötvös numbers. With liquid-liquid systems such limitation is not necessary, since it is remembered that none of the given correlations can be used if $N_{Eo} < 500$, and in this way a lower limit is automatically imposed on the Eötvös numbers (approximately $N_{Eo} = 0.7$). In the case of gas bubbles however the use of Equations (16) and (17) is not recommended for Eötvös numbers lower than 1.0.

It has been mentioned that in the region of spherical cap-shaped particles ($N_{Eo} > 40$) the shape is independent of the particle size; therefore as expected, the C^*/C_{∞} ratio is a constant (see Figure 1.) On the basis of the measurements of Rosenberg (40) and

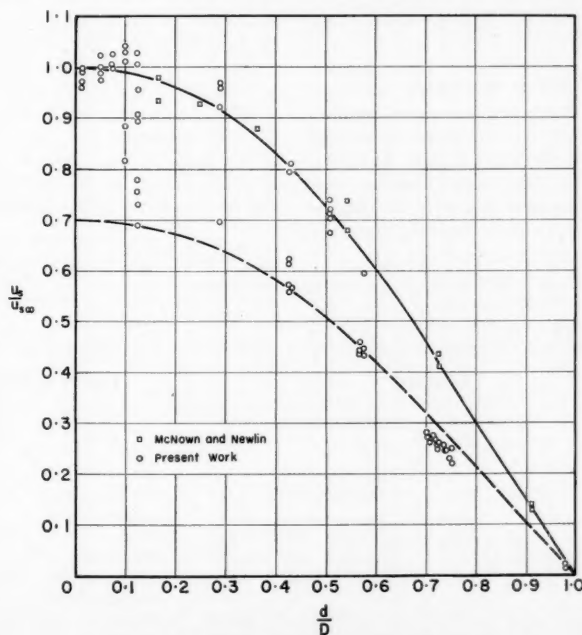


Fig. 3. Velocity of falling spheres in restricted media.

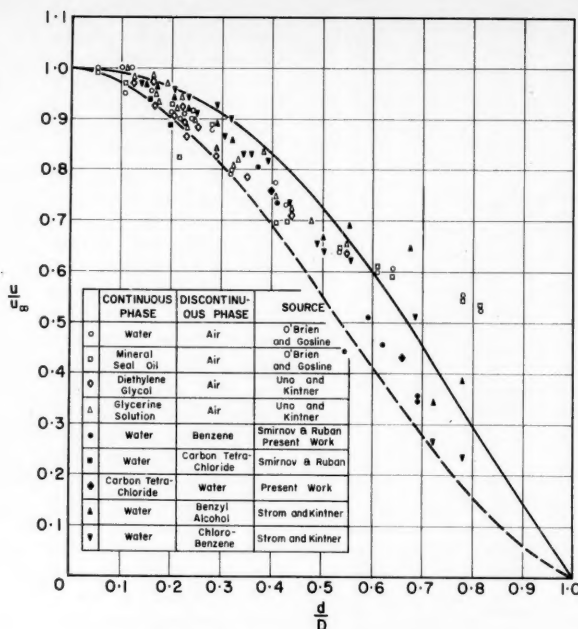


Fig. 4. Velocity of fluid particles in restricted media.

Haberman and Morton (16) the value of the constant is $2.6/0.44 = 5.91$, which is reached after a fairly long transitional region ($13 < N_{Re} < 40$) in which the variation of C_{∞}^*/C_{xx} is very slow.

Applying Equation (10) for the region of spherical cap-shaped particles, one gets

$$\frac{u_{\infty}}{u_{xx}} = 0.411 (N_{Re} > 40) \quad (18)$$

in agreement with the observations of several research workers (9, 16, 38, 40).

SHAPE OF FLUID PARTICLES

If one accepts the general practice of characterizing the shape of a fluid particle by the ratio of the horizontal diameter to the vertical length, then as an alternative form for Equation (41) of Appendix 1 one can write

$$\frac{a}{b} = \phi_1(N_{Re}) \quad (19)$$

However if one tries to use the data reported in the literature (1, 2, 12, 16, 26, 27, 31, 40, 45) to plot a/b against the Eötvös number, a mass of widely scattered points will result, as shown in Figure 2. This enormous spread is undoubtedly due to shape oscillation, which, as the photographs taken by Licht and Narasimhamurty (31) show, may cause the a/b ratio for a given particle size to vary in a range with an upper limit three times as large as the lower limit. Under such conditions a multitude of photographs are required to determine the true average shape.

There is however another way of finding the explicit form of Equation (19). The wind-tunnel measurements of Riabouchinsky (24, 39) show that in the fully turbulent range of flow the drag coefficient of an oblate spheroid can be expressed in the following form:

$$\frac{C_{Re}}{C_{xx}} = 1 + \left(1 - \frac{b}{a}\right) \left(\frac{C_{Re}}{C_{xx}} - 1\right) \quad (20)$$

Owing to the spiraling, zigzagging motion, shape oscillation, and deviations from the true spheroidal form, the drag coefficient of a fluid particle will be expressed as

$$C_{\infty} = \epsilon C_{Re} \quad (21)$$

By combining Equations (4), (20), and (21) and substituting $C_{xx} = 0.44$ and $C_{Re} = 1.10$, one obtains

$$\frac{C_{\infty}}{C_{xx}} = \epsilon \beta^2 \left(2.5 - 1.5 \frac{b}{a}\right) \quad (22)$$

Figure 2 is a graphical representation of this equation. It has been based on the C_{∞}^*/C_{xx} vs. N_{Re} correlation shown in Figure 1 and the following assumptions:

1. Up to $N_{Re} = 15$ the fluid particle is spheroidal [that is, β is substituted from Equation (5)] and ϵ is independent of N_{Re} and equals 1.15.
2. Above $N_{Re} = 40$ the particle is spherical cap shaped [that is, Equation (6) describes the correlation between β and a/b], and since the motion is practically rectilinear, $\epsilon = 1.0$.
3. In the range $15 < N_{Re} < 40$ the shape gradually changes from spheroid to spherical cap and ϵ from 1.15 to 1.0.

It is seen that for the spherical-cap region $a/b = 3.85$, in good agreement with Rosenberg's experimental value 4.02 (40).

EFFECT OF WALL PROXIMITY

Since in practice the extent of the continuous medium around the moving fluid particle is always more or less restricted, it is extremely important to know the effect of the wall proximity on the particle. In fact a new variable enters the problem of particle motion—the diameter (or equivalent diameter) of the container D . This will result in the appearance of a new dimensionless variable in Equation (13), and according to the basic theorem of the dimensional analysis this new variable is d/D . The more complete form of Equation (13) is therefore

$$\frac{u}{u_{xx}} = \phi \left(N_{Re}, \frac{d}{D} \right) \quad (23)$$

Since the particles for which $N_{Re} \rightarrow 0$ behave like solid spheres, it seemed reasonable to start the investigation by studying the effect of cylindrical wall on the motion of solid spheres.

Several publications deal with the velocity (or drag) of spheres moving (or suspended) in the axis of a cylindrical channel under turbulent flow conditions (10, 18, 34, 49). In practice however the spheres rarely move along the axis of the cylinder; therefore the author thought it necessary to carry out a few experiments with spheres falling freely in tubes filled with different liquids.

TABLE 1. DIAMETER AND DENSITY OF SPHERES AND LIQUID COLUMNS USED

Spheres								Liquid columns			
No.	Material	d , cm.	ρ_D , g./cc.	No.	Material	d , cm.	ρ_D , g./cc.	No.	Material	D , cm.	ρ_C , g./cc.
1	Plastic 1	1.571	1.049	8	Plastic 2	0.931	1.167	1	Methanol	2.184	0.789
2	Plastic 1	1.565	1.053	9	Plastic 2	0.934	1.170	2	Carbon tetra- chloride	2.202	1.590
3	Plastic 2	1.534	1.184	10	Plastic 2	0.929	1.172	3	Water	2.174	0.998
4	Plastic 2	1.249	1.171	11	Plastic 2	0.937	1.172	4	Methanol	1.264	0.789
5	Plastic 2	1.240	1.169	12	Glass	0.634	2.283	5	Carbon tetra- chloride	1.248	1.590
6	Plastic 2	1.234	1.176	13	Glass	0.158	2.283	6	Water	1.243	0.998
7	Plastic 2	0.935	1.162	14	Steel Alloy	0.635	7.948	7	Water	12.40	0.998

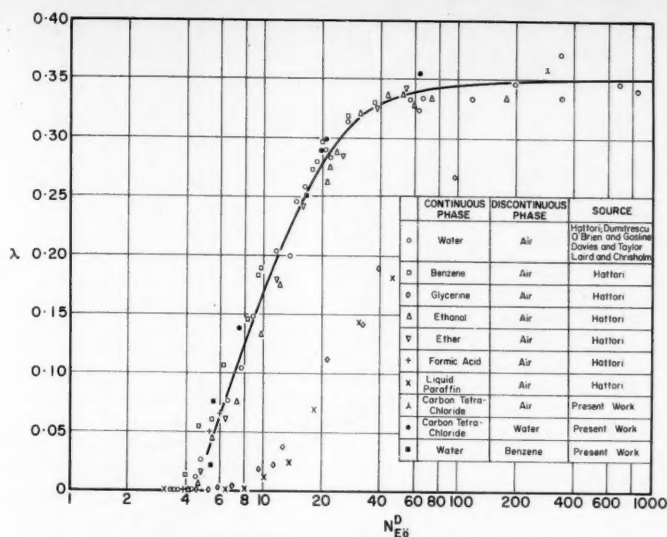


Fig. 5. Velocity coefficient of cylindrical particles.

Table 1 contains information about the diameter of spheres and tubes and the density of the spheres and liquids used in the experiments. In most cases the beads of a necklace of unknown plastic materials (denoted as plastic 1 and plastic 2) were used for spheres because of their convenient density and very good sphericity. The hole in them was partly filled with cement, accounting for the small spread in their density.

The time of fall of the spheres was measured on a 90- or 100-cm. distance with a stop watch. It was assumed that after 30 cm. of fall the spheres closely approached their terminal velocities. The measured velocities ranged from 0.94 cm./sec. to 83.4 cm./sec.

Points calculated from the experimental results of the author are plotted in Figure 3. A few other points, determined from the drag coefficient measurements of McNown and Newlin (34) for the range $7,000 < N_{Re} < 20,000$, are also shown. It is seen that part of the points, those representing the spheres falling in rectilinear or very

steep helical paths, closely follow a curve, the equation of which is

$$\frac{u_s}{u_{ss}} = \frac{1 - \left(\frac{d}{D}\right)^2}{\sqrt{1 + \left(\frac{d}{D}\right)^4}} \quad (24)$$

or for $\frac{d}{D} < 0.5$

$$\frac{u_s}{u_{ss}} \approx 1 - \left(\frac{d}{D}\right)^2 \left(\frac{d}{D} < 0.5\right) \quad (25)$$

Equation (24) was developed in a semiempirical way in Appendix 3*. Many other correlations were also examined, but none of them could follow the course of those points satisfactorily in the whole $0 < d/D < 1$ interval.

A considerable number of the points, representing the badly oscillating, zigzagging spheres or those not

* Appendix 3 has been deposited as document 6265 with the American Documentation Institute, Photoduplication Service, Library of Congress, Washington 25, D. C., and may be obtained for \$1.25 for photoprints or for 35-mm. microfilm.

TABLE 2. SYSTEMS USED FOR STUDYING WALL EFFECT AND CYLINDRICAL PARTICLE VELOCITY

No.	Continuous phase	Discontinuous phase	D , cm.	ρ_c , g./cc.	ρ_d , g./cc.	σ , dynes/cm.
1	Carbon tetrachloride	Water	2.202	1.590	0.998	45.0
2	Carbon tetrachloride	Water	2.184	1.590	0.998	45.0
3	Carbon tetrachloride	Water	1.264	1.590	0.998	45.0
4	Carbon tetrachloride	Water	1.248	1.590	0.998	45.0
5	Carbon tetrachloride	Water	0.765	1.590	0.998	45.0
6	Carbon tetrachloride	Air	2.202	1.590	0.001	26.3
7	Water	Benzene	2.184	0.998	0.877	35.0
8	Water	Benzene	1.264	0.998	0.877	35.0
9	Water	Benzene	1.248	0.998	0.877	35.0

oscillating but rolling down on the tube wall, are located along a curve passing about 30% lower (see the dotted curve of Figure 3) than the curve of Equation (24). At large d/D ratios the zigzagging spheres frequently knocked against the tube wall; probably this fact accounts for the additional velocity drop at large d/D values.

Some spheres started as zigzagging, but later their paths straightened out. Points pertaining to such cases lie between the above-mentioned two curves.

An investigation into the nature and causes of oscillation was beyond the scope of this work. However it did not require too much attention to realize that the strong zigzagging was caused by the reaction of the wake, disturbed by the proximity of wall, on the spheres. This reaction is obviously less for fast-moving spheres; therefore the intensity of oscillation is a function of the absolute velocity, as well as the d/D ratio.

No general rule on the behavior of spheres in the proximity of the wall can be given. Sometimes even the deliberately eccentrically released balls seemed to steer themselves after a few oscillations to the axis of the tube. In other instances the almost concentrically dropped spheres turned to the wall and rolled down on it throughout.

Theoretical considerations, empirical formulas (18), and observations (48, 49) equally support the view that in the region concerned the terminal velocity reduction caused by the wall effect is practically independent of the shape of the particle if the a/D ratio is used instead of d/D . If one combines this fact with the observation that increasing d/D ratio increases the deformation of fluid particles, as well as the tendency of zigzagging, and thus decreases the u/u_s ratio beyond that predicted by Equation (24), then one can make a rough estimation of the velocity of fluid particles in media of restricted extent.

In Figure 4 the variation of the terminal velocity of fluid particles can be seen with increasing d/D ratio. The majority of the points represent data taken from the literature (35, 46, 48, 49). A few other points have been located on the basis of the author's measurements. Systems 2, 3, 5, 7, and 8 of Table 2 were used in the experiments. The values of the surface or interfacial tension have been taken from the literature (19, 37).

The particle diameter was calculated either from the volume measured in a capillary tube before release or, in case of droplets issued under quasi-static conditions, from the orifice diameter by means of Equation (43) of

Appendix 2. Two orifices were used, one of 0.353 and the other of 0.487-cm. diameter.

Whenever available, experimentally determined values of u_{∞} (16, 48, 49) were used for calculating the u/u_{∞} ratio. In the rest of the cases u_{∞} was computed by means of Equation (17).

It is seen that up to about $d/D \approx 0.45$ the majority of the points in Figure 4 lie somewhat below the curve representing Equation (24) developed for solid spheres. The decrease of velocity due to the increased zigzagging tendency in restricted media is apparently much less for fluid particles than it was for solid spheres. The explanation is probably that in the turbulent range of spheroidal shapes the fluid particles always keep spiraling or zigzagging, even if $d/D = 0$, but the solid spheres move smoothly enough in infinite media.

The plotted points correspond to a size range of $0.31 < d < 4.45$ cm. and an Eötvös number range of $0.75 < N_{Eo} < 519$. Because of the considerable spread of the points the apparently slight effect of the Eötvös number on the u/u_{∞} ratio cannot be detected from the figure. From the quality of the correlation found by Uno and Kintner (49) between u/u_{∞} and σ on the one hand and u/u_{∞} and D on the other, one can conclude however that u/u_{∞} does in fact depend on the Eötvös number. On the basis of a study of their observations, and of the location of points in Figure 4, it seems to be a very plausible assumption that the lower the Eötvös number the nearer the u/u_{∞} vs. d/D curve passes to that of the solid spheres. This fact is expressed in the following empirical equation:

$$\frac{u}{u_{\infty}} = \frac{1 - \left(\frac{d}{D}\right)^2}{\sqrt{1 + \left(\frac{d}{D}\right)^4}} \times \left[1 - \frac{2}{3} \frac{N_{Eo}}{1 + N_{Eo}} \left(\frac{d}{D}\right)^{3/2}\right] \quad (26)$$

The curve pertaining to Eötvös numbers approaching infinity is also shown in Figure 4 as a dotted line.

Combining Equations (16) and (26) yields an explicit form for Equation (23):

$$\frac{u}{u_{\infty}} = \frac{0.88}{N_{Eo}^{3/4}} \frac{1 - \left(\frac{d}{D}\right)^2}{\sqrt{1 + \left(\frac{d}{D}\right)^4}} \times \left[1 - \frac{2}{3} \frac{N_{Eo}}{1 + N_{Eo}} \left(\frac{d}{D}\right)^{3/2}\right] \quad (27)$$

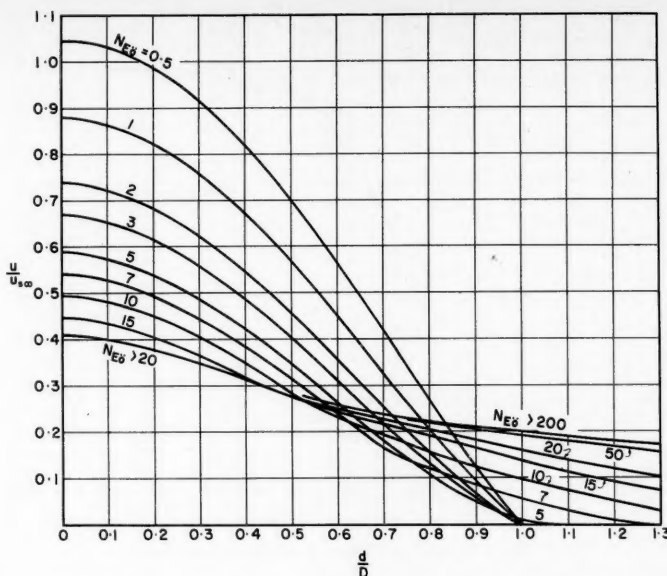


Fig. 6. Generalized chart for calculating the velocity of fluid particles.

which is applicable whenever

$$\frac{d}{D} < 1.0 \quad \text{for } N_{Eo} \leq 4.5$$

$$\frac{d}{D} < 1 - 0.175\sqrt{N_{Eo} - 4.5}$$

$$\text{for } 4.5 < N_{Eo} < 20$$

$$\frac{d}{D} < 0.31 \quad \text{for } N_{Eo} \geq 20$$

(28)

From Figure 4 it can be observed

that above $d/D = 0.45$ the spread of the points becomes more and more noticeable because part of the particles assume velocities which are no longer dependent on their size but on the tube diameter.

CYLINDRICAL BUBBLES AND DROPS

A number of papers (9, 11, 21, 28, 35) concerned with the description and velocity of cylindrical bubbles have been published. The general conclusion is that the velocity of cylindri-

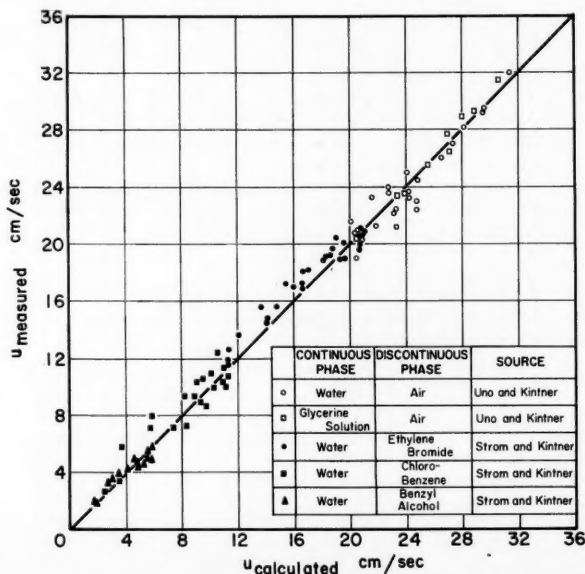


Fig. 7. Comparison of measured and calculated velocities.

cal bubbles is practically independent of the bubble volume and can be expressed as

$$u = \lambda \sqrt{\frac{g\Delta\rho D}{\rho_c}} \quad (29)$$

where λ has been recognized by Dumitrescu (11) as being a function of the $D\sqrt{g\Delta\rho/\sigma}$ group [which in this notation is identical with $(N_{Eo}^D)^{1/2}$].

To study the variation of λ , the experimental data of the above-mentioned authors have been used to plot λ against N_{Eo}^D in Figure 5. A few points representing average values of the writer's measurements with cylindrical drops (so far not studied) and bubbles are also plotted. The systems used in these experiments are those denoted by numbers 1, 3, 4, 5, 6, 7, 8, and 9 in Table 2.

The majority of the points follow a definite course, regardless of whether they represent gas bubbles or liquid drops. The best curve through these points seems to have a horizontal asymptote of $\lambda = 0.35$.

The points of two systems with continuous phases of very high viscosity are located on a different curve which would probably approach the same asymptote. It seems therefore that N_{Eo}^D is not the only variable on which λ depends; the other variable (or variables) however plays no significant part if the viscosity of the continuous phase is in the common range. The motion of cylindrical fluid particles in very viscous continuous phase will not be discussed further here.

Hattori (21) has defined a critical tube diameter (corresponding to $N_{Eo}^D = 3.36$) below which the gas bubbles are no longer capable of moving in the tube filled with liquid. It is improbable that such a critical diameter can be found for liquid-liquid systems because of the higher tendency of the drops to wet the tube wall if the velocity is sufficiently low. Around $N_{Eo}^D \approx 5$ the reproducibility of the drop velocities becomes generally very poor.

If Equation (29) is rewritten in the form

$$\frac{u}{u_{sz}} = \lambda \left(\frac{N_{Eo}}{(d)^2} \right) \frac{1}{1.74 \sqrt{d/D}} \quad (30)$$

one has an explicit form of Equation (23) for the range of cylindrical fluid particles. Values taken from the continuous curve of Figure 5 can be used for λ in Equation (30), which is applicable if

$$\frac{d}{D} > 1 - 0.175 \sqrt{N_{Eo} - 4.5}$$

for $4.5 < N_{Eo} < 20$

$$\frac{d}{D} > 0.31 \quad \text{for } N_{Eo} \geq 20 \quad (31)$$

An interesting feature of Equation (30) is that, although it was derived for cylindrical fluid particles, in the case of large Eötvös numbers it holds good even in regions where the particles are far from being cylindrical.

Figure 6 is a graphical representation of Equations (27) and (30) over the appropriate intervals and offers a quick way for the determination of the velocity of fluid particles in liquids in the range $0 \leq d/D \leq 1.3$, which is most frequently met in practice. Again it should be emphasized that this graph must not be used below $N_{Eo} = 500$, and in the case of gas bubbles it is not recommended for $N_{Eo} < 1$.

In Figure 7 the velocities calculated by the use of the above u/u_{sz} vs. d/D and N_{Eo} graph are compared with those measured by Strom and Kintner (48) and Uno and Kintner (49). The

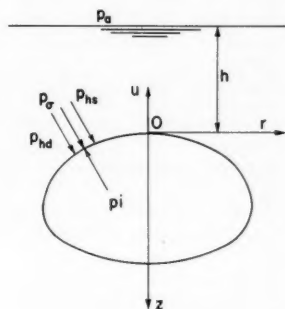


Fig. 8. Forces acting on surface of fluid particles.

systems used in this plot are of widely different properties. The Eötvös number varies between 0.66 and 75, the d/D ratio between 0.01 and 0.78. The spread of the points is generally well within the limits of reproducibility of the measurements.

ACKNOWLEDGMENT

The assistance of E. O. Porteous in the experiments is sincerely appreciated.

NOTATION

- a = horizontal diameter of particle, cm.
- A = $a^2\pi/4$, area of particle projected on a horizontal plane, sq.cm.
- b = vertical size of particle, cm.
- C = drag coefficient, dimensionless
- d = spherical diameter, equivalent

lent diameter of nonspherical particle, cm.

- D = tube diameter, cm.
- D_o = orifice diameter, cm.
- F = drag, g.cm./sec.² (= dyne)
- g = acceleration due to gravity, 981 cm./sec.²
- h = distance from liquid surface, cm.
- K = factor defined by Equations (8) and (9), dimensionless
- N_{Eo} = $g\Delta\rho d^2/\sigma$, Eötvös number, dimensionless
- N_{Eo}^D = $g\Delta\rho D^2/\sigma$, Eötvös number referred to tube diameter, dimensionless
- $N_{Eo}^{D_o}$ = $g\Delta\rho D_o^2/\sigma$, Eötvös number referred to orifice diameter, dimensionless
- N_{Re} = $u_{sz}d\rho_c/\mu$, Reynolds number, dimensionless
- p = pressure, g./cm.² (sec.²) (= dynes/sq.cm.)
- \bar{p} = $p/(\rho_c \frac{u^2}{2})$, dimensionless
- r = variable (see Figure 8), cm.
- \bar{r} = r/d , dimensionless
- R = curvature of particle surface, cm.
- \bar{R} = R/d , dimensionless
- R_1, R_2 = principal curvatures of particle surface, cm.
- \bar{R}_1, \bar{R}_2 = $R_1/d, R_2/d$, respectively, dimensionless
- u = terminal velocity, cm./sec.
- \bar{z} = variable (see Figure 8), cm.
- \bar{z} = z/d , dimensionless

Greek Letters

- α = latitude on the particle surface, dimensionless
- β = factor defined by Equation (3), dimensionless, function of particle shape
- ϵ = factor defined by Equation (21), dimensionless, function of Eötvös number
- κ = factor defined by Equation (48), of Appendix 3, dimensionless
- λ = factor defined by Equation (29), dimensionless
- μ = viscosity, g./cm.sec (= poise)
- ρ = density, g./cc.
- $\Delta\rho$ = $|\rho_o - \rho_p|$, density difference, g./cc.
- σ = surface tension or interfacial tension, g./sec.² (= dynes/cm.)
- ϕ, ϕ_1, ϕ_2 , etc. = function

Subscripts

- a = atmospheric
- C = of continuous phase
- D = of discontinuous phase
- E = of oblate spheroid
- hd = hydrodynamic
- hs = hydrostatic
- i = inside

- O = at $z = 0$
P = of circular disk
s = of sphere
w = due to wall effect (in Appendix 3)
 ∞ = in infinite media
 σ = due to surface or interfacial tension

Superscripts

- * = area of $d^2\pi/4$

LITERATURE CITED

- Allawala, M. A., M.Sc. thesis, Illinois Inst. Technol., Chicago, (1952).
- Blanchard, D. C., *Trans. Am. Geophys. Union*, **31**, 836 (1950).
- Bond, W. N., *Phil. Mag.* (7), **4**, 889 (1927).
- , and D. A. Newton, *ibid.*, **5**, 794 (1928).
- Boussinesq, J., *Ann. Chim. Phys.*, **29**, 364 (1913).
- Christiansen, R. M., *Dissertation Abstr.*, **15**, 1810 (1955).
- Datta, R. L., D. H. Napier, and D. M. Newitt, *Trans. Inst. Chem. Engrs. (London)*, **28**, 14 (1950).
- Davies, C. N., *Proc. Phys. Soc.*, **51**, 259 (1945).
- Davies, R. M., and Sir G. Taylor, *Proc. Roy. Soc. (London)*, **A200**, 375 (1950).
- Dubs, R., *Schweiz. Bauz.*, **97**, 169, 183 (1931).
- Dumitrescu, D. T., *Z. angew. Math. u. Mech.*, **23**, 139 (1943).
- Farmer, W. S., U.S. Atomic Energy Comm., CRNL-635, Oak Ridge Natl. Lab. (1950).
- Freud, B. B., and W. D. Harkins, *J. Phys. Chem.*, **33**, 1217 (1929).
- Garner, F. H., *Trans. Inst. Chem. Engrs. (London)*, **28**, 88 (1950).
- Gunn, R., and G. D. Kinzer, *J. Meteorol.*, **6**, 243 (1949).
- Haberman, W. L., and R. K. Morton, *The David W. Taylor Model Basin Report* 802, NS 715-102 (1953).
- Hadarnard, J., *Compt. rend. acad. sci. Paris*, **152**, 1735 (1911).
- "Handbook of Aeronautics," Vol. I, p. 90, Sir Isaac Pitman & Sons Ltd., London, England (1938).
- "Handbook of Chemistry and Physics," 35 ed., p. 1984, Chemical Rubber, Cleveland, Ohio (1954).
- Harmathy, Tibor, *Acta. Tech. Acad. Sci. Hung.*, **12**, 209 (1955).
- Hattori, S., *Rept. Aeronaut. Research Inst., Tokyo Imp. Univ.*, No. 115 (1935).
- Hayworth, C. B., and R. E. Treybal, *Ind. Eng. Chem.*, **42**, 1174 (1950).
- Hu, Shengen, and R. C. Kintner, *A.I.Ch.E. Journal*, **1**, 42 (1955).
- Hughes, R. R., and E. R. Gilliland, *Chem. Eng. Progr.*, **48**, 497 (1952).
- Johnson, A. I., and L. Braida, *Can. J. Chem. Eng.*, **35**, 165 (1957).
- Keith, F. W., and A. N. Hixson, *Ind. Eng. Chem.*, **47**, 258 (1955).
- Klee, A. J., and R. E. Treybal, *A.I.Ch.E. Journal*, **2**, 444 (1956).
- Laird, A. D. K., and D. Chrisholm, *Ind. Eng. Chem.*, **48**, 1361 (1956).
- Laws, J. O., *Trans. Am. Geophys.*

Union, Part III, p. 709, 22 Annual Meeting (1941).

- Lewis, J. B., I. Jones, and H. R. C. Pratt, *Trans. Inst. Chem. Engrs. (London)*, **29**, 126 (1951).
- Licht, William, and G. S. R. Narasimhamurthy, *A.I.Ch.E. Journal*, **1**, 366 (1955).
- Lohnstein, T., *Ann. Physik*, **20**, 237 (1906).
- Merrington, A. C., and E. G. Richardson, *Proc. Phys. Soc.*, **59**, 1 (1947).
- McNown, J. S., and J. T. Newlin, *Proc. First U.S. Natl. Cong. Appl. Mech.*, p. 801 (1951).
- O'Brien, M. P., and J. E. Gosline, *Ind. Eng. Chem.*, **27**, 1436 (1935).
- Peebles, R. N., and H. J. Garber, *Chem. Eng. Progr.*, **49**, 88 (1953).
- Perry, J. H., "Chemical Engineers' Handbook," 3 ed., p. 363, McGraw-Hill, New York (1950).
- Prandtl, L., "Essentials of Fluid Dynamics," p. 329, Hafner, New York (1952).
- Riabouchinsky, D. P., *Aerodyn. Inst. Koutchino Bull.*, **5**, 73 (1921).
- Rosenberg, B., *The David W. Taylor Model Basin Report* 727, (1950).
- Rybczynski, W., *Bull. Acad. Sci. Cracovie*, **A**, 40 (1911).
- Saffman, P. G., *J. Fluid Mech.*, **1**, 249 (1956).
- Savic, P., *Natl. Res. Council (Canada)*, Rept. No. MT-22 (1953).
- Siemes, W., *Chem.-Ing.-Tech.*, **26**, 479 (1954).
- Ibid.*, **614** (1954).
- Smirnov, N. I., and V. L. Ruban, *Zhur. Priklad. Khim.*, **22**, 1068 (1949).
- Ibid.*, **26**, 110 (1953).
- Strom, J. R., and R. C. Kintner, *A.I.Ch.E. Journal*, **4**, 153 (1958).
- Uno, Seiji, and R. C. Kintner, *ibid.*, **2**, 420 (1956).
- Warshay, M., E. Bogusz, M. Johnson, and R. C. Kintner, *Can. J. Chem. Eng.*, **37**, 29 (1959).

Manuscript received March 25, 1959; revision received October 26, 1959; paper accepted October 29, 1959.

APPENDIX 1

The shape of fluid particles is determined by the forces acting along their surface. For the sake of simplicity a particle is examined which, when moving upward with its terminal velocity, is a body of revolution around the vertical axis, and its meridian curve is $r = r(z)$ (Figure 8).

The equilibrium of the forces is expressed by

$$p_i = p_{hs} + p_{\sigma} + p_{hd} \quad (32)$$

where

$$p_i = p_{io} + \rho_0 gz \quad (33)$$

$$p_{hs} = p_a + \rho_c gh + \rho_c gz \quad (34)$$

$$p_{\sigma} = \sigma \left(\frac{1}{R_1} + \frac{1}{R_2} \right) \quad (35)$$

and under turbulent flow conditions

$$p_{hd} = \rho_c \frac{u^2}{2} \bar{p}_{hd}(\text{shape}, \alpha) \quad (36)$$

For $z = 0$, $R_1 = R_2 = R_0$, and $\bar{p}_{hd} = 1$; thus

$$p_{io} = p_a + \rho_c gh + \frac{2\sigma}{R_0} + \rho_c \frac{u^2}{2} \quad (37)$$

Combining Equations (32) to (37) one has

$$\begin{aligned} (\rho_c - \rho_0)gz + \sigma \left(\frac{1}{R_1} + \frac{1}{R_2} - \frac{2}{R_0} \right) \\ - \rho_c \frac{u^2}{2} [1 - \bar{p}_{hd}(\text{shape}, \alpha)] = 0 \end{aligned} \quad (38)$$

When one uses d as a characteristic length and the $\bar{r} = r/d$, $\bar{z} = z/d$, $\bar{R}_0 = R_0/d$, $\bar{R}_1 = R_1/d$, and $\bar{R}_2 = R_2/d$ dimensionless quantities, the dimensionless form of Equation (38) becomes

$$\begin{aligned} \frac{g\Delta\rho d^2}{\sigma} \bar{z} + \frac{1}{\bar{R}_1} + \frac{1}{\bar{R}_2} - \frac{2}{\bar{R}_0} - \frac{1}{2} \frac{\rho_c d u^2}{\sigma} \\ \times [1 - \bar{p}_{hd}(\text{shape}, \alpha)] = 0 \end{aligned} \quad (39)$$

After one substitutes for \bar{R}_1 and \bar{R}_2 expressions in terms of \bar{r} and \bar{z} , Equation (39) will be the one which, in principle, can be used for determining the $\bar{r} = \bar{r}(\bar{z})$ correlation, that is the shape of the fluid particle. But instead of getting into a hopelessly involved trial-and-error calculation, one should only draw the conclusion that in Equation (39) the following relationship is expressed:

$$\phi_0 \left(\text{shape}, \frac{g\Delta\rho d^2}{\sigma}, \frac{\rho_c d u^2}{\sigma} \right) = 0 \quad (40)$$

Here the third group is the well-known Weber number. The second group can be recognized as a dimensionless form of the Laplace constant and plays an important part in such problems as the quasi-static bubble formation [see (13, 32, 44)], the formation of droplets among packing elements (30) or by breakup of jets (6), and the inception of internal circulation in liquid particles (3, 4, 8, 14, 43). It is suggested that this group be called *Eötvös number*.

A substitution for u from Equations (7) and (9) indicates however that in the turbulent region at a given particle shape and Eötvös number the Weber group does not impose an additional restriction on Equation (39), so that the shape of fluid particles moving in infinite media depends solely on the Eötvös group:

$$\text{shape} = \phi_0(N_{Eo}) \quad (41)$$

APPENDIX 2

On the basis of Siemes's study (44) on quasistatic bubble formation the following equation can be developed:

$$\frac{N_{Eo}^3}{N_{DN_{Eo}}} = 21.6 \quad (42)$$

or, if solved for d

$$d = 1.67 \sqrt{\frac{D_{NS}}{\Delta\rho g}} \quad (43)$$

The validity of this equation for liquid-liquid systems can be proved by the application of Hayworth and Treybal's correlation (22) to very slowly forming droplets.

Mass Transfer Coefficients for Solids Suspended in Agitated Liquids

JAMES J. BARKER and ROBERT E. TREYBAL

New York University, New York, New York

The mass transfer coefficient in covered, right-cylindrical tanks full of liquid, turbulently agitated at various speeds by turbines with six flat blades, was measured by the rate of solution of suspended solids in water and in 45% sucrose solutions.

Screened crystals in the following U. S. mesh sizes were used: boric acid: 18/20, 16/18, 16/20, 14/16, 12/14, 10/12, 8/10, 6/8; rock salt: 6/8, 4/6. Pellets were benzoic acid: 0.126 in. long by 0.218-in. diam.; salt: 0.565-in. diam. by 0.531-in. long (over rounded ends). Tanks were 6, 12, 18, and 30 in. Turbines were 2, 3, 4, 6, 9, and 12 in. in diameter, centrally located. Four full-length baffles 10% of the tank diameter wide were spaced at 90 deg. A few runs were made without baffles.

The coefficient of mass transfer was found to be independent of particle size and Schmidt number ($N_{Sc} = 735$ to 62,000) and could be correlated with turbine Reynolds number in each tank, with larger tanks yielding smaller coefficients at the same N_{Re} . An empirical equation which fits all the data from the baffled tanks within about 4% (in the range $0.1 < k < 2$) is

$$\ln(10k) = I_2 + 0.85 V^{0.02975} \ln(N_{Re}/10')$$

where $I_2 = 0.8235 - 1.544 V^{1/3} + 0.115 V^{2/3}$

The variance of estimate for this expression is 0.0383, in units of $[\ln(10k)]^2$.

For extrapolation outside the experimental range of vessel sizes it is recommended that $I_2 = 0.676 - 1.266 V^{1/3}$ be used in place of I_2 . $N_{Re} = \pi T n / \nu$. The results indicate that power per unit volume for a given k goes through a maximum, with the following relative values for the 6-, 12-, 18- and 30-in. tanks: 1, 1.73, 1.78, 0.62.

A treatment of the data according to dimensionless groups provides another correlation:

$$kd/D = 0.02 N_{Re}^{0.533} N_{Sc}^{0.5}$$

It is shown that for the systems used $1/D$ is essentially proportional to $N_{Sc}^{0.5}$, and so the effect of diffusivity here is only apparent.

A recent review of the available information for computing the stage efficiency of mixer-settler extractors (19) revealed the severe limitations of our knowledge of the mass transfer coefficients for the continuous phase which surrounds the dispersed particles in the mixer. For baffled vessels

it was even necessary to resort to the use of coefficients for the continuous phase in contact with the surface of the vessel itself. This paper attempts to fill this gap by studying the rate of dissolution of particulate solids in agitated liquids under circumstances such that the surface area is known.

In 1897 Noyes and Whitney (15) formulated a durable theory for the dissolution of solids in liquids, which is summarized by

$$N = k(c_s - c) \quad (1)$$

Since then a number of investigators have attempted to correlate k by dimensional analysis with the apparent variables, such as particle size, turbine parameters, vessel geometry, fluid properties, density difference between solid and liquid, and ratio of the phases.

Murphree (13), Hixson and co-workers (3, 4, 5), and White (20) assumed no effect of particle size, but others (1, 21, 8, 16, 7, 9, 18) either found or assumed an effect.

A great variety of impeller types have been investigated, but relatively little information is available on flat-blade turbines, and no systematic investigation of the effect of ratio of turbine diameter to tank diameter has been made. The effect of speed for fully suspended particles has ranged from n^0 (1, 8, 12, 20) to $n^{0.6}$ (6), as well as intermediate effects (3, 11, 16, 12, 14, 7).

Essentially all the work has been done in unbaffled vessels with an air-liquid interface. Mack and Marriner (11) and others (8, 20, 14, 16, 12, 6, 7) worked with baffled vessels, but the effect of baffles is not established; neither is the shape of the vessel.

The significant fluid properties are kinematic viscosity, which in the usual dimensional-analysis treatment enters into Reynolds numbers and Schmidt number, and diffusivity, which is included in the latter and the Sherwood number. The effect of kinematic viscosity in the Reynolds number is usually the same as that of speed, which has been mentioned above. Hixson and Baum additionally related (kd/D) to $(\nu/D)^{0.5}$, but the exponent 0.5 was suggested by the results of gas-liquid contact in wetted-wall towers rather than by their own data. Others (8, 16, 6) have assumed the same relationship, but Akselrud (1) changes this to $(\nu/D)^{1/3}$. No systematic study of the effect has been made.

Most investigators assumed no effect of density difference. Akselrud (1) suggests $k \sim [(\Delta\rho)/\rho]^{1/4}$ and Kneule (8) $[(\Delta\rho)/\rho]^{1/3}$, both of which lead

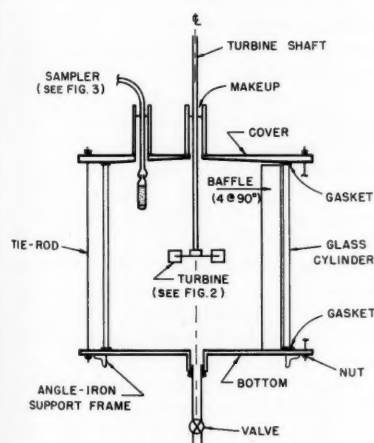
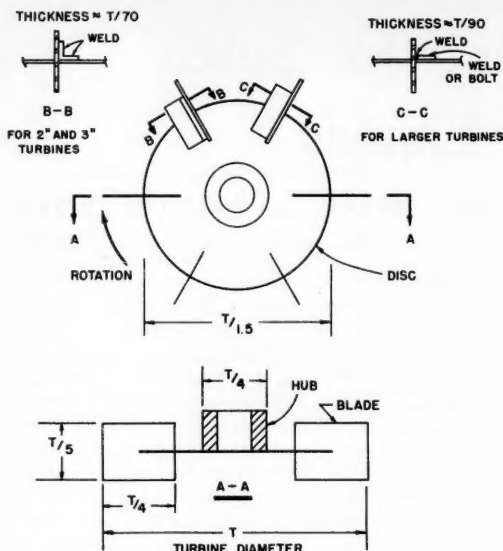


Fig. 1. Typical sketch for 6-, 12-, and 18-in. vessels. (See Table 1 for dimensions, etc.)

TABLE 1. VESSEL DIMENSIONS AND MATERIALS

Nominal size of vessel, in.	6	12	18	30
Height, inside wall, in.	5.95	12	18.1	30
Diameter, inside, in.	5.45	11.2	17.4	30
Volume, inside, cu. ft.	0.0806	0.685	2.481	12.22
Wall material	Pyrex	Pyrex	Pyrex	316 stainless steel
Baffle width, in.	0.55	1.12	1.74	3
thickness, in.	1/16	1/16	1/16	1/4



TURBINE DIAMETER, INCH.	2	3	4	6	9	12 3/8
SHAFT DIA., INCH	1/2	1/2	1/2	1/2	1	1

Fig. 2. Sketch of turbines.

to unreasonable values of k as $\Delta\rho$ approaches zero. Koláv (9) suggests $(\rho_s/\rho)^2$.

Most of the work has been done with dilute suspensions, with no attempt to study phase ratio. Wilhelm (21) however finds k decreasing with decreasing percentage of solids.

The effects of the variables on k are clearly not well established.

APPARATUS AND PROCEDURE

Figure 1 and Table 1 give the design and dimensions of the vessels used; Figure 2 summarizes the turbine dimensions.

Carefully screened fractions of boric acid and rock salt, as well as pellets of salt and of benzoic acid, were dissolved in water or 45% sucrose solutions in water under the circumstances outlined in Table 2. Table 3 summarizes Schmidt numbers and density differences.

Following is an outline of the procedure for each run. Fill the vessel and make-up reservoir with liquid of the same concentration. Measure the liquid temperature and adjust the turbine speed to proper range. Stop the turbine, remove a portion of liquid, add weighed solids, and replace the liquid. Quickly insert the sampling filter, start the turbine, and, as soon as solids are fully suspended—almost immediately with small amounts of solids, and within a few seconds in any usable instance—start the stop watch. Ten or fifteen seconds later draw the first sample as follows (refer to Figure 3). Open the stopcock on the sampler 1 sec. before the recorded time, directing the flow into a waste bottle. At recorded time divert the flow into the proper test tube by maneuvering the hard copper tubing extending through the flexible polyethylene neck

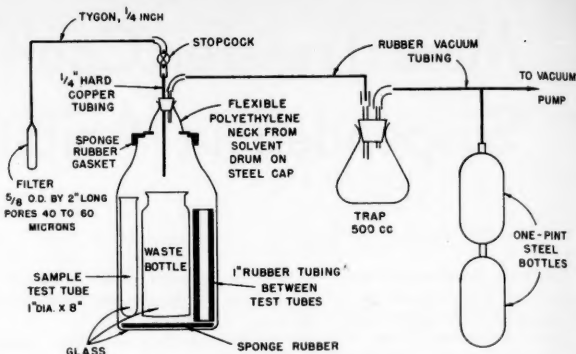


Fig. 3. Sampling system.

rial at a slightly different concentration, a correction was applied to account for the difference whenever necessary. In most cases the correction was negligible. The average surface area was calculated by estimating the amount of material that had dissolved up to the mid-point of the time interval and then calculating the relationship between the weight of the particles and their surface area. Most of the runs were made with crystalline materials that were more like parallelepipeds than like cubes or spheres. Therefore a relationship between surface area and volume was derived for such bodies on the assumption that each face of a crystal dissolved at the same rate per unit area. This leads to a rate of change in surface area which is less than the familiar two-thirds power of the volume that is associated with equidimensional bodies.

In addition to the rate of solution measurements, such physical properties of the liquids as were unavailable in the literature (diffusivity, density, viscosity, solubility) were also determined.

RESULTS

The results are summarized in Figures 4 through 10. Detailed data are given in reference 2.

Baffled Vessels

Figure 4 shows the correlation for the baffled 6-in. vessel and the 2-in. turbine. The coordinates are defined, and the 95% confidence limits of the least-squares line through the data are indicated by the dashed curve above the line. (The lower confidence limit, which would be located a similar distance below the line, is not shown, to keep the figures uncluttered.) In subsequent plots this information is labeled in abbreviated form. The equations for the least-squares lines are also given in the figures.

Figure 5 shows the correlation for the baffled 12-in. vessel, including all the first-interval data for all the turbines and all the solids. Figure 6 compares the data for the three turbines and indicates the solids used in each run. Figures 7 and 8 are similar plots for the 18-in. vessel. Figure 9 is a plot of the data from the 30-in. vessel; the

on the cover of the vacuum bottle; about 40 ml. or 1 sec. later, whichever is less, stop the flow by shutting the stopcock. If the sample volume is not replaced automatically from the reservoir, add the make-up. (This applies only to early runs on the 12-in. vessel.) Draw the second sample after the interval listed in the last column of Table 2, and the third sample a similar interval after that. For example in the first run indicated in Table 2, samples were drawn 10, 35, and 60 sec. after the particles were suspended. Read the turbine speed by a tachometer and the temperature by a thermometer between and/or after samples. Withdraw the filter and place it in distilled water, read the temperature, stop the turbine, drain and clean the vessel. Meanwhile break the vacuum and remove the sample bottle. Rinse and dry the filter with an auxiliary bottle. Pipette two or three 10-ml. portions from each sample and titrate; rinse and dry the pipette in an oven between samples. Measure the remaining volumes of samples in test tubes and the volume of liquid in the waste bottle. A total of 128 such runs were made. In most of the runs additional samples were drawn at intervals after the first. Only the data from the first interval, which were the more reliable, are reported here.

Experimental conditions were chosen so that only a small fraction of the initial solids was dissolved during a run. This permitted estimation of the interfacial area and consequently allowed calculation of true mass transfer coefficients from the following simple equation:

$$\ln\left(\frac{c_s - c_t}{c_s - c}\right) = \frac{kA}{V}(t - t_i) \quad (2)$$

Since the material removed from the vessel for a sample was replaced with mate-

TABLE 2. RANGES OF VARIABLES

Vessel size, in.	Turbine Diameter, in.	Speed, rev./min.	Liquid phase	Material	Solid Volume, %†	Particle sizes‡	Time between samples, sec.
6	2	578 to 1,440	Water	Boric acid	2.4	10/12, 18/20	25
		531 to 1,410	Sucrose*	Boric acid	1.65	8/10, 18/20	25, 35, 45, 60
12	3	589 to 1,206	Water	Boric acid	0.8, 2.4	12/14, 14/16, 16/20, 18/20	25
		610 to 1,170	Sucrose	Boric acid	1.63	12/14, 16/20	30, 60
		1,161	Brine	Salt	1.81	50-grain pellet	180
	Unbaffled 4	397 to 1,065	Water	Boric acid	0.8	16/20	25, 30
		422 to 1,106	Sucrose	Boric acid	3.3	16/20	30, 60
	4	333 to 865	Water	Boric acid	0.66, 0.8, 2.4, 4.9	10/12, 12/14, 14/16, 16/20, 18/20	25, 30
		368 to 621	Water	Benzoic acid	0.5, 9.3	0.1-g. pellet	45, 60, 420
		253 to 402	Sucrose	Benzoic acid	1.9, 9.3	0.1-g. pellet	240, 300, 420
		346 to 895	Sucrose	Boric acid	1.6, 3.3, 6.1, 23.2	10/12, 16/20	30, 60
	6	172 to 422	Water	Boric acid	0.8, 1.4, 1.5, 1.6, 2.4	6/8, 8/10, 16/18	25, 60
		171 to 177	Water	Benzoic acid	0.5, 9.3	0.1-g. pellet	60, 420
		170	Sucrose	Benzoic acid	1.9, 9.3	0.1-g. pellet	60, 420
		172 to 428	Sucrose	Boric acid	1.6, 6.1, 23.2	8/10, 12/14, 16/18	30, 60
		225 to 240	Brine	Rock salt	3.8	4/6	25, 117
18	6	196 to 677	Water	Boric acid	2.4	6/8, 14/16	25, 30, 60
		196 to 671	Sucrose	Boric acid	1.6	6/8, 8/10, 18/20	40, 60
		366 to 659	Brine	Rock salt	3.8	6/8	25, 40
	9	92 to 243	Water	Boric acid	2.4	8/10, 16/18, 18/20	25, 30, 60
		104 to 254	Sucrose	Boric acid	1.6	8/10, 16/18	60
		251 to 254	Brine	Salt	3.8, 4.4	4/6, 50-grain pellet	30, 60
	12	90 to 161	Water	Boric acid	2.4	10/12, 18/20	25, 30, 45, 60
		44 to 151	Sucrose	Boric acid	1.6	10/12, 18/20	60, 90, 120
		160	Brine	Salt	3.8, 4.4	4/6, 50-grain pellet	30, 60
	9	257 to 260	Brine	Rock salt	3.8	4/6, 6/8	30
30	12	141	Water	Boric acid	2.4	16/18	40
		145	Water	Benzoic acid	0.5	0.1-g. pellet	420
		136	Brine	Rock salt	3.6	6/8	30

* 45 wt. % sucrose in water.

† (initial volume of solids/volume of vessel) 100.

‡ 10/12 indicates through U.S. mesh 10, on 12; 50-grain pellets were 0.565-in. diam. by 0.531-in. long (over rounded ends); 0.1-g. pellets were 0.218-in. diam. by 0.126-in. long.

basis for the line through these data, which was obtained differently owing to the relatively few data points, is explained below. It should be noted that high values of k on the preceding plots are frequently those obtained from pellets, which had some tendency to disintegrate.

Figure 10 shows the least-squares lines for each vessel on the same plot. It is seen that the slopes are markedly similar and that, at a given Reynolds number, the larger the vessel the smaller the mass transfer coefficient.

The slopes of the lines for the 6-,

12-, and 18-in. vessels were plotted vs. the cube root of the volume of the vessel, which was chosen as the characteristic dimension because the height-to-diameter ratios were not exactly constant. Extrapolation of the least-squares line through these points indicated that the slope of the $\ln k$ vs. $\ln N_{Re}$ line for the 30-in. vessel should be 0.912. The lines for the 30-in. vessel shown on Figures 9 and 10 have this slope and are positioned so that the sum of the squares of the deviations of the points from the line is a minimum.

A plot of the intercepts of the $\ln k$ vs. $\ln N_{Re}$ lines as a function of $V^{1/3}$ was used to yield least-squares equations relating the intercepts to $V^{1/3}$.

With the above approximations the experimental results for the baffled vessels may be expressed by

$$\ln(10k) = (I_1 \text{ or } I_2) + 0.85 V^{0.02075} \ln(N_{Re}/10^4) \quad (3)$$

where

$$I_2 = 0.8235 - 1.544 V^{1/3} + 0.115 V^{2/3}, \text{ recommended for interpolations with vessels between 6 and 30 in.}$$

$$I_1 = 0.676 - 1.266 V^{1/3}, \text{ recommended for extrapolation to vessels less than 6 or more than 30 in.}$$

The variance of estimate for all the first-interval data from Equation (3) is 0.0383, in units of $[\ln(10k)]^2$.

Unbaffled Vessels

The results for the unbaffled 12-in. vessel with the 4-in. turbine are summarized by

$$\ln(10k) = 0.747 \ln(N_{Re}/10^4) - 0.671 \quad (4)$$

TABLE 3. SCHMIDT NUMBERS AND DENSITY DIFFERENCES

System	Density difference, solid minus liquid, g./cc.	Schmidt number range, dimensionless
Benzoic acid-water	0.26	1,138 to 1,328
Benzoic acid-sucrose solution	0.06	62,000
Salt tablets-brine	0.71	826 to 989
Rock salt-brine	0.99	740 to 926
Boric acid-water	0.42	735 to 1,182
Boric acid-sucrose solution	0.23	27,400 to 55,000

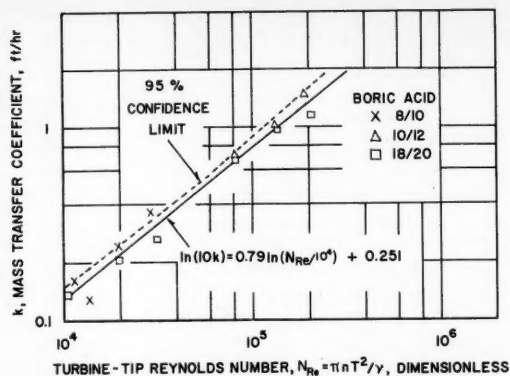


Fig. 4. Mass transfer coefficient vs. turbine-tip Reynolds number, 6-in. vessel, baffled, 2-in. turbine.

The mass transfer coefficients in the unbaffled vessel are smaller than those in the baffled vessel, in the region under study.

EFFECTS ON k

All of the generalizations stated in this section refer to the baffled vessels.

Particle Size

The data indicate that there is no systematic variation of mass transfer coefficient with particle size. The 50-grain salt tablets, which were the largest particles used, exhibited high coefficients, but this is ascribed to a tendency for these tablets to disintegrate rather than to any fundamental effect of particle size.

Density Difference

The difference in density between solid and liquid does not appear to influence the mass transfer coefficient.

Schmidt Number

Schmidt number, despite the large range studied, does not appear to influence the mass transfer coefficient to any great extent. Since kinematic viscosity appears in both the Reynolds and the Schmidt numbers, when the Schmidt number is high the Reynolds number tends to be low and vice versa. Therefore it is difficult to obtain a wide range of Schmidt numbers at a given value of Reynolds number. This is especially true when either suspension of particles or prevention of emulsification are auxiliary requirements. Therefore it seems unnecessary to include both N_{Re} and N_{Sc} to account for the variation in k , since N_{Re} alone appears adequate.

Ratio of Turbine Diameter to Tank Diameter

The ratio of turbine diameter to tank diameter exerts a negligible influence on the mass transfer coefficient over a wide range of the ratio (0.27 to 0.54 in the 12-in. vessel, 0.34 to 0.7 in the 18-in. vessel).

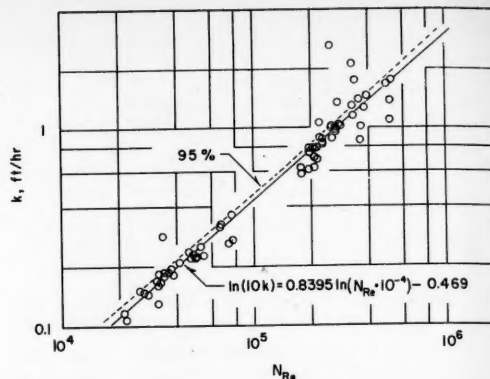


Fig. 5. k vs. N_{Re} , 12-in. vessel, baffled, 3-, 4-, 6-in. turbines.

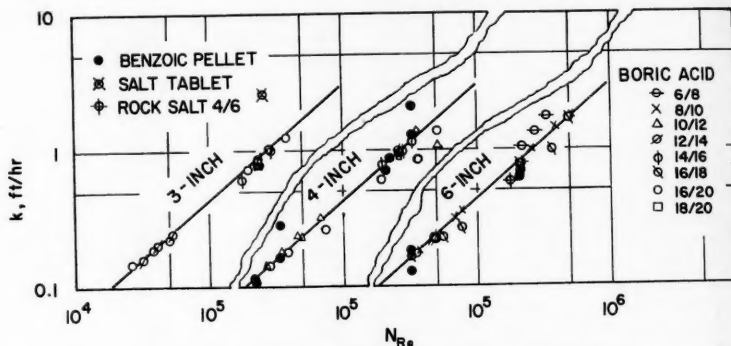


Fig. 6. k vs. N_{Re} , 12-in. vessel, baffled, comparison of turbines.

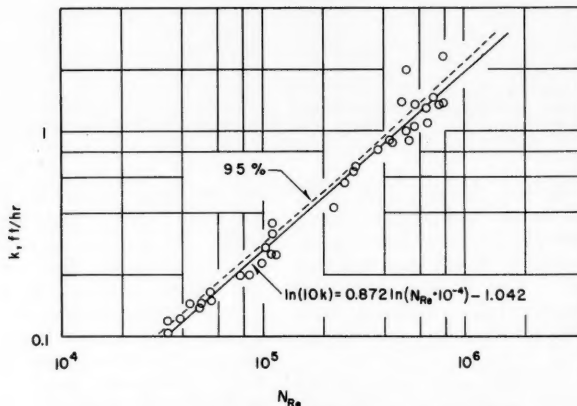


Fig. 7. k vs. N_{Re} , 18-in. vessel, baffled, 6-, 9-, 12-in. turbines.

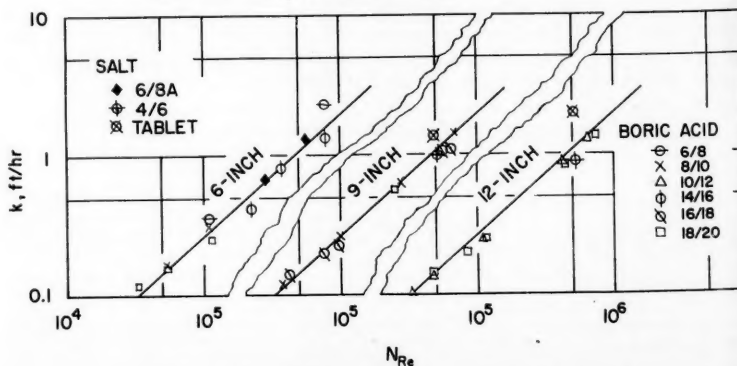


Fig. 8. k vs. N_{Re} , 18-in. vessel, baffled, comparison of turbines.

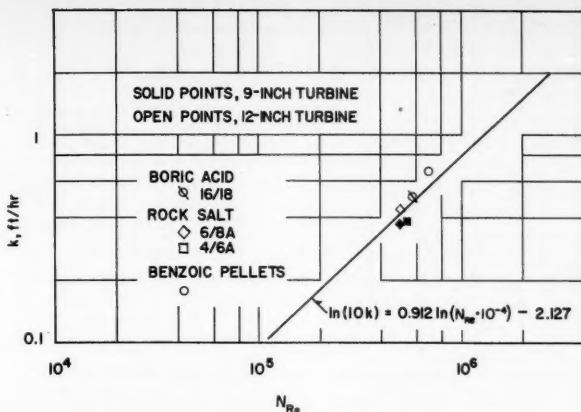


Fig. 9. k vs. N_{Re} , 30-in. vessel, baffled, 9-, 12-in. turbines.

Reynolds Number

The data indicate that k increases with the Reynolds number raised to a power between about 0.8 and 0.9, with the larger vessels favoring the larger exponents.

Vessel Size

Larger vessels give smaller mass transfer coefficients at the same Reynolds number.

Inventory of Solids

There is a tendency toward somewhat larger coefficients when the inventory of solids is increased, with other conditions held constant. However this is believed to be caused by a greater relative proportion of fines in those runs with the large inventories. This could be caused by the greater difficulty of removing fines from the larger inventory before it was added to the vessel, or by the increased collision frequency, and consequently greater attrition rate, in the larger inventory cases. In any event the effect of inventory is not large.

Power per Unit Volume

Rushton (17) has shown that for Reynolds numbers greater than about 10^4 the power number in open, baffled vessels equipped with six bladed turbines is constant. Laity and Treybal (10) have demonstrated that this is likewise true for similar vessels when

run covered and full of liquid. Under these circumstances, with all other things the same, the power per unit volume in two different vessels may be expressed as

$$\frac{(P/V)_1}{(P/V)_2} = \frac{V_2}{V_1} \left(\frac{N_{Re1}}{N_{Re2}} \right)^3 \frac{T_2}{T_1} \quad (5)$$

Table 4 compares the power per unit volume for the four vessels at $k = 0.5$ ft./hr. Since the slopes of the curves of k vs. N_{Re} are all about the same, the comparison would be approximately the same at other values of k .

Power per unit volume apparently exhibits a maximum with vessel size.

When applied to the same vessel with turbines of different sizes, Equation (5) indicates that, for the same power input, a higher Reynolds number is obtained with a larger turbine. Since k increases with N_{Re} independent of turbine size, a larger turbine will effect a given amount of mass transfer for a smaller expenditure of power. Whether this will also correspond to a

TABLE 5. MASS TRANSFER COEFFICIENTS PREDICTED BY AKSEL RUD'S EQUATION

Particle diameter, in.	k , ft./hr. for boric acid in	
	Water	Sugar solution
0.02	3.82	0.424
0.20	2.15	0.238

more economical operation depends on many other factors that in turn depend on the specific application under consideration.

Conventional Treatment of Data

The new data are also amenable to treatment through the use of the customary dimensionless groups. The slopes of the lines of Figure 10 are nearly equal, at an average value of 0.833, and at a given N_{Re} the product kd is practically constant for all vessels. Here d is the diameter of a cylinder of equal height and diameter and of the same volume as the vessel. Therefore kd is proportional to $(N_{Re})^{0.833}$. When $(kd/D)/(N_{Re})^{0.833}$ is plotted against N_{Re} on logarithmic paper, the points can be represented by a straight line whose slope might be anywhere between 0.45 and 0.55, owing to the scatter of the data. A value of 0.5 was chosen, so that the correlation of Figure 11 results. The dimensionless-group equations which describe all the data reasonably well are then

$$N_{Sh} = 0.02 (N_{Re})^{0.833} (N_{Sc})^{0.5} \quad (6)$$

or, in terms of the more conventional Reynolds number $N_{Re}' = T^2 n / \nu$,

$$N_{Sh} = 0.052 (N_{Re}')^{0.833} (N_{Sc})^{0.5} \quad (7)$$

The dependence of the mass transfer rates on diffusivity which these equations imply is only apparent. The ratio of the group $D\mu$ to temperature, which has long been used to correlate diffusivities, indicates that D varies as $1/\mu$. Since the densities of common liquids

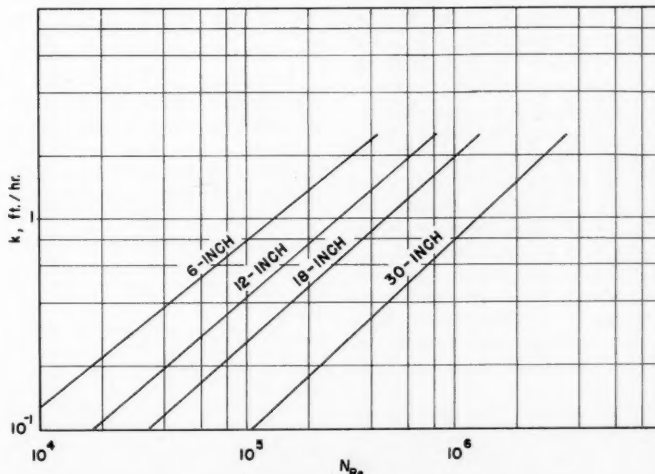


Fig. 10. k vs. N_{Re} , all vessels, baffled.

TABLE 4. COMPARISON OF POWER PER UNIT VOLUME IN VARIOUS VESSELS AT THE SAME VALUE OF

Vessel size, in.	Ratio: Power per unit volume in 6-in. vessel to power per unit volume in other vessel
6	1
12	1.73
18	1.78
30	0.62

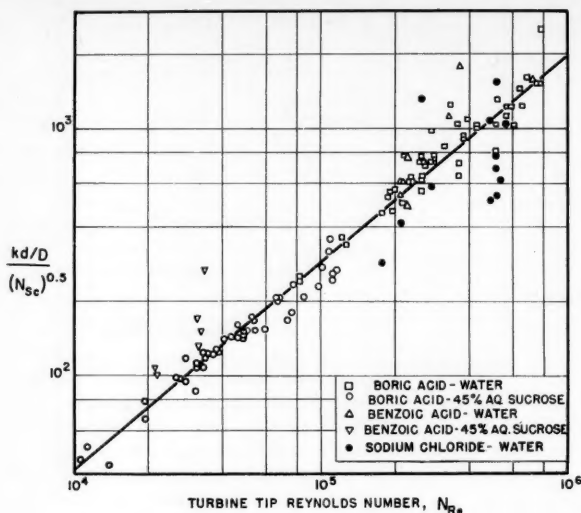


Fig. 11. Dimensionless correlation for baffled vessels.

lie within a narrow range, it follows that $1/D$, which is contained in N_{sh} , can be expected to relate to $(N_{sc})^{0.5}$. This is the case for the large range of Schmidt numbers employed here, as demonstrated in Figure 12, where the data are reasonably well described by the straight line of slope 0.5. It follows that $1/D$ and $(N_{sc})^{0.5}$ essentially cancel from Equations (6) and (7) and that Figure 11 is practically a plot of kd against N_{Re} . The empirical equation developed earlier more correctly reflects the observed role of diffusivity.

COMPARISONS WITH DATA OF OTHERS

Mass Transfer Coefficients

Hixson and Baum (3) worked in unbaffled vessels with propeller agitators. The mass transfer coefficients for one of the systems of this study predicted by their equation were compared with the unbaffled data obtained in the present work. Their equation predicts a k about 1.9 times that observed for the sugar solutions ($N_{sc} \approx 28,000$) and about 1.3 times that observed for the aqueous solutions ($N_{sc} \approx 830$). Their agitators were located closer to the bottom of the vessel and acted to lift the particles through the propeller, which could promote better mass transfer in an unbaffled tank.

Akselrud's (1) equation has been used to estimate the mass transfer coefficients to be expected with boric acid in the experimental range of interest. The results are shown in Table 5.

Despite the obvious apparent shortcomings of Akselrud's equation, the magnitudes of the predicted values of the mass transfer coefficient are correct.

Wilhelm, Conklin, and Sauer (21) found the coefficients shown in Table 6 when dissolving rock salt in water, using a three bladed propeller at a constant speed in an unbaffled crock. Equation (4) predicts a k of 0.9 ft./hr. for these conditions, ignoring the differences in geometry, which is a surprisingly good check.

Turbine Speed

One of the experiments by Nagata, Adachi, and Yamaguchi (14), using a four bladed paddle close to the bottom and benzoic acid pellets of 0.04 g. each dissolving in caustic solution, was done with 15% baffles in a 0.8-liter vessel. They found reciprocal neutralization time proportional to $n^{0.872}$ in the region of full suspension, and their unbaffled data show less dependence on speed.

Humphrey and Van Ness (6) found the mass transfer coefficient varied as the 0.87 power of the speed of rotation.

Suspension Point

Zwietering (22) presents a correlation for the amount of mixing required for full suspension of solid particles in tanks of various sizes, based on experiments using salt and sand in various liquids and with various types of agi-

TABLE 6. COEFFICIENTS FOUND BY WILHELM, CONKLIN, AND SAUER*

Particle size, in.	k , ft./hr.
0.0748	0.984
0.13	1.023
0.173	1.122
0.232	1.181
0.303	1.338

*Initial charge of rock salt 40% of that required to saturate the 10 liters of water used at 15°C.

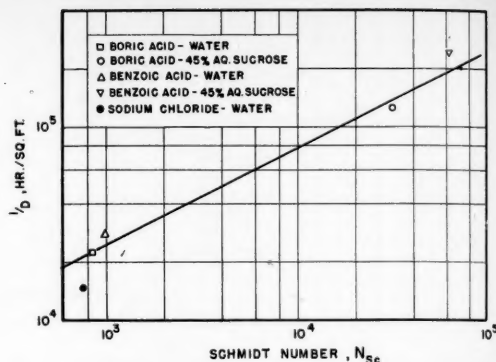


Fig. 12. Relation between diffusivities and Schmidt numbers, 25°C. The line has a slope 0.5.

tators. In the case of each run with salt in the study reported here a comparison was made between the agitator speed predicted by Zwietering's correlation and the actual speed used. The ratio of actual speed to that required by Zwietering's correlation ranges from 0.48 to 1.18. The mass transfer coefficients for those runs where the ratio is low, however, fit the correlation of Equation (3) equally as well as those for which the ratio is high. It is therefore concluded that if Zwietering's criterion is satisfied, suspension is full as far as mass transfer is concerned. But even if Zwietering's criterion is not satisfied, suspension may still be adequate for mass transfer purposes. In other words Zwietering's criterion predicts a point of adequate agitation for mass transfer but not the point of inadequate agitation.

COMMENTS ON TURBULENCE

The motion inside the baffled vessels was definitely turbulent. It is therefore not so surprising that the mass transfer coefficient turns out to be independent of Schmidt number, or molecular diffusivity. At the present time, however, not enough is known about the details of turbulent motion in baffled vessels to be able to predict the mass transfer coefficients from data on other properties of the fluid motion. In fact the problem may be turned around, and the mass transfer coefficients may be used as a measure of the average level of turbulence in the vessels.

The general equation for turbulent transfer may be expressed as

$$Q = -v l \frac{d\theta}{dh} = -E \frac{d\theta}{dh} \quad (8)$$

In mass transfer θ becomes the concentration, and the flux of mass may be expressed as

$$N = -E \frac{dc}{dh} = E \left(\frac{c_s - c}{l} \right) = k (c_s - c) \quad (9)$$

$$\therefore k = \frac{E}{l} = v \quad (10)$$

This expression indicates that the turbulent mass transfer coefficient is equal to the mean fluctuating velocity. Anything that promotes fluctuations in velocity should promote mass transfer.

It has been observed that the mass transfer coefficient in unbaffled vessels is less than that in baffled vessels, with other conditions equal. The pattern of motion in an unbaffled vessel, which consists of a rotational swirl superimposed on the turbine pattern, allows packets or eddies of fluid to take long flights between collisions with objects that promote velocity fluctuations. Therefore it is not unreasonable that the mass transfer coefficient should be smaller. Under conditions when the turbine speed is insufficient to lift the particles, on the other hand, others have observed that the coefficient in unbaffled vessels is greater than that in baffled vessels. (In other words the slopes of k vs. N_{Re} persist to low N_{Re} , and eventually k unbaffled $>$ k baffled.) A possible explanation for this may be that the swirling velocity in the unbaffled vessels, which can build up to appreciable magnitudes, by tumbling the particles on the vessel bottom actually exposes more surface and provides a greater relative velocity between solid and liquid than is produced in the baffled vessels.

It should be noted that it is apparently not sufficient to have eddy diffusivity large with respect to molecular diffusivity for the latter to be negligible in mass transfer. According to Equations (9) and (10), when the film concept of molecular diffusion is recalled, one sees that it is necessary to have

$$\frac{E}{l} \gg \frac{D}{B} \quad (11)$$

before molecular diffusion becomes negligible. This is a more stringent condition than $E \gg D$, since certainly $l \gg B$.

It is well known that in pipes ($E/l \sim (N_{Re})^{0.9 \text{ to } 1}$), with the exponent on the Reynolds number tending toward unity as the roughness of the pipe increases. The present results indicate that $k = E/l \sim (N_{Re})^{0.8 \text{ to } 0.9}$. If $l \sim (N_{Re})^{0.1}$ in the baffled tanks, then the eddy diffusivity in pipes and in baffled vessels is similar. This would imply that l increases as N_{Re} increases, which makes the condition expressed by Equation (11) even more stringent.

An attempt was made to compare the eddy diffusivities obtained in fluidized beds with those obtained in this work, without too much success because of fundamental differences. Eddy diffusivity goes through a maximum as

the velocity increases and the bed expands from the packed condition to a highly dilute state. A plausible explanation of this behavior may be as follows. When the velocity is low, the distance between particles is small, and since $E \sim N_{Re}$, E is small; as the bed expands, N_{Re} increases, and therefore E also increases; eventually E becomes independent of the distance between particles and approaches that characteristic of the pipe. The picture is complicated because the particles themselves generate turbulence in the fluid, accounting for the maximum in the curve of E vs. velocity, rather than a monotonic increase toward the diffusivity characteristic of the pipe.

ACKNOWLEDGMENT

The authors thank James Harte and Salvatore Bartolotta for help in building the equipment. The Hooker Chemical Corporation donated the benzoic acid, which was pelletized by Nysco Laboratories, Inc.

This paper is a condensation of a thesis by J. J. Barker in partial fulfillment of the requirements for the degree of Doctor of Engineering Science at New York University.

NOTATION

a	= a constant, dimensionless
\bar{A}	= average surface area of particles, sq. ft.
b	= slope of least squares line of $\ln k$ vs. $\ln N_{Re}$
B	= film thickness, ft.
c	= concentration, moles/unit volume
c_s	= solubility, moles/unit volume
d	= differential
d	= diameter of vessel, ft.
D	= molecular diffusivity, sq. ft./hr.
E	= eddy diffusivity, sq. ft./hr.
h	= distance, ft.
I	= intercept of least-squares line on plot of $\ln(10k)$ vs. $\ln(N_{Re}/10^4)$, k in ft./hr.
I_1	= first-order approximation to I
I_2	= second-order approximation to I
k	= mass transfer coefficient, ft./hr.
l	= mixture length, ft.
n	= speed of rotation of turbine, rev./hr.
N	= flux of mass, moles/hr., sq. ft.
P	= power for agitation, hp.
Q	= mean rate of transfer of a property per unit time per unit area
N_{Re}	= Reynolds number, $n\pi T^2/\nu$, dimensionless, $N_{Re}' = N_{Re}/\pi$
N_{Sc}	= Schmidt number, ν/D , dimensionless
N_{Sh}	= Sherwood number, kd/D , di-

mensionless

t	= time, hr.
T	= turbine diameter, ft.
V	= volume of vessel, cu. ft.

Greek Letters

μ	= viscosity, lb./ (ft.) (hr.)
ν	= kinematic viscosity, sq. ft./hr.
v	= root-mean-square velocity fluctuation, ft./hr.
ρ	= density of liquid, lb./cu. ft.
ρ_s	= density of solid, lb./cu. ft.
$\Delta\rho$	= $(\rho_s - \rho)$ = difference in density, solid minus liquid, lb./cu. ft.
θ	= property
π	= 3.14159

Subscript

i	= beginning of an interval
-----	----------------------------

LITERATURE CITED

1. Akselrud, G. A., *Nauch. Zapiski*, **29**, No. 1, 63 (1955).
2. Barker, J. J., thesis, New York Univ., New York (April, 1959).
3. Hixson, A. W., and S. J. Baum, *Ind. Eng. Chem.*, **33**, 478 (1941); **34**, 120 (1942).
4. ———, and J. H. Crowell, *ibid.*, **23**, 923, 1002, 1160 (1931).
5. ———, and G. A. Wilkins, *ibid.*, **25**, 1196 (1933).
6. Humphrey, D. W., and H. C. Van Ness, *A.I.Ch.E. Journal*, **3**, 283 (1957).
7. Kafarov, V. V., and V. D. Podoima, *Khim. Prom.*, **86** (1957).
8. Kneule, F., *Chem.-Ing. Tech.*, **28**, 221 (1956).
9. Koláv, V., *Chem. Listy*, **52**, 852 (1958).
10. Laity, D. S., and R. E. Treybal, *A.I.Ch.E. Journal*, **3**, 176 (1957).
11. Mack, D. E., and R. A. Marriner, *Chem. Eng. Progr.*, **45**, 545 (1949).
12. Mattern, R. V., Oleg Bilous, and E. L. Piret, *A.I.Ch.E. Journal*, **3**, 497 (1957).
13. Murphree, E. V., *Ind. Eng. Chem.*, **15**, 148 (1923).
14. Nagata, S., M. Adachi, and I. Yamaguchi, *Mem. Fac. Eng., Kyoto Univ.*, **20**, 72 (1958).
15. Noyes, A. A., and W. R. Whitney, *J. Am. Chem. Soc.*, **19**, 930 (1897).
16. Oyama, Y., and K. Endoh, *Soc. Chem. Eng. (Japan)*, **20**, 575 (1956).
17. Rushton, J. H., *Chem. Eng. Progr.*, **47**, 485 (1951).
18. Steidl, H., *Chem. Listy*, **52**, 1411 (1958).
19. Treybal, R. E., *A.I.Ch.E. Journal*, **4**, 202 (1958).
20. White, E. W., Ph.D. thesis, Lehigh Univ., Bethlehem, Pa. (1951).
21. Wilhelm, R. H., L. H. Conklin, and T. C. Sauer, *Ind. Eng. Chem.*, **33**, 453 (1941).
22. Zwietering, Th. N., *Chem. Eng. Sci.*, **8**, 244 (1958).

Manuscript received September 28, 1959; revision received November 6, 1959; paper accepted November 9, 1959. Paper presented at A.I.Ch.E. St. Paul meeting.

Mechanisms by Which Ultrasonic Energy Affects Transfer Rates in Liquid-Liquid Extraction

H. A. WOODLE, JR., and F. C. VILBRANDT

Virginia Polytechnic Institute, Blacksburg, Virginia

Concurrent and spray-tower studies have been accomplished that illustrate the effects of ultrasonic insonation on transfer rates in liquid-liquid extraction. Stage efficiencies and over-all transfer rates in the system toluene-methyl alcohol-water were determined with and without insonation of the system at frequencies of 40 and 800 kc.

Insonation was shown to have a positive effect on mass transfer in both concurrent and spray-tower operations. Insonation of the system provides for increased interfacial area between the two phases, removal of relatively stagnant liquid layers at the interface, and increased circulation currents within a single liquid phase. Low-frequency insonation favors local agitation and mixing of the phases, and high-frequency insonation favors induced circulation currents.

The majority of the proved industrial uses of ultrasonics are of the nature of nondestructive testing and thickness measurement (4, 13), degassing of liquids (8), improved cleaning methods for finely-machined parts (14, 23), and formation of emulsions and homogenized mixtures (5, 7, 17). A field that is gradually becoming interesting commercially is the utilization of high frequency sound waves in extraction operations (8, 17).

In this investigation, in addition to the obvious purpose of comparing extraction rates obtained in the presence of ultrasonic waves with rates obtained without insonation, a secondary objective was that of presenting a picture more complete than formerly available of the mechanisms by which insonation affects mass transfer rates in a two-phase, three-component liquid system.

DIFFUSION OF ALKALI THROUGH A CELLOPHANE MEMBRANE

Rees (18) reports an increase of 30% for the dialysis constant in the transport of alkali through a cellophane membrane when subjected to insonation. A similar investigation by Bakhshi (2) indicated that insonation was responsible for increases of up to 80% in the over-all mass transfer coefficient for the system. Baumgartl (3)

H. A. Woodle, Jr., is with E. I. du Pont de Nemours and Company, Inc., Richmond, Virginia.

found that the diffusion of 5% sodium chloride was increased by a factor of 2 under the influence of ultrasonics.

Liquid-Solid Extraction

Grove (11) has reported increased extraction of protein from brewer's yeast with a 5% sodium chloride solution in the presence of audible sound waves. A patent (20) was granted for a process whereby audible and inaudible insonation was applied to the extraction of oil from fish materials. Increased extraction of flavor from hops in the brewery industry through application of ultrasonic vibrations has been reported in several instances (5, 6). Thompson and Sutherland (21) found that insonation of the system *n*-hexane and peanuts increased extraction of the peanut oil 2.76 times that of control samples.

Liquid-Liquid Extraction

With insonation at a frequency of 570 kc. Haul, Rust, and Lutzow (12) reported an increase of 76% in the extraction of phenanthrene from methanol by gasoline in a small spray tower.

Murray (15) investigated the effects of 400 kc. insonation on the extraction of acetone from carbon tetrachloride with water, finding an increase in stage efficiency of approximately 20% when the system was insonated at high power levels. In subsequent work (16) Murray studied the system benzene-acetic acid-

water at the same frequency as before and found that with insonation at high power levels the stage efficiency increased approximately 30% over control tests.

Aeroprojects, Incorporated (1) has reported stage efficiencies of $90 \pm 10\%$ when working with frequencies from 15 to 30 kc. The particular extractor employed consisted of an ultrasonic device for emulsifying the two phases and a separate chamber for breaking the emulsion with a standing wave pattern.

The postulation has been made that ultrasonic energy may affect mass transfer in a liquid-liquid extraction system in a positive direction by at least three mechanisms, simultaneously occurring but separate in nature (21): increasing conductance of the interface by decreasing interfacial resistance to mass transfer, increasing interfacial area between two liquid phases by reducing size and increasing number of dispersed-phase particles, and increasing concentration gradients across the interface by decreasing the concentration gradient within a single phase.

EXPERIMENTAL

Two-Phase, Three-Component Liquid System

The system toluene-methyl alcohol-water was used because of component

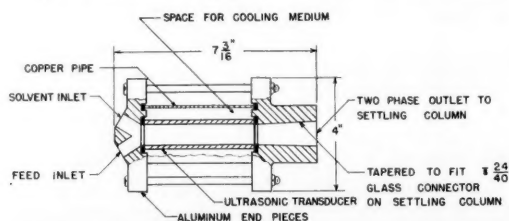


Fig. 1. Concurrent extractor used in extraction studies.

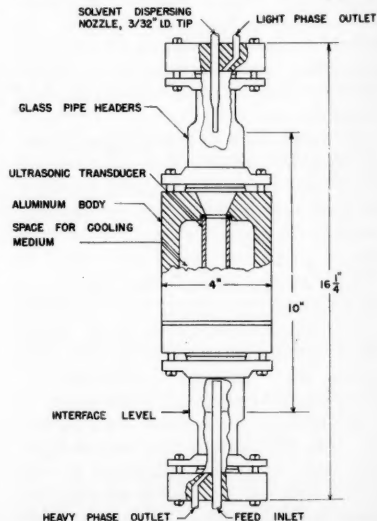


Fig. 2. Spray column used in extraction studies.

availability, noncorrosive nature, and ease of composition analysis. Methyl alcohol was considered as the solute, being extracted from the toluene with distilled water. A.C.S. reagent-grade toluene and methyl alcohol were used to prepare the feed mixture, and distilled water was used as solvent. All feed mixtures were in the concentration range of 14.4 to 14.8 weight % methyl alcohol in toluene, with the mixture saturated with distilled water. Composition analysis of samples was accomplished by refractive-index measurements.

Ultrasonic Equipment

Two cylindrical barium-titanate transducers, one 40-kc. radial frequency and one 800-kc. radial frequency, were utilized for this study. Both transducers were 4 in. long. The outside diameter of the 40-kc. transducer was 1½ in., and of the 800-kc. transducer 1 in. The 40-kc. transducer, powered by a Rich-Roth 400 generator, was used only in the spray column. The 800-kc. transducer was powered by a Brush Hypersonic generator but was used in both the concurrent extractor and the spray column. General construction features of the extractors are shown in Figures 1 and 2.

Procedure

The approximate power delivered to the liquid system from a transducer for any given generator setting was measured through a thermal calibration of each transducer and generator arrangement. The temperature rise of a known flow rate of distilled water going through the transducer was measured for various generator settings. Power output of the transducer was calculated from this data.

A solvent-to-feed ratio of 1.23:1.00 by weight was used for all concurrent tests, and a ratio of 1.00:7.00 was used for the spray-column tests. Feed rates of 40, 52, 85, and 122 g./min. were used for the concurrent tests. Time of contact was taken as the time required for a given cross-sectional plane of the two liquid phases to pass from one end of the transducer to the other, with plug flow condi-

tions assumed. A single feed rate of 105 g./min. was used for the spray-column tests, in which solvent was the dispersed phase. Temperature of the solvent and feed was maintained between 25° and 27°C. by constant-temperature-circulation.

In all cases final samples of extract and raffinate streams were taken only after steady state conditions had been reached in the extractor, as indicated by continual analysis of the exit streams. Stage efficiency was used for comparison of tests with the concurrent extractor, and the over-all transfer rate of methyl alcohol was used for comparison of tests conducted with the spray column. A strong beam of light was directed through interfacial regions and dispersed drops to aid in observation of concentration gradients and liquid currents.

Data and Results

A summation of data and results for the concurrent tests is presented in Figure 3. Figure 4 represents a summation for the spray-column tests. Observations of the physical conditions occurring at a liquid-liquid interface both with and without insonation are represented in Figure 5.

DISCUSSION

Stage efficiencies resulting from concurrent tests at various contact times without insonation varied only slightly over the range of contact times studied (Figure 3, zero insonation power). From this result it can be reasoned that the stage efficiencies resulting from tests with insonation are truly indicative of the effect of insonation, with little or no interaction effect from the various contact times.

As illustrated by Figure 3, for a threefold increase in contact time at a constant insonation power, 5.9 to 18 sec. at 20 w., the increase in stage efficiency obtained was about three times, 15 to 45%. For a threefold increase in insonation intensity at a constant contact time, 20 to 60 w. at 18 sec.,

the maximum increase in stage efficiency was about 1.3 times, 45 to 59%. These results bear out the general opinion that, in cavitation processing, an insonation power level sufficiently high to produce cavitation generally serves the same purpose as a much more intense field and is often more economical to produce.

Three major effects of insonation that contribute to extraction increases were observed in this two-phase system: agitation or mixing of opposite phases, induced-circulation currents within a single liquid phase, and removal of stagnant liquid areas in vicinity of the interface between the two liquid phases. All three effects probably occur concurrently at high levels of insonation power, although intense mixing of the two phases makes observation of any circulation currents or stagnant areas difficult. As temperature rise of a liquid during insonation is an inherent characteristic of such treatment, no effort was made to separate this thermal effect from the mechanical effects that led to increased extraction rates.

At levels of 55- to 70-w. insonation power the two liquid phases in the insonation zone were thoroughly mixed by the sound waves, leaving no truly single interface between the two phases. The increase in extraction observed at these power levels may have resulted primarily from increased interfacial area and improved mixing of the two phases. With mild insonation at 5- to 10-w. power there was no apparent bulk mixing or dispersion of one phase in another; there was a slight increase in interfacial area as a result of ripples in the interface. Observation and rough measurement of the depth of these ripples led to an estimate of a maximum increase of about 10%, not nearly a sufficient increase to account for the extraction increase observed.

Observations of interfacial conditions

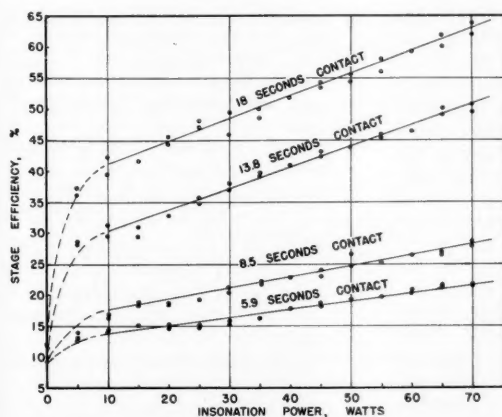


Fig. 3. Relationship between stage efficiency and insonation power at various contact times for concurrent extraction with an 800-kc. transducer.

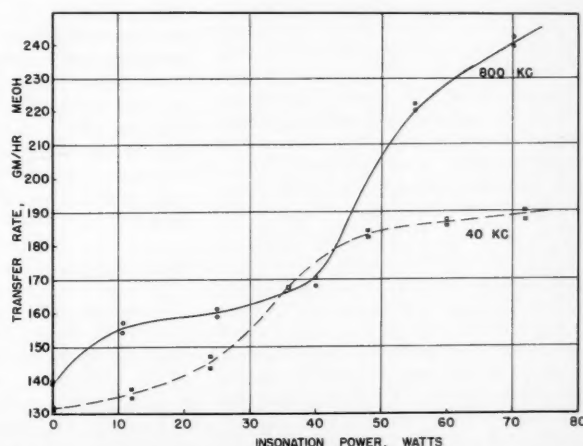


Fig. 4. Relationship between transfer rate and insonation power for spray-column extraction with 40- and 800-kc. transducers.

during concurrent extraction tests both with and without insonation are presented in Figure 5. In case A the two phases were observed to be in viscous flow. Liquid at the extreme top of the light phase and bottom of the heavy phase was not disturbed nor brought into contact with the opposite phase, and for all practical purposes these liquid portions were not a part of the extraction operation. The zone of high methyl alcohol concentration in the solvent was clearly distinguishable, with no noticeable turbulence. Over an observed travel distance of about 2 in. this high-concentration region increased in thickness from approximately $\frac{1}{8}$ to $\frac{3}{16}$ in. Molecular diffusion was apparently responsible for all solute transfer between the different liquid regions under these conditions.

Case B (Figure 5) shows the effects of ultrasonic waves on a liquid-liquid interface. The high-concentration region of methyl alcohol in the solvent was considerably decreased in thickness to about $\frac{1}{16}$ in. and was relatively constant at this value over the 2 in. of observed travel. Circulation currents immediately within this small zone were also observed. Interfacial agitation and mixing encompassing a liquid layer about $\frac{1}{32}$ in. thick was observed through use of a hand magnifying glass. Fresh portions of feed and solvent were continually presented to the interface by circulation currents created in the bulk phases by the ultrasonic waves.

Over the range of 10- to 35-w. insonation power for the spray-column tests (Figure 4) the increased transfer rates were probably a result of internal circulation currents in the dispersed-solvent drops and a pronounced prolate-oblate oscillation of the falling drops, both effects produced by the insonation. Circulation currents in the drop interior gave the same effect of "cleaning" the solvent side of the interface as was noticed in the concurrent tests. Minor internal circulation currents were observed in tests without insonation. (Circulation currents inside the drops were observed with the aid of a beam of light directed through the area in question, the regions of different solute concentration showing up clearly.) It has been demonstrated in other studies that these two actions, internal-circulation currents (10, 19) and prolate-oblate oscillation of drops (9), enhance transfer rates in a dispersed-phase system.

Data have been accumulated to show that a large portion of the over-all extraction accomplished in a spray tower occurs as the dispersed phase is formed in drops at the nozzle tip (22). In the spray-column tests formation time for drops in the 800-kc. tests was approximately 0.8 sec. and for the 40-kc. tests 0.3 sec. This formation time did not vary significantly between insonated

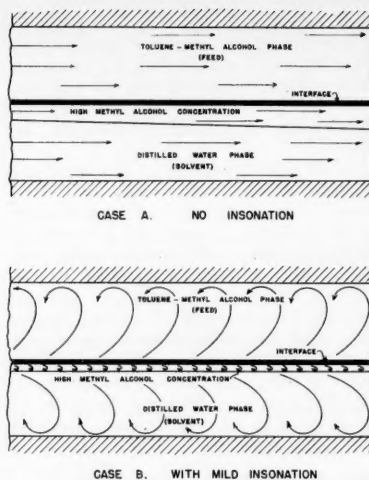


Fig. 5. Physical conditions at liquid-liquid interface with and without insonation.

and noninsonated tests, and the longer formation time in the 800-kc. test (800-kc. column had only 36% of the cross-sectional area in the 40-kc. column) probably accounts for the slightly higher transfer rate at zero insonation power as illustrated in Figure 4. Circulation currents in the drops as a result of insonation were very prominent during this formation period and unquestionably affected mass transfer rates in a positive manner during this time.

At insonation powers of 35 to 55 w. single drops formed at the nozzle tip were dispersed further into numerous small drops, increased transfer rates being a consequence of this increased interfacial area. Circulation currents were still evident at this point and should receive partial credit for the high transfer rates.

At the highest insonation powers studied, approximately 70 w., single drops released from the nozzle were dispersed into fifty or seventy-five smaller drops. (The number of drops was estimated from the relation between diameter of the small drops and the diameter of the original one drop.) Internal circulation currents probably had less effect in these smaller drops than in the larger ones. Apparently the increase in interfacial area was sufficient to maintain the higher transfer rates.

CONCLUSIONS

Insonation of a two-phase, three-component liquid system with ultrasonic waves in the frequency range of 40 to 800-kc./sec. effects an increase in mass transfer rates in such a system.

Basically the same mechanisms are responsible for the mass transfer increases in a concurrent system and in a dispersed-phase system. The mechanical

actions or results of insonation that have been shown to increase mass transfer rates are increase in interfacial area between phases through agitation and mixing, removal of minute stagnant liquid layers at the interface through cavitation-induced microagitation and circulation currents, and a continual supply of fresh material from both phases to the interface through bulk phase circulation currents. Local agitation and mixing appear to be favored by low-frequency insonation, and circulation currents appear to be favored by high-frequency insonation.

ACKNOWLEDGMENT

This investigation was made possible through the support of the Virginia Engineering Experiment Station and through the support of a research grant furnished by E. I. du Pont de Nemours and Company, Inc.

LITERATURE CITED

1. Aerochemicals, Inc., A.E.C. Contract AT(30-1)-1798, Rept. NYO 7489, First Interim Rept. (Dec. 1955).
2. Bakhshi, N. N., Ph.D. thesis, Va. Polytech. Inst., Blacksburg (1956).
3. Baumgartl, F., *Artz. Forsch.*, **3**, 525 (1949).
4. Boyce, C. W., *Fac. Man. Maint.*, **111**, No. 3, 84 (1953).
5. *Chem. Eng. News*, **33**, 1024 (1955).
6. *Chem. Week*, **76**, No. 7, 52 (1952).
7. *Ibid.*, **79**, No. 9, 46 (1955).
8. Davis, A. S., *Food Eng.*, **29**, No. 3, 119 (1957).
9. Garner, F. H., and A. H. P. Skelland, *Ind. Eng. Chem.*, **46**, 1255 (1954).
10. ———, *Chem. Eng. Sci.*, **4**, 149 (1955).
11. Grove, H. D., Jr., M. Sc. thesis, Univ. Iowa, Iowa City (1948).
12. Haul, R. H., H. Rust, and J. Lutzow, *Naturwissenschaften*, **37**, 523 (1950).
13. Hueter, R. F., and R. H. Bolt, "Sonics," Chap. 8, John Wiley, New York (1950).
14. Meyer, C. F., *Fac. Man. Maint.*, **109**, No. 9, 119 (1951).
15. Murray, L. P., Jr., M. Sc. thesis, Va. Polytech. Inst., Blacksburg (1954).
16. ———, Ph. D. thesis, Va. Polytech. Inst., Blacksburg (1956).
17. Rapp, H., *Food Eng.*, **29**, No. 9, 97 (1957).
18. Rees, J. H., M. Sc. thesis, Mass. Inst. Technol., Cambridge (1949).
19. Sherwood, T. K., J. E. Evans, and J. V. A. Longcor, *Ind. Eng. Chem.*, **31**, 1144 (1939).
20. Shropshire, R. F., U.S. Patent 2,473,453 (June 14, 1949).
21. Thompson, Dudley, and D. G. Sutherland, *Ind. Eng. Chem.*, **47**, 1167 (1955).
22. Treybal, R. E., "Mass-Transfer Operations," p. 435, McGraw-Hill, New York (1955).
23. *Ultrasonic News*, **1**, No. 4, 11 (1957).

Manuscript received March 31, 1959; revision received September 28, 1959; paper accepted October 8, 1959. Paper presented at A.I.Ch.E. Atlantic City meeting.

Burning Rates of Solid Propellants

J. M. SMITH

Northwestern University, Evanston, Illinois

A model is proposed for the burning of solid propellants which takes into account heat transfer, diffusion, and chemical reaction processes. The chemical step influencing the rate is postulated to be a reaction between a gaseous molecule and a solid component occurring at the solid-gas interface. The combination of expressions for the rates of the heat transfer, diffusion, and reaction steps leads to relatively simple equations for the burning rate in terms of (1) the physical properties of the propellant; (2) the transport coefficients; (3) the operating conditions of the burning process, temperatures, and pressure; and (4) chemical characteristics of the gas-solid reaction, activation energy, frequency factor, and heat of reaction.

The well-established facts concerning burning rates, the effect of pressure and initial temperature, and the phenomenon of erosive burning are predicted by the proposed theory. Also specific experimental data for burning potassium and ammonium perchlorate composite propellants can be predicted from the theory. The values of the variables necessary to obtain agreement between observed and predicted results are generally realistic. However it should be emphasized that conclusions regarding the detailed mechanism of the burning process cannot be obtained from comparison with burning-rate data. Elucidation of the kinetic steps in the process will require experimental investigation of the intermediate products of combustion and a detailed study of the burning surface and gaseous flame zone.

Solid propellants used in rocket propulsion are primarily of the composite type; that is, they consist of a powdered crystalline oxidizer dispersed in a continuous phase of plastic fuel. The rate of burning of the propellant is of basic importance in determining the performance of the rocket motor. The linear burning rate is defined as the velocity of the gas-solid interface (the burning surface) as the propellant is converted into gaseous combustion products. This linear rate is related to the mass burning rate per unit surface by the density of the propellant and to the mass burning rate of component C of the propellant by its mass fraction:

$$r = \frac{m}{\rho} = \frac{m_c}{n_c} \left(\frac{1}{\rho} \right) \quad (1)$$

The primary physical variables which can influence the burning rate in the rocket motor are pressure, initial temperature of the propellant, gas velocity parallel to the burning surface, and the characteristics of the propellant. Among the significant characteristics are the kind, size, and shape of the oxidizer crystals; the fuel-oxidizer ratio; the catalyst that may be incorporated in the propellant; and the nature of the manufacturing process for the propellant. The desirable goal is the development of a theory of burning which would explain the effects of all these variables and enable the manufacturing chemist to produce a propellant for specific burning properties.

The objective of this investigation is to propose a theory for the over-all aspects of the burning process which can lead to theoretical expressions for the burning rate. The processes of chemical reaction and energy and mass

transport are occurring simultaneously during the burning process, and perhaps all with finite and different resistances. The basic problem is to combine these three rate processes in such a way as to allow for the proper significance of each.

Owing to the molecular complexity of the propellant system of fuel and oxidizer it is extremely difficult to determine the separate chemical reactions which, taken together, explain the sequence of steps that lead from reactants to final combustion products. The experimentation necessary for this resolution of the chemical kinetics of propellant burning has not been accomplished at present, nor is there any evidence to suggest that the evidence will be obtained in the near future. For example after a long period of study on double-base propellants (for example the colloidal mixtures of nitroglycerin and nitrocellulose used in guns) only the general nature of the first step in the combustion process has been reasonably well elucidated (1). Because of this situation it has been necessary in previous studies to make assumptions regarding both the nature of the chemical steps and their relative rates. This procedure is adopted in the theory proposed in the following sections. Hence the results apply only to the over-all results of the burning process and pretend no information about the mechanism of the chemical steps.

The model proposed for the over-all burning process attempts to account for all three transport steps. In principle it is not necessary to assume that either chemical reaction, energy, or mass transfer is the controlling feature of the process. A steady state solution of the equations provides this more

general solution. However the resultant burning-rate equation would perhaps be too complicated for useful application. As an illustration of the kind of specific expression that is possible from the theory the burning-rate equation is developed for the particular postulate that the mass transfer processes occur at close to equilibrium conditions.

A number of theoretical models of the burning process have been proposed in earlier investigations, particularly for the burning of double-base propellants. These results are briefly summarized in the following paragraphs.

PREVIOUS WORK

Geckler (6) has reviewed the unclassified experimental and theoretical work on burning colloidal and composite propellants up to about 1952 and included a list of references. Some of the most important theoretical contributions are those of Wilfong, Penner, and Daniels (11); Rice and Ginel (8); Parr and Crawford (7); Friedman and co-workers (5); Summerfield *et al.* (10); and Corner (3).

Wilfong, Penner, and Daniels (11) proposed that a solid-phase chemical reaction at the propellant surface was the controlling chemical step. Experimental burning-rate data show that pressure may have a strong effect. The coefficient ϵ in the empirical representation of the pressure effect

$$r = b p^{\epsilon} \quad (2)$$

may vary from 0 to 1.0. In the Wilfong theory the pressure does not affect the rate of the solid-phase reaction. Rice and Ginel (8) considered the burning rate to be controlled by a combination of the kinetics of the initial solid-phase reaction, the rate of heat transfer to the solid by conduction (erosive burning was not considered), the kinetics of the combustion processes in the gas phase, and diffusion from the surface to the bulk gas. This theory leads to results showing the burning rate to increase with pressure as shown by experiment. The magnitude of the pressure effect was dependent upon the order of the gas-phase reactions. Experimental burning-rate data can be correlated by the theory, although the resultant expressions are not convenient to use. The procedure used by Rice and Ginel di-

vides the gaseous burning region into several somewhat arbitrary zones and is based primarily upon observations of the flame zone in composite propellants by Crawford and co-workers (2, 4).

Parr and Crawford (7) used the same concept of successive chemical reactions occurring in different zones of the flame. Their treatment was made more general by reducing the assumptions pertaining to the position of each separate zone, but more restricted by neglecting diffusion. As in the work of Rice and Ginell, the results do not lead to usable expressions unless the processes in all but one zone are neglected.

Summerfield *et al.* (10) observed (by microphotography) the burning region using ammonium perchlorate propellants. Their interpretation was that the burning surface was dry and the gaseous reaction zone thin. From this it was concluded that chemical reactions at the solid surface did not occur. Rather it is supposed that the reactants stream from the surface unmixed and unreacted. Presumably the rate is controlled by the kinetics of the gaseous combustion reaction and diffusion and energy transfer in the boundary layer near the propellant surface. From these concepts empirical expressions for the burning rate are obtained for two extreme cases: diffusion resistances are negligible with respect to that of a second-order combustion reaction, and the reactions occur at near equilibrium conditions.

MODEL OF THE BURNING PROCESS

Rather than following the separate-zone concept of Rice and Ginell (8) it will be supposed that the significant combustion reactions are of two types. As in the theory of Wilfong, Penner, and Daniels (11) it is postulated that the primary, significant reaction is at the surface; however in contrast to their concept it is proposed that this reaction is between a gaseous molecule A and a solid substance C to form intermediate, gaseous products of combustion. Prior to this other physical and chemical changes may occur, such as melting or preliminary decomposition of the solid fuel. Nevertheless it is supposed that these prior steps do not exert an important effect on the rate of the over-all process. In formulating a rate equation for the over-all burning it is not necessary to describe in detail the nature of the gaseous and solid components reacting at the surface.

The second step is the conversion in the gas phase of the intermediate components into the end combustion products. The gas phase near the solid surface will be at a temperature much higher than that of the propellant surface because the greatest energy release will be for the final steps in the combustion process. The difference in temperature between the core of gas in the rocket motor and the propellant surface exists because of the large resistance to heat transfer in the gaseous

boundary layer next to the surface. Because of the relatively higher temperature of the gas phase near the propellant surface it is postulated that the second stage of the combustion occurs at conditions near equilibrium. Hence the kinetics of this second stage gaseous reaction are not important in establishing the rate of burning. The pressure effect on the rate must then originate from the kinetics of the first step, the heterogeneous reaction on the propellant surface. This concept differs in this respect from the theory of Summerfield *et al.* (10). On the other hand Friedman and co-workers (5) have proposed that the initial decomposition at the solid surface is the controlling step in the decomposition of pure ammonium perchlorate.

It may be observed that the postulated model of the chemical changes does not specify that the gaseous reactions constituting the second step occur in any particular zone away from the surface. Also since they occur at near equilibrium conditions, it is not important whether they take place as a set of successive reactions, parallel steps, or a combination of both.

The physical processes that take place simultaneously with the chemical steps complete the model. The first is the energy transfer to the solid surface as a result of the temperature difference between the core gas at T_c and the interface at T^* . In using a constant temperature T_c for the gas phase it is again supposed that essentially all the resistance to energy transfer occurs in the thin boundary layer of gas adjacent to the solid surface. The magnitude of this resistance will be affected by the thickness and turbulence in the boundary layer. It is in its effect on the heat transfer characteristics of the boundary layer that gas velocity parallel to the propellant surface (erosive burning) will be a significant variable.

The energy transferred to the propellant from the gas increases the temperature of a surface layer of propellant from its original temperature T_s to its reaction temperature T^* . As a consequence of this increase in solid temperature a fusion process may be involved, increasing the energy requirement. T^* is the temperature at which the initial chemical step occurs. Its value is fixed by the characteristics of the propellant (fuel-oxidizer ratio, kind and size of oxidizer crystals, etc.) and by the resistances of the other individual steps, both chemical and physical, that in combination result in the over-all combustion process. For a fixed system of propellant and rocket motor operating conditions T^* should not change. If the heat transfer coefficient between surface and gas changes during the burning process, owing for

example to a change in the velocity of core gas, or if the pressure changes, it is expected that T^* would likewise change.

While it is not essential to describe specifically the nature of the components taking part in the surface reaction, it is necessary to postulate how the oxidizing component A is formed. Two possibilities exist: A may be formed at the burning surface by decomposition of the oxidizer, or if A is an intermediate product of combustion, it will be transferred to the burning surface through the boundary layer of gas in the same way as the energy transfer occurs. If A is formed at the surface, its rate of formation does not affect the burning rate because the process is postulated to occur near equilibrium conditions. If A is transferred from the core gas through the boundary layer, a diffusional resistance may be introduced. This is identified in the list of rate equations for the individual steps formulated in the next section.

RATE EQUATIONS FOR INDIVIDUAL STEPS

1. Energy Transfer to Propellant Surface

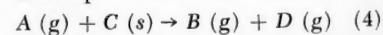
The rate of energy transfer from the core gas to the propellant surface per unit area per unit time may be written as

$$q = h (T_c - T^*) \quad (3)$$

The heat transfer coefficient represents the result of the combination of conduction, convection, and radiation contributions to the energy transfer. Its value increases with the velocity of the core gas parallel to the propellant surface.

2. Mass Transfer of Component A to Propellant Surface

The burning rate will be formulated first in terms of the mass of propellant component C which reacts per unit area per unit time, that is m_c . Species C is the fuel component which reacts with gaseous A in the primary combustion step



If A reaches the solid surface from the core gas, its rate of transfer per unit area of propellant surface is given by the diffusion expression

$$m_A = k_A (p_g - p_{A_i}) \quad (5)$$

In accordance with Equation (4) the molal rates of disappearance of A(g) and C(s) are equal. Hence the mass burning rate of component C is related to m_A by the ratio of the molecular weights:

$$m_c = m_A \frac{M_c}{M_A} = \frac{M_c}{M_A} k_A (p_g - p_{A_i}) \quad (6)$$

3. Effect of Energy Transfer on the Propellant

The energy transfer rate to the propellant surface is related to the disposition of the energy in the solid by

$$q = [\Delta H + C_p(T^* - T_s)] \quad (7)$$

If n_c is the mass fraction of C in the solid propellant, Equation (7) may be written in terms of m_c :

$$q = \frac{m_c}{n_c} [\Delta H + C_p(T^* - T_s)] \quad (8)$$

Equation (8) takes into account possible fusion of parts of the propellant prior to the primary reaction by considering ΔH to be the heat of fusion plus heat of primary reaction per total mass of propellant.

4. Primary Chemical Reaction at Propellant Surface

The burning rate in terms of the disappearance of C may be formulated according to the kinetics of the surface reaction between gaseous A and solid C [Equation (4)]. If the activation energy for this primary chemical step is E , the rate is

$$m_c = M_c \gamma C_s P_{A1} e^{-E/RT^*} \quad (9)$$

The concentration of active centers for reaction on the solid surface is designated as C_s . The value of C_s is dependent upon the specific propellant and how it is produced. However C_s should be constant during the burning process.

5. Diffusion of Products of Primary Combustion

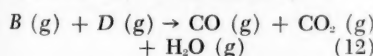
The components B (g) and D (g) produced in the surface reaction [Equation (4)] diffuse out into the core gas. The mass rates of these processes in terms of m_c are

$$m_c = M_c k_B (P_{B1} - P_{Bp}) \quad (10)$$

$$m_c = M_c k_D (P_{D1} - P_{Dp}) \quad (11)$$

6. Secondary Combustion in the Gas Phase

The secondary combustion reactions are postulated to occur in the core gas at a relatively high temperature. The reactions may be illustrated by



+ other final combustion products

At the elevated temperature these reactions take place at near equilibrium conditions, so that their kinetics are unimportant in formulating the burning rate.

BURNING-RATE EQUATIONS

An expression for the burning rate m_c can be obtained in terms of initial and final quantities by combining the

equations for rates of the individual steps as listed in the preceding section. At steady state burning the rates of all the steps are equal. Hence Equations (3), (6), (8), (9), (10), and (11) form a group of simultaneous equations which may be used to eliminate the intermediate and nonmeasurable quantities, such as T^* , q , P_{A1} , etc. However this steady state solution method leads to a complicated result not readily usable. Useful expressions can be obtained by considering some of the individual steps to be of negligibly low resistance with respect to the others. This procedure can lead to a large number of distinct expressions for the burning rate, each based upon a particular choice for the set of individual steps which control the over-all process. Provided sufficient experimental data are at hand, it is possible in principle to test the various suppositions.

It is not the aim here to develop and test a number of separate equations for the burning rate. The chief objective is to illustrate how the proposed model can be employed to determine burning-rate equations. As experimental data accumulate concerning the detailed characteristics of the combustion process, it should be possible to draw conclusions about the significance of individual steps in the over-all process. At present one choice of controlling steps will be assumed and the resultant equation compared with observed rate data.

Because it seems well established that the mass velocity of core gas affects the rate, and also that the original propellant temperature exerts a small effect, steps 1 and 3 in the previous section will be considered significant. It will also be supposed that the diffusion of reactant A and its rate of reaction at the propellant surface are important steps in determining the burning rate. The diffusion of the products and the secondary combustion will be assumed to take place at near equilibrium conditions.

Under these conditions Equations (3), (6), (8), and (9) define the rate. Eliminating q from Equation (3) and (8) one gets for T^*

$$T^* = \frac{h T_p + \frac{m_c}{n_c} (C_p T_s - \Delta H)}{h + \frac{m_c}{n_c} C_p} = \frac{h T_p + r \rho (C_p T_s - \Delta H)}{h + r(\rho C_p)} \quad (13)$$

where Equation (1) has been utilized to introduce the linear burning rate.

The partial pressure of A at the solid surface may be obtained from Equation (6) and used in Equation (9) to obtain m_c in terms of the bulk partial pressure of A. This latter quantity is equal to the total pressure multiplied by the mole fraction of A in the core gas. The product $p y_A$ should be constant during the burning process but a function of the propellant composition and perhaps the oxidant grain size. With these concepts Equations (6) and (9) yield

$$r = \gamma C_s \frac{y_A}{n_c \rho} \left[p - \frac{M_A n_c \rho}{M_c y_A k_A} r \right] e^{-E/RT^*} \quad (14)$$

In the formulation of Equation (14), the linear burning rate is again substituted for m_c through Equation (1).

Equations (13) and (14) determine the burning rate as a function of the parameters of the system. The transport coefficients h and k_A are affected by the conditions of the gas boundary layer at the surface and would increase with core-gas velocity, as in erosive burning. The core-gas temperature is very nearly the adiabatic flame temperature for the propellant. The quantities ΔH , C_p , ρ , n_c , y_A , and the activation energy are properties of the propellant. The surface-kinetics constants γC_s and E depend upon the propellant system and the characteristics of its manufacture, for example oxidant grain size.

Equation (14) is simplified considerably if either the diffusion of A to the solid surface occurs at near equilibrium conditions, or it is postulated that A arises from preliminary decomposition processes at the surface. In either case Equation (14) becomes

$$r = \frac{\gamma C_s y_A}{n_c \rho} p e^{-E/RT^*} = I p e^{-E/RT^*} \quad (15)$$

The quantity I is composed of factors, $\gamma C_s y_A / n_c \rho$, which are invariant during the burning but dependent upon the nature of the fuel and oxidizer, their composition, and the physical characteristics (grain size, etc.) of the composite propellant charge.

Examination of Equation (15) indicates that the rate should be directly proportional to the pressure except as modified by the variation of T^* with pressure. At low pressures the rate will

TABLE I. AMMONIUM PERCHLORATE PROPELLANT DESCRIPTIONS (10)

Oxidizer Wt. %	Particle size, μ	Values of parameters in Equation (15)	
		E , cal./g. mole	I , cm./ (atm. sec.)
75	16	11,400	7.7
75	120	8,000	3.1
80	16	14,800	154.0
80	120	10,800	19.3

be low, and T^* , according to Equation (13), will be high, with T_s as an upper limit. Conversely at high pressures, where the rate is high, T^* will be dominated by the second term in Equation (13). It will have a low value, approaching $(T_s C_p - \Delta H)/C_p$ as a limit. The net result is that the rate will increase rapidly with pressure at low values and more slowly at high pressures. This is in agreement with observed data and with the widely used empirical expression [Equation (2)].

Experimentally it has been found by Green and co-workers (9) that the phenomenon of erosive burning is more pronounced at low burning rates than high ones. In the proposed theory the effect of erosive burning is due to the influence of the heat transfer coefficient on T^* in Equation (13). An increase in h results in an increase in T^* and hence an increase in burning rate according to Equation (15). The magnitude of this effect will be larger the lower the rate and therefore the smaller the second term in the numerator and denominator of Equation (13) in comparison with the first. Finally the effect of initial temperature of propellant is to increase the value of T^* in Equation (13). This in turn results in an increased rate.

COMPARISON WITH EXPERIMENTAL DATA

Because of the large number of parameters involved it is not difficult to fit burning-rate data for various propellants with Equations (13) and (14) or even (13) and (15). More critical tests of the theory are whether the predictions of the effects of important variables are correct as described in the previous section, and whether the values of the parameters needed to fit the equations to the data are realistic.

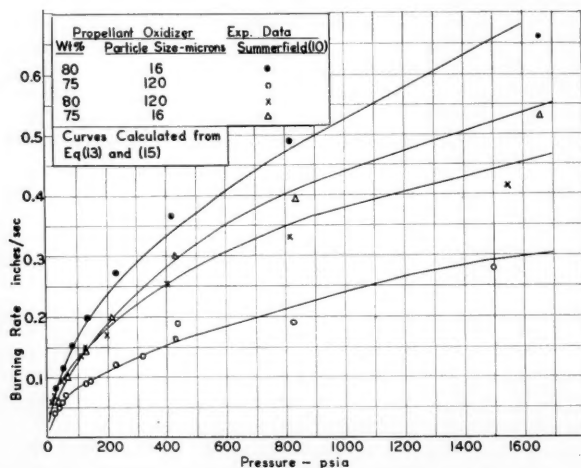


Fig. 1. Burning rates of ammonium-perchlorate propellants.

Effect of Pressure and Temperature

Geckler (6) presented burning-rate data for an asphalt-potassium perchlorate propellant containing 76.5 wt. % oxidizer. Its density was 1.77 g./cc. and the flame temperature 2,040°K. At 15°C. ($T_s = 288^\circ\text{K.}$) the observed pressure effect on the burning rate could be represented by

$$r = 0.103 p^{0.715} \quad (p = 100 \text{ to } 200 \text{ atm.}) \quad (16)$$

The best estimates of available information suggest a value of $C_p = 0.35$ cal./g. °C. The data correlated by Equation (16) were obtained from firings of rocket motors by means of cigarette-burning grains of propellant. Hence the mass velocity of gases past the surface was not as large as in burning solid charges of propellant in a rocket motor. Therefore the heat transfer coefficient between gas and propellant surface would be somewhat, but not greatly, larger than the value corresponding to no flow of gas past the surface. A value of $h = 8.0 \times 10^{-2}$ cal./(sec.) (sq. cm.) (°C.) was chosen to use in Equation (13). Under these conditions Equations (13) and (15) fit the data [Equation (16)] with the following values for the other parameters: $\Delta H = -200$ cal./g., $E = 14,900$ cal./g. mole, and $I = 1.23 \times 10^6$ cm./ (atm.) (sec.).

The temperature of the burning surface obtained from Equation (13), is slightly dependent upon the pressure but is in range 880° to 900°K. from 100 to 211 atm. The melting point of pure potassium perchlorate is about 883°K.

Equation (16) can be represented by other sets of values for the parameters than those listed. The specific choice was made on the basis that the numbers should be realistic. For the

same propellant Geckler (6) presents data on the effect of initial temperature of propellant on the rate. The approximate result is given in the form

$$\frac{d \ln r}{dT_s} = 0.013 \quad (17)$$

Equations (13) and (15), with the given values for the parameters, predict a somewhat greater increase in rate with T_s than Equation (17). The predicted value of the constant in Equation (17) is about 0.005 to 0.006 or about the same as observed for colloidal propellants (2).

Summerfield *et al.* (10) measured burning rates of ammonium perchlorate-styrene polyester propellants over the pressure range 14.7 to 2,000 lb./sq. in. abs. The measurements were obtained in a bomb with square strands of propellant. Data were observed for four mixtures containing different weight fractions and particle sizes of oxidizer as shown in Table 1.

Since there was no forced motion of the combustion gases in the apparatus, the heat transfer coefficient would be considerably lower than would exist in an actual rocket motor and somewhat less than employed in analyzing the data for the potassium perchlorate-asphalt propellant. For comparison of Equation (13) and (15) with Summerfield's data a value of $h = 3.0 \times 10^{-2}$ cal./(sec.) (sq. cm.) (°C.) was employed. The flame temperature was measured and found to be about 2,670°K. Information was not given about the other conditions, so that the following values were employed: $T_s = 298^\circ\text{K.}$, $\rho = 1.8$ g./cc., and $C_p = 0.45$ cal./g. °K.

The initial heat effect would probably not involve a heat of fusion, since the melting point of ammonium perchlorate is high (1,200°K.). However the heat evolved in the initial decomposition reactions might well be higher. In the computations ΔH was taken as -200 cal./g., the same as for the po-

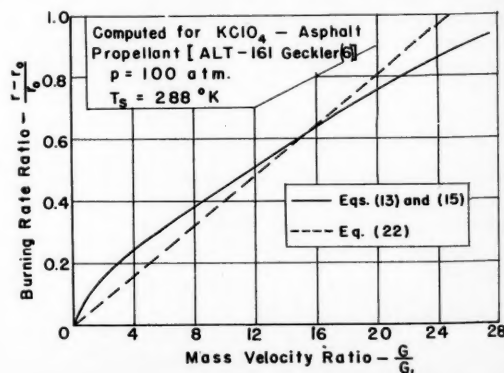


Fig. 2. Effect of gas velocity on burning rate (erosive burning).

tassium perchlorate—asphalt propellant.

Since temperature-coefficient data were not obtained, it was not possible to check the suitability of the values proposed for C_p and ΔH . However the pressure vs. rate data did permit the determination of values of E and I , which along with the chosen numbers for the other parameters best fit the data. These values are given in the last two columns of Table 1. The computed burning rate vs. pressure curves are compared with the experimental measurements in Figure 1. It is seen that some of the curves cross at low pressures. This explains the lack of systematic variation in the activation energy and the modified frequency factor I . However, as in the case of the data of Geckler, it is clear that Equations (13) and (15) can show a pressure effect that is in agreement with experiment. Chemical significance cannot be attached to the free-energy and frequency-factor numbers in Table 1 because of the complexity of combustion at the solid surface. Stated differently, the model used in developing Equations (13) and (15) is much too simple to be true in detail. All that can be said is that such a model leads to predictions that in an over-all sense (burning rates vs. pressure) agree with observation.

Effect of Gas Velocity

The numerical magnitude of the effect of heat transfer rate on the burning velocity can be evaluated from Equations (13) and (15) by considering variations in h . If the heat transfer coefficient is related to the mass velocity, the significance of erosive burning results. Such computations were carried out for the potassium chlorate propellant studied by Geckler (6).

Since potassium perchlorate gives high burning rates, the effect of erosive burning would not be as important for this propellant as for some others. Nevertheless increasing the mass velocity should increase the burning rate for any propellant, although the effect may be small in some instances. Using the property values given previously for the asphalt-potassium perchlorate propellant one can compute the rate from Equations (13) and (15) for various values of h , as shown in Table 2. Heat transfer coefficients for turbulent flow in tubes have been found to be proportional to the 0.8 power of the mass velocity. When one assumes this relationship, the heat transfer coefficient can be written in terms of G by

$$h = h_0 + a G^{0.8} \quad (18)$$

The quantity h_0 is the coefficient at zero velocity and hence represents pri-

TABLE 2. EFFECT OF GAS MASS VELOCITY ON BURNING RATE FOR PROPELLANT ALT-161 [GECKLER (6)]

h , cal./ (sec.) (sq. cm.) (°K.)	G/G_0 , mass velocity ratio calculated from Equa- tion (20)	r , cm./sec.	$\frac{r-r_0}{r_0}$
0.030	0	2.54	0
0.046	1	2.80	0.10
0.080	4.1	3.19	0.25
0.139	11.1	3.75	0.48
0.193	18.3	4.36	0.71
0.242	25.2	4.80	0.89

marily the contribution of radiation and natural convection to the energy-transfer rate. The value of h found to correlate the experimental data of Geckler (6) in rocket motors was 0.08 cal./ (sec.) (sq. cm.) (°K.). As noted previously the velocity was not large in these measurements. Therefore h_0 will be chosen a small amount less than this value and the same as h_0 used with Summerfield's data; that is $h_0 = 0.03$. Applying Equation (18) at two mass velocities and dividing gives

$$\frac{h-h_0}{h_1-h_0} = \left(\frac{G}{G_1} \right)^{0.8} \quad (19)$$

Choosing $h_1 = 0.046$, the second value in Table 2, one may obtain the heat transfer coefficient at any mass velocity from

$$\frac{h-0.030}{0.046-0.030} = \left(\frac{G}{G_1} \right)^{0.8} \quad (20)$$

The ratio G/G_1 is plotted in Figure 2 vs. the burning-rate ratio $(r-r_0)/r_0$. The curve shows that the rate increases rapidly at low values of G and more slowly at high velocities. This is to be expected, since the burning rate is influenced less by the resistance to energy transfer as this resistance decreases, that is as the velocity increases.

A common empirical means of correlating erosive burning data is the expression (9)

$$\frac{r-r_0}{r_0} = k \frac{G}{G^*} \quad (21)$$

This equation may be written

$$\frac{r-r_0}{r_0} = \left(\frac{k G_1}{G^*} \right) \frac{G}{G_1} \quad (22)$$

Plotted on the coordinates used in Figure 2, Equation (22) suggests a linear relationship as illustrated by the dotted line, when one assumes that the erosion constant does not change. The theoretical curve in Figure 2 appears preferable to the empirical dotted line, since the effect of erosion should decrease at higher mass velocities.

Stated differently, the erosive constant should decrease as the velocity increases.

CONCLUSION

A theory of burning of solid propellants has been presented which agrees with the observed effects of measurable properties upon the burning rate. However without detailed and exacting experimental studies of the several stages in the over-all combustion process it is hazardous to draw conclusions about the mechanisms involved. Hence the proposed, simple model is best regarded as a basis for developing rate equations and correlating burning-rate data.

ACKNOWLEDGMENT

Permission of the Jet Propulsion Laboratory, California Institute of Technology, to publish this work is appreciated.

NOTATION

- $A(g)$, $C(s)$, $B(g)$, $D(g)$ = components of the primary surface reaction
 C_p = specific heat of the solid propellant, cal./g. °K.
 C_s = concentration of active centers on surface of propellant, g./sq. cm.
 E = activation energy for primary surface reaction, cal./g. mole
 G = mass velocity of core gas, g./sq. cm. sec.
 G^* = mass velocity corresponding to Mach number = 1.0
 h = heat transfer coefficient between core gas and propellant surface, cal./sq. cm. sec. °K.
 ΔH = heat of fusion plus heat of reaction for primary surface reactions per unit mass of propellant, cal./g.
 I = constant during burning equal to $(\gamma C_s y_A)/(n_c \rho)$, cm./ (atm.) (sec.)
 k_A = mass transfer coefficient for component A, g./ (sec.) (sq. cm.) (atm.)
 k = erosion coefficient, defined by Equation (21)
 M = molecular weight
 m = mass burning rate, g. of propellant/sec. sq. cm.
 m_c = mass burning rate of component C of propellant, g. of C/sec. sq. cm.
 n_c = mass fraction of component C in propellant
 p = total pressure, atm.
 p_A = partial pressure of component A, atm.
(subscript g denotes the core gas; i denotes the solid surface)

q = rate of energy transfer to propellant surface, cal./sec. sq. cm.
 R = gas constant, cal./g. mole °K.
 r = linear burning rate, cm./sec.; r_0 = burning rate at zero gas velocity
 T^* = temperature of primary reaction (propellant surface temperature during burning, °K.)
 T_i = initial temperature of propellant, °K.
 T_g = temperature of core gas during burning, °K.
 y_A = mole fraction A in gas phase
 ϵ = pressure coefficient in empirical burning rate, Equation (2)
 γ = frequency factor in Arrhenius' representation of chemical rate equation
 ρ = density of solid propellant, g./cc.

Subscripts

A, B, D = components in the primary surface reaction
 g = core gas
 i = gas-solid interface

LITERATURE CITED

1. Adams, G. K., and L. A. Wiseman, "The Combustion of Double-Base Propellants," p. 275, Butterworth's Scientific Publications, London, England (1954).
2. Crawford, B. L., C. Huggett, F. Daniels, and R. E. Wilfong, *Anal. Chem.*, **19**, 630 (1947).
3. Corner, J., *Trans. Faraday Society*, **43**, 635 (1947).
4. Crawford, B. L., C. Huggett, and J. J. McBrady, *J. Phys. Chem.*, **54**, 854 (1950).
5. Friedman, N., R. G. Nugent, K. E. Pimbel, and A. C. Scurlock, "Deflagration of Ammonium Perchlorate,"

- p. 612, Reinhold, New York (1956).
6. Geckler, R. E., "The Mechanism of Combustion of Solid Propellants," p. 289, Butterworth Scientific Publications, London, England (1954).
 7. Parr, R. G., and B. L. Crawford, *J. Phys. Chem.*, **54**, 929 (1950).
 8. Rice, O. K., and R. Ginell, *ibid.*, **54**, 885 (1950).
 9. Schultz, R., L. Green, and S. S. Penner, "Combustion Reviews (AGARD)," Butterworth Scientific Publications, London, England (1958).
 10. Summerfield, M., G. S. Sutherland, M. J. Webb, H. J. Taback, and K. P. Hall, paper presented at 13th Annual Meeting American Rocket Society, New York (November, 1958).
 11. Wilfong, R. E., S. S. Penner, and F. Daniels, *J. Phys. Chem.*, **54**, 863 (1950).

Manuscript received June 1, 1959; revision received October 26, 1959; paper accepted October 28, 1959. Paper presented at A.I.Ch.E. Atlanta meeting.

Continuous-Throughput Rectification of Organic Liquid Mixtures with Thermal-Diffusion Columns

DAVID R. LONGMIRE

University of Wisconsin, Madison, Wisconsin

Experiments were carried out with cylindrical thermal-diffusion columns in which the separation chambers were sufficiently narrow so that curvature effects might be ignored. For both open and closed operation, results were obtained for the two binary systems benzene-carbon tetrachloride and *n*-heptane-benzene as well as the ternary mixture *n*-heptane-methylcyclohexane-toluene. For the binary systems, correlations are given in terms of dimensionless combinations which arise when the equations of conservation are placed in dimensionless form. The thermal-diffusion coefficients used in the correlations are literature values determined in steady-state-cell (no convection) measurements.

The historical background of thermal diffusion has been covered by Powers and Wilke (1). Except for the many steady-state-cell experiments (no convection), studies with liquids generally have been confined to the vertical or inclined countercurrent thermal-diffusion column conceived by Clusius

and Dickel (2). Although for continuous throughput the product positions on a Clusius-Dickel column are usually at the extremities, with the feed position at an intermediate point, recent arrangements by A. L. Jones and his associates (3 to 12) include concurrent flat-plate columns operated vertically or horizontally with or without membranes as well as apparatus

with porous walls. Studies have been reported recently on the Clusius-Dickel column operated with packing as well as centrifugal force (13, 14).

In addition to the work of Powers and Wilke (1), the principal quantitative investigations covering thermal-diffusion columns operated with a continuous throughput have been those of Heines, Larson, and Martin (15) and

David R. Longmire is with Texas Butadiene and Chemical Corporation, Channelview, Texas.

Thomas and Watkins (16, 17). The former have contributed a large number of data for the system *n*-heptane-benzene, and their results have been expressed in terms of a dimensionless group $FL/4K_c$, which appears in the earlier theoretical developments of Furry, Jones, and Onsager (18). The thesis by Heines (19) was the first experimental study on continuous-throughput operation for liquids presented as a dimensionless-group correlation. The study of Powers and Wilke (1) was carried out with the system ethanol-water as well as *n*-heptane-benzene. Variables examined were feed rate, length of column, wall spacing, temperature difference between walls, and the angle of inclination of the apparatus, which was of the flat-plate type. By extrapolation to zero throughput of curves describing the difference of top and bottom product concentrations vs. throughput constants H and K_c for the Furry, Jones, and Onsager (18) equations were determined. Curves then calculated from the equations were generally in good agreement with experimental results. The failure of the equations at high throughputs led Powers and Wilke (1) to a novel theory modification which assumes a linear variation of vertical concentration gradient with the horizontal cartesian coordinate. Thomas and Watkins (17) have presented the first experimental results for continuous-throughput operation of thermal-diffusion columns with concentrated mixtures of ternary gaseous mixtures.

For binary systems this study differs from previous ones in several respects, essentially, in the thermal-diffusion coefficients utilized in the correlations, in the method of developing the correlations, and in the correlations themselves. In view of the disagreement between thermal-diffusion coefficients determined from column experiments (20 to 23) and those arising from steady state thermal-diffusion-cell experiments without convection (24, 25, 26), coefficients which have resulted from steady-state-cell measurement, a more fundamental type of determination, have been used in the correlations. The binary systems benzene-carbon tetrachloride and *n*-heptane-benzene were selected because of the availability of data on ordinary diffusion (27, 28) and thermal-diffusion coefficients (24, 26). On account of the many assumptions in the classical derivation of Furry, Jones, and Onsager (18); Waldmann (29); and de Groot (30) and in the more recent modification of Powers and Wilke (1), quantitative expressions more general in application were sought. The unintegrated dimensionless equation of mass con-

servation revealed the dimensionless groups and combinations thereof for treatment of operating data.

The study of ternary systems was intended for observation of continuous throughput operation with concentrated solutions for which a composition analysis for each component could be made. Previous investigations for concentrated three-component liquid mixtures are the closed-column experiments of Jones and Milberger (31) as well as of Begeman and Cramer (32).

THEORETICAL CONSIDERATIONS

Fundamental Theoretical Expressions

The theoretical relations are founded on the partial-differential equations of fluid mechanics which describe the

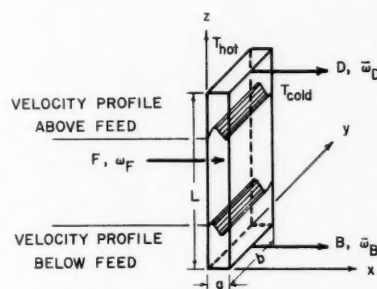


Fig. 1. Vertical flat plate, open thermal-diffusion column.

laws of conservation of mass, momentum, and energy. The nomenclature for the equations, fluxes, and transport coefficients is not given here, but it is identical to that in the review article by Bird (33). The coordinate arrangement is the three-dimensional, orthogonal system of Figure 1.

Application to the Vertical,

Countercurrent Thermal Diffusion Column

Physical problem. The column consists of two flat plates, one at a high temperature and one at a low temperature, as described by Figure 1. Both plates of vertical length L and horizontal length b are spaced parallel to each other with a horizontal separation a . The quantity ω is the mass fraction of that component in a binary mixture which migrates toward the hot wall and the top of the column. The definition of $\bar{\omega}$ is

$$\bar{\omega} = \frac{1}{ab} \int_0^b \left[\int_0^a \omega dx \right] dy \quad (1)$$

Before beginning the dimensional analysis of the equations of change, the author omits some of the terms according to the following physical assumptions:

1. Steady state, realized experimentally
2. No chemical reaction, realized experimentally
3. Laminar flow, realized experimentally
4. Pressure and external force diffusion absent, realized experimentally
5. No viscous heat effects, negligible effects at low velocities
6. Insignificance of Dufour effects, radiation heat flux, and flux due to intrinsic energy carried by diffusing species
7. $p = p(z)$
8. $T = T(x)$
9. No variations in the y direction

The Dufour effect is neglected for lack of a descriptive expression as well as the probability that it is small (33). The equation for radiation heat flux is valid only if the flux is in equilibrium with the matter, a prerequisite which usually does not exist (33). This energy flux has been ignored in the past and is not accounted for here. Intrinsic energy carried by diffusing species is discussed in the application of the equation of energy balance in the analysis of the final correlations. The significance of its effect is not known (34).

Dimensionless relations. When analytical solutions of the partial differential equations of fluid mechanics are not easily found, the equations and their boundary conditions can serve as a guide to physical behavior. In the examination of the conservation equations Schlichting's (35) procedure for handling problems in fluid mechanics has been applied. The equations of change and their boundary conditions are placed in dimensionless form, and the resulting dimensionless groups of physical quantities are noted. The groups are the coefficients of the dimensionless derivatives and of other variable terms in the equations of change and their boundary conditions. These dimensionless groups of physical quantities are parameters of any analytical solution to the dimensionless equations of change, no matter how difficult that solution might be.

Above the feed point dimensionless variables are defined as follows:

$$\begin{aligned} x^* &= x/a & \omega^* &= \frac{\omega - \omega_F}{(\omega_D - \omega_F)_{ce}} \\ z^* &= z/L \\ T^* &= \frac{T - T_{cold}}{T_{hot} - T_{cold}} & v_z^* &= v_z / (v_{av})_D \end{aligned} \quad (2)$$

Although such a procedure is not entirely sound, for simplicity μ , D_{12} , D_{13} , ρ , and β are assumed constant. In

open-column operation above the feed point

$$(v_{av})_D = \frac{1}{a} \int_0^a (v_z)_D dx \quad (3)$$

A similar relation would define $(v_{av})_B$ below the feed point. For closed-column cases above the feed point

$$\lim_{D \rightarrow 0} (v_{av})_D = \lim_{D \rightarrow 0} \frac{1}{a} \int_0^a (v_z)_D dx \quad (4)$$

with $(v_{av})_B$ being defined by a like relation below the feed point. Dimensionless numbers are formulated as follows:

$$(N_{Re})_D = \frac{a(v_{av})_D}{\mu} \rho \text{ Reynolds number}$$

$$N_{Gr} = \frac{a^3 \rho^2 \beta g \Delta T}{\mu^2} \text{ Grashof number}$$

$$N_{Sc} = \frac{\mu}{\rho D_{12}} \text{ Schmidt number}$$

$$N_a = \frac{T_{av} D_{12}}{D_{12}} \text{ Thermal-diffusion factor}$$

$$N_{\Delta T} = \frac{\Delta T}{T_{av}} \quad (5)$$

The quantity T_{av} denotes the arithmetic mean temperature of the hot and cold walls, and ΔT is $T_{hot} - T_{cold}$.

For the given assumptions the equations of change and their boundary conditions have been set down by others (1, 18, 20, 30) and are repeated here in dimensionless form. The equation of energy conservation is

$$\frac{d^2 T^*}{dx^{*2}} = 0 \quad (6)$$

with boundary conditions

$$\begin{aligned} T^* &= 1 \quad \text{at } x^* = 0 \\ T^* &= 0 \quad \text{at } x^* = 1 \end{aligned} \quad (7)$$

The equation of momentum conservation can be simplified to

$$\frac{d^2 (v_z^*)_D}{dx^{*2}} = - \frac{N_{Gr}}{(N_{Re})_D} \quad (8)$$

for which the boundary conditions are

$$\begin{aligned} (v_z^*)_D &= 0 \quad \text{at } x^* = 0, 1 \\ \int_0^1 (v_z^*)_D dx^* &= 0 \quad \int_0^1 (v_z^*)_D dx^* = 1 \end{aligned}$$

closed column open column

The equation of mass conservation becomes

$$[v_z^*(x^*)]_D \frac{\partial \omega^*}{\partial z^*}$$

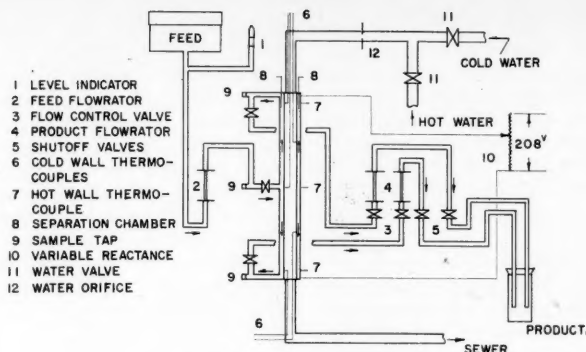


Fig. 2. Process flow scheme.

$$\begin{aligned} &= \frac{1}{(N_{Re})_D N_{Sc} N_{a/L}} \frac{\partial^2 \omega^*}{\partial x^{*2}} \\ &+ \frac{N_{a/L}}{(N_{Re})_D N_{Sc}} \frac{\partial^2 \omega^*}{\partial z^{*2}} \\ &+ \frac{N_a N_{\Delta T}}{(N_{Re})_D N_{Sc} N_{a/L}} \frac{\partial \omega^*}{\partial x^*} \\ &\{1 - 2[(\bar{\omega}_D - \omega_F)_{cc} \omega^* + \omega_F]\} \frac{\partial \omega^*}{\partial x^*} \end{aligned} \quad (10)$$

$$\begin{aligned} &= \left[f_1^*(x^*) + \frac{(N_{Re})_D}{N_{Gr}} f_2^*(x^*) \right] \frac{\partial \omega^*}{\partial z^*} \\ &= \frac{1}{N_{Gr} N_{Sc} N_{a/L}} \frac{\partial^2 \omega^*}{\partial x^{*2}} \\ &+ \frac{N_{a/L}}{N_{Gr} N_{Sc}} \frac{\partial^2 \omega^*}{\partial z^{*2}} + \frac{N_a N_{\Delta T}}{N_{Gr} N_{Sc} N_{a/L}} \frac{\partial \omega^*}{\partial x^*} \\ &\{1 - 2[(\bar{\omega}_D - \omega_F)_{cc} \omega^* + \omega_F]\} \frac{\partial \omega^*}{\partial x^*} \end{aligned} \quad (13)$$

and has the boundary conditions

$$\begin{aligned} &\frac{\partial \omega^*}{\partial x^*} + \left[\omega^* + \frac{\omega_F}{(\bar{\omega}_D - \omega_F)_{cc}} \right] \\ &\{1 - [\omega^*(\bar{\omega}_D - \omega_F)_{cc} + \omega_F]\} \\ &N_a N_{\Delta T} = 0 \quad \text{at } x^* = 0, 1 \end{aligned} \quad (11)$$

$$\begin{aligned} &\frac{\bar{\omega}_D - \omega_F}{(\bar{\omega}_D - \omega_F)_{cc}} = \frac{\omega_F}{(\bar{\omega}_D - \omega_F)_{cc}} \\ &(-1 + \int_0^1 \omega^* v_z^* dx^*) + \int_0^1 \omega^* v_z^* dx^* \\ &- \frac{N_{a/L}}{(N_{Re})_D N_{Sc}} \int_0^1 \frac{\partial \omega^*}{\partial z^*} dx^* \\ &\text{at } z^* = 1 \\ &\omega^* = 0 \quad \text{at } z^* = z_F^* \end{aligned}$$

above the feed point.

Solutions to the equations of energy and momentum conservation, Equations (6) and (8), have been established by previous investigators (1, 18, 20, 30), although not explicitly in this nomenclature. The integration of Equation (6) gives a linear variation of T with x . Above the feed point the solution for Equation (8) and its boundary conditions (9) becomes

$$[v_z^*(x^*)]_D = \frac{N_{Gr}}{(N_{Re})_D} f_1^*(x^*) + f_2^*(x^*) \quad (12)$$

Although Equation (8) can easily be integrated, the general expression, Equation (12), suffices for this illustration. Substitution of Equation (12) for $[v_z^*(x^*)]_D$ in Equation (10) gives

For Equation (13) and its boundary conditions (11) an analytical solution of the form $\omega^* = \omega^*(x^*, z^*)$ is difficult because of the nonlinearity of both the partial differential equation and its boundary conditions. Although they have been carried through with ingenuity (1, 18, 29, 30), existing solutions are approximate and of the form $\omega^* = \omega^*(z^*)$.

With $N_{a/L}$ being of the order 10^{-3} , terms with coefficients of $(N_{a/L})/(N_{Gr} N_{Sc})$ were neglected in accordance with Schlichting's procedure for comparing dimensionless terms (35). Then any solution to Equation (13) and its boundary conditions must be a relation of the following type:

$$\begin{aligned} \omega^* &= \omega^* \left[x^*, z^*, \frac{\bar{\omega}_D - \omega_F}{(\bar{\omega}_D - \omega_F)_{cc}}, \right. \\ &\left. (\bar{\omega}_D - \omega_F)_{cc}, \omega_F, \frac{(N_{Re})_D}{N_{Gr}}, \right. \\ &\left. N_a N_{\Delta T}, \frac{N_a N_{\Delta T}}{N_{Gr} N_{Sc} N_{a/L}} \right] \end{aligned} \quad (14)$$

Actually when physical properties of liquids in the column vary to some extent as they did here, particularly on the z axis, these properties might be described as dimensionless variables with boundary conditions corresponding to $\rho_D, \rho_F, (D_{12})_D$, etc. Then dimensionless ratios such as ρ_D/ρ_F , etc., would become parameters of a solution to the dimensionless equations of

TABLE 1. BINARY SYSTEMS—OPERATING DATA FOR CLOSED COLUMN RUNS

System	Run	T_{av} , °C.	ΔT , °C.	L , cm.	a , cm.	$\bar{\omega}_D$	$\bar{\omega}_B$	ω_F
$C_6H_6-CCl_4$	I-C-2	39.8	33.5	183	0.043	0.968	0.004	0.337
	I-C-7	40.1	34.6	183	0.079	0.523	0.175	0.337
	I-C-9	40.2	34.3	36.6	0.079	0.930	0.899	0.903
$nC_7-C_6H_6$	II-C-1	33.5	36.0	183	0.043	0.965	0.004	0.577
	II-C-2	38.9	37.8	36.6	0.079	0.609	0.540	0.549

change. The experimental data have been examined only with the aid of the groups incorporated in Equation (14). The group $N_a N_{\Delta T} / (N_{Gr} N_{Re} N_{a/L})$ multiplied by $9! / 6!$ is identical with the quantity HL/K_c , which results from an integration of the Furry, Jones, and Onsager (18) transport equation for the vertical closed column in the steady state with longitudinal diffusion neglected.

EXPERIMENTAL WORK

Experimental Apparatus

Thermal-diffusion column. The column consisted of two concentric tubes. Except for physical dimensions, it was similar to the multiple port device described by Jones and Milberger (31), the annulus between the two tubes serving as the separation chamber. The tubes were of 304 stainless steel and formed a separation chamber 183 cm. in length. Annulus width, varied by use of alternate inside tubes, was either 0.043 or 0.079 cm. The outside tube was equipped with iron-constantan thermocouples, one at the center and one near each extremity of the tube. A nichrome heating element was wrapped on the outside tube, the inside wall of which served as the hot wall of the annulus. Each of the two tubes which could be used as the inside tube was equipped with five copper-constantan thermocouples installed at equal intervals in the tube wall as shown in Figure 2.

Cooling. The inside wall of the annular space was maintained at lower temperatures than the hot wall by cold water

passing in turbulent flow through one of the two center tubes available for this purpose. The temperature of the cold water could be varied by mixing it with hot water.

Feed and product lines. From the feed reservoir copper tubing led through a rotameter and stainless steel needle valve into one of the column ports. The two ports at the extremities of the column served as product ports to which copper tubing lines were connected. The product lines each led through stainless steel needle valves to upper and lower product-line rotameters and finally to a product reservoir. Construction materials exposed to the chemical systems studied were copper, brass, stainless steel, glass, and Teflon.

Instruments. A precision potentiometer indicated thermocouple potentials. For closed-column runs a six-point recording potentiometer was used during periods of absence by the operator. Although steady state throughput was indicated by rotameters, actual flow rates were measured by allowing liquid product to pass into small sealed bottles placed at the ends of the product lines, which otherwise emptied into a large collection bottle used for replenishing the feed reservoir. The small bottles were weighed on an analytical balance, collection time having been measured with a stop clock.

Power devices. A variable reactance controlled voltage across the column heating element. A household type of electric fan placed about 6 ft. from the center of the column and turning at a low speed helped to equalize the temperatures along the hot wall. At larger values of ΔT layers of Fiberglas insulation added near the

column extremities reduced the heat leak and temperature gradient between the midpoint and ends of the column.

Analytical equipment. The two binary systems were analyzed with a refractometer at 25°C. The first six runs with the ternary system were analyzed with a double-beam infrared recording spectrophotometer. The remaining ternary-system runs were analyzed with a vapor fractometer.

Equipment Operation

Continuous throughput runs. The increase in temperature of the cooling water was about 1.5°C. or less. The cold-wall temperature fluctuation was not greater than $\pm 0.1^\circ\text{C}$. Lengthwise the hot-wall variation in temperature was about 2°C . or less with fluctuations of about $\pm 0.2^\circ\text{C}$. at any one of the three thermocouple positions. The rotameter floats were held to a fluctuation of 2 to 4% of the indicated float level. A run was considered complete when liquid compositions at the ends of the product lines were the same as, or within 1% of, those at the sample taps on the upper and lower ends of the column.

Closed-column runs. Before such experiments were begun, the top and bottom product lines leading from the column were disconnected and the port caps designed for those ports were put in place, the connection between the center feed port and feed reservoir being maintained. After the annulus had been filled with liquid, the valve at the feed port was closed and operation commenced.

When the operator was absent, the average hot-wall temperature might fluctuate as much as 2°C . for ΔT values of about 35°C . For lower ΔT values the fluctuation in average hot-wall temperature was proportionally lower. Usually at the end of 48 hr. any change in $\omega_D - \omega_B$, the composition difference between the top and bottom of the column, would be less than 0.5% over a period of 12 hr.

DISCUSSION OF EXPERIMENTAL RESULTS

Binary Systems

Separation curves. Conditions which were varied were feed rate, temperature difference, wall spacing, column length, and feed concentration. For continuous throughput runs the quantity F was varied, with all other conditions remaining constant when each of the quantities ΔT , a , L , or F was studied. Curves describing $\bar{\omega}_D - \bar{\omega}_B$ vs. F appear elsewhere (36) and are similar in form to those reported by other investigators (1, 15). Samples of the closed column and continuous throughput operating results are given by Tables 1 and 2, in which ω refers to benzene in the system benzene-carbon tetrachloride and to n -heptane for the combination n -heptane-benzene.

Construction of correlations. The results for the two-component systems

TABLE 2. BINARY SYSTEMS—OPERATING DATA FOR CONTINUOUS THROUGHPUT RUNS

System	Run	D , g./sec.	B , g./sec.	L , cm.	a , cm.
$C_6H_6-CCl_4$	I-5	0.00210	0.00162	183	0.043
	I-12	0.00188	0.00197	183	0.043
	I-17	0.00383	0.00375	183	0.043
	I-51	0.00544	0.00528	183	0.079
	I-55	0.0109	0.0108	183	0.079
$nC_7-C_6H_6$	II-18	0.00456	0.00406	183	0.043
	II-24	0.00656	0.00658	183	0.079

System	Run	T_{av} , °C.	ΔT , °C.	$\bar{\omega}_D$	$\bar{\omega}_B$	ω_F
$C_6H_6-CCl_4$	I-5	39.8	33.6	0.560	0.157	0.328
	I-12	40.2	22.0	0.458	0.186	0.331
	I-17	39.7	9.4	0.350	0.310	0.331
	I-51	40.2	34.5	0.464	0.207	0.337
	I-55	40.2	34.5	0.443	0.234	0.337
$nC_7-C_6H_6$	II-18	35.5	35.0	0.597	0.520	0.562
	II-24	38.9	37.2	0.629	0.532	0.577

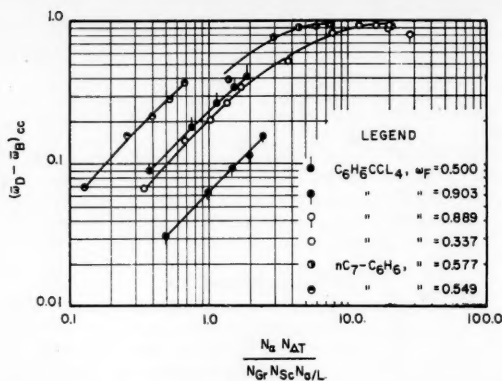


Fig. 3. Binary-system correlation of closed-column separations with parameter of feed composition.

have been expressed in the form of correlations constructed from the dimensionless quantities included within Equation (14). Literature sources were utilized for the transport coefficients and density data which made the correlations possible. For the system benzene-carbon tetrachloride the thermal-diffusion coefficients had been determined in cells by Tichacek, Kmak, and Drickamer (26), the ordinary diffusion coefficients by Caldwell and Babb (27), the coefficients of shear viscosity by Thorpe and Rodger (37), and the density by Hubbard (38). For the system *n*-heptane-benzene the thermal-diffusion coefficients had been measured in cells by Huse, Trevo, and Drickamer (24), the ordinary diffusion coefficients by Trevo and Drickamer (28), and both viscosity and density by Heines (19). In the correlations absolute values of thermal-diffusion coefficients are used.

The closed-column correlation is discussed initially. In the experiments the composition measurements correspond to w_D , w_B , and w_F . Therefore for

closed-column operation and for Equation (14)

$$\int_0^1 \omega^* dx^* = 1 \quad \text{at } z^* = 1$$

and $(\bar{w}_D - \bar{w}_F)_{cc}$ becomes a function of

$$\omega_F, N_a N_{\Delta T}, \frac{N_a N_{\Delta T}}{N_{Gr} N_{Sc} N_{a/L}} \quad (15)$$

a similar statement being possible for $(\bar{w}_F - \bar{w}_B)_{cc}$ below the feed. In the dimensionless numbers average fluid properties have been taken at the

TABLE 3. BINARY SYSTEMS—THERMAL DIFFUSION FACTORS N_a USED IN CORRELATIONS

System	ω	$T_{av}, ^\circ\text{C.}$	N_a	Ref.
$\text{C}_6\text{H}_6\text{-CCl}_4$	0.113	40.0	1.37	26
	0.336	40.0	1.43	26
	0.670	40.0	1.48	26
$n\text{C}_7\text{-C}_6\text{H}_6$	0.561	38.7	0.342 to 0.371	24

arithmetic mean temperature and arithmetic mean composition for that portion of the column above or below the feed point. After a combination of dimensionless numbers had been computed for both top and bottom portions of the column, the arithmetic average of the two computations was used in the correlations. The group N_{re}/N_{Gr} has not been considered, since the average value of N_{re} is zero at any position z for the closed column operating in the steady state. The closed-column separation, $(\bar{w}_D - \bar{w}_B)_{cc}$, has been plotted vs. $N_a N_{\Delta T} / (N_{Gr} N_{Sc} N_{a/L})$ in Figure 3. The sets of points appear to be stratified according to the feed concentration ω_F . The quantity $\omega_F(1 - \omega_F)$ has been used to form the group $[\omega_F(1 - \omega_F)]^{1.3} N_a N_{\Delta T} / (N_{Gr} N_{Sc} N_{a/L})$ which has been plotted against $(\bar{w}_D - \bar{w}_B)_{cc}$ in Figure 4. Included is a closed-column separation reported by Trevo and Drickamer (22) with a column 4 in. in height. The upper line corresponds to *n*-heptane-benzene and the lower to benzene-carbon tetrachloride.

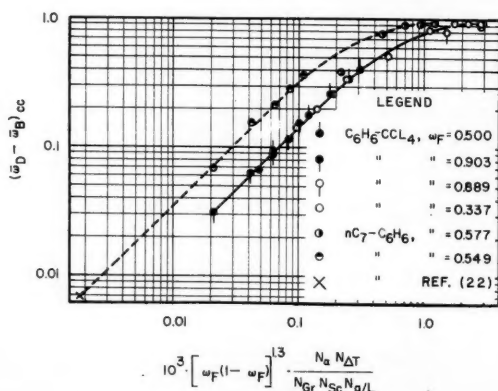


Fig. 4. Binary-system closed-column correlation with feed composition incorporated.

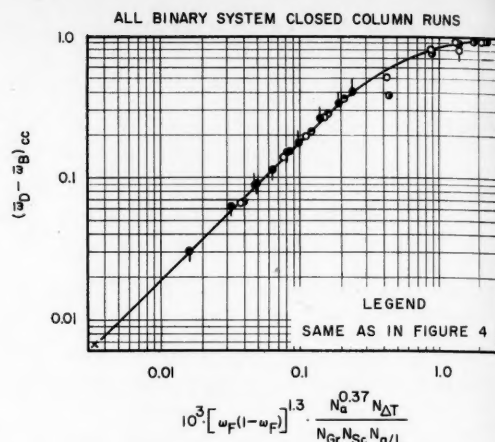


Fig. 5. Final closed-column correlation for two binary systems.

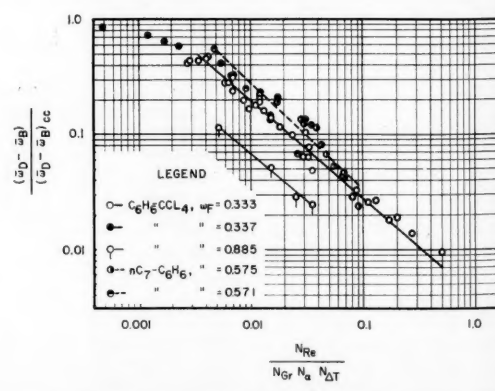


Fig. 6. Correlation of continuous throughput separations with parameter of feed composition.

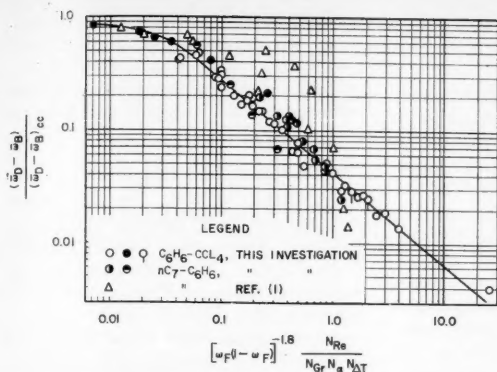


Fig. 7. Final binary-system continuous-throughput correlation with feed composition incorporated.

The dimensional analysis of the equations of change gives N_a in either of the two groups $N_a N_{\Delta T}$ or $N_a N_{\Delta T} / (N_{Gr} N_{Re} N_{a/L})$. If the terms of the equation of energy conservation containing partial molal enthalpy are omitted in the solution of the equations of change, N_a never occurs alone and cannot be obtained by intermultiplication of the groups which remain. It is possible to merge the two sets of points of Figure 4 by multiplying the abscissas of the points by a factor of $N_a^{-0.63}$ to give the result in Figure 5, which is presented with the reservation that N_a and $N_{\Delta T}$ occur only as $N_a N_{\Delta T}$ unless the terms containing partial molal enthalpy are accounted for.

The continuous throughput results have been related to the closed-column separations. In the theoretical discussion concentration was defined

$$\omega^* = \frac{\omega - \omega_F}{(\bar{\omega}_D - \omega_F)_{cc}}$$

One reason is that in a series of runs for which the only factor varied is the feed rate, the closed column, steady state concentration difference between the top and feed point $(\bar{\omega}_D - \omega_F)_{cc}$ is greater than that for any run with a throughput. Furthermore, Heines (15) has had success with a correlation by beginning at this point. He has introduced the following expression which is conveniently in terms of the product compositions of the experimental runs:

$$\frac{\bar{\omega}_D - \bar{\omega}_B}{(\bar{\omega}_D - \bar{\omega}_B)_{cc}} \quad (16)$$

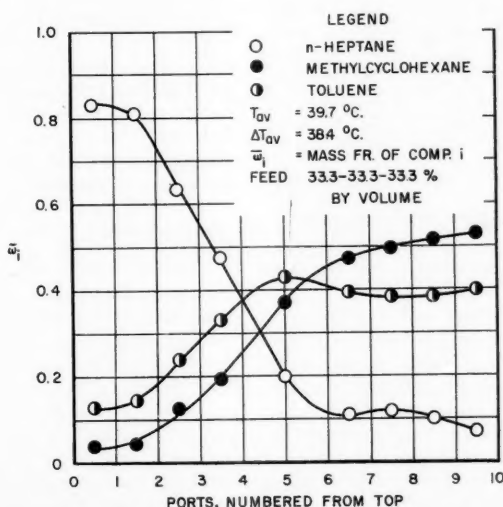


Fig. 8. Closed-column separation for ternary mixture; $a = 0.043$ cm.

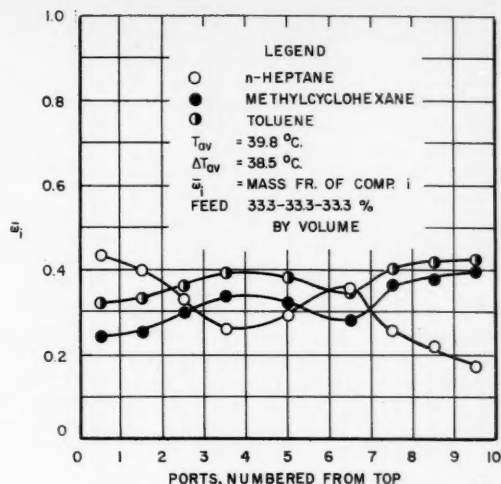


Fig. 9. Closed-column separation for ternary mixture; $a = 0.079$ cm.

Except for four runs for which no values of $(\bar{\omega}_D - \bar{\omega}_B)_{cc}$ were determined, the concentration data for all the continuous-throughput, two-component runs have been placed in the form of the ratio (16).

Since feed rate was varied in all of the sets of continuous-throughput runs, the dimensionless group into which the feed rate could be incorporated, N_{Re}/N_{Gr} , was investigated initially. The ratio has been averaged in the following manner:

$$\frac{N_{Re}}{N_{Gr}} = \frac{1}{2} \left[\left(\frac{N_{Re}}{N_{Gr}} \right)_D + \left(\frac{N_{Re}}{N_{Gr}} \right)_B \right] \quad (17)$$

In a series of runs in which the ratio of product rates, B/D or D/B , in the two sections of the column was varied with F being approximately constant, the Powers (20) data for ratios in the range 1 to 1 through 1.5 to 1 show a variation in rectification between top and bottom fractions of perhaps several per cent of total rectification. In this investigation similar behavior was noted, and an attempt was made to keep the ratios of product rates as close to unity as possible.

As N_{Re}/N_{Gr} was increased, the ratio $(\bar{\omega}_D - \bar{\omega}_B) / (\bar{\omega}_D - \bar{\omega}_B)_{cc}$ decreased for both binary systems with considerable scattering of points for benzene-carbon tetrachloride. The plots are given elsewhere (36). Although the points for one system appeared to be displaced from those of the other by a factor almost equal to N_a , the ratio $(\bar{\omega}_D - \bar{\omega}_B) / (\bar{\omega}_D - \bar{\omega}_B)_{cc}$ has been plotted vs. $N_{Re} / (N_{Gr} N_a N_{\Delta T})$ for both binary systems in Figure 6, since N_a occurs as $N_a N_{\Delta T}$ in the dimensionless groups. In Figure 6 between the

abscissa values of 0.0025 and 1, the straight lines are least-squares representations of the data. The four points toward the lower left-hand region of Figure 6 correspond to runs for a dilute solution of carbon tetrachloride in benzene. The forms D/H and B/H which occur in the Furry, Jones, and Onsager developments (18) include a constant 6!. Except for this constant, the combination $N_{re}/(N_{gr} N_a N_{\Delta T})$ is similar to D/H and B/H .

The quantity $\omega_F (1 - \omega_F)$ has been used together with Figure 6 to form the combination $[\omega_F (1 - \omega_F)]^{-1.8} N_{re}/N_{gr} N_a N_{\Delta T}$ which is the abscissa of Figure 7. The *n*-heptane-

$$\frac{(\bar{\omega}_D - \bar{\omega}_B)_{cc}^{2.8}}{[\omega_F (1 - \omega_F)]^{3.5}} \quad (18)$$

The possible error in N_a if determined from closed-column experiments as conducted in this investigation can be as high as 30%; the most probable error is about 16%. For definitions of these errors see reference 39.

One shortcoming of the continuous-throughput correlation is that the exponent -1.8 on $\omega_F (1 - \omega_F)$ is heavily influenced by the points corresponding to runs conducted with dilute solutions. Also in the experiments no assurance was made that the feed was equally distributed about the circumference of the annulus. Although the arithmetic mean circumference b does not enter into the group $N_{re}/(N_{gr} N_a N_{\Delta T})$, it is necessary to use b to compute N_{re} from the top and bottom product rates. Short-circuiting would cause the effective b to be smaller than its true value if any tendency exists for the solution concentration to vary circumferentially. This problem has been studied by Jones (40), but nothing quantitative appears to have been established.

For the convection effect due to the x direction concentration gradient it is possible to define a Grashof group different from that given by Boelter (41). It is

$$N_{gr}^{\omega} = \frac{a^2 \rho^2 \beta_c g (\Delta \omega)_{\text{constant } z}}{\mu^2} \quad (19)$$

In neither the continuous throughput nor the closed-column correlations does the group N_{gr}^{ω} appear. An accurate measurement of the derivative $\partial \omega^*/\partial x^*$ would be essential for calculating N_{gr}^{ω} . By the use of theoretical relations of de Groot (30) for the system benzene-carbon tetrachloride the ratio N_{gr}^{ω}/N_{gr} was estimated to be about 0.10. Since the effect of N_{gr}^{ω} must be greater for benzene-carbon tetrachloride than for *n*-heptane-benzene, the curves of Figure 4 probably should be closer together, which would modify the exponent on N_a for Figure 5. Dimensionless terms such as $\frac{N_{gr}}{N_{sc} N_{\Delta T}}$

$\left[\frac{1}{M_1 C_p T_{av}} \frac{\partial H_1}{\partial x^*} \right]$ and M_1/M_2 arise (36) when partial molal enthalpy is treated in the dimensionless equation of energy conservation, partial molal enthalpies being a function of temperature, pressure, and composition (42). How these groups would affect the correlations is not known. As has been pointed out, variations in physical properties such as μ , D_{12} , etc., introduce additional parameters which have not been included in the dimension-

less-group treatment. In the correlations the absolute value of N_a is used. In the strict meaning N_a would have a negative value when that component which migrates toward the hot wall is considered.

Ternary System

Separation curves. For the ternary combination *n*-heptane-methylcyclohexane-toluene the factors studied were F and a . The closed-column runs are reported in Figures 8 and 9. When placed in the thermal-diffusion column under closed-column conditions 50 mole % methylcyclohexane-toluene mixtures had little tendency to separate, a result observed by others (31, 32). Figures 8 and 9 show an improvement in the rectification of methylcyclohexane and toluene by the addition of the third component *n*-heptane.

For the continuous-throughput runs an attempt was made to maintain the product rates as nearly alike as possi-

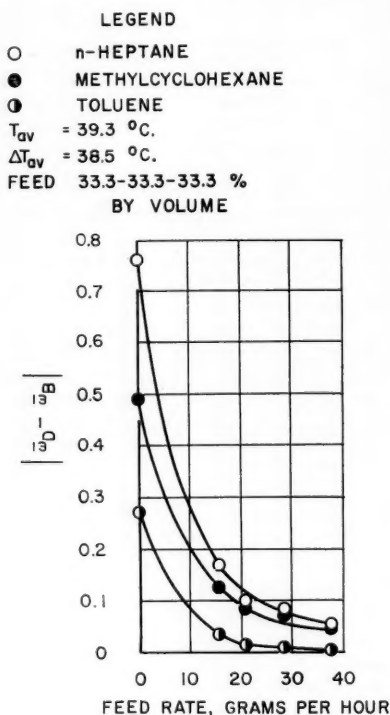


Fig. 10. Continuous-throughput separations for ternary mixture; $a = 0.043$ cm.

benzene points of Powers and Wilke (1), also shown on Figure 7, were not included in the least-squares computation for the straight portion of the line. The values of $(\bar{\omega}_D - \bar{\omega}_B)_{cc}$ for the Powers and Wilke points were estimated from the closed-column correlation of Figure 4.

Analysis of correlations. In Figures 4 and 5 the variation in N_{gr} was about twenty-five-fold, N_{sc} 1.7 fold, N_a four-fold, $N_{a/L}$ ninefold, and ω_F from 0.34 to 0.90 fold. For the straight portion of the curve in Figure 5

$$N_a = 1.2 \times 10^{-9} \left(\frac{N_{gr} N_{sc} N_{a/L}}{N_{\Delta T}} \right)^{2.7}$$

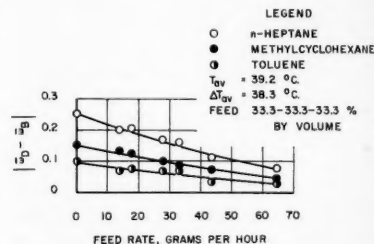


Fig. 11. Continuous-throughput separations for ternary mixture; $a = 0.079$ cm.

ble for each run. The absolute value of the difference in mass fraction between the top and bottom ports for each component in the mixture has been plotted vs. feed rate in Figures 10 and 11. At high feed rates the separations tended to be smaller. The separations for larger annulus width were greater than those for smaller annulus width at the higher throughputs. This behavior for annulus width and throughput is similar to that observed with binary systems.

CONCLUSIONS

For the binary solutions benzene-carbon tetrachloride and *n*-heptane-benzene and for the conditions under which they were studied in this investigation it is possible to correlate thermal-diffusion-column operating variables on the basis of thermal-diffusion coefficients determined in cell experiments. The correlating combinations of dimensionless groups can be obtained from the equations of conservation and their boundary conditions in dimensionless form. With the

ternary system *n*-heptane-methyleyclohexane-toluene, variations in feed rate and wall spacing gave results similar to those observed in binary systems.

ACKNOWLEDGMENT

The author is especially grateful to R. Byron Bird, whose guidance and encouragement made both this study and the paper possible. The advice of V. W. Meloche of the Department of Analytical Chemistry, Wayne K. Neill, and James R. Brock (University of Wisconsin) was essential, and the financial aid furnished at various times during the project by the Shell Fellowship Committee, Celanese Corporation of America, Hercules Powder Company, and the Wisconsin Alumni Research Foundation is sincerely appreciated.

NOTATION

a = distance between hot and cold walls
 B = bottom product rate, mass per unit time
 b = arithmetic mean circumference of hot and cold walls forming an annulus in a cylindrical thermal-diffusion column or horizontal width of heat transfer plates for a flat column
 C_p = heat capacity per unit mass at constant pressure
 D = top product rate, mass per unit time
 D_{12} = concentration diffusion mass transport coefficient in a binary mixture of components 1 and 2
 D_1^T = thermal diffusion mass transport coefficient for component 1 in a binary mixture
 F = feed rate, mass per unit time
 f^* = arbitrary function, dimensionless
 g = acceleration of gravity
 H = thermal-diffusion-column parameter from physics literature
 H_1 = partial molal enthalpy of component 1 in a binary mixture
 K_e = thermal-diffusion-column parameter from physics literature
 L = vertical length of column
 M = molecular weight
 T = absolute temperature
 T_{ar} = arithmetic mean temperature of hot and cold walls
 v = mass average velocity
 x = Cartesian coordinate perpendicular to heat transfer surfaces
 y = horizontal cartesian coordinate parallel to the heat transfer surface

z = Cartesian coordinate parallel to the heat transfer surface and perpendicular to the x , y plane

Greek Letters

β = volumetric coefficient of thermal expansion
 β_w = volumetric coefficient of expansion from concentration variation
 μ = coefficient of shear viscosity
 ρ = mass density
 ω = mass fraction of that component in a binary mixture which migrates toward the warm wall and is enriched toward the top of the column

Dimensionless Variables

T^* = $(T - T_{cold}) / (T_{hot} - T_{cold})$
 v_z^* = v_z / v_{ar}
 x^* = x/a
 z^* = z/L
 ω^* = $(\omega - \omega_F) / (\omega_D - \omega_F)_{cc}$

Dimensionless Numbers

N_{Gr} = Grashof number for heat transfer
 N_{Gr}^w = Grashof number for mass transfer
 N_{Re} = Reynolds number
 N_{Sc} = Schmidt number
 N_{Pr} = Prandtl number
 N_α = thermal-diffusion factor (calculated α in physics literature)
 $N_{a/L}$ = a/L , geometric factor

Subscripts

B = quantity pertaining to the bottom product
 D = quantity pertaining to the top product
 F = quantity pertaining to the feed
 1 = component in a binary mixture which migrates toward hot wall
 2 = component in a binary mixture which migrates toward cold wall
 cc = closed column

LITERATURE CITED

1. Powers, J. E., and C. R. Wilke, *A.I.Ch.E. Journal*, **3**, 213 (1957).
2. Clusius, Karl, and G. Dickel, *Naturwissenschaften*, **26**, 546 (1938).
3. Jones, A. L., U. S. Patent 2,720,976 (1955).
4. ———, U.S. Patent 2,720,979 (1955).
5. ———, U.S. Patent 2,723,034 (1955).
6. ———, and P. S. Fay, U. S. Patent 2,723,033 (1955).
7. Jones, A. L., R. A. Gardner, and C. W. Seelbach, U. S. Patent 2,720,978 (1955).
8. Jones, A. L., and E. C. Hughes, U. S. Patent 2,734,633 (1956).
9. Jones, A. L., and E. C. Milberger, U. S. Patent 2,712,386 (1955).

10. Jones, A. L., C. W. Seelbach, and David Frazier, U. S. Patent 2,720,975 (1955).
11. Gary, J. H., U. S. Patent 2,751,082 (1953).
12. Thomas, J. W., U. S. Patent 2,720,980 (1955).
13. Sullivan, L. J., T. C. Ruppel, and C. B. Willingham, *Ind. Eng. Chem.*, **47**, 208 (1955).
14. *Ibid.*, **49**, 110 (1957).
15. Heines, T. S., Jr., O. A. Larson, and J. J. Martin, *ibid.*, p. 1911.
16. Thomas, W. J., and S. B. Watkins, *Chem. Eng. Sci.*, **5**, 34 (1956).
17. *Ibid.*, **6**, 26 (1956).
18. Furry, W. H., R. C. Jones, and L. Onsager, *Phys. Rev.*, **55**, 1083 (1939).
19. Heines, T. S., Jr., Ph. D. thesis, Univ. Mich., Ann Arbor (1954).
20. Powers, J. E., UCRL 2618, U. S. Atomic Energy Comm., Washington, D. C. (1954).
21. Prigogine, I., L. de Brouckere, and R. Amand, *Physica*, **16**, 577 (1950).
22. Trevo, D. J., and H. G. Drickamer, *J. Chem. Phys.*, **17**, 1120 (1949).
23. Velden, P. F., van, H. G. P. van der Voort, and C. J. Gorter, *Physica*, **12**, 151 (1946).
24. Huse, E. S., D. J. Trevo, and H. G. Drickamer, *Rev. Sci. Instr.*, **21**, 60 (1950).
25. Thomaes, G., *Physica*, **17**, 885 (1951).
26. Tichacek, L. J., W. S. Kmak, and H. G. Drickamer, *J. Phys. Chem.*, **60**, 660 (1956).
27. Caldwell, C. S., and A. L. Babb, *ibid.*, **51** (1956).
28. Trevo, D. J., and H. G. Drickamer, *J. Chem. Phys.*, **17**, 1117 (1949).
29. Waldmann, Ludwig, *Z. Physik*, **114**, 53 (1939).
30. Groot, S. R. de, *Physica*, **9**, 801 (1942).
31. Jones, A. L., and E. C. Milberger, *Ind. Eng. Chem.*, **45**, 2689 (1953).
32. Begeman, C. R., and P. L. Cramer, *ibid.*, **47**, 202 (1955).
33. Bird, R. B., in "Advances in Chemical Engineering," Vol. 1, Academic Press, New York (1956).
34. ———, private communication (1956).
35. Schlichting, Hermann, "Boundary Layer Theory," pp. 248-253, Pergamon Press, New York (1955).
36. Longmire, D. R., Ph. D. thesis, Univ. Wis., Madison (1957).
37. Thorpe, T. E., and J. W. Rodger, *J. Chem. Soc. (London)*, **71**, 360 (1897).
38. Hubbard, J. C., *Z. Phys. Chem.*, **74**, 207 (1910).
39. Sherwood, T. K., and C. E. Reed, "Applied Mathematics in Chemical Engineering," 1 ed., pp. 368-378, McGraw-Hill, New York (1939).
40. Jones, A. L., U. S. Patent 2,720,977 (1955).
41. Boelter, L. M. K., *Trans. Am. Inst. Chem. Engrs.*, **39**, 557 (1943).
42. Hougen, O. A., K. M. Watson, and R. A. Ragatz, "Chemical Process Principles," Part 1, 2 ed., Wiley, New York (1954).

Manuscript received September 26, 1958; revision received October 16, 1959; paper accepted October 19, 1959.

Momentum and Heat Transfer in Laminar Boundary-Layer Flows of Non-Newtonian Fluids Past External Surfaces

ANDREAS ACRIVOS, M. J. SHAH, and E. E. PETERSEN

University of California, Berkeley, California

A theoretical analysis for the laminar flow past arbitrary external surfaces of non-Newtonian fluids of the power-law model is presented. The main problem which is considered is how to predict the drag and the rate of heat transfer from an isothermal surface to the fluid. Inspectional analysis of the modified boundary-layer equations yields a general relationship both for the drag coefficient and for the Nusselt number as functions of the generalized Reynolds and Prandtl numbers. The flow past a horizontal flat plate is studied in detail numerically.

Considerable attention has lately been devoted to the problem of how to predict the behavior of non-Newtonian fluids in motion. The main reason for this is probably that fluids, such as molten plastics, pulps, slurries, emulsions, etc., which do not obey the Newtonian postulate that the stress tensor is directly proportional to the deformation tensor, are produced industrially in increasing quantities and are therefore in some cases just as likely to be pumped in a plant as the more common Newtonian fluids.

It is well known, though, that a chief difficulty in the theoretical study of non-Newtonian fluid mechanical phenomena, and in the correct interpretation of experimental results, is that so far no definite relationship between the stress tensor and the deformation tensor, valid for all fluids, has been discovered. This means that, except for simple cases, a generalized form of the Navier-Stokes equations, obeyed by all fluids in motion, cannot be written down, and so theoretical studies in this area are limited not so much by the mathematical complexity of the basic equations as by the inability to arrive at their correct form. It is fortunate however that certain simple problems in this field can be attacked successfully, either theoretically or experi-

mentally, and thereby provide a basis for the analysis of the more complicated physical situations usually encountered in practice.

The flow in pipes and channels has been primarily studied so far because of its importance and relative simplicity. The laminar-flow equations have been solved (4, 10, 11) for various non-Newtonian models, characterized by the empirically observed relationship between shear stress and velocity gradient, and a generalization of the Poiseuille formula for pressure drop has been derived. In addition, some experimental work has been carried out in the turbulent regime for fluids which obey the power-law model (11, 13), and a tentative extension of the familiar Fanning friction-factor plot has been proposed (2, 11, 13, 16). The analogous laminar heat transfer problem has also been studied (5, 9, 10), and generalized j factor plots for power-law fluids have been made available (12).

It is thus seen that the flow inside pipes of non-Newtonian fluids, especially those obeying the power-law model, has been covered both theoretically and experimentally rather well, although it is realized that further work in the turbulent regime would be both desirable and most useful. Other

investigations have been restricted to rather specialized problems, for example the design of an extruder for a pseudoplastic fluid (1).

It is surprising to note however that, according to the authors' best knowledge, no analysis of the flow of non-Newtonian fluids past external surfaces has ever been published. Such systems have, aside from their practical applications, considerable theoretical interest, for, especially when the geometry of the external surface is simple, they can be examined more carefully and in more detail than internal flows and thus yield fundamental information about the behavior of non-Newtonian fluids in motion.

In the present paper a theoretical analysis will be presented of the laminar flow of non-Newtonian fluids which obey the power-law model past an arbitrary two-dimensional surface. The main problem considered is that of predicting the drag and the rate of heat transfer from an isothermal surface to the fluid. Inspectional analysis of the modified boundary-layer equations yields a general relationship both for the drag coefficient and for the Nusselt number as functions of the generalized Reynolds and Prandtl numbers. Also included is a rather detailed numerical study of the flow past a horizontal flat plate.

BASIC LAMINAR BOUNDARY-LAYER EQUATIONS AND THEIR INSPECTIONAL ANALYSIS

The laminar flow of a non-Newtonian fluid past the arbitrary two-

dimensional surface, shown in Figure 1, is considered. Analysis will be restricted to the case where the usual boundary-layer assumptions can be made that gradients in the normal direction are much larger numerically than the corresponding gradients in the transverse, or x , direction. This allows simplifying the exact basic equations of conservation of momentum, mass, and energy and transforming them into the boundary-layer equations. For a constant property fluid and in the absence of the dissipation function in the energy equation, which may usually be neglected to a first approximation, these are (14)

$$u \frac{\partial u}{\partial x} + v \frac{\partial u}{\partial y} = U_i \frac{dU_i}{dx} + \frac{1}{\rho} \frac{\partial \tau_{xy}}{\partial y} \quad (1)$$

$$\frac{\partial u}{\partial x} + \frac{\partial v}{\partial y} = 0 \quad (2)$$

$$u \frac{\partial T}{\partial x} + v \frac{\partial T}{\partial y} = \frac{k}{\rho c_p} \frac{\partial^2 T}{\partial y^2} \quad (3)$$

The symbols have the usual meaning. The boundary conditions are

$$\begin{aligned} \text{At } y = 0, u = 0, v = 0, T = T_s \\ \text{At } y = \infty, u = U_i(x), T = T_\infty \\ \text{At } x = 0, u = U_i(0), T = T_s \end{aligned} \quad (4)$$

It now remains to express τ_{xy} in terms of the velocity gradients by means of some empirical equation of state. It was pointed out in the introduction that a generally acceptable definite relationship between the components of the stress tensor and those of the deformation tensor has not yet been proposed. In accordance with the boundary-layer theory, however, $\partial u / \partial y$ is numerically much larger than all the other velocity gradients. It follows therefore that for boundary-layer flows τ_{xy} is a function of $\partial u / \partial y$ only, which, as is well known, is exact for the fully developed flow in pipes and channels where all the velocity gradients, except for $\partial u / \partial y$, are identically zero.

Generally the form of the function relating τ_{xy} to $\partial u / \partial y$ is quite complicated. It has been found however that the two-parameter equation of state

$$\tau_{xy} = K \left(\frac{\partial u}{\partial y} \right)^n \quad (5)$$

is adequate for many non-Newtonian fluids (10). This is the well-known power-law model which will be used in the remaining part of this paper.

Equations (1 to 5) possess now a unique solution that will depend on the surface geometry, which, as is well known from potential theory, estab-

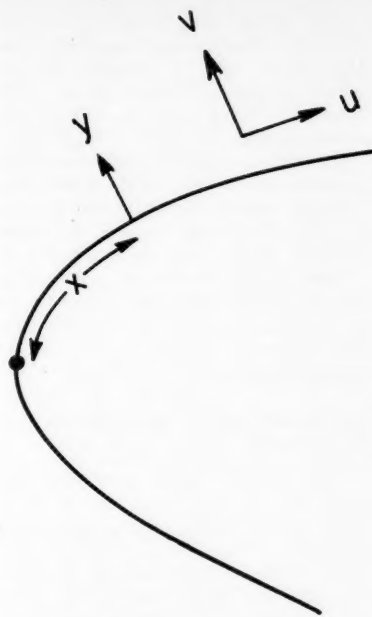


Fig. 1. The directions of the coordinates x and y and the velocities u and v with respect to the surface.

lishes the function $U_i(x)$, as well as on the characteristic parameters of the fluid, K, n, ρ, c_p and k . First, however, important and general results can be obtained, without solving the equations, by means of inspectional analysis. This is sometimes referred to in the literature as the stretching of the boundary-layer coordinates. If the following transformations are made,

$$x_1 \equiv \frac{x}{L}; \quad u_1 \equiv \frac{u}{U_\infty}; \quad \phi(x_1) \equiv \frac{U_i(x_1)}{U_\infty};$$

$$\theta \equiv \frac{T - T_\infty}{T_s - T_\infty}; \quad y_1 \equiv \left[\frac{\rho U_\infty^{2-n} L^n}{K} \right]^{\frac{1}{1+n}} \frac{y}{L};$$

$$v_1 \equiv \left[\frac{\rho U_\infty^{2-n} L^n}{K} \right]^{\frac{1}{1+n}} \frac{v}{U_\infty};$$

$$N_{Re} \equiv \left[\frac{\rho U_\infty^{2-n} L^n}{K} \right];$$

$$\text{and } N_{Pr} \equiv \frac{N_{Pe}}{N_{Re}^{2/(1+n)}}$$

$$\equiv \frac{c_p U_\infty \rho L}{k N_{Re}^{2/(1+n)}} \quad (6)$$

the boundary-layer equations become

$$\begin{aligned} u_1 \frac{\partial u_1}{\partial x_1} + v_1 \frac{\partial u_1}{\partial y_1} &= \phi \frac{d\phi}{dx_1} \\ &+ \frac{\partial}{\partial y_1} \left(\frac{\partial u_1}{\partial y_1} \right)^n \end{aligned} \quad (7)$$

$$\frac{\partial u_1}{\partial x_1} + \frac{\partial v_1}{\partial y_1} = 0 \quad (8)$$

$$u_1 \frac{\partial \theta}{\partial x_1} + v_1 \frac{\partial \theta}{\partial y_1} = \frac{1}{N_{Pr}} \frac{\partial^2 \theta}{\partial y_1^2} \quad (9)$$

while the boundary conditions are changed into

$$\begin{aligned} \text{At } y_1 = 0, u_1 = 0, v_1 = 0, \theta = 1 \\ \text{At } y_1 = \infty, u_1 = \phi(x_1), \theta = 0 \\ \text{At } x_1 = 0, u_1 = \phi(0), \theta = 0 \end{aligned} \quad (10)$$

It therefore follows immediately that if τ_s is the shear stress at the wall and the Nusselt number is defined in the usual manner as

$$N_{Nu} \equiv -L \left(\frac{\partial \theta}{\partial y_1} \right)_{y_1=0}$$

then

$$\begin{aligned} \frac{\tau_s}{\rho U_\infty^2} &= (N_{Re})^{-\frac{1}{1+n}} \left(\frac{\partial u_1}{\partial y_1} \right)_{y_1=0}^n \\ &= (N_{Re})^{-\frac{1}{1+n}} F_1(x_1, n) \end{aligned} \quad (11)$$

and

$$\begin{aligned} N_{Nu} &= (N_{Re})^{\frac{1}{1+n}} \left(\frac{\partial \theta}{\partial y_1} \right)_{y_1=0} \\ &= (N_{Re})^{\frac{1}{1+n}} F_2(x_1, N_{Pr}, n) \end{aligned} \quad (12)$$

In many instances, however, one is interested in the average values of τ_s and N_{Nu} , which are calculated from Equations (11) and (12) by integrating over that part of the surface where the boundary-layer equations apply. Thus for non-Newtonian fluids of the power law type

$$\frac{\tau_s}{\rho U_\infty^2} = (N_{Re})^{-\frac{1}{1+n}} F_3(n) \quad (13)$$

and

$$N_{Nu} = (N_{Re})^{\frac{1}{1+n}} F_4(N_{Pr}, n) \quad (14)$$

where $F_3(n)$ depends on n and $F_4(N_{Pr}, n)$ is also a function of the Prandtl number which, as will be shown later on, can be simplified still further.

It should also be noted here that Equations (13) and (14) are themselves of considerable interest, for they prove that in laminar boundary-layer flows the two groups $(\tau_s / \rho U_\infty^2) (N_{Re})^{1/(1+n)}$ and $N_{Nu} (N_{Re})^{-1/(1+n)}$ are both independent of the Reynolds number, since F_3 and F_4 depend only on the geometry of the surface and in the case of F_4 the Prandtl number. Therefore when the boundary-layer equations are too involved and cannot be solved, Equations (13) and (14) can be used for the analysis and the correlation of experimental data. It also should be quite evident that all the results presented so far reduce to

the corresponding expressions for Newtonian fluids when $n = 1$.

LIMITATIONS OF THE BOUNDARY-LAYER THEORY

It must be remembered that the boundary-layer equations are not exact but are the asymptotic forms of the basic hydrodynamic relations when the Reynolds number is large. It would be of interest to examine under what conditions laminar boundary-layer type of flows would be expected to occur.

It has already been seen that the characteristic Reynolds number for a power law non-Newtonian fluid is

$$N_{Re} = \frac{\rho U_\infty^{2-n} L^n}{K}$$

from which it follows that only if $n < 2$ is N_{Re} a monotonic increasing function of U_∞ . It is apparent therefore that for $n < 2$ laminar boundary-layer flows may be produced by making U_∞ sufficiently large. For $n > 2$ however a boundary-layer configuration will not be formed if U_∞ is too large, since N_{Re} decreases with increasing U_∞ . And although the above expression predicts that for $n > 2$, $N_{Re} \rightarrow \infty$ as $U_\infty \rightarrow 0$, boundary-layer flows do not occur when the characteristic velocity is small because the power-law model

$$\tau_{xy} = K \left(\frac{\partial u}{\partial y} \right)^n$$

is valid only when the velocity gradient component $\partial u / \partial y$ is relatively large (Figure 3 reference 10). Thus when U_∞ , and therefore $\partial u / \partial y$, is small, then, as with Newtonian fluids, τ_{xy} must be a linear function of $[(\partial u) / (\partial y) + (\partial v) / (\partial x)]$ for two-dimensional flows, since on physical grounds τ_{xy} is analytical and for sufficiently small values of $\partial u / \partial y$ and $\partial v / \partial x$ can be expressed by a power series in these variables. One can conclude from this discussion then that:

1. All fluids approach Newtonian behavior if U_∞ is sufficiently small and, in accordance with the well-known argument of Stokes, the inertia terms of the equations of motion may be neglected.

2. For $n < 2$ boundary-layer type of flows can be obtained if U_∞ is large, and therefore the Reynolds number is made sufficiently large.

3. For $n > 2$ and moderate values of U_∞ the boundary-layer approximations may be introduced provided that $N_{Re} \gg 1$. For large values of U_∞ the inertia terms may again be neglected since $N_{Re} \rightarrow 0$; however the stress-strain-velocity relations would have to be made more elaborate than the simple power-law form.

It is evident therefore that when $n > 2$ the boundary-layer flow is not an asymptotic state of laminar motion which is approached as U_∞ is made sufficiently large. At best there may be an intermediate state of high Reynolds number, where the boundary layer approximations are valid, which lies between regions characterized by the fact that the inertia terms in the equations of motion may be neglected. It follows then that when $n > 2$ laminar boundary-layer flows are probably not of much practical interest because their range of validity appears to be rather limited.

THE FLOW PAST A HORIZONTAL FLAT PLATE

The analysis of the horizontal flat plate will be considered now in some detail. It is divided into two parts: the solution of Equations (7) and (8) which will yield the velocity distribution and the local value of the shear stress at the wall, and the determination of the local rate of heat transfer from the surface to the main part of the fluid.

The velocity distribution and the drag on a flat plate

For the flow past a flat plate $\phi = 1$, and a Blasius type of similarity transformation can be used to reduce Equations (7) and (8) into an ordinary differential equation. Thus if

$$\eta = \frac{y_1}{x_1^{1/(1+n)}} \text{ and } u_1 = f'(\eta) \quad (15)$$

it can be shown, from Equations (7) and (8), that

$$v_1 = \frac{1}{n+1} x_1^{-n/(n+1)} [\eta f' - f] \quad (15a)$$

and

$$n(n+1)f''' + (f')^{2-n}f = 0 \quad (16)$$

Incidentally an analogous transformation can also be used for the flow past a wedge, for which $\phi = x_1^m$.

Equation (16), which for $n = 1$ will be recognized as the familiar Blasius equation (14), is nonlinear in f except when $n = 2$. It must be solved numerically, subject to the usual boundary conditions:

$$\begin{aligned} f &= f' = 0 & \text{at } \eta &= 0 \\ f' &= 1 & \text{at } \eta &= \infty \end{aligned}$$

Also by the use of a technique first introduced by Töpfer (15) in connection with the Blasius equation, no trial and error is required. One can easily see however that when $n \geq 2$ a function which will satisfy both Equation (16) and the above conditions cannot be found. Therefore the boundary conditions must be changed into the more general form

$$\begin{aligned} f &= f' = 0 & \text{at } \eta &= 0 \\ f' &= 1 \text{ and } f'' = 0 & \text{for } \eta &\geq \eta_c \end{aligned} \quad (17)$$

Of course $\eta_c = \infty$ for $n < 2$, but η_c is finite for $n \geq 2$. This interesting phenomenon of a finite boundary-layer thickness is never encountered in the laminar flow of Newtonian fluids. It was pointed out however that when $n > 2$, laminar boundary-layer flows are probably not of much practical interest, since their range of validity appears to be rather limited; therefore the numerical calculations for $n > 2$, which are included here for completeness, seem to be of secondary significance only. On the other hand Equation (16) simplifies as $n \rightarrow 0$, for if

$$f'(\eta) = f'_1(\eta/n) \quad (18)$$

f_1 becomes independent of n and is obtained from

$$f''_1 + [f'_1]^2 f_1 = 0 \quad (18a)$$

This limiting expression is accurate when $n < 0.1$ in the sense that both Equations (16) and (18a) yield essentially identical solutions.

Velocity profiles, calculated from Equations (16) and (17), are seen plotted in Figures 2 and 3 for dilatant ($n > 1$) and pseudoplastic fluids ($n < 1$). Generally however it is the shear stress at the wall and not the complete velocity profile which is of prime interest. From Equations (11) and (15)

$$\begin{aligned} \frac{\tau_o}{\rho U_\infty^2} &= (N_{Re})^{-\frac{1}{1+n}} \frac{[f''(0)]^n}{x_1^{\frac{n}{1+n}}} \\ &= c(n) (N_{Re})^{-\frac{1}{1+n}} \end{aligned}$$

where $c(n) \equiv [f''(0)]^n$ and $N_{Re} \equiv (\rho U_\infty^{2-n} x_1^n) / K$ (a Reynolds number based on x).

The shear-stress coefficient can be determined exactly from the numerical solution of Equation (18) or approximately by a momentum integral method, analogous to the one developed by Pohlhausen for Newtonian fluids (14). Owing to its relative simplicity and good accuracy this Pohlhausen method is very frequently used in boundary-layer problems, where the exact solution of the basic equations would be too involved and time consuming to be carried out. It is therefore of considerable interest to compare the results of the integral method and those of the exact numerical solution for the flow past a flat plate. This is done to obtain some feeling as to the accuracy of the approximate procedure and as to whether or not it could be used with the same degree of confidence for non-Newtonian as well as Newtonian fluids.

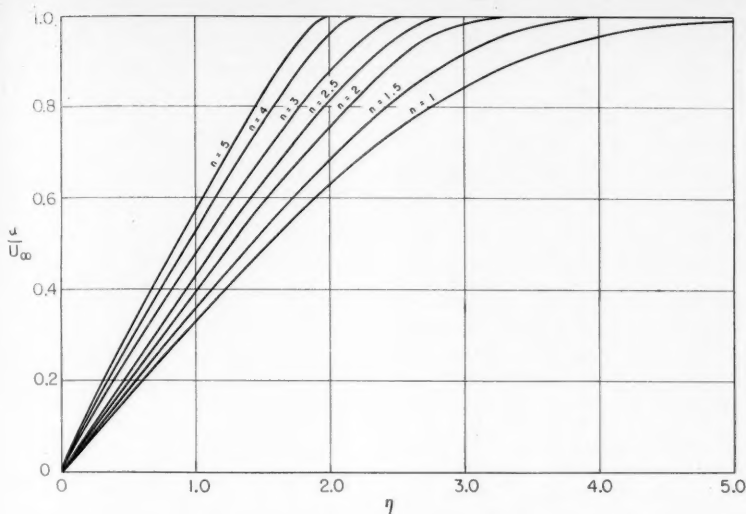


Fig. 2. Velocity profile over a flat plate for dilatant fluids:

$$\tau_{xy} = K \left(\frac{\partial u}{\partial y} \right)^n, n \geq 1, \eta \text{ given by Equation (15).}$$

The approximate momentum-integral method

If Equations (7) and (8), with $\phi = 1$ for flat plate, are multiplied through by dy_1 and integrated from 0 to ∞ , they reduce to

$$\frac{d}{dx_1} \int_0^\infty (1 - u_1) u_1 dy_1 \quad (20)$$

which will be solved now by the Pohlhausen method (14, p. 201).

A commonly used profile, for the flow past a flat plate, is

$$u_1 = \frac{3y_1}{2\delta} - \frac{y_1^3}{2\delta^3} \text{ for } y_1 \leq \delta \quad (21)$$

$$u_1 = 1 \text{ for } y_1 \geq \delta$$

This gives, when substituted into Equation (20),

TABLE 1. COMPARISON BETWEEN THE EXACT VALUES OF $c(n)$ AND EQUATION (22)

n	$c(n)$ exact	$c(n)$ from Equation (22)
0.05	1.017	0.926
0.1	0.969	0.860
0.2	0.8725	0.75
0.3	0.7325	0.655
0.5	0.5755	0.518
1.0	0.33206	0.323
1.5	0.2189	0.238
2.0	0.1612	0.169
2.5	0.1226	0.133
3.0	0.09706	0.109
4.0	0.06777	0.079
5.0	0.05111	0.061

$$u_1 = \sin \frac{\pi y_1}{2\delta} \text{ for } y_1 \leq \delta$$

gave results very close to those of Equation (22). However the comparison between the numerically calculated values of $c(n)$ and those obtained from the momentum integral method shows that the latter is of acceptable accuracy when $n \leq 3$ and that the best results can be expected where n is approximately 1. Moreover from experience with this method for Newtonian fluids one should also expect that the inaccuracy of the Pohlhausen method will be larger for more complicated surfaces and that still poorer results would be obtained if this method were used to predict the location of the separation point. For it is known that even for Newtonian fluids the separation point cannot be calculated accurately by means of integral methods.

Table 1 will also show that the modified Pohlhausen method is unable, when n is small, to predict the numerical value of $f''(0)$ with reasonable accuracy. This must be considered as a serious disadvantage of the momentum-integral approach because, as will be brought out in the next section, an accurate knowledge of $(\partial u / \partial y)_{y=0}$ is essential for most heat transfer calculations involving non-Newtonian fluids. It can be stated in conclusion therefore that the Pohlhausen method appears to be less accurate in general for non-Newtonian than it is for Newtonian fluids, but for $n < 3$ it could be used to predict τ_w , although not $(\partial u / \partial y)_{y=0}$, with acceptable accuracy. It seems probable in addition that this integral method would turn out to be quite

and therefore from Equations (11) and (19)

$$\frac{\tau_w}{\rho U_\infty^2} = c(n) (N_{Re})^{-\frac{1}{n+1}}$$

where

$$c(n) = \left[\frac{39}{280} \cdot \frac{1.5}{n+1} \right]^{\frac{n}{n+1}} \quad (22)$$

A comparison between the exact values of $c(n)$ and Equation (22) is shown in Figure 4 and Table 1.

Similarly the profile

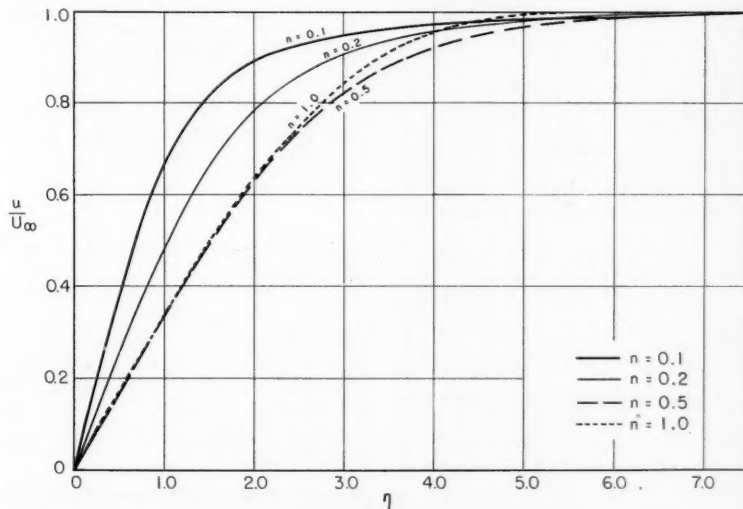


Fig. 3. Velocity profile over a flat plate for pseudoplastic fluids:

$$\tau_{xy} = K \left(\frac{\partial u}{\partial y} \right)^n, 0 < n \leq 1, \eta \text{ given by Equation (15).}$$

unreliable for the calculation of the separation point.

THE RATE OF HEAT TRANSFER FROM AN ISOTHERMAL SURFACE

Once the velocity distribution past a surface has been determined, u_1 and v_1 can be substituted in Equation (9). The solution of this linear equation will then yield the rate of heat transfer from the surface, and also the temperature profile, which usually however is of little interest. Equation (9) cannot generally be solved by elementary means, and an exact solution can at present be obtained only by a numerical finite-difference procedure. Most such problems for Newtonian fluids are therefore solved approximately by a standard momentum-integral method (6, 14) similar to that of Pohlhausen, which was briefly described earlier. This method can also be applied, without any modifications, to non-Newtonian fluids because, as is obvious, Equation (9) is perfectly general and not restricted to any particular class of fluids. On the other hand the local rate of heat transfer can also be calculated by means of a closed-form expression first obtained by Lighthill (8). Strictly speaking it is exact only for very large Prandtl numbers, but, as Lighthill has shown for Newtonian fluids, it can be used with good accuracy for $N_{Pr} \geq 1$. This formula is apparently not well known to chemical engineers, and therefore a derivation of it is presented below which is simpler than that given originally by Lighthill. As was first pointed out by Fage and Falkner (3) the temperature boundary layer is much thinner over a given surface than the momentum boundary layer for large Prandtl numbers. Therefore essentially all the temperature drop occurs in a very narrow region close to the wall, where the velocity u_1 is given by the first term of a power series expansion in y_1 :

$$u_1 = \beta(x_1)y_1 \quad (23)$$

This is then substituted in Equation (9) which can readily be transformed into

$$\beta y_1 \frac{\partial \theta}{\partial x_1} - \frac{\beta^2 y_1^2}{2} \frac{\partial \theta}{\partial y_1} = \frac{\partial^2 \theta}{\partial y_1^2} \quad (24)$$

where

$$y_1 \equiv (N_{Pr})^{1/3} y_1 \quad (24a)$$

It can be shown now that Equation (24) can be reduced to an ordinary differential equation by a similarity transformation. Thus if θ equals a function of z only, where

$$z \equiv \frac{\beta(x_1)}{2t^{2/3}} y_1^2, \quad t(x_1) = \int_0^{x_1} \sqrt{2\beta} dx_1 \quad (25)$$

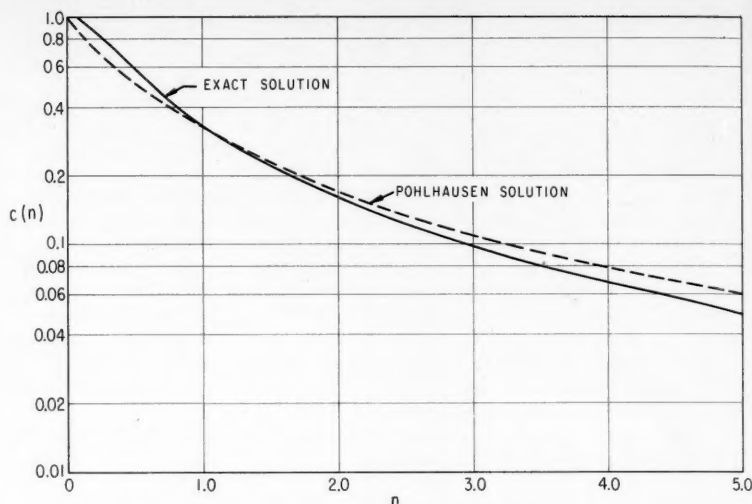


Fig. 4. A comparison between the exact and the approximate solution for $c(n)$.

then Equation (24) becomes

$$\frac{d^2 \theta}{dz^2} + \left(\frac{1}{2z} + \frac{2z^{1/2}}{3} \right) \frac{d\theta}{dz} = 0 \quad (26)$$

The solution, which satisfies the boundary conditions

$$\theta = 0 \text{ at } z = \infty, \quad \theta = 1 \text{ at } z = 0$$

is

$$\theta = \frac{1}{\Gamma(1/3)} \int_{4z^{3/2}}^{\infty} x^{-2/3} e^{-x} dx \quad (27)$$

It follows that

$$-\left(\frac{\partial \theta}{\partial y_1} \right)_{y_1=0} = \frac{1}{0.8930} \left(\frac{N_{Pr}}{9} \right)^{1/3} \frac{\sqrt{\beta(x_1)}}{\left[\int_0^{x_1} \sqrt{\beta} dx_1 \right]^{1/3}} \quad (28)$$

which is the Lighthill formula. For large Prandtl numbers therefore Equation (14) can be simplified to

$$\overline{N_{Su}} = (N_{Re})^{1/3} (N_{Pr})^{1/3} F_2(n) \quad (29)$$

where $F_2(n)$ is a function only of n and the surface geometry. It is seen then that for non-Newtonian fluids as well the average Nusselt number is again asymptotically proportional to the $1/3$ power of the Prandtl number, although it should be kept in mind that the Lighthill formula should not be expected to hold near the separation point, where $\beta = 0$.

The rate of heat transfer from a horizontal flat plate

By means of Equation (28) an expression for the rate of heat transfer from a horizontal flat plate will now

be obtained. One can readily show from Equations (15) and (19) that

$$\beta(x_1) = [c(n)]^{1/n} x_1^{1/(1+n)} \quad (30)$$

where $c(n)$ is given in Figure 4 and Table 1. Therefore in accordance with Equation (28)

$$-\left(\frac{\partial \theta}{\partial y_1} \right)_{y_1=0} = \frac{1}{0.8930} \left[\frac{c(n)^{1/n} N_{Pr}}{9} \frac{1+2n}{2+2n} \right]^{1/3} x_1^{1/(1+n)} \quad (31)$$

so that the local value of the Nusselt number based on the distance from the leading edge is

$$N_{Su} \equiv -x \left(\frac{\partial \theta}{\partial y} \right)_{y=0} = \frac{(N_{Re})^{1/3}}{0.8930} \left[\frac{c(n)^{1/n} N_{Pr}}{9} \frac{1+2n}{2+2n} \right]^{1/3} x_1^{1/(1+n)} \quad (32)$$

It remains now to determine whether Equation (28) is applicable along the whole surface of the flat plate or only along part of it. One finds from Equation (15) that the momentum boundary-layer thickness is proportional to $x_1^{1/(1+n)}$ and from Equation (25) that the temperature boundary-layer thickness is proportional to $x_1^{2n/(3(1+n))}$. Therefore the ratio of the temperature to the momentum boundary-layer thickness is proportional to $x_1^{n-1/(3(1+n))}$.

For Equation (28) to be accurate, this ratio must be very small, so that for $n < 1$, Equation (31) is valid as $x_1 \rightarrow \infty$; for $n > 1$, Equation (31) is valid as $x_1 \rightarrow 0$.

It can be shown now that for $n < 1$ there exists a region near the leading edge where the momentum boundary-layer thickness is much smaller than that of the temperature. When one calculates the rate of heat transfer for $x_1 \rightarrow 0$ and $n < 1$, therefore, the velocity distribution in the boundary may be disregarded. Thus by setting $u_1 = 1$ and $v_1 = 0$ in Equation (9) and solving the resulting expression by elementary means one finds that

$$-\left(\frac{\partial \theta}{\partial y_1}\right)_{y=0} = \frac{1}{\sqrt{\pi}} x_1^{-1/2} (N_{Pr})^{1/2} \quad (33)$$

and

$$N_{Nu_x} = \frac{x_1^{1/2}}{\sqrt{\pi}} (N_{Re})^{\frac{1}{1+n}} (N_{Pr})^{1/2} \quad (33a)$$

Two asymptotic formulas, Equations (32) and (33a) have been derived then for N_{Nu_x} . It has been found from experience however that for such heat transfer problems it is usually sufficiently accurate to set N_{Nu_x} equal to either Equation (32) or (33a), whichever is appropriate. Let therefore x_1^* be defined as the intersection of these two asymptotes, so that

$$\frac{(x_1^*)^{1/2}}{\sqrt{\pi}} (N_{Re})^{\frac{1}{1+n}} (N_{Pr})^{1/2} = \frac{(N_{Re})^{\frac{1}{1+n}}}{0.8930} \left[\frac{c(n)^{1/n} N_{Pr}}{9} \frac{1+2n}{2+2n} \right]^{1/2} x_1^{\frac{1+2n}{2(1+n)}} \quad (34)$$

With good accuracy then

1. For $n < 1$, N_{Nu_x} is given by Equation (33a) for $0 \leq x_1 \leq x_1^*$ and by Equation (32) for $x_1 \geq x_1^*$.

2. For $n > 1$, N_{Nu_x} is obtained from Equation (32) for $0 \leq x_1 \leq x_1^*$ and from Equation (33a) for $x_1 \geq x_1^*$.

One observes however that as $N_{Pr} \rightarrow \infty$, $x_1^* \rightarrow 0$ for $n < 1$, and $x_1^* \rightarrow \infty$ for $n > 1$; therefore for large Prandtl numbers Equation (28) is applicable essentially over the whole surface of the flat plate. This is very convenient, since the Prandtl number is usually quite large, as will be shown by the following numerical example.

In the flow of a lime-water suspension, the rheological properties of which are (10) $n = 0.17$, $K = 5.48$ lb.-mass sec.⁻ⁿ/ft., $\rho = 90$ lb.-mass cu. ft., $c_p = 0.7$ B.t.u./lb.-mass °F., and $k = 0.7$ B.t.u./ft. °F. hr. $U_\infty = 18,000$ ft./hr., $L = 1$ ft., $c(n)^{1/n} = f''(0) = 0.504$. Therefore $N_{Re} = 312$, $N_{Pr} = 86.2$, and from Equation (34) $x_1^* \sim 10^{-5}$.

Since Equation (28) is general, these results can be generalized to arbitrary surfaces, provided that the function $\beta(x_1)$ can be obtained first from the solution of the equations of motion. Since for most problems involving non-Newtonian fluids N_{Pr} is large, the Lighthill formula, Equation (28), can be used for calculating the local rate of heat transfer over that part of a surface where the boundary-layer equations apply. It is true that, as was shown above, one should expect Equation (28) to break down over a portion of the surface where the momentum boundary-layer thickness is smaller than that of the temperature. This is especially true when $n \rightarrow 0$, as is clear from Equation (18). Under these conditions the velocity distribution in the boundary layer can be overlooked, and the fluid may be assumed ideal for the purpose of obtaining the rate of heat transfer with standard procedures (7). In general however the Prandtl number is quite large, and this region is so small that its existence can for all practical purposes be disregarded.

ACKNOWLEDGMENT

This work was supported in part by a grant from the National Science Foundation and a grant from the Petroleum Research Fund administered by the American Chemical Society. Grateful acknowledgment is hereby made to the foundation and to the donors of said fund.

Thanks are also extended to Eugene J. Fenech for assisting with the numerical calculations.

NOTATION

$c(n)$ = shear-stress coefficient defined by Equation (19)
 c_p = specific heat
 f = defined by Equation (15)
 F_1, F_2 = functions of indicated variables, which have to be obtained from the solution of Equations (7) to (9)
 k = thermal conductivity
 K, n = parameters in the power law model, Equation (5)
 L = characteristic length
 N_{Nu} = Nusselt number
 $N_{Pr} = (c_p U_\infty \rho L) / (k (N_{Re})^{2/(1+n)})$, the Prandtl number
 $N_{Re} = (\rho U_\infty^{2-n} L^n) / K$, the Reynolds number
 N_{Pe} = conventional Peclet number
 T = temperature
 T_s = temperature of the surface
 T_∞ = temperature of the bulk of the fluid
 $U_1(x)$ = the velocity component outside the boundary layer
 U_∞ = a characteristic velocity
 u = velocity component along x
 u_1 = dimensionless velocity com-

ponent defined by Equation (6)
 v = velocity component along y
 v_1 = dimensionless velocity component defined by Equation (6)
 x = distance along the surface from the leading edge
 x_1 = dimensionless distance defined by Equation (6)
 x_1^* = defined by Equation (34)
 y = distance normal to the surface
 y_1 = dimensionless distance defined by Equation (6)

Greek Letters

$\beta(x_1)$ = defined by Equation (23)
 $\Gamma(1/3)$ = the gamma function of $1/3 = 1.3541$
 δ = parameter in the Pohlhausen profile, Equation (21)
 η = defined by Equation (15)
 θ = dimensionless group defined by Equation (6)
 ρ = density
 τ_{xy} = the shear stress
 τ_w = the shear stress at the wall
 ϕ = dimensionless group defined by Equation (6)

LITERATURE CITED

- De Haven, E. S., paper presented at the A.I.Ch.E. meeting in Montreal, Canada (April, 1958).
- Bird, R. B., *A.I.Ch.E. Journal*, **2**, 428 (1956).
- Fage, A., and Y. M. Falkner, *Rept. Mem. Aeronaut. Res. Comm. London*, No. 1314 (1931).
- Frederickson, A. G., and R. B. Bird, *Ind. Eng. Chem.*, **50**, 347 (1958).
- Grigull, U., *Chem.-Ing. Tech.*, **28**, 553 (1956).
- Goldstein, S., "Modern Developments in Fluid Dynamics," Vol. II, Oxford Press (1938).
- Grosh, R. J., and R. D. Cess, *Trans. Am. Soc. Mech. Engrs.*, **80**, 667 (1958).
- Lighthill, M. J., *Proc. Roy. Soc. (London)*, **A202**, 359 (1950).
- Lyche, B. C., and R. B. Bird, *Chem. Eng. Sci.*, **6**, 35 (1956).
- Metzner, A. B., in "Advances in Chemical Engineering," ed. by T. B. Drew and J. W. Hoopes, Jr., Vol. I, pp. 79-150, Academic Press, New York (1956).
- , and J. C. Reed, *A.I.Ch.E. Journal*, **1**, 434 (1955).
- Metzner, A. B., R. D. Vaughn, and G. L. Houghton, *ibid.*, **3**, 92 (1957).
- Metzner, A. B., *Ind. Eng. Chem.*, **49**, 1429 (1957).
- Schlichting, Hermann, "Boundary Layer Theory," McGraw-Hill, New York, (1955).
- Töpfer, C., *Z. Math. u. Phys.*, **60**, 397 (1912).
- Weltmann, R. N., *Ind. Eng. Chem.*, **48**, 386 (1956).

Manuscript received May 4, 1959; revision received September 28, 1959; paper accepted October 5, 1959.

Use of Momentum Balance in Calibrating Orifices for Flow of Gases

J. J. MARTIN and V. R. PABBI

University of Michigan, Ann Arbor, Michigan

A method of determining the absolute calibration of a gas-flow orifice without the use of gas holders or any comparative device is described. The method is based on the application of the momentum balance, as well as the energy balance, to the flow of the gas. The application requires the measurement of pressures on the face of the orifice in addition to the usual pressure-drop measurements along the axis of flow.

Orifice coefficients determined by the force-momentum principle are shown to agree within an average deviation of 1.4% with those determined by other standard techniques. Also the application of the force-momentum principle demonstrates clearly why orifice coefficients are much less than unity.

The absolute calibration of an orifice for gas-flow measurement usually requires somewhat awkward and bulky equipment, particularly if the flow rates are high. This is due to the fact that large volumes of gas must be collected and measured at constant pressure. To avoid building a large gas holder with a constant pressure control system, one is inclined to calibrate an orifice by comparison with some other device which has previously been given an absolute calibration. The reliability of the comparison calibration therefore depends upon the accuracy with which the original absolute calibration was made. This may not always be completely satisfactory to the user of an orifice, who would prefer his own absolute calibration.

This study was undertaken to develop a procedure for calibrating a gas-flow orifice by measuring pressure only. In the conventional treatment of an orifice an energy balance is applied to the flowing stream. In the following treatment emphasis is placed on the application of the momentum balance and on the determination of the forces which are exerted on the flowing stream.

THEORY

Figure 1 is a diagrammatic sketch of the flow through a circular thin-plate orifice of standard design (1). Point 1 is taken at least one pipe diameter upstream, where the flow is not appreciably affected by the orifice; point 2 is in the plane of the upstream face of the orifice opening itself; point 3 is at the vena contracta, the narrowest section of the rapidly moving stream; and point 4 is taken several pipe diameters downstream, where maximum pressure recovery has been obtained.

For flow of a gas where the pressure drop across the orifice is not more than one-tenth the absolute upstream pressure, experimental studies show that the following assumptions are reasonable. (1) There is almost negligible friction between points 1 and 3; the bulk of the friction loss occurs between

points 3 and 4 during the irreversible expansion of the moving stream. (2) The pressure at the vena contracta point 3 is little different from the pressure immediately on the downstream side of the orifice plate. For a freely discharging orifice, such as one in which there is no pipe downstream from the orifice (that is discharge is directly to a large chamber), this assumption is exact. (3) The density of the gas may be assumed constant at the average pressure and temperature between points 1 and 3, since for small pressure drops the density does not vary much. (4) The pressure exerted backward by the upstream face of the orifice plate is uniform over the plate and equal to P_1 . This assumption will later be modified slightly.

With the above assumptions one may write momentum, energy, and mass balances for the fluid between points 1 and 3:

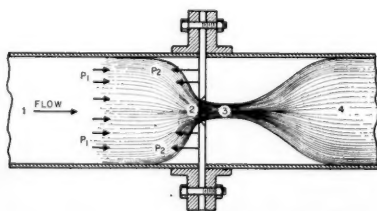


Fig. 1. Diagrammatic sketch of flow through a thin-plate orifice.

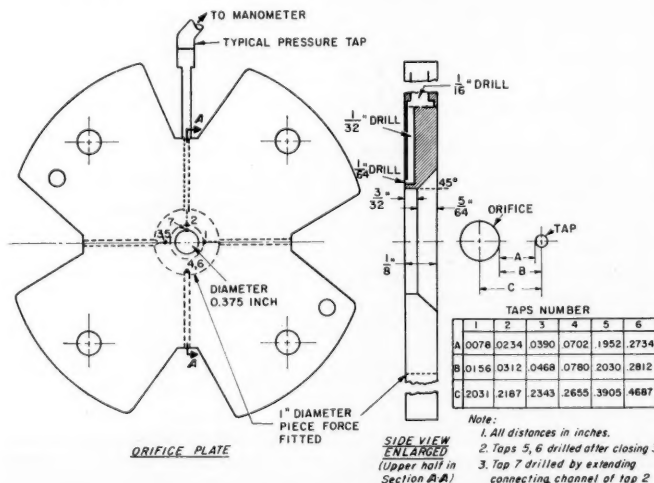


Fig. 2. Experimental orifice plate.

TABLE 1

Ratio orifice diameter pipe diameter	K, experimental (Amer. Soc. Mech. Engrs.)	Equation (6)
		$K = \frac{1}{2 \sqrt{1 - \frac{A_2}{A_1}}}$
0	—	0.5
0.125	0.6015	0.503
0.4	0.609	0.545
0.5	0.625	0.577
0.6	0.652	0.625

TABLE 2

Run	Pressure differential = in. of water						
C ^a →	0.2031	0.2187	0.2343	0.2655	0.3905	0.4687	0.1033
1	24.8	27.95	29.0	30.0	—	—	31.2
2	17.6	19.85	20.7	21.3	22.1	22.15	22.1
3	11.6	13.2	13.7	14.1	14.6	14.65	14.7
4	23.8	25.8	26.9	27.6	28.5	28.5	28.6
5	5.2	5.8	6.0	6.1	6.12	6.27	6.4
6	19.35	22.2	22.9	23.05	—	—	23.6
7	15.22	17.15	17.9	18.4	—	—	19.2
8	11.75	13.27	13.95	14.2	14.6	14.65	14.7
9	5.0	5.55	5.9	6.0	6.12	6.27	6.35
10	12.15	13.85	14.30	14.75	14.70	14.92	15.30

^a C = Distance between tap and orifice in inches shown in Figure 2. Average air temperature = 82°F. Average barometric pressure = 29.9 in. Hg.

Momentum balance

$$\frac{u_1 \rho A_1}{g_c} (u_3 - u_1) = P_1 A_1 - P_1 (A_1 - A_2) - P_2 A_2 = A_2 (P_1 - P_2) \quad (1)$$

Energy balance

$$\frac{u_1^2}{2g_c} + \frac{P_1}{\rho} = \frac{u_3^2}{2g_c} + \frac{P_2}{\rho} \quad (2)$$

Mass balance

$$u_1 A_1 \rho = u_2 A_2 \rho = u_3 A_3 \rho \quad (3)$$

It is to be noted in Equation (1) that the pressure applies over the whole orifice area and not merely over the cross-sectional area at point 3, in line with the second assumption.

From Equations (1) and (3), u_1 may be eliminated to give

$$u_3^2 = \frac{u_2^2 A_2^2}{A_1^2} + \frac{(P_1 - P_2) g_c A_2^2}{u_2^2 \rho} + \frac{2(P_1 - P_2) g_c A_2}{\rho A_1} \quad (4)$$

In the same manner Equations (2) and (3) may be combined to give

$$u_3^2 = \frac{u_2^2 A_2^2}{A_1^2} + \frac{(P_1 - P_2) 2g_c}{\rho} \quad (5)$$

If now the last two equations are equated to eliminate u_3 , there results after simplification

$$u_2 = \frac{1}{2 \sqrt{1 - \frac{A_2}{A_1}}} \sqrt{\frac{2g_c(P_1 - P_2)}{\rho}} \quad (6)$$

Experimental values of the coefficient in the equation

$$u_2 = K \sqrt{\frac{2g_c(P_1 - P_2)}{\rho}} \quad (7)$$

are given for orifice Reynolds numbers above 10,000. These may be compared with the theoretical prediction of Equation (6), as shown in Table 1.

It is seen that although the theory predicts the order of magnitude of K , and indeed why K is nowhere near unity, still the agreement with experimental

values is not sufficiently good to recommend the use of the theoretical K 's for accurate measurement of flow. It was suspected that the major discrepancy was due to the fourth assumption above. The backward pressure of the orifice plate would hardly be uniform all the way from the edge of the pipe to the edge of the orifice opening. It would seem reasonable that this pressure would be equal to P_1 at the edge of the pipe but would fall rapidly in the immediate vicinity of the orifice.

If the average pressure along the upstream side of the orifice plate is taken as something less than P_1 , say $0.9 P_1$, the momentum balance Equation (1) becomes

$$\frac{u_1 \rho A_1}{g_c} (u_3 - u_1) = P_1 A_1 - 0.9 P_1 (A_1 - A_2) - P_2 A_2 = A_2 (P_1 - P_2) + 0.1 P_1 (A_1 - A_2) \quad (8)$$

Since $A_1 - A_2$ is positive, the right side of (8), which is the net force acting on the fluid, is greater than $A_2 (P_1 - P_2)$ alone. Therefore it is said that the net force is $m A_2 (P_1 - P_2)$, where $m > 1$. If this quantity is used for the right side of (8), and Equations (2) and (3) are combined with it in the same manner as before, the result is

$$u_2 = \frac{m}{2 \sqrt{1 - \frac{m A_2}{A_1}}} \sqrt{\frac{2g_c(P_1 - P_2)}{\rho}} = K \sqrt{\frac{2g_c(P_1 - P_2)}{\rho}} \quad (9)$$

To use Equation (9) it is necessary to evaluate the quantity m . The following describes the experimental deter-

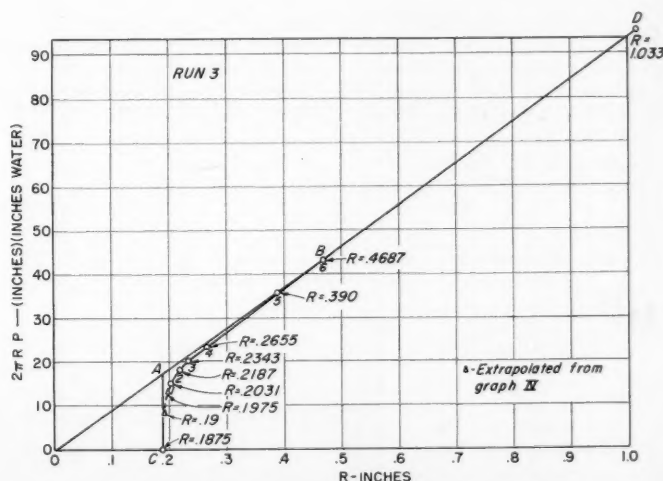


Fig. 3. Data for run 3 to give resisting force of orifice plate.

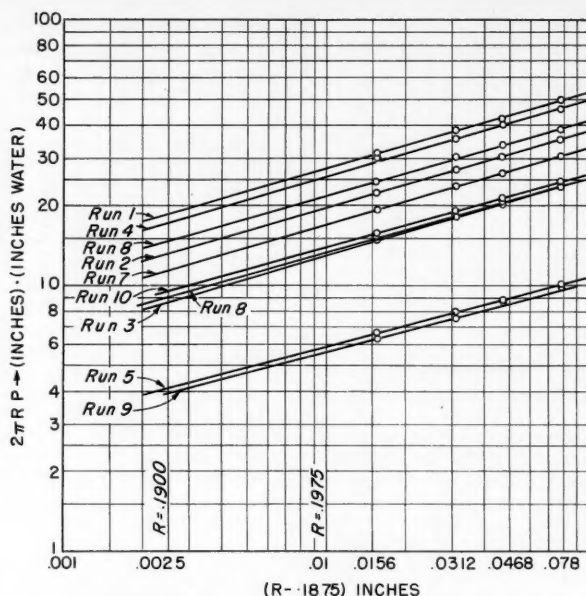


Fig. 4. Extrapolation of orifice-plate pressures to points closer to orifice radius.

mination of m and subsequently the coefficient calculated from it.

EXPERIMENTAL WORK

The orifice plate was constructed according to specifications (1) to permit comparison with the experimental values of K . A $\frac{1}{8}$ -in. brass plate was used with a $\frac{1}{8}$ -in. orifice hole drilled in the center, as shown in Figure 2. The hole was beveled at an angle of 45 deg. on the downstream side so that the cylindrical portion along the axis of flow was $3/64$ -in. long.

On the upstream face of the orifice four small holes, $1/64$ -in. diameter, were drilled to a depth of $1/32$ -in. at varying distances from the orifice opening. These were connected to small holes running parallel to the plane of the plate, permitting pressure communication to outside manometers. The distances between the pressure-tap holes in the upstream face and the orifice are shown in the table on Figure 2. It is noted that the hole closest to the orifice has its edge

only 0.0156 in. from the edge of the orifice. Getting the pressure hole this close to the orifice posed a very difficult problem. Also accurate drilling was required to make each hole perfectly circular and to meet it properly with the $1/32$ -in. hole parallel to the plate. This was done by building the orifice plate in two parts. A center section of 1-in. diameter was prepared with its $1/64$ -in. pressure holes and $1/32$ -in. connecting holes. The outer section was made with $1/16$ -in. holes leading to the manometer tubing connections. This section had a hole in center just 1 in. in diameter, into which the center section was force fitted and soldered. In addition to the four pressure taps shown, two extra holes were drilled later to get better spacing of pressure data across the upstream face of the orifice.

The finished orifice plate was mounted between standard flanges in a 2-in. schedule 40 pipe. The calming section of pipe preceding the orifice was 4 ft. long. The orifice was fed air from a compressed air line and discharged directly into the

room. The pressure taps were connected to manometer tubes which could measure up to 32 in. of water pressure drop with a precision of ± 0.05 in.

DATA

Pressure readings at various taps are presented in Table 2 for ten runs. A separate run with tap 7 right inside the orifice opening showed the pressure there to be that of the room.

RESULTS

Discharge coefficients evaluated from Equation (9) are summarized in Table 3 and compared with those taken from the American Society of Mechanical Engineers report. The method of calculation of K in Equation (9) can be explained by reference to Figure 3 which for run 3 plots $2\pi RP$ vs. R . The area under a curve on this plot constitutes a force according to the integral

$$F = \int_{R_1}^{R_2} 2\pi RP dR \quad (10)$$

The area under the straight line, $OABD$, represents the total force at the upstream position pushing the fluid toward the orifice. The area under ABD is the force from the orifice plate opposing the flow if the pressure over the plate were uniformly the same as the upstream pressure. The area under the curve, CBD , is the actual measured force of the orifice plate opposing the flow. The area of the triangle, $OACO$, is the net force accelerating the fluid in the idealized case where the pressure on the orifice plate is uniform and equal to the upstream pressure. The area of the irregular shape, $OABCO$, is the net force determined experimentally, and it is clearly seen how this force is greater than that in the idealized case.

It is noted on Figure 3 that the experimental pressure points across the orifice plate extend down to a radius of $R = 0.2031$ in. To obtain pressures closer to the orifice radius of 0.1875 in., where the pressure must go to zero, the quantity $2\pi RP$ was plotted vs. $R - 0.1875$ on logarithmic coordinates as shown in Figure 4. For all runs the curves on this graph yielded straight lines, so that extrapolation to points closer to the orifice opening was justified. In this manner the pressures at $R = 0.1975$ and 0.1900 in. were obtained for use on Figure 3.

In the specific case of run 3 the area $OABCO$ was found to be 1.890 units, while $OACO$ gave 1.595 units. This made $m = 1.890/1.595 = 1.185$. Using this in Equation (9) with $A_2/A_1 = (0.375/2.067)^2 = 0.0329$ one determines K as 0.604.

The Reynolds number in the orifice

TABLE 3

Run	Reynolds number in orifice	K from equation (9)	K from R (1)	Percentage deviation $\left(\frac{K_0 - K_{A.S.M.E.}}{K_{A.S.M.E.}} \right)$
1	70,400	0.616	0.598	+3.01
2	59,000	0.596	0.599	-0.50
3	48,500	0.604	0.601	+0.50
4	62,400	0.607	0.599	+1.34
5	32,000	0.593	0.602	-1.49
6	61,000	0.587	0.598	-1.84
7	55,000	0.609	0.600	+1.50
8	48,500	0.597	0.601	-0.67
9	32,000	0.600	0.602	-0.33
10	49,500	0.617	0.601	+2.66

was calculated in the usual way as $D_0 \rho u_s / \mu$. Air was assumed to behave as an ideal gas at the low pressures employed in this work.

DISCUSSION AND CONCLUSIONS

The agreement between the measured orifice coefficients according to the American Society of Mechanical Engineers report and those determined by use of the momentum balance is considered quite good. It would be desirable in a more complete study to try other ratios of orifice to pipe diameter. However it is believed that the agreement in this experiment demonstrates the applicability of the momentum balance and the assumptions employed. The study shows rather graph-

ically why the orifice coefficient is in the neighborhood of 0.6.

If an orifice is to be used to measure gas flow and there is no convenient way to make a calibration, the technique of measuring a few pressures on the upstream face of the orifice plate should prove useful. The most serious drawback would be the mechanical problem of making pressure taps close to the orifice opening. However this problem can be solved as shown here.

NOTATION

A = area
 D = diameter
 F = force
 g_c = conversion factor = 32.17 (lb.-mass/lb.-force) (ft./sec.²)

K = orifice discharge coefficient
 m = ratio of net force in actual case to that in idealized case
 P = pressure
 R = radius
 u = velocity
 μ = viscosity

Subscripts

1 = upstream position
 2 = orifice opening
 3 = vena contracta

LITERATURE CITED

1. Am. Soc. Mech. Engrs., "Fluid Meters, Their Theory and Application," 4 ed. (1937); Am. Soc. Mech. Engrs., "Flow Measurement," Part 5 (1940).

Manuscript received June 17, 1959; revision received September 28, 1959; paper accepted October 1, 1959. Paper presented at A.I.Ch.E. Kansas City meeting.

The Mechanics of Vertical Moving Fluidized Systems: IV. Application to Batch-Fluidized Systems with Mixed Particle Sizes

ROBERT F. HOFFMAN, LEON LAPIDUS, and J. C. ELGIN

Princeton University, Princeton, New Jersey

The present paper extends the previous investigations from this laboratory on ideal fluidized systems to a system which is somewhat nonideal. Mixtures of different but well-defined glass spheres are fluidized by water to ascertain whether the principles developed for a single particle size still hold. The analysis indicates that the ideal prediction method gives a reasonable representation of the batch-expansion curves for mixed sizes.

In a previous publication from this laboratory (3) a detailed theoretical analysis was presented for predicting the behavior of all types of vertical

moving fluidized systems. The basic postulate of this development was the proposal that a simple unique relationship exists between the slip velocity and the holdup for any system. The slip velocity is defined as the relative velocity between the particles and the fluid and can be represented mathematically as

$$V_s = \text{slip velocity} \\ = \frac{V_f' - V_s'}{1 - \epsilon} \quad (1)$$

In accordance with the theory, the holdup can be calculated for any mode of fluidization once the relationship between the slip velocity and the holdup has been determined. Figure 1 gives a typical relationship.

The generalized theory has however been proved only for ideal systems (1,

11, 12, 14). An ideal system is one of uniform rigid spheres fluidized with a liquid having a density not too different from that of the particles. Such a system was termed *particulate fluidization* by Wilhelm and Kwauk (16).

The present investigation was undertaken to study the behavior of a

TABLE 1. PHYSICAL PROPERTIES OF GLASS SPHERES USED

Particle	U.S. screen	Average diameter, in.	Average deviation from average diameter, %	Density, lb./cu. ft.
1	40	0.0183	4.1	157.6
3	60	0.0106	4.5	155.2
6	170	0.00382	3.8	152.0
7	140	0.00475	4.9	154.0
8	80	0.00752	3.5	153.9

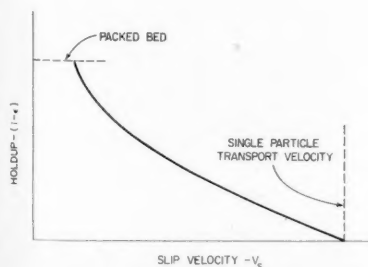


Fig. 1. Typical holdup slip velocity for an ideal batch fluidized bed.

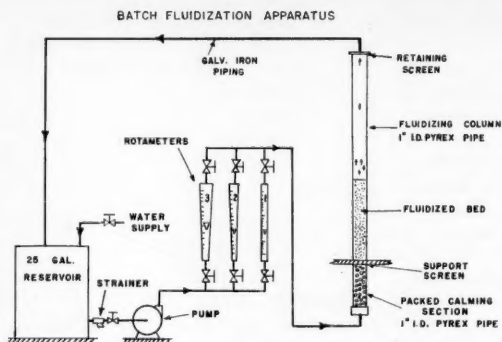


Fig. 2. Schematic diagram of fluidization apparatus.

batch or nonfed bottom restrained fluidized system which was somewhat nonideal, the nonideality occurring because of nonuniform particle size. To develop the necessary principles, mixed beds consisting of two or three distinct measurable particle sizes rather than a spectrum of sizes were used. The experimental work was intended to provide basic information on a batch system which could be used for a possible extension or modification of the generalized theory to include nonideal systems.

LITERATURE SURVEY

Some work has been done previously by other investigators dealing with fluidized beds with mixed particle sizes. These data however are few and in some cases conflicting. No previous systematic study of the effect of particle-size distribution on the batch expansion curves (Figure 1) has apparently been made.

Lewis, Gilliland, and Bauer (6) and Morse (10) report the use of an average particle diameter in correlating data from batch expansion with mixed sizes along with uniform particle data. Such correlations are in the form of modified-drag-coefficient-Reynolds-number plots. However no numerical size distributions within the bed were reported.

Mixtures of various-sized particles have been separated by passing a fluid upward through a suspension of mixed size particles, effecting a transport of the smaller-sized particles from the mixture. In a batch-fluidized system McCune and Wilhelm (7), Lewis and Bowerman (5), and Richardson and Zaki (13) observed a size distribution within the bed, the fines being removed to the top of the bed. Richardson and Zaki further found that for one experiment with a binary mixture of particle sizes the holdup could be calculated as the weighted sum of the holdups of each individual particle size.

Mertes and Rhodes (8, 9) mention briefly the possibility of attacking the problem of holdup-slip-velocity relationship for mixtures of sizes but do not present any experimental work.

More recently Furukawa and Tsutoma (2) have performed miscibility experiments for fluidized beds with binary mixtures of various-sized sand and charcoal. They observed size separation within the fluidized bed and the formation of two layers consisting of each component of the mixture, respectively. The reported separation, however, was found to be only a partial one. Their work did not include the effect of mixed sizes on the actual batch expansion curves.

The recent work of Andrieu (4) is probably the most complete and thorough

available at the present time on segregation of solids.

Previous work is not sufficiently complete to permit the prediction of batch expansion curves but does indicate the possibility of size separation.

EXPERIMENTAL

Fluidization Apparatus

The fluidization apparatus consisted of a glass fluidizing column, a pump, a water reservoir, rotameters, and interconnecting piping as shown schematically in Figure 2.

The fluidizing column was constructed of 1-in. Pyrex pipe, at either end of which was a retaining screen made of U.S. 170 bronze-wire cloth. Below the fluidizing column was a 12-in. packed section which minimized velocity gradients at the inlet to the fluidizing column. The pump was a three-stage centrifugal one.

Glass Spheres

Binary and ternary mixtures of particle sizes were made from known quantities of glass spheres, each having a uniform diameter. These were obtained by a careful screening of glass beads. Table 1 lists the pertinent physical properties of the particles used.

By means of a calibrated micrometer eyepiece, the beads were examined microscopically to check the sphericity and to

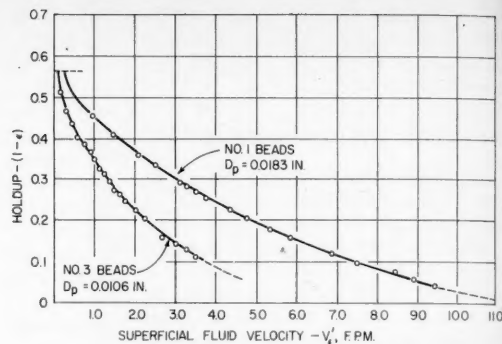


Fig. 4. Batch expansion curves for glass beads 1 and 3 in water.

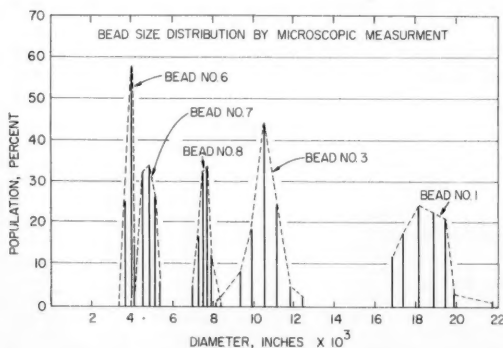


Fig. 3. Graphical representation of bead-size distribution as determined by microscopic measurement.

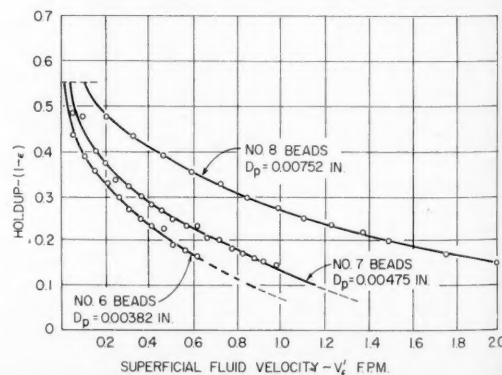


Fig. 5. Batch expansion curves for glass beads 6, 7, and 8 in water.

TABLE 2. PARTICLE MIXTURE USED IN PRESENT EXPERIMENTS

	Particle mixture		D_a/D_b	Quantity in mixture, % B
	A	B		
I	Particle 1	Particle 3	1.73	50
II	Particle 1	Particle 3	1.73	80
III	Particle 8	Particle 7	1.58	33.3
IV	Particle 8	Particle 7	1.58	50
V	Particle 7	Particle 6	1.24	33.3
VI	Particle 7	Particle 6	1.24	70
VII	Particle 3, 8 and 7		2.23/1.58/1.0	33.3% of each

determine size distribution. The average diameter and size distribution were obtained from measurement of a random sample of one hundred beads. The spectra of size distribution is shown graphically in Figure 3. Although a spread of diameters is seen in this diagram, the average percentage deviation from the average particle diameter is less than 5%. This narrow size distribution is the closest approximation to uniformly sized beads that can be approached by standard screening techniques.

The density of each bead size was determined by water displacement.

Glass-Bead Coloring Procedure

To observe the extent of the segregation during fluidization of binary and ternary mixtures, one size of beads in a mixture was colored by a process originally proposed for dyeing glass fibers (15). The fibers are heated with various ionic solutions, and supposedly the ions are absorbed in the glass by a base exchange of the solution ions with the alkali and alkaline earth metals in the glass. It was found that a blue coloration, produced by the formation of Prussian blue, was most easily reproduced on the beads. Density measurements after coloration showed that the coloring process had no significant effect upon the bead density.

Fluidization Procedure

Each uniform size of glass beads (No. 1, 3, 6, 7, and 8) was fluidized separately to determine the individual batch expansion curves. The procedure used in the fluidization of the individual-sized beads was as follows:

1. A given weight of beads was fluidized in the column until the bed had expanded to the full height of the column.

2. The water rate was decreased incrementally, with the height of the fluidized bed and the fluid rate being measured after each increment. Time was allowed for the system to reach equilibrium at each fluid rate.

3. The water temperature was maintained at 22° to 23°C. throughout each run.

A similar experimental technique was used in the fluidization of the mixed particle sizes. In this latter case, however, each bead size was of a different color, and the heights of the individual segments of the bed (blue and white layers) were measured in addition to over-all height.

RESULTS

Individual Batch Curves

The batch-expansion curves obtained for each individual bead size, shown in Figures 4 and 5, are presented in terms of superficial fluid velocity, rather than slip velocity, to facilitate the prediction of the batch expansion curves for binary and ternary mixtures, as will be described later.

Size Separation in Mixtures of Sizes

The six binary mixtures and one ternary mixture which were fluidized in this investigation are presented in Table 2.

Two types of size separation were observed in the experiments with mixed sizes. First, in the case where the beads were of widely different diameters (I, II, III, IV, and VII), a

very sharp size separation was noted. When steady state was reached, two distinct layers were seen with a very clearly defined interface between the layers. This layer formation was easily observed, since each size of bead was a different color. The separation into sizes was essentially complete, with few if any particles of one size detectable in the zone of the other.

In the second case (V and VI), where the beads were of nearly the same diameter, only a partial separation into layers was observed. In this case a transition region existed between the two layers. The height of this transition region varied with the fluid velocity. As the fluid velocity was decreased, the upper layer became smaller, while the height of the upper interface remained almost constant. Thus the fraction of the bed height occupied by the transition region increased with decreasing fluid velocity. The behavior of this fluidized system suggests strongly the analogous behavior of liquid mixtures which may be partially or completely immiscible and in which the degree of miscibility is determined by the temperature (here in the form of fluid velocity or energy).

Prediction of Batch Expansion Curves for Mixtures of Sizes

If a perfect size separation occurs in a fluidized bed of mixed particle sizes of the same density, the total height of the bed will be the sum of the heights of the individual particle-size layers. The height of each layer is given by

$$L_i = \frac{W_i}{\rho_i} \cdot \frac{1}{A} \cdot \frac{1}{(1 - \epsilon_i)} \quad (2)$$

and the total holdup defined as

$$(1 - \epsilon_t) = \frac{W_t}{\rho_t} \cdot \frac{1}{A} \cdot \frac{1}{L_t} \quad (3)$$

In terms of individual particle-layer weights the holdup thus becomes

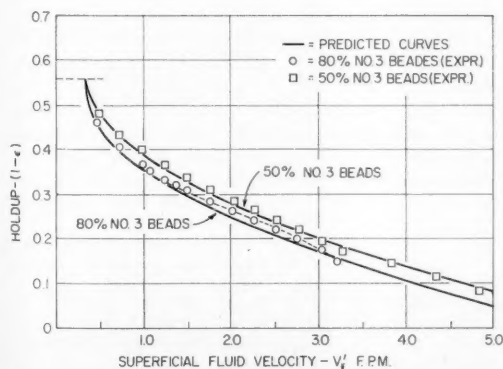


Fig. 6. Comparison of experimental data with predicted batch expansion curves for binary mixtures of glass beads 1 and 3.

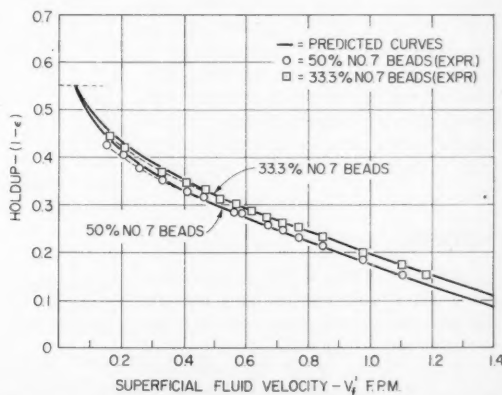


Fig. 7. Comparison of experimental data with predicted batch expansion curves for binary mixtures of glass beads 7 and 8.

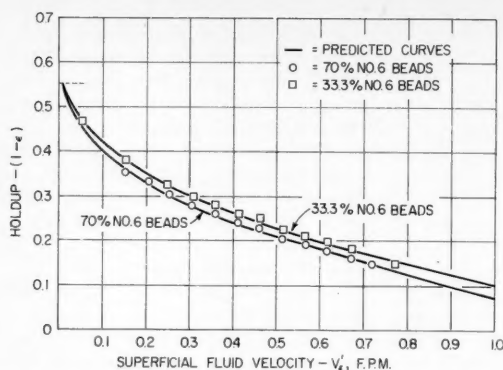


Fig. 8. Comparison of experimental data with predicted batch expansion curves for binary mixtures of glass beads 6 and 7.

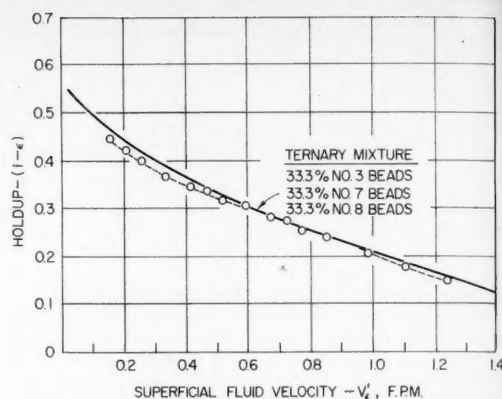


Fig. 9. Comparison of experimental data with predicted batch expansion curves for a ternary mixture of glass beads 3, 7, and 8.

$$(1 - \epsilon_i) = \frac{1}{\frac{X_1}{1 - \epsilon_1} + \frac{X_2}{1 - \epsilon_2} + \dots + \frac{X_i}{1 - \epsilon_i}} \quad (4)$$

$$= \frac{1}{\sum_{n=1}^i \frac{X_n}{1 - \epsilon_n}}$$

The comparison between experimental holdup-fluid velocity curves for mixed particle sizes and those calculated by means of Equation (4) and the experimentally determined slip velocity-holdup curves measured for the individual particle sizes is shown in Figures 6 to 9. For the most part the experimental expansion data give excellent agreement with the theoretical curves as predicted from the single-size-particle data. The error calculated for the majority of the points is of the order of 3% or less with the maximum error being 7 to 8%. It is seen that in some cases the experimental data curves contain some discontinuities in the form of bumps or dips, which are believed to be the result of nonidealities in the individual layers of the fluidized bed. Such nonidealities can produce higher or lower holdups in each layer than were observed for a fluidized bed of uniform particle size.

An important result is that the calculated and experimental curves agree extremely well for the partially segregated beds having closely sized particles.

DISCUSSION

The nonidealities of the individual layers which produce in some of the mixtures deviations from the over-all predicted curves may be the result of one of two factors. First, the individual layers of the mixtures may behave as partially restrained systems. When the uniformly sized beads are fluidized,

there is no restriction at the top of the bed, while at the bottom there is a fixed restraint in the form of the bed support screen. In a two- or three-layer mixture, however, the lower layer is partially restrained at the top by the presence of the upper layer, and this restraint can cause a higher holdup in the lower region. In addition, the upper layer is no longer totally restricted at the bottom, since the only restriction is the variable height of the lower layer. Second, there may be some degree of mixing between layers, causing a mixture of sizes within each individual holdup from the ideal case.

In spite of these nonidealities, in most cases the ideal prediction curve, Equation (4), gives excellent agreement with the experimental data. The actual random motion which takes place on the individual particle level in a fluidized bed is an extremely complex phenomenon, and any prediction method must be a simplification of the actual process. Recognizing this fact, one must make the general conclusion that the ideal prediction method gives a reasonable representation of the batch expansion curves for mixed sizes. As a result it is possible to predict the holdup curves for mixed particle sizes through the use of Equation (4) and any one of the several correlations available for the batch expansion curve.

NOTATION

A = cross-section area of fluidizing column
L = height of fluidized bed
 V'_f = superficial fluid velocity
 V'_d = superficial net particle velocity through fluidized bed

V_s = slip velocity
W = weight of particles having a diameter D_i
X = weight fraction
 ϵ = void fraction of fluidized bed
(1 - ϵ) = holdup of fluidized bed
 ρ_i = density of particles having a diameter D_i

Subscript

n = nth particle diameter in the mixture

LITERATURE CITED

1. Flinn, D. R., M. S. thesis, Princeton Univ., Princeton, N. J. (1954).
2. Furukawa, J., and O. Tsutoma, *Ind. Eng. Chem.*, **50**, 821 (1958).
3. Lapidus, Leon, and J. C. Elgin, *A.I.Ch.E. Journal*, **3**, 63 (1957).
4. Leva, Max, Personal communication.
5. Lewis, E. W., and E. W. Bowerman, *Chem. Eng. Progr.*, **48**, 603 (1952).
6. Lewis, W. K., E. R. Gilliland, and W. C. Bauer, *Ind. Eng. Chem.*, **41**, 1104 (1949).
7. McCune, L. K., and R. H. Wilhelm, *ibid.*, 1124 (1949).
8. Mertes, T. S., and H. B. Rhodes, "Fluid-Particle Behavior," Sun Oil Company, Marcus Hook, Pa.
9. ———, *Chem. Eng. Progr.*, **51**, 429, 517 (1955).
10. Morse, R. D., *Ind. Eng. Chem.*, **41**, 1117 (1949).
11. Price, B. G., Leon Lapidus, and J. C. Elgin, *A.I.Ch.E. Journal*, **5**, 93 (1959).
12. Quinn, J., Ph.D. thesis, Princeton Univ., Princeton, N. J. (1958).
13. Richardson, J. F., and W. N. Zaki, *Trans. Inst. Chem. Eng., (London)*, **32**, 35 (1954).
14. Struve, D. L., Leon Lapidus, and J. C. Elgin, *Can. J. Chem. Eng.*, **36**, 141 (1958).
15. U.S. Patent 2,245,783 (1941).
16. Wilhelm, R. H., and Mooson Kwauk, *Chem. Eng. Progr.*, **44**, 201 (1948).

Manuscript received January 19, 1959; revision received September 15, 1959; paper accepted September 17, 1959.

Point Source Turbulent Diffusion in a Pipe

DUANE L. FLINT, HISAO KADA, and THOMAS J. HANRATTY

University of Illinois, Urbana, Illinois

Turbulent diffusion from a small source located in the center of a 3-in. pipe was studied. Hydrogen and carbon dioxide were mixed in air, and potassium chloride solution was mixed in water. Eddy diffusion coefficients calculated from the data are correlated by plotting $(E)/(2u'x)$ vs. N_{Re} . Differences from other data in the literature are discussed. The results could not be used for determining the form of the correlation coefficient because of inaccuracies in the measurements for small diffusion times.

Many processes involving turbulent transport of heat and mass may be described in terms of a number of sources and sinks of heat or mass in the flow field being considered. For example in the transfer of heat from a hot wall to a cold wall through a turbulently flowing fluid the hot wall may be considered as consisting of a series of infinitesimal heat sources, and the cold wall may be considered as consisting of a series of infinitesimal sinks of heat (7). A better understanding of turbulent transfer processes therefore may be obtained by studying the behavior of sources of heat and mass in a turbulent field. In this paper data are presented on the diffusion of mass from a small source located in the center of a pipe through which water or air is flowing.

A foreign substance is injected into the flow through a small tube. Samples are withdrawn from the flow stream at different positions along a diameter in a plane downstream of the source plane over a time period which is long compared with the time scale of the turbulence and are analyzed for the concentration of the diffusing substance. The spread of the diffusing material is characterized by the x -component of the mean-squared displacement of the material from its centroid, designated by the symbol \bar{X}^2 . By carrying out such measurements for different distances between the plane of the injector and the plane of the sampling tube the rate of spread of the diffusing material can be obtained. The data presented in this paper are compared with results of investigations by Towle and Sherwood (18) and by Mickelsen (14) for air flows in a pipe. Disagreement amongst the three investigations is noted, and possible explanations are discussed.

THEORY

Taylor's statistical description of turbulent diffusion (17) is used to present the results of this investigation. This treatment has been described in an excellent review by Frenkiel (6)

and in numerous other articles which have appeared in the literature (1, 12, 13, 20, 8); only a brief outline will be presented here. Taylor's description of turbulent diffusion is valid only for a homogeneous isotropic field. Since pipe flows are neither homogeneous nor isotropic, the justification for its use is that it provides a convenient framework for presenting the results of this research.

Taylor considered the diffusion of a particle with the same properties as the fluid. He described the average behavior of a large number of these particles which originate from a fixed point in the field in terms of the variation with time of the x component of the mean-squared displacement from the origin. He related this variation to the properties of the turbulence through two parameters, the intensity of the velocity fluctuations in the x direction, and the scale, which is a measure of the lifetime of the eddies responsible for turbulent diffusion. This scale is defined by

$$\tau = \int_0^\infty R ds \quad (1)$$

where

$$R = \frac{u_x u_{x+s}}{u'^2} \quad (2)$$

All of the above averages are taken with respect to a large number of excursions of single particles through the field. The x component of the mean-squared displacement is given as a function of time by

$$\bar{X}^2 = 2\bar{u}^2 \int_0^t (t-s) R(s) ds \quad (3)$$

As time approaches zero, the correlation coefficient approaches unity and the above integral approaches

$$\bar{X}^2 = \bar{u}^2 t^2 \quad (4)$$

If the time interval is long compared with the Lagrangian time scale, Equation (3) becomes

$$\bar{X}^2 = 2\bar{u}^2 \tau t + \text{constant} \quad (5)$$

or

$$\frac{1}{2} \left(\frac{d\bar{X}^2}{dt} \right)_{t \gg \tau} = \bar{u}^2 \tau \quad (6)$$

The above equation is analogous to the Einstein equation (2) for the molecular diffusion coefficient

$$\frac{1}{2} \frac{d\bar{X}^2}{dt} = \text{constant} = D \quad (7)$$

However unlike Equation (6) the last expression is always valid. A turbulent diffusivity may be defined analogous to the molecular diffusion coefficient as

$$E = \bar{u}^2 \tau \quad (8)$$

The relation between \bar{X}^2 and t for intermediate times depends on the form of the correlation coefficient. As yet turbulence theory is unable to predict the dependency of the correlation coefficient on time. Likewise its experimental determination is quite difficult. Three forms for R which have been used are

$$R(s) = e^{-\alpha s} \quad (9)$$

$$R(s) = e^{-\alpha s^2} \quad (10)$$

$$R(s) = 1 - \alpha s \quad s < \frac{1}{\alpha} \quad (11)$$

$$R(s) = 0 \quad s > \frac{1}{\alpha}$$

First consider the form $R = e^{-\alpha s}$. From the definition of τ the constant α can be evaluated:

$$\tau = \int_0^\infty e^{-\alpha s} ds = \frac{1}{\alpha}$$

$$\alpha = \frac{1}{\tau} \text{ and } R(s) = e^{-\frac{s}{\tau}} \quad (12)$$

Substituting into Equation (3) and integrating one obtains

$$\bar{X}^2 = 2\bar{u}^2 \tau \left[t - \tau \left(1 - e^{-\frac{t}{\tau}} \right) \right] \quad (13)$$

For times large in comparison with τ

$$\bar{X}^2 = 2\bar{u}^2 \tau t - 2\bar{u}^2 \tau^2 \quad (14)$$

If $R = e^{-\alpha s^2}$ is employed, the following equations are obtained:

$$\alpha = \frac{\pi}{4\tau^2}; R(s) = e^{-\frac{s^2}{4\tau^2}} \quad (15)$$

Duane L. Flint is now with the Union Oil Company, Brea, California, and Hisao Kada is with the Monsanto-Kasei Chemical Company, Ltd., Tokyo, Japan.

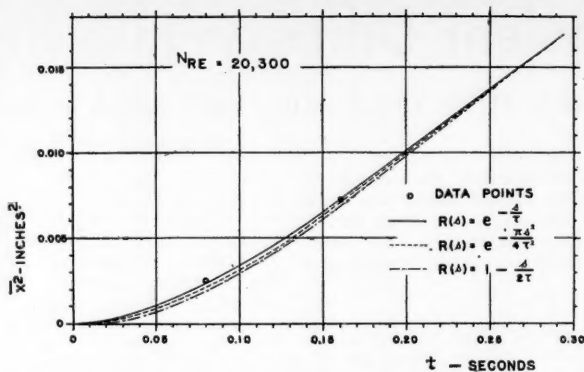


Fig. 1. Comparison of equations for the correlation coefficient at small times.

$$\bar{X}^2 = 2 \bar{u}^2 \tau \left[t \operatorname{erf} \left(\frac{\sqrt{t}}{2\tau} \right) + \frac{2\tau}{\pi} \exp \left(-\frac{\pi^2 t^2}{4 \tau^2} \right) - \frac{2\tau}{\pi} \right] \quad (16)$$

$$\bar{X}^2 = 2 \bar{u}^2 \tau t - \frac{4}{\pi} \bar{u}^2 \tau^2 \quad t \gg \tau \quad (17)$$

For the third form of the correlation coefficient considered

$$\alpha = \frac{1}{2} \tau; R(s) = 1 - \frac{s}{2\tau} \quad 0 \leq s \leq 2\tau$$

$$R(s) = 0 \quad s \geq 2\tau \quad (18)$$

$$\bar{X}^2 = \bar{u}^2 \left(t^2 - \frac{t^3}{6\tau} \right) \quad 0 \leq t \leq 2\tau \quad (19)$$

$$\bar{X}^2 = 2 \bar{u}^2 \tau t - \frac{4}{3} \bar{u}^2 \tau^2 \quad 2\tau \leq t \quad (20)$$

Equations (12) and (18) are known to be incorrect for very small values of s , since the correlation coefficient should vary as s^2 at small times (20). However despite this inaccuracy they have been used as empirical descriptions of the correlation coefficient.

Equations (13), (16), (19), and (20) are plotted in Figure 1; only two data points are shown, since most of the measurements reported in this paper were made at larger times, or larger distances from the injector, than are represented by the abscissa. The parameters τ and \bar{u}^2 used in calculating the curves were obtained from the slope and intercept of the asymptote to the experimental data at large times. It can be seen that the form of the \bar{X}^2 vs. time curve is not sensitive to the form of the correlation coefficient. However the turbulent intensity calculated by fitting Equations (13), (16), (19), and (20) to experimental data will vary somewhat depending on the correlation coefficient used. For the curves in Figure 1 $R = e^{-s^2/4\tau}$ gives $\sqrt{\bar{u}^2}/U_c = 0.057$, $R = e^{-(\pi^2 s^2)/(4\tau^2)}$ gives

$\sqrt{\bar{u}^2}/U_c = 0.046$, and $R = 1 - s/2\tau$ gives $\sqrt{\bar{u}^2}/U_c = 0.045$. Very accurate measurements at small diffusion times would be needed to discern which of the assumed correlation coefficients best describes point-source diffusion. Such accuracy is difficult to attain in mass diffusion studies, and therefore it is not likely that such studies will establish the correct form of the correlation coefficient.

APPARATUS FOR STUDYING DIFFUSION IN AIR

Point source turbulent diffusion in air was studied by injecting hydrogen or carbon dioxide in the center of a flowing air stream. Figure 2 shows a schematic diagram of the equipment used in this study. The test section was made of two lengths of 3½-in. O.D. and 3.15-in. I.D. smooth copper pipe which were connected by a soldered collar to give a total length of 20 ft. This gave an entry section of about 72 pipe diameters prior to the test section to allow for full development of the velocity profile. The pipe was positioned in a vertical direction, and air was supplied to the top from a gear type of rotary pump. High flow rates were measured by a venturi meter attached to the lower end of the copper pipe, and low flow rates were measured with an orifice meter. Hydrogen or carbon dioxide was metered and fed to a ¼-in. steel tube extending through a fitting at the top of the 20-ft. pipe section so that the velocity of the injected gas would be approximately equal to the air velocity in the pipe. Riders consisting of three knife-edged legs were attached to the steel tubing to position it in the center of the pipe. An 8-in. length of ⅜-in. brass tubing with an inside diameter of 0.060 in. was soldered to the end of the injector tube. An additional 1½ in. of 1/16-in. hypodermic tubing was attached to the ⅜-in. brass tubing. For a few runs a total of 9½ in. of ⅜-in. brass tubing was used as the final section of the injector. The tips of the injectors were cut off at a right angle and beveled from the inside so that a sharp protruding edge was presented to the flow. The distance between the plane of the injector and the

plane of the sampling tube was varied by moving the injector tube up and down the center of the pipe. A scale was etched directly on the top portion of the ¼-in. steel tube so that the exact position of the injector could be determined. Two sampling probes which could move across diameters at 90 deg. to each other were located 1 ft. from the lower end of the copper pipe. The probes were attached to a carriage that was moved by a micrometer screw. The probes consisted of a length of ⅜-in. brass tubing attached to the carriages and 1½-in. extensions silver soldered at right angles to the brass tubing. The 1½-in. extensions were either 1/16-in. hypodermic tubing or 1/8-in. thin walled nichrome tubing. The ends of the extensions were cut at right angles and were beveled in the same manner as the injector tubes.

Gas samples were withdrawn through the sampling tubes at a carefully controlled velocity which was less than the velocity of the air in the pipe. The gas composition was measured with a thermal conductivity bridge. Chambers containing thermistor elements constituted two legs of the bridge circuit. Pure air obtained from a fixed probe located halfway up the test section was passed through one of these chambers; the gas sample to be analyzed was passed through the other chamber. The gas flows were carefully controlled at a constant value and were metered by measuring the pressure drop over a constriction. These constrictions and the chambers containing the thermistor elements were immersed in a constant-temperature bath controlled to $\pm 0.005^\circ\text{C}$. The line leading into the chambers containing the thermistors consisted of several coils of ¼-in. copper tubing which were immersed in the constant-temperature bath. The variation of the relative resistance of the two thermistors was measured by the off balance of the bridge circuit. Since the two thermistor elements were not exactly matched, a variable resistance in series with one of the thermistors was adjusted so that the bridge was balanced when air was in both thermistor

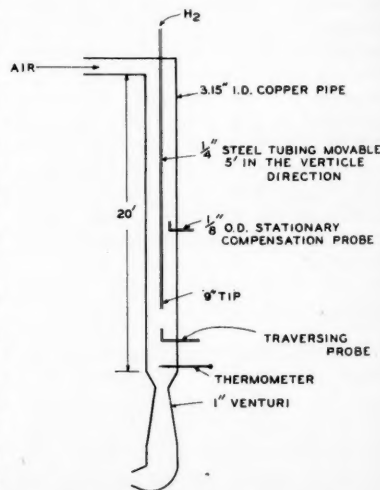


Fig. 2. Apparatus for studying diffusion in air.

chambers. The other two legs of the bridge were a 25-kohm. resistor and a 25-kohm. helipot. The voltage source to the bridge was two 12-v. storage cells. The current was controlled at a fixed value of 1.300 ma. by a variable resistance in series with the storage cells and measured by a potentiometer from the voltage drop across a 10-ohm resistor. The off balance of the bridge was measured with a potentiometer which had a range of 0 to 80 mv. By use of the helipot this range was extended to 8,000 mv. without changing the sensitivity, and a much larger concentration range could be conveniently measured. The helipot is a precision variable resistor on which the variable tap can be moved by definite increments (4). The constriction used to meter the hydrogen and carbon dioxide was calibrated by a water-displacement method. This calibration was used as a basis for the calibration of the orifice and venturi meters and of the conductivity cells.

APPARATUS FOR STUDYING DIFFUSION IN WATER

The basic design of the apparatus for studying point source turbulent diffusion in water was the same as that used for air. A schematic drawing of the experimental setup is shown in Figure 3. The study was carried out in a 3-in. I.D. vertical Pyrex pipe. One normal potassium chloride solution was injected into the system at approximately the same velocity as the water in the pipe through a tube which could be moved up and down the center of the pipe. A length of about 75 pipe diameters preceded the test section so that the flow was fully developed in the test section. Samples were removed from the flow stream at different locations along a diameter by a stainless steel tube positioned by a micrometer screw and were analyzed for potassium chloride content by measuring their electroconductivity. Demineralized water was used to increase the sensitivity of the electroconductivity measurements. As it was impractical to

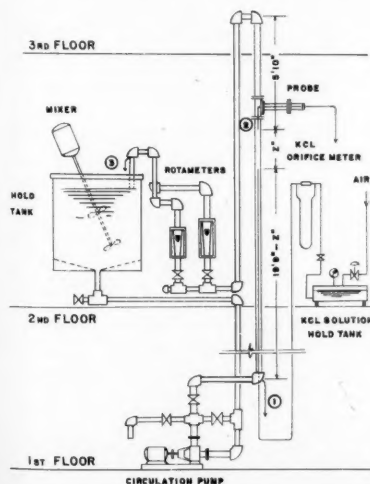


Fig. 3. Equipment for studying diffusion in water.

TABLE 1. CONCENTRATION PROFILE DATA FOR DIFFUSION OF HYDROGEN AND CARBON DIOXIDE

Reynolds number = 72,000
Inside pipe diameter = 3.15 in.
Gas temperatures = 28.5 to 33.7°C.
Gas pressures = 77.8 to 79.0 cm. Hg
 r_c = center of the concentration profile
 Z = distance between the plane of the injector and the plane of the traverse

Run I-102			Run II-92		
$Z = 5$ in.			$Z = 5$ in.		
r_c	Vol. %		r_c	Vol. %	
in.	H ₂		in.	CO ₂	
0.0000	3.69		0.0000	2.65	
0.0500	3.65		0.0250	2.55	
0.1000	3.08		0.0500	2.22	
0.1250	2.70		0.0750	1.98	
0.1500	2.31		0.1000	1.65	
0.1750	1.89		0.1250	1.31	
0.2000	1.487		0.1500	1.05	
0.2250	1.110		0.1750	0.73	
0.2500	0.805		0.1875	0.61	
0.2750	0.584		0.2000	0.49	
0.3000	0.400		0.2125	0.49	
0.3250	0.268		-0.2750	0.49	
0.3500	0.168		-0.2625	0.56	
0.4000	0.060		-0.2500	0.66	
0.4500	0.014		-0.2250	0.89	
0.5000	0.005		-0.2000	1.20	
-0.4500	0.000		-0.1750	1.53	
-0.4000	0.019		-0.1500	1.85	
-0.3500	0.093		-0.1250	2.17	
-0.3000	0.235		-0.1000	2.40	
-0.2750	0.355		-0.0750	2.61	
-0.2500	0.529		-0.0500	2.71	
-0.2250	0.762		-0.0250	2.71	
-0.2000	1.025				
-0.1750	1.333				
-0.1500	1.704				
-0.1250	2.09				
-0.1000	2.49				
-0.0750	2.85				
-0.0500	3.25				
-0.0250	3.56				

discharge the water after sampling, the water was recirculated through the system. Mixed average samples of the inlet feed were taken throughout a run, and the electroconductivity of this sample was subtracted from the electroconductivity of the probe sample to give a net conductivity due to the newly injected potassium chloride solution.

The water was circulated with a pump and metered by two rotameters. Two rubber-tube connectors, attached to the main flow line at the outlet of the glass lined holding tank, absorbed the vibration of the holding tank caused by the mixer mounted on the tank. The injector tube was made of 5/64-in. I.D., 1/4-in. O.D. stainless steel tubing. Several fins attached to the injector fixed it at the center of the pipe. A fine glass tube of 0.0327-in. I.D. and 0.070-in. O.D. was attached to the top of the stainless steel tube. The potassium chloride solution was fed to the injector from a pressurized tank lined with acid-proof paint. The sampling probe was constructed of the same size stainless steel tubing as the injector. A fine glass tube having an opening of 0.076 in. was attached to it.

The equipment used for electroconductivity measurements consisted of a bridge,

a conductivity cell, an oscillator, and an oscilloscope. The four ratio arms of the bridge consisted of two fixed resistors, one adjustable standard resistor, and the conductivity cell dipped in the sample of unknown potassium chloride concentration. The resistance of the solution between two electrodes of the conductivity cell was measured by this bridge, and the conductivity could be calculated from this resistance. Alternating voltage of 1,000 cycles/sec. and about 24 v. was applied to the bridge, and the bridge was balanced by regulating the adjustable resistor. The balance point was detected by an oscilloscope which showed a flat image when the bridge was balanced. The components consisted of a shielded ratio box, an adjustable air capacitor, and a five-dial shielded a.c. resistance box. The samples were immersed in a constant-temperature bath during measurements.

TREATMENT OF DATA

Under the conditions of the experiments diffusion in the longitudinal direction had a negligible effect upon the concentration profiles (4, 5, 6). Likewise measurements were confined to the central portion of the pipe, where the average fluid velocity was approximately constant. Therefore the material in a plane at a distance Z from the injector could be considered as being in the field a time $t = Z/U_c$. All of the profiles except those for gas flows 2 in. from the source or closer were Gaussian. Data on a few traverses are tabulated in Table 1. For Gaussian profiles the concentration is described by the equation

$$c = \frac{Q}{2\pi U_c X_m^2} e^{-\frac{r^2}{2X_m^2}} \quad (21)$$

$$Q = \pi a^2 V c_{AV} \quad (22)$$

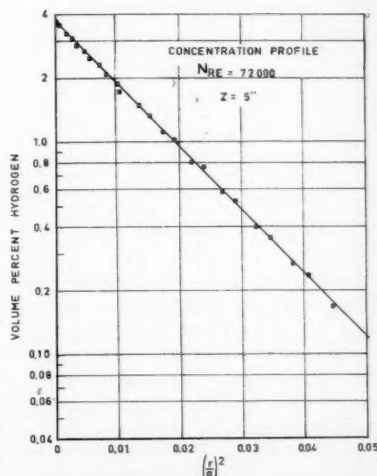


Fig. 4. Concentration profile for diffusion of hydrogen in air.

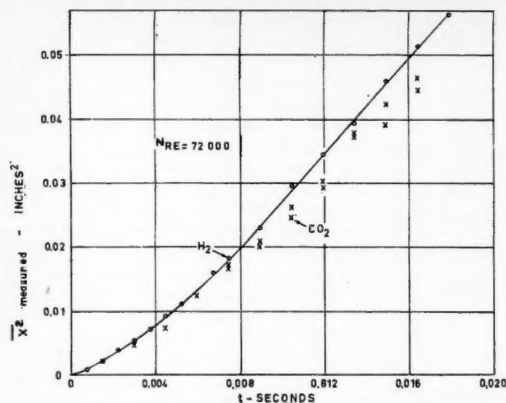


Fig. 5. Comparison of uncorrected hydrogen data with carbon dioxide data.

or

$$\frac{c}{c_{AV}} = \frac{a^2 V}{2 U_c \bar{X}_m^2} e^{-\frac{r^2}{2 \bar{X}_m^2}} \quad (23)$$

The quantity \bar{X}_m^2 was calculated from the slope of a plot of either c or c/c_{AV} vs r^2 . A typical plot of the data is shown in Figure 4. The mean-squared displacement could also be calculated from the intercept of such plots at $r = 0$. However the calculation from the intercept is not as reliable as the calculation from the slope, since low values of the center concentration or high values of the calculated \bar{X}_m^2 will result by measuring a concentration profile which does not go through the center of the diffusing plume. For the cases in which a Gaussian profile was not measured the \bar{X}_m^2 was evaluated by graphically integrating the following equations:

$$\bar{X}_m^2 = \frac{\bar{R}^2}{2} = \frac{\int_0^R 2\pi r^3 c dr}{2 \int_0^R 2\pi r c dr} \quad (24)$$

or

$$\bar{X}_m^2 = \frac{\int_0^R r^3 \frac{c}{c_{AV}} dr}{2 \int_0^R r \frac{c}{c_{AV}} dr} \quad (25)$$

From a series of concentration traverses at different distances from the injector a plot of \bar{X}^2 vs. t could be constructed. Taylor's description of turbulent diffusion was formulated for a point source of material. Batchelor (1) has shown that for finite sources the displacement can be considered as increased over the displacement for a point source by a constant amount \bar{X}_0^2 . The quantity \bar{X}_0^2 is approximately

equal to the displacement in the original source. If the initial source is of diameter d and if the concentration is uniform over the source

$$\bar{X}_0^2 = \frac{d^2}{16} \quad (26)$$

In actual experiments it is not likely that such an ideal initial source will be obtained. In the correlation of the data for the air experiments \bar{X}_0^2 was calculated for a d of 1/16 in., and for the water experiments \bar{X}_0^2 was based on a d of 0.083 in. The values of \bar{X}_0^2 were small enough so that the finite injector size had a negligible effect on the plot of \bar{X}^2 vs. t . However the correction \bar{X}_0^2 did have an effect on the root mean-square displacements at small times.

The effect of molecular diffusion was negligibly small for the runs with water because of the low molecular diffusion coefficient of the diffusing substance. However in the runs with air molecular diffusion was affecting the data as can be seen in Figure 5, where data with hydrogen and carbon dioxide are compared. The carbon dioxide did not diffuse as fast as the hydrogen as can be seen by comparing the \bar{X}_m^2 for carbon dioxide and for hydrogen at a fixed diffusion time. An exact theory to predict the role of molecular diffusion in the turbulent-diffusion process is not yet available. Taylor (17) suggested that the turbulent- and molecular-diffusion processes are independent and additive:

$$\bar{X}_m^2 = \bar{X}^2 + 2 Dt \quad (27)$$

This equation was used to correct all the data presented in this paper. For example by subtracting $2 Dt$ from the two sets of data in Figure 5 the results were brought into approximate agreement. It is expected that such a correction is valid for diffusing material with

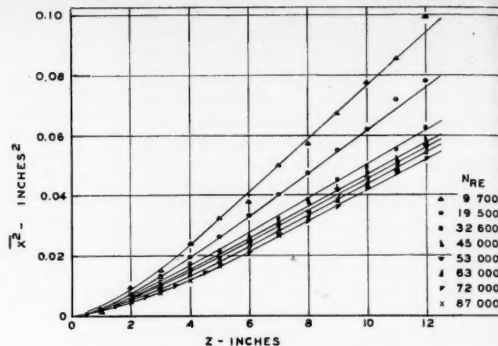


Fig. 6. Mean-square displacement data for air.

a small molecular-diffusion coefficient; however it is quite likely that it would be incorrect when the ratio of the molecular-diffusion coefficient to the turbulent-diffusion coefficient is relatively large. Hinze (9) discusses a theory of Burgers which suggests that turbulent diffusion is decreased by molecular diffusion owing to the escape of the diffusing property from fluid particles moving through the field. Townsend (19) has proposed a theory of accelerated diffusion for small diffusion times such that the spread of material would be larger than is predicted by Equation (27). Neither of these theories have been completely verified experimentally. It was not feasible to compare Townsend's theory with the data in this research, since the data at very small diffusion times were not accurate enough to justify such a comparison. Since no significant difference in the turbulent-diffusion coefficients for potassium chloride in water and for hydrogen and carbon dioxide in air were obtained with

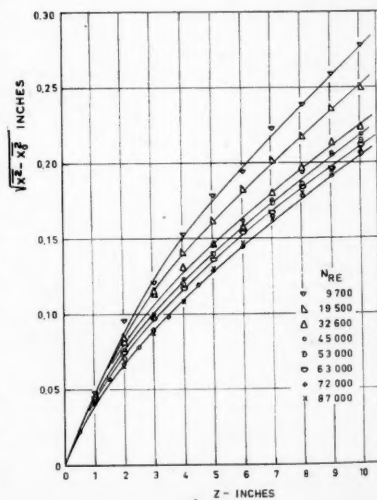


Fig. 7. Root-mean-square displacement data for air.

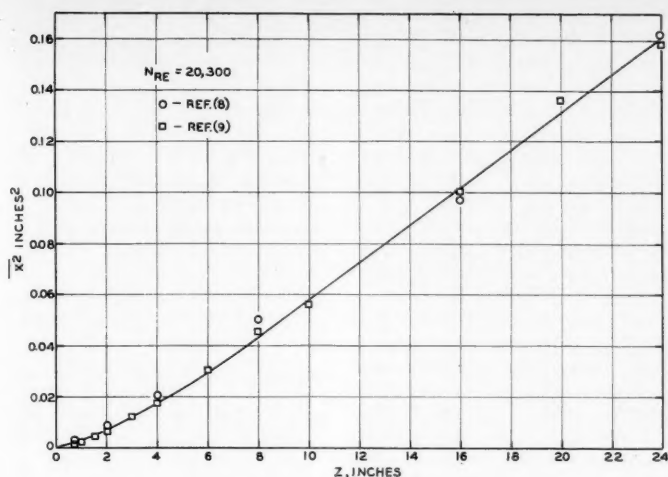


Fig. 8. Mean-square displacement data for water.

Equation (27) used to correct the data, Burger's theory could not be compared with the data.

A turbulent diffusivity, $E = \overline{u^2} \tau$, was calculated from the slope of the $\overline{X^2}$ vs. t curve at large times. From Equation (6) it can be seen that the slope is equal to twice the turbulent diffusivity.

The turbulent intensity or the Lagrangian time scale could not be evaluated from the results of this research as reliably as the turbulent diffusivity. Accurate data close to the source are needed for such an evaluation; such data are not readily obtained in mass diffusion experiments because of disturbances caused by the introduction of the diffusing substance and by the closeness of the probe and the injector. Values of $\overline{u^2}$ were calculated in two ways. From Equation (4) it can be seen that the intensity is the initial slope of a plot of $\sqrt{\overline{X^2} - \overline{X^2_0}}$ vs. t . Values of the intensity were also calculated by assuming forms for the correlation coefficient given by Equations (12), (15), and (18). From the t axis intercept of the limiting asymptote of the $\overline{X^2}$ vs. t curve and the slope of the asymptote $\overline{u^2}$ could be evaluated by means of Equations (14), (17), and (20).

RESULTS

Measurements with air with hydrogen used as the tracer gas were made for a total of eight runs which covered a range of Reynolds numbers from 9,700 to 87,000. For one Reynolds number (72,000) runs were made with both hydrogen and carbon dioxide used as the tracer gases. Measurements were made with water for Reynolds numbers of 20,300 and 50,500.

Plots of $\overline{X^2}$ vs. Z and of $\sqrt{\overline{X^2} - \overline{X^2_0}}$ vs. Z for the data with air are shown in Figures 6 and 7; plots of $\overline{X^2}$ vs. Z for water are shown in Figures 8 and 9. The two sets of data points at $Re = 20,300$ in Figure 8 were obtained at different times. Their agreement shows the reproducibility of the experiments.

Data points shown in Figures 6, 8, and 9 that were obtained at distances greater than $1\frac{1}{2}$ to 2 pipe diameters from the injector could be approximated by the asymptotic equation for large times [Equation (5)]. As is shown in reference 4 for the air runs and in Figure 8 for the water runs the linear relation between $\overline{X^2}$ and Z extends to a distance of about 8 pipe diameters from the source. For distances greater than this the data appear to be affected by the nonuniform velocity distribution in the pipe.

Turbulent-diffusion coefficients calculated from the slopes of the $\overline{X^2}$ vs. Z curves at large Z are plotted in Figure 10 along with the data of Towle and

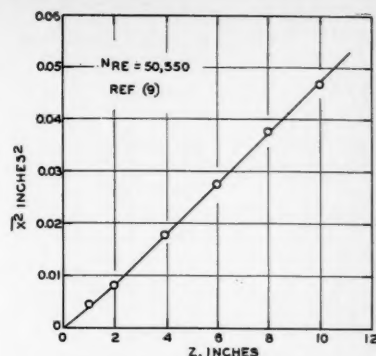


Fig. 9. Mean-square displacement data for water.

Sherwood and of Mickelsen. Mickelsen's measurements were made in a larger pipe (8 in.) than the ones presented in this work. Owing to the dilution of the injected material he did not obtain many measurements in the region in which Equation (5) approximates the data. On the basis of the slope of the $\overline{X^2}$ vs. Z curves obtained in this research values of E were obtained from Mickelsen's results by drawing a straight line through his measurements of $\overline{X^2}$ at distances from the injector greater than 2 pipe diameters. In each of his runs only three data points could be used.

Calculated values of the turbulent intensity for air are compared in Figure 11 with the hot wire anemometer measurements of Sandborn (15) in the center of a pipe. Intensities calculated from the initial slope of the $\sqrt{\overline{X^2} - \overline{X^2_0}}$ vs. t curve and from the different forms of the correlation coefficient are higher than measurements with a hot wire. The correlation coefficient $R = e^{-u^2 \tau^2}$ gave intensities quite close to the values calculated from the initial slopes. The $\overline{X^2}$ vs. t curves were represented by $R = e^{-u^2 \tau^2}$ a little better than the other two forms tested.

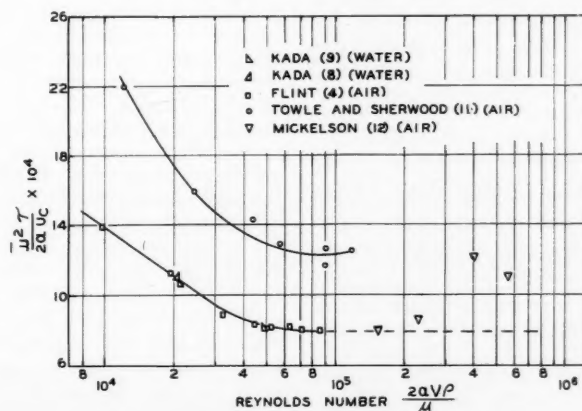


Fig. 10. Correlation of data on turbulent diffusion coefficients.

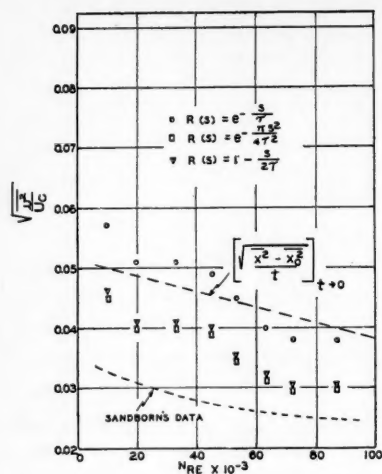


Fig. 11. Comparison of intensities with hot-wire data.

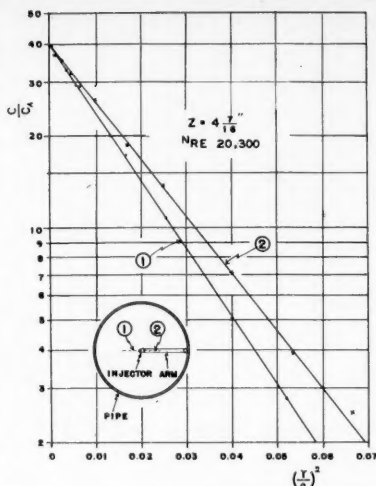


Fig. 12. Concentration profile for test injector.

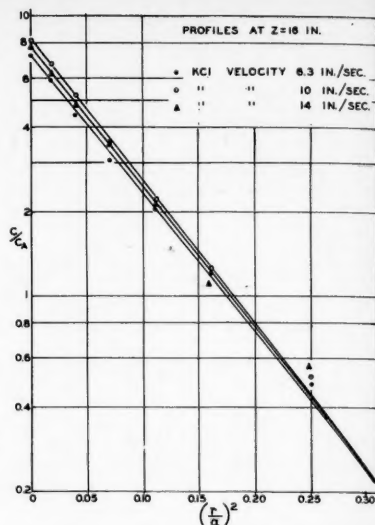


Fig. 13. Effect of injection velocity on concentration data.

DISCUSSION OF RESULTS

The good agreement between the results for air and water in Figure 10 suggests that the plot of the diffusion data in the dimensionless form of $E/2aU_c$ vs. $2aV\rho/\mu$ produces a general correlation which should be valid for other systems. The group $E/2aU_c$ decreases with Reynolds numbers and at a Reynolds number of about 50,000 levels out to a constant value of about 0.0082. The data of Mickelsen yield values of $E/2aU_c = 0.0081$ at $N_{Re} = 167,000$ and $E/2aU_c = 0.0087$ at $N_{Re} = 250,000$. His low Reynolds number runs are in fair agreement with the results of this research. However the increase in $E/2aU_c$ with increasing N_{Re} is not to be expected. Data on velocity profiles in a pipe (16) show that the dimensionless form of the eddy viscosity $E_m/2aU_c$ becomes approximately constant for large N_{Re} . It seems likely that the turbulent-diffusion coefficient obtained from point source diffusion measurements should show similar behavior. Therefore it is expected that the data from this research should extrapolate to higher Reynolds numbers as indicated by the dashed line in Figure 10. Since the turbulent-diffusion coefficient may be viewed as the product of an intensity term $\sqrt{u^2}$ and a scale $\sqrt{u^2\tau}$, the constancy of $E/2aU_c$ implies the constancy of the two terms $\sqrt{u^2}/U_c$ and $\sqrt{u^2\tau}/2a$. Mickelsen used an entrance section of only 36 pipe diameters prior to the test section. As he pointed out in his paper, the flow in his test section might not have been fully developed and free from entry disturbances. The data of Towle and Sherwood are about 60% higher than

the results of this research. The reason for this difference is not entirely clear. A possible explanation is the lack of symmetry in the concentration profiles reported by Towle and Sherwood. They used injectors supported by horizontal arms of 1/4-in. O.D. for a 6-in. duct and of 3/8-in. O.D. for a 1-ft. duct. In run series (K) (Kh) concentration profiles measured along diameters at right angles to one another were quite different. The plot of $\ln C$ vs r^2 produced a larger turbulent-diffusion coefficient for the profile in line with the injector support than for the profile perpendicular to the line of the support. However in series (B) the profiles appear to be symmetrical. Because of the possibility of a lack of symmetry in their data Towle and Sherwood used only the center-line concentrations to calculate the eddy-diffusion coefficient [see Equation (21)].

The agreement amongst the data for diffusion of hydrogen and carbon dioxide in air and for diffusion of potassium chloride in water indicates that the correction for molecular diffusion used in Equation (27) was valid for the data obtained in this research for large diffusion times and for Reynolds numbers greater than 20,000. At a Reynolds number of 20,000 the ratio of the molecular-diffusion coefficient to the turbulent-diffusion coefficient was 0.17 for the runs with hydrogen. At a Reynolds number of 9,700 this ratio would be about 0.30. Since no data were obtained with carbon dioxide or with potassium chloride at $N_{Re} = 9,700$, it is not certain whether Equation (27) was valid for hydrogen diffusion at this Reynolds number.

To investigate the effect of injector design some experiments were performed with the injector shown in Figure 12. This injector was a 1/8-in. O.D. brass tube. It was brought into the system through the packing in the flange just before the sampling station. The tube came down along the inside wall of the glass pipe and had two right angle bends so that the outlet faced downstream in the center of the pipe. At $N_{Re} = 20,300$ and at a distance of 4.7/16-in. the asymmetrical concentration profile shown in Figure 12 was obtained for a traverse along the line parallel to the support arm. Traverses perpendicular to the support arm were symmetrical and in agreement with the results obtained with the injector used in this research. It appears as if the horizontal support arm disturbed the flow.

Slight variations in the injection velocity did not appear to affect the results. This is indicated in Figure 13 by the fact that injection velocities of 6.3 in./sec., 10 in./sec., and 14 in./sec. gave approximately the same result.

The effect of the inlet condition at the bottom of the pipe used for water runs on the concentration profiles was also tested. A 1 ft. thick packed bed consisting of two layers was placed at the inlet. The lower layer was 6 in. thick and made of 1/4-in. Berl saddles. The upper layer was 6-in. and consisted of 1/4-in. diameter glass spheres. Diffusion data obtained with this system agreed with data obtained without a packed section at the bottom of the pipe.

In the type of experiments reported in this paper it is impossible to elimi-

nate all disturbances created in the flow stream by the injection system. It is also quite difficult to say exactly how these disturbances are affecting the results. It has been assumed that at large distances from the injector the diffusion rate is unaffected by the presence of the injector. If in these regions the concentration profile is Gaussian and is distributed symmetrically around the center of the pipe (as was true in this research), then the change in the distribution of the diffusing material will be the same as if it had originated from a point source in an undisturbed stream at some time which is different from the actual time the material has been in the field. Since the turbulent-diffusion coefficient is calculated from the slope of the \bar{X}^2 vs. t curve at large times, it should not be affected by disturbances created by the injector unless these disturbances are propagated a large distance downstream. Some preliminary runs (4) on diffusion in air with an injector twice as large as the one used to obtain the data presented in this paper yielded slightly higher (7% at $N_{Re} = 30,000$ and 17% at $N_{Re} = 70,000$) values of E than those in Figure 10. It is not certain whether this disagreement results from inaccuracies in these measurements which cannot be accounted for at this time or whether it results from increased disturbance due to the use of a larger injector. The calculation of a turbulent intensity from data at small diffusion times or from the intercept on the time axis of the asymptote to the \bar{X}^2 vs. t curve at large times would be affected by disturbances in the neighborhood of the injector. This is probably the reason for the lack of agreement with intensities obtained from hot wire anemometer measurements shown in Figure 10. This conclusion is supported by the results obtained by Mickelsen. He did his experiments with a pipe which was almost three times as large as the one used in this research and with an injector of the same size. Therefore the region over which Equation (4) should approximate the data was larger in his experiments, and more accurate values of the turbulent intensity should be obtained from diffusion data. He found close agreement between turbulent intensities from diffusion data and those measured with a hot-wire anemometer.

Some experiments (2) have been performed at a Reynolds number of 10,000 to obtain a more direct measure of the extent of the disturbances introduced by the presence of injectors of the type used in this research. A heating wire of 0.0126-in. diameter was extended across the pipe 3 in. downstream from a 20 in. length of $\frac{1}{8}$ -in.

diameter tubing located in the center of the pipe. Temperature measurements made downstream of the injector were compared with measurements obtained without the tubing at the pipe center. Close to the heating wire a larger spread of heat was obtained with the tubing present. This result supports the conclusion that the discrepancy between intensities measured by the diffusion technique and by the hot-wire anemometer was due to disturbances introduced by the injector. Far downstream from the heating wire no significant difference was noted in measurements made with and without the injector being present. Figure 14 presents data at a distance of 12 in. The measurements indicate that disturbances introduced by the injector were not propagated far enough downstream to affect the calculation of the limiting slope of the \bar{X}^2 vs. z curve at large distances from the injector.

ACKNOWLEDGMENT

The authors are grateful to the Office of Ordnance Research for supporting this work.

NOTATION

a	= radius of pipe
c	= concentration of diffusing substance
c_{AV}	= mixed average concentration of diffusing material
d	= inside diameter of injector
D	= molecular-diffusion coefficient
E	= turbulent-diffusion coefficient = $\bar{u}^2 \tau$
N_{Re}	= Reynolds number = $2aV\rho/\mu$
Q	= quantity of diffusing material injected per unit time
r	= radial distance
R	= Lagrangian correlation coefficient

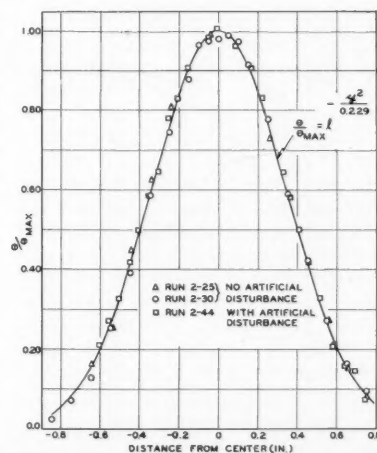


Fig. 14. Effect of artificial disturbance on diffusion of heat.

s	= time increment
t	= time
u	= turbulent velocity fluctuation in the x direction
\bar{u}^2	= mean-square turbulent velocity fluctuation in the x direction
V	= mixed average fluid velocity
U_c	= time average fluid velocity at the center of the pipe
\bar{X}^2	= x component, the mean-square displacement of particles due to turbulent diffusion
\bar{X}_{me}^2	= measured value of \bar{X}^2
\bar{X}_c^2	= correction used to account for finite source
Z	= distance in the direction of flow between the injector plane and the sampling plane
θ	= temperature
μ	= fluid viscosity
ρ	= fluid density
τ	= time scale characterizing turbulence = $\int_0^{\infty} R ds$

LITERATURE CITED

1. Batchelor, G. K., *Australian J. Sci. Research Ser. A*, **2**, 437 (1949).
2. Crum, C. F., to be published as part of Ph.D. thesis, Univ. Ill., Urbana.
3. Einstein, Albert, *Ann. Physik*, **17**, 549 (1905); **19**, 371 (1906).
4. Flint, D. L., M.S. thesis, Univ. Ill., Urbana (Oct., 1956).
5. ———, Ph.D. thesis, Univ. Ill., Urbana (Jan., 1958).
6. Frenkiel, F. N., "Advances in Applied Mechanics," vol. 3, Academic Press, New York (1953).
7. Hanratty, T. J., *A.I.Ch.E. Journal*, **2**, 42 (1956).
8. ———, George Latinen, and R. H. Wilhelm, *ibid.*, 372 (1956).
9. Hinze, J. O., "Turbulence," p. 304, McGraw-Hill, New York (1959).
10. Kada, Hisao, M.S. thesis, Univ. Ill., Urbana (Oct., 1957).
11. ———, Ph.D. thesis, Univ. Ill., Urbana (March, 1959).
12. Kalinske, A. A., and E. R. Van Driest, "Fifth International Congress for Applied Mechanics," Wiley, New York (1938).
13. ———, and C. L. Pien, *Ind. Eng. Chem.*, **36**, 220 (1944).
14. Mickelsen, W. R., *Natl. Advisory Comm. Aeronaut. Tech. Note* 3570 (1955).
15. Sandborn, V. A., *ibid.* 3266 (1955).
16. Schlichting, Hermann, "Boundary Layer Theory," p. 408, McGraw-Hill, New York (1955).
17. Taylor, G. I., *Proc. Roy. Soc. (London)*, **A151**, 421 (1935).
18. Towle, W. L., and T. K. Sherwood, *Ind. Eng. Chem.*, **31**, 457 (1939).
19. Townsend, A. A., *Proc. Roy. Soc. (London)*, **A224**, 487 (1954).
20. Uberoi, M. S., and Stanley Corrsin, *Natl. Advisory Comm. Aeronaut. Rept.* 1142 (1953).

Manuscript received May 18, 1959; revision received October 30, 1959; paper accepted November 2, 1959.

Correlating Criteria for Liquid-Phase Adsorption

HERBERT L. JONES, JR., and EDWARD B. STUART

University of Pittsburgh, Pittsburgh, Pennsylvania

A correlating equation for selective adsorption in the liquid phase has been extended to predict accurately the benzene-cyclohexane equilibrium data on silica gel. Gel pore diameters range from approximately 25 to 150 Å. and temperatures between the boiling and freezing points of the pure components.

The ability to select the best adsorbent and conditions for the most effective separation of a particular system of liquid components can yield real savings in time and manpower. Before chromatographic columns, percolation columns, or other types of countercurrent liquid-phase contacting equipment can be designed, the knowledge of the optimum conditions for separation is absolutely necessary. Whether the operation involves separation of organic liquids or merely decoloration, there is a definite need for data which indicate the effects of pore diameter and system temperature on separation efficiency. The utility of an expression relating these factors was recently shown when Weatherford (8) and Somers (6) successfully used the equation proposed in this paper in predicting wave-front compositions for the separation of benzene and cyclohexane on silica gel and alumina in chromatographic columns.

An equation was suggested by Stuart and Coull (7) by which one could predict equilibrium data for a particular system for all liquid-phase temperatures and pore diameters after a measurement of only four equilibrium points. This present work is an extension and modification of the original equation and its application.

EXPERIMENTAL PROCEDURE

The container for the equilibrium solution and adsorbent was a dried 125-ml. Erlenmeyer flask fitted with a 24/40 ground-glass top. There were two outlets from the top, one fitted with a serum cap and the other having a No. 1 tapered stopcock. The activation of the gel was conducted by placing 5 g. of adsorbent in the flask and heating at 550°F. for 15 hr. While it was at this temperature the top was inserted into the flask with the serum cap in place and the stopcock closed to ensure as little contamination from gas or moisture as possible. The unit was cooled under vacuum.

About 10 g. of a premixed solution of pure benzene and cyclohexane (R.I. \pm 0.00005) was placed in the flask. By inserting an 18-gauge, 6-in. syringe needle attached to a 30-cc. medicinal syringe

filled with about 15 cc. of solution through the serum cap to a position above this gel and depositing the solution.

The solution in the flask assembly was placed in a constant-temperature bath at a predetermined temperature and gently agitated by means of a wrist-action shaker for at least 30 min. Clear samples were then removed from the slurry by inserting a syringe needle fitted with a syringe filter through the serum cap to withdraw about a cubic centimeter of liquid. The sample was placed in a refractometer at 33°C., and the refractive index was determined. From data by Stuart and Coull (7) the benzene concentration was determined. At least three identical readings were taken from each flask before a run was considered complete. Descriptive dimensional parameters of the silica gels studied are shown in Table 1.

EQUILIBRIUM EQUATIONS

When a binary solution is shaken with a solid adsorbent, one of the components may be preferentially adsorbed, resulting in a decrease in the mole fraction of the component in solution. The adsorption may take place in one of the following ways

1. One component will be adsorbed on a single layer in the adsorbent pore, and the rest of the pore will be filled with equilibrium binary solution.

2. Both components will be adsorbed in a single layer and the remaining pore volume filled with solution.

3. Both components will be adsorbed in multilayers with the degree of selectivity decreasing as the distance from the surface is increased.

Jones and Mill (3) have advocated the use of the multilayer concept in analyzing data. However this method involves the use of partial molar volumes in the adsorbed phase, and as such quantities are extremely difficult to determine experimentally, discussion will be confined to monolayer adsorption only.

On the basis of the adsorption of one component, Eagle and Scott (2) suggested the use of adsorption capacity in calculating the weight of this adsorbed component:

$$G = \frac{W_s(X_s - X)}{W_a(1 - X)} \quad (1)$$

Assuming that all the adsorption takes place in a monolayer and that the rest of the pore is filled with binary solution, one may calculate the over-all

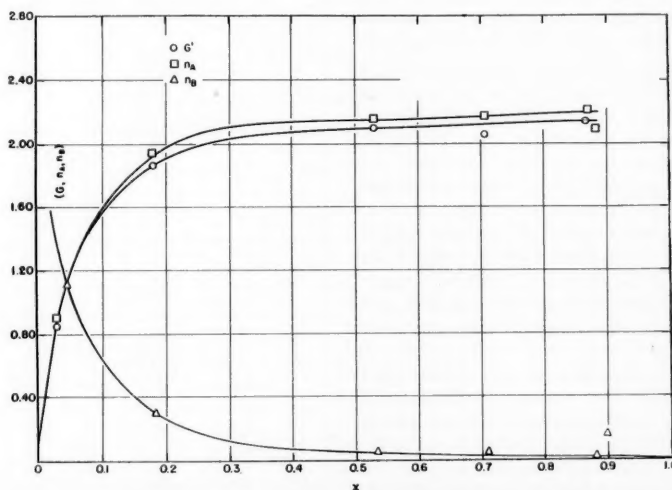


Fig. 1. Adsorption (G , n_A , n_B), moles benzene adsorbed per gram of adsorbent x , mole from benzene in equilibrium liquid: benzene-cyclohexane-silica gel (No. 922) at 8.0°C.

Herbert L. Jones, Jr., is with Hercules Powder Company, Young Development Division, Rocky Hill, New Jersey.

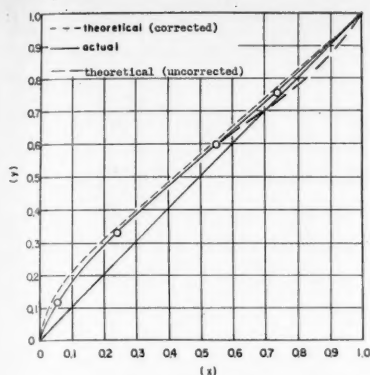


Fig. 2. Mole fraction of benzene in adsorbed phase (y) vs. mole fraction of benzene in equilibrium phase (x): benzene-cyclohexane-silica gel (No. 70) at 8.0°C.

TABLE 1. ADSORBENT PROPERTIES

	Silica gel No. 922	Silica gel, 70 Å.	Silica gel No. 70
Pore volume, cc./g.	0.429	0.562	1.0876
*Surface area, sq. m./g.	698.8	321.0	290.0
Average pore diameter, Å.	24.6	70.0	149.5
Mesh size	-200	100-200	+10

* B.E.T. method.

TABLE 2.

Pore diameter, Å.	Azeotrope mole fraction
24.6	1.000
30.0	0.980
32.0	0.917
40.0	0.865
70.0	0.710
149.5	0.690

composition of all the liquid in the pore using

$$Y = \frac{G + \left(V_p - \frac{G}{\rho_0} \right) \rho_s X}{G + \left(V_p - \frac{G}{\rho_0} \right) \rho_s} \quad (2)$$

When the correlating equation (Stuart equation) was used to predict equilibrium data for gels having diameters over 30 Å, an inversion in selectivity, that is an azeotrope, was predicted to occur at higher mole fractions, as shown in Table 2.

The actual data interpreted by the use of the G -factor concept indicated no such change in selectivity. This lack of agreement between estimated values and actual equilibrium data was attributed either to inaccurate interpretation of equilibrium data by the equations above or to an error in the correlating equation.

TABLE 3. BENZENE-CYCLOHEXANE-SILICA GEL No. 922 (Equilibrium Data Taken at 8°C.)

Weight of solution, g. W_B	Refractive index		Weight fraction benzene after X	Weight of silica gel, g. No. 922 W_a	Selective adsorption, g. benzene/g. gel G	n_A , m.-moles/g.	n_B , m.-moles/g.	G' , m.-moles/g.
12.3245	1.4224	1.4203	0.0279	7.7477	0.0663	0.895	1.168	0.850
10.7102	1.4332	1.4281	0.1729	7.7730	0.1452	1.927	0.295	1.862
11.3801	1.4531	1.4509	0.5160	4.3716	0.1624	2.142	0.052	2.082
12.6449	1.4682	1.4652	0.6934	0.2200	0.1592	2.149	0.044	2.041
12.4305	1.4817	1.4802	0.8629	8.6170	0.1652	2.179	0.010	2.118

A more realistic interpretation of the data was undertaken by assuming the adsorption of both components in a single layer. Such a relationship was suggested empirically by Williams (9) and later adopted by Kipling and Tester (4):

$$\frac{n}{W_a}(x_a - x) = \frac{n \Delta x}{W_a} = n_A(1 - x) - n_B x \quad (3)$$

The essential unknowns in this equation are n_A and n_B ; they can be determined only by solving this equation simultaneously with a second equation.

If the adsorption took place in a monolayer, the following equation could be used as a second relationship between n_A and n_B to solve the Williams equation:

$$n_A A_A + n_B A_B = S_T \quad (4)$$

By combining Equations (3) and (4) with the mole-fraction form of Equation (1) one obtains

$$n_A = \frac{\frac{n \Delta x}{W_a(1-x)} + \frac{S_T}{A_B} \left(\frac{x}{1-x} \right)}{1 + \frac{A_A}{A_B} \left(\frac{x}{1-x} \right)} \quad (5)$$

$$= \frac{G' + \frac{S_T}{A_B} \left(\frac{x}{1-x} \right)}{1 + \frac{A_A}{A_B} \left(\frac{x}{1-x} \right)}$$

From these equations one may calculate the molal concentration in the monolayer:

$$y_{(m)} = \frac{n_A}{n_A + n_B} \quad (6)$$

Robert (5) determined the area of an adsorbed benzene molecule, and Blackburn, Kipling, and Tester (1) measured the ratio of the adsorbed areas of cyclohexane and benzene. With these data and the surface area of the adsorbent, a corrected concentration in the pore was calculated by means of the following relationship:

$$(y'_m) = \frac{n_A + \left[V_p - \frac{M_{(m)}(n_A + n_B)}{(\rho_s)_m} \right] \rho_s \frac{x}{M_x}}{n_A + n_B + \left[V_p - \frac{M_{(m)}(n_A + n_B)}{(\rho_s)_m} \right] \frac{\rho_s}{M_x}} \quad (7)$$

Figure 1 and Table 3 show the comparative calculated values of n_A , n_B , and G for a typical system.* It is apparent from these data that the two methods of calculation are almost identical and that the original interpretation of equilibrium data was correct.

CORRELATING EQUATIONS

Stuart and Coull (7) proposed the following equation as a means of correlating liquid-phase adsorption-equilibrium data:

$$\left(\frac{y}{1-y} \right) = e^{ik/r} \left(\frac{x}{1-x} \right) \left(1 - \frac{y}{x} \right) \quad (8)$$

In logarithmic form this may be written as

$$\ln \left(\frac{y}{1-y} \right) = \ln \left(\frac{x}{1-x} \right) \left[1 - \frac{\psi}{T} \right] + \frac{\xi k}{T} \quad (9)$$

where

$$\psi = \frac{2 a_s \Delta p_s}{R \ln \left(\frac{x}{1-x} \right)} \quad (10)$$

$$\xi = \left(\frac{D}{D-d} \right)^2 = \left(\frac{2r}{2r-d} \right)^2 \quad (11)$$

$$k = \frac{2 a_s \Delta p_y}{R} \quad (12)$$

where a_s is a measure of the attractive force (attractive force constant) between molecules of both components and the equilibrium binary solution, a_s is a measure of the force of attraction between the solid and a binary solution at composition y , Δp_s and Δp_y are

* Data pertaining to all of the gels studied are filed with the American Documentation Institute, Photoduplication Service, Library of Congress, Washington 25, D. C., as document 6263 and may be obtained for \$3.75 for photoprints or \$2.00 for 35-mm. microfilm.

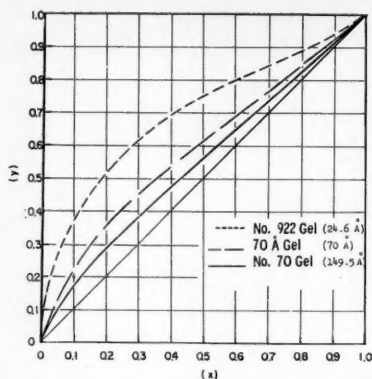


Fig. 3. Equilibrium data as a function of pore diameter: benzene-cyclohexane-silica gel (No. 922) at 8.0°C.

the density differences of the adsorbed components and equilibrium liquids, a_y is the attractive force constant between both components and the adsorbate, and d is an effective distance between the adsorbent surfaces and the adsorbed layer of molecules.

The term a_x has been viewed as a weak function of $\ln(x/1-x)$, and a_y is dependent on y , the over-all concentration of benzene in the adsorbed phase. The terms a_y and a_x may be related as follows:

$$a_y = a_o \left(\frac{D}{D-d} \right) = \xi a_o \text{ or } \frac{a_y}{a_o} = \xi \quad (13)$$

Equation (8) may be used for predicting equilibrium data by making a log-log plot of $y/1-y$ vs. $x/1-x$ and determining the slope and intercept. Calling the slope M and the intercept C , one obtains

$$C = \frac{\xi k}{T} \quad (14)$$

and

$$M = 1 - \frac{\Psi}{T} \quad (15)$$

A plot of M vs. $1/T$ yields Ψ ; this factor requires the use of only two equilibrium points at one temperature.

Values of d and k are determined as follows:

$$C = \frac{\xi k}{T} = \left(\frac{D}{D-d} \right)^2 \quad (16)$$

and

$$\left(\frac{CT}{k} \right)^{1/2} = \frac{D}{D-d} \quad (17)$$

then

$$\frac{1}{D} = \frac{1}{d} - \frac{1}{d} \left(\frac{1}{CT} \right)^{1/2} \quad (18)$$

A plot of $1/D$ vs. $(1/CT)^{1/2}$ is made from data obtained at a minimum of either two pore diameters or temperatures. This requires at least four equi-

TABLE 4. ADSORBENT CONSTANTS

Con- stants	Silica gel No. 922	Silica gel 70 Å.	Silica gel No. 70
d , Å.	14.5	14.5	14.5
ξ	5.932	1.590	1.226
k , °K.	54.2	54.2	54.2
ψ_{15} , °K.	77.5	71.70	55.37
ψ_{25} , °K.	77.5	20.52	15.82
$\xi k/\psi_1$	4.2	1.20	1.20
$\xi k/\psi_2$	4.2	4.20	4.20

librium points. It is advisable however when establishing a completely new system that two temperatures and two pore sizes be investigated. Values for the constants for the benzene-cyclohexane-silica gel system were determined Stuart (7).

At smaller pore diameters the above form of the equation as originally derived and applied predicts equilibrium data satisfactorily. However with larger diameter gels the equations will predict azeotropes at higher benzene concentrations.

This faulty indication of azeotropes was corrected by altering the $\xi k/\Psi$ factor above and below benzene concentrations of 50%. This is done by first determining the $(\xi k)/\Psi$ factor as originally suggested by Stuart and Coull (7). If the correlation is to be applied below a mole fraction of strongly adsorbed component of 0.50, the $(\xi k)/\Psi$ ratio must be equal to a value of at least 1.2. If it is less, the Ψ constant is adjusted to bring the ratio up to 1.2. If the correlating equation is to be applied to data above 0.50, the $(\xi k)/\Psi$ ratio must be equal to 4.2. Again if the calculated values are less, then the Ψ factor is reduced accordingly. Figure 2 shows the results of adjustment on actual data for a typical gel. Table 4 lists the constants used for all the gels.

A partial theoretical justification for the adjustment of the $(\xi k)/\Psi$ ratio is based on the comparative attractive force between surface and solution. It may be seen from Figure 3 that the adsorption capacity, or the attractive force between the surface and a molecule, falls off for gels above 25 Å. in diameter. Further it would seem that this force becomes very low for adsorption in macropores (pores over 100 Å.). Therefore the effects of the relative cohesive energy densities of the adsorbed phases on a molecule would become more important as the diameter increased. In terms of the previously mentioned attractive force constants a relationship between these two energy terms would be

$$\frac{f(\text{cohesive energy density of adsorbate})}{f(\text{cohesive energy density of solution})} = \frac{f(a_y)}{f(a_x)} \quad (19)$$

In terms of Stuart constants

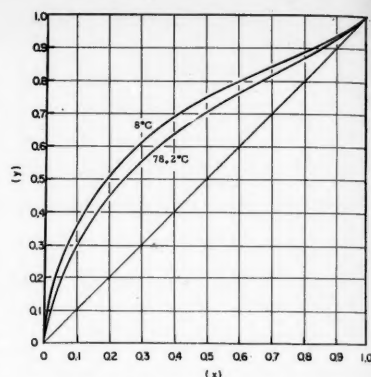


Fig. 4. Variation of equilibrium data with temperature: silica gel (No. 922).

$$\begin{aligned} \frac{\xi k}{\Psi} &= \frac{\left(\frac{D}{D-d} \right) k}{\frac{\Psi}{a_y/a_o(2a_o \Delta p_y/R)}} \\ &= \frac{2a_o \Delta p_y/R \ln \frac{x}{1-x}}{f(a_y)} \cdot \phi(x) \quad (20) \end{aligned}$$

Since a_x is a function of $\ln(x/1-x)$, it is felt that this partially negates the effect of $\phi(x)$ and yields

$$\frac{\xi k}{\Psi} = \frac{f(a_y)}{f(a_x)} \quad (21)$$

It would seem reasonable then that when $a_o \rightarrow a_x$, the ratio of $(\xi k)/\Psi$ must be greater than 1.

TEMPERATURE EFFECTS

The work of Stuart and Coull was extended to include temperatures covering the entire range between the boiling and freezing points of the pure liquids. The effect of temperature on equilibrium data for a typical gel is shown in Figure 4.

SUMMARY AND CONCLUSIONS

It is shown that for the benzene-cyclohexane-silica gel system the concept of monomolecular adsorption in a single layer followed by pore filling with equilibrium solution is as valid as the assumption of bimolecular adsorption. A correlating equation has been proposed which can satisfactorily predict equilibrium data for the benzene-cyclohexane system and similar systems for adsorption on adsorbents over a wide pore-diameter range. The equation relates only to liquid adsorption

and includes the effects of tempera-

ture. A theoretical mechanism for the adsorption-based cohesive-energy-density differences is suggested.

NOTATION

A = liquid component A, the more highly adsorbed component (benzene in this case)
 A_A = effective area occupied by a mole of component A in a monolayer (sq. m./g.)
 A_B = effective area occupied by a mole of B in a monolayer (sq. m./g.)
 a_o = attractive force constant between components and adsorbent surface
 a_s = attractive force constant between binary solution and components
 a_y = attractive force constant between binary solution and pore
 B = liquid component B, component (cyclohexane in this case)
 C = Stuart slope of $\ln y/1-y$ vs. $\ln x/1-x$
 D = adsorbent pore diameter, Å.
 d = constant in Stuart equation
 G = selective adsorption capacity (g. of component A adsorbed/g. of adsorbent)
 G' = moles of component A adsorbed /g. of adsorbent
 k = constant in Stuart equation
 M = Stuart intercept of plot $\ln y/1-y$ vs. $\ln x/1-x$

$M_{(m)}$ = average molecular weight of binary solution in monolayer
 $M_{(s)}$ = average molecular weight of equilibrium solution
 n = moles of total original solution
 n_A = moles of component A adsorbed /g. of adsorbent
 n_B = moles of component B adsorbed /g. of adsorbent
 R = universal gas constant
 r = pore radius, Å.
 S_T = adsorbent surface area, sq. m./g.
 T = temperature, °K.
 V_p = adsorbent pore volume cc./g.
 W_o = weight of original solution, g.
 W_s = adsorbent weight, g.
 X = equilibrium weight fraction of adsorbed component (bulk solution)
 X_o = weight fraction of stronger adsorbed component in original solution
 x = equilibrium mole fraction of adsorbed component (bulk solution)
 x_o = mole fraction of more highly adsorbed component in original solution
 Y = weight fraction of component A in equilibrium solution
 $y_{(m)}$ = mole fraction of component A in monolayer calculated by the use of Williams equation
 $y'_{(m)}$ = equilibrium mole fraction of

component A in the pore as calculated by the Williams equation

Greek Letters

ξ = constant in Stuart equation
 ρ_b = density of benzene, g./cc.
 $\rho_{s(m)}$ = density of binary mixture in monolayer, g./cc.
 ρ_s = density of equilibrium solution, g./cc.
 $\Delta\rho_s$ = density differences between the equilibrium liquid components, g./cc.
 $\Delta\rho_y$ = density difference between adsorbate components, g./cc.
 Ψ = constant in Stuart equation

LITERATURE CITED

- Blackburn, A., J. J. Kipling, and D. A. Tester, *J. Chem. Soc. (London)*, 2373 (May, 1957).
- Eagle, S., and J. W. Scott, *Petroleum Processing*, 4, 888 (1949).
- Jones, D. C., and G. S. Mill, *J. Chem. Soc. (London)*, 213 (January, 1957).
- Kipling, J. J., and J. Tester, *ibid.*, 4123 (1952).
- Robert, Louis, *Compt. Rend.*, 234, 2066 (1952).
- Somers, Alan E., M.S. thesis, Univ. Pittsburgh, Pittsburgh, Pa. (1958).
- Stuart, E. B., and James Coull, *A.I.Ch.E. Journal*, 4, 383 (Dec., 1958).
- Weatherford, W. D., Jr., Ph.D. thesis, Univ. Pittsburgh, Pittsburgh, Pa. (1954).
- Williams, Medd. K. *Vetenskapsakad. Nobel-Inst.*, 2, No. 27 (1913).

Manuscript received September 22, 1958; revision received September 30, 1959; paper accepted October 12, 1959.

Calculation Procedures for Binary Batch Rectification

CHARLES E. HUCKABA and DONALD E. DANLY

University of Florida, Gainesville, Florida

A rigorous mathematical description, consisting of differential-difference equations, is presented for binary batch rectification in the plate type of column. Two approaches are taken to solving these equations for the condition of constant reflux ratio: an integration by numerical means employing an IBM 650 computer, and a hand calculation procedure that involves trial-and-error computation of batch-rectification curves, which is of interest primarily where high-speed computing equipment is not available.

Enthalpy balances are used to avoid assumption of equal rate of overflow in the tower; weight units are used instead of mole units; means for accounting for holdup in the condenser-accumulator system are described. Criteria of convergence and stability of the numerical solution are presented. The validity of the results of the proposed calculation procedures is substantiated by the close agreement of experimental and calculated batch-rectification curves.

Interest in batch-rectification calculations has grown during recent years, as evidenced by the contributions which have appeared in the technical

Donald E. Danly is at present with the Chemstrand Corporation, Pensacola, Florida.

literature. For a review of most of this work it is recommended that the reader consult the work of Rose and Rose (1) and Rose and Johnson (2). Rose, Johnson, and Williams (3) also give a brief

historical outline of many of the accomplishments in the field.

The mathematical model describing batch rectification is inherently very complex even for the case of a binary mixture. Batch-rectification calculation procedures, comparable in rigor to methods for continuous steady state distillation calculations, have therefore led to long and tedious procedures. Simplification for convenience, on the other hand, has tended to restrict applicability of the results to the conditions embodied within the simplifying assumptions. For instance, the use of

some of the traditional assumptions frequently employed in continuous steady state distillation has in most cases not met with great success in batch-rectification computations. It should be generally recognized now that because of the assumptions required the McCabe-Thiele (4) method can lead to gross errors in batch-rectification calculations where appreciable holdup is present in the tower. This was pointed out by Colburn and Stearns (5) and has been discussed by Van der Hoeven (6) and Rose *et al.* (7). Huckaba and Tour (8) presented further confirmation of the wide divergence which can exist by comparing experimentally determined batch-rectification operating lines with the corresponding lines calculated by both the McCabe-Thiele and Ponchon-Savarit (9, 10) methods.

Rose and Johnson (2) made a very comprehensive study of the various non-idealities which might have to be considered in batch-rectification calculations. They suggested approaches for handling variable relative volatility, plate efficiency less than 100%, non-adiabatic operation, condenser holdup, and variation of column holdup with time. Huckaba and Tour (8) pointed out the advantages of using weight units in batch-rectification computations and showed that equality of plate-to-plate overflow in batch rectification would not usually occur on either a mole or weight basis.

The investigation reported in this paper represents a continuation of the work of Huckaba and Tour (8), who, emphasizing rigor rather than convenience, presented design procedures that were tedious and time consuming.

The work has proceeded along two lines of approach. The hand-calculation method of Huckaba and Tour was simplified in order to be of more practicable value for those workers who do not have access to a high-speed computing machine. The other portion of the work was devoted to the adaptation of the solution of the basic equations to a medium-speed digital computer. Confirmation of the hand and machine procedures was obtained through direct comparison of calculated and experimental curves.

THEORETICAL ANALYSIS

To select the proper operating conditions and number of plates required in designing a batch-rectification column to perform a given separation, it is necessary to predict the composition of the distillate and kettle liquid as a function of the fraction of the batch distilled. This can be accomplished by solving a series of simultaneous differential-difference equations, based on

enthalpy and material balances around the individual plates. These balances consist of merely an extension of the work of Sorel (11) to transient conditions. Most of the previous work has involved material balances, but only Rose and Johnson (2) and Huckaba and Tour (8) have written the enthalpy balances.

For a column having N -plates $N + 1$ differential material balances of the more volatile component can be written, one around each plate and one around the kettle. A corresponding number of enthalpy balances can also be made. Several authors (2, 5, 7, 12) have discussed the possible assumptions upon which these balances can be written. The basic assumptions made in setting up the differential equations in this paper are (1) the holdup of vapor in the column is small compared with that of the liquid; (2) heat losses from the column are negligible; (3) holdup per plate is constant; (4) liquid composition on a tray is uniform.

Under these conditions a differential material balance for the more volatile component and a differential enthalpy balance around plate n (section A in Figure 1), written as suggested by Pigford *et al.* (13) in terms of fraction distilled, give respectively

$$\frac{V_{n+1} y_{n+1}}{D} - \frac{L_n x_n}{D} + \frac{L_{n-1} x_{n-1}}{D} - \frac{V_n y_n}{D} = \frac{H_n}{S_o} \frac{dx_n}{d\phi} \quad (1)$$

$$\frac{V_{n+1} I_{n+1}}{D} - \frac{L_n i_n}{D} + \frac{L_{n-1} i_{n-1}}{D} - \frac{V_n I_n}{D} = \frac{H_n}{S_o} \frac{di_n}{d\phi} \quad (2)$$

Similar material and enthalpy balances around the kettle (section B in Figure 1) yield

$$\begin{aligned} \frac{L_N x_N}{D} - \frac{V_S y_S}{D} &= \frac{d(x_S S/S_o)}{d\phi} \\ &= \frac{d(x_S(1-\phi))}{d\phi} \\ \frac{L_N i_N}{D} - \frac{V_S I_S}{D} &= \frac{d(i_S S/S_o)}{d\phi} - \frac{Q_S}{D} \end{aligned} \quad (3)$$

It is the solution of this group of differential equations which is sought, given the boundary conditions for $\phi = 0$, that is the steady state conditions at the end of the warmup period. In addition to the initial steady state conditions, it is also necessary to prescribe the value of one of the variables as a function of ϕ . This may be the specification of L_n/D , for operation of constant reflux ratio, or, alternately, a con-

stant or prescribed variation of y_1 with ϕ might be the given condition. These two alternatives are the ones most commonly met in industrial applications, but a number of other possibilities exist. However care must be taken to set up a boundary condition which will lead to a physically significant solution.

The solutions developed in this investigation are for constant reflux ratio. If the reflux to the column is below its boiling point, i_n is not only a function of x_n but also of the degree of subcooling, which must be known.

It should be noted that in developing the basic equations it was not necessary to stipulate constancy of D , $(V_S - L_N)$, Q_n , or, in fact, any mass or heat flow rates. Thus a varying boilup rate throughout a batch-rectification run would result in the same curve of overhead composition vs. fraction distilled as a constant boilup rate, providing the plate-efficiency relationships were not affected.

To make the solution as general as possible the equilibrium and plate-efficiency relationships are taken as

$$y^* = f(x_n) \quad (5)$$

and

$$y_n = E_{MVn} y^* + (1 - E_{MVn}) y_{n+1} \quad (6)$$

or

$$x^* = f(y_n) \quad (7)$$

$$x_n = E_{MLn} x^* + (1 - E_{MLn}) x_{n-1} \quad (8)$$

With a functional relationship between E_{MVn} (or E_{MLn}) and x_n , there are a sufficient number of equations available to solve the set of differential equations. If H_n cannot be assumed constant, there are N additional variables, H_1, H_2, \dots, H_N , but since each of these is a function only of the corresponding compositions, x_1, x_2, \dots, x_N , the solution of the differential equations can still be accomplished.

Consideration of Condenser and Accumulator Holdup

In most actual batch-rectification systems the holdup of material in the condenser-accumulator system cannot be neglected. Consideration of this holdup was omitted from the previous section on derivation of the basic equations, since there is some question as to the manner in which this holdup should be treated.

As pointed out by Rose *et al.* (14), the overhead holdup can be broken down as follows: holdup of vapor in the line between the top of the column and the condenser, holdup of vapor and condensate in the condenser, liquid holdup in the lines between the condenser and accumulator and between the accumulator and reflux inlet of the column, and accumulator holdup. For the first three types of holdup

listed, the assumption of slug flow with no back mixing definitely seems to be better than that of complete mixing; however, the degree of mixing in the accumulator can be expected to vary widely from one installation to the next depending on the shape of the vessel, the position of the inlet and outlet nozzles, and the liquid flow rate.

One of the following assumptions could be made concerning condenser-accumulator holdup: (1) the entire holdup of the condenser-accumulator system is completely mixed, or (2) all flow through the overhead system is free of back mixing. Based on what little information is available on the applicability of these alternate assumptions, the assumption of no back mixing appears to be the better founded of the two. If an analytical solution of the design equations were to be attempted, material- and enthalpy-balance equations written around section C of Figure 1 would have to be used to relate x_R with y_1 . However in solving the equations by numerical methods, as will be shown later, the value of x_R when $\phi = k\Delta\phi$ can readily be determined, since it is equal to the value of y_1 when $\phi = k\Delta\phi - (\Delta\phi)_0$ where $(\Delta\phi)_0$ is the time lag expressed in terms of ϕ for a small increment of material to pass through the condenser-accumulator system.

Since C is the mass of the overhead holdup and $(R+1)D$ is the mass rate of flow, the time lag between entering and leaving the condenser-accumulator system is $C/(R+1)D$. To express this lag in terms of ϕ it must be multiplied by D/S_0 :

$$(\Delta\phi)_0 = \frac{C}{S_0} \frac{1}{(R+1)} \quad (9)$$

From $\phi = 0$ to $\phi = C/S_0(R+1)$, that is the time required to displace completely the original contents of the overhead system, the composition of the reflux is equal to the composition of the vapor leaving the top plate at steady state. For larger values of ϕ the appropriate value of x_R can be determined from the portion of the y_1 vs. ϕ curve already developed in the calculation.

The assumption of no back mixing was verified experimentally by taking samples simultaneously from each end of the condenser-accumulator system during the batch-rectification runs described below and establishing that the difference in compositions of the two samples did, in fact, correspond to a lag between entering and leaving the system of $C/S_0(R+1)$.

Derivation of the Over-all Material-Balance Equation

When it is assumed that the amount of holdup on each tray is equal and

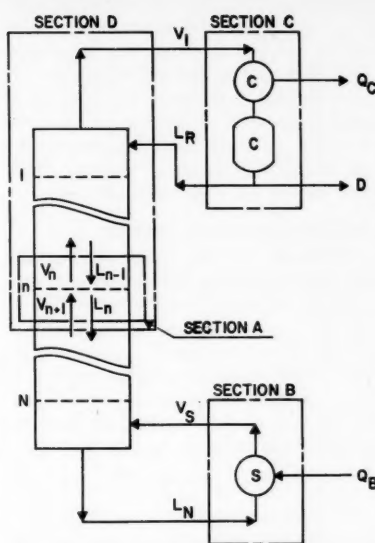


Fig. 1. Sections of the batch-rectification system about which material and enthalpy balances are made.

constant, a material balance of the more volatile component around the entire system shown in Figure 1 leads to

$$\frac{d(S/S_0)}{dx_s} - \frac{S/S_0}{x_D - x_s} = \frac{1}{x_D - x_s} \left(\frac{H_T}{S_0} \frac{dx_{HT}}{dx_s} + \frac{C}{S_0} \frac{d\bar{x}_C}{dx_s} \right) \quad (10)$$

This equation is a linear, first order differential equation in the variable S/S_0 , and so its solution can be expressed as

$$\frac{S}{S_0} = e^{-M} \left[1 + \int_{x_{s0}}^{x_s} \frac{e^M}{x_D - x_s} \left[\frac{H_T}{S_0} \frac{dx_{HT}}{dx_s} + \frac{C}{S_0} \frac{d\bar{x}_C}{dx_s} \right] dx_s \right] \quad (11)$$

$$\text{where } M = \int_{x_{s0}}^{x_s} \frac{dx_s}{x_D - x_s}$$

This equation is very similar to the one

$$y_{n+1} = \frac{\beta x_n + [(x_R - x_n) + (R+1)(y_1 - x_R) + \sum_{j=1}^n (H_j/S_0) dx_j/d\phi]}{\beta - g[(x_R - x_n) + (R+1)(y_1 - x_R) + \sum_{j=1}^n (H_j/S_0) dx_j/d\phi]} \quad (17)$$

obtained by Rose (15).

If dx_{HT}/dx_s , $d\bar{x}_C/dx_s$, and x_D are known as a function of x_s , the value of S/S_0 corresponding to any given value of x_s can be found by a double

graphical integration. First, e^M is determined graphically as a function of x_s , and then the integral of Equation (11) can be evaluated graphically. For H_T and C equal to zero the integral term vanishes and the conventional Rayleigh type of equation results.

Simplification of the Basic Equations

Plate-to-plate calculations based on the use of both material and heat balances around a plate normally involve a trial-and-error procedure. In calculating down a column, y_{n+1} must be determined from x_n . However this requires a knowledge of V_{n+1} , which in turn depends on y_{n+1} .

For a number of systems, however, the enthalpy-composition relationships are essentially linear, and simplified equations can be derived expressing y_{n+1} directly as a function of x_n , the rates and composition of the streams entering and leaving the top of the column, and the rate of change of holdup of the more volatile component on plates 1 through n .

In this paper the enthalpies of the saturated vapor and saturated liquid are expressed by

$$I_n = A + By_n \quad (12)$$

$$i_n = a + bx_n \quad (13)$$

A material balance for the more volatile component and an enthalpy balance around section D shown in Figure 1 gives

$$V_{n+1}y_{n+1} - L_nx_n + L_Rx_R - V_1y_1 = \sum_{j=1}^n \frac{H_j dx_j}{d\theta} \quad (14)$$

$$V_{n+1}I_{n+1} - L_ni_n + L_Ri_R - V_1I_1 = \sum_{j=1}^n \frac{H_j di_j}{d\theta} \quad (15)$$

The degree of subcooling of the reflux below its boiling point is given by

$$\Delta T = (a + bx_R - i_R)/C_p \quad (16)$$

Substitution of the above together with the linear expressions for I_n and i_n into Equation (15) and combining with Equation (14) gives

where $\beta = (R+1)(1+gy_1) + RC_p\Delta T/(A-a)$, $g = (B-b)/(A-a)$, and $R = L_R/D$.

The above equation relates y_{n+1} to x_n and thus represents the operating-line

equation. At steady state $dx_i/d\theta = 0$ and $y_i = x_{R_i}$ and so for use in steady state warm-up calculations the equation becomes

$$y_{n+1} = \frac{\beta x_n + (x_R - x_n)}{\beta - g(x_R - x_n)} \quad (18)$$

Use of either the unsteady state or steady state forms of the above equation eliminates the trial-and-error procedure normally required in plate-to-plate calculations employing enthalpy balances. It should be restated, however, that the applicability of these simplified equations is limited to systems having essentially linear enthalpy-composition relationships.

CALCULATION PROCEDURES

Two approaches to the solution of the basic differential-difference equations were taken. The first involved a numerical integration of the differential equations in the direction of increasing ϕ with the conditions at the end of the steady state start-up period used as the boundary conditions. The second approach was based on the method of Huckaba and Tour (8), in which the finite-difference equations are integrated step by step in the direction of increasing n and in which it is necessary to establish the relationship between x_n and ϕ by trial and error.

Selection of Units

Distillation calculations are generally carried out with compositions and flow rates expressed in mole units, since for many binary systems it is possible to assume constant molal liquid overflow from tray to tray. Since this assumption is rather restrictive, it was obviated in the derivation of the basic unsteady state equations by inclusion of enthalpy balances around the individual plates. If it is not necessary to assume constant molal overflow, there is no particular advantage in the use of molar units; in fact there is a definite disadvantage in their use, since flowmeters and level gauges cannot be used to measure molar rates and quantities directly.

The reason for using weight units is that the pounds of holdup per plate is generally much less dependent on composition of the plate liquid than is the moles of holdup. Strictly speaking, it is probably the volume of holdup that is least dependent upon composition, but since volumetric flow rates of liquid mixtures are not necessarily additive, the use of weight units appears preferable. As the range of liquid densities normally encountered is much narrower than the range of molecular volumes, the assumption of constant weight of holdup would seem for most

cases to be better than that of constant moles holdup. However for those cases in which the moles of holdup do not vary greatly with time, if it should be desired to work in mole units, the calculation procedures described in this paper can be employed without alteration except for conversion of units.

Solution by Numerical Methods

Solution of the $N+1$ differential equations relating the dependent variables x_1, x_2, \dots, x_N , and x_S with the independent variable ϕ can be accomplished by conventional techniques for numerical integration. The simplest of these, known as the Euler method, assumes that $dx_n/d\phi$ is constant over the increment from ϕ_k to ϕ_{k+1} , so that

$$x_{n;k+1} = x_{n;k} + (dx_n/d\phi)_k \Delta\phi \quad (19)$$

A considerably better assumption is that $dx_n/d\phi$ is linear between ϕ_k and ϕ_{k+1} . This corresponds to the assumption that the curve of x_n vs. ϕ can be fitted by a second-degree polynomial in ϕ over a single $\Delta\phi$ increment. In this case the numerical formula is

$$x_{n;k+1} = x_{n;k} + \frac{\Delta\phi}{2} [(dx_n/d\phi)_k + (dx_n/d\phi)_{k+1}] \quad (20)$$

Since the derivative $(dx_n/d\phi)_{k+1}$ cannot be determined until $x_{n;k+1}$ is known, an iterative process is necessary to satisfy the above equation.

This method, known as the modified Euler method, was the one selected for use in starting the solution of the unsteady state distillation equations, since it could be applied beginning with the very first increment in ϕ . Methods based on a past history are obviously not applicable over the first few increments, where no past history yet exists.

The great disadvantage in the modified Euler method is that under certain circumstances many iterations may be necessary for the prescribed degree of satisfaction of Equation (20). This is undesirable from the standpoint of the calculating time required.

Consequently in most of the calculations the modified Euler method was used over only the first few increments, and the simple Euler method was employed thenceforth for numerical integration of Equations (1) and (3).

Convergence and Stability of the Numerical Formulas

Rose *et al.* (7) and Rosenbrock (17) have pointed out the necessity of ensuring convergence and stability in calculations of this type. In the application of the numerical formulas the size of the increment in ϕ that could be employed in the solution was found to be limited by one or the other of

two factors. When the modified Euler method was used, there was an increment size above which the iterative process, common to all numerical formulas of the closed type, would not converge. On the other hand, the increment size used in the simple Euler method was limited by the stability of the solution; that is, the use of too large an increment size caused successive values of x_n to oscillate about the true curve with ever increasing amplitude, resulting ultimately in completely absurd values of x_n .

By a derivation similar to that given by Hildebrand (18) for the case of a single dependent variable, it can be shown that the limiting increment size for convergence of the modified Euler method is defined by

$$\Delta\phi < \frac{H_n/S_n}{(R_n + 1)m + R_n} \quad (21)$$

In the derivation of the limiting value of $\Delta\phi$ it is necessary to assume that R_n and m are constant over a range of two plates. Under these conditions it can further be shown that the limiting condition for stability of the simple and modified Euler methods is also given by Equation (21).

Equation (21) was not derived until most of the computer runs had been completed, and consequently this equation was not used in the work described in the following sections. However the need for a relationship by which a satisfactory increment size could be estimated became increasingly apparent as the work progressed, and more and more hours of computer time were wasted because an increment size was used which ultimately led to divergence or instability.

The validity of Equation (21) for convergence of the modified Euler method was demonstrated by a series of calculations over the first increment in ϕ . The values of x_{n+1} were punched out by the computer for n from one to N following each of eight to ten iterations, and from these data it was possible to determine whether the iterative process was converging or diverging. The enthalpy data used in the program for this calculation was chosen such that R_n was constant, since this was assumed in the derivation of the limiting increment size for convergence. In addition, the operating conditions and equilibrium data were chosen to minimize the variation of m .

In one series of runs, in which H/S was taken as 0.012, R was 2.0 and m varied from 0.520 at the bottom of a twelve-plate column to 0.500 at the top; $\phi = 0.0035$ was found to give convergence, whereas $\phi = 0.0040$ gave divergence. When the maximum value of m is used, the limiting $\Delta\phi$ predicted

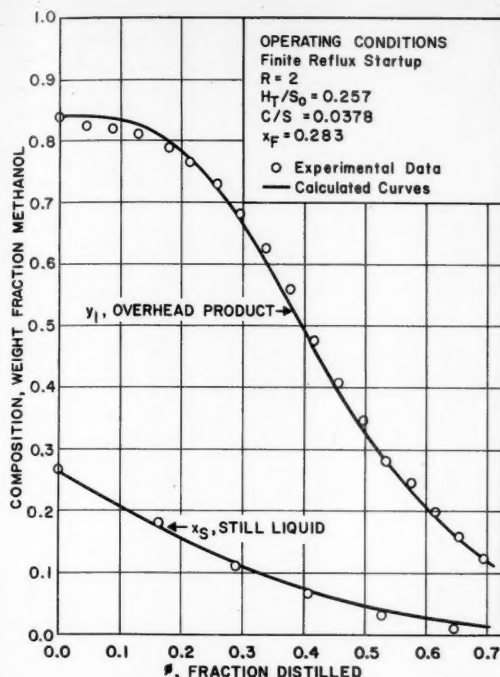


Fig. 2. Comparison of calculated and experimental data—run B-1.

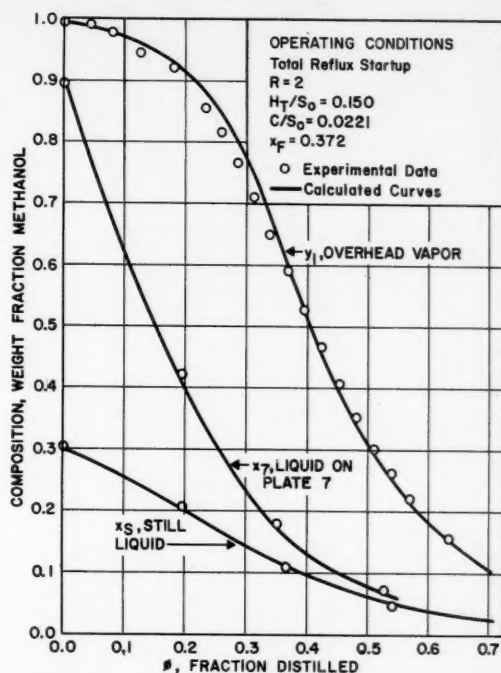


Fig. 3. Comparison of calculated and experimental data—run B-4.

by Equation (21) is $\phi < 0.00343$. Thus the predicted value of $\Delta\phi$ would give convergence of the iterative process but is only slightly less than the maximum usable value, determined by trial and error to lie between 0.0035 and 0.0040.

For the general case where R_n and m vary from plate to plate, use of the maximum value of the term $(R_n + 1)m + R_n$ in Equation (21) was found, in some instances, to predict a value of $\Delta\phi$ which gave divergence, and values 20 to 30% less than the predicted maximum were found to be necessary for convergence. Thus in general Equation (21) can be used to determine only a first approximation of the maximum increment size for convergence and stability and is exact only if R_n and m are constant. The equation does however give the right order of magnitude for the maximum value of $\Delta\phi$ that can be used and can therefore save a large portion of the trial and error involved in establishing the increment size.

The Computer Program

The numerical integration of the $N + 1$ differential equations was programmed on an IBM 650 data-processing machine. This was desirable since the extremely small increment size required for convergence and stability made a hand-calculated solution entirely impractical. The initial, steady state calculation was also included in the program, and so a minimum

number of data is needed for calculation of the complete batch-rectification curves. Danly (19) has presented a detailed discussion of this program.

The computing time on the IBM 650 required for the unsteady state calculation is approximately 0.5 sec./plate/ $\Delta\phi$ increment when the simple Euler method is used and about two to four times as long with the modified Euler method, depending on the number of iterations necessary. In the calculations made for comparison with the experimental runs described below, the modified Euler method was used for only the first twenty increments ($\Delta\phi = 0.0005$), and the enthalpy data were assumed linear. About 2½ hr. was required to reach a value of $\phi = 0.70$.

EXPERIMENTAL WORK

Mixtures of methanol and tertiary butyl alcohol were distilled at about atmospheric pressure in a twelve-plate, bubble-cap column. The column had an internal diameter of 10 in. and a plate spacing of 12 in. Five 2-in. O.D. bubble caps were contained on each plate. Sample outlets on each plate were positioned to allow withdrawal of samples of the liquid just prior to entry into the downcomer. The entire column was insulated to minimize heat losses.

A 40-gal. jacketed kettle served as the still pot. A rotary pump was used to circulate the contents of the kettle during runs to ensure adequate mixing.

The accumulator was designed to keep a constant liquid head on the reflux to

the column to allow close control of the reflux rate. The split of condensate into reflux and product was controlled manually by means of a valve in the reflux line. The portion of the flow from the condenser that was not returned as reflux overflowed to the product receivers. An electric immersion heater in the reflux line was provided for reheating the reflux.

After passing through the product rotameter, the product stream could be directed into either one of two receivers or returned to the kettle. A bypass line was installed between the vapor line from the kettle and the condenser. This line enabled the column holdup to be determined at various operating conditions, since the column could be completely isolated from the system by directing the vapor flow from the kettle through the bypass, instead of through the column, and by closing valves in the reflux line and column-bottoms line.

Experimental Procedure

The experimental runs were of two different types. First a preliminary set of runs was made to investigate the effects of liquid composition, vapor velocity, and reflux ratio on the plate efficiencies. The second series, the batch-rectification runs, comprised the major part of the experimental program. The purpose of these runs was to determine sets of experimental curves of product and kettle composition vs. fraction distilled for comparison with calculated curves.

Since the initial conditions for the batch runs were those of steady state, two types of batch runs were possible. One involved an initial steady state start-up at the same finite reflux ratio as that used for the unsteady state portion of the run, returning the product stream directly to the

Euler
incre-
ative
erical
d not
ne in-
Euler
ity of
f too
acces-
at the
mpli-
com-

given
of a
n be
t size
Euler

(21)

value
at R_n
ge of
ons it
miting
simple
also

until
been
this
work
ctions.
nship
t size
creased,
puter
incre-
ately

) for
Euler
series
ement
nched
one to
itera-
possi-
erative
erging,
ogram
such
s was
limite-
ce. In
s and
mini-

H/S,
and m
n of a
at the
re con-
gave
value
dicted

kettle. Alternately, the column could be allowed to come to equilibrium at total reflux for the start-up condition. The latter mode of operation is the one more commonly employed in industry. All runs were made at constant reflux ratio during the unsteady state portion of the run.

In the batch runs when equilibrium had been reached, the twelve plates, kettle, and reflux were sampled. The unsteady state portion of the run was then initiated either by diverting the product stream from the kettle to a product receiver (for finite-reflux start-up) or by cutting down on the reflux rate to begin withdrawal of product to a receiver (for total-reflux start-up). At regular time intervals the product flow was switched from one product receiver to the other, and the liquid was immediately drained from the partially full receiver into a tared container.

During an entire run about fifteen to twenty samples of the overhead condensate and about half as many kettle samples were withdrawn at recorded times. In some runs samples were also taken from selected plates directly after each change in product receivers.

When about 5 gal. of liquid remained in the kettle, the run was terminated. Following shutdown the liquid drained from the accumulator and associated lines was weighed. From these weights, along with those of the intermediate product accumulations, a material balance could be made, and in turn the relationship between time and fraction distilled could be determined. From the refractive-index measurements of the liquid samples, it was then possible to make plots of composition vs. fraction distilled. The determination of these plots for a variety of operating con-

ditions constituted the main objective of the experimental program.

Comparison of Calculated and Experimental Results

In making the calculations for comparison with the experimental data the following empirical relationships were employed to represent the binary-system data:

Plate-Efficiency Data

$$E_{M/Ln} = 0.845 - 0.740 x_n, \quad 0.000 < x_n < 0.224 \quad (22)$$

$$E_{M/Ln} = 0.763 - 0.374 x_n, \quad 0.224 < x_n < 1.000 \quad (23)$$

Equilibrium Data

$$x_n^* = 0.6184 y_n, \quad 0 < y_n < 0.3234 \quad (24)$$

$$x_n^* = (y_n - 0.0355)/1.4393, \quad 0.3234 < y_n < 0.4670 \quad (25)$$

$$x_n^* = \frac{y_n + 0.406}{4.232 - 2.826 y_n}, \quad 0.4670 < y_n < 1 \quad (26)$$

Enthalpy Data

$$i_n = 115.0 - 44.0x_n \quad (27)$$

$$I_n = 349.8 + 194.2y_n \quad (28)$$

Heat-Capacity Data for Saturated Liquid

$$C_p = 0.880 - 0.244x \quad (29)$$

The plate-efficiency data were obtained experimentally for the desired

rate of throughput as a function of liquid composition. Equilibrium data were obtained with a Fenske (20) still. Basic thermal data were obtained from Perry (21) and Parks and Anderson (22).

Comparisons of calculated and experimental batch-rectification curves are given in Figures 2 through 4. It is seen that in general the agreement is excellent. A number of other experimental plots were determined with mutual agreement comparable to the runs shown. The ranges of operating variables studied were $1 < R < 4$ and $0.119 < H_T/S_o < 0.257$.

The close agreement obtained in these comparisons substantiates the validity of the numerical calculation procedure for the ranges of variables considered. Thus it is believed that this procedure provides a generally satisfactory means for making accurate batch-rectification calculations provided that electronic computation equipment is available. Without such equipment however this method is too lengthy, and for hand computations an alternative procedure is recommended.

Solution by the Huckaba-Tour Method

The basic difference between the numerical solution previously described and the Huckaba-Tour method (8) is that in the former a series of differential equations is integrated in the direction of increasing ϕ , whereas

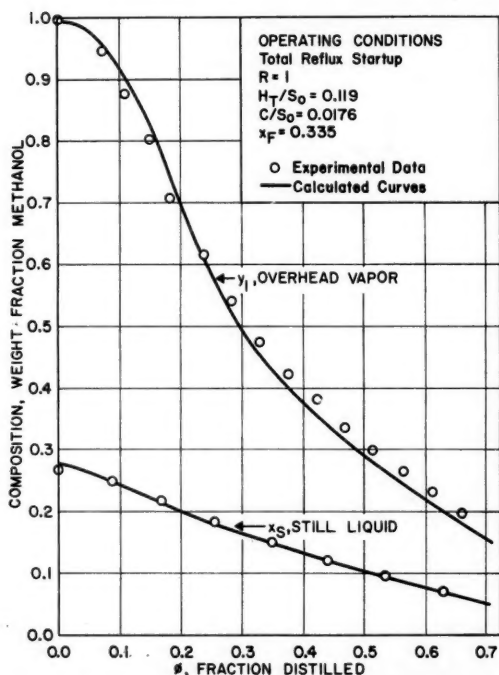


Fig. 4. Comparison of calculated and experimental data—run B-6.

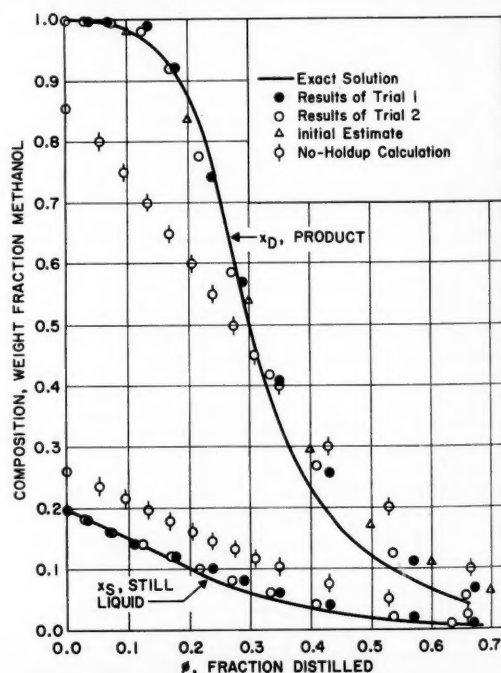


Fig. 5. Calculated batch-rectification curves illustrating the Huckaba-Tour method.

TABLE I. SUMMARY OF RESULTS OF SECOND TRIAL CALCULATION IN ILLUSTRATIVE PROBLEM BY THE USE OF THE HUCKABA-TOUR METHOD

Composition, weight fraction methanol								
ϕ	0.0	0.1	0.2	0.3	0.4	0.5	0.6	0.7
x_D	0.9995	0.991	0.874	0.543	0.302	0.170	0.096	0.059
y_1	0.9995	0.989	0.845	0.515	0.284	0.160	0.090	0.057
x_C	0.9995	0.990	0.860	0.529	0.293	0.165	0.093	0.058
x_{HT}	0.8370	0.563	0.268	0.129	0.067	0.037	0.021	0.014
x_S	0.1962	0.154	0.112	0.076	0.045	0.027	0.016	0.011

x_S	x_D	e^w	$\frac{H_T}{S_o} \frac{dx_{HT}}{dx_S}$	$\frac{C}{S_o} \frac{dx_C}{dx_S}$	$-f_1$	f_2	ϕ
0.1962	0.9995	1.000	0.318	0.000	0.396	0.000	0.000
0.1800	0.998	0.980	0.591	0.005	0.745	0.009	0.029
0.1600	0.995	0.956	1.189	0.012	1.504	0.033	0.075
0.1400	0.981	0.934	1.062	0.040	1.403	0.062	0.125
0.1200	0.920	0.912	0.900	0.163	1.459	0.090	0.170
0.1000	0.775	0.888	0.606	0.282	1.481	0.119	0.218
0.0800	0.585	0.858	0.445	0.262	1.632	0.150	0.271
0.0600	0.417	0.818	0.298	0.243	1.852	0.185	0.334
0.0400	0.269	0.763	0.228	0.211	2.518	0.227	0.411
0.0200	0.125	0.666	0.193	0.211	5.77	0.303	0.536
0.0100	0.055	0.568	0.193	0.211	15.82	0.397	0.658

$$f_1 = \frac{e^w}{x_D - x_S} \left[\frac{H_T}{S_o} \frac{dx_{HT}}{dx_S} + \frac{C}{S_o} \frac{dx_C}{dx_S} \right]$$

$$f_2 = \int_{x_{S_0}}^{x_S} f_1 dx_S$$

in the latter an integration of a series of finite-difference equations is performed in the direction of increasing n . One basic advantage of the Huckaba-Tour approach is that only N increments need be taken in the n direction, with x_n evaluated only at as many values of ϕ as are necessary to draw in the curve of x_n vs. ϕ , whereas in the numerical solution as many as 2,000 to 10,000 increments may be required in the integration in the ϕ direction for a stable solution. Thus the Huckaba-Tour method finds applicability where high-speed computers are not available.

However this method also has one serious drawback, in that the boundary condition relating x_D as a function of ϕ cannot be established in advance. Therefore it is necessary to assume a curve of x_D vs. ϕ , corresponding to specified values of N and R , from which curves of x_1, x_2, \dots, x_n , and x_S vs. ϕ can successively be determined. Then an over-all material balance is made to give a corrected curve of x_D vs. ϕ . This iterative process is continued until the assumed and calculated curves are in satisfactory agreement.

The steps involved in the calculation procedure are

1. Assume a curve of x_D vs. ϕ based on a knowledge of the initial value of x_D (that is the steady-state value of x_D existing at end of warm-up period)

and the relationship between the area under the entire curve and the over-all composition of the material charged to the still.

2. At discrete values of ϕ , for example, 0.05, 0.10, 0.15, . . . , determine the values of y_1 from the curve of x_D vs. ϕ and the condenser lag ($\Delta\phi$).

3. Calculate the corresponding values of x_1 from the equilibrium and plate-efficiency relationships. If the plate efficiency varies with x , trial and error will be necessary.

4. Plot x_1 vs. ϕ and evaluate the slopes $dx_1/d\phi$ at the selected values of ϕ . Then determine the corresponding value of $di/d\phi$ from the composition-enthalpy relationship.

5. Calculate y_2 by Equation (1) with V_1/D used as a first approximation of V_2/D .

6. Calculate V_2/D by Equation (2) and compare with the value used in step 5. Repeat steps 5 and 6, if the agreement is not satisfactory.

7. Determine x_2 from the equilibrium and plate-efficiency relationships, as done for x_1 in step 3. Calculate on down the column in this manner until y_n has been determined.

8. Calculate x_S as the liquid in equilibrium with y_S .

9. Integrate Equation (11) graphically to relate x_S with S/S_o . Since for constant holdup $S/S_o = 1 - \phi$, x_S and the corresponding value of x_D can then be related with ϕ . Compare the calculated curve of x_D vs. ϕ with that assumed in step 1 and repeat the entire calculation procedure if necessary.

culated curve of x_D vs. ϕ with that assumed in step 1 and repeat the entire calculation procedure if necessary.

If the enthalpy-composition relationships are linear, then Equation (17) can be used to calculate y_{n+1} from x_n , avoiding the necessity for the iterative procedure described in steps 5 and 6.

Illustrative Problem

A batch-rectification design calculation was carried out by the Huckaba-Tour method with the following data assumed:

- | | |
|-------------------------------|-------|
| 1. Relative volatility | 2.0 |
| 2. Reflux ratio | 2.0 |
| 3. Number of plates | 12 |
| 4. Enthalpy constant, g | 1.0 |
| 5. Reflux subcooling | 0 |
| 6. Plate efficiency, E_{ML} | 1.0 |
| 7. Plate holdup H/S_o | 0.012 |
| 8. Condenser holdup C/S_o | 0.030 |
| 9. Charge composition x_F | 0.295 |

Total reflux start-up was assumed; therefore the operating-line relationship for the steady state period was merely $y_{n+1} = x_n$. Although the steady state calculation for total reflux is straightforward, a trial-and-error approach was necessary in order to find the set of still, plate, and condenser compositions which has a composite value equal to that of the liquid charged to the system.

The initially assumed curve of x_D vs. ϕ is shown in Figure 5. The value of x_D at $\phi = 0$ was determined in the steady state calculation, and then a curve was drawn through this point such that the total area under the curve was approximately $x_F (1 - H_N/S_o - C/S_o)$. This relationship follows by equating the amount of the more volatile component initially in the system to that removed in the product when the contents of the kettle have been depleted, with the liquid on the plates and in the condenser assumed to be essentially pure high boiler at $\phi = 1.0$. Values of $y_1, x_1, y_2, x_2, \dots, y_n, x_n$ were calculated successively at a number of values of ϕ as described earlier. Following the plate-to-plate calculations the values of the average plate holdup \bar{x}_{HT} and the average condenser holdup \bar{x}_C were determined corresponding to each value of ϕ . Plots were then made of \bar{x}_C and x_{HT} vs. x_S , and the slopes dx_C/dx_S and dx_{HT}/dx_S were evaluated. The relationship between e^w and x_S was found from the area under the curve of $(x_D - x_S)^{-1}$ vs. x_S , between x_{S_0} and x_S . Then S/S_o was related to x_S by graphically integrating Equation (11). Since each value of x_S had associated with it a value of x_D , the curve of x_D vs. ϕ could be plotted for comparison with the curve assumed initially.

The entire procedure was then repeated with the results of the first trial calculation for the relationship between x_D and ϕ used. The results of the second trial are summarized in Table 1.* The values of x_D and x_S determined in the first and second trial calculations are shown in Figure 5, together with the points defining the

* Tabular material showing results of the first trial has been deposited as document 6262 with the American Documentation Institute, Photoduplication Service, Library of Congress, Washington 25, D. C., and may be obtained for \$1.25 for photoprints or 35-mm. microfilm.

initial estimate of the x_D vs. ϕ curve and the results of the computer solution, based on numerical integration of the basic differential equations. The increment in ϕ used in the numerical integration was sufficiently small ($\Delta\phi = 0.0005$) that this solution can be considered as exact for all practical purposes. Also shown in Figure 5 is the gross error resulting from completely neglecting column holdup in this batch-rectification calculation.

Ideally one would like to be able to repeat the trail calculations until the resulting curve of x_D vs. ϕ falls directly on top of the one assumed at the beginning of the trail calculation. However in general such perseverance would probably not be justified, owing to the excessive amount of calculating time required. There can be little doubt however that some accounting of holdup is absolutely essential and that the above method does provide a possible approach to the problem where electronic computers are not available.

SUMMARY

Two approaches to the solution of the basic batch-rectification equations have been demonstrated and verified by experimental data. The first involves integration of the basic differential equations by conventional numerical methods. The extremely small increments in fraction distilled that are required for stability of the numerical formulas requires the use of an electronic computer. A medium-speed computer gave rapid and accurate results.

For designers who do not have access to an electronic computer, the approach of Huckaba and Tour (8) as modified in this investigation is much faster than attempting a numerical integration with a desk calculator or slide rule.

Both of the approaches assume that the holdup per plate is constant, but use of these methods is not restricted to any particular set of units. In many cases the use of weight units appears to be satisfactory with respect to constancy of holdup and is preferable from the design standpoint of applying economic data directly to the results of the calculation. Methods of accounting both for enthalpy effects and for condenser-accumulator holdup in batch-rectification calculations have been demonstrated. Also an approach to the development of quantitative criteria for ensuring convergence and stability in the numerical machine computations has been presented.

It is believed that the two calculation procedures presented herein provide the designer with tools for development of batch-rectification curves, which are in general both convenient and valid and as such allow a high degree of confidence in batch-rectification designs in which they are applied.

NOTATION

a	= y intercept in the linear liquid-enthalpy equation, $i_n = a + bx_n$, B.t.u./lb.
A	= y intercept in the linear vapor enthalpy equation $I_n = A + By_n$, B.t.u./lb.
b	= slope in the linear liquid-enthalpy equation B.t.u./lb.
B	= slope in the linear vapor enthalpy equation, B.t.u./lb.
C	= holdup in the condenser-accumulator system, lb.
C_p	= mean heat capacity of reflux between its subcooled temperature and boiling point, B.t.u./lb. °F.)
D	= flow rate of distillate from the system, lb./hr.
E_{ML}	= Murphree liquid-plate efficiency
E_{MV}	= Murphree vapor-plate efficiency
g	= $(B - b)/(A - a)$, enthalpy constant
H	= total liquid and vapor holdup per plate, lb.
i	= enthalpy of the liquid, B.t.u./lb.
I	= enthalpy of the vapor, B.t.u./lb.
k	= number of increments in ϕ between $\phi = 0$ and $\phi = \phi$
L	= liquid flow rate down the column, lb./hr.
m	= slope of the curve of y_n vs. x_n
M	= $\int_{x_{B_0}}^{x_B} -dx_s/(x_D - x_s)$
N	= number of plates in the column
Q	= heat flow rate, B.t.u./hr.
R	= reflux ratio, L_R/D
R_n	= internal reflux ratio, L_n/D
S	= quantity of liquid in the still, lb.
ΔT	= temperature difference between the boiling point of the reflux and the temperature at which it is introduced into the column, °F.
x	= liquid composition, weight fraction more volatile component
\bar{x}_c	= average composition of condenser-accumulator holdup, weight fraction more volatile component
y	= vapor composition, weight fraction more volatile component
β	= $(R + 1)(1 + gy_1) + RC_p\Delta T / (A - a)$
θ	= time, hr.
ϕ	= fraction distilled, defined as $1 - S/S_0$

Subscripts

1, 2, . . . , $n-1$, $n+1$, . . . , N = top plate, second plate from the

top, . . . , plates $n-1$, n , and $n+1$, . . . , and the bottom plate

$k-1$, k	= integral number of increments in fraction distilled, $(k-1)\phi$, $(k)\phi$, and $(k+1)\phi$
B	= reboiler
C	= condenser-accumulator system
D	= distillate (pertains to instantaneous value)
F	= feed charged to the still initially
HT	= total holdup in the column
o	= original ($\phi = 0$)
R	= reflux stream
S	= still material
T	= total

LITERATURE CITED

- Rose, Arthur and E. Rose, "Technique of Organic Chemistry," Vol. IV, pp. 1-174, Interscience, New York (1951).
- , and R. C. Johnson, *Chem. Eng. Progr.*, **49**, 15 (1953).
- , and T. J. Williams, *ibid.*, **48**, 549 (1952).
- McCabe, W. L., and E. W. Thiele, *Ind. Eng. Chem.*, **17**, 605 (1925).
- Colburn, A. P., and R. F. Stearns, *Trans. Am. Inst. Chem. Engrs.*, **37**, 291 (1941).
- Van der Hoeven, B. J. C., *ibid.*, 727 (1941).
- Rose, Arthur, R. C. Johnson, and T. J. Williams, *Ind. Eng. Chem.*, **42**, 2145 (1950).
- Huckaba, C. E., and R. S. Tour, paper presented at A.I.Ch.E. Annual Meeting St. Louis, Missouri (December, 1953).
- Ponchon, M., *Tech. moderne*, **13**, 20 (1921).
- Savarit, R., *Arts et metiers*, pp. 65, 142, 178, etc. (1922).
- Sorel, E., "La Rectification de l'alcohol," Paris, France (1893).
- Robinson, C. S., and E. R. Gilliland, "Elements of Fractional Distillation," 4 ed., pp. 370-392 McGraw-Hill, New York (1950).
- Pigford, R. L., J. B. Tepe, and C. J. Garrahan, *Ind. Eng. Chem.*, **43**, 2592 (1951).
- Rose, Arthur, R. C. Johnson, and T. J. Williams, *ibid.*, 2459 (1951).
- Rose, Arthur, *ibid.*, **32**, 675 (1940).
- , and T. J. Williams, *ibid.*, **42**, 2494 (1950).
- Rosenbrock, H. H., *Brit. Chem. Eng.*, **3**, 432 (1958).
- Hildebrand, F. B., "Introduction to Numerical Analysis," p. 212, McGraw-Hill, New York (1956).
- Danly, D. E., Ph.D. Dissertation, Univ. Fla., Gainesville (1958).
- Fenske, M. R., *Ind. Eng. Chem.*, **39**, 1322 (1947).
- Perry, J. H., "Chemical Engineers' Handbook," 3 ed., pp. 216, 228, McGraw-Hill, New York (1950).
- Parks, G. S., and C. T. Anderson, *J. Am. Chem. Soc.*, **48**, 1506 (1926).

Manuscript received February 10, 1959; revision received October 9, 1959; paper accepted October 12, 1959.

COMMUNICATIONS TO THE EDITOR

Design of Catalysts: Application of Crystal-Face Orientation

HOWARD F. RASE and R. R. PADHYE

University of Texas, Austin, Texas

Remarkable strides in the past few years have provided the chemical engineer with valuable information and tools for use in selecting and improving catalysts. Briefly these include three major theories and several measuring techniques useful in gaining insight into catalyst characteristics.

THEORIES

1. The electronic factor in catalysis.
2. The influence of crystal face on catalytic activity.
3. Balandin's theory of surface geometry (volumes 7 and 10 of "Advances in Catalysis" give good summaries of these theories and associated experimental work.)

MEASURING TECHNIQUES

1. Thermal emf
2. Electrical conductivity
3. Electron microscopy
4. Electron diffraction
5. X-ray diffraction
6. Differential thermal analysis

STATUS

At the present state of development it is clear that none of the theories can be successfully applied to all catalytic phenomena. It must be concluded that they are empirical rules resulting from some yet undiscovered general theories. The literature will therefore continue to contain numerous contradictions as well as magnificent substantiations of the several factors said to govern catalytic activity. Complete resolution of this complex problem is not in sight.

THE INFLUENCE OF CRYSTAL FACE

As an example of engineering application, concepts proposed by Gwathmey, Beeck, and others (1, 4, 6) related to the effect of crystal face on catalysis are being applied in these laboratories in the postulation of a more active nickel-hydrogenation catalyst. Whether such a catalyst is needed is not the burden of this study. Our goal is the demonstration of a technique which can have many useful applications.

BACKGROUND

The reader is referred to other sources (1 to 4) for a detailed review of the literature of this field. The relevant facts related to nickel as a hydrogenation-dehydrogenation catalyst follow.

1. Beeck and his associates (3) in studying evaporated metal films found that the hydrogenation activity for ethylene on (110) oriented nickel films was five times that on unoriented films. The diffraction measurements used to establish orientation were made on fresh films (films not used in the reaction).

2. Sachtler and associates (5) found the (111) faces active in hydrogenation but not the (110) as found by Beeck. In this work Sachtler studied the orientation *in situ*.

3. Gwathmey and Cunningham (4) prepared single crystals and measured ethylene hydrogenation rates on the different crystal faces. They found the (321) face most active followed by the (111) face. Single crystals were prepared large enough so that individual faces might be identified and studied. Their data suggested that any tendency toward unoriented films particularly at low temperature would increase catalyst activity. This is contrary to Beeck's work on ethylene but can be explained by the fact that Beeck identified crystal faces on samples

which were not used in the reaction studies. The very nature of Gwathmey and Cunningham's experiments suggests more careful control of the variables.

4. Schuit and van Reijen (6) have shown that the kinetics, activation energy, and specific rate constant do not differ greatly between nickel-on-silica catalysts and nickel films. Relative activities for other metals were found to be substantially equal for the two types of catalysts.

A TECHNIQUE FOR APPLICATION TO CATALYST DESIGN

The above outlined observations when used to propose various theories and hypotheses may generate numerous controversies. When used as empirical facts obtained by competent workers as a guide in the development of a catalyst, there should be no objection. Perhaps the most obvious application, and the one suggested here, is the creation or improvement of a catalyst by means of studies made with metal films.

The slower rate of propylene hydrogenation made it more convenient for use in our laboratories and further served to illustrate the extrapolation of the ethylene observations to an analogous system. Experimental procedures are described at the end of this paper. The results and thereby the proposed technique are outlined here.

1. On the assumption that hydrogenation activity is determined by the arrangement of crystal faces, an attempt was made to produce the optimum result suggested by Gwathmey's work. His findings indicated that a randomly oriented (unoriented) film might be the more active. Foreign atoms introduced in the film could produce both a change in the normal

R. R. Padhye is with Indian Explosives, Ltd., Gomio, Indiana.

structural pattern of the film and the desired randomness.

2. A simple empirical procedure for finding such foreign atoms is to evaporate readily available commercial alloys of nickel and test their activity. The results of such a procedure are tabulated for batch hydrogenation of propylene in Table 1 as activities relative to nickel film at various conversion levels. The films prepared from nickel-chromium and nickel-chromium-iron alloys were the most active.

3. X-ray diffraction studies showed all films to be oriented in the (111) plane, but the nickel-chromium and nickel-chromium-iron films (the most active) showed some random orientation in agreement with the original hypothesis. Results were reproducible. Further studies could lead to even more randomly oriented and thus more active films.

4. The next step is the application of the findings of the film experiments to supported catalysts prepared by precipitation of mixtures of metal salts on kieselguhr followed by decomposition and subsequent reduction. It is postulated that nickel-chromium and nickel-chromium-iron supported catalysts will exhibit comparable superiority over nickel catalysts as that shown by the film studies. This work will be done, but these thoughts are presented here with the hope that other workers may be stimulated in employing orientation studies as a means of suggesting improved or new catalysts.

TABLE 1. ACTIVITIES OF VARIOUS NICKEL FILMS
COMPARED WITH COMMERCIAL PURE NICKEL FILMS

Conversion level	Film designation					
	A	B	C	D	E	F
0.05	1.625	1.625	0.590	0.650	0.650	0.325
1.10	1.750	1.780	0.700	0.700	0.700	0.437
0.15	1.830	1.830	0.758	0.735	0.772	0.550
0.20	1.935	1.870	0.788	0.792	0.788	0.631
0.25	1.950	1.900	0.808	0.805	0.808	0.704

1. Activities expressed as ratio of reaction times at constant conversion for the pure nickel film to those of alloy film.

2. Designations indicate percentage of metal evaporated

A: 79.5 nickel, 13 chromium, 6.5 iron
B: 80 nickel, 20 chromium
C: 67 nickel, 30 copper, 1.4 iron, 1 manganese
D: 66 nickel, 29 copper, 2.75 aluminum, 0.9 iron
E: 95.5 nickel, 4.5 manganese

EXPERIMENTAL METHODS

Briefly, the films were evaporated from a tungsten filament to a 500-ml. flask with nickel and nickel-alloy wires wrapped around the helical filament. Other significant data include:

Vacuum: 0.1 μ
Flask wall temperature: 103°F.
Current: 30 to 32 amp. at 10 v.

The reaction was carried out in the flask without prior contact with the atmosphere. Pretreatment for 6 hr. with hydrogen or propylene eliminated the induction period and permitted comparison of films on an equal basis.

ACKNOWLEDGMENT

This work was financed in part from a grant by the University Research Institute of the University of Texas.

LITERATURE CITED

1. Beeck, Orin, *Advances in Catalysis*, **2**, 151 (1950).
2. ———, *Discussions Faraday Soc.*, **8**, 118 (1950).
3. ———, A. E. Smith, and A. Wheeler, *Proc. Roy. Soc. (London)*, **A177**, 62 (1940).
4. Gwathmey, A. T., and R. E. Cunningham, *Advances in Catalysis*, **10**, 242 (1958).
5. Sachtleer, W. M. H., L. Dargelo, and W. J. van der Knaap, *Chim. Phys.*, **51**, 491 (1954).
6. Schuit, G. C. A., and L. L. van Reijen, *Advances in Catalysis*, **10**, 242 (1958).

The Effect of Velocity Profile on Axial Dispersion in Packed Beds

A. O. CONVERSE

University of Delaware, Newark, Delaware

To my knowledge no treatment of axial dispersion in packed beds which accounts for the effect of the velocity profile has been published. Yet it seems possible that some of the axial dispersion observed in packed beds is caused by the combined influence of velocity profile and radial diffusion. Consider a pulse of dye flowing through a packed bed. The variation of axial velocity with radius causes the pulse to spread axially; however radial diffusion counteracts this by causing the dye that has

been carried ahead in the faster flow to diffuse radially into slower flow, and likewise dye that has been held back in the very slow flow diffuses into faster flow. As the ratio of the bed diameter to the particle diameter is increased, these two counteracting effects vary as follows. The velocity profile becomes flatter and tends to cause less dispersion. The radial diffusion is also reduced because the particles are smaller in relation to the radius of the bed. This however tends

to cause more dispersion. The following work is an attempt to evaluate these effects by calculating the N_{Pe} from a theoretical development similar to that used by Taylor (*1*) to evaluate these effects in pipe-line flow.

A material balance around a differential annular shell that moves with the mean superficial velocity of the stream yields

$$\frac{\partial}{\partial z} \left[zE \left(-\frac{\partial c}{\partial z} \right) \right]$$

$$+ zR^2(u-U)\frac{\partial c}{\partial x} + zR^2\frac{\partial c}{\partial t} = 0 \quad (1)$$

Although the consideration of axial convection and radial diffusion is a two-dimensional problem, the resulting axial dispersion is only one-dimensional. The transition is obtained mathematically through using an effective axial diffusivity and writing material balances [Equations (2) and (5)] where axial convection and radial diffusion are replaced by an imagined axial diffusion. The next equation is obtained from a material balance around a cylindrical element which moves with the mean superficial velocity of the stream and is of differential length dx and finite radius R :

$$\frac{\partial}{\partial x} \left[\epsilon \left(-\frac{\partial \bar{c}}{\partial x} \right) \right] + \frac{\partial \bar{c}}{\partial t} = 0 \quad (2)$$

When one assumes $\partial \bar{c} / \partial x$ to be constant, Equation (2) shows that $\partial \bar{c} / \partial t = 0$; when one assumes $\partial \bar{c} / \partial t = \partial c / \partial t$, Equation (1) becomes

$$\frac{\partial}{\partial z} \left[zE \left(\frac{\partial c}{\partial z} \right) \right] = zR^2(u-U)\frac{\partial c}{\partial x} \quad (3)$$

When one assumes that $\partial c / \partial x$ is constant, the integration of Equation (3) gives

$$c - c_0 = (\partial c / \partial x) \int_0^z \frac{1}{Ez'} dz' \quad (4)$$

These assumptions apply rigorously only when radial diffusion is so fast compared with axial convection that there is no axial dispersion. When there is no dispersion, $\partial c / \partial t = 0$, $\partial c / \partial x = \text{constant}$ (where x is a coordinate that moves with the mean superficial velocity of the stream), and $c \neq c(z)$. In essence the above development relaxes the last restriction and yet holds the first two. Therefore the solution applies only when the time for flow is much greater than the time for decay of the radial concentration gradient due to diffusion. Taylor showed that this is equivalent to

$$\frac{L}{u} \gg \frac{R^2}{D(3.8)^2}$$

In McHenry's (2) equipment, which provides the only experimental data for the comparison with this work, $L/u =$

1 to 3 sec. when $u = 1$ ft./sec. and $R^2/D(3.8)^2 = 0.42$ sec. Hence the validity of the above assumptions needs experimental verification but is not obviously false.

The net flow of tracer through a disk that forms a boundary of the tracer pulse at the inlet and which moves with the mean superficial velocity of the stream is given by the following two expressions.

$$2\pi R^2 \int_0^1 (u-U) cz dz = -\epsilon \pi R^2 \frac{\partial c}{\partial x} \quad (5)$$

By substituting Equation (4) for c in Equation (5) one obtains the following equation, thus permitting the evaluation of the effective axial diffusion coefficient.

$$\epsilon = -2R^2U^2 \int_0^1 \left(\frac{u}{U} - 1 \right) z$$

$$\int_0^z \frac{1}{Ez'} \int_0^{z'} \left(\frac{u}{U} - 1 \right) z'' dz'' dz \quad (6)$$

(Note: $\int_0^1 (u-U) cz dz = 0$)

ϵ was evaluated from Equation (6) by numerical integration, with the velocity

TABLE 1

D/δ_p	Re	$f\ddagger$	N_{Pe} , calc.	N_{Pe} , exp. ²
10.7	221	.37	3.2	
15.7	200			1.85
16.0	147	.36	1.7	
21.3	110	.35	10.4	

\ddagger Estimated from reference 4.

profiles measured by Collins (3) used. The experimental velocity measurements were extended beyond $z = 0.95$ with the following correlation:

$$\left(\frac{u}{U} \right) - \frac{u}{U} = a + b \ln(1-z) \quad (7)$$

The radial Peclet number was assumed to be 10, and the radial diffusivity was evaluated from

$$E = D + \frac{\delta_p u}{10} \quad (8)$$

The results of these calculations are summarized in Table 1.

The resulting N_{Pe} do not vary monotonically with D/δ_p because of the offsetting effects of velocity profile and radial diffusion. D/δ_p was varied experimentally by Collins by using 3/8, 1/4, and 1/16-in.-diameter spheres in

a 4-in.-diameter bed. The velocity profiles corresponding to the 3/8 and 1/4-in. spheres show little change; yet E [Equation (8)] is smaller for the 1/4-in. spheres, and hence the N_{Pe} is lower. The velocity profile for the 1/16-in. spheres is flatter, hence the higher N_{Pe} .

The agreement between the calculated value at $D/\delta_p = 16$ and the experimental value is probably fortuitous because the theory is based on the assumption that axial dispersion is small, and the velocity near the wall, not well known in this case, has a strong influence on the result (5). Nevertheless this analysis does show that N_{Pe} is a function of D/δ_p in beds where the velocity profile is not flat. Although this analysis does not yield information about the dependence of N_{Pe} on the radial position, the action of the velocity profile might bring about such a dependence.

NOTATION

a, b	= experimental constants
c	= concentration
\bar{c}	= mean concentration = $2 \int_0^1 cz dz$
D	= bed diameter
E	= radial diffusivity
f	= void fraction
L	= length of bed
N_{Pe}	= Peclet number based on the mean superficial velocity
N_{Pe}	= Peclet number based on the mean interstitial velocity
o	= center line
R	= bed radius
R_p	= Reynolds number based on the particle diameter
t	= time
u	= point superficial velocity
U	= mean superficial velocity
x	= spatial coordinate along the axis of the bed
z	= r/R where r varies between 0 and R
δ_p	= diameter of the particles
D	= molecular diffusivity between the tracer and the carrier gases
ϵ	= effective axial diffusivity

LITERATURE CITED

1. Taylor, G. I., *Proc. Roy. Soc. (London)*, **A223**, p. 446 (1954).
2. McHenry, K. W., and R. H. Wilhelm, *A.I.Ch.E. Journal*, **3**, No. 1, p. 83 (1957).
3. Collins, M., B.S. thesis, Univ. Del., Newark (1957).
4. Leva, Max, *U.S. Bur. Mines Bull.* 504 (1951).
5. Tichacek, L. J., C. H. Barkeley, and Thomas Baron, *A.I.Ch.E. Journal*, **3**, No. 4, p. 439 (1957).

The Internal Consistency of Simultaneous Heat and Mass Transfer Relationships

DONALD R. OLANDER

University of California, Berkeley, California

In illustrating some of the fundamental difficulties encountered in the analysis of chemical engineering problems, White and Churchill (1) discussed an apparent inconsistency in the treatment of simultaneous heat and mass transfer in a vapor-liquid dehumidifier. The anomaly, they claimed, was due to the fundamental incompatibility of potential-difference and potential-gradient models in describing the rate of heat and mass transport. In this brief note an attempt will be made to show that the inconsistency stems from a much more prosaic source, namely that some of the relationships involved are approximations. The offending equations however are enthalpy balances, which care not a whit whether the heat fluxes therein are expressed as functions of differences or gradients of temperature; one need only retain these heat-flux terms as unspecified q 's to prove that the inconsistency remains. Specifically, Equations (26) and (27) of reference 1 each lack one term which, because of its relatively small magnitude, has been universally disregarded. Naturally, the neglected terms become apparent when the internal consistency of the entire set of equations is examined.

It was pointed out that the equations

$$dL = GdH \quad (1)$$

$$GdH = -N_a dZ \quad (2)$$

$$-Gs dt = h_a (t - t_i) dZ \quad (3)$$

$$LC_i d t_i = h_a (t_i - t_i) dZ \quad (4)$$

$$h_a (t - t_i) + h_a (t_i - t_i) = -N_a \lambda_i \quad (5)$$

can be appropriately combined to yield

$$G [s dt + \lambda_i dH] = LC_i d t_i \quad (6)$$

Equation (6) was then compared to the differential enthalpy balance over both phases, which, with the thermodynamic identity,

$$\lambda_{t_1} + C_i (t_1 - t_2) = \lambda_{t_2} + C_v (t_1 - t_2) \quad (7)$$

can be written as

$$G [s dt + [\lambda_i + C_i (t - t_i)] dH] = LC_i d t_i \quad (8)$$

The authors indicated that Equations (6) and (8) could be combined to yield results which suggested the impossibility of operating a cooling tower with hot water and cold dry gas. The reason given for this anomaly indicated that Equations (3) through (5) were incompatible and that Equations (3) and (4) did not adequately represent the sensible heat fluxes required by the enthalpy balance.

It is a great relief to find that, after years of misuse, the logically misleading approximations to the gas- and liquid-phase differential enthalpy balances [Equations (3) and (4)] and the equally meaningless flux balance around the interface [Equation (5)] have finally been exposed. As a further impetus to the speedy demise of these relations the present author would like to point out the apparent source of the difficulty.

Equations (1), (2), and (8) are perfectly straightforward expressions of conservation of mass and the first law of thermodynamics. The prime error in attempting to combine these relations

with Equations (3), (4), and (5) is that one too many restrictions have been imposed upon the system; that is, if sensible heat fluxes are defined by Equations (3) and (4) (whether these definitions are useful and/or well-founded is another matter), then we are not at liberty to specify the relationship between these fluxes, as Equation (5) assumes. The so-called "flux balance at the interface" is not an independent relation but is an auxiliary expression derivable from Equations (2) through (4) and (8). Thus if we consider the definitions of Equations (3) and (4), then Equation (5) must be of the form

$$h_a (t - t_i) + h_a (t_i - t_i) = -N_a [\lambda_i + C_i (t - t_i)] \quad (9)$$

Nevertheless both Equations (5) and (9) are logically superfluous statements of the behavior of the system. Moreover Equation (5) is incorrect.

Next we might inquire as to the origin of Equations (3) and (4). From what basic principle were they derived? Are they exact statements of that principle or convenient approximations?

Consider a differential slice of a dehumidifier, as sketched in Figure 1.

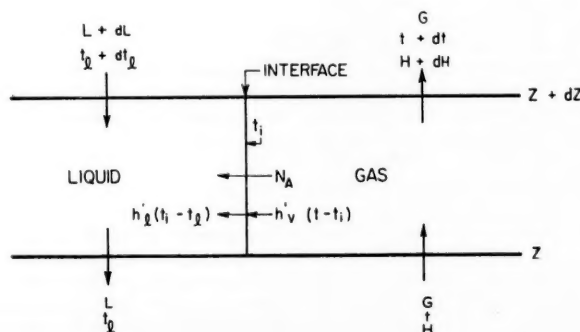


Fig. 1. Flows, compositions, and temperatures in a differential slice of a contactor undergoing simultaneous heat and mass transfer.

* $N_A = k_p M_v (p - p_i)$. Note the inversion of p and p_i compared with Equation (23) of reference 1.

An enthalpy balance over the vapor phase up to but not including the interface proper would contain the following terms:

$$\text{Rate of enthalpy in} = G \bar{C}_{sg}(t - t_r) + G H [C_v(t - t_r) + \lambda_r]$$

The rate of enthalpy removal must contain the contribution of the diffusing vapor, which leaves the control volume at a rate $N_a a dZ$ (per unit cross section of tower) at a temperature t_i :

$$\begin{aligned} \text{Rate of enthalpy out} &= G \bar{C}_{sg} \\ & (t + dt - t_r) + G(H + dH) \\ & [C_v(t + dt - t_r) + \lambda_r] \\ & + N_a a dZ [C_v(t_i - t_r) + \lambda_r] \end{aligned}$$

The difference in these enthalpy rates is properly attributed to a sensible heat flux from the vapor phase toward the liquid. With Equation (2) there results

$$h'_a a (t - t_i) dZ = -G s dt - G dH C_v (t - t_i) \quad (10)$$

Similarly, an enthalpy balance over the liquid phase up to but not including the interface yields

$$h'_i a (t_i - t_r) dZ = L C_l dt_i - G dH C_l (t_i - t_r) \quad (11)$$

In Equation (11) the contribution of the diffusive flux entering the control volume as a liquid at temperature t_i has been included.

Returning to Equations (3) and (4) one can see that these relations differ from the enthalpy balances just considered in their omission of the right-

hand term of Equations (10) and (11). Equations (3) and (4) are therefore approximations of exact enthalpy balances which have been in use so long that they have acquired the aura of fundamental relationships. By their inexact nature they can only lead to anomalies when the internal consistency of the entire set of equations describing the simultaneous heat and mass transfer in the dehumidifier is considered. Their usefulness in the practical task of analyzing this type of contactor depends on the magnitude of the omitted term. The heat transfer coefficients h'_a and h'_i are more nearly equal to those obtainable from correlations of heat transfer experiments conducted in the absence of simultaneous mass transfer [appropriately corrected by the method of Ackermann (2)]. This is generally not true of h_a and h_i .

It can easily be demonstrated that combining Equations (2), (8), (10), and (11) will lead to a "flux balance at the interface" given identically by Equation (5). Nevertheless the flux balance at the interface is still a superfluous concept. The proper enthalpy and material balances are the necessary and sufficient relations for a complete and internally consistent description of the process.

NOTATION

- a = interfacial area for both heat and mass transfer per unit volume, sq.ft./cu.ft.
 C_l = liquid heat capacity, B.t.u./ (lb.) (°F.)
 C_v = heat capacity of the condensable vapor, B.t.u./ (lb.) (°F.)

- \bar{C}_{sg} = average heat capacity of the carrier gas, B.t.u./ (lb.) (°F.)
 G = mass velocity of carrier gas, lb./ (hr.) (sq.ft.)
 H = humidity, lb. vapor/lb. carrier gas
 h_i, h'_i = liquid-phase heat transfer coefficient defined by Equations (4) and (11) respectively, B.t.u./ (hr.) (sq.ft.) (°F.)
 h_a, h'_a = gas-phase heat transfer coefficients, defined by Equations (3) and (10) respectively, B.t.u./ (hr.) (sq.ft.) (°F.)
 k_g = gas-phase mass transfer coefficient, lb. mole/ (hr.) (sq.ft.) (atm.)
 L = mass velocity of liquid, lb./ (hr.) (sq.ft.)
 M_v = molecular weight of the condensable vapor, lb./lb.mole
 N_a = rate of mass transfer, lb./ (hr.) (sq.ft.)
 p, p_i = partial pressure of the condensable vapor in the gas phase and at the interface respectively, atm.
 s = humid heat, equal to $\bar{C}_{sg} + H C_v$, B.t.u./ (lb.) (°F.)
 t = gas-phase temperature, °F.
 t_i = liquid-phase temperature, °F.
 t_i = temperature of interface, °F.
 t_r = reference temperature for enthalpy balance, °F.
 Z = height, ft.
 λ = heat of vaporization, B.t.u./ lb.

LITERATURE CITED

- White, R. R., and S. W. Churchill, *A.I.Ch.E. Journal*, 5, No. 3, 354 (1959).
- Ackermann, G., *Forschungsheft*, 382, 1 (1937).

Effectiveness of Mixing Tanks in Smoothing Cyclic Fluctuations

EDGAR B. GUTOFF

Brown Company, Berlin, New Hampshire

Mixing tanks are useful in smoothing out fluctuations in continuous process streams. If perfect mixing is assumed in the mixing tank, calculation of the effectiveness of the tank in reducing cyclic fluctuations can be fairly straightforward, as was shown by Danckwerts and Sellers (4), Kramers

and Alberda (8), Gutoff (6), and Walker and Cholette (13).

When, on the other hand, the assumption of perfect mixing is not justified, it is extremely difficult to calculate the mixing tank effectiveness, for the fluid regime is very complex. [Danckwerts (2, 3) describes how experimental data on a given tank can be used for this calculation.] Cholette and

Cloutier (1) assumed that in part of the tank volume perfect mixing takes place, that part is stagnant, and that some plug flow and short circuiting of feed occur. However it is difficult to calculate beforehand what the magnitude of these factors will be. The model presented below is believed to be more fundamental in that it takes into account the behavior of the agitator.

Edgar B. Gutoff is with Ionics, Incorporated, Cambridge, Massachusetts.

Either laminar or turbulent flow may take place in the mixing tank. However for longitudinal blending laminar flow is more efficient (9), for there is a greater velocity gradient across the flow path. This velocity gradient causes longitudinal flow and thus promotes the longitudinal blending. The transverse gradients set up by the longitudinal flow are removed by the strong transverse mixing that takes place at the agitator itself. With turbulent flow, on the other hand, the velocity profile is more nearly flat, and there is less back mixing.

If we are conservative, and assume turbulent flow conditions in the mixing tank, and further assume that the turbulent flow can be approximated by a flat velocity profile with no relative longitudinal flow, then the mixing-tank efficiency can be calculated from a simple difference equation. This flow condition may be approximated in practice by a propeller agitator located at the bottom of a draft tube in a tank and also in the case of mixing of certain types of slurries, such as wood pulp. In other cases it is clear that there is a great deal of return of the rising fluid to the agitator at all levels above the propeller, not only at the top. This short-circuiting of the fluid thus aids the longitudinal mixing. The assumed model therefore gives a limiting case, and this case is the conservative limit. Being a conservative limit, the model should prove useful in defining the worst conditions. If short-circuiting is to be taken into account, the mathematics become extremely involved and so far have not been solved.

A turbine agitator provides a radically different flow pattern in the tank. The fluid flows radially outward at the agitator, up and down the sides to the top and bottom of the tank respectively, and then along the axis of the tank back to the turbine. A tank with a turbine agitator is thus similar to two tanks like those described above, but each would be half the height and they would be placed bottom to bottom. Although the back mixing of the fluid is greater in this case, the assumption of a flat velocity profile will lead to the identical conservative results obtained with the first model. Figure 1 is equiv-

alent to the above models, but here the agitation takes place by recycling some of the product back to the input stream. The mathematics below refers to Figure 1.

The material at the entrance point at t is a mixture of the input, $Fc_i(t)$, and the recycle, $(P-F)c_o(t)$. When one assumes a flat velocity profile, all of this takes time T to move through the system, to give the output flow just before the take-off point of $Pc_o(t+T)$ at time $t+T$. Thus

$$\sigma_o = \frac{bc}{\sqrt{2} \left[1 + \frac{2H}{T} \left(\frac{H}{T} - 1 \right) (1 - \cos 2\pi T/\lambda) \right]^{1/2}} \quad (8)$$

$$c_o(t+T) = \frac{F}{P} c_i(t)$$

$$+ \frac{(P-F)}{P} c_o(t) \quad (1)$$

and for the input, from Equation (2)

$$\sigma_i = \frac{bc}{\sqrt{2}} \quad (9)$$

Therefore the effectiveness of the mixing tank is found as

$$1 - E = \frac{\sigma_o}{\sigma_i} = \frac{1}{\left[1 + \frac{2H}{T} \left(\frac{H}{T} - 1 \right) (1 - \cos 2\pi T/\lambda) \right]^{1/2}} \quad (10)$$

This is a difference equation and may be solved by standard methods (7).

The steady state solution may be found by the method of undetermined coefficients (7). If the input function is assumed to vary sinusoidally,

$$c_i(t) = \bar{c} (1 + b \sin 2\pi t/\lambda) \quad (2)$$

then the output function will be of the form (7)

$$c_o(t) = A + B \sin 2\pi t/\lambda + C \cos 2\pi t/\lambda \quad (3)$$

and

$$c_o(t+T) = A + B \sin 2\pi (t+T)/\lambda + C \cos 2\pi (t+T)/\lambda \quad (4)$$

Substituting Equations (2), (3), and (4) into Equation (1) and equating constant coefficients, coefficients of $\sin 2\pi t/\lambda$, and coefficients of $\cos 2\pi t/\lambda$ gives three simultaneous equations involving A , B , and C . Solving these equations and simplifying yields the desired result,

The effectiveness of the mixing tank in smoothing the input fluctuations may be expressed most conveniently by the reduction in the root mean square value of the deviations from the mean (4). This is the standard deviation σ . When

$$c - \bar{c} = a \sin \theta + b \cos \theta \quad (6)$$

then

$$\sigma = \sqrt{(a^2 + b^2)/2} \quad (7)$$

Therefore from Equation (5)

When the turnover time approaches zero, perfect mixing is approached; the cosine function can be replaced by the first terms in its series expansion:

$$1 - \cos 2\pi T/\lambda \approx (2\pi T/\lambda)^2/2 \quad (11)$$

$(H/T - 1)$ approaches H/T , and Equation (10) reduces to

$$1 - E = \frac{\sigma_o}{\sigma_i} = \frac{1}{[1 + (2\pi H/\lambda)^2]^{1/2}} \quad (12)$$

This is the equation for the effectiveness of a mixing tank with perfect mixing (4), such that the concentration in the tank is at all times equal to the output concentration.

The mixing-tank effectiveness calculated from Equation (10) is plotted as a function of H/λ , the ratio of holdup time to the cycle time of the fluctuations, for various values of H/T , the ratio of holdup time to turnover time,

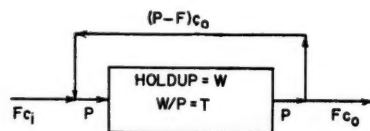


Fig. 1. Equivalent model of a continuous mixer, with throughput rate F and agitator turnover time T .

$$\frac{c_o - \bar{c}}{bc} = \frac{-\left[1 - \frac{1}{H/T} - \cos 2\pi T/\lambda \right] \sin 2\pi t/\lambda}{2 \left(\frac{H}{T} - 1 \right) \left[1 + \frac{1}{2H \left(\frac{H}{T} - 1 \right)} - \cos 2\pi T/\lambda \right]} - \frac{\sin 2\pi T/\lambda \cos 2\pi t/\lambda}{2 \left(\frac{H}{T} - 1 \right) \left[1 + \frac{1}{2H \left(\frac{H}{T} - 1 \right)} - \cos 2\pi T/\lambda \right]} \quad (5)$$

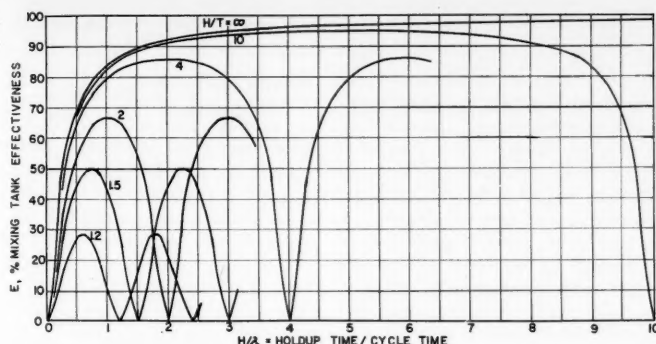


Fig. 2. Effectiveness of mixing tanks in reducing cyclic fluctuations as a function of the ratio of tank holdup time to the cycle time of the fluctuations. H/T is the ratio of the holdup time to the agitator turnover time.

in Figure 2. The ratio of H/T is also equal to P/F , the ratio of agitator pumping rate to throughput rate. It is seen that the effectiveness increases as the turnover time decreases relative to the holdup time, or as perfect mixing is approached, and also increases as the ratio of holdup time to cycle time increases.

As the ratio of holdup time to cycle time increases, the effectiveness goes through the maxima and then decreases to zero at integral values of T/λ , equal to $H/\lambda \div H/T$. This occurs only because the proposed model assumes a flat velocity profile, with no short-circuiting back to the agitator, and the flow in the mixer is in phase with the frequency of the fluctuations. In an actual mixing tank it is extremely doubtful whether these maxima would appear, because of the back mixing that takes place. Certainly the effectiveness would not drop to zero at values of $T/\lambda = 1, 2$, and higher integers.

EFFECTIVENESS OF AGITATION

The effectiveness of agitation measuring the approach to perfect mixing, may be defined as the mixing-tank effectiveness divided by the tank effectiveness if perfect mixing took place (5), E^* or

$$E = E_a E^* \quad (13)$$

The effectiveness of agitation is plotted in Figure 3 as a function of H/T , the ratio of the holdup time to the turnover time, for various values of T/λ . It is noticed that the lines of constant T/λ are asymmetrical with respect to $T/\lambda = 0.5$. Looking again at Figure 2, one notices that although the curves of tank effectiveness are symmetrical (about the point $T/\lambda = 0.5$), the value of tank effectiveness with perfect

mixing keeps rising with increasing values of H/λ , and so the degrees of agitation are lower for values of T/λ above 0.5 than for those under 0.5.

The effectiveness of agitation, as defined above, is thus dependent on the cycle time of the fluctuations. Whether this dependence exists in practice or is only a result of using an approximate model is not known. Certainly, the dependence would not be so great as shown in Figure 3.

The effectiveness of agitation is above 90% in most cases when the turnover time is less than one fifth of the holdup time (H/T above 5).

AGITATOR PUMPING RATES

So far no mention has been made here of the determination of agitator

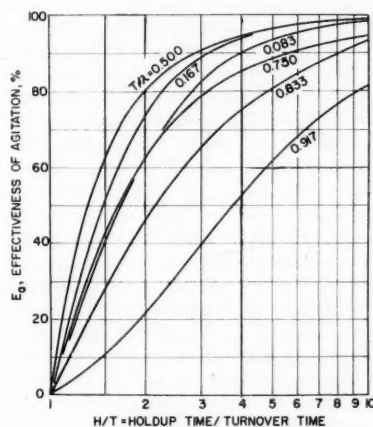


Fig. 3. Effectiveness of agitation in continuous mixing tanks as a function of the ratio of tank holdup time to agitator turnover time. T/λ is the ratio of turnover time to the cycle time of fluctuations. The effectiveness of agitation measures the approach to perfect mixing.

pumping rates. The subject is complex; some work has been done, and more needs to be done. Rushton and co-workers (9, 10) presented some equations to calculate this pumping rate, for both propellers (9) and turbines (10). They pointed out that the total fluid pumped was greater than the discharge from the agitator and discussed (9) the application of the work of Folsom and Ferguson (5) on jet entrainment to this problem. Van de Vusse (12) derived equations enabling one to calculate the pumping rates for turbines, paddle stirrers, and propellers. It is hoped that this paper will stimulate more studies in this field.

NOTATION

- A, a = constants
 B, b = constants
 b = maximum fractional deviation of c_i from \bar{c} , or $[(c_i - \bar{c})/\bar{c}]_{max}$
 C = constant
 c_i = input concentration or other additive intensive property
 c_o = output concentration
 \bar{c} = time average concentration, in and out
 E = mixing-tank effectiveness, equal to $1 - (\sigma_o/\sigma_i)$
 E^* = mixing-tank effectiveness with perfect mixing
 E_a = degree of agitation, equal to E^*/E
 F = flow rate in and out of mixing tanks, lb./min.
 H = holdup time in mixing tank, equal to W/F , min.
 P = agitator pumping rate, lb./min.
 T = turnover time in mixing tank, equal to W/P , min.
 t = time, min.
 W = holdup in mixing tank, lb.
 λ = cycle time of fluctuations, min.
 σ_i = standard deviation of input fluctuations
 σ_o = standard deviations of output fluctuations
 σ_o^* = standard deviations of output fluctuations with perfect mixing

LITERATURE CITED

- Chollette, A., and L. Cloutier, *Can. J. Chem. Eng.*, **37**, 105 (1959).
- Danckwerts, P. V., *Ind. Chemist.*, **30**, 102 (1954).
- , *Chem. Eng. Sci.*, **2**, 1 (1953).
- , and E. S. Sellers, *Ind. Chemist*, **27**, 395 (1951).
- Folsom, R. G., and C. K. Ferguson, *Trans. Am. Soc. Mech. Engrs.*, **71**, 73 (1949).
- Gutloff, E. B., *Ind. Eng. Chem.*, **48**, 1817 (1956).

7. Hildebrand, F. B., "Methods of Applied Mathematics," pp. 237-44, Prentice-Hall, New York (1952).
8. Kramers, H., and G. Alberda, *Chem. Eng. Sci.*, **2**, 173 (1953).
9. Rushton, J. M., *Chem. Eng. Progr.*, **50**, 587 (1954).
10. ———, and J. Y. Oldshue, *ibid.*, **49**, 161, 267 (1953).
11. Sachs, J. P., and J. H. Rushton, *ibid.*, **50**, 597 (1954).
12. Van de Vusse, J. G., *Chem. Eng. Sci.*, **4**, 178, 209 (1955).
13. Walker, O. J., Jr., and A. Cholette, *Pulp Paper Mag. Can.*, **59**, 113 (1958).

CHEMICAL ENGINEERING PROGRESS SYMPOSIUM SERIES ABSTRACTS

The Chemical Engineering Progress Symposium Series is composed of papers on specific subjects conveniently bound in individual books, which are published at intervals. The books are 8½ by 11 inches, paper covered, and cost \$3.50 to members, \$4.50 to nonmembers. They may be ordered from the Secretary's Office, the American Institute of Chemical Engineers, 25 West 45 Street, New York 36, New York.

The *A. I. Ch. E. Journal* will publish, from time to time, abstracts of the articles appearing in the Symposium Series volumes. Recently published volumes are abstracted below.

NUCLEAR ENGINEERING—PART VI, Vol. 55, No. 23, 1959.

A Digital Program to Evaluate Transients for Nuclear Power Plant Design, F. J. Scheib and A. J. Arker. The design limitations of a nuclear power plant for mobile use often depend on the transients which the plant undergoes during normal or casualty operation. Examples of decisions which depend on transient evaluation in the design of a pressurized water plant are given, and the model digital computer program used to analyze such transients is described. Important features of this program are nonsymmetrical and variable flow operation of the two coolant loops, use of nonanalytic input data, and flexibility for alteration. **Control of the PRTR-A Gas-Balance Method With Supplementary Mechanical Shims**, J. F. Fletcher. The Plutonium Recycle Program, a comprehensive research and development program, has as its goal the development of safe, economical methods of using plutonium fuels in power reactors. The Plutonium Recycle Test Reactor is a test facility essential to this program designed to have a high degree of versatility and to be capable of operating under a great variety of experimental conditions. The control system used provides an unusual degree of reactor safety. **A Study**

of the Feasibility of a Tracer System for Locating a Fuel-Element Failure in a Pressurized Water Reactor, Meyer Pobereskin, Duane N. Sunderman, Aaron Eldridge, George D. Calkins, and Walston Chubb. This investigation indicated that a system of tracer elements for location of fuel-element failure merited development. The method consists in adding small amounts of different pairs of elements to the fuel alloy of each subassembly. When a fuel-element failure occurs, a portion of the coolant is analyzed radiochemically for the elements added to the fuel as tracers. The radioactive species of the elements detected indicate the subassembly in which the failure has occurred. Eleven elements were found to be suitable tracers. **Coolant Temperature Rise in a Pressurized Water Reactor During a Loss of Flow Incident**, Joel Weisman, Shepard Bartnoff, and G. C. Tirellis. A method is described for calculating the coolant temperature at the reactor outlet as a function of time following a loss of pumping power and the consequent loss of coolant flow. The effects of negative temperature coefficient and delayed gamma radiation on the heat production rate of the reactor are considered and contributions to the total coolant temperature rise calculated from both the nucleate boiling region

and the nonnucleate boiling region of the core. **Reprocessing Costs for Fuel From a Single-Region Aqueous Homogeneous Reactor**, A. C. Jealous and R. J. Klotzbach. The cost is estimated for a fuel-reprocessing plant to recover fissionable, fertile, and moderator materials from irradiated slurry fuel of the Pennsylvania Advanced Reactor (PAR). The estimate is based on a reprocessing plant designed to process 47 kg. of thorium per day for return to the reactor plant. Off-site solvent-extraction decontamination of PAR fuel in A.E.C. multipurpose plant would cost more than complete-on-site reprocessing. **Pilot Plant Fluorination of Uranium Fuel Elements by Bromine Trifluoride**, Gerald Strickland, F. L. Horn, and Richard Johnson. The dissolution of uranium in bromine trifluoride at 250°F. was investigated in continuous equipment on a pilot plant scale. In particular the autocatalytic effect of the UF_6 concentration on the dissolution time of unirradiated B.N.L. reactor slugs was determined. A series of nine runs is described in which the UF_6 concentration progressed from 0 to 4.5 mole %. **Reprocessing Uranium-Zirconium-Alloy Reactor Fuel Elements**, C. B. Leek, R. B. Lemon, and F. K. Wrigley. The process employed for the recovery of uranium from uranium-zirconium alloy reactor fuel ele-

ments at the Atomic Energy Commission's Idaho chemical processing plant is described, and the results of the initial processing and decontamination operations are summarized. **Effect of Geometrical Shape on the Continuous Dissolution of Aluminum in Mercury-Catalyzed Nitric Acid**, A. F. Boeglin and J. A. Buckham. The results of a study of the effect of geometrical shape of aluminum-reactor fuel elements on the dissolution rate in mercury-catalyzed nitric acid are presented. Statistical analysis of the data showed that the main effects, feed rates, catalyst concentration, and shape, and all first-order interaction effects had a significant effect on dissolution rate. A mathematical relationship between dissolution rate and feed rate, catalyst concentration and the catalyst concentration by feed-rate interaction was graphically developed for each shape. **General Economics of Chemical Reprocessing Using Solvent Extraction Processing**, F. L. Culler, Jr. The competitive requirement of producing electricity at 8 mills/kw.-hr. in the United States places limitations on the over-all recycle costs of irradiated fuel and fertile material. Based on buy-back prices published by the A.E.C. the residual value of fissionable and fertile material in irradiated fuel is almost always greater than the cost of recycle. Reprocessing probably will always be required.

NUCLEAR ENGINEERING—PART VII, Vol. 55, No. 27, 1959

Radiochemical Research in the U.S.S.R., Victor Spitsyn. A survey of the state of the art in the U.S.S.R. from the time of initial studies of radioactive elements soon after the discovery of radioactivity to the present (date of article is 1958). **The Use of Tracer Atoms in the Physicochemical Study of Some Inorganic Polycompounds**, Victor Spitsyn. Tracer atoms were used to ascertain in the primary stages of formation of aquopoly and heteropoly compounds, and to study their properties and structure by isotopic exchange, and other physical and chemical methods of research. It has been suggested that the process of formation of aquopoly and heteropoly compounds is related to the appearance of hydrogen bonds between the anions of acids, which participate in the said interaction. The existence of oxonium groups in the structure of aquopoly anions may also be assumed. **Effect of Gamma Radiation Intensity on the Polymerization of Ethylene**, B. G. Bray, R. A. Carstens, O. A. Larson, J. J. Martin, and K. K. G. Sikchi. In the

field of photochemical reactions it is suggested that the reaction-rate constant often varies as the square root of the intensity of the radiation field. For the two-step mechanism proposed in this study it was found that the initiating reaction constant was directly proportional to the intensity of radiation. A secondary reaction constant was found. **Blast Effects Tests of a One-Quarter-Scale Model of the Air Force Nuclear Engineering Test Reactor**, Wilfred E. Baker. The results of a series of nuclear accidents to a one-quarter scale model reactor simulated by explosives and propellants are presented. The accuracy of simulation of these power excursions and the applicability of laws of scaling blast loading and corresponding transient structural response are discussed. **Heavy-Water Reactors for Power Production**, David P. Herron. From a nuclear standpoint, heavy water is the most attractive moderator for thermal reactors because its high moderating ratio permits excellent fuel economy. The principal factors affecting the fuel-cycle and capital in design of heavy-water reactors are reviewed, and several possibilities for reducing the power cost of this type of reactor are discussed. **Conversion of Uranium Hexafluoride to Uranium Tetrafluoride**, S. H. Smiley and D. C. Brater. The atomic energy program has a need for large quantities of uranium metal and uranium salts of various uranium-235 assays for nuclear reactors. Since enriched uranium is usually available as the hexafluoride, it is necessary to convert this compound to uranium tetrafluoride as an intermediate step in the preparation of most of the desired reactor fuel materials. Contrary to published literature the single-step reduction of UF_6 to UF_4 with hydrogen was found to be quantitative; further a highly efficient, safe, economical was developed and adapted for large-scale production use. **High-Temperature Processing of Molten Fluoride Nuclear Reactor Fuels**, Warren R. Grimes, James H. Shaffer, Newman V. Smith, Richard A. Strehlow, Wilfred T. Ward, and George M. Watson. The removal of certain undesirable fission-product fluorides from reactor fuels consisting of molten mixtures of uranium tetrafluoride with other fluorides has been successfully accomplished in small-scale experiments by precipitation techniques which may be adaptable to large-scale application. Data relating to the solubility of xenon and other rare gases are presented and are pertinent to the ease of removal of such gaseous fission-product poisons. **Summary Report: Economic Comparison of Zircaloy and Stainless Steel in Nuclear Power Reactors**, Manson Bene-

dict. In most nuclear reactors being designed for commercial power production, it is technically feasible to use either stainless steel, zirconium, or one of its alloys as structural material, fuel cladding, or fuel diluent. When zirconium is used within the neutron flux of the reactor, its low neutron-absorption cross section gives zirconium an important economic advantage over stainless steel. On the other hand, zirconium and its alloys cost more. This study was made to assist reactor designers in determining when it is advantageous to consider zirconium. **Boiling-Heavy-Water Reactor for Process Steam and Power**, Patrick J. Selak and George B. Humphreys. For a hypothetical reactor plant located in the United States there is no significant difference in the net fuel cycle cost or the cost of steam produced, whether the reactor is operated with fuel element reprocessing or on a throw-away basis. This suggests the suitability of this reactor for remote mining and processing operations. **Laboratory Facilities for Nuclear Engineering Education at MIT**, T. J. Thompson. A comprehensive program of graduate study in nuclear engineering is intended primarily for students with undergraduate degrees in physics, chemistry, or metallurgy or chemical, civil, electrical, or mechanical engineering. For those interested in specializing in nuclear engineering, the program leads to the degree of M.S. in nuclear engineering or Sc.D. Courses taught are outlined. **Conceptual Design of Pyrometallurgical Reprocessing Plant**, Louis Basel and Joseph Koslov. A pyrometallurgical reprocessing plant for handling fuel from a 500-Mw. fast-breeder reactor is described. Also included are capital and operating costs and a discussion of problems requiring further investigation. **The Nitrophos Extraction Process for the Separation of Zirconium and Hafnium**, Wayne H. Keller and Irwin S. Zonis. The several possible systems for separating Zr and Hf are reviewed briefly. The reasons for selecting the Nitrophos liquid-liquid extraction process are discussed. The laboratory and pilot plant experiments are described and the data presented. Under the conditions studied, reactor-grade zirconium can be prepared in a column with less than ten theoretical stages. The commercial plant design is described and preliminary operating results are given. **Natural-Circulation Boiling Reactor With Tapered Coolant Channels**, S. G. Bankoff. It is suggested that some of the heat transfer characteristics of natural-circulation boiling reactors might be improved by employing tapered coolant channels. A previously developed flow model for straight

channels is used to predict frictional losses in tapered channels with uniform and with cosine heat-flux distributions. **Temperature Rise in Underground Storage Sites for Radioactive Wastes**, R. S. Schechter and E. F. Gloyna. An attempt is made to determine the limits of the temperature increase resulting from the release of energy by high-level radioactive wastes stored in underground spherical cavities. This determination is accomplished by calculating the temperature rise on the basis of two models, one fixing the upper limit of temperature increase and the other the lower limit. The results of these calculations are presented in a generalized graphical form to facilitate design calculations. **A Technical and Economic Analysis of the Separation of Plutonium and Fission Products from Irradiated Nuclear Reactor Fuels**, H. A. Ohlgren, J. G. Lewis, M. E. Weech, and G. W. Wensch. The technical background for chemical processing of irradiated nuclear reactor fuels is discussed, and aqueous solvent extraction methods for the separation of uranium from plutonium and fission products are briefly described. Estimated capital and operating costs are presented for an aqueous separation of plutonium and fission products from irradiated fuel elements of a fast-breeder power reactor.

REACTION KINETICS AND UNIT OPERATIONS,

Vol. 55, No. 25, 1959

Reaction Rates in Chemical Engineering Science, Hugh M. Hulburt. Chemical reactions consist in the redistribution of electrons between nuclei. The laws which govern their interactions are concisely summarized in the Schrödinger equation and the postulate of Coulomb's law for the force between charged particles. **Transport Processes With Chemical Reactions**, Stephen Prager. The general transport equations, after discussion, are applied to (1) reactions with bulk flow only, (2) reactions accompanied by diffusion and heat conduction, both with and without the assumption of local chemical equilibrium, (3) diffusion-controlled surface reactions, (4) systems in which reactions give rise to volume changes, and (5) the steady state. For systems with nonlinear kinetics the method of moments is shown to give good results with a relatively small amount of effort. **Turbulent Transport in Chemical Reactors**, John Beek, Jr., and R. S. Miller. To predict the behavior of a reactor under specified conditions, one must be able to calculate not only the rates of

whatever chemical reactions are going on but also the rates of whatever transport processes are involved. This paper lists and discusses the transport processes. **Intraparticle Diffusion in Catalytic Systems**, Paul B. Weisz. Diffusion transport may have various effects on the measured rate of conversion. Application of diffusion equations to chemical rate processes is discussed, and examples of various cases of intraparticle chemical conversion and generally useful methods of evaluating diffusion effects are given. Diffusion-transport criteria can often be used to investigate reaction kinetics involving intermediate species. **Stability of Chemical Reactors**, C. H. Barkelew. It has been common practice to base the stability aspects of reactor design primarily on pilot plant or laboratory experience. Recently, however, several analyses of the thermal behavior of reactors have been published in the hope that a suitable theoretical treatment could save expensive experimentation. This paper presents a new method of designing stable tubular reactors. **Chemical Reaction-System Dynamics**, Alan S. Foss. Recent developments in the dynamics of chemical-reaction systems contributing toward improved control of today's chemical processes are reviewed in some detail, with emphasis on the methods and techniques of analysis, and some means of filling the gaps in our present knowledge are suggested. **Progress in the Fundamentals of Heat Transfer**, M. T. Cichelli. Progress in heat transfer science during the past fifty years is briefly reviewed, with emphasis on those developments which have had the greatest impact on chemical engineering practice in this country. **Future Trends in Heat Transfer Technology**, Donald Q. Kern. Future developments in thermal process technology will be derived from the design practices employed in nuclear reaction, cryogenics, rocketry, missile technology; from extensions of current chemical engineering techniques; and from the adaptation of advanced mathematical tools to computer solutions. Rockets and related problems predominate in outmoding current thermal processing concepts. **Mass, Heat, and Momentum Transfer Between Phases**, T. K. Sherwood. Mass may be transferred, as by evaporation of a liquid into a gas in a wetted-wall tower; heat is transferred if tube and fluid are not at the same temperature; and momentum transfer from the fluid results in a shear stress at the tube wall, causing a decrease in fluid pressure along the tube length. The subject of the present paper is the interrelationships of these three transfer processes. **Progress in Fractional Distillation**, R. L. Geddes. A brief outline

of important developments that contribute to present knowledge of design of fractionators is given in historical sequence. Some comments on the present status and future problems from a chemical engineer's viewpoint are offered. **Liquid-Liquid Extraction: Theory and Practice**, Robert B. Beckmann. In this presentation of the theory and practice of solvent extraction—its history, current practice, and a few prognostications for the future—the enormity of the general field has limited discussion of the fundamentals of mechanism and theory as they pertain to liquid-liquid extraction in general and specifically to presently popular commercial extraction equipment. **Progress in Separation by Sorption Operations—Adsorption, Dialysis, and Ion Exchange**, G. P. Monet and Theodore Vermeulen. The object of this paper is to outline briefly the present status of quantitative knowledge about adsorption, dialysis, and ion exchange. First, general effects which are believed to apply to all three fields are discussed, and then are considered specific effects which are caused by the sorbent materials used. **Principles of Gas-Solids Separations in Dry Systems**, S. K. Friedlander. The mechanics of fluid-particle systems are used to explain the functioning of each class of device developed to handle the wide range of problems encompassed within suspension concentrations and particle-size limits. Emphasis is on recent advances in the field and on areas which may prove fruitful for further research. **The Art and Science of Liquid Filtration**, H. P. Grace. This paper describes the present state of theoretical knowledge as applied to solution clarification and to cake filtration and its limitations, considers the major problems in measurement techniques and their potential solutions, and points out the potential areas of development that are most likely to yield significant improvements in filtration performance. **Separation by Crystallization**, Robert A. Findlay and Dwight L. McKay. Crystallization could be the basis of a separation method of wide usefulness, particularly in the field of organic chemicals, as it minimizes the decomposition of heat-sensitive substances and separates organic isomers which can be separated practically in no other way. Application has been hindered by lack of chemical engineering development. **Mixing of Liquids**, J. H. Rushton and J. Y. Oldshue. Mixing of fluids in chemical processing usually involves an intimate and homogeneous distribution of all liquid components, gases, and particulate solids which may be involved. The most common device to bring about

(Continued on page 3J)

(Continued from page 352)

mixing is some form of rotating impeller, driven by a shaft attached to a power-transmission device connected to an electric or other motor. **Mixing of Solids**, Sherman S. Weidenbaum. High lights of solids-mixing studies are given, based on a critical and interpretive review of American and foreign literature and other pertinent material. Degree of mixing, theoretical frequency distributions, rate studies, and equipment are discussed. Areas for future investigation are suggested. **Size Reduction**, Lincoln T. Work. The creation and control of particle size goes under many names, some pointing to the production of particles in a desired range of sizes. This paper will discuss the aspects of solids only, with particular reference to size reduction and some reference to size enlargement. **Drying—Its Status in Chemical Engineering in 1958**, W. R. Marshall, Jr. Historically, drying is one of the oldest operations in chemical engineering, and yet at this date its theoretical development has not progressed so far as many other chemical engineering operations. The objectives of a drying operation can be manifold, and it is difficult to name a common objective, other than moisture removal. Consequently, drying problems generally involve a variety of secondary objectives.

Errata

The equations given below are corrected versions of those published in "Heat Transfer in Cylinders with Heat Generation" by Leonard Topper, *A.I.Ch.E. Journal*, 1, 463 (1955). The help of Dr. P. J. Schneider and of Professor R. Byron Bird is acknowledged by the author.

$$\frac{t - t_s}{t_0 - t_s} = \sum_{n=1}^{\infty} N_n J_0(\lambda_n w) e^{-\lambda_n^2 (\alpha / s^2) (x/s)} + \frac{Bs^2 \left(1 + 2 \frac{k}{sh} - w^2 \right)}{4\alpha (t_0 - t_s)} \quad (7)$$

$$\frac{t - t_s}{t_0 - t_s} = 1 = \sum_{n=1}^{\infty} N_n J_0(\lambda_n w) + \frac{Bs^2 \left(1 + 2 \frac{k}{sh} - w^2 \right)}{4\alpha (t_0 - t_s)} \quad (11)$$

$$N_n = \frac{2 \frac{hs}{k}}{\left[\lambda_n^2 + \left(\frac{hs}{k} \right)^2 \right] J_0(\lambda_n)} \left[1 - \frac{Bs^2}{\alpha \lambda_n^2 (t_0 - t_s)} \right] \quad (12)$$

$$\frac{t - t_s}{t_0 - t_s} = \frac{Bs^2 \left(1 + 2 \frac{k}{sh} - w^2 \right)}{4\alpha (t_0 - t_s)} + 2 \frac{hs}{k} \sum_{n=1}^{\infty} \frac{J_0(\lambda_n w) e^{-\lambda_n^2 (\alpha / s^2) (x/s)}}{\left[\lambda_n^2 + \left(\frac{hs}{k} \right)^2 \right] J_0(\lambda_n)} \left[1 - \frac{Bs^2}{\alpha \lambda_n^2 (t_0 - t_s)} \right] \quad (13)$$

$$t + \frac{B}{A} = \left(t_s + \frac{B}{A} \right) \frac{J_0 \left[\left(\frac{As^2}{\alpha} \right)^{1/2} w \right]}{J_0 \left[\left(\frac{As^2}{\alpha} \right)^{1/2} \right]}$$

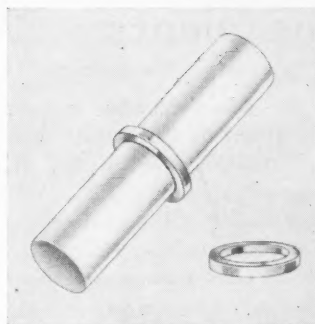
IMPORTANT NOTICE

If your address has changed, please fill out this form and mail to A.I.Ch.E. JOURNAL, 25 West 45th Street, New York 36, New York.

EFFECTIVE DATE OF NEW ADDRESS		DATE OF THIS NOTICE	
PREVIOUS ADDRESS			
STREET NUMBER, STREET NAME, POST OFFICE BOX NUMBER		NAME OF STATE	
NAME OF CITY OR TOWN		ZONE NO.	
NEW ADDRESS			
STREET NUMBER, STREET NAME, POST OFFICE BOX NUMBER		NAME OF STATE	
NAME OF CITY OR TOWN		ZONE NO.	
PRINT NAME & MEM. REF. NO.		SIGN NAME HERE	

spinbars

magnetic stirring bars



Pivot Ring at no extra cost.

teflon®
kel-f®
tygon®
polyethylene
high temp

The most widely accepted, lowest priced stirring bars on today's market.

Four years in research... research that has developed Spinbars with a powerful Alnico V Magnet encased in a solid one-piece capsule, each electrically and vacuum tested and absolutely leak proof. Available at any Laboratory Supply House.

SPINBARS, TEFLON	SPINBARS, KEL-F	SPINBARS, TYGON	SPINBARS, POLYETHYLENE
5/16" Dia. 1/2" Lg. to 2" Lg.	1/4" Dia. 1/2" Lg. to 7/8" Lg.	3/8" Dia. 3/8" Lg. to 2 1/4" Lg.	5/16" Dia. 1/2" Lg. to 2" Lg.
3/8" Dia. 3/8" Lg. to 2 1/4" Lg.	5/16" Dia. 1/2" Lg. to 2" Lg.	3/8" Dia. 1 3/4" Lg.	3/8" Dia. 3/8" Lg. to 2 1/4" Lg.
1/2" Dia. 1 1/4" Lg. to 3" Lg.	3/8" Dia. 3/8" Lg. to 2 1/4" Lg.		
5/8" Dia. 1 3/8" Lg. to 1 7/8" Lg.	1/2" Dia. 1 1/4" Lg. to 3" Lg.		
	3/8" Dia. 1 3/8" Lg. to 1 7/8" Lg.		

*Trademarks
DuPont
Kellogg
U. S. Stoneware

Stirring Bars for every requirement in Teflon, Kel-F, Tygon and Polyethylene—all leak proof, laboratory tested.

Spinbars are available, like all better products through Laboratory Supply Houses.

SPINBARS... designed for greater movement and agitation.



LABORATORY PLASTICWARE FABRICATORS

714 BALTIMORE • P. O. BOX 213 • KANSAS CITY 5, MO.

(Continued from preceding page)

$$+ \sum_{n=1}^{\infty} \left[\frac{2 \left(t_0 + \frac{B}{A} \right)}{\beta_n J_1(\beta_n)} + N_n \right] J_0(\beta_n w) e^{(\pi/V)[A - \alpha(\beta_n/s)^2]} \quad (14)$$

$$\frac{t - t_s}{t_0 - t_s} = \frac{\left(t_s + \frac{B}{A} \right)}{(t_0 - t_s)} \left\{ \frac{J_0 \left[\left(\frac{As^2}{\alpha} \right)^{1/2} w \right]}{J_0 \left[\left(\frac{As^2}{\alpha} \right)^{1/2} \right]} - 1 \right\} + \frac{2 \left(t_s + \frac{B}{A} \right)}{(t_0 - t_s)} \sum_{n=1}^{\infty} \frac{J_0(\beta_n w) e^{(\pi/V)[A - \alpha(\beta_n/s)^2]}}{\beta_n J_1(\beta_n)} \cdot \left[\frac{\left(t_0 + \frac{B}{A} \right)}{\left(t_s + \frac{B}{A} \right)} + 1 - \frac{\beta_n^2}{\left(\beta_n^2 - \frac{As^2}{\alpha} \right)} \right] \quad (17)$$

$$\frac{t - t_s}{t_0 - t_s} = \frac{\left(t_s + \frac{B}{A} \right)}{(t_0 - t_s)} \left\{ \frac{J_0 \left[\left(\frac{As^2}{\alpha} \right)^{1/2} w \right]}{J_0 \left[\left(\frac{As^2}{\alpha} \right)^{1/2} \right] - \frac{k}{sh} \left(\frac{As^2}{\alpha} \right)^{1/2} J_1 \left[\left(\frac{As^2}{\alpha} \right)^{1/2} \right]} - 1 \right\} + \frac{2 \left(t_s + \frac{B}{A} \right)}{(t_0 - t_s)} \frac{hs}{k} \sum_{n=1}^{\infty} \frac{J_0(\lambda_n w) e^{(\pi/V)[A - \alpha(\lambda_n/s)^2]}}{\left[\lambda_n^2 + \left(\frac{hs}{k} \right)^2 \right] J_0(\lambda_n)}$$

$$\cdot \left[\frac{\left(t_0 + \frac{B}{A} \right)}{\left(t_s + \frac{B}{A} \right)} + 1 - \frac{\lambda_n^2}{\left(\lambda_n^2 - \frac{As^2}{\alpha} \right)} \right] \quad (21)$$

The equation given below is the corrected version of that published in "Phase Equilibria in Mixtures of Polar and Nonpolar Compounds: Derived Thermodynamic Quantities for Alcohols and Hydrocarbons" by Cline Black, *A.I.Ch.E. Journal*, 5, 249 (1959).

$$\log \theta_i = [(P - P_i^0)/2.3RT] \cdot [b_i - V_i' - a_i \xi_i^0/RT] + (P/2.3R^2T^2) [(\sum G_{ij}Y_j) + (\sum \bar{G}_{ij}Y_j)] \quad (2)$$

The notation given below is the corrected version of that published in "Thermodynamic Consistency of Binary Liquid-Vapor Equilibrium Data When One Component Is Above Its Critical Temperature" by S. B. Adler, Leo Friend, R. L. Pigford, and G. M. Rosselli, *A.I.Ch.E. Journal*, 6, 108 (1960).

$$Z'' \equiv Z^L + Z_1^a y_1 (1/K_2 - 1/K_1) - Z^V/K_2$$

SAFETY in air and ammonia plants

—may save a life! This publication contains articles which appeared in **CHEMICAL ENGINEERING PROGRESS**—plus reports on A.I.Ch.E. Symposia held in 1956, 1957, 1958. 84 pages, paper bound. Prices: 1-4 copies: Members, \$1.50; Nonmembers, \$1.75; 5 or more copies, \$1.25 each. Postage extra when payment does not accompany order.

American Institute of Chemical Engineers
25 West 45 Street, New York 36, N. Y.

Send copies of *Safety in
Air and Ammonia Plants* to

PRINT NAME _____

COMPANY _____

STREET _____

CITY _____

ZONE _____

STATE _____

Member ☐ Nonmember ☐
Check enclosed ☐ Bill me ☐

SAVE THOSE BACK ISSUES!

Every so often an unprecedented demand for a particular issue, or an unexpected influx of new subscribers and members puts the editor in the embarrassing position of running out of copies of *A.I.Ch.E. Journal*. This has happened several times in our short history and if members have copies of any of the following issues, we would be glad to purchase them.

The issue which we need and for which we will pay \$1.50 each is: March 1960.

All these issues were overprinted to the usual extent, but because popular features spurred single copy sales, our reserves are exhausted.

Help fellow members by sending your back numbers of the issues specified above to:

Mrs. E. PLATTNER
A.I.Ch.E. Journal
25 West 45 St.
New York 36, N. Y.

A.I.Ch.E. RESEARCH COMMITTEE

Final Report from the University of Michigan

Tray Efficiencies in Distillation Columns

PUBLISHED JUNE 1960

Members of A.I.Ch.E. \$5.00

Non-members \$10.00

Paper Bound

Final Report from North Carolina State College

PUBLISHED SEPTEMBER 1959

Members of A.I.Ch.E. \$2.00

Non-members \$4.00

Paper Bound

Final Report from the University of Delaware

PUBLISHED DECEMBER 1958

Members of A.I.Ch.E. \$5.00

Non-members \$10.00

Paper Bound

Bubble-Tray Design Manual

prediction of fractionation efficiency

by the Distillation Subcommittee of the Research Committee

1. Enables the engineer to predict efficiencies for commercial bubble trays used in multicomponent fractionation. 2. Contains sample calculations made on plant-scale columns. 3. Includes calculation form sheets for the use of the reader. (Additional sheets may be purchased.) Members of A.I.Ch.E., \$5.00; Non-members, \$10.00; Calculation form sheets, \$.25. (One bound in book but also available for separate purchase). Hard covers, gold stamped, 6 $\frac{1}{2}$ " x 9 $\frac{1}{4}$ ", 94 pages, attractively designed and printed.

American Institute of Chemical Engineers

25 West 45 Street

New York 36, New York

Enclosed is my check for _____ (Add 3% sales tax for delivery in New York City.)

- () Final Report from the University of Michigan
- () Final Report from North Carolina State College
- () Final Report from the University of Delaware
- () Bubble Tray Design Manual

Name _____

Address _____

Member () Non-member ()

STAND and be counted

for the SYMPOSIUM SERIES

A STANDING ORDER

ensures your not missing a needed book
and saves you 10% on each book

Each book in the Series is a collection of papers in a specific field of chemical engineering. Some papers have been presented at A.I.Ch.E. symposia during national meetings; some have been submitted directly for publication. All are reviewed by experts in the particular fields and revised before publication.

During 1959 eight books were published—on heat transfer; nuclear engineering; computer techniques, chemical engineering education; reaction kinetics; adsorption, di-

alysis, and ion exchange.

At least six more are planned for 1960—on rockets and missiles, computer techniques, nuclear engineering, and heat transfer.

This Series is produced in an attractive but economical format—8½ x 11 inch volumes, paper covered, averaging 150 to 200 pages. It is priced as close to cost as possible for Members and about one-third higher for others.

MONOGRAPH & SYMPOSIUM SERIES

29-S. Heat Transfer—Chicago: The A.I.Ch.E.-sponsored papers presented at the Joint Heat Transfer Conference in 1958. \$4.00 to members, \$5.00 to nonmembers.

28-S. Nuclear Engineering, Part VIII: The A.I.Ch.E.-sponsored papers presented at the 1958 Nuclear Congress, together with additional papers from A.I.Ch.E. Symposia. \$3.50 to members, \$4.50 to nonmembers.

26-S. Chemical Engineering Education—Academic and Industrial: The new philosophies behind both graduate and undergraduate curricula, together with descriptions of successful programs held in industry. \$3.00 to members, \$4.00 to nonmembers.

25-S. Reaction Kinetics and Unit Operations: 23 surveys of the basic fields in chemical engineering, covering the most recent developments and future trends. \$3.50 to members, \$4.50 to nonmembers.

24-S. Adsorption, Dialysis, and Ion Exchange: Detailed discussion of the use of these operations in fractionation and other operations, with emphasis on the chemical viewpoint. \$3.50 to members, \$4.50 to nonmembers.

18-S. Heat Transfer—Louisville: Studies of vertical tubes, forced-circulation boiling, cross-flow cooling tower, burn-out, boiling liquids, metal vapors, condensation, large temperature differences, single-baffle exchangers. Vol. 52; paper bound; about 125 pp.; \$3.00 to members, \$4.00 to nonmembers.

17-S. Heat Transfer—St. Louis: Data on surface boiling, liquid metals, gas-solid contact, convection; solids melting, immiscible liquids, nonisothermal flow, and jacketed agitated kettles. Vol. 51; paper bound; 125 pp.; \$3.00 to members, \$4.00 to nonmembers.

9-S. Heat Transfer—Research Studies: Data on fluidized systems, free convection between horizontal surfaces, temperature-level and radiation effects, liquid-solid sus-

pensions, two-phase, two-component flow, pyrolysis-coil designs, and metal wetting and gas entrainment. Vol. 50; paper bound; 67 pp.; \$1.50 to members, \$2.25 to nonmembers.

5-S. Heat Transfer—Atlantic City: Studies of heated tubes, liquid metals, fluidized beds, three-fluid exchangers, etc. Vol. 49; paper bound; 162 pp.; \$3.00 to members, \$4.00 to nonmembers.

22-S, 23-S, and 27-S Nuclear Engineering—Parts V, VI, and VII: In all, 63 papers on the chemical engineering aspects of the nuclear field. Most of the A.I.Ch.E.-sponsored papers presented at the 1958 Nuclear Congress are included in Part VI. \$3.50 each to members, \$4.50 each to nonmembers.

19-S. Nuclear Engineering, Part IV: Containing papers sponsored by the A.I.Ch.E. at the second nuclear engineering and science congress, in Cleveland, this volume of 206 pages contains more on reactors, solvent extraction systems, economic design of power packages, neutron flux in critical assemblies, engineering design, reactor site selection, metallurgy, etc. Vol. 52; paper bound; \$3.00 to members, \$4.00 to nonmembers.

13-S. Nuclear Engineering, Part III: The third volume from the Ann Arbor meeting covers pulsed-column techniques; the breeder reactor; recovery of uranium from pitchblende; radiochemical processes; a series of articles on the impact of the atomic field on health, safety of individuals, education, etc.; materials testing reactor, radioisotope utilization. Vol. 50, 274 pp., paper bound; \$3.00 to members, \$4.00 to nonmembers.

12-S. Nuclear Engineering, Part II: The second volume from the first nuclear engineering congress, held at Ann Arbor, continues the technology of the first volume—reactors, analog computing techniques for reactor analysis, evaluation of reactor coolants, metallurgy, waste disposal, radiation damages and effects on structural materials. Vol. 50, 259 pp., paper bound; \$3.00 to members, \$4.00 to nonmembers.

11-S. Nuclear Engineering, Part I: The first volume from the first nuclear engineering congress, held at Ann Arbor, contains articles on the metallurgy of zirconium, beryllium, thorium, uranium, heat transfer studies in the nuclear field; and articles on reactors including the Swedish reactor; chlorination of aromatics under gamma radiation; gamma-ray polymerization of styrene and methyl methacrylate. Vol. 50, 280 pp., paper bound; \$3.00 to members, \$4.00 to nonmembers.

16-S. Mass Transfer—Transport Properties: Studies of gas bubbles, gas-film transfer, nonisothermal systems, liquid drops, thermal diffusion, gas viscosity, rotating cylinders, intermolecular forces. Vol. 51; paper bound; 125 pp.; \$3.00 to members, \$4.00 to nonmembers.

15-S. Mineral Engineering Techniques: Studies of the separation techniques of flotation, fine sizing, and sink and float and various related concentrating devices, together with cost and design considerations, assembled with a view toward acquainting the chemical engineer with the possibility of applying these techniques in his own field. Vol. 50; paper bound; 85 pp.; \$2.50 to members, \$3.75 nonmembers.

14-S. Ion Exchange: Data on mixed-bed deionization rare-earth separation, adsorption and stripping, economic evaluation, hydroxide-cycle operations, asymptotic solution of mechanisms, use of gross components. Vol. 50; paper bound; 134 pp.; \$3.00 to members, \$4.00 to nonmembers.

20-S. Liquid Metals Technology, Part I: A volume on liquid metals problems of special interest to the chemical engineer, it contains ten articles (84 pages) on the manufacture and availability of alkali metals, sodium heat transfer, sampling analysis for impurities, description of high-temperature loops, material transport, corrosion and mass transfer, thermal conductivity, etc. Vol. 53; paper bound; \$3.00 to members, \$4.00 to nonmembers.

7-S. Applied Thermodynamics: Experimental data, largely on hydrocarbons, and the results of various calculation programs covering enthalpies of mixtures, vapor liquid equilibria, and the thermodynamic properties of single components. Vol. 49; paper bound; 165 pages; \$3.00 to members, \$4.00 to nonmembers.

6-S. Phase-Equilibria—Collected Research Papers: Papers on the methane-nitrogen ethane-ethylene, and ethyl alcohol-water systems; reduced crudes at subatmospheric pressures; hydrocarbon mixtures; integral calculation, and graphical methods for distillation. Vol. 49; paper bound; 113 pp.; \$3.00 to members, \$4.00 to nonmembers.

3-S. Phase-Equilibria—Minneapolis and Columbus: Studies of pressure-vapor temperature relations, solubility, graphical techniques, solvent extractions, etc. Vol. 48; paper bound; 122 pp.; \$3.00 to members, \$4.00 to nonmembers.

2-S. Phase-Equilibria—Pittsburgh and Houston: Studies of vapor-liquid equilibria under such topics as flash vaporization, nomographs, extraction, thermodynamics, isothermal and isobaric equations. Vol. 48; paper bound; 138 pp.; \$3.00 to members, \$4.00 to nonmembers.

4-S. Reaction Kinetics and Transfer Processes: Data on transfer phenomena in heterogeneous systems, including studies of fixed and fluidized beds, catalytic dehydration, alcoholysis, and diffusion. Vol. 48; paper bound; 125 pp.; \$3.00 to members, \$4.00 to nonmembers.

1-S. Ultrasonics—Two Symposia: Papers examining possibilities and limitations of applied acoustics in chemical processes and unit operations. Vol. 47; paper bound; 87 pp.; \$2.00 to members, \$2.75 to nonmembers.

8-S. Communications: Papers stressing accuracy and clarity in written and spoken communication and treating corollary problems such as sound psychological approaches, proper routing of correspondence and information, better accounting and statistical reports, and scientific organization of paper work. Vol. 49; paper bound; 57 pages; \$1.00 to members, \$1.50 to nonmembers.

21-S. Computer Techniques in Chemical Engineering: 12 papers, primarily on digital-computer techniques in use in the chemical industry. \$3.00 to members, \$4.00 to nonmembers.

1-M Reaction Kinetics in Chemical Engineering by Olaf A. Hougen: A survey of the historical development of chemical kinetics as applied to process design, of the present state of this technology, and of the most promising fields therein for immediate investigation. Vol. 47; paper bound; 78 pp.; \$2.25 to members, \$3.00 to nonmembers.

2-M. Atomization and Spray Drying by W. R. Marshall, Jr.: Covering the theory of spray drying and its industrial applications. Vol. 50; paper bound; 122 pp.; \$3.00 to members, \$4.00 to nonmembers.

To be certain receiving all the Symposium Series volumes from now on, return the **STANDING ORDER** coupon now.

AMERICAN INSTITUTE OF CHEMICAL ENGINEERS
25 West 45 Street, New York 36, New York

Enroll us in your Symposium Series **STANDING ORDER GROUP** to receive all future publications as soon as published, and bill them at 10% discount. Ship books to attention of the following person who will be acquainted with this operation:

PRINT NAME _____

ORGANIZATION _____

STREET _____

CITY _____ ZONE _____ STATE _____

Member () Nonmember ()

If you would like to start with some of the earlier publications you may have missed, enter the numbers here:

ONE responsible source...

Successfully operating industrial plants mark the path of Stearns-Roger development from the earliest days of process engineering. Stearns-Roger provides every service through one responsibility—one order. Rely on the experience and facilities of Stearns-Roger for design, fabrication and construction—new plant or modification.

Stearns-Roger
THE STEARNS-ROGER BUILDING, NEW YORK, N.Y.

DENVER
HOUSTON
SALT LAKE CITY

Stearns-Roger Engineering Co., Ltd. Calgary

• ENGINEERS • CONSTRUCTORS • MANUFACTURERS

INDEX OF ADVERTISERS

Computer Systems, Inc.	178
E. I. du Pont de Nemours, Inc.	
Outside Back Cover	
Hevi-Duty Electric Company	2J
Laboratory Plasticware Fabricators	3J
Stearns-Roger Mfg. Company	8J
Vulcan-Cincinnati, Inc.	
Inside Front Cover	

Advertising Officers

New York 36—Paul A. Jolcuvar, Adv. Sales Mgr., Carl G. Lassen, Asst. Adv. Sales Mgr., Donald J. Stroop, Dist. Mgr., Robert S. Bugbee, Dist. Mgr.; 25 W. 45th St., COLUMBUS 5-7330.

Philadelphia—Lee W. Swift, Jr., Dist. Mgr.; 1207 Broad-Locust Bldg., PENNYPACKER 5-5560.
Chicago 4—Martin J. Crowley, Jr., Dist. Mgr.; Robert Kliesch, Dist. Mgr.; 53 West Jackson Blvd., Room 504, HARRISON 7-3760.
Cleveland 15—Harry L. Gebauer, Dist. Mgr.; 1501 Euclid Ave., Superior 1-3315.
Pasadena 1, Calif.—Richard P. McKey, Dist. Mgr.; 465 Converse Place, MURRAY 1-0685.
Dallas 18—Richard E. Hoierman, Dist. Mgr.; 9006 Capri Drive, DIALMOND 8-1229.
Birmingham 9, Ala.—Fred W. Smith, Dist. Mgr.; 1201 Forest View Lane, VESTHAVEN, TREMONT 1-5762.

(Continued from page 2J)

libria, and chemical reaction equilibria. Also discussed in individual sections are power plant cycles, internal combustion engines, and refrigeration processes.

Aside from the reviewer's feeling that overemphasis has been placed on generalized correlations insofar as learning thermodynamics is concerned, the present volume represents an improvement in both content and coverage over the previous edition. The topics are well presented and well illustrated, and the text is certainly to be recommended for general use.

John B. Butt
Yale University

Computer Program Abstracts

Readers of the *A.I.Ch.E. Journal* who are interested in programming for machine computation of chemical engineering problems will find in each issue of *Chemical Engineering Progress* abstracts of programs submitted by companies in the chemical process industries. Collected by the Machine Computation Committee of the A.I.Ch.E., these programs will be published as manuals where sufficient interest is indicated. The following abstracts have appeared this year:

CEP (January, 1960), p. 86

Equilibrium Flash Vaporization (012)
 Equilibrium Flash Distillation (035)
 Smoker Distillation Program (037)

CEP (February, 1960), p. 90

Electric Log Interpretation (039)
 Solution of Counterflow Water Cooling Tower (040)
 Operational Characteristics of Isothermal Tubular Flow Reactors (041)

CEP (March, 1960), p. 86

Nonlinear Regression by Criterion of Least Squares (034)
 Batch Rectification of Binary Mixtures (042)
 Enthalpy Lookup (043)

CEP (April, 1960), p. 80

Multicomponent Extraction of Heavy Metal Nitrates with Tributyl Phosphate Solvents (045)
 General Analysis of Variance (047)
 Thermodynamic Functions of Diatomic Gases (048)

ilibria.
ections
com-
eration

feeling
ed on
ar as
erned,
n im-
cover-
The
well
nly to

butt
ersity

urnal
ng for
al en-
each
Prog-
nitted
rocess
chine
the
pub-
nt in-
g ab-

ization

(035)
(037)

(39)
Cool-

Iso-
actors

on of
Mix-

heavy
Phos-

(047)
Di-

1960